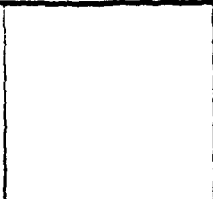


AD-A260 224



DTIC ACCESSION NUMBER



LEVEL



INVENTORY

AFOSR-TR-92-0514

DOCUMENT IDENTIFICATION

22 May 92

DISTRIBUTION STATEMENT

Approved for public release  
Distribution Unlimited

DISTRIBUTION STATEMENT

DTIC  
ELECTE  
FEB 8 1993  
S C D

DATE ACCESSIONED

DTIC		<input checked="" type="checkbox"/>
FRAC		<input type="checkbox"/>
UNANNOUNCED		<input type="checkbox"/>
DISTRIBUTION		<input type="checkbox"/>
BY		
DISTRIBUTION		
AVAILABILITY CODES		
DISTRIBUTION	AVAILABILITY AND/OR SPECIAL	
A-1		

DISTRIBUTION STAMP

DTIC QUALITY INSPECTED 3

DATE RETURNED

DEFENSE TECHNICAL INFORMATION CENTER



9301941

34928  
RICKARD

REGISTERED OR CERTIFIED NUMBER

DATE RECEIVED IN DTIC

PHOTOGRAPH THIS SHEET AND RETURN TO DTIC-FDAC

93 22 038

# REPORT DOCUMENTATION PAGE

Form Approved  
OMB No. 0704-0188

Public reporting burden for this collection of information is estimated to average 1 hour per response, including the time for reviewing existing data sources, gathering and maintaining the data needed, and completing and reviewing the collection of information. Send comments regarding this burden estimate or any other aspect of this collection of information, including suggestions for reducing this burden, to Washington Headquarters Services, Directorate for Information Operations and Reports, 1215 Jefferson Davis Highway, Suite 1204, Arlington, VA 22202-4302, and to the Office of Management and Budget, Paperwork Reduction Project (0704-0188), Washington, DC 20503.

1. AGENCY USE ONLY (Leave blank) 2. REPORT DATE: May 22, 1992 3. REPORT TYPE AND DATES COVERED: Final 1/1/91-12/31/91

4. TITLE AND SUBTITLE: Organization of the 1991 Optical Society of America Photonic Science Topical Meeting Series Oct 16  
5. FUNDING NUMBERS: G - AFOSR-91-0176

6. AUTHOR(S): Jarus W. Quinn

7. PERFORMING ORGANIZATION NAME(S) AND ADDRESS(ES): Optical Society of America  
2010 Massachusetts Ave. NW  
Washington, DC 20036  
8. PERFORMING ORGANIZATION REPORT NUMBER: AFOSR-TR-92-0014

9. SPONSORING/MONITORING AGENCY NAME(S) AND ADDRESS(ES): US Air Force Office of Scientific Research  
Department of the Air Force  
Bolling Air Force Base  
Washington, DC 20332-6448 Schlossberg  
10. SPONSORING/MONITORING AGENCY REPORT NUMBER: 2305/A1 NE

11. SUPPLEMENTARY NOTES:

12a. DISTRIBUTION / AVAILABILITY STATEMENT: Approved for public release  
Distribution unlimited  
12b. DISTRIBUTION CODE:

13. ABSTRACT (Maximum 200 words): Attach list of reports supported by Optical Society of America  
Photorefractive Materials, Effects, and Devices  
Integrated Photonics Research  
Nonlinear Guided Wave Phenomena  
Optical Amplifiers and Their Applications  
Optical computing  
Picosecond Electronics and Optoelectronics  
Quantum Optoelectronics  
Photonic Switching  
Microphysics of Surfaces: Beam Induced Processes  
Soft X-ray Projection Lithography  
Short Wavelength Coherent Radiation, Generation & Applications  
Persistent Spectral Hole-Burning: Science & Applications

14. SUBJECT TERMS 15. NUMBER OF PAGES  
16. PRICE CODE

17. SECURITY CLASSIFICATION 18. SECURITY CLASSIFICATION 19. SECURITY CLASSIFICATION 20. LIMITATION OF ABSTRACT

# **PERSISTENT SPECTRAL HOLE- BURNING: SCIENCE AND APPLICATIONS**

*Sponsored by*  
**Optical Society of America**

**1991 TECHNICAL DIGEST  
SERIES VOLUME 16**

**SEPTEMBER 26-28, 1991  
MONTEREY, CALIFORNIA**



# Persistent Spectral Hole-Burning: Science and Applications

*Summaries of papers presented at the Persistent Spectral  
Hole-Burning: Science and Applications Topical Meeting*

September 26–28, 1991  
Monterey, California

1991 Technical Digest Series  
Volume 16

CONFERENCE EDITION

*Sponsored by*  
Optical Society of America

*Partial support provided by*  
Air Force Office of Scientific Research

The organizers of the conference wish  
to acknowledge contributions by  
IBM and Coherent Laser Group

Optical Society of America  
2010 Massachusetts Avenue, NW  
Washington, DC 20036

Articles in this publication may be cited in other publications. In order to facilitate access to the original publication source, the following form for the citation is suggested:

Name of Author(s), "Title of Paper," in Technical Digest on Persistent Spectral Hole-Burning: Science and Applications, 1991 (Optical Society of America, Washington, D.C., 1991), Vol. 16, pp. xx-xx.

**ISBN Number**

Conference Edition	1-55752-204-9 (softcover)
Postconference Edition	1-55752-205-7 (hardcover)
(Note: Postconference Edition includes postdeadline papers.)	
1991 Technical Digest Series	1-55752-192-1 (hardcover)

**Library of Congress Catalog Card Number**

Conference Edition	90-64482
Postconference Edition	90-64481

Copyright © 1991, Optical Society of America

Individual readers of this digest and libraries acting for them are permitted to make fair use of the material in it, such as to copy an article for use in teaching or research, without payment of fee, provided that such copies are not sold. Copying for sale is subject to payment of copying fees. The code 1-55752-192-1/91/\$2.00 gives the per-article copying fee for each copy of the article made beyond the free copying permitted under Sections 107 and 108 of the U.S. Copyright Law. The fee should be paid through the Copyright Clearance Center, Inc., 21 Congress Street, Salem, MA 01970.

Permission is granted to quote excerpts from articles in this digest in scientific works with the customary acknowledgment of the source, including the author's name and the name of the digest, page, year, and name of the Society. Reproduction of figures and tables is likewise permitted in other articles and books provided that the same information is printed with them and notification is given to the Optical Society of America. Republication or systematic or multiple reproduction of any material in this digest is permitted only under license from the Optical Society of America; in addition, the Optical Society may require that permission also be obtained from one of the authors. Address inquiries and notices to Director of Publications, Optical Society of America, 2010 Massachusetts Avenue, NW, Washington, DC 20036. In the case of articles whose authors are employees of the United States Government or its contractors or grantees, the Optical Society of America recognizes the right of the United States Government to retain a nonexclusive, royalty-free license to use the author's copyrighted article for United States Government purposes.

The views and conclusions contained in this document are those of the author(s) and should not be interpreted as necessarily representing the official policies or endorsements, either expressed or implied, of the Air Force Office of Scientific Research or the U.S. Government.

# CONTENTS

Advance Program.....	v
ThA Spectral Diffusion: Observables and Dynamics.....	1
ThB Optical Processing and Holography: 1 .....	23
ThC Optical Processing and Holography: 2 .....	37
ThD External Fields.....	55
ThE Poster Session: 1 .....	73
FA High Temperature and Photon Gating.....	133
FB Time Domain.....	163
FC Mechanisms: 1 .....	185
FD Mechanisms: 2.....	201
FE Poster Session: 2.....	219
SA Linewidth and Relaxation .....	277
SB Novel Spectroscopies and Systems .....	299
Key to Authors and Presiders.....	323

## TECHNICAL PROGRAM COMMITTEE

**W. E. Moerner, Chair**  
*IBM Almaden Research Center*

**Michael Fayer**  
*Stanford University*

**J. Friedrich**  
*University of Mainz, Federal Republic of Germany*

**Dietrich Haarer**  
*University of Bayreuth, Federal Republic of Germany*

**Kazuyuki Horie**  
*The University of Tokyo, Japan*

**Michael Jefferson**  
*IBM Almaden Research Center*

**Roger Macfarlane**  
*IBM Almaden Research Center*

**Masaharu Mitsunaga**  
*NTT Basic Research Laboratories, Japan*

**Thomas W. Mossberg**  
*University of Oregon*

**R. I. Personov**  
*Moscow Institute of Spectroscopy, USSR*

**K. Rebane**  
*Estonian Academy of Sciences, USSR*

**Seishiro Saikan**  
*Osaka University, Japan*

**Kazuaki Sakoda**  
*Toray Industries, Inc., Japan*

**Gary Scott**  
*University of California, Riverside*

**Albert Sievers**  
*Cornell University*

**Robert Silbey**  
*Massachusetts Institute of Technology*

**James Skinner**  
*University of Wisconsin*

**G. J. Small**  
*Iowa State University*

**Toshiro Tani**  
*Electrotechnical Laboratory, Japan*

**S. Volker**  
*University of Leiden, The Netherlands*

**Urs Wild**  
*ETH, Switzerland*

**William M. Yen**  
*University of Georgia*

WEDNESDAY, SEPTEMBER 25, 1991

PORTOLA LOBBY

6:30 pm-8:00 pm REGISTRATION

DeANZA III

6:30 pm-8:00 pm INFORMAL RECEPTION

THURSDAY, SEPTEMBER 26, 1991

PORTOLA LOBBY

7:30 am-6:00 pm REGISTRATION/SPEAKER &  
PRESIDER CHECK-IN

DeANZA III

8:30 am-10:30 am

ThA, SPECTRAL DIFFUSION: OBSERVABLES AND DYNAMICS

D. L. Huber, *University of Wisconsin, Presider*

8:30 am (Invited)

ThA1 Spectral diffusion of optical transitions in doped polymer glasses below 1 K, D. Haarer, K.-P. Muller, *U. Bayreuth, F.R.G.* We have performed optical hole-burning experiments in the temperature range between 25 and 500 mK and found a linear temperature law which we ascribe to spectral diffusion. Implications to the theory of TLS are discussed. (p. 2)

9:00 am (Invited)

ThA2 Time dependent hole-burning and optical coherence experiments as probes of spectral diffusion in low temperature glasses, Michael D. Fayer, *Stanford U.* Time dependent hole-burning experiments (10  $\mu$ sec to 10,000 sec) and photon echo and stimulated echo experiments performed on chromophores in low temperature glasses are used to investigate spectral diffusion. (p. 6)

9:30 am

ThA3 Frequency dependence of IR radiation-induced spectral diffusion in hole-burning systems, W. Richter, *U. Bayreuth, F.R.G.* Spectral width and area of persistent photochemical holes in polymeric matrices show different light-induced spectral diffusion behavior depending on the frequency of the infrared light. (p. 10)

9:45 am

ThA4 Time-resolved hole-burning in  $YLiF_4:Er^{3+}$  with Zeeman scanning, Y. P. Wang, R. S. Meltzer, *U. Georgia*; R. Wannemacher, R. M. Macfarlane, *IBM Almaden Research Center.* The observed spectral diffusion is modeled with a computer simulation that includes the dynamics of a frozen core of  $F$  nuclear spins. (p. 12)

THURSDAY, SEPTEMBER 26, 1991—Continued

10:00 am

ThA5 Photon echo and time-resolved fluorescence anisotropy measurements of organically doped solgel glasses, Drew M. L'Esperance, Robert A. Crowell, Eric L. Chronister, *UC-Riverside.* We present time resolved measurements of homogeneous dephasing of organic dopants in inorganic solgel glasses. Organically doped solgel glasses have been synthesized and their dynamics investigated. (p. 15)

10:15 am

ThA6 Ultrafast dephasing of resorutin in *D*-ethanol glass from 1.8 to 35 K studied by incoherent photon echo, N. V. Gruzdev and Yu. G. Vainer, *Institute of Spectroscopy of the Academy of Sciences U.S.S.R.* The  $T$ -dependence of the optical dephasing in doped organic glass was measured by incoherent photon echoes. The difference between picosecond and incoherent photon echoes results was obtained. (p. 18)

PORTOLA LOBBY

10:30 am-11:00 am COFFEE BREAK

DeANZA III

11:00 am-12:00 m

ThB, OPTICAL PROCESSING AND HOLOGRAPHY: 1

Masaharu Mitsunaga, *NTT Basic Research Laboratories, Japan, Presider*

11:00 am (Invited)

ThB1 Error-corrective recall of digital optical images in neural network models by photoburning of spectral holes, Karl K. Rebane, Olavi Ollikainen, *Estonian Academy of Sciences, U.S.S.R.*; Alexander Rebane, *Swiss Federal Institute of Technology.* We discuss the concept and present experimental implementation of hole-burning memory coded as 2-D and 4-D parallel digital autoassociative interconnections matrices which has error-correcting capability. (p. 24)

11:30 am

ThB2 Persistent spectral hole-burning uses for massive optical neural network computers, Philip D. Henshaw, Steven A. Lis, *SPARTA, Inc.* Persistent spectral hole-burning materials can be utilized for optical interconnections. Our device uses the additional dimension of wavelength to fully connect two 2-D planes. (p. 28)

11:45 am

ThB3 Time-and-space-domain holography and shaping of light pulses by spectral hole-burning filters; new developments, Rein Kaarli, Peeter Saari, Heiki Sonajalg, *Estonian Academy of Sciences, U.S.S.R.* Time-domain interference of accumulated photon echoes, its use in time-domain holography, and problems of pulse shaping via temporal filters are investigated theoretically and experimentally. (p. 32)

12:00 m-1:30 pm LUNCH BREAK (on your own)

THURSDAY, SEPTEMBER 26, 1991—Continued

DeANZA III

1:30 pm–3:00 pm

**ThC, OPTICAL PROCESSING AND HOLOGRAPHY: 2**  
Michael Jefferson, *IBM Almaden Research Center, Presider*

1:30 pm (Invited)

**ThC1 Molecular computing**, Urs P. Wild, Alois Renn, *Swiss Federal Institute of Technology*. The concept of molecular computing is based on spectral hole-burning, the shift of molecular energy levels in an electric field, and on holography. The spectroscopic properties of dye molecules in a polymer film enable data storage as well as data processing in a single system. (p. 38)

2:00 pm (Invited)

**ThC2 Holograms in time and space: imaging through a scattering medium**, Alexander Rebane, *Swiss Federal Institute of Technology*; J. Feinberg, *U. Southern California*. We demonstrate imaging through an opaque screen using temporal holography in a persistent spectral hole-burning medium. (p. 42)

2:30 pm

**ThC3 Holographic optical data storage of 2000 images by photochemical hole-burning**, Bern Kohler, Stefan Bernet, Alois Renn, Urs P. Wild, *Swiss Federal Institute of Technology*. High-density holographic storage of 2000 grayscale images has been performed in a polymer thin film using a novel frequency-domain spectral hole-burning technique. (p. 46)

2:45 pm

**ThC4 Holography in frequency selective media: hologram phase and causality**, Stefan Bernet, Bern Kohler, Alexander Rebane, Alois Renn, Urs P. Wild, *Swiss Federal Institute of Technology*. Diffraction properties of holograms stored in persistent spectral hole-burning media are shown to be directly related to causality principles and are studied experimentally by using a frequency-tunable narrowband laser. (p. 50)

PORTOLA LOBBY

3:00 pm–3:30 pm COFFEE BREAK

DeANZA III

3:30 pm–5:30 pm

**ThD, EXTERNAL FIELDS**  
Gary Scott, *University of California, Riverside, Presider*

3:30 pm (Invited)

**ThD1 Applications of electric field effects on persistent spectral holes**, Max Maier, *U. Regensburg, F.R.G.* Basic principles and applications of the effects of an electric field on spectral holes of dye molecules in crystalline and disordered solids are discussed, including optical data storage, modulation and pulse forming of laser beams, and hybrid optical bistability. (p. 56)

THURSDAY, SEPTEMBER 26, 1991—Continued

4:00 pm (Invited)

**ThD2 Hole-burning and external-field effects: principles, recent results and new systems (superfine films)**, R. I. Personov, *Institute of Spectroscopy of the Academy of Sciences, U.S.S.R.* Recent results on Stark and Zeeman effects in organic molecules in amorphous solids studied by the hole-burning method are reviewed. The latest results for Langmuir-Blodgett films are discussed. (p. 60)

4:30 pm

**ThD3 Stark splitting in mixed crystals: octatetraene in *n*-alkanes**, Gerhard Gradl, Bryan E. Kohler, Curtis Westfield, *U. California-Riverside*. We have studied the effects of externally applied electric fields on narrow photochemical holes that can be burned in the zero-phonon component of the 0–0 transition of octatetraene substituted in various *n*-alkane crystals. (p. 62)

4:45 pm

**ThD4 Electric-field effects on hole spectra in doped polymers: a step toward 2-D optical spectroscopy**, L. Kador, *U. Bayreuth, F.R.G.* The linear Stark effect of hole spectra depends on the position in the inhomogeneous absorption band. This yields additional information on the dye-matrix interaction. (p. 65)

5:00 pm (Invited)

**ThD5 Spectral holes under pressure: proteins and glasses**, J. Friedrich, J. Zollfrank, *U. Mainz, F.R.G.* Pressure tuning of spectral holes enables the determination of solvent shift and compressibility. Its use with proteins allows an estimation of their volume fluctuations. (p. 68)

DeANZA III

5:30 pm–7:00 pm

**ThE, POSTER SESSION: 1**

**ThE1 Correlation between the relative zero-phonon electronic transition probabilities (Debye-Waller factors) and the matrix-induced spectral shifts of molecular impurity centers doped into amorphous hosts**, I. Renge, *Estonian Academy of Sciences, U.S.S.R.* Weak electron-phonon coupling of porphyrins is correlated with the small solvent shifts ( $< 200 \text{ cm}^{-1}$ ). Systems with solvent shifts  $> 2200 \text{ cm}^{-1}$  are not suitable for hole burning. (p. 74)

**ThE2 Persistent hole-burning study of core antenna of photosystem II**, M. Vacha, F. Adamec, M. Ambroz, J. Dian, J. Hala, Charles U., *Czechoslovakia*; L. Nedbal, *CSAV Institute of Microbiology, Czechoslovakia*. The role of the protein environment and the efficiency of excitation energy transfer in photosystem II core antenna in glass and polymer hosts are compared. (p. 78)

**ThE3 Hole-burning in the organic triplet state: side holes in an amorphous glass**, Hans Riesen, Elmars Krausz, *Australian National University*. Structured persistent holes are burned in the triplet phosphorescent state of organic molecules, both free and, we believe for the first time, as ligands in inorganic complexes. (p. 82)

**ThE4 Spectral hole-burning: dynamic approach to spectral diffusion**, I. S. Osadko, *Lenin State Pedagogical U., U.S.S.R.* The spectral diffusion problem is analyzed within the scope of a dynamic approach. It yields results that differ from those obtained with a stochastic approach. (p. 86)

**ThE5 Hole-burning optical magnetic resonance imaging**, Stephan Schiller, R. L. Byer, *Stanford U.* A theoretical study of spatial imaging of rare earth ions by projection reconstruction using transient hole-burning spectroscopy in magnetic field is presented. (p. 90)

**ThE6 Photon-gated photochemical hole-burning in a zinc-tetrabenzoporphyrin/aromatic cyanide system**. Lizeng Zhao, Zhengzhong Lu, Xiulang Zhang, Dongxiang Zhang, Xin Mi, Yuxin Ni, Duoyuan Wang, Lingzhi Hu, Huizhu He, Jie Xie, Junyi Zhang, *Academy of Sciences of China*. Photon-gated persistent spectral hole-burning was performed for zinc-tetrabenzoporphyrin molecules in the presence of aromatic cyanide in a poly(methyl methacrylate) host matrix at 4.2 K. (p. 94)

**ThE7 Preparation and properties of solgel thin films with porphines**, Hiroyuki Inoue, Takashi Iwamoto, Akio Makishima, Makoto Ikemoto, Kazuyuki Horie, *U. Tokyo, Japan*. Amorphous silica films doped with the porphine derivative were prepared by the solgel method and used for photochemical hole burning. It was found that the porphyrins in the films could be heat-treated up to 200°C. (p. 98)

**ThE8 Optimized read/write conditions of PHB memory**, Norio Murase, *Hitachi, Ltd., Japan*. Kazuyuki Horie, *U. Tokyo, Japan*. Photochemical hole-burning memory is proved theoretically to have the potential ability to achieve both high recording density and high speed readout in optimized read/write conditions. (p. 102)

**ThE9 Hole multiplexing in quinone derivative photochemical hole-burning systems**, Motomu Yoshimura, Tetsuya Nishimura, Eiji Yagyu, Noriaki Tsukada, Tetsu Takeyama, *Mitsubishi Electric Corp., Japan*. We have been investigating the hole-burning reaction of quinone derivatives to elucidate the effects on hole multiplexing, hole formation wavelength range, and electric-field effect. (p. 106)

**ThE10 Antihole formation in intramolecular tunnel systems**, G. Gradl, A. Feis, J. Friedrich, *Johannes Gutenberg U. Mainz, F.R.G.* Hole-burning in dimethyl-s-tetrazine doped *n*-octane leads to very sharp perfectly Lorentzian antiholes from which the rotational tunnel splitting of the methyl group can be determined. (p. 110)

**ThE11 Subnanosecond time-resolved study of accumulated photon echoes in chlorin-doped polymer films at 1 K**, Hansruedi Gygax, Ekkehard Gortlach, Alexander Rebane, Urs P. Wild, *Swiss Federal Institute of Technology*. Photochemically accumulated photon echoes can be detected over more than 5 orders of magnitude with a time resolution of 40 ps using time-correlated single photon counting. (p. 114)

**ThE12 Spectral hole-burning between 2 K and room temperature in Sm<sup>2+</sup> doped substitutionally disordered microcrystals**, Keith Holliday, Changjiang Wei, Mauro Croci, Urs P. Wild, *Swiss Federal Institute of Technology*. Photochemical hole-burning has been investigated in Sm<sup>2+</sup> doped crystalline powders of the form  $M_xM_{1-x}FCl_{0.5}Br_{0.5}$  ( $M =$  group II ion) between 2 K and room temperature. (p. 118)

**ThE13 Optical filter based on spectral hole-burning in dye-doped amorphous solids**, R. Billmers, J. Davis, M. Squicciarini, *U.S. Naval Air Development Center*. The triplet trapping mechanism responsible for hole-burning is investigated in several dye/host combinations. Rhodamine 6G seems to be a possible filter candidate to match doubled Nd:YAG at 532 nm. (p. 122)

**ThE14 Hole-burning of the exciton-coupled antenna complex of *Rhodobacter sphaeroides***, N. R. S. Reddy, G. J. Small, *Iowa State U.* Nonphotochemical hole-burned spectra of the two protein-pigment complexes of *Rb. sphaeroides* were obtained and used to provide new insights on excitonic interactions and the temperature dependence of energy transfer. (p. 125)

**ThE15 Free volume model of thermally induced spectral diffusion**, Jun Tsuchiya, Jun-ichi Takahashi, Hiroshi Tanaka, *Idemitsu Kosan Co., Ltd., Japan*. We report thermally induced spectral diffusion (TISD) results of some dye/polymer systems and correlation between TISD and polymer properties. (p. 129)

FRIDAY, SEPTEMBER 27, 1991

FRIDAY, SEPTEMBER 27, 1991—Continued

**PORTOLA LOBBY**

7:30 am-6:00 pm **REGISTRATION/SPEAKER & PRESIDER CHECK-IN**

**DeANZA III**

8:30 am-10:30 am  
**FA, HIGH TEMPERATURE AND PHOTON GATING**  
A. J. Sievers, *Cornell University, Presider*

8:30 am (Invited)  
**FA1 Room temperature persistent spectral hole-burning using dielectric particles as photonic atoms**, Steve Arnold, *Polytechnic U. NY*. We show both theoretically and experimentally that a 2-D collection of fluorescent spherical microparticles acts as a persistent spectral hole-burning memory at room temperature. (p. 134)

9:00 am  
**FA2 Room temperature persistent spectral hole-burning in distributions of optical cavities: a simple Fabry-Perot model**, Dee W. Pack, *Aerospace Corp.*; Steve Arnold, *Polytechnic U. NY*. A theory of room temperature, persistent spectral hole-burning in distributions of optical cavities doped with photoreactive molecules is discussed. Cavity Q factors and size distributions determine the detailed hole shapes. (p. 138)

9:15 am  
**FA3 Inhomogeneous broadening and persistent spectral hole-burning of divalent samarium ions in alkaline earth metal halides**, Jiahua Zhang, Shihua Huang, Jiaqi Yu, *Changchung Institute of Physics of the Academy of Sciences, China*; Xiangjun Wang, *Tianjin Institute of Technology, China*. A more broadened inhomogeneous line and hole-burning was observed in a mixture at 77 K. The ratio of inhomogeneous to homogeneous linewidth reaches 130. (p. 142)

9:30 am  
**FA4 Room temperature persistent spectral hole-burning in  $\text{Sm}^{2+}:\text{SrFCl}_{0.5}\text{Br}_{0.5}$** , R. Jaaniso, H. Bill, *U. Geneva, Switzerland*. Two-photon reversible hole-burning is observed at 296 K in  $^5D_1 \rightarrow ^7F_0$  and  $^5D_0 \rightarrow ^7F_0$  transitions of  $\text{Sm}^{2+}$  ions in the partially disordered  $\text{SrFCl}_{0.5}\text{Br}_{0.5}$  single crystals showing ratio of an inhomogeneous and homogeneous linewidths of 20-25. (p. 146)

9:45 am  
**FA5 Suppression of dephasing by deuteration of amorphous host materials: porphyrin-doped polymers**, Kazuaki Sakoda, Masayuki Maeda, *Toray Industries, Inc., Japan*. Photochemical holes burned in porphyrin-doped deuterated polyvinylalcohol below  $\sim 80$  K are shown to be narrower than those in protonated polyvinylalcohol by 30-50%. (p. 150)

10:00 am  
**FA6 Photon-gated photochemical hole burning by two-color-sensitized photoreaction**, Kazuyuki Horie, Shinjiro Machida, Takashi Yamashita, *U. Tokyo, Japan*. A new type of photon-gated photochemical hole burning by a two-color-sensitized photoreaction is provided with zinc-tetratolyltetra-benzoporphine in glycidyl azide polymer with a gating ratio of  $> 500$ . (p. 154)

10:15 am  
**FA7 Persistent photon-gated spectral hole-burning in a new donor-acceptor electron transfer system**, Mingzhen Tian, Baozhu Luo, Wenlian Li, Shihua Huang, Jiaqi Yu, *Changchun Institute of Physics of the Academy of Sciences of China*. Photon-gated spectral hole-burning in a new donor-acceptor electron transfer system composed of *me.al*-tetrabenzoporphyrin derivatives (donors) and a solid acceptor is reported. (p. 158)

**PORTOLA LOBBY**

10:30 am-10:45 am **COFFEE BREAK**

**DeANZA III**

10:45 am-12:30 pm  
**FB, TIME DOMAIN**  
W. M. Yen, *University of Georgia, Presider*

10:45 am (Invited)  
**FB1 Temporal accessing of frequency-domain optical storage: specific approaches and general considerations**, Thomas W. Mossberg, *U. Oregon*. The basic principles of temporal access to frequency-domain optical storage are discussed. Comparison and contrasts with approaches employing direct spectral accessing of information are made. (p. 164)

11:15 am (Invited)  
**FB2 Time-domain optical data storage using  $\text{Eu}^{3+}$  ions in crystals**, Masaharu Mitsunaga, *NTT Basic Research Laboratories, Japan*. Recent progress in time-domain optical data storage using  $\text{Eu}^{3+}$  in  $\text{YAlO}_3$  and  $\text{Y}_2\text{SiO}_5$  is reviewed. Topics include cw photon echo, bit-by-bit storage, and spectral programming. (p. 170)

11:45 am  
**FB3 Incoherent light read-out of spectral holograms**, A. Debarre, J. C. Keller, J. L. Le Gouet, P. Tchenio, *Laboratoire Aime Cotton, France*. Optically stored spectral holograms are probed by long duration broadband light pulses. A field cross-correlation technique is used to sample the signal with subpicosecond time resolution. (p. 173)

12:00 m  
**FB4 Frequency-domain measurements of spectral hole patterns burned with phase coherent pulses**, C. Michael Jefferson, Alfred J. Meixner, *IBM Almaden Research Center*. We have measured and calculated ground-state population gratings created in the inhomogeneously broadened absorption band of  $\text{Eu}^{3+}:\text{YAlO}_3$  by pulse pairs whose relative phases could be varied. (p. 176)

FRIDAY, SEPTEMBER 27, 1991—Continued

12:15 pm

**FB5 Photon echo in Er-doped fibers: a new approach to femtosecond time-domain optical signal processing.** V. L. da Silva, Y. Silberberg, J. P. Heritage, E. W. Chase, M. A. Saifi, M. J. Andrejco, *Bellcore*. We report the observation of femtosecond accumulated photon echo in erbium-doped fibers and investigate its use in time-domain optical signal processing. (p. 180)

12:30 pm–2:00 pm LUNCH BREAK (on your own)

DeANZA III

2:00 pm–3:15 pm

FC MECHANISMS: 1

C. J. Small, *Iowa State University*, *Presider*

2:00 pm (Invited)

**FC1 Hole burning in the vibrational spectrum of crystals and glasses.** A. J. Sievers, *Cornell U.* Persistent IR spectral holes have been generated inside the inhomogeneously broadened vibrational absorption bands of small molecules matrix isolated in crystals and glasses. (p. 186)

2:30 pm

**FC2 Hydrogen bonds in a polymer investigated by picosecond infrared hole-burning.** H. Graener, *U. Bayreuth, F.R.G.* Hole burning with ultrashort pulses provides detailed insight in the structural and dynamic properties of hydrogen bonded polymers. Comparison with persistent holes shows interesting similarities. (p. 189)

2:45 pm

**FC3 Spectral and temporal dynamics of nonequilibrium phonons in YAG:Pr<sup>3+</sup>.** Xiao-jun Wang, W. M. Dennis, *U. Georgia*. We investigate the spectral and temporal evolution of decay products from monochromatic phonon generation in YAG:Pr<sup>3+</sup>. The temperature dependence associated with phonon decay is also determined. (p. 193)

3:00 pm

**FC4 Persistent spectral hole burning induced by ion tunneling in hydrogenated CaF<sub>2</sub>:Pr<sup>3+</sup> and SrF<sub>2</sub>:Pr<sup>3+</sup> crystals.** R. J. Reeves, *Oklahoma State U.*; R. M. Macfarlane, *IBM Almaden Research Center*. We have observed persistent spectral hole-burning due to light-induced hydrogenic ion motion in CaF<sub>2</sub>:Pr<sup>3+</sup>:D<sup>-</sup> and SrF<sub>2</sub>:Pr<sup>3+</sup>:D<sup>-</sup> and used this to measure ground-state hyperfine splittings. (p. 197)

PORTOLA LOBBY

3:15 pm–3:45 pm COFFEE BREAK

FRIDAY, SEPTEMBER 27, 1991—Continued

DeANZA III

3:45 pm–5:15 pm

FD, MECHANISMS: 2

Urs P. Wild, *Swiss Federal Institute of Technology*, *Presider*

3:45 pm (Invited)

**FD1 Linear electron-phonon interaction in dye-doped polymers: Boson peak frequencies in polymers.** Seishiro Saikan, *Osaka U., Japan*. Temperature dependences of the Debye-Waller factor and the homogeneous spectrum of dye-doped polymers have been investigated with femtosecond accumulated photon echo. (p. 202)

4:15 pm

**FD2 Iron-free cytochrome-C and myoglobin in buffer glass as a weakly coupling mesoscopic molecular system: hole-burning, absorption, and fluorescence spectra and their temperature properties.** Toshiro Tani, Youich Sakakibara, Hisao Takahashi, Kyonosuke Yamamoto, *Electrotechnical Laboratory, Japan*. Persistent spectral holes, antiholes and their temperature dependences of protoporphyrin cytochrome-C and myoglobin in buffer glasses are described with absorption and fluorescence observations. (p. 206)

4:30 pm

**FD3 Weak linear electron-phonon coupling in iron-free heme proteins.** J. W. I. Lin, T. Tada, Seishiro Saikan, T. Kushida, *Osaka U., Japan*; Toshiro Tani, *Electrotechnical Laboratory, Japan*. The femtosecond accumulated photon echoes of iron-free myoglobin and iron-free cytochrome-C reveal that the linear electron-phonon coupling is extremely weak in these materials. (p. 210)

4:45 pm (Invited)

**FD4 Spectral hole-burning in the storage hierarchy?** Roger F. Hoyt, *IBM Almaden Research Center*. The challenges and opportunities for a spectral hole-burning-based storage device are discussed in the environment of contemporary computer systems that rely on a hybrid storage hierarchy for high capacity and performance. (p. 214)

DeANZA III

5:15 pm–6:45 pm

FE, POSTER SESSION: 2

**FE1 Persistent hole-burning spectroscopy applications on phthalocyanine Langmuir-Blodgett films.** F. Adamec, M. Ambroz, J. Dian, M. Vacha, J. Hala, *Charles U., Czechoslovakia*; E. Brynda, *CSAV Institute of Macromolecular Chemistry, Czechoslovakia*. The excited-state lifetimes strongly influenced by fast excitation energy transfer within phthalocyanine Langmuir-Blodgett multilayers are determined from excitation hole-burning spectra. (p. 220)

**FE2 Kinetics of hole-burning in inhomogeneously broadened spectra: origin of nonexponentiality and problem of burning efficiency dispersion.** E. I. Alshits, B. M. Kharlamov, N. I. Ulitsky, *Institute of Spectroscopy of the Academy of Sciences U.S.S.R.* A method is developed which permits correct measurement of burning efficiency dispersion in strongly inhomogeneously broadened spectra. (p. 224)

**FE3 Spectral diffusion decay for strongly interacting spins in glasses.** U. Zurcher, R. Silbey, *Massachusetts Institute of Technology.* We study the spectral diffusion for large strain fields in a glass. We examine the relevant time scales for dephasing processes. (p. 228)

**FE4 Electrooptical multistable switches based on persistent spectral holes.** David M. Hanson, *SUNY-Stony Brook.* An external electric field can provide a nonlinear response in sample transmission, absorption, or diffraction to produce novel electrooptical devices. (p. 232)

**FE5 Marker mode structure in the primary donor state of bacterial reaction centers.** P. Lyle, G. J. Small, *Iowa State U.*; T. J. DiMugno, J. R. Norris, *U. Chicago.* Marker mode structure is characterized by photochemical hole-burning for the primary donor absorption profile (P870) of fully deuterated *Rhodobacter sphaeroides* and compared to that of the protonated form. (p. 233)

**FE6 Solvation effects of organic dyes in polymers: wavelength dependence of the Stark effect.** Eric Vauthey, Keith Holliday, Changjiang Wei, Alois Renn, Urs P. Wild, *Swiss Federal Institute of Technology.* The wavelength dependence of the dipole moment difference between the ground and excited states of two polar dyes has been measured and attributed to solvation effects. (p. 236)

**FE7 Elucidation of photophysics and photochemistry in polyacene photoadducts.** Mark A. Iannone, Gary W. Scott, *UC-Riverside.* Photoadducts of anthracene with tetracene and of 9-bromoanthracene with tetracene are studied by photochemical hole-burning (PHB) and emission spectroscopy. The low temperature photochemical decomposition mechanism, excited vibronic level energies, and PHB hole depth vs intensity are reported. (p. 240)

**FE8 Fluorine spin diffusion barrier in Pr<sup>3+</sup>:LaF<sub>3</sub>, observed by cross relaxation.** L. L. Wald, E. L. Hahn, *UC-Berkeley*; M. Lukac, *Josef Stefan Institute, Yugoslavia.* We report Pr-F cross relaxation rates in Pr<sup>3+</sup>:LaF<sub>3</sub>, indicating nearly complete detuning of the fluorine spins near the optical ion. (p. 244)

**FE9 Crystalline model systems probing dynamics and electric-field effects.** T. Attenberger, U. Bogner, *U. Regensburg, F.R.G.* Spectral holes and antiholes in crystalline systems such as perylene/*n*-heptane were used to study dynamics in double-well potentials and electric field-induced level shifts. (p. 248)

**FE10 Light- and thermo-induced spectral diffusion in organic amorphous systems measured via hole-burning Stark spectroscopy.** E. I. Alshits, B. M. Kharlamov, N. I. Ulitsky, *Institute of Spectroscopy of the Academy of Science, U.S.S.R.* Light- and thermo-induced spectral diffusion (LISD and TISD) are investigated by hole-burning Stark spectroscopy on chlorin in polyvinylbutyral films. LISD is nonefficient in the investigated case; TISD has an activation character. (p. 252)

**FE11 Stark effect on persistent spectral holes measured by the electric-field modulation technique.** Toshiyuki Shimada, Hiroyuki Suzuki, *NTT Optoelectronics Laboratories, Japan.* The Stark effect on spectral holes is measured using the electric-field modulation technique. It enables us to detect a small spectral change caused by a weak field. (p. 256)

**FE12 New systems of organic photon-gated photochemical hole-burning.** Duoyuan Wang, Lingzhi Hu, Huizhu He, Lizeng Zhao, Xin Mi, Yuxin Ni, *Academy of Sciences, China.* Multiple photon-gated photochemical hole-burning is performed by donor-acceptor electron transfer for mesotetraphenyl (tetrabenzoporphyrinato) zinc in the presence of aromatic cyanide in poly (methylmethacrylate) at 4.2 K. (p. 260)

**FE13 Effect of intersystem crossing enhancement on the hole-burning process of metal-free porphyrin.** Youichi Sakakibara, Toshiro Tani, *Electrotechnical Laboratory, Japan*; Youkoh Kaizu, *Tokyo Institute of Technology, Japan.* Lifetime modification by intersystem crossing enhancement changed the population of energy levels of metal-free porphyrin and influenced the quantum yield of hole formation. (p. 264)

**FE14 Photon echo decay and optical storage in Pr-doped YAlO<sub>3</sub>.** Stefan Kroll, *Lund Institute of Technology, Sweden*; Ravinder Kachru, *SRI International.* Photon echoes in Pr-doped YAlO<sub>3</sub> demonstrate excitation-energy dependent homogeneous dephasing inconsistent with instantaneous spectral diffusion and time-domain optical storage using 200 pJ/bit. (p. 268)

**FE15 Hole-burning of long chain molecular aggregates.** R. Hirschmann, J. Friedrich, *Johannes Gutenberg U. Mainz, F.R.G.* A special feature of pseudoisocyanine aggregates is their excitonic states. Hole-burning is an excellent tool to study the homogeneous, inhomogeneous, and motional narrowing phenomena associated with these states. (p. 272)

SATURDAY, SEPTEMBER 28, 1991

PORTOLA LOBBY

8:00 am-12:30 pm REGISTRATION/SPEAKER &  
PRESIDER CHECK-IN

DeANZA III

8:30 am-10:30 am

SA, LINEWIDTH AND RELAXATION

Michael Fayer, *Stanford University, Presider*

8:30 am (Invited)

SA1 Molecular theory of inhomogeneous broadening in glasses, J. L. Skinner, *U. Wisconsin-Madison*. We describe a statistical mechanical theory of inhomogeneous broadening, focusing on quantities that can be directly measured in a variety of nonlinear optical experiments. Theory, together with experiment, provides information about the structure of glasses. (p. 278)

9:00 am (Invited)

SA2 Time-resolved transient hole-burning in disordered systems, Silvia Volker, *U. Leiden, The Netherlands*. Microsecond-living transient holes have been burned and probed, as a function of time and temperature, with a diode laser. Results are discussed in terms of spectral diffusion and compared with experiments on longer time scales in glassy and crystalline systems. (p. 281)

9:30 am

SA3 Accumulated photon echoes as a probe of radiationless relaxation processes in Nd-doped glasses, Keith W. Ver Steeg, Roger J. Reeves, Richard C. Powell, *Oklahoma State U.* The results of wavelength and temperature dependent measurements of accumulated photon echoes in Nd<sup>3+</sup>-doped fluoride, germanate, and silicate glasses are presented. (p. 282)

9:45 am

SA4 Persistent spectral hole-burning of Pr<sup>3+</sup> ions in (ZrO<sub>2</sub>)<sub>1-x</sub>(Y<sub>2</sub>O<sub>3</sub>)<sub>x</sub> mixed crystals, Koichiro Tanaka, Tsuyoshi Okuno, Tohru Suemoto, *U. Tokyo, Japan*; Hiroo Yugami, Mareo Ishigame, *Tohoku U., Japan*. Persistent spectral hole burning has been observed in Pr<sup>3+</sup>-doped (ZrO<sub>2</sub>)<sub>1-x</sub>(Y<sub>2</sub>O<sub>3</sub>)<sub>x</sub> mixed crystals. The homogeneous linewidth of the <sup>3</sup>H<sub>4</sub>-<sup>1</sup>D<sub>2</sub> transition is found to have a T<sup>1.24 ± 0.1</sup> dependence. (p. 286)

10:00 am

SA5 Optical pumping detection of anomalous NQR spectra of Pr<sup>3+</sup> in Pr<sup>3+</sup>:LaF<sub>3</sub>, L. L. Wald, E. L. Hahn, *UC-Berkeley*; M. Lukac, *Joseph Stefan Institute, Yugoslavia*. NQR frequency and linewidth variations of Pr hyperfine levels are reported for different positions within the main inhomogeneous optical line and satellite transitions of Pr<sup>3+</sup>:LaF<sub>3</sub>. (p. 290)

SATURDAY, SEPTEMBER 28, 1991—Continued

10:15 am

SA6 Hole-burning study of optical heating in low temperature glasses, A. A. Gorokhovski., *CUNY*; G. S. Zavr. V. V. Palm, A. L. Stolovich, *Estonian Academy of Sciences, U.S.S.R.* The spectral hole in the 0-0 band of an impurity molecule in a polymer ( $T = 0.6-5$  K) is influenced by non-equilibrium phonons generated through optical excitation within the vibronic band of another impurity. (p. 294)

PORTOLA LOBBY

10:30 am-11:00 am COFFEE BREAK

DeANZA III

11:00 am-1:00 pm

SB, NOVEL SPECTROSCOPIES AND SYSTEMS

W. E. Moerner, *IBM Almaden Research Center, Presider*

11:00 am (Invited)

SB1 Applications of spectral hole-burning spectroscopies to the excited electronic states and transport dynamics of photosynthetic units, G. J. Small, *Iowa State U.* Hole-burning methodologies suitable for the study of excited electronic state structure, energy and electron transfer dynamics, electron-phonon coupling, and heterogeneity of photosynthetic units are discussed. (p. 300)

11:30 am

SB2 Microwave-induced hole burning of the 638-nm zero-phonon transition and frequency-dependent dephasing of the N-V center in diamond, Max Glasbeek, Eric van Oort, *U. Amsterdam, The Netherlands*. Microwave-induced hole burning of an optical transition is demonstrated. Coherent transients show that the inhomogeneous broadening of the optical transition is due to microscopic strain. (p. 304)

11:45 am

SB3 Hole-burning of dye molecules adsorbed on metal oxide powders, T. Basche, C. Brauchle, *U. Munich, F.R.G.* Adsorbed dye molecules were investigated with spectral hole-burning between 1.6 and 77 K. In particular, we report on the temperature dependence of the holewidth and the Debye-Waller factor. (p. 308)

12:00 m (Invited)

SB4 Fluorescence excitation of single molecules, M. Orrit, J. Bernard, *U. Bordeaux I, France*. For small volumes of pentacene-doped terphenyl crystal, fluorescence excitation lines of single impurity molecules are resolved and studied according to light power and temperature. (p. 312)

12:30 pm (Invited)

SB5 Observation of spectral diffusion in solids using a single molecule, W. P. Ambrose, T. Basche, W. E. Moerner, *IBM Almaden Research Center*. Spontaneous spectral jumping and wandering of the optical resonance frequency for single pentacene defects in *p*-terphenyl crystals has been observed from 1.5 to 6 K using highly efficient fluorescence excitation spectroscopy. (p. 316)

NOTES

Thursday, September 26, 1991

# Spectral Diffusion: Observables and Dynamics

**ThA** 8:30am–10:30am  
DeAnza Room

D. L. Huber, *Presider*  
*University of Wisconsin*

# Spectral Diffusion of Optical Transitions in Doped Polymer Glasses below 1° K

D. Haarer and K.-P. Müller

Institute of Physics and BIMF, University of Bayreuth,

Postfach 101251, D-8580 Bayreuth, Germany

Photochemical and photophysical hole burning is a well established technique for eliminating the large inhomogeneous broadening of electronic transitions, which dominates the optical spectroscopy of amorphous solids. With the possibility of measuring the quasi-homogeneous width  $\Gamma_{qh}$  of electronic transitions, dye molecules can be used as probes for dynamical processes in amorphous solids [1][2]. The temperature dependence of the electronic linewidth of a given dye molecule in a crystalline lattice as compared to its linewidth in an amorphous solid shows large differences in both, its absolute value and its broadening behavior. This is due to the different origin of the dominant line broadening mechanisms: Interaction with phonons in a crystalline host and with two level systems (TLS) in an amorphous solid.

For different dye molecules in amorphous, organic matrices the quasihomogeneous linewidths have been measured as  $\Gamma_{qh} \propto T^\alpha$  with  $1 \leq \alpha \leq 2$  in the temperature range between 0.3K and 20K [3][4][5]. This is in contrast to temperature dependencies scaling with  $T^4$  [3] or  $\exp(-\Delta E/k_B T)$  [5] as obtained for similar dye molecules in crystalline matrices.

Various theories have been proposed for explaining the different exponents of the measured temperature dependencies. They differ in the model assumptions concerning the nature of the coupling between the TLS and the phonon bath on one hand and the coupling between the TLS and the electronic system on the other hand.

In order to decide which of these theories, if any, describes the broadening mechanism in amorphous solids it is important to investigate the behavior of optical linewidths at very low temperatures, at which the differences between phonon-like

and TLS-like excitations are expected to become very significant. For this reason we have constructed a  $^3\text{He}/^4\text{He}$  dilution refrigerator with optical windows for transmission spectroscopy. With this cryostat we were able to perform experiments on optical linewidths down to  $25\text{mK}$ , a temperature regime in which only very few optical data exist [6] [7].

Ref. [7] for instance contains the only published hole burning data in the temperature regime below  $300\text{mK}$ . These data exhibit a very puzzling temperature dependence, where the authors claim two crossovers of the exponent  $\alpha$  in one temperature decade. Furthermore a dependence of this exponent upon the location in the inhomogeneous absorption band was observed. In contrast to this, our measurements show no sign of a crossover and yield a linear dependence over the hole temperature range and no dependence of  $\alpha$  upon the wavelength. These new results should be quite relevant in the discussion of the multitude of theoretical models which have been suggested.

We investigated polystyrene (PS) doped with free-base phthalocyanine ( $\text{H}_2\text{Pc}$ ) and polymethylmethacrylate (PMMA) doped with tetra-4-tert-butyl phthalocyanine ( $\text{H}_2\text{Pc}^*$ ). The samples had optical densities of 0.55 and 0.42 respectively at a typical thickness of  $3.3\text{mm}$  and  $2\text{mm}$  respectively. The samples were prepared by bulk polymerisation of the solution of the dye in the monomer. The temperature dependence of the hole width is shown in figure 1 on a linear plot. Two observations are worth mentioning and are reported for the first time with good experimental evidence :

1. Both systems exhibit a linear temperature dependence over the whole temperature range down to  $25\text{mK}$  and no crossover to a constant linewidth is seen. This indicates that dynamical processes occur in amorphous systems even at these ultra-low temperatures.

2. A residual linewidth is found which is nearly the same for both systems, reconfirming that in an amorphous system the linewidth reaches the lifetime limited value  $\Gamma_h = 1/2\pi T_1$  (Heisenberg limit) of the electronic transition only in the limit  $T \rightarrow 0\text{K}$ . This limit is reached within 10% !

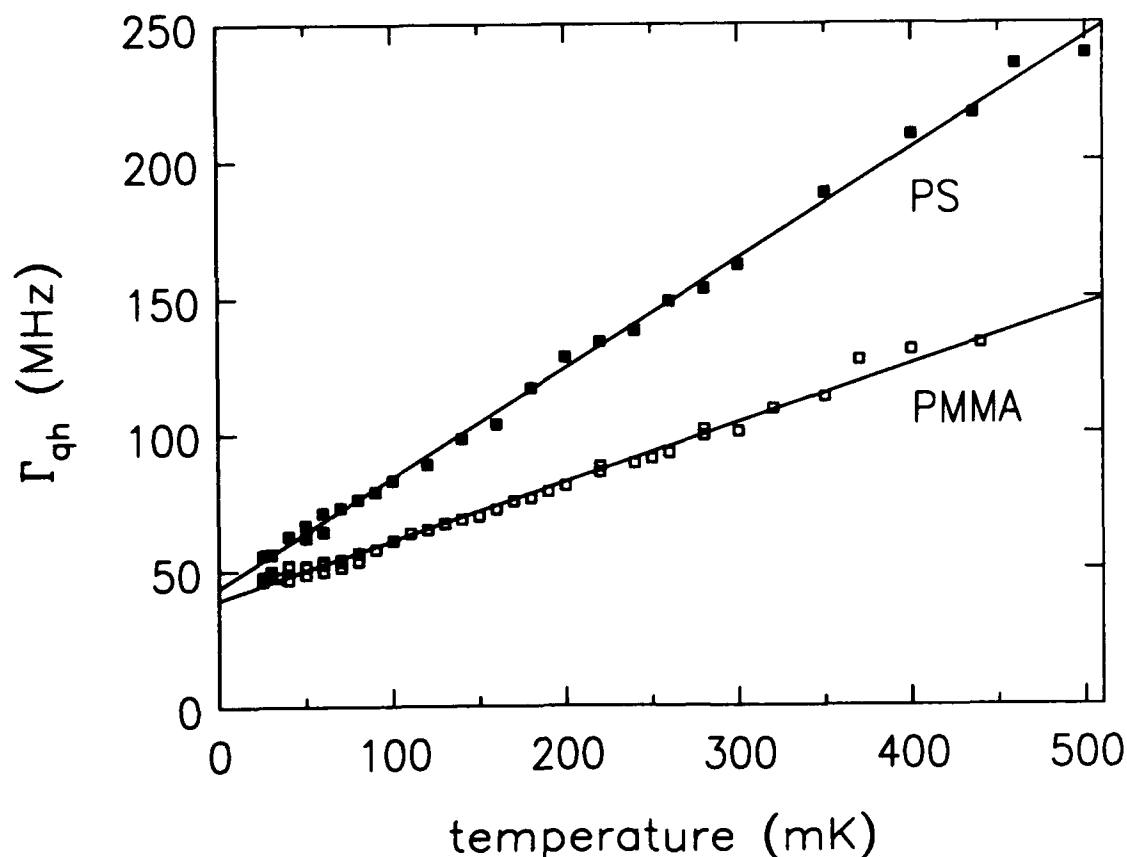


Figure 1: Temperature dependence of the quasi-homogeneous hole width  $\Gamma_{qh}$  for the  $S_1 \leftarrow S_0$  transition of  $H_2Pc$  and  $H_2Pc^*$  in the amorphous polymers PS and PMMA between 25 mK and 500 mK [10].

It is commonly assumed that the homogeneous linewidth of a dye molecule embedded in a solid matrix can be described as [2, pp 79]:

$$\Gamma_h = \frac{1}{2\pi T_1} + \frac{1}{\pi T_2^*} \quad (1)$$

In equation 1 the parameter  $T_1$  contains all energy relaxation processes and is assumed to be constant at low temperatures. The temperature dependence is therefore caused by the dephasing time  $T_2^*$ . In order to explain hole-burning data at temperatures between 1 K and 20 K in the polymer matrices PMMA, PS, and PE dephasing via local modes was assumed [8]. The measured linewidth can therefore be written as [8]:

$$\Gamma_{qh} = 2\Gamma_h + \Gamma_{SD} \quad (2)$$

where  $\Gamma_{SD}$  is the spectral diffusion part of the linewidth. The factor of two in equation

2 indicates that hole burning can be considered as a tandem two photon process, yielding twice the homogeneous linewidth [2]. Using our own experimental data we could verify this factor by comparing  $\Gamma_{qh}(T \rightarrow 0K) = 2\Gamma_h$  with the fluorescence lifetime of the electronic excitation. If we take the model of Black and Halperin [9] we can derive the following temperature dependence [10]:

$$\Gamma_{SD} = \frac{2\pi^2}{3\hbar} \langle |C_{ij}^{\Delta m}| \rangle \bar{P}(\lambda - \lambda_{min}) k_B T \quad (3)$$

The data of Figure 1 show beyond doubt that the density  $\bar{P}(\lambda - \lambda_{min})$  of TLS with tunneling parameters  $\lambda$  in the appropriate range can be considered constant for the two amorphous host polymers.

## References

- [1] J.Friedrich and D.Haarer, *Angew. Chem.* **96**, 96 (1984);  
*Angew. Chem. Int. Ed. Engl.* **23**, 113 (1984).
- [2] 'Persistent Spectral Hole-Burning: Science and Applications' W.E. Moerner (ed.) Springer, N.Y. (1987).
- [3] A.A.Gorokhovskii, Ya.V. Kikas, V.V. Pal'm, and L.A. Rebane, *Sov. Phys. Solid State* **23**(4) 602 (1981).
- [4] A. Burkhalter, G.W. Suter, U.P. Wild, V.D. Samoilenko, N.V. Rasumova, and R.I. Personov, *Chem. Phys. Lett.* **94**(5) 483 (1983).
- [5] H.P.H. Thijssen, R.E. van den Berg, and S. Völker, *Chem. Phys. Lett.* **103**(1) 23 (1983).
- [6] M.M. Broer, B. Golding, W.H. Haemmerle, J.R. Simpson, and D.L. Huber, *Phys. Rev. B* **33**(6) 4160 (1986).
- [7] A. Gorokhovskii, V. Korrovits, V. Palm, and M. Trummal, *Chem. Phys. Lett.* **125**(4) 355 (1986).
- [8] G. Schulte, W. Grond, D. Haarer, and R. Silbey, *J. Chem. Phys.* **88**(2) 679 (1988).
- [9] J.L. Black and B.I. Halperin, *Phys. Rev. B*, **16**, 2879 (1977).
- [10] K.-P. Müller and D. Haarer, *Phys. Rev. Lett.*, in print

Time Dependent Hole Burning and Optical Coherence Experiments as Probes  
of Spectral Diffusion in Low Temperature Glasses

Michael D. Fayer

Department of Chemistry  
Stanford University, Stanford, CA 94305

Dynamics and interactions in low temperature glasses can be studied with optical line narrowing techniques applied to chromophores embedded in glassy hosts. Prior to the use of optical methods, a wide variety of classical methods, such as heat capacities, were applied to the study of glasses. Results have been successfully interpreted in terms of a model of the glass potential surface described in terms of Two Level Systems (TLS). Because of the very large extent of inhomogeneous broadening in glassy systems, it is necessary to apply line narrowing methods to provide information on the dynamics and interactions of atoms and molecules with their environments.

A number of optical line narrowing methods have been developed to remove inhomogeneous broadening. Among these are hole burning, fluorescence line-narrowing, accumulated grating echoes, stimulated photon echoes, and photon echoes. The photon echo and the stimulated photon echo are the direct optical analogs of the magnetic resonance spin echo and stimulated spin echo. In magnetic resonance it is known that the spin echo measures the homogeneous dephasing time,  $T_2$ , and that the stimulated echo can have additional contributions to the dephasing time from spectral diffusion occurring on time scales slower than  $T_2$ . Until recently hole burning and fluorescence line narrowing have been the line narrowing techniques applied to the study of glasses. Various workers have defined the observables of these techniques as the homogeneous linewidth. Each technique, however, is sensitive to processes over a different range of time scales and, in general, will yield different linewidths.

The line narrowing experiments have been treated as if they are absorption experiments using optical absorption formalisms. The line narrowed lineshape was taken to be related to the Fourier transform of the two-time transition dipole-moment correlation function. However, the two time correlation function is insufficient to describe actual line-narrowing experiments, such as hole-burning, that are performed on glasses. In fact the two time correlation function description of experiments has been misleading. It indicated that all of the line narrowing experiments measured the same observable, the homogeneous line. It caused the fundamentally distinct nature of different experiments, i.e., the characteristic time scale associated with each experiment, to be absent from the theoretical treatments. Using the correct description of the different experiments makes it possible to obtain information on the broad distribution of rates of dynamical processes in complex systems.

A theoretical formalism has been developed by Berg et al. and extended by Bai and Fayer that relates the experimental observables in the various types of line narrowing experiments to details of the dynamics and intermolecular interactions in complex systems such as glasses. Each line-narrowing technique can be regarded as a specific case of a four-wave mixing experiment in which three input beams induce and subsequently interfere with a polarization in a medium to generate a fourth (signal) beam. The frequency domain experiments have specific time domain analogs obtained through Fourier transforms. The differences between the techniques are reduced to the timing between the pulses in the time domain description. It has also been shown that all of the line-narrowing experiments currently being performed on glasses are describable in terms of

correlation functions which are variants of the stimulated echo four time correlation function. In a stimulated echo, three pulses are applied at times, 0,  $\tau$  and  $\tau+T_w$ . A fourth pulse, the signal, emerges at time  $2\tau+T_w$ . The correlation function is usually specified by the time intervals between the pulses, i.e.,  $\tau$ ,  $T_w$ , and  $\tau$ . The detailed analysis shows that the differences among the various line narrowing experiments is the duration of the interval  $T_w$ , which has a major influence on the observables in the experiments.

First consider the photon echo experiment. It is the limit of a stimulated echo experiment with  $T_w=0$ . The second and third pulses in the sequence are time coincident. Inhomogeneous broadening is eliminated by the echo pulse sequence. The polarization in the sample decays as the separation between the two excitation pulses is increased. If the homogeneous line shape is Lorentzian, the polarization decays as  $\exp[-2\tau/T_2]$  and the signal intensity decays as  $\exp[-4\tau/T_2]$  where  $T_2$  is the homogeneous or transverse dephasing time. In addition to the dephasing induced by dynamics, population decay also contributes to the coherence loss. The pure dephasing time,  $T_2^*$  can be obtained by removing the population decay contribution.

In a stimulated echo, a pulse excites the chromophores as before but at time  $\tau$ , the second pulse is split into two pulses separated by the interval  $T_w$ . The echo appears as a fourth pulse. The stimulated photon echo is sensitive to homogeneous dephasing during the interval  $\tau$  between the first and second pulses and between the third and echo pulses. It is also sensitive to frequency fluctuations (spectral diffusion) that occur on the slower time scale,  $T_w$ .

Hole burning is a frequency domain line narrowing experiment. In a hole burning experiment, a narrowband laser excites a narrow transition frequency subset of the chromophores in the inhomogeneous line. A spectrum bracketing the point of excitation will show reduced absorption, the hole. Molecules that were excited by the laser can contribute to the hole, these being ones either initially on resonance with the laser, or ones which had fluctuations in energy during the hole burning period which brought them into resonance with the laser. In the time interval between burning and reading the hole, fluctuations in transition energies can bring molecules into the frequency region of the hole. Therefore, fluctuations in frequency which occur on the time scale from burning through reading the hole will determine the hole width. Since this time scale is typically long (seconds), the experiment will be sensitive to very slow dynamical processes (very slow spectral diffusion). It has been formally proven that hole burning is the frequency domain equivalent of the stimulated echo experiment. The spectrum of the hole is determined by the Fourier transform of the stimulated echo correlation function. Hole burning is a frequency domain stimulated echo experiment. In a hole burning experiment,  $T_w$  is essentially the time required to do the experiment, from burning through reading. The typical time scale for a photon echo experiment is 100 ps. Fluctuations occurring on a  $\mu$ sec or msec time scale are static on the time scale of a photon echo experiment, and do not contribute to the measured dephasing time. In contrast,  $\mu$ sec and msec time scale fluctuations are rapid on the seconds time scale of a hole burning experiment, and contribute to the measured dephasing time. Therefore, echo and hole burning experiments should not measure the same dephasing times in systems which have broad distributions of fluctuation rates. Changing  $T_w$ , the time scale of experiments, provides a path for the examination of dynamics over a very wide range of times from psec to 10,000 sec, or longer.

The dephasing time measured by photon echoes is substantially longer than the dephasing time measured by hole burning experiments. The additional broadening of a hole arises from slow time scale spectral diffusion. At low temperature, the ratio of the hole line width to echo determined line width is

proportional to the integral of the fluctuation rate distribution,  $P(R)$ , from time scale of the homogeneous dephasing time to the time,  $T_w$ , associated with the hole burning experiment.  $P(R)$  is the probability of having a dynamical process of rate  $R$  in the glass. Thus if  $T_w$  (time between burning and reading the hole) is varied over a range of times in which some rates are active, i. e.,  $1/R$  falls within the experimental time range, the holewidth will change. The change in holewidth can be used to quantitatively determine  $P(R)$ .

Recently we performed experiments of this nature. We examined cresyl violet in ethanol, ethanol-d, and glycerol glasses and resorufin in ethanol. For example, holes were measured at different times after burning in the cresyl violet/ethanol system. As the time between burning and reading increased, the hole broadens. For cresyl violet in ethanol at 1.30 K the holes broadened from 2.2 GHz to 3.2 GHz between 100 msec and 7000 sec. The holewidth was observed to vary over the entire range of study, but the change in width is most pronounced in the range of 50 seconds.

By performing a detailed theoretical analysis of the four time correlation function for hole burning, the dependence of the hole width on the waiting time,  $T_w$ , was obtained. It is possible to determine the fluctuation rate distribution by examining the holewidth, or the dephasing time in time domain experiments, as a function of  $T_w$ . A log normal distribution (Gaussian on a log time scale) was found to be the form of  $P(R)$  that fit the data well. Other functions will also fit the data, but not as well, e. g., a rectangular distribution. However, all functions which fit the data have three features in common: identical center frequencies, identical areas under the curve, and the same characteristic widths. At low temperatures, TLS relaxation is caused by phonon assisted tunneling. For this case, a log normal distribution of fluctuation rates is equivalent to a Gaussian distribution of tunneling parameters.

The experiments were repeated on resorufin in ethanol, and identical results were obtained. This proves that the dynamics in this time range are an intrinsic property of the glass, independent of the chromophore. Experiments on glycerol glass covering the same range of  $T_w$  displayed no hole broadening. Again demonstrating that the dynamics observed in ethanol glass is an intrinsic property of the glass and not a function of the experimental procedures.

The experiments described above used a conventional hole burning procedure, i. e., the hole was burned and following a time  $T_w$ , the hole was read out by sweeping the laser frequency. We have extended the measurements to  $T_w$ s (time between burning and reading) as fast as 10  $\mu$ sec. To accomplish this we measure the entire time response at a given frequency and then repeat this for a number of frequencies. This avoids the necessity of sweeping the reading frequency across the hole. To do this we employ a 300 MHz acousto-optic modulator (AOM). The narrow band dye laser beam is split, one part becomes the burning beam. This is passed through two AOMs which are used to turn it on and off rapidly to make the burning pulse. The other part of the dye laser beam passes through the 300 MHz AOM. The diffracted beam is shifted from the burning beam by exactly 300 MHz. To read at 600 MHz, the diffracted beam is passed back through the AOM. The beam is again diffracted, and is now shifted 600 MHz from the burn frequency. This process can be repeated up to six times with a single AOM with more than sufficient intensity to read the hole. Thus reading frequencies of 0, 300, 600, 900, 1200, 1500, and 1800 MHz shift from the center frequency are obtained. This can be done on either side of the line by taking either the +1 or -1 diffraction order.

At each probe frequency the full time dependence is measured. The holes used are transient, presumably triplet bottle neck holes, which refill on the 100 msec time scale for cresyl violet in ethanol. Therefore, about 1000 shots can be

averaged to obtain good quality data. Great care is taken to test for saturation, heating and other unwanted side effects.

The holes at 10  $\mu$ sec are 1.2 GHz compared to 3.2 GHz measured at 7000sec. Between 10  $\mu$ sec and 100 msec the increase in width plotted on a log time scale is well fit by a straight line, indicating a  $P(R) = 1/R$  distribution. Therefore, using hole burning we have examined hole widths from 10  $\mu$ sec to 10,000 sec, i. e., over 9 decades of time.

On fast time scales we have employed photon echo and stimulated echo experiments. The photon echo experiments demonstrates that the fluctuation rate distribution from 1 psec to 1 nsec also has the form  $P(R) = 1/R$ . Extrapolation of the msec to  $\mu$ sec hole burning data to the nsec time scale produces essentially perfect agreement with the photon echo data. This indicates that a  $1/R$  distribution exists in ethanol from psecs to 100 msec, i. e., over 11 decades of time.

As discussed above, the hole burning experiments are the Fourier transform of the stimulated echo experiment. To work on fast time scales it is preferable to work in the time domain rather than the frequency domain. To extend the short time echo experiments to longer times, to avoid the necessity of doing very fast hole burning experiments, and to fill in the gap between  $\mu$ sec time scale hole burning experiments and psec time scale photon echo experiments, we are using the stimulated photon echo. Because of spectral diffusion on a fast time scale, the stimulated echo decay is faster than the two pulse echo decay. This is equivalent to the classic NMR experiments that compare spin echoes and stimulated echoes to measure spectral diffusion. Until now, the only information on  $P(R)$  for fast fluctuation rates (short times) has come from the functional form of the echo decays. An exponential decay indicates a  $1/R$  distribution. By performing three pulse stimulated echo experiments for relatively short  $T_w$ s (time between the second and third pulses of the echo sequence; the time between the first and second pulse is scanned)  $P(R)$  can be determined in the same manner that measuring  $T_w$  dependent hole widths determines  $P(R)$ . The results indicate that  $P(R)$  is, in fact,  $1/R$  for fast fluctuation rates.

The net result is the observation of hole broadening over 9 decades of time and the determination of the low temperature ethanol glass fluctuation rate distribution over 16 decades of time. The increase in observed dynamical line widths by a factor of approximately 8 from the psec time scale to the 10,000 sec time scale is caused by spectral diffusion induced by the fluctuating Two Level System structure of glasses. The data is analyzed using a detailed theoretical description of the four time correlation functions that describe the various line narrowing experiments.

#### Reference Publications

"Probing Organic Glasses at Low Temperatures with Variable Time Scale Optical Dephasing Measurements", L.R. Narasimhan, K.A. Littau, D.W. Pack, Y.S. Bai, A. Elschner, and M.D. Fayer, Chem. Rev. 90 439 (1990).

"Probing Low Temperature Glass Dynamics by Fast Generation and Detection of Optical Holes", K.A. Littau and M.D. Fayer, Chem. Phys. Lett. 176 551 (1991).

"Observation of Fast time Scale Spectral Diffusion in a Low Temperature Glass: Comparison of Picosecond Photon and Stimulated Echo Experiments", L.R. Narasimhan, Y.S. Bai, M.A. Dugan, and M.D. Fayer, Chem. Phys. Lett. 176 335 (1991).

## Frequency Dependence of IR Radiation-Induced Spectral Diffusion in Hole-Burning Systems

W. Richter, M. Lieberth, D. Haarer  
 University of Bayreuth, Physical Institute  
 D-8580 Bayreuth, Germany

Persistent spectral holes burnt in polymeric matrices such as polyethylene (PE) and polymethylmethacrylate (PMMA), doped with metal-free phthalocyanine ( $H_2Pc$ ), show infrared (IR) light-induced spectral diffusion (Fig. 1) /1,2/.

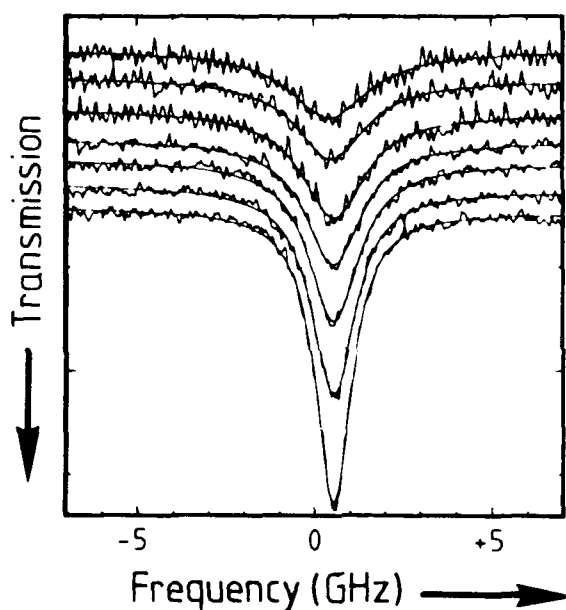


**Fig. 1:** Evolution of a photochemical hole at different times after burning and under infrared irradiation with an intensity of  $350 \mu W/cm^2$ . The solid lines are fitted Lorentzian line profiles.

With respect to the energy dose of the IR irradiation, the hole broadening exhibits no saturation, whereas the hole filling saturates at a level of 70-90% of the initial hole area, the exact value being dependent on the frequency of the infrared light.

Previous experiments with a broadband infrared source in the spectral region between  $2.5 \mu m$  and  $13 \mu m$  unravelled spectral diffusion processes which are strongly dependent on the matrix material. In the PMMA system, the increase of the hole width as a function of the IR energy dose is larger by a factor of 60 as compared to the PE system. Even the low-intensity room temperature blackbody radiation gives rise to strong hole broadening and hole filling phenomena.

Frequency-selective IR irradiation allows us to study the microscopic origin of these light-induced spectral-diffusion processes. Fig. 2 shows the hole broadening upon irradiation of different infrared frequencies but constant energy doses. Around  $3550\text{ cm}^{-1}$  there is a clear resonance in the broadening behavior. The bandwidth of the irradiated IR light was about  $100\text{ cm}^{-1}$ . The hole filling behavior is characterized by resonant spectral contributions in a broader frequency range between  $3450\text{ cm}^{-1}$  and  $3650\text{ cm}^{-1}$ .

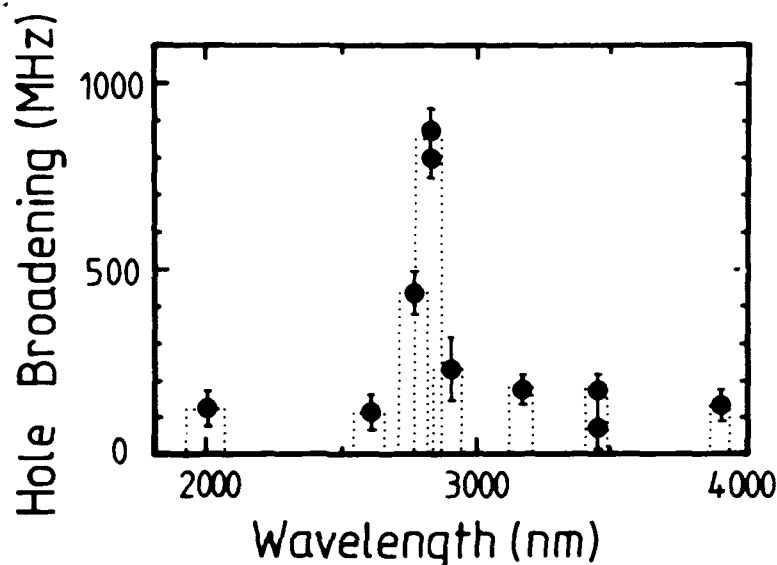


**Fig. 2:** Broadening of a photochemical hole in  $\text{H}_2\text{Pc/PMMA}$  as a function of the frequency of the irradiated IR light. The width of the rectangles give the spectral bandwidth of the light source.

Experiments with a deuterated PMMA matrix as well as the measured frequency dependence of the hole broadening leads us to exclude contributions of the C-H or the C-D stretching vibrations.

The measured contribution to the spectral diffusion in the near-infrared regime can be correlated with two fundamental vibrations of water molecules and with the first harmonic of the C=O stretching vibration in PMMA. Hole filling and hole broadening, which respond in different ways to the IR irradiation, seem to be caused by different types of vibrations in the matrix. Some model assumptions concerning Raman- and IR-aktiv modes will be discussed.

### References

- /1/ W. Richter, Th. Sesselmann, D. Haarer, Chem. Phys. Lett. 159, 235 (1989)
- /2/ A.A. Gorokhovskii, G.S. Zavg, V.V. Palm, JETP Lett. 48, 369 (1988)

TIME-RESOLVED HOLEBURNING IN  $\text{YLiF}_4:\text{Er}^{3+}$  WITH ZEEMAN SCANNING

Y. P. Wang and R. S. Meltzer

Department of Physics and Astronomy

University of Georgia

Athens, Georgia 30602 U.S.A.

Tel:404/542-5515 Fax:404/5422492

and

R. Wannemacher and R. M. Macfarlane

IBM Almaden Research Laboratory

San Jose, CA 95120 U.S.A.

We report the results of time-resolved optical holeburning of  $\text{Er}^{3+}$  ions in  $\text{YLiF}_4$  (0.02%). In earlier work for  $H//c$  we described the time evolution of holes burned at 33kG using laser scanning over a frequency of  $40\text{MHz}^1$  and we reported, using larger scans, the occurrence of optical side holes. We now describe results for  $H\perp c$  with scans  $> 400\text{MHz}$  using a new Zeeman technique for frequency scanning the optical transition frequencies which allow one to study the time evolution of the holes and their associated sideholes. The hole lineshapes evolve with time reaching a linewidth of  $\approx 10\text{MHz}$  after  $600\mu\text{s}$ . We identify the source of the time evolution of the hole shape as spectral diffusion resulting from mutual spin flips of the surrounding fluorine nuclei whose flip rates are strongly modified from the bulk rates by the presence of the large magnetic moment of the  $\text{Er}^{3+}$  ion which produces a "frozen core". A computer simulation which takes into account the details of the dynamics of the frozen core successfully describes the time evolution of the holes, confirming the dominant role of F nuclear spin flips.

Saturation holes are burned (pulse duration  $5\mu\text{s}$ ) with a single frequency tunable dye laser tuned to the  $^4I_{15/2} \rightarrow ^4F_{9/2}$  transition between the lowest crystal field levels of the two manifolds. The sample is placed in a large D.C. magnetic field and the transition between the lowest Zeeman sublevels is selected. The Zeeman scanning is accomplished by surrounding the sample with a small Helmholtz pair of copper coils (18 turns each coil) whose axis is parallel to the D.C. field. The hole is burned with a small current,  $I_0$ , in the coils which adds to the large D.C. field. After a delay, a weaker probe pulse is gated to the sample with an acousto-optic modulator while at the same time a ramped current is applied to the coil. When the current reaches the value  $I_0$ , the hole is on resonance with

the laser. Thus the optical frequency of the  $\text{Er}^{3+}$  ion transition,  $\nu$ , is scanned with the current to the coil. The frequency shift of the transition is given by

$$d\nu/dI = 1/2(g-g')\beta dH/dI \quad (1)$$

where  $g$  and  $g'$  are the  $g$ -values of the ground and excited states, respectively, and  $\beta$  is the Bohr magneton. For  $H_{\perp c}$ ,  $g_{\perp} = 8.3$  and  $g'_{\perp} < 1$ . For a maximum current of 10 A, this yields a scan range of over 2 GHz which can be accessed in 5  $\mu\text{s}$ .

Typical time-resolved holeburning spectra in a D.C. field of 29.5 kG for  $H_{\perp c}$  are shown in Fig. 1 for various time delays. The sideholes result from transitions in the burn or detection pulses in which nuclear spin flips of the adjacent F or Li nuclei occur accompanying the electronic transitions as discussed previously for  $H//c$ .<sup>2</sup>

The local field produced by nuclear spin flips on adjacent F nuclei is  $\approx 1$  G producing frequency shifts of the  $\text{Er}^{3+}$  transitions of  $\approx 5$  MHz. The linewidth of the holeburning spectra indicate that nearby F spin flips occur within the first 500  $\mu\text{s}$ . Dynamics of other  $\text{Er}^{3+}$  electron spins cannot contribute to the linewidth at the .02% concentration and 30 kG magnetic field since the nearest  $\text{Er}^{3+}$  in the excited spin state is  $> 1000$  Å from any  $\text{Er}^{3+}$  ion in its ground spin state. The local field change produced by the flip of such a distant nuclear spin is too small to make an observable contribution to the hole width.

The dynamics of the spectral hole is modeled with a computer simulation which considers mutual spin flips of  $\approx 1000$  surrounding F nuclear spins. The bulk nuclear spin flip rate is known to be about  $5 \times 10^3 \text{ s}^{-1}$ . However, the mutual flip rate of the nearby F spins, perturbed by the  $\text{Er}^{3+}$  magnetic moment, is greatly reduced. The rate is calculated assuming a magnetic dipole-dipole interaction where the spin flip energies of the two spins are out of resonance by an amount  $\Delta$ , calculated from the local fields produced by the  $\text{Er}^{3+}$  spin at the F sites. For the calculation the nuclear spin resonance linewidths are assumed to have the same value as that of the bulk spins ( $\approx 20$  kHz).

The time history of the local field at a typical  $\text{Er}^{3+}$  site is calculated by cycling through the lattice of F nuclear spins a large number of times, allowing the spins to undergo mutual spin flips stochastically, based on their calculated mutual spin flip rates. The time history of the transition frequency of  $\approx 10000$   $\text{Er}^{3+}$  spins, whose initial frequency distribution describes the hole spectrum immediately after burning, are obtained by starting the time evolution of each  $\text{Er}^{3+}$  spin at a different time in the typical time

history. This yields a predicted spectral evolution which agrees reasonably well with experiment. However the results suggest that the strongly perturbed nearby F spins flip somewhat more rapidly than predicted by the simple mutual spin flip model described above. This may result from 4 spin mutual flips or the role of the Li spin which have been ignored.

We acknowledge the support of the National Science Foundation, Grant DMR-9015468.

#### REFERENCES

1. R. Wannemacher, R. S. Meltzer and R. M. Macfarlane, *J. Lumin.* **45**, 307 (1990).
2. R. Wannemacher, R. M. Macfarlane, Y. P. Wang, D. Sox, D. Boye and R. S. Meltzer, *J. Lumin.* **48/49**, 309 (1991)

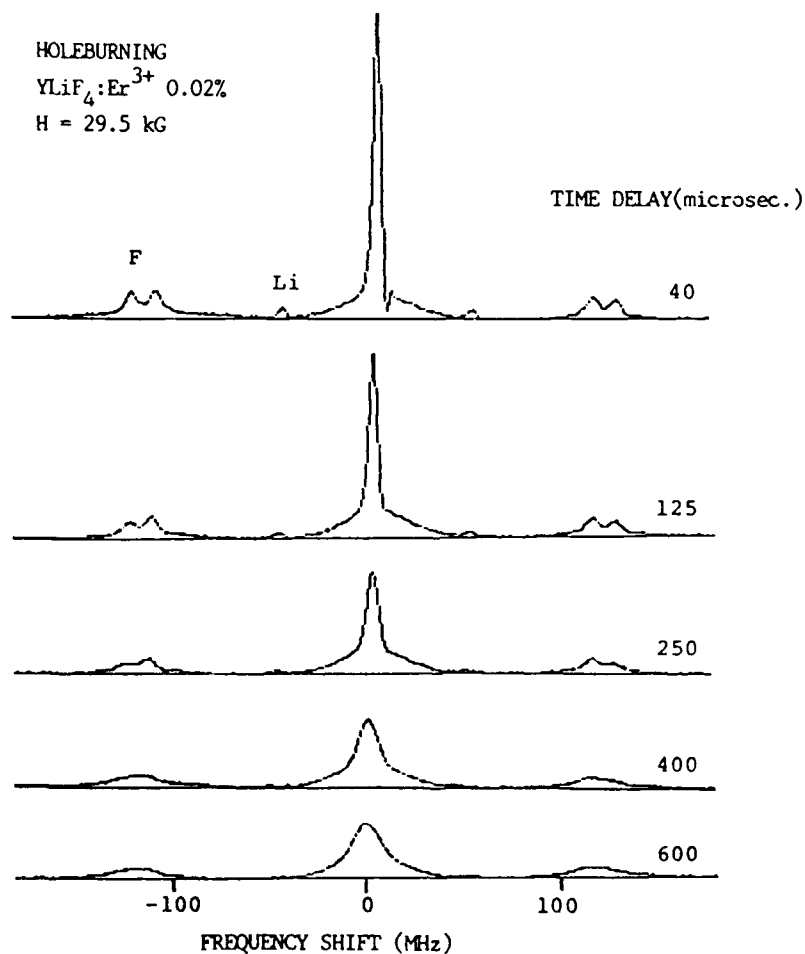


Fig. 1. Time-resolved holeburning spectra for the magnetic field perpendicular to the c axis using Zeeman scanning. Sideholes associated with spin flips of Li and F nuclei are indicated.

## Photon Echo and Time-Resolved Fluorescence Anisotropy Measurements of Organically Doped Sol-Gel Glasses

Drew M. L'Esperance, Robert A. Crowell and Eric L. Chronister  
Department of Chemistry, University of California, Riverside, CA 92521  
(714) 787-3288

### Introduction

We present time resolved measurements of homogeneous dephasing of organic dopants in inorganic sol-gel glasses. A variety of organically doped sol-gel glasses have been synthesized and their dynamics investigated by time-resolved photon echo and fluorescence anisotropy measurements. The homogeneous dephasing rate of the chromophore is determined from photon echo measurements at low temperature ( $T = 1.4$  K), while thermally activated homogeneous dephasing mechanisms are investigated by temperature dependent photon echo measurements. Our results are contrasted with recent hole-burning experiments on doped sol-gel glasses. Aluminosilicate (ASE) and tetraethoxy silane (TEOS) glasses have been doped with rhodamine dyes, polyaromatics, cresylviolet, resorufin and a wide range of chromophores with different nonradiative electronic relaxation rates. A small list includes naphthalene (170ns), rhodamine 6G (2ns), Rose Bengal (500ps), stilbene (70ps), azulene (2ps), as well as quinizarin and chlorin. The visible absorption spectra of some organically doped sol-gel glasses is shown in Figure 1. The low temperature homogeneous dephasing rate for chromophores doped into TEOS and in ASE sol-gel glasses has been measured utilizing photon echo measurements, as shown in Figure 2.

The dynamics of the sol-gel matrix giving rise to spectral diffusion is analyzed in terms of a distribution of two-level systems which can model the local fluctuations characteristic of the non-equilibrium glassy state. The covalent nature of the host polymer structure differs from van der Waals solids (e.g. ethanol glasses and molecular crystals) and is much more branched than typical organic polymers (such as PMMA). Thus one expects the barrier height distribution for local structural changes to be quite different. It is not yet clear whether the sol-gel barrier height distribution has a functional form different from the (barrier height)<sup>-1/2</sup> dependence seen in other glassy systems. [1]

### Time-Resolved Photon Echo Spectroscopy

Photon echo spectroscopy is utilized to obtain homogeneous dephasing rates. At higher temperatures, thermally populated low frequency modes of the solid or low frequency modes of the dopant molecule induce thermally activated dephasing processes. Temperature dependent photon echo measurements in glasses are complex due to the dynamics of the glass as well as the dynamics of the chromophore within the glassy matrix. [2] Thus, temperature dependent photon echo spectroscopy is being used as a sensitive probe of how organic chromophores interact with the inorganic sol-gel host matrix.

For example, time-resolved photon echo measurements have yielded the homogeneous lifetime of cresylviolet doped into TEOS and ASE glasses. We observe a photon echo decay time of  $t_{pe}=180ps$  for a cresylviolet doped ASE glass at 1.4 K, which corresponds to  $T_2=720ps$ . Our

results for cresylviolet doped TEOS are similar except that the nonresonant intensity spike at zero delay relative to the long time decay is much greater for this system. One possibility for this difference is that vibronic transitions become more dominant in the TEOS matrix. Our photon echo results can be compared with hole-burning experiments performed on cresylviolet adsorbed onto porous silica at a similar temperature. [3] A homogeneous linewidth of 8GHz (corresponding to a dephasing time of  $\sim 20$ ps) was reported for cresylviolet adsorbed onto porous silica at 1.7K [3] yet our measured dephasing time is an order of magnitude longer. Thermally activated homogeneous dephasing can occur due to coupling of the electronic excitation to delocalized chromophore vibrations as well as due to local rearrangement of the sol-gel structure (i.e. spectral diffusion). [2] Temperature dependent photon echo measurements are currently being performed to separate these effects.

### Time-Resolved Fluorescence Anisotropy

In addition to relaxation and dephasing processes energy transfer can occur between chromophores and will be very important in determining the dynamics of mixed chromophore systems. When the electronic energy transfer occurs between molecules with randomly oriented transition dipoles the resulting fluorescence is depolarized to some degree. Since the energy transfer mechanism is sensitive to the proximity of neighboring molecules, we utilize time-resolved fluorescence depolarization to investigate the average spatial distribution of dopant molecules within the host glass as well as to probe the dynamics of energy transfer. [4]

Room temperature and 77K fluorescence anisotropy measurements have been made on several of the doped glasses listed in Figure 1 and due to their low concentration only a small change in anisotropy is observed over a timescale of twice the fluorescence lifetime (not shown). However, one can use these initial results to conclude that the dopant distribution function does not have a large number of close neighbors (as might be the case if a fraction of dopant molecules were localized in what used to be solvent pores). Instead, the dopants appear randomly distributed, as if in a frozen liquid. In addition, we have yet to see any dispersion in the time-resolved anisotropy measurements (both at room temperature and 77K) indicating that  $\Delta v_{\text{homo}}$  is large enough to prevent donor trapping of the excitation to occur. [5] We are continuing these experiments on sol-gels doped to higher concentrations where we expect to see more efficient energy transfer.

### References

- [1] J. Friedrich, Personal communication.
- [2] K.A. Littau, Y.S. Bai, and M.D. Fayer, *J. Chem. Phys.* **92** (1990) 4145;  
D.W. Peck, L.R. Narasimhan, and M.D. Fayer, *J. Chem. Phys.* **92** (1990) 4125;  
A. Elschner, L.R. Narasimhan, and M.D. Fayer, *Chem. Phys. Lett.* **171** (1990) 19.
- [4] K.A. Peterson, M.B. Zimmt, S. Linse, R.P. Domingue, and M.D. Fayer, *Macromolecules* **20** (1987) 168; and *Molecular Dynamics in Restricted Geometries*, edited by J. Klafter and J.M. Drake (Wiley, New York, 1989).
- [3] R.Locher, A.Renn and U.P. Wild, *Chem. Phys. Lett.* **138** (1987) 405.
- [5] A.D. Stein, K.A. Peterson, and M.D. Fayer, *J. Chem. Phys.* **92** (1990) 5622.

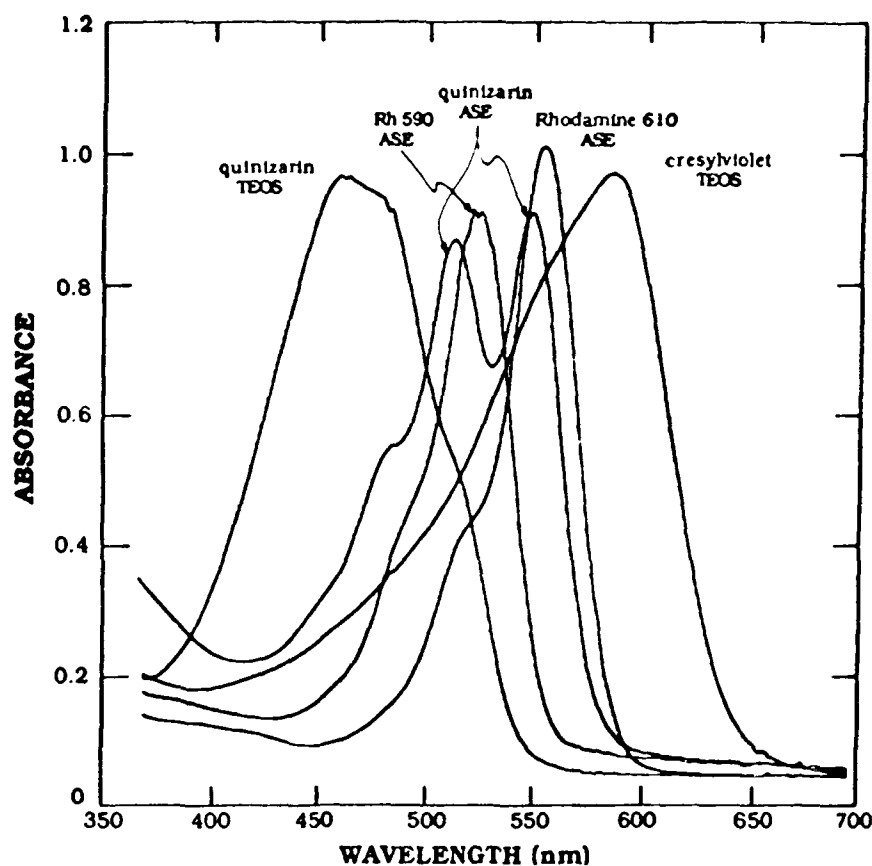


Figure 1. A variety of organic dyes have been incorporated into both silicate (TEOS) and aluminosilicate (ASE) sol-gel glasses. The visible absorption spectrum of several of these doped sol-gel glasses are shown to the left.

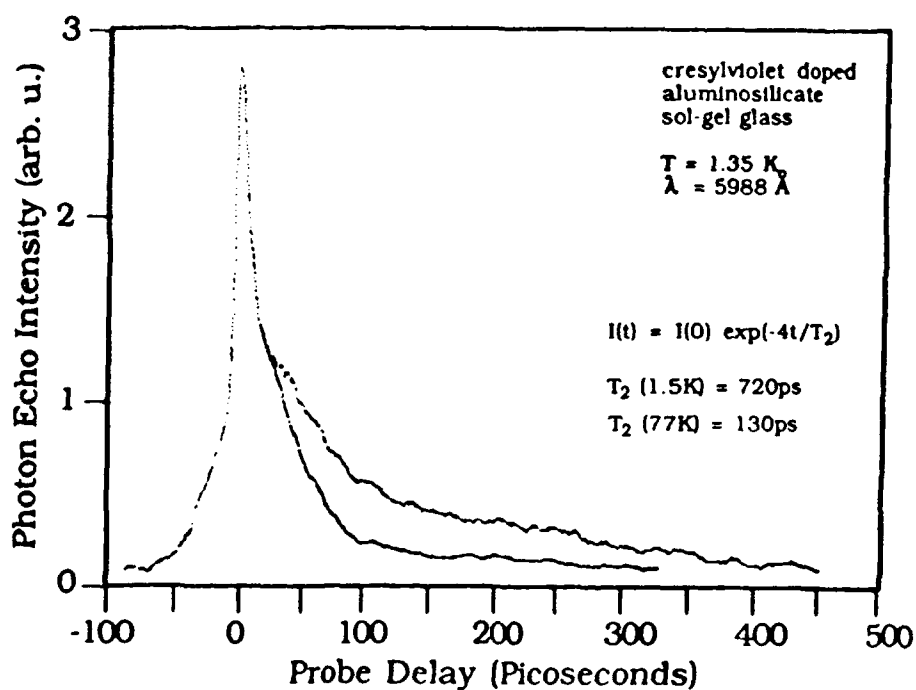


Figure 2. As a means of measuring the homogeneous dephasing rate for chromophores doped into inhomogeneous sol-gel glasses we have performed picosecond photon echo experiments. The results for cresylviolet doped ASE at two different temperatures is shown to the left. The 720ps homogeneous dephasing time at 1.5K is shorter than the 3ns fluorescence lifetime. Thus, the homogeneous dephasing of cresylviolet in ASE at 1.4K occurs due to a combination of spectral diffusion and population relaxation mechanisms.

ULTRAFAST DEPHASING OF RESORUFIN IN D-ETHANOL GLASS  
FROM 1.8 - 35 K STUDIED BY INCOHERENT PHOTON-ECHO

N.V. Gruzdev and Yu.G. Vainer

Institute of Spectroscopy, USSR Academy of Sciences,  
142092, Troitzk, Moscow Region, USSR, tel.: 334-02-36

Optical dephasing studies of organic glasses and polymers provide the valuable information about an amorphous system's dynamics. In the recent years hole-burning and two-pulse picosecond photon-echo were widely used for these purposes. These methods have different characteristic times: minutes and more - for hole-burning, picoseconds - for two-pulse picosecond photon-echo. As a result, in the case of amorphous systems, data obtained by using of these methods correspond to different time scales and are not equivalent [1]. The comparison between the results obtained by these different methods can provide additional information about a dynamical processes in amorphous systems (for example, about spectral diffusion).

Up to now the most experimental investigations of optical dephasing in organic glasses and polymers were made at small temperature region and only in two time scales: picosecond and minutes and more. It was interesting to investigate organic amorphous systems in nanosecond and microsecond time regions and at more wide temperature region.

We report the results of our experimental study of the optical dephasing in organic glasses by nontraditional photon-echo method, with incoherent laser source of light [2,3]. The main advantage of this method is potentially very high time resolution (up to femtoseconds), because in this method time

resolution is not determined by the laser pulse duration but by the correlation time of the laser light. This permits to measure the optical dephasing at the higher temperatures.

The characteristic time of incoherent photon-echo is determined by minimum from two times: pulse duration and  $T_1$  [4] and can differ from characteristic times of hole-burning and two-pulse photon-echo. It permits to obtain information about spectral diffusion in other time scale then in the cases of above-mentioned methods.

The experimental setup was created on the base of special developed broadband dye laser system. Its parameters: time resolution 20 - 30 fs, region of time delays from 10 fs up to nanoseconds, spectral region 450 ÷ 860 nm, spectral width of laser light up to  $300 \text{ cm}^{-1}$ , laser pulse duration  $\sim 15 \text{ ns}$  and energy up to 1 mJ.

Measurements were made at  $2 - 3 \times 10^{-4} \text{ mol/l}$  solutions of resorufin in d-ethanol in cuvette with 1 mm thickness, placed in temperature regulated helium cryostat. The samples were cooled rapidly ( $\geq 1 \text{ K/s}$ ). A number of precautionary measures and control measurements have been performed to exclude optical density effects and to obtain reproducible results.

The scheme of experiment is shown in Fig.1. Additional beam was introduced to have simultaneously two signals: first - from photon-echo with variable optical delay (main signal) and second - from photon-echo with constant delay (additional signal). Additional signal was used for calibration of the photon-echo signal intensity. It permitted us to improve the precision of our measurements.

The results of our experimental study are demonstrated in Fig.2. For comparison, the results of hole-burning [5] and picosecond photon-echoes [1,5] experiments are demonstrated too

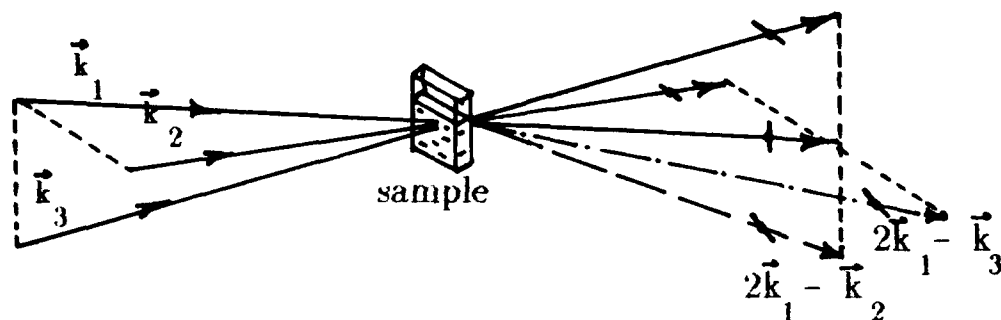


Fig.1.  $\vec{k}$  - common beam,  $\vec{k}_1$  - beam with variable delay,  $\vec{k}_3$  - beam with constant delay,  $2\vec{k}_1 - \vec{k}_2$  - main photon-echo signal beam,  $2\vec{k}_1 - \vec{k}_3$  - calibration photon-echo beam, - - denote direction of beam polarization.

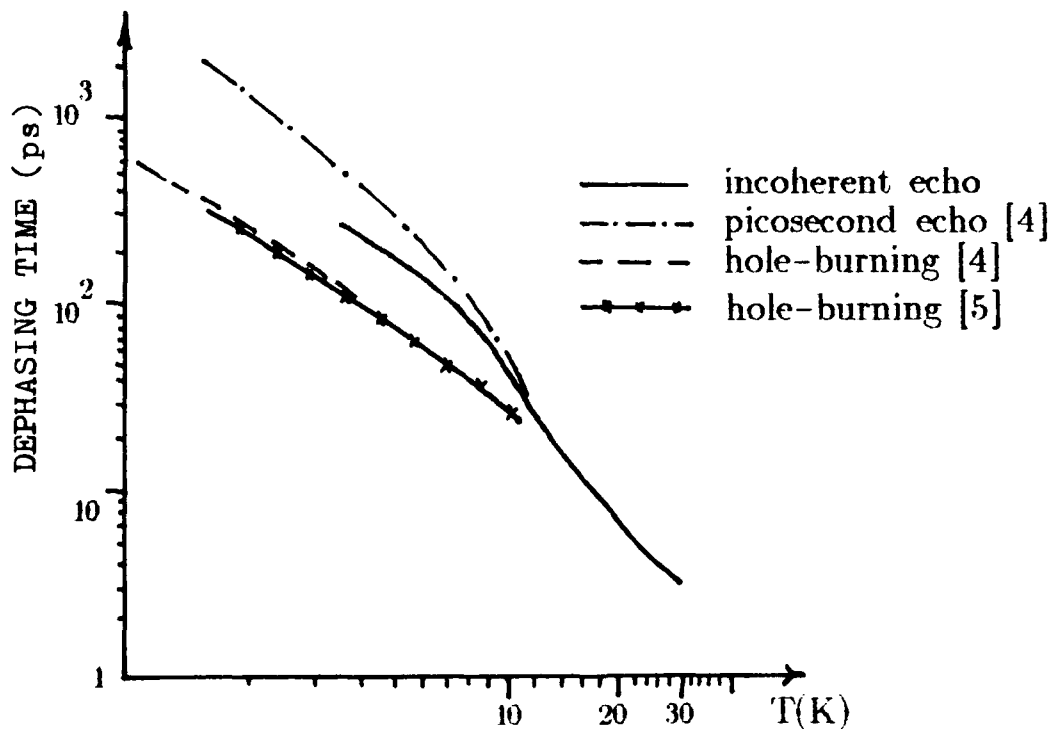


Fig.2. Temperature dependence of dephasing times for resorfin in d-ethanol glass.

At  $T \sim 11$  K all results are practically coincide. At  $T$  between 8 - 11 K our results coincide with picosecond photon-echoes results. At  $T$  below 8K we can see the difference between our and picosecond photon-echoes and hole-burning results.

The coincidence of the all optical dephasing values at 11 K is readily explained. At this temperature and more the contribution of spectral diffusion in dephasing value is, most likely, negligible. The coincidence of picosecond and incoherent photon-echoes results between 8 - 11 K signify that in investigated system in the nanosecond time scale the contribution of spectral diffusion obviously is sufficiently small. Good agreement in this temperature region of picosecond and incoherent photon-echoes data, obtained by the two essentially different methods in different laboratories and with different samples, indicates a high reliability of these data and an absence of some artefacts in above-mentioned experiments. The difference between our and picosecond photon-echoes results below 8 K indicates, for our opinion, on the presence of spectral diffusion process in nanosecond time scale. In accordance with most of theoretical models this difference is increasing when the temperature is decreasing.

The obtained high temperature dephasing time data (up to 35 K) permits us to analyze more precisely contributions to the dephasing different mechanisms: interactions with pseudolocal modes, TLS, acoustic and optical phonons.

- [1] Y.S. Bai and M.D.Fayer, Chem.Phys.**128**,135 (1988)
- [2] R.Beach and S.R.Hartmann, Phys.Rev.Lett.**53**,663 (1984)
- [3] N.Morita and T.Yajima, Phys.Rev.**A30**,2525 (1984)
- [4] M.Berg, C.A.Walsh, L.R.Narasimhan, K.A.Littau and M.D.Fayer, J.Chem.Phys.**88**,1564 (1988)
- [5] R.van den Berg and S.Völker, Chem.Phys.Lett.**137**,201 (1987)



Thursday, September 26, 1991

# Optical Processing and Holography: 1

**ThB** 11:00am–12:00m  
DeAnza Room

Masaharu Mitsunaga, *Presider*  
*NTT Basic Research Laboratories, Japan*

## Error-Corrective Recall of Digital Optical Images in Neural Networks Models by Photoburning of Spectral Holes

Karl K. Rebane, Olavi Ollikainen, and Alexander Rebane<sup>#</sup>

Institute of Physics, Estonian Academy of Sciences, 142 Riia Street, Tartu, Estonia 202400, USSR, tel. 01434/ 281-75

<sup>#</sup> Present address: Physical Chemistry Laboratory, Swiss Federal Institute of Technology, ETH-Zentrum, Universitätstrasse 22, CH - 8092, Zürich, Switzerland  
tel. +41-1/ 256-43-92

The neural-network-like scheme of data storage and processing of N-bit sequences of information needs a memory of about  $N^2$  elements (interconnections). In digital auto-associative memories /1/ the useful data is presented usually as a set of S different words,  $v^{(s)}$  ( $s= 1, \dots, S$ ), each word being a sequence of N bits. Simple mathematical rule /2/, given originally by Hopfield /3/, can serve as an algorithm to calculate the values of the  $N^2$  elements of the memory matrix, T. Recall of the memory gives an output word,  $v^{(out)}$ , which results from a thresholded inner product between the interrogating input word,  $v^{(in)}$ , and the memory matrix. The readout procedure can be expressed mathematically,

$$v^{(out)} = \text{TRH} \{ T \cdot v^{(in)} \},$$

where TRH{...} stands for the thresholding procedure.

The remarkable property of associative memories is that the input words,  $v^{(in)}$ , can comprise errors (certain number of error bits) without loss of the essential information: the recall automatically corrects for the errors towards the closest matching amongst the memorized words,  $v^{(s)}$ . By arranging feedback loops (i.e. if the thresholded output is fed back into the input) multi-step approximation error-corrective recalls can be obtained.

Optical realizations of digital associative memories /4/ make use of the advantage that optics has over conventional electronics in performing the necessary massive matrix multiplication procedure. Optical means allow the multiplication to be carried out simultaneously in many parallel channels if the memory matrix is coded as a spatial transparency or a hologram. However, the conventional optical storage, utilizing the spatial coordinates (x, y, z), fails if a very large memory capacity is needed, e.g., for processing of image information. Also, if we want direct input/output of images presented in two-dimensional format, the optical multiplication process will need an additional, fourth degree of freedom, difficult to realize by conventional means.

Hole burning (HB) /5, 6/ provides in addition to the spatial coordinates (x, y, z) the frequency  $\omega$  (and time t) dimensions and opens new prospects to increase the storage capacity by a

factor up to  $10^4 - 10^6$ . The possibility of fully parallel optical access to the stored data, even if the information is partially (or completely) coded in the frequency and/or time dimensions //, makes the application of hole burning materials for associative parallel processing especially attractive.

In this paper we present a concept and first experimental implementation of a hole burning optical memory which is coded as a multidimensional digital auto-associative interconnections matrix and which has error-correcting capability. In our experiments the memory stores two 12-bit words ( $v^{(1)} = 100101101001$ ,  $v^{(2)} = 101000101110$ ). The mathematical algorithm which we use to calculate the associative memory matrix is discussed in detail in /8/. The memory consists of  $(12 \times 12) = 144$  elements and its content is shown graphically in Fig.1. The white and the shaded squares represent, correspondingly, 1 and 0.

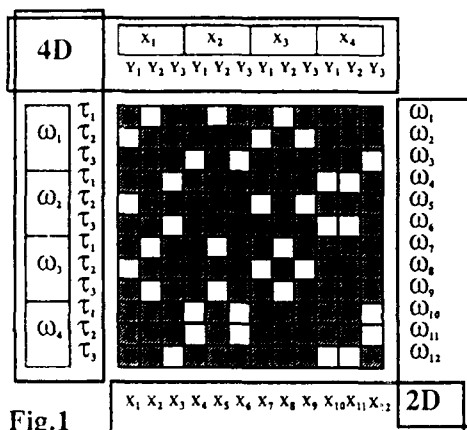


Fig. 1

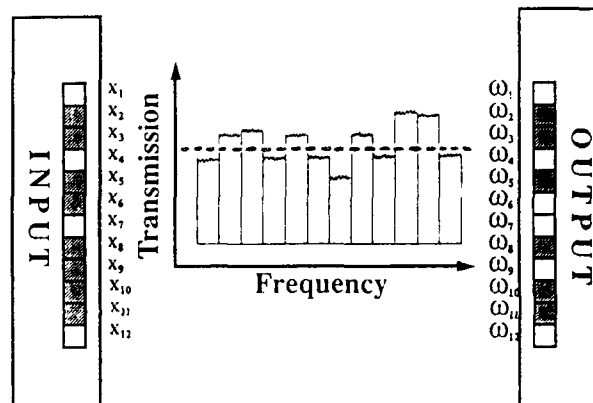


Fig. 2

In the experiment we use photoburning media that comprises two different organic impurity molecules (octaethylporphine and protoporphyrine). The partially overlapping inhomogeneous absorption bands of the two impurities gives us a nearly "flat" absorption frequency interval of a width of about  $150 \text{ cm}^{-1}$  where the transmission of the sample (measured before the write-in exposures) varies between 1% and 2%; at the working temperature of 2K the narrowest hole-width is about  $0.05 \text{ cm}^{-1}$  for both types of impurities. The spatial dimensions of the sample (block polystyrene) are  $3 \times 3 \text{ cm}$  across and 4 mm in thickness. As a laser source we use a picosecond Rhodamine 6G dye laser synchronously pumped by an Ar ion laser. The wavelength of the laser is tuned in steps between a set of prefixed values within the  $150 \text{ cm}^{-1}$  "flat" spectral storage interval. The temporal analysis of the signals is performed with a synchroscan streak camera (20 ps time resolution). Details about the experiment are given in /8/.

In the first example the memory matrix is materialized by using the coordinate  $x$  and the frequency  $\omega$ . The corresponding 2D partition of the memory matrix is shown in Fig. 1. The variable

$x$  corresponds to 12 horizontal stripes arranged perpendicularly to the  $x$ -coordinate of the PSHB plate. The variable  $\omega$  corresponds to 12 different frequencies where holes are burnt in the transmission spectrum.

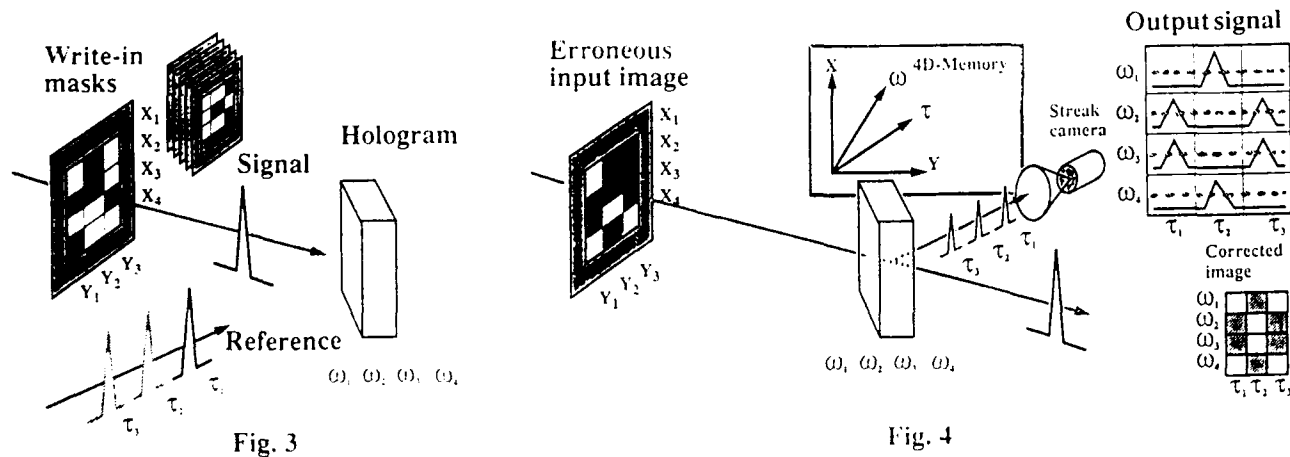
To write in the memory we tune the laser sequentially to 12 different burn-in frequencies. At each frequency the sample is exposed through a certain mask slide (prepared according to each of the rows of the memory matrix) with 12 transparent and opaque stripes that are projected upon the storage plate.

Once the memory is stored it can be read out by illumination through a mask with a bit structure of an interrogating word and by measuring the spatially integrated transmission at the prefixed wavelengths. The information contained in the spectrum can be obtained either by using a spectrally broad light source (and measuring the spectrum at the output) or, which is more convenient in the present experiment, by tuning the laser wavelength. Fig. 2 schematically illustrates the read-out procedure and presents the read-out signal when the memory is interrogated through a mask resembling one of the stored words,  $v^{(l)}$ , but with two error bits. The error-free output is obtained after applying an appropriate thresholding level (dashed horizontal line in Fig. 2).

In the second example the memory is stored by using four variables: two orthogonal spatial coordinates ( $x$  and  $y$ ), frequency  $\omega$ , and delay  $\tau$ . The delay corresponds to time-domain hologram signal (photochemically accumulated stimulated photon echo). The 4D partition of the memory matrix is shown in Fig. 1.

Formatting of the memory into a 4D matrix gives us the possibility to present the input signals also as digital 2D images by coding them, e.g., in the  $x$  and  $y$  coordinates. The optical recall of the memory is also two-dimensional and is coded in the frequency dimension,  $\omega$ , and in the time dimension,  $\tau$ .

Fig. 3 illustrates the procedure of storing of the 4D memory. Spatial coding is carried out



by using masks with precalculated 4x3 bit binary patterns positioned in the write-in signal beam. The signal beam is projected upon the PSHB sample so that each spatial element of the mask coincides with the corresponding spatial element of the hologram. The frequency-domain assignment corresponds to four different (fixed) wavelengths,  $(\omega_1, \omega_2, \omega_3, \omega_4)$ , accessed by tuning the dye laser. At each wavelength three time-domain photochemically accumulated stimulated photon echo holograms are stored, each using a different delay value,  $\tau$ , between the signal and the reference beam ( $\tau_1 = 40$  ps,  $\tau_2 = 100$  ps,  $\tau_3 = 180$  ps). The reference beam has a plain wave front and it illuminates uniformly the whole storage area.

The read-out of the memory is carried out by illuminating the hologram with the picosecond signal beam (reference beam is blocked) through a two-dimensional interrogating mask according to the scheme presented in Fig. 4. The image pattern of the mask corresponds to an input word with two error bits. At the output of the memory the diffracted holographic signal is focussed on the entrance slit of a streak camera. By the translation theorem of Fourier transform the time delay between the write-in signal and the reference pulse corresponds to multiplying the complex amplitude transmission coefficient of the time-space hologram by a factor of  $\exp(i\omega\tau)$ . The hologram time domain response measured at the output of the memory reproduces the values of the time delays. Again, for the purpose of experimental convenience, the recall of the hologram at different wavelengths is measured sequentially by tuning the laser. In principle, simultaneous time-resolved detection of all spectral components is also feasible. When arranged into a (4x3) matrix so that the vertical coordinate corresponds to the frequency,  $(\omega_1, \omega_2, \omega_3, \omega_4)$ , and the horizontal coordinate corresponds to the delay,  $(\tau_1, \tau_2, \tau_3)$ , the resulting (thresholded) read-out data reproduces the true stored 2D image.

In conclusion, we have demonstrated a new principle of parallel optical data storage and processing by making use of the spectral selectivity properties of hole burning materials. In the first example the HB media acts as a spatial-spectral filter. In the second example the data is coded into a hologram written by two spatially, spectrally and temporally modulated intercrossing laser beams. Holographic scheme has as an advantage of a reduced background signal level during the readout but requires more complicated memory writing procedure.

#### References

1. T. Kohonen, *Self-Organization and Associative Memory* (Springer-Verlag, Berlin, Heidelberg, 1987).
2. I. Shariv, and A. A. Friesem, *Optics Lett.* **14** (1989) 485.
3. J. J. Hopfield, *Proc. Natl. Acad. Sci. USA* **79** (1982) 2554.
4. N. Farhat, D. Psaltis, A. Prata, and E. Paek, *Applied Optics* **24** (1985) 1469.
5. W.E. Moerner, ed., *Persistent Spectral Hole Burning: Science and Applications* (Springer-Verlag, Berlin, Heidelberg, 1988) and refs. therein.
6. L. A. Rebane, A. A. Gorokhovskii, and J. V. Kikas, *Appl. Phys. B* **29** (1982) 235.
7. A. Rebane, *Optics Commun.* **65** (1988) 175.
8. A. Rebane, and O. Ollikainen, *Optics Commun.* (accepted for publication)

## Persistent Spectral Hole Burning Applications for Massive Optical Neural Network Computers

Philip D. Henshaw and Steven A. Lis

SPARTA, Inc.

24 Hartwell Avenue

Lexington, MA 02173

(617) 863-1060

### Introduction

Neural networks require two types of operations; interconnections, which define how the output of one state affects the input of the next, and non-linear operations, which relate the inputs of a state to its output. Interconnections, which require many signals passing through the same space, are best performed with photons, which do not interact with one another. Non-linear operations require interaction (i. e., cross products) between the various inputs to a state, and are best performed with electrons, which interact strongly through their electrical charge. In a typical neural network architecture, almost all of the computation required is associated with the interconnections, and only a tiny fraction is associated with the non-linear operations (sigmoidal response or thresholding) performed at each state.

In this paper we will present an architecture which uses both photons and electrons in a natural manner to perform all the functions required for a complete neural network architecture. A schematic of this architecture is shown in Figure 1. Almost all of the computations are performed optically in parallel, providing the capability to implement extremely large neural networks.

### Statement of the Problem

Conventional 3D volume holograms are unable to record independent interconnections between pairs of points in two fully-populated two-dimensional planes. Solutions to this problem, such as fractal patterns of input and output points,[1] greatly restrict the number of input and output points which can be used. For large numbers of input and output points, only a tiny fraction of the total space-bandwidth product of the input spatial light modulator and output detector arrays can be used.

### The 4D Interconnect Concept

The four-dimensional interconnect concept we have proposed is able to completely connect two two-dimensional input and output planes. This concept makes use of the three spatial dimensions available to volume holograms plus the fourth dimension of frequency available using persistent spectral hole burning materials.

### Applications

The projected capabilities of electronic and optical technologies to implement extremely large neural networks have been estimated by a DARPA-funded study.[2] Single- and multichip electronics are projected to provide up to  $10^9$  interconnects and  $10^{12}$  interconnects per second. Optical techniques, including volume (3D) hologram storage of interconnect values, which are less well-developed, are projected to provide  $10^{10}$  interconnects and  $10^{13}$  interconnects per second. The projected capabilities of our 4D interconnect method exceed these projections by several orders of magnitude ( $10^{12}$  interconnects and  $10^{15}$  interconnects per second). A number of significant applications, including robot vision and real-time imaging radar processing will require performance similar to that which can be provided by our neural network. In addition, most

living organisms have estimated capabilities well beyond those projected for existing electronic and optical neural networks. Our method will be able to implement networks capable of being trained to be at least as smart as a honeybee. (Current Cray computers are estimated to approach the intelligence of a garden slug in a neural network configuration.)

### **Recent Experimental Results**

SPARTA recently performed an early experimental verification of hologram recording and playback in a true volume configuration. This experiment demonstrates optical recording in an SHB material sufficiently thick to provide significant sensitivity to the reference beam angle of incidence during hologram playback. This sensitivity is necessary to achieve the high recording density required for both 4D optical interconnects and holographic optical mass storage.

The holograms were recorded in a  $5 \times 5 \times 5$  mm sample of polystyrene doped with chlorin cooled to a temperature of 5K using a liquid He cryostat, a copper cold finger, and a pressed indium thermal contact. The recording and playback were performed with an 8 mW He-Ne laser illuminating a  $5 \times 5$  mm area of a standard Air Force resolution chart. Approximately 0.4 mW of radiation reached the sample. Holograms with diffraction efficiencies of approximately  $10^{-4}$  were recorded with exposure times of 8 minutes.

The recording sensitivity of the medium and the quality of the recorded holograms can be improved considerably with several simple changes in the SHB sample preparation. First, a longer heating cycle to completely dissolve the chlorin in the polystyrene will reduce the scattering of the sample, which limits the signal to noise in the results shown here. Second, the sample of optical density 1.2 was not optimized for highest hologram reconstruction efficiency. An optical density of 0.8 will produce superior results. Finally, a narrower laser spectral width of 100 MHz will be used in a typical system. This width may produce as much as a factor of  $10 \times$  improvement in sensitivity over the 1 GHz width of the He-Ne laser used to record the holograms in this experiment. We are confident the results of these improvements will support our previous analysis which predicts a storage capacity of  $10^{12}$  bits/cm<sup>3</sup> or  $10^{12}$  interconnects in a single hologram recording medium.[3]

The experimental setup used for hologram recording is shown in Figure 2. Figure 3 shows the original object and the reconstruction of a hologram recorded using this setup.

### **Summary**

In this paper we will discuss the problem with existing optical interconnect concepts, our solution, the 4D interconnect concept, the architecture of a neural network computer based on this concept, the capabilities and applications of this concept, and the most recent experimental results of our ongoing investigation.

This work has been funded by the Air Force Office of Scientific Research under contract F49620-91-C-0002 and monitored by Alan Craig of AFOSR.

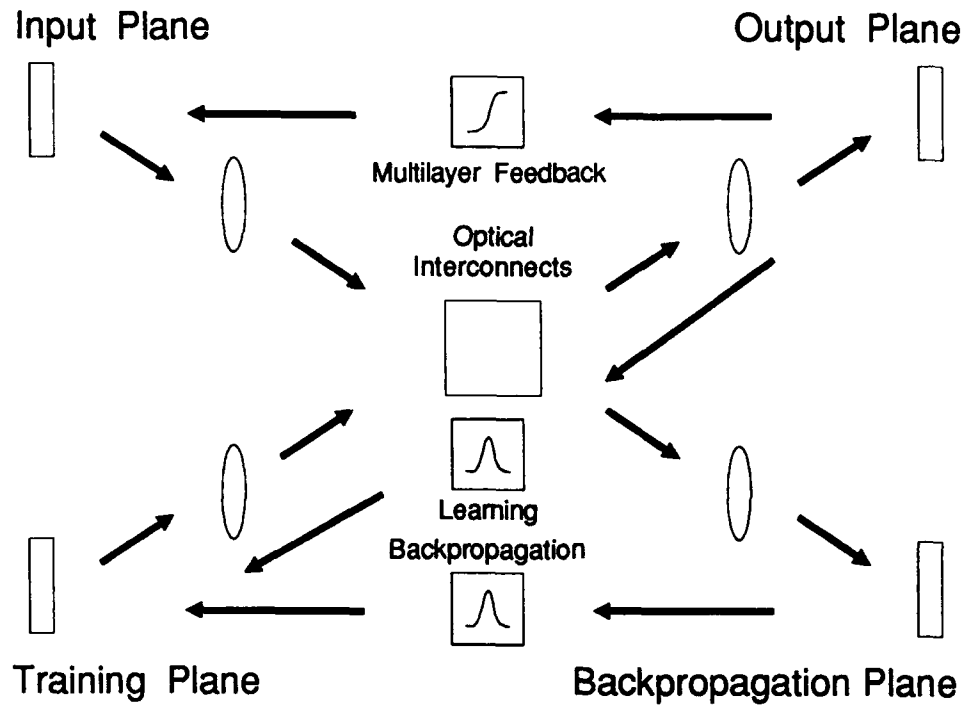


Figure 1. Architecture of an optical neural network computer.

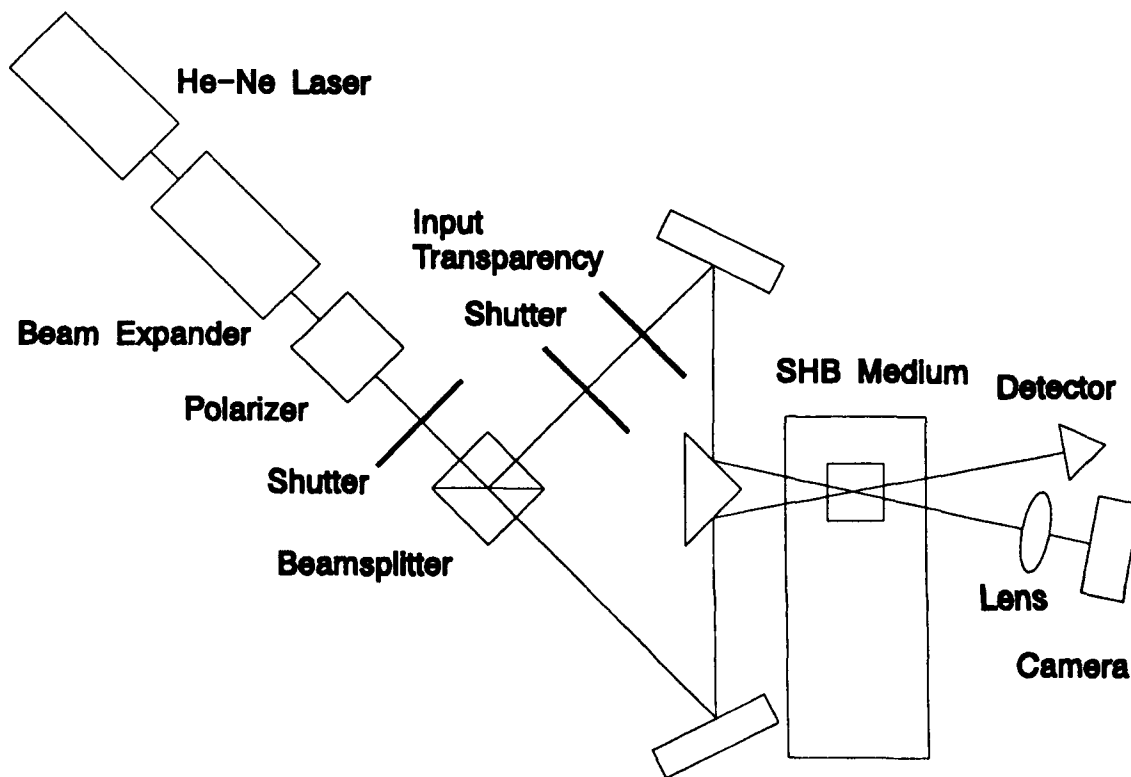
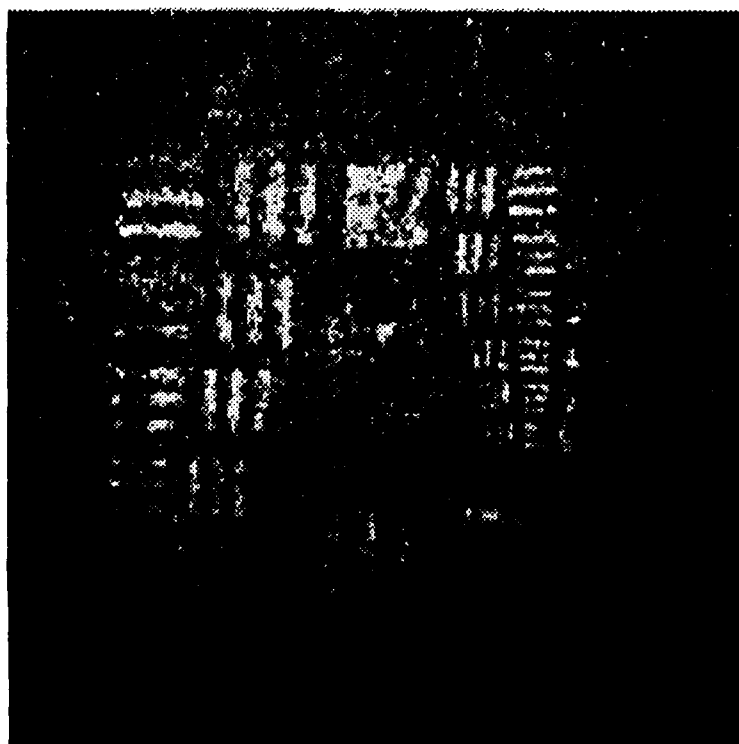


Figure 2. Experimental setup for hologram recording in SHB materials.



*a. Original object - 5 × 5 mm section of Air Force resolution chart.*



*b. Hologram recorded in chlorin-doped polystyrene at 5K. Estimated diffraction efficiency  $10^{-4}$ .*

*Figure 3. Volume hologram recording in SHB materials.*

## NEW DEVELOPMENTS IN TIME-AND-SPACE-DOMAIN HOLOGRAPHY AND SHAPING OF LIGHT PULSES BY SPECTRAL HOLE-BURNING FILTERS

Rein Kaarli, Peeter Saari, and Heiki Sõnajalg  
Institute of Physics, Estonian Acad. Sci., Tartu 202400, Estonia

### 1. INTRODUCTION

Photochemically instable dye molecules in low-temperature polymers are distributed not only spatially in the medium but also spectrally along the axis of resonant optical transition frequencies and orientationally with reference to the polarization of the transition. Consequently, such composite organic materials -- spectral hole burning media<sup>1-4</sup> -- can be considered as novel optical materials possessing not only three-dimensional photosensitivity but also sensitivity to the wavelength and polarization of the incident light.

The distribution function of the resonance frequencies of dye molecules determines the dielectric permittivity of the material and hence the amplitude and phase transmittance of the sample after exposure to light. Exposure to spatially modulated and pulsed, spectrally swept or otherwise nonmonochromatic polarized light gives rise to a four-dimensional anisotropic hole, or grating pattern, in the distribution function. Consequently, the function determines the temporal behaviour of the linear impulse response of the sample (pulse-excited macroscopic polarization or free induction decay in terms of optical transients; time-domain diffraction in terms of Fourier optics)<sup>5-6</sup>. On this basis common holography has been generalized, which results in a holography that precisely corresponds to the exact meaning of the term -- "complete recording", i.e. it results in a 4-D holography where the restored light fields are completely identical to the stored ones and play<sup>6-9</sup> back both spatial and temporal dependences of the object field vector. Time-domain holography and time-domain frequency-selective data storage, based upon transient stimulated photon echoes, which allows no persistent storage, are considered in a number of papers, see e.g.<sup>5,10-14</sup>. The essentials of 4-D holography or time-and-space-domain holography are discussed briefly in Sec.2

By making use of special features of 4-D holograms (originating from causality principle, see) and controlled time-domain interference of accumulated photon echoes, the method of a segmentwise storage and reconstruction of light signals in predetermined time interval has been demonstrated. These results and discussion about some other potential applications of photon echo interference are presented in Sec.3.

In much the same way as spatial shaping of a light beam can be accomplished by a kinoform, spectral hole burning media can be used for temporal shaping of ultrashort pulses. The results on an experimental realization of time-domain kinoform shapers and theoretical analysis of pulse shaping by isotropic and anisotropic spectral filters appear in Sec.4.

### 2. 4-D HOLOGRAPHY OF VECTOR FIELD OPTICAL SIGNAL

In the general setup of 4-D holography the reference and object pulses, which are not overlapping in time, are incident on the sample in an off-axis scheme<sup>7-9</sup>. By means of selective excitation of the molecules inside the inhomogeneously-broadened absorption band and photoburning of spectral holes, after the exposure the Fourier-spectrum of the incident radiation is recorded in every  $\lambda$ -sized spot of the sample, due to the modulation of the

complex permittivity of the latter. The original temporal and spatial dependences of the signal beam are restored by a delayed scattering of the readout laser pulse from the resulting spectral hologram. If the incident field is not polarized, then in spite of the absorbing molecules of the photochromic plate being orientated at different angles  $\Omega$ , the hologram-grating in the isotropic medium still remains isotropic. If the incident field is polarized, the process of hologram formation through spectrally-selective photobleaching is governed by the spectral amplitude  $\vec{A}(\vec{r}, \omega)$  of the pair of pulses given by the Fourier transformation of the sum  $\vec{A}(\vec{r}, t) = \vec{S}(\vec{r}, t) + \vec{R}(\vec{r}, t)$ , where  $\vec{S}(\vec{r}, t)$  is object (signal) pulse of arbitrarily time- and space-dependent amplitude, phase and polarization state, and  $\vec{R}(\vec{r}, t)$  is a short ( $\delta$ -like in comparison with signal) planewave reference pulse. The probability of photobleaching is proportional to  $|\vec{A}(\vec{r}, \omega) \cdot \vec{e}_\Omega|^2$ , where  $\vec{e}_\Omega$  is the unit vector along the axis of the dipole momentum. As a direct consequence of the latter, anisotropy of the complex permittivity and that of the transmittance of the hologram plate appears. The polarization state of the reconstructed wave in its turn is governed by the polarization of the reading pulse and the induced anisotropy of the complex transmittance of the hologram. A theoretical examination has revealed that the object wave is completely restored including its original variations of the polarization state, if the reference and read-out pulses are of the same state of circular polarization. Here the conjugated signal appears in case of counterrotating circular polarization. A detailed derivation and interpretation of general formulae for 4-D holography of vector fields is given in<sup>8,9</sup>. An experimental improvement of the theoretical conclusions including complete polarization-preserving phase conjugation and<sup>8</sup> time reversal of an arbitrarily polarized pulsed optical signal is presented in<sup>8</sup>.

### 3. SEGMENTWISE STORAGE IN 4-D HOLOGRAPHY BY THE INTERFERENCE OF ACCUMULATED PHOTON ECHOES

Standard procedure of 4-D holography allows us to record temporal behaviour of ultrafast events. During reconstruction the part of the signal event, incident onto the frequency-selective sample before the reference pulse, is restored as a conjugated wave and the part, incident after the reference pulse is played back directly. These parts can easily be separated and thus we can tell that spectral hologram can distinguish between "future" and "past". Quite logically the following problem arises: can a shorter segment be separated from a signal to be recorded by means of time- and space-domain holography? As shown theoretically<sup>15</sup> and experimentally, it is possible. In order to accomplish such a separation one has to record a double-exposure spectral hologram by applying, in successive exposures, different reference pulses incident onto the sample in slightly different directions and at different delays  $t_1$  and  $t_2$  with respect to signal pulse. Experimental streak-camera traces of model signal and reference pulses are depicted in Fig.1a and b. Applying now, during reconstruction, both reference pulses simultaneously to the multiplex spectral hologram, at the output of the hologram one can observe simultaneously the responses of both holograms which, starting from the moment  $t_2$ , interfere. As the two reference pulses are separated spatially one can easily control their mutual phase. If there is no extra phase-shift between read-out pulses, constructive interference appears (Fig.1c). If an extra delay of  $\lambda/2$  is introduced into the path of one of the read-out pulses, at the output of the hologram only a segment of the signal with

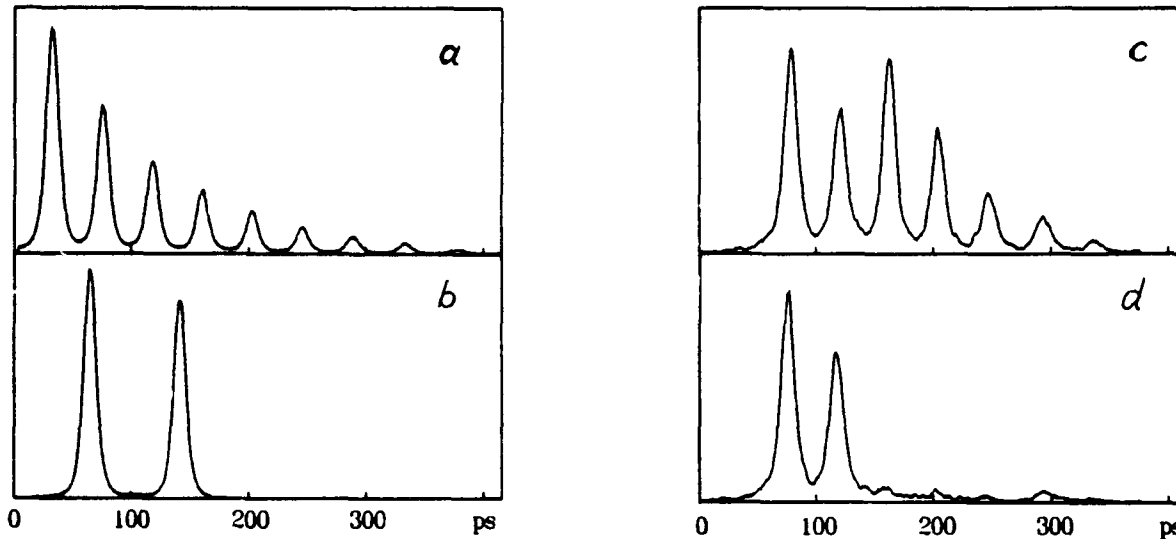


Fig.1. Streak-camera traces of: original signal pulse sequence (a), pair of reference (or readout) pulses (b), constructive (c) and destructive (d) interference pattern of reconstructed signals.

duration from  $t_1$  to  $t_2$  appears, see Fig.1d. In doing so the part preceding the first reference pulse, is cut off due to the general quality of spectral holograms, while the part after the second reference pulse vanishes due to a destructive interference between the signals from both reference pulses. Variation of the phase delay between the two restored signals allows us to control the interference phase.

Further analysis reveals that utilization of the reading pulses counterpropagating the reference ones allow also the observation of the interference between the phase-conjugated replicas of the signal pulse and the recall of its phase-conjugated segments. Concerning other possible applications, controlled interference of accumulated photon echoes enables oneto perform operations of addition and subtraction of vectorial functions and, in principle, allows the formation of polarized light pulses of pico- and femtosecond scale with the shapes determined by the linear combination of vector functions with phase-sensitive multipliers.

#### 4. OPTICAL PULSE SHAPING BY LINEAR SPECTRAL FILTERS

Spectral hole-burning serves also as a unique method of "engineering" the absorption spectrum of an optical material. By a preprogrammed tuning of monochromatic irradiation over a relevant spectral range of photochromic material one can design a filter with a predetermined absorption spectrum of a complex shape. If a short laser pulse is passed through such a synthesized linear spectral filter, it is modified according to the filter amplitude-frequency and phase-frequency characteristics, and its temporal shape is determined by the Fourier transformation of the filter frequency response.<sup>16,17</sup> As one can see from the model experiments carried out with isotropic spectral filters in picosecond time scale (see Fig.2),<sup>17</sup> the measured curves fit well with the responses calculated from actual transparency spectra (via Hilbert<sup>18</sup> and Fourier transformations).

Recent theoretical analysis<sup>18</sup> has revealed that, as the possibilities of forming continuous spectral profiles of refractive index (phase response of the filter) are restricted by the Hilbert transformation (dispersion

relations), light pulses of an arbitrary temporal shape cannot be formed by isotropic spectral filters. Only the pulses with the rising rear part intensity are allowed. To overcome this restriction anisotropic spectral filters and polarized input pulses have to be utilized<sup>18</sup>.

By combining the temporal shaping proposed within the common kinoform approach, one obtains a time-invariant scanner in which not only the direction of the output beam but also the spot shape and polarization are time-dependent.

It has been shown theoretically that in an optically thick sample the shape of the temporal response of the spectral hole filter is determined by the peculiarities of the burning process<sup>19</sup>. The effect has also been studied experimentally and considered for 4-D holography.

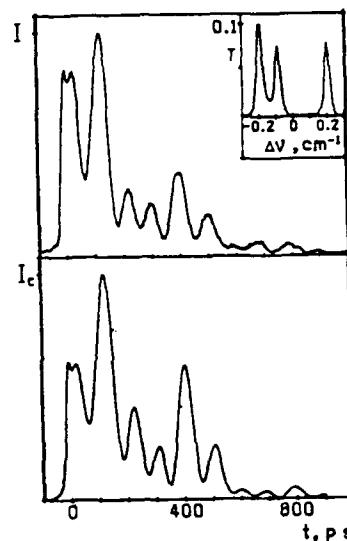


Fig.2. Transparency spectrum of the filter  $T(\Delta\nu)$  ( $\nu_0 = 16140 \text{ cm}^{-1}$ , upper insert); respective streak-camera image (upper main frame), calculated response  $I_c(t)$  (bottom).

#### REFERENCES

1. A.A.Gorokhovskii, R.K.Kaarli, L.A.Rebane, *JETP Lett.* 20 (1974) 474.
2. B.M.Kharlamov, R.I.Personov, L.A.Bykovskaya, *Optics Comm.* 12 (1974) 191.
3. *Persistent Spectral Hole-Burning: Science and Applications*, W.E.Moerner, Ed. Springer Series Topics in Current Physics, Vol.44. , Springer-Verlag, 1988.
4. *Zero-phonon lines and spectral hole burning in spectroscopy and photochemistry*, Eds. O.Sild and K.Haller, Springer-Verlag, 1988.
5. T.W.Mossberg, *Opt. Lett.* 7 (1982) 77.
6. A.Rebane, R.Kaarli, P.Saari, A.Anijalg, K.Timpmann, *Opt. Commun.* 47 (1983) 173.
7. P.Saari, R.Kaarli and A.Rebane, *J.Opt.Soc.Am. B* 3 (1986) 527.
8. P.M.Saari, R.K.Kaarli, R.V.Sarapuu and H.R.Sõnajalg, *IEEE J. Quant. Electr.* 25 (1989) 339.
9. R.V.Sarapuu and P.M.Saari, *Proc. Acad. Sci. Estonian SSR*, 37 (1988) 269.
10. N.W.Carlson, Y.S.Bai, W.R.Babbitt, T.W.Mossberg, *Phys.Rev.A*, 30 (1984) 1572.
11. W.R.Babbitt, T.W.Mossberg, *Opt.Comm.* 65 (1988) 185.
12. W.H.Hesselink, D.A.Wiersma, *Phys.Rev.Lett.* 43 (1979) 1991; D.A.Wiersma and K.Duppen, *Science* 237 (1987) 1147.
13. M.K.Kim, R.Kachru, *Opt. Lett.* 12 (1987) 593.
14. M.Mitsunaga and N.Uesugi, *Opt. Lett.* 15 (1990) 195.
15. R.Sarapuu, *Diploma thesis*, Tartu University, Estonia, 1986.
16. G.C.Bjorklund, U.S.Patent N.4,306,771,1981.
17. H.Sõnajalg, A.Gorokhovskii, R.Kaarli, V.Palm, M.Rätsep and P.Saari, *Opt. Commun.*, vol.71, N.6, pp.377-380, 1989.
18. H.Sõnajalg, *Opt. Commun.*, 80 (1990) 76.
19. E.Malkin, J.Kikas, *Opt. Commun.*, 75 (1990) 295.



Thursday, September 26, 1991

## Optical Processing and Holography: 2

**ThC** 1:30pm-3:00pm  
DeAnza Room

Michael Jefferson, *Presider*  
*IBM Almaden Research Center*

# Molecular Computing

Urs P. Wild, and Alois Renn

Physical Chemistry Laboratory, Swiss Federal Institute of Technology, ETH-Zentrum  
CH-8092 Zurich, Switzerland, Tel.: ++41 1 256-4381; Fax: ++41 1 252-3402

## Introduction

Each dye molecule embedded in an amorphous material such as a polymer host experiences a specific molecular environment which strongly influences its electronic transition energies. At low temperatures the different microenvironments result in an inhomogeneously broadened absorption band. The invention of the laser brought new spectroscopic techniques based on energy selection, such as fluorescence line narrowing and spectral hole-burning [1]. These techniques enable convenient addressing of thousands of molecular subsets selected by their transition energy.

## Holographic Image Storage

Combining spectral holeburning with holography [2] has led to frequency and electric field selective image storage [3, 4], allowing for the storage of up to thousands of images within a single piece of polymer film. In a typical experimental set-up [3] the beam of a tunable single mode dye laser is split into *reference and object beams* and a holo-

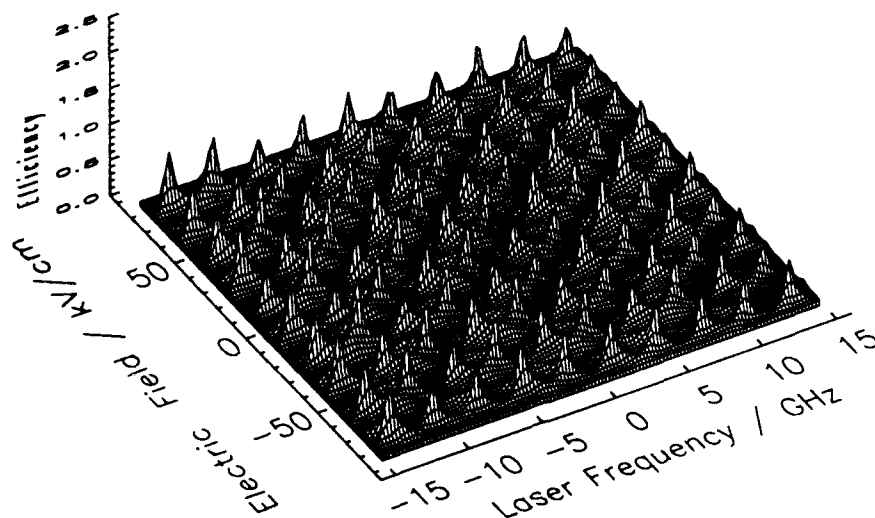


Fig. 1 Storage of 100 images within a single wavenumber. The integrated diffraction efficiency is plotted as a function of the read-out parameters: electric field and laser frequency. Each peak corresponds to a stored image.

gram is formed by exposing the sample to the interference pattern formed by spatially overlapping the two beams. Images of size 50x50 mm are introduced into the object beam either as slides or by using a liquid crystal TV. They are focussed on the photocathode of a video camera. For retrieval the sample is illuminated by the reference beam alone. The addressing of the individual images is performed by adjusting the laser frequency and the electric field to the values used during recording. The image information is displayed on a video monitor and the integrated diffraction efficiency is measured by a photomultiplier.

An electric field applied to the sample represents a new storage dimension and further increases the storage capacity [5]. In Fig. 1 the storage of 100 holograms in the absorption spectrum of chlorin (2,3-dihydroporphyrin) in polyvinylbutyral is presented. A wavelength range as small as a single wavenumber in combination with an electric field range of  $\pm 100\text{kV/cm}$  was used. Each of the peaks represents the integrated diffraction efficiency of a stored image. Typical images corresponding to individual peaks were recorded with the video camera and are shown in Fig 2.

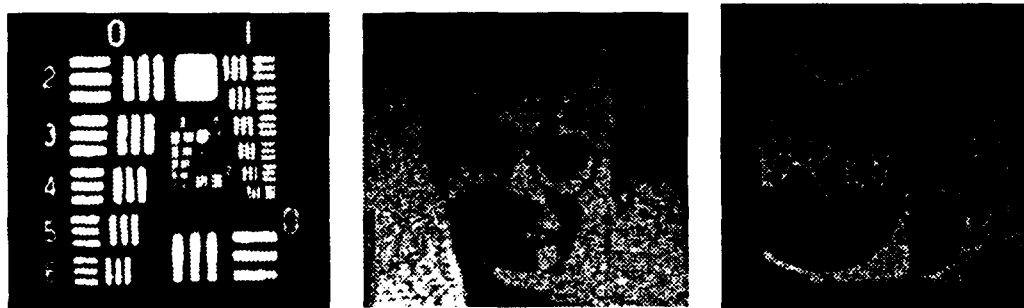


Fig. 2 Images demonstrating the spatial resolution and grey scale capabilities of the recording medium.

### Superposition of Images

The frequency - electric field plane allows pairs of holograms to be stored in different combinations, they can be burned either with a small frequency separation at the same electric field strength or at the same burning frequency at slightly different electric field strengths (Fig 3). The separation of the burning coordinates is chosen such that the hole contours overlap within an accessible frequency and electric field range. In Fig 3 the maxima of the Stark components are indicated by dashed lines and the burning coordinates are represented by filled circles. At the burning coordinates the stored images can be reconstructed separately. At the regions where the dashed lines intersect, marked by squares in Fig. 3, the phase properties of the holograms must be taken into account. In fig. 2 the result of image superposition is shown. The images were recorded at different values of the electric field,  $E_1$  and  $E_2$ , at the laser frequency,  $\nu$ . A horizontal

bar was stored at the position  $(\nu, E_1)$  and a vertical bar at  $(\nu, E_2)$ . Both images can be reconstructed individually by adjusting the experimental parameters used during recording. The superposition of the images can be reconstructed at the frequency,  $\nu_1$  or  $\nu_2$ , and the electric field,  $(E_1 + E_2)/2$ .

The results of the image superposition are shown in Fig 3 for phase differences of 0 and  $\pi$ . Constructive interference (phase difference 0) leads to an increase of the image intensity in regions where the images overlap - the images are added. Destructive interference (phase difference  $\pi$ ) results in a "subtraction" of the images [6,7,8]. Logical operations corresponding to AND or XOR functions can be derived with appropriate discrimination. In Fig. 4 the use of destructive interference for the implementation of a parallel XOR processor is shown [9]. The images, (a,b), corresponding to bit patterns have been stored according to Fig. 3 at different electric field strengths. The experimental result of the destructive interference is given in (c) and after discrimination in (d). It corresponds to a parallel XOR operation of the initially stored bit patterns.

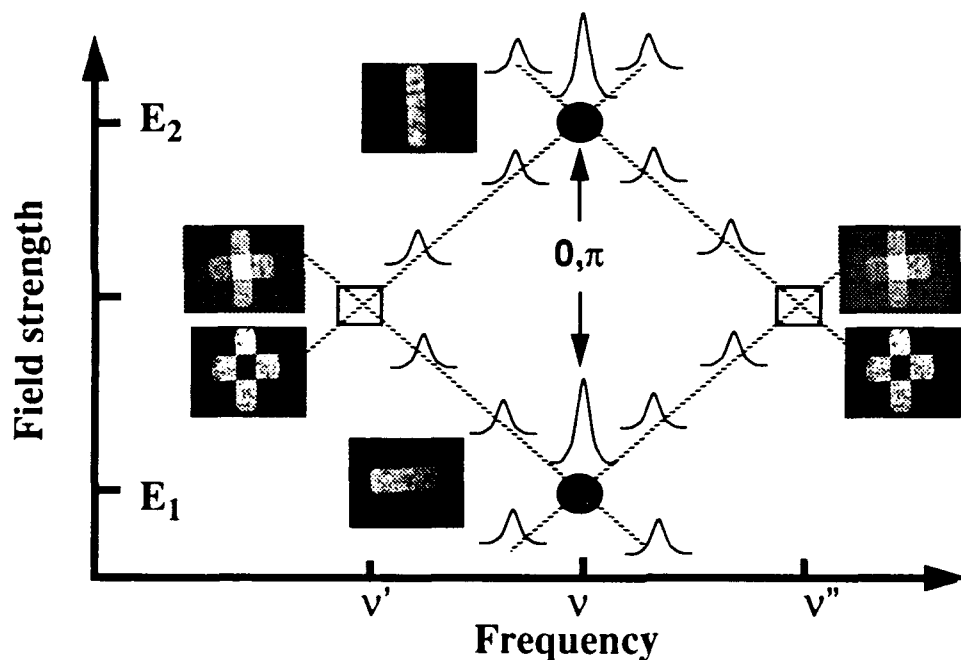


Fig. 3 Two images have been stored holographically in a plane defined by the laser frequency and the electric field at different values of the electric field ( $E_1, E_2$ ). The recording parameters are indicated by circles. Due to the Stark splitting of the spectral holes the holograms are made to overlap at the regions indicated by the squares. The reconstructed images show the result of the superposition: constructive interference, when a phase difference of zero was adjusted and destructive interference when a phase difference of  $\pi$  was chosen during the initial recording of the holograms.

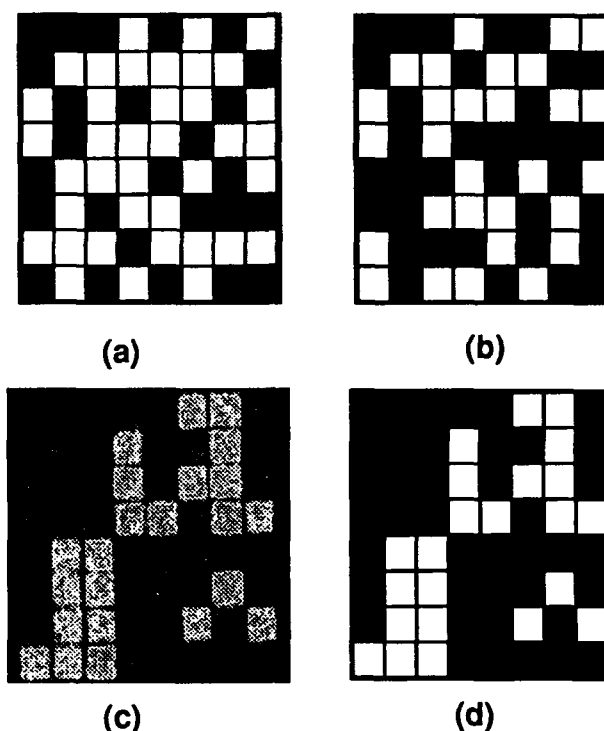


Fig. 4 Logical operations by superposition of images. Destructive interference (c) is used to perform a "XOR" operation (d) of the stored bitpatterns (a,b).

Whereas electronic processing of data is based on the properties of electrons in an electric field, the molecular processor introduced here relies on spectroscopic properties - the behavior of molecular energy levels in an electric field. The molecular system itself becomes a parallel information processor - a molecular computer.

### References

- 1 F.A. Burkhalter, G. W. Suter, U. P. Wild, V. D. Samoilenko, N. V. Rasumova, and R. I. Personov, Chem. Phys. Lett. **94** (1983) 483.
- 2 A. Renn, A.J. Meixner, U.P. Wild and F.A. Burkhalter, Chem. Phys. **93** (1985) 157.
- 3 A. Renn and U.P. Wild, Appl. Opt. **26** (1987) 4040.
- 4 C. De Caro, A. Renn, and U.P. Wild, Ber. Bunsenges. Phys. Chem. **93** (1989) 1395.
- 5 U.P. Wild, S. E. Bucher, and F.A. Burkhalter, Appl. Opt. **24** (1985) 1526.
- 6 A. Renn, A.J. Meixner, and U.P. Wild, J. Chem. Phys. **93** (1990) 2299.
- 7 U.P. Wild, A. Renn, Cosimo De Caro, and Stefan Bernet, Appl. Opt. **29** (1990) 4329.
- 8 U.P. Wild and A. Renn, J. Mol. Electr. **7** (1991) 1.
- 9 S. Bernet, A. Renn, and U.P. Wild, to be published.

## Holograms in Time and Space: Imaging Through a Scattering Medium

**Alexander Rebane\* and Jack Feinberg**

Department of Physics, University of Southern California,  
Los Angeles, CA 90089-0484, USA, Phone: (213)-740-1134

\*Present address: Laboratory of Physical Chemistry, Swiss Federal Institute of  
Technology, ETH - Zentrum, CH-8092 Zurich, Switzerland Phone: 011-41-1-256-43-92.  
Permanent Address: Institute of Physics, Estonian Academy of Sciences, 142 Riia  
Street, Tartu, Estonia

As an image-bearing wave traverses a scattering medium, the phase of the wave becomes severely distorted. Although most of the light is multiply scattered, a small fraction of the light will be scattered much less than average, and so may still contain information about the original incident wave front. Because this barely-scattered light is extremely weak, it is usually overwhelmed by the multiply-scattered light, so that no image can be observed by eye. Note, however, that the wave that is barely scattered (or not scattered at all) travels a shorter path to the observer's eyes than does the multiply-scattered part of the wave. If the original image-bearing beam is an ultrashort pulse, then in principle, by replacing the eye with a fast, time-resolving detector, one could discriminate between the unscattered, image-containing part of the transmitted light and the multiply-scattered background light. One might use this technique to observe objects embedded in a strongly scattering medium, such as living tissue, if only a fast enough "shutter" could be developed to cut off the strong background of scattered light.

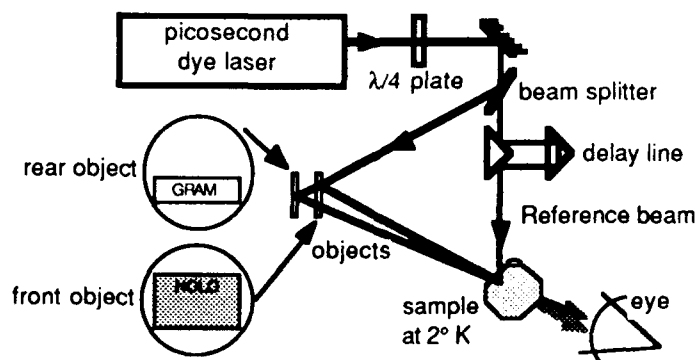
Recently streak cameras have been employed to study ultrashort laser pulses passed through a scattering medium and to discriminate in time between the multiply-scattered light and the less-scattered light /1/. However, streak cameras have a limited temporal resolution and do not allow two-dimensional imaging. An alternative, two-dimensional holographic technique was recently used to produce shadowgrams of objects embedded in a scattering medium /2/. This "holographic shutter" operates by interfering a short reference pulse with the signal wave. The arrival time of the reference pulse is adjusted to coincide with the arrival time of the unscattered portion of the image-bearing wave at the hologram recording plane, which was an electronic CCD camera. However, in this case increasing the temporal resolution inevitably decreases the physical overlap region and consequently the spatial information content of the final image.

Here we demonstrate that recording time-and-space-domain holograms in a persistent spectral hole burning (PSHB) medium /3-7/ can serve as a universal "time shutter" with sub-picosecond time resolution. We use this technique to image through a scattering medium based on the arrival time of various portions of the incident light at the holographic medium. In our case the spatial image quality does not degrade if the coherence length of the illuminating laser pulses is decreased. Clear images are obtained even if the wave fronts of the signal and the reference pulses do not overlap in time in the PSHB medium.

The basic principle of time-and-space-domain holography can be explained by

a simple model of holographic temporal recall given by Longuet-Higgins /8/. Consider a holographic recording material consisting of a bank of lightly-damped resonators, with each resonator tuned to a slightly different frequency. In the case of the PSHB medium, each resonator corresponds to the homogeneously-broadened, purely electronic, zero-phonon line of the photochemically active impurity, while the bank of resonators is equivalent to the inhomogeneously broadened ensemble of such lines. Consider two optical beams F and G incident on a PSHB holographic recording medium, and let the two beams each consist of a light pulse of finite duration. The bank of resonators records the interference pattern of two pulses F and G even if the pulses are never present in the material at the same time. The optical electric field of the first light pulse excites the resonators, which then continue to "ring" each at their own natural frequency. The optical electric field of the second light pulse then transfers energy either into or away from each resonator depending on the relative phase between the resonator's oscillation and the electric field of the second pulse. Due to the photochemical bleaching of the PSHB medium, the transfer of energy into a resonator decreases its subsequent absorption by an amount proportional to the energy absorbed. Later, when the hologram recording process is complete, this alteration can be read out by a third laser pulse, which causes any absorbing resonators to re-emit. For the case of a PSHB medium, such a response has been given the name "photochemically accumulated stimulated photon echo"/5/. If pulse F arrives  $\tau_0$  seconds before pulse G, then reading the resulting "hologram" with a read-out light pulse identical to pulse F will produce, after a delay time of  $\tau_0$ , a replica of pulse G (especially if pulse F is much shorter in duration than pulse G). This resembles the geometry of conventional off-axis holography, where a reference beam is used to reconstruct a virtual image of the original object. However, if the material is sufficiently thick, the reading of the hologram with pulse G will not reproduce pulse F. The hologram knows the direction of time's arrow: an early pulse will reproduce a later pulse, but not the other way around. By using a slightly different geometry to read the hologram one can instead reproduce the earlier information and cut off the later information.

In our experiment the recorded scene consisted of two objects (Fig. 1).



The nearby object was a 1.0-mm thick glass slide with the letters "HOLO" attached to its front surface. The distant object was a white paper screen carrying the letters "GRAM", which was pressed against the back of the transparent slide, so the separation between the two objects was about 1 mm. In order to increase the

amount of light scattered by the slide, its front surface was coated with a frosting aerosol spray. The slide was illuminated from the front by light pulses from a synchronously-pumped picosecond dye laser. Of the scattered light from the slide reaching the hologram recording sample (a polystyrene block doped with protoporphyrin, cooled to 2° K), about 80% came from the front sprayed surface of the slide, and only 20% came from the rear surface. If one viewed by eye the laser-illuminated slide from the position of the polystyrene block one could clearly read the letters "HOLO", but the intense glare from the front surface almost completely obscured the letters "GRAM" located near the back of the slide.

Light from the laser reached the front of the slide 5 picoseconds before it reached the back of the slide. Consequently, light from the front of the slide (containing the letters "HOLO") reached the storage medium 10 picoseconds (twice the glass travel-through time) before the light from the back of the slide (containing the letters "GRAM"). Further details about the experiment are listed in /8/. Read-out of the holograms was performed by blocking the light coming from the object and illuminating the hologram with only the reference beam. Light Bragg-scattered by the hologram contained a virtual image of the original scene, and this image was viewed by eye and recorded by a camera. The intensity of the reference beam was decreased during read out to reduce bleaching of the storage medium, and thereby prolong the viewing time of the hologram to tens of minutes. In the dark the holograms last for as long as the sample is kept cold.

Figure 2a shows the reconstructed image when the hologram was recorded

Fig. 2a

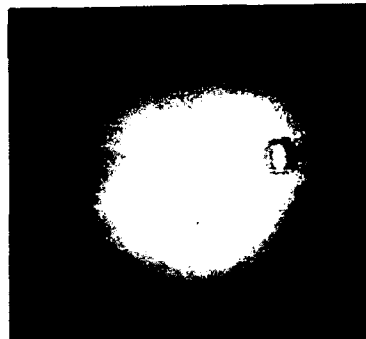


Fig. 2b



using a reference beam that arrived a few picoseconds before any of the light from the glass slide. The letters HOLO on the front of the slide are plainly visible, but the glare from the front of the slide all but obscures the letters GRAM located near the back of the slide. Figure 2b shows the reconstructed image when the reference beam pulse was set to arrive after light from the distant object but before the light from the nearby object. Now only the distant object is reconstructed, and the nearby object has been eliminated from the scene. We emphasize that the light from these objects need not arrive at the polystyrene block at the same time as light in the reference pulse in order for the hologram to be recorded. In fact, because the coherence time of the light pulses is only 0.5 ps, and because we set the reference beam to arrive at the storage medium about 5 ps before the light from the back of the slide, the reference and the object beams could not have produced a conventional intensity interference pattern in the storage medium. The maximum time delay allowed between the object and the reference beams is determined by the phase decay time of

the material, which was  $T_2 = 10^3$  ps for our sample.

The time resolution of the "shutter" is limited in our experiment by the coherence time of the laser pulses. For laser pulses become shorter than ~70 femtoseconds, the inhomogeneous bandwidth becomes the limiting factor. One way to overcome this limitation is to use a PSHB medium with a broader inhomogeneous bandwidth, or to prepare composite samples by combining impurities that absorb at different wavelengths. Note also that the light pulses need not be short in the time domain. The sharpness of the shutter's temporal edge is determined not by the duration of the light pulses but by the inverse of their spectral bandwidth. Frequency-chirped pulses or even a frequency scanning continuous-wave laser could be used to record spatial and temporal holograms.

In the experiment reported here we were able to selectively display those objects that sent light to the hologram *after* the reference pulse had arrived. However, for some applications, such as imaging objects embedded inside a scattering medium, it is desirable to do the opposite, and so recreate light that arrived *before* the reference pulse. This selection of early light over late light can be accomplished by simply altering the direction of the read-out beam used in the experiments above. Instead of using a read-out beam that is in the same direction as the reference beam, one should use a read-out beam that is directed exactly opposite to the direction of the original reference beam. (Also the phase front of the read-out beam should be a phase-conjugate replica of the phase front of the reference beam). This is the "four-wave mixing" geometry used in traditional phase conjugation experiments, and it will produce a real, phase conjugate image of the original object /10/. However, in contrast to phase conjugation using a conventional nonlinear medium, with the spectral hole burning medium only those portions of the object that arrive before the reference beam will be reconstructed in the final image. We point out that this scheme requires a large dynamic range for the spectral hole-burning medium if the scattered light is much stronger than the unscattered light. We estimate that shadowgrams with contrast as small as 1/1000 of the background light intensity could be seen using this technique. Experiments to demonstrate such selective imaging are in progress.

#### References

1. Yoo, K.M., and Alfano, R. R., *Opt. Lett.* 15, 320-322 (1990).
2. Chen, H., Chen, Y., Dilworth, D., Leith, E., Lopez, J., and Valdmanis, J., *Opt. Lett.* 16, 487-489 (1991).
3. Moerner, W. E., ed., *Persistent Spectral Hole Burning: Science and Applications* (Springer, Berlin, Heidelberg, 1988).
4. Mossberg, T. W. *Opt. Lett.* 7, 77-79 (1982).
5. Rebane, A., Kaarli, R., Saari, P., Anijalg, A., and Timpmann, K., *Opt. Commun.* 47, 173-176 (1983).
6. Saari, P., Kaarli, R., Rebane, A., *J. Opt. Soc. Amer.* B3, 527-533 (1986).
7. Rebane, A., Aaviksoo, J., and Kuhl, J., *Appl. Phys. Lett.* 54, 93-95 (1989).
8. Longuet-Higgins, H. C., *Nature* 217, 104 (1968).
9. Rebane, A., and Feinberg, J., *Nature* (May 30, 1991 issue).
10. Hellwarth, R. W., *J. Opt. Soc. Amer.* 67, 1-3 (1977)

# Holographic optical data storage of 2000 images by photochemical hole burning

Bern Kohler, Stefan Bernet, Alois Renn, and Urs P. Wild

*Physical Chemistry Laboratory, Swiss Federal Institute of Technology, ETH-Zentrum, CH-8092 Zurich, Switzerland, Tel. 41 (1) 256 4381*

## 1. Introduction

In addition to its importance for the optical spectroscopy of solids, photochemical spectral hole burning (PSHB) has attracted great interest due to its potential use in high density optical data storage [1]. By encoding information as a function of frequency an enormous increase in storage is possible compared to conventional optical storage materials. The most optimistic estimates predict an increase given by the ratio of the inhomogeneous linewidth to the homogeneous linewidth of the optical transition responsible for hole burning. Until now, however, there have been relatively few investigations of the practical limitations to storing a large number of spectral holes [2,3]. We describe here a recent experiment in which 2000 grayscale images were successfully recorded as holograms in the PSHB material chlorin in polyvinylbutyral. In holographic spectral hole burning the relative phase of the interfering light waves used to prepare the hologram has a strong influence on diffraction properties and, hence, on crosstalk between adjacent holograms [4]. By controlling the phase and frequency during burning in a novel manner, we have minimized crosstalk between the stored images.

## 2. Experimental details

The experimental setup is illustrated in Figure 1. The chlorin-doped polymer film was prepared as described previously [5]. The 65  $\mu$  thick sample was held between transparent electrodes in a liquid helium bath cryostat at 1.7 K. Two thousand video frames were digitized from an animated film and stored as 512 x 512 x 8 bit deep grayscale images on a real-time magnetic disk. Under the control of a Sun 4/330 computer each image was displayed on an LCD TV positioned in the object beam. A polarizer positioned after the LCD TV resulted in an amplitude-modulated object wave which was recorded holographically by interference with the plane-wave reference beam inside the sample.

A tunable dye laser (Coherent autoscan 899) running in single-frequency mode with the laser dye sulforhodamine B was used to store the holograms. Holograms were burned for 4 seconds using approximately 150  $\mu$ W / cm<sup>2</sup> of laser power in each beam. During burning the laser frequency was linearly swept over a range of 1.5 Ghz about the average burning frequency. Simultaneously, the phase of the object beam was linearly swept by  $2\pi$  radians by moving a mirror with a piezoelectric translator as shown in Figure 1. This technique minimizes crosstalk as discussed below.

By applying an electric field, the zero phonon lines of the impurities undergo Stark splitting, providing an additional technique for increasing the storage density [5]. At each frequency

five holograms were stored at evenly spaced electric field values on the range  $-150 \text{ kV/cm}$  to  $+150 \text{ kV/cm}$ . After recording a group of images, the laser frequency was increased by 10 GHz and the next group of five images was recorded. In this fashion, 2000 images were recorded in  $4000 \text{ GHz}$  ( $133 \text{ cm}^{-1}$ ) between 631.1 and 636.5 nm under total computer control.

During readout the object beam was blocked and the reference beam was used to holographically reconstruct the object wave. After selecting the appropriate laser frequency and electric field combination, the read-out image was detected using a CCD camera and digitized for later analysis.

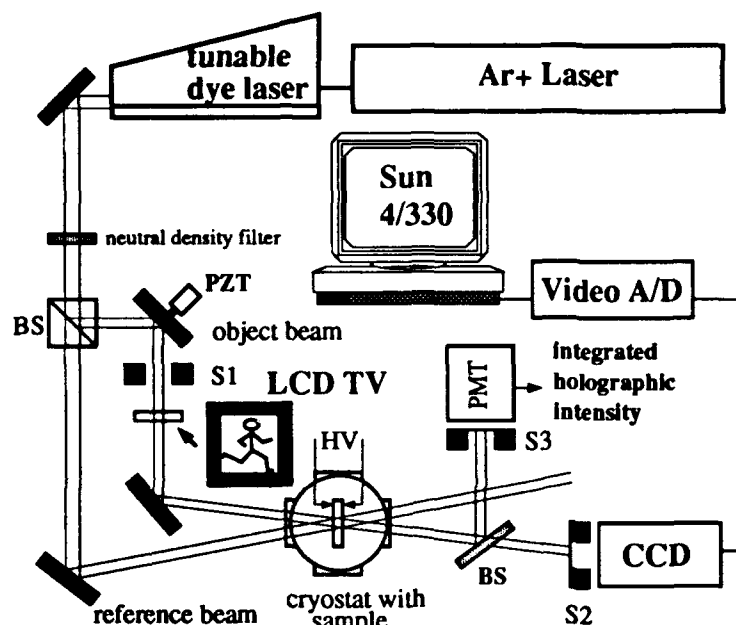


**Figure 1.** The experimental setup used for holographic image storage and readout. A static electric field is applied to the sample by a high voltage source, HV. During recording an image is displayed with the LCD TV, resulting in an amplitude-modulated object beam. The phase of this beam is swept during burning using a piezoelectric translator, PZT. For readout the hologram is reconstructed using only the reference wave by closing shutter S1 and opening shutters S2 and S3. Finally, a video digitizer records the reconstructed image detected by a CCD camera.

### 3. Results

Figure 2 shows the improved characteristics of spectral holes recorded by sweeping phase and frequency as described above. The dashed curve shows the diffraction efficiency vs. frequency for a hole recorded by burning at a single frequency. The solid curve shows the diffraction efficiency for a hole burned by sweeping the phase of the object beam while simultaneously sweeping the laser frequency over a 1 GHz range. The total light exposure was the same in both cases. The 'swept' hole has steeper edges and less intense wings than the simple hole. This permits holograms to be stored closer together by reducing crosstalk. A detailed analysis of the burning technique will be presented elsewhere [6]. We emphasize that merely sweeping the laser frequency while burning is insufficient to produce these effects. The phase of the object wave relative to the reference wave must be controlled as well [4].

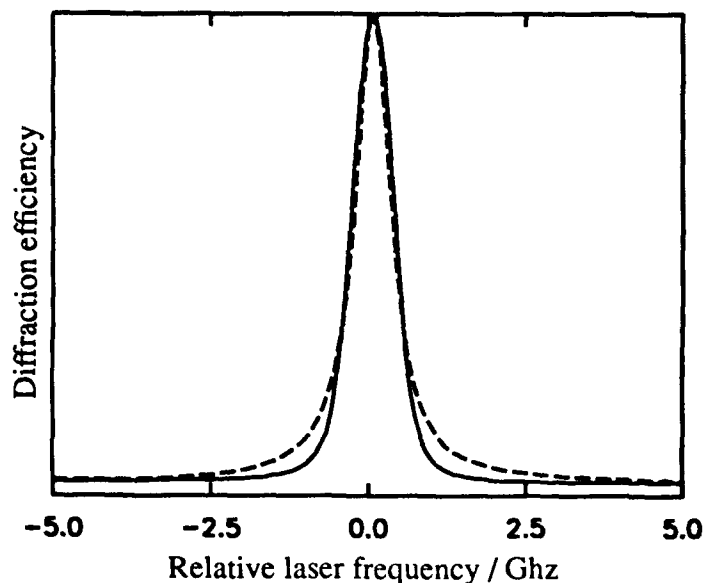


**Figure 2.** Comparison of the holographic efficiency of a spectral hole burned at a single frequency (dashed curve) with a hole burned by sweeping the laser frequency over a range of 1.0 Ghz about the hole middle while sweeping the phase of the object beam by  $2\pi$  radians (solid curve). The swept hole has significantly less intensity in the wings, reducing the amount of crosstalk between spectrally adjacent holograms.

In Figure 3, a single recalled image is reproduced together with the image originally transmitted by the object beam. The latter image provides an indication of the imaging quality inherent in the optical setup. Clearly, the quality of the read-out image is excellent when compared to the original object wave. There is no evidence of crosstalk from neighboring images. Although the stored images span most of the inhomogeneously broadened absorption band of the chlorin impurity molecules, we saw no evidence that the burning of additional holes had any effect on previously recorded holes. Two material parameters which are significant in this respect are the



**Figure 3.** Comparison of a typical holographic image reconstructed using only the reference beam (a) with the original image information carried by the object beam (b). Both images were digitized from the video signal output from a CCD camera.

large Debye-Waller factor of the optical transition used, and the fact that the photoproduct absorbs outside the band of the photoeduct. The first property minimizes the depletion of educt molecules by phonon sideband absorption, while the second property insures that the absorption characteristic at a particular frequency is not corrupted by subsequent writing.

#### 4. Conclusions

Two thousand grayscale images, corresponding to an 80 second film, have been stored in a PSHB material. Using a holographic setup, the bits which make up each image were stored and recalled in a completely parallel manner. Due to the enormous capacity of a PSHB optical memory, parallel recording is indispensable for practical implementation. By sweeping the laser phase and frequency during burning, it was possible to store the holograms without crosstalk. The images were stored across the entire inhomogeneously broadened band of chlorin with no deleterious effects from phonon-side band absorption. Finally, we believe that our spacing of holograms (10 Ghz along the frequency axis, 60 kV / cm along the electric field axis) was generous, and that a higher image storage density is possible in this material. This has great practical importance for a variety of optical processing applications of current interest, including optical data storage, optical neural networks and holographic interconnects.

We wish to thank Markus Traber for valuable technical assistance. The work was supported by the Swiss National Science Foundation.

#### REFERENCES

1. W. E. Moerner (Ed.), *Persistent Spectral Hole Burning: Science and Applications*, Springer Verlag, Berlin, 1988.
2. Ya. V. Kikas, R. K. Kaarli, and A. K. Rebane, *Opt. Spektrosk.* **56** (1984) 238.
3. A.R. Gutierrez, J. Friedrich, D. Haarer, and H. Wolfrum, *IBM J. Res. Dev.* **26** (1982) 198.
4. A. Renn, A. J. Meixner, and U. P. Wild, *J. Chem. Phys.* **92** (1990) 2748.
5. U. P. Wild, S. E. Bucher, and F. A. Burkhalter, *Appl. Opt.* **24** (1985) 1526.
6. A. Rebane, S. Bernet, A. Renn and U. P. Wild, (1991) submitted. to *Opt. Comm.*

# Holography in Frequency Selective Media: Hologram Phase and Causality

Stefan Bernet, Bern Kohler, Alexander Rebane, Alois Renn, and Urs P. Wild

Physical Chemistry Laboratory, Swiss Federal Institute of Technology, ETH-Zentrum  
CH-8092 Zurich, Switzerland, Tel.: +41 1 256-4389; Fax: +41 1 252-3402

## Introduction

Persistent spectral hole burning [1] in conjunction with holography (PSHB) opens new prospects for high density optical information storage and processing. In the holographic approach, hole burning is carried out with two -crossed coherent laser beams which bleach out a narrow frequency domain hole in an inhomogeneously broadened absorption band recording, at the same time, a spatial holographic fringe pattern. During read out of the hologram diffraction from this spatial fringe pattern occurs, and a holographic image is reconstructed, reflecting the changes of the absorption coefficient and the refractive index introduced by the spectral hole [2].

The variation of the refractive index as a function of the frequency extends further than the corresponding absorption coefficient change. If many holograms are recorded at adjacent frequencies, the refractive index gratings cause interference between the holographic signals recorded at different frequencies. A possible way to avoid interaction, and to suppress the buildup of a spectrally non-selective background signal, is to control the relative phase of the holograms. It has been shown, that relative phase changes of  $\pi$  between adjacent holograms in the frequency domain as well as in the electric field dimension result in a considerable reduction of this background [3]. In this case, however, the holograms stored at different frequencies should have similar spatial structure and contrast.

If a PSHB hologram is written in a thin polymer film with a narrow band laser at a fixed frequency so that the sample comprises only one grating with a narrow spectral width then the hologram diffracts light symmetrically into the positive and the negative diffraction orders. When a second hologram is added at an adjacent frequency, interference effects take place depending on the relative phases of the holograms [4]. If the phase changes are  $\pi/2$  or  $-\pi/2$  an asymmetry between these holographic signals has been observed. This is due to the interference arising from the interaction of the absorption coefficient of the one hologram with the refractive index contribution of the other, and to the changing sign of the refractive index part [4,5].

In general, the dispersion relations can be derived fundamentally from the causality principle. Thus, the asymmetry arising from the interaction of the absorption coefficient

and the refractive index of spectrally adjacent holograms must be related to causality. From time domain holography it is known that a time delay  $\tau \gg (\Delta\omega_{\text{laser}})^{-1}$  between the write-in beams ( $\tau$  is equivalent to an optical path length difference of  $d = \tau c$ ), produces signals which appear either only in the positive or only in the negative (conjugated) orders of diffraction, depending on the temporal ordering of the pulses [6]. This temporal order of reference and object beam is recorded in a frequency dependent phase change  $\Delta\phi(\omega) = \tau\Delta\omega$ . In a previous paper we investigated experimentally this causality property of PSHB holograms [7]. The spectral profile of a hologram was varied by using a tunable single mode dye laser and the efficiency of holographic image reproduction was compared when a glass block (10 cm) causing a time delay was inserted in one of the write-in beams. In this paper we demonstrate that frequency dependent phase changes corresponding to arbitrary path differences can be easily introduced by moving a mirror mounted on a piezoelectric transducer.

### Experimental Results

The PSHB material we use to record holograms is polyvinylbutyral doped with chlorin at a concentration  $10^{-3} M$ . The hologram sample is a  $65\mu$  thick film and is positioned inside an optical bath cryostat. The PSHB active inhomogeneous absorption band has a maximum at the wavelength of 633 nm with a width of  $130 \text{ cm}^{-1}$ . The minimum hole width obtained at the temperature of 1.7 K is  $\sim 300 \text{ MHz}$ .

The lay-out of the experimental scheme is depicted in Fig. 1. The tunable single mode dye laser (CR 899-29 autoscan ring laser) and the signal detection system we use

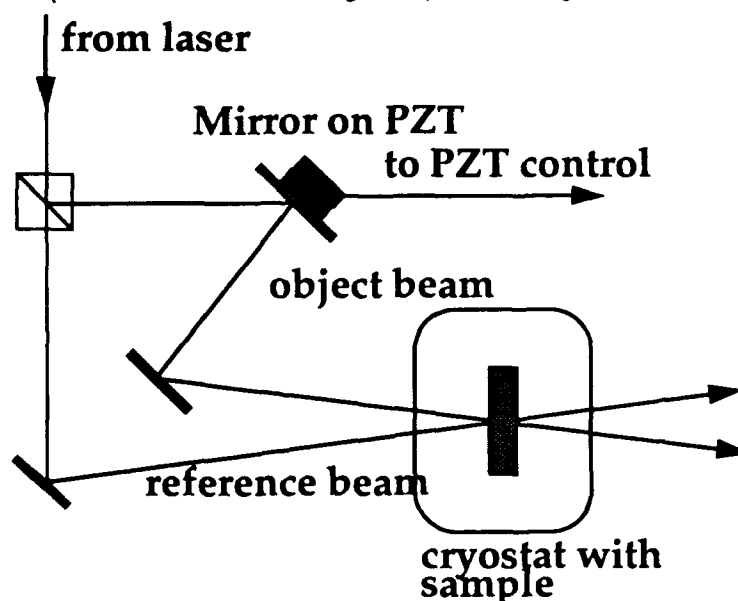


Fig 1 Optical lay-out of the hologram recording scheme. The optical delay is accomplished by the mirror mounted on the piezo electric transducer.

in this experiment are interfaced via GPIB bus to a SUN 4/330 work station. The optical path lengths of the reference and of the object beams are roughly equal within a precision of about 1 mm. The "optical delay," either in the reference or in the object arm of the interferometer is simulated by moving the mirror under computer control. The moving mirror allows for adjusting arbitrary delay values  $|\tau|$  between the writing beams related to the phase dispersion  $\tau = d\phi(\omega) / d\omega$ . The delay is considered to be positive if the object beam is delayed. According to the discussion presented above the inverse value of the delay  $|\tau|^{-1}$  has to be smaller than the frequency range where the hologram is stored. On the other hand, the delay should not be larger than the inverse value of the homogeneous hole width: if  $\Gamma_{\text{hom}}^{-1} \ll |\tau|$  then the spectral response of the PSHB media is unable to record the fringe pattern and the contrast of the hologram will vanish. In our experiments the frequency scan width during burning the holograms was in the range of 3.5 GHz, approximately twelve times the minimum hole width of 300 MHz. During burning the laser frequency and the hologram phase were synchronously swept. For the read-out of the hologram the object beam is blocked, the reference beam attenuated by a factor of 4 by inserting a neutral density filter, and the hologram efficiency was measured as a function of the read out frequency.

Fig. 2 presents experimental results of the frequency dependence of the diffracted signal for holograms burned with positive delay (a), no delay, (b), and negative delay.

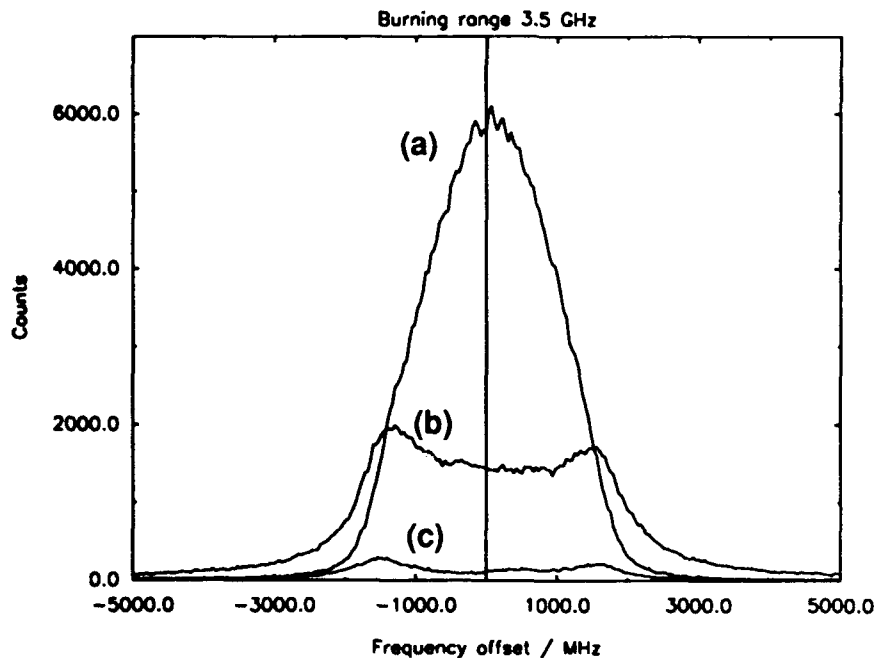


Fig 2 Hologram efficiency spectra for opposite phaseshifts applied during burning. Positive delay results in an amplification of the hologram efficiency, whereas negative delay leads to causality induced attenuation.

The scan width applied during burning of the holograms is 3.5 GHz and the phase change applied is  $2\pi$  and  $-2\pi$ , respectively. This corresponds to an optical delay of 8.7 cm or 0.29 ns. Whereas for positive delay the diffraction efficiency is considerably enhanced with respect to the delayless hologram the diffraction efficiency is strongly inhibited for negative delay, i. e. when the reference beam is delayed with respect to the object beam. Note also the different behavior of the diffraction efficiency in the wings of the "undelayed" signal (b) and the signal with positive delay (a).

Let us also point out that the minimum spectral width at which the causality property of the PSHB holograms can still have effect is about twice the value of the minimum (homogeneous) hole width. This means, in fact, that by applying the hologram storage method discussed in this paper the cross-talk between the different holograms in spectrally selective media can be eliminated by sacrificing approximately one half of the total spectral storage capacity. On the other hand, if we consider that the amplitude diffraction efficiency of the holograms (thin as well as thick holograms) is in this case, by a factor of two higher, the actual loss in the storage and processing capacity of the medium will be compensated.

In conclusion, these experiments show that causality-related cancellation of certain diffraction orders, previously demonstrated only for spectrally broad, time-domain holograms, also applies to holograms synthesized by a tunable narrow CW laser beam. Control of the grating phase opens a path to reduce crosstalk between holograms recorded at different frequencies and enables direct manipulating of the diffraction efficiency of holographic images. The experimental results presented here show that the hologram phase is a new and important variable in hole burning holography opening a wide field of exciting experiments.

### References

- 1 W. E. Moerner (Ed.), *Persistent Spectral Hole Burning: Science and Applications*, Springer Verlage, Berlin, 1988.
- 2 A. Meixner, A. Renn, and U.P. Wild, *J.Chem.Phys.* **91**, 6728 (1989).
- 3 C. De Caro, A. Renn and U.P. Wild, *Appl.Optics*, (1991) in print.
- 4 A. Renn, A. J. Meixner, and U.P. Wild, *J.Chem.Phys.* **92**, 2748 (1990).
- 5 K. Holliday, C. Wei, A. J. Meixner, and U. P. Wild, *J.Luminescence*, **48/49**, 329 (1991).
- 6 P. Saari, R. Kaarli, and A. Rebane, *J.Opt.Soc.Am.* **B3**, 532 (1986).
- 7 A. Rebane, S. Bernet, A. Renn and U.P. Wild, (1991) *subm. to Opt.Comm.*



Thursday, September 26, 1991

## External Fields

**ThD** 3:30pm–5:30pm  
DeAnza Room

Gary Scott, *Presider*  
*University of California, Riverside*

## Applications of Electric Field Effects on Persistent Spectral Holes

Max Maier

Naturwissenschaftliche Fakultät II – Physik,  
Universität Regensburg, W-8400 Regensburg, F.R.G.

We studied the effects of an external electric field on persistent spectral holes in an inhomogeneously broadened optical transition of dye molecules embedded in crystalline or disordered solids.<sup>1</sup> The results are applied to optical data storage in the electric field dimension, modulation and pulse forming of laser beams,<sup>1,2</sup> and hybrid optical bistability.

When an electric field is applied to molecules a spectral line or band shifts, splits or broadens because of the shifts of the electronic levels in the electric field (Stark effect). The frequency shift contains a term linear in the electric field  $\vec{E}$  which is proportional to the difference  $\Delta\vec{\mu}$  of the electric dipole moments of the excited and ground states of the molecules. It has been shown for various dye-matrix systems that even for centrosymmetric dye molecules, where  $\Delta\vec{\mu} = 0$  for the free molecule, a linear electric field induced frequency shift is observed. This effect has been ascribed to the influence of the environment on the dye molecules in the solid. A simple mechanism is usually discussed for polar solids. It is assumed that the polar groups of the surrounding matrix induce a dipole moment difference in the dye molecules which interacts with the applied electric field leading to a linear electric field effect. In a more generally applicable mechanism it is assumed that the large gas-to-matrix shift of the involved electronic transition is slightly changed by the applied electric field and causes the observed electric field effects.

We investigated the effects of an electric field on a persistent spectral hole in the inhomogeneously broadened  $S_0-S_1$  transition of the centrosymmetric dye molecule perylene in the nonpolar Shpol'skii matrix *n*-heptane, where perylene occupies distinct substitutional sites. A splitting of the spectral hole was observed which was linear in the electric field. It is ascribed to electric field induced variations of the gas-to-matrix shift, which is caused by the dispersion interaction in this dye-matrix system.

When perylene is embedded in an amorphous matrix, e.g. the polymer polyvinylbutyral (PVB), the spectral hole is broadened and reduced in depth in the electric field. The observed linear electric field effect is usually described by an effective electric dipole moment difference  $\Delta\vec{\mu}^*$ . The broadening of the spectral hole is explained by a statistical distribution of the magnitudes and directions of  $\Delta\vec{\mu}^*$ . For sufficiently high electric field strengths the spectral hole appears to be filled. It is possible to burn a further hole, which is also filled by sufficiently changing the field, etc. In this way it is possible to burn holes at different electric field strengths, i.e. in the electric field dimension. We term these holes field holes. They are important for applications of hole burning.

The following applications will be discussed: optical data storage in the electric field dimension, modulation and pulse forming of laser beams, and hybrid optical bistability.

In the usual method of optical data storage the information is stored by burning spectral holes in the frequency dimension. We used the electric field domain as a storage dimension in the dye-matrix system 9-aminoacridine-PVB. The information is written (or read) by burning (or detecting) holes with a fixed frequency laser at different electric field strengths, which correspond to different memory locations. The

memory locations in the electric field dimension are addressed by the voltage applied to the sample. This method is distinguished by its simplicity and speed. The combined use of the electric field dimension and the frequency dimension will be discussed also.

We studied a laser beam modulator in an experimental configuration which can be used in integrated optics. The laser light is coupled from an optical fiber to a thin perylene-doped PVB film which acts as a waveguide. The modulator operates in the following way. Without voltage the absorption in the center of the spectral hole is low leading to a high transmission of the laser light. The application of a voltage to the sample fills the center of the spectral hole and increases the absorption of the sample. When an alternating voltage is applied the transmission of the sample is modulated by the time-varying absorption. The response time of the investigated waveguide modulator was measured to be less than 300 ps. The limitation of the response time of the modulator by the width of the spectral hole is discussed.

We have used the effects of an electric field on a spectral hole for pulse forming of laser beams. The essential point in this application is that the T-U characteristic curve, which describes the dependence of the sample transmission T on the applied voltage U, can be adjusted to obtain the desired pulse shape. This is achieved by using proper conditions during hole burning. We present examples of different pulse shapes obtained with this method.

We have investigated a hybrid optical bistable device which uses voltage controlled changes of a persistent spectral hole in the dye-matrix system perylene-PVB. The hybrid optical bistability is based on the nonlinear dependence of the sample transmission on the applied voltage in conjunction with an external electrical feedback mechanism. In our case, the nonlinear transmission function is realized by the effects of the voltage on the persistent spectral hole. The feedback is created by detecting the

zero-phonon fluorescence light of the perylene molecules with a photomultiplier, the signal of which is amplified. The resulting voltage is applied across the sample. The application of the voltage increases the absorption at the probing laser frequency because the center of the hole is filled. This leads to an increase of the zero-phonon fluorescence intensity, which is fed back as a voltage rise to the sample. When the transmitted laser power was measured as a function of the incident laser power a bistable region was observed. In this region, the transmitted laser power was high or low at the same incident laser power depending on the fact whether the incident laser power was increased or decreased during the measurement. Under appropriate operating conditions transition to optical instability and chaos has been observed. Conditions for a bistable system based on increasing absorption bistability will be discussed. Optical bistable systems offer the possibility of performing logic functions. Under appropriate operating conditions they can serve as an optical amplifier, limiter, discriminator, and oscillator.

In conclusion, electric field effects on persistent spectral holes allow the construction of a versatile electrooptic processor which may serve for optical data storage, modulation and pulse forming of laser beams, and as a hybrid optical bistable device.

1. M. Maier, Appl. Phys. B 41, 73 (1976).
2. N. Hartmannsgruber, U. Bogner, and M. Maier, J. Mol. Electron. 5, 193 (1989);  
Opt. Quant. Electron. 23, 361 (1991), and references therein.

## Hole-Burning and External Field Effects: Principles, Recent Results and New Systems (Superfine Films)

R.I. Personov

Institute of Spectroscopy, USSR Academy of Sciences,  
142092, Troitzk, Moscow Region, USSR, phone:3340236

The possibility to investigate the influence of external electric and magnetic fields on complex molecules in amorphous solids is essentially limited by a large width of their spectral bands ( $\Delta\nu=10^2\text{-}10^3\text{ cm}^{-1}$  even at liquid helium temperature). Hole-burning opens up new excellent opportunities for using the Stark and Zeeman effects in spectroscopy of molecules and solids and their different applications [1]. Owing to the small hole width ( $\Delta\nu=10^{-1}\text{-}10^{-2}\text{ cm}^{-1}$  at 2-5 K) the sensitivity of measurements increases by several orders of magnitude.

In this report we shall:

- give a brief overview of principal peculiarities of the hole behaviour when the external field is applied; discuss two types of measurements, namely of (i) spectral shape of the hole  $\Delta D(\nu)$  at different fields  $F$  and (ii) the optical density  $\Delta D(F)$  as function of  $F$  at fixed frequency;
- discuss the results on the Stark effect for polar and unpolar dye molecules in polymers and glasses and estimations of internal fields in disordered materials;
- illustrate some new applications of the Stark effect on the holes for the high sensitive and precise investigations of the homogeneous line width and kinetics of hole-burning with the hole depth ( $\Delta D/D$ ) much less than 1% [2];

- discuss recent results on the strong (up to 500 k $\Theta$ ) magnetic field effect on S-S transitions in organic molecules (including such molecules as metalloporphyrins with degenerate S<sub>1</sub>-states [3]) studied via hole burning;
- present the latest results on the electric field effect on the holes in spectra of cadmium behenate Langmuir-Blodgett films doped with cyanine dye [4,5] and discuss new methods to study orientations of chromophores and internal electric fields in Langmuir-Blodgett systems.

### References

1. R.I. Personov. *Izv. Akad. Nauk SSSR, Ser. Fiz.* **52**, 628 (1988) (in russian).
2. E.I. Al'shits, B.M. Kharlamov and N.I. Ulitsky. (to be published).
3. N.I. Ulitsky, B.M. Kharlamov and R.I. Personov. *Chem. Phys.*, **141**, 441 (1990).
4. M. Orrit, J. Bernard, A. Mouhsen, H. Talon, D. Möbius and R.I. Personov. *Chem. Phys. Lett.*, (to be published) (1991).
5. J. Bernard, D. Möbius, M. Orrit and R.I. Personov. (to be published).

Photochemical Hole Burning Stark Effect Studies  
on  
Octatetrane n-Alkane Mixed Crystals

Gerhard Gradl, Bryan E. Kohler and Curtis Westerfield  
Chemistry Department  
University of California  
Riverside, CA 92521  
U.S.A.

Given the enormous increase in resolution that can be realized in hole burning studies, the application of these techniques to determine the spectroscopic consequences of applied electric fields was a natural extension.[1] Much of the work in this area has focused on organic dye molecules in disordered glasses.[1-3] For most of these systems, the application of an electric field most often just broadens the persistent hole, although it has been shown that, in certain cases the orientation averaged effect of a randomly oriented solvent field plus a fixed applied field can lead to a partial splitting of the hole profile.[1,4]

There are several aspects of linear polyene electronic structure that make Stark experiments on these molecules especially informative. First, these molecules are intrinsically nonpolar. Of course, in the centrosymmetric all-trans conformation symmetry demands that there be no permanent dipole moments. However, noncentrosymmetric isomers are also expected to have vanishingly small diagonal dipole moment matrix elements because of the charge neutrality of the carbon skeleton. This is expected from simple molecular orbital considerations and is born out in more elaborate theoretical treatments.

Second, the gap between  $S_1$  and  $S_2$  is relatively small (3400  $\text{cm}^{-1}$  for all-trans octatetraene in n-hexane) and the off diagonal dipole moment matrix element between these states is symmetry allowed and relatively large. The observed vibronic development of the optical spectra are consistent with the idea that the Franck-Condon factors for the mixing of higher lying  $1^1B_u$  levels will only be significant for the C=C double bond stretch

vibrations. Since the frequencies of these vibrations are almost as large as the electronic gap, this means that, with respect to hole burning studies on the  $1^1A_g$  to  $2^1A_g$  origin, the primary effect of an applied electric field is to mix the  $2^1A_g$  and  $1^1B_u$  zero point levels. Thus, it is reasonable to treat the data in terms of a two level model with known energy gap parameterized in the local field and the  $2^1A_g-1^1B_u$  transition dipole.

Third, because of the long lifetime of the excited  $2^1A_g$  state, the intrinsic hole width is extremely narrow (3.2 MHz HWHM for octatetraene in n-hexane[5]). This means that the effects of applied electric fields can be registered with very high resolution which removes ambiguity from the interpretation of the observed effects.

We have measured the effects of applied electric fields on the linear polyene octatetraene substituted in various n-alkane matrixes. These are systems where there is a high degree of order in the environment of a given octatetraene molecule but the sample consists of randomly oriented microcrystals. This is to some extent the inverse of the more usual situation. Instead of a dye molecule seeing the vector sum of a fixed magnitude but randomly oriented laboratory field plus a solvent field whose orientation and magnitude are both also randomly distributed, the octatetraene molecule sees the vector sum of a fixed magnitude but randomly oriented laboratory field plus a solvent field whose magnitude and orientation are both fixed.

In consequence, the application of an electric field to a polycrystalline octatetraene in n-alkane sample which has been labeled by photochemical hole burning produces a splitting whose detailed form depends on the polarizations of the excitation and observation channels with respect to the applied field. This splitting is quantitatively fit by a simple two level model parameterized in the magnitude of the  $S_1$  to  $S_2$  transition dipole and the projection of the local solvent field along this transition dipole. An example hole profile for octatetraene in n-hexane is compared to the profile calculated from the model below.

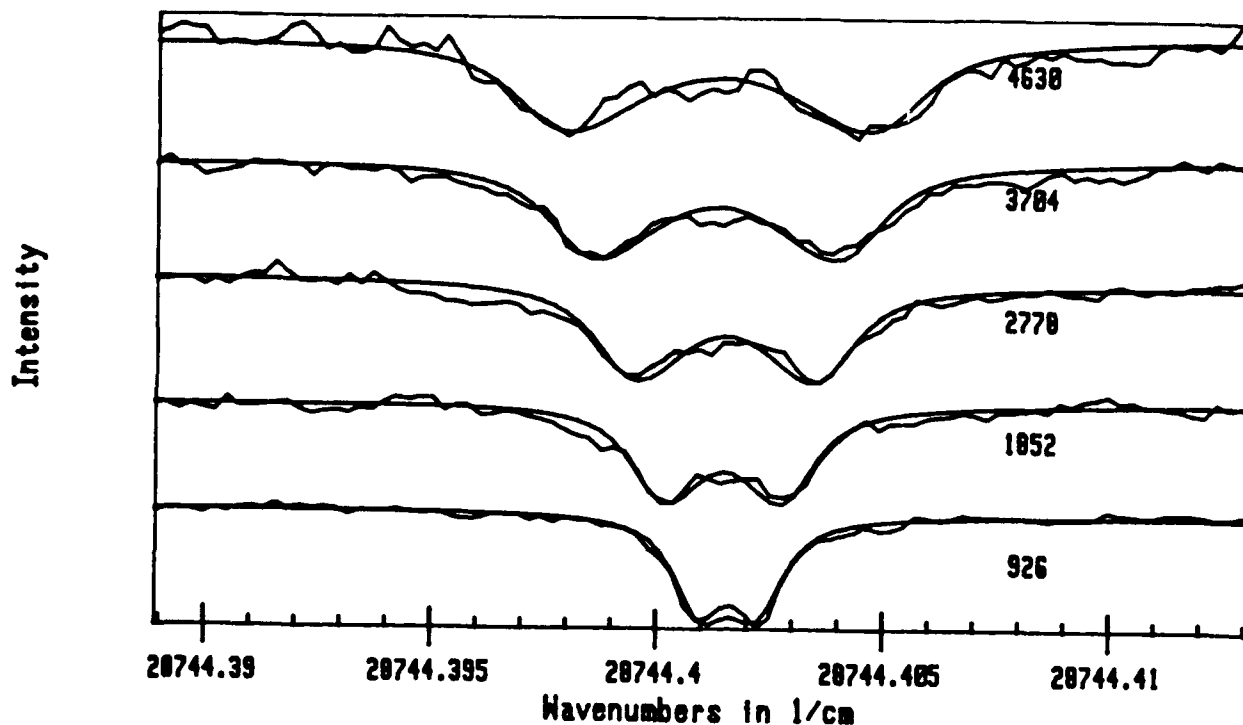


Figure 1: Hole profiles for all-trans octatetraene in n-hexane as a function of electric field in  $\text{V cm}^{-1}$  which labels the curves. There is good agreement between the measured profiles (noisy lines) and those calculated from the 2-level model for a transition dipole of 2.3 Debye and internal field projection of  $10^6 \text{ V cm}^{-1}$  (smooth lines).

This talk will summarize the observed dependence of photochemical hole profile on such experimental variables as applied field strength and orientation with respect to the polarization of excitation and detection channels and give further details of the model used to quantitatively interpret these results.

1. A.J. Meixner, A. Renn, S.E. Bucher and U.P. Wild, *J. Phys. Chem.* **90**, 6777 (1986).
2. U. Bogner, P. Schatz, R. Seel and M. Maier, *Chem. Phys. Lett.* **102**, 267 (1983).
3. L. Kador, D. Haarer and R. Personov, *J. Chem. Phys.* **86**, 5300 (1987).
4. P. Schatz and M. Maier, *J. Chem. Phys.* **87**, 809 (1987).
5. G. Adamson, G. Gradl and B.E. Kohler, *J. Chem. Phys.* **90**, 3038 (1989).

# Electric-Field Effects on Hole Spectra in Doped Polymers: A Step towards Two-Dimensional Optical Spectroscopy

L. Kador

*University of Bayreuth, Physical Institute and  
Bayreuther Institut für Makromolekülforschung (BIMF),  
P. O. Box 10 12 51, W-8580 Bayreuth, Fed. Rep. Germany  
Phone (0921) 55-3261*

Optical absorption bands of organic dye molecules or inorganic ions in condensed matter are affected by inhomogeneous broadening [1] and are thus usually much broader than the corresponding homogeneous lines. In disordered systems, the difference can amount to several orders of magnitude at low temperatures. In order to detect the effects of external perturbations such as hydrostatic pressure or electric fields on an inhomogeneous band, the perturbations must therefore have very large magnitudes. The sensitivity can be greatly enhanced by investigating the changes of hole-burning spectra caused by the external fields. In amorphous matrices, an external electric field gives rise to a symmetrical broadening of spectral holes due to the linear Stark effect. This was shown to be true even in the case of centrosymmetric dopant molecules where the first-order Stark effect is ascribed to matrix-induced dipole moments [2] (see Fig. 1). The magnitude of the broadening yields thus information on the electrostatic dye-matrix interaction.

Measurements performed at various frequency positions within the inhomogeneous band showed that the matrix-induced dipole moment differences between excited and ground state increase from the blue to the red edge of the band for a large number of dye-matrix systems. As an example, Fig. 2 shows the data for a symmetrically substituted zinc tetrabenzoporphin in poly(vinyl butyral). In order to interpret these results, a stochastic theory of the dye-matrix interaction [3] was extended to take the van der Waals and the electrostatic intermolecular interactions into account. According

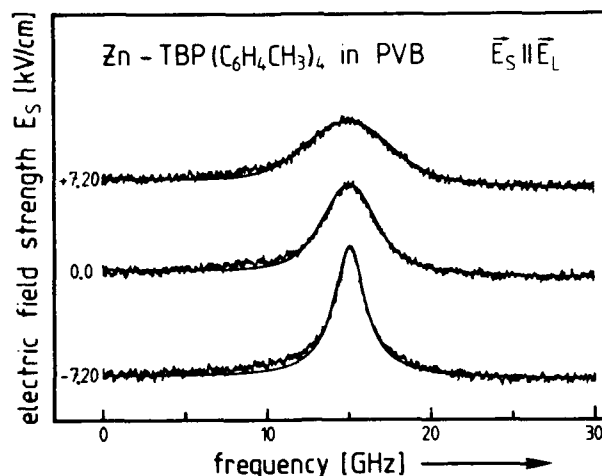


Figure 1: Hole spectra of apolar dye molecules (a symmetrically substituted zinc tetrabenzoporphin) in a polar polymer [poly(vinyl butyral)], recorded in three different electric field strengths. The field strength values are indicated in kV/cm on the left side of the traces. The hole was burned with  $-7.20$  kV/cm applied.

to the theory, the measurements can be viewed as a sort of two-dimensional optical spectroscopy, since they are characterized by two different frequency scales: the change of the hole width in the electric field, which is roughly given by the homogeneous linewidth, and the width of the inhomogeneous band. Hence, the broad inhomogeneous distribution that has long been the main obstacle to performing sensitive spectroscopic experiments in amorphous materials, can be utilized to obtain additional physical information.

Nevertheless, the interpretation of the data is more difficult than in the case of, for example, two-dimensional NMR spectroscopy. The reason is that molecules in solution which are investigated by magnetic resonance, consist of a certain number of atoms whose arrangement and distances are exactly identical in all molecules under study. This gives rise to strong, discrete features in the spectra. The ensemble of dopant molecules in a disordered solid, on the other hand, is characterized by broad, continuous distributions of the salient physical quantities, since essentially all of them have different local environments. The stochastic theory predicts

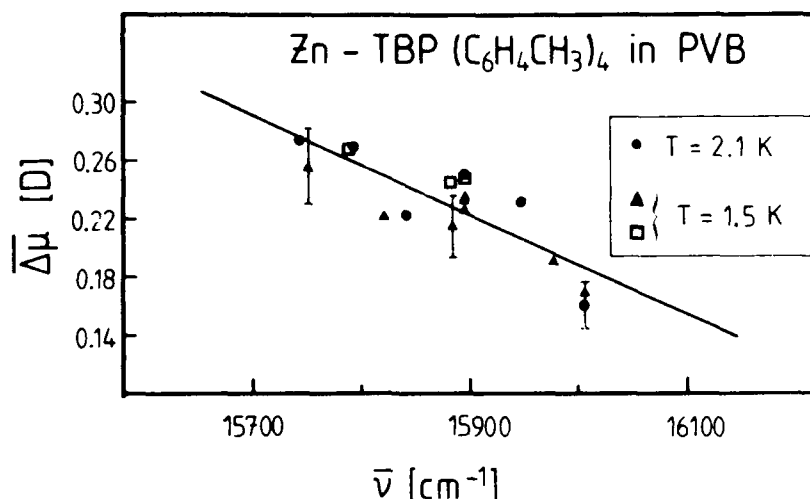


Figure 2: Experimental data of the average matrix-induced dipole moment difference  $\bar{\Delta\mu}$  as measured at different optical frequencies within the inhomogeneous absorption band. The sample was poly(vinyl butyral) doped with a symmetrically substituted zinc tetrabenzoporphin

the distribution of linear Stark shifts for each optical frequency within the inhomogeneous band to be given by a profile whose shape is very close to Gaussian and whose width increases from higher to lower frequencies. While this is in qualitative agreement with experiment, the predicted variation across the absorption band is too small by a factor of 2 ... 5, although the so-called Gaussian approximation is not applied which would restrict the validity of the calculation to systems with high densities of the matrix molecules. Possible reasons for the deviation are discussed.

## References

- [1] A. M. Stoneham, *Rev. Mod. Phys.* **41**, 82 (1969).
- [2] U. Bogner, P. Schätz, R. Seel, and M. Maier, *Chem. Phys. Lett.* **102**, 267 (1983).
- [3] B. B. Laird and J. L. Skinner, *J. Chem. Phys.* **90**, 3274 (1989).

## SPECTRAL HOLES UNDER PRESSURE: PROTEINS AND GLASSES

**J. Zollfrank, J. Friedrich**

Institut für Physikalische Chemie, Johannes Gutenberg-Universität

W-6500 Mainz, Germany

Phone: (06131)-39-2447

Fax: (06131)-39-3768

Pressure tuning of spectral holes /1/ provides, in a way, a link between gas-phase and solid state spectroscopy. Generally speaking, the shift of a spectral hole under isotropic pressure conditions, allows for a determination of three system parameters. These are: the vacuum frequency  $\nu_{\text{vac}}$  of the molecular probe, the solvent shift  $\nu_s$  which the probe experiences when embedded into a lattice and the compressibility  $\kappa$  of the host material.

The first of these three quantities,  $\nu_{\text{vac}}$ , is the link to the gas-phase spectroscopy. We consider the possibility of a determination of  $\nu_{\text{vac}}$  from a host matrix spectrum as important with respect to quantum chemical calculations of the probe transition energies and the guest-host interaction. Both quantities,  $\nu_{\text{vac}}$  and  $\nu_s$ , can be obtained on an absolute scale from the pressure tuning properties of the hole /2/. Note, that for many guest-host systems it is impossible to determine  $\nu_{\text{vac}}$  from a gas-phase experiment. For some systems, the probe may not exist at all in the gas-phase. For other systems the probe is modified, physically or chemically, through the interaction with the host. This often happens for dye probes embedded in proteinaceous environments. In this case, too, a gas phase experiment cannot be performed or does not provide the desired information. As far as proteins are concerned, the third of the above mentioned quantities, namely the compressibility  $\kappa$ , is of special interest. Since in a pressure tuning hole burning experiment, the compressibility is determined from the change of the interaction in the compressed lattice with the probe molecules, the experiment actually measures the compressibility of a local environment of the probe. For a homogeneous medium, this local compressibility is identical with the bulk compressibility, but for a nonhomogeneous medium it is not. Solutions of chromoproteins in a host glass can be considered as non-homogeneous solutions. The local environment is determined by the protein and, hence, the compressibility of individual protein molecules can be directly determined from the

properties of the pressure tuned hole. The compressibility, in turn, determines the volume fluctuations of the protein, which is an important quantity with respect to its function /3/.

Consider a photoreactive dye probe dissolved in a glassy medium. The interaction of this probe with a solvent molecule at position  $R_i$  changes its vacuum absorption frequency by an amount  $\nu(R_i)$ . We assume that the dominant contributions to this interaction is due to the attractive part of the Lennard-Jones potential, which falls off as  $R^{-6}$ . The repulsive part concerns only a few solvent molecules because of its short range. Provided that the sample around the dye probe is isotropic and homogeneous within the interaction range of the dispersion forces, the changes in  $\nu(R)$  due to application of pressure is /4/

$$\Delta\nu = -\frac{R}{3} \kappa \frac{\delta\nu}{\delta R} \Delta p \quad . \quad (1)$$

Since we assume  $\nu(R) \propto R^{-6}$ , equation (1) becomes

$$\Delta\nu = 2\kappa \nu(R) \Delta p \quad . \quad (2)$$

A hole burning experiment is frequency selective. Hence, equation (2) has to be averaged over those configurations of solvent molecules, which lead to a probe absorption as selected by the laser frequency:

$$\langle \Delta\nu \rangle_c = 2\kappa \langle \nu(R) \rangle_c \Delta p \quad . \quad (3)$$

$\langle \Delta\nu \rangle_c$  is the pressure induced shift of the burnt in hole, and the configurationally averaged perturbation of the transition frequency  $\langle \nu(R) \rangle_c$  is the solvent shift of the laser selected probe molecules. The solvent shift  $\nu_s$ , on the other hand, is the difference between the vacuum frequency  $\nu_{vac}$  and the absorption frequency  $\nu$  (which coincides, of course, with the laser frequency). Hence, we have

$$\nu_s \equiv \langle \nu(R) \rangle_c = \nu - \nu_{vac} \quad (4)$$

and

$$s \equiv \frac{\langle \Delta\nu \rangle_c}{\Delta p} = 2\kappa (\nu - \nu_{vac}) \quad . \quad (5)$$

Equation (5) tells us that the quantity  $s$ , i.e. the hole shift per unit pressure, changes in a linear fashion as the burning frequency  $\nu$  is tuned across the inhomogeneous band (4). The slope factor of the corresponding straight line is determined by the compressibility of the host  $\kappa$ . Moreover, there exists a frequency, namely  $\nu_{\text{vac}}$ , where the pressure induced hole shift vanishes.

We investigated quite a series of soft organic glasses by applying pressure tuning hole burning spectroscopy. All these experiments showed that the above model describes the observed spectral features qualitatively correct. In some cases, where the parameters of the model,  $\kappa$  or  $\nu_{\text{vac}}$ , were known from other experiments, it could be cross-checked that even the quantitative predictions were correct within a reasonable range of accuracy. In a few cases we found that  $\nu_{\text{vac}}$  was within the inhomogeneous band, hence, we could directly show that there is a frequency which does not shift under pressure. Scanning the burn frequency across  $\nu_{\text{vac}}$  the slope factor changes sign, i.e. the pressure induced line shift turns from a red to a blue shift (or vice versa). As an example we show the data for resorufin in ethyleneglycol/water glass.

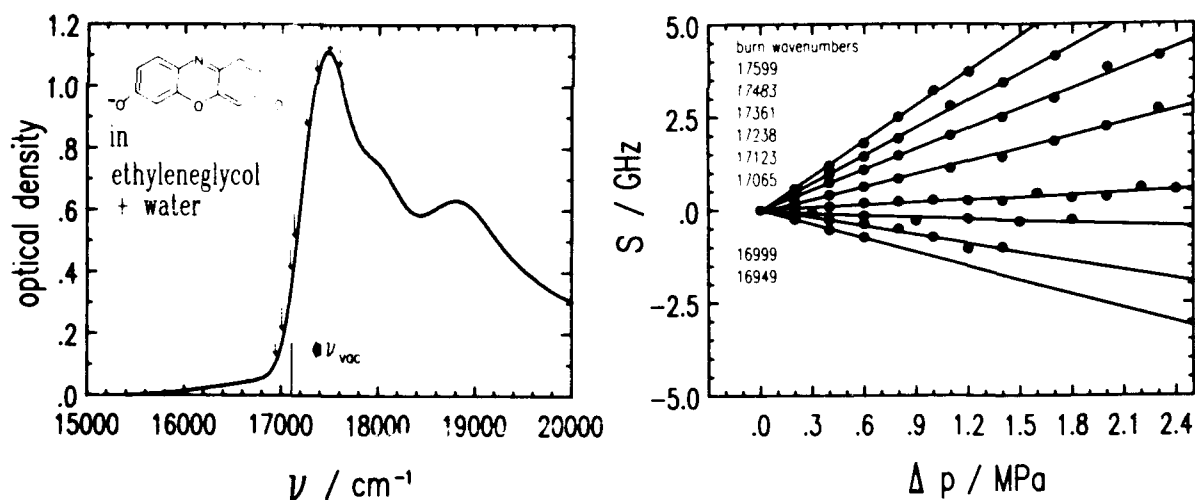


Fig. 1: Left: Absorption spectrum of resorufin in ethyleneglycol/water glass. Arrows mark the hole burning frequencies. Right: Frequency shift of a hole under pressure for the various burn frequencies.

Figure 1 shows the absorption at He-temperature. The arrows mark the positions where burning was performed. The hole shift as a function of pressure is plotted in Figure 1 (right). Clearly, there is a well defined frequency, where the lineshift changes sign. According to the model above, this frequency is identified as  $\nu_{\text{vac}}$ .

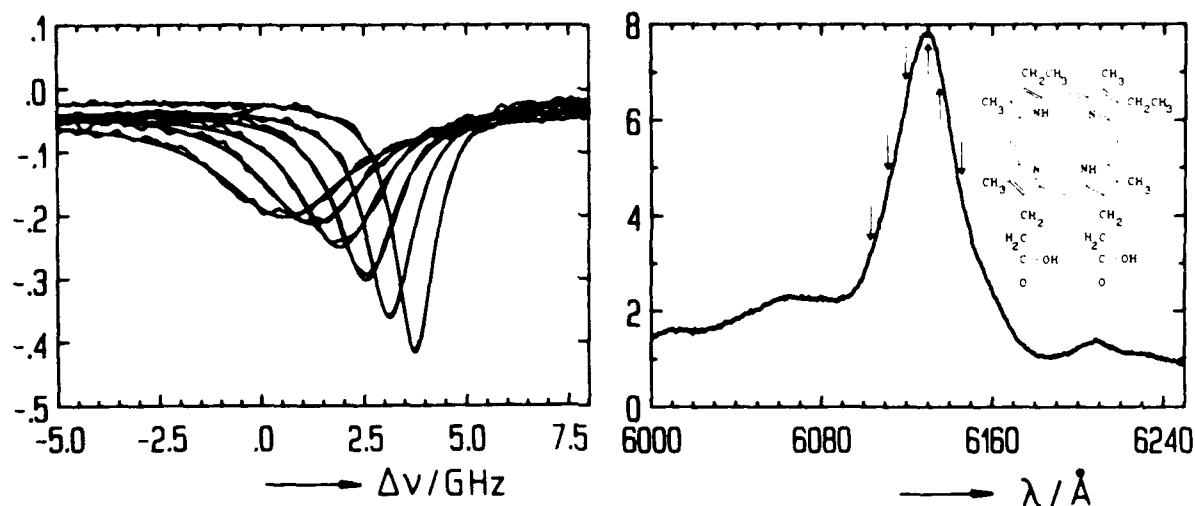


Fig. 2: Left: The behavior of a typical hole under pressure.  
 Right: Excitation spectrum of mesoporphyrin IX substituted horseradish peroxidase.  
 Arrows mark hole burning frequencies.

Figure 2 shows pressure tuning hole burning data for a chromoprotein, namely mesoporphyrin IX substituted horseradish peroxidase (HRP) /3/. Again the burning positions are marked by arrows. From the data, the compressibility of the protein molecule could be determined according to equation (5). We found  $\kappa_p \approx 0.11 \text{ GPa}^{-1}$ . For a protein molecule, this is a very interesting quantity because its volume fluctuations  $\sigma_V$  can be determined, once  $\kappa$  is known:

$$\sigma_V = \sqrt{\frac{kT\kappa}{V}} \quad (6)$$

$V$  is the volume of a single HRP molecule which can be estimated from its molecular weight. It is on the order of  $10^5 \text{ \AA}^3$ . Hence,  $\sigma_V$  is, at ambient temperature, on the order of 3%. This is a lower estimate, because  $\kappa$  increases with temperature. However, this value seems to be already large enough for a proper functioning of the protein as an oxidizing enzyme for small aromatic molecules. This oxidation takes place in the protein crevice. Rather large volume fluctuations are required so that the protein can provide enough space for incorporating the substrate molecule.

## References

- /1/ Th.Sesselmann, W.Richter, D.Haarer, H.Morawitz, Phys.Rev.**B36**, 7601 (1987)
- /2/ G.Gradl, J.Zollfrank, W.Breinl, J.Friedrich, J.Chem.Phys., May 15, 1991
- /3/ J.Zollfrank, J.Friedrich, J.Fidy, J.Vanderkooi, J.Chem.Phys., accepted
- /4/ B.B.Laird, J.L.Skinner, J.Chem.Phys. **90**, 3274 (1989)



Thursday, September 26, 1991

## Poster Session: 1

**ThE** 5:30pm–7:00pm  
DeAnza Room

CORRELATION BETWEEN THE RELATIVE ZERO-PHONON ELECTRONIC TRANSITION PROBABILITIES (DEBYE-WALLER FACTORS) AND THE MATRIX-INDUCED SPECTRAL SHIFTS OF MOLECULAR IMPURITY CENTERS DOPED INTO AMORPHOUS HOSTS

Indrek RENGE

Institute of Physics, Estonian Academy of Sciences, 142 Riia, 202400 Tartu, Estonia; Phone: 01434-28882

The attainable contrast in spectrally highly selective photochromic materials critically depends on the Debye-Waller factors (DWF)/1/. The search for better hole-burning systems requires simple criteria for the selection of suitable dopants and hosts on the basis of molecular structure and, preferably, of room-temperature spectroscopy. The accumulated experimental data allow to establish reasonable relationships between the DWF and the differences of intermolecular interaction parameters in the ground and excited state (dipole moments, polarizabilities).

According to the Franck-Condon principle, the probability of exciting low-frequency intermolecular vibrations in the course of an electronic transition is higher when the minima of the intermolecular interaction potentials are displaced. Small DWF values are expected in the case of large differences between the van der Waals forces in the ground and excited state and vice versa. On the other hand, the matrix-induced transition frequency shift depends on the relative stabilization of the respective electronic levels upon transfer of the free molecule into the condensed phase/2/. For instance, the strengthening of the interaction with the surroundings in the  $S_1$  state results in the downward shift of the  $S_1-S_0$  transition frequency. The strongest zero-phonon transitions should therefore occur in the systems with small matrix shifts.

The DWF values were collected from the literature (Table 1). In several cases the DWF-s have been estimated by us as a relative saturated depth of a spectral hole burned near the band maximum. The matrix shift was calculated as a difference between the resonance origin of a free molecule seeded in the supersonic jet ( $\nu_0$ ) and the frequency at which the spectral hole was burned or, alternatively, between  $\nu_0$  and the absorption band maximum. The  $\nu_0$  values for ionic dyes have been obtained from the liquid-phase solvatochromic measurements.

The non-specific solvent-induced shifts of absorption band maxima can be described according to the equation/19/:

$$\nu = \nu_0 + pP + yY, \quad (1)$$

where  $Y = (\epsilon - 1) / (\epsilon + 2)$  is the solvent polarity,  $\epsilon$  is the dielectric constant at 20°C,  $P = (n^2 - 1) / (n^2 + 2)$  is the solvent polarizability,  $n$  is the refractive index for the Na D-line at 20°C.

TABLE 1

Debye-Waller factors and the matrix shifts of purely electronic transitions ( $\Delta\nu = \nu_0 - \nu_{\text{burn}}$ ) for the hole-burning systems

Dopant	Matrix	DWF	T, K	$\nu_{\text{burn}}$ , cm <sup>-1</sup>	$\Delta\nu^a$ , cm <sup>-1</sup>
Tetraphenylporphine	PMMA	0.9	4.2	15549/3/	68/4/
Phthalocyanine	polystyrene	0.72 $\pm$ 0.1	4-16	14362/5/	770/6/
Perylene	PVB	0.5 $\pm$ 0.1	1.2	22647/7/	1390/8/
Rhodamine 640(101)	PVA	0.35- 0.48	2/9/		$\sim$ 800
Oxazine 4	PVB	$\sim$ 0.3	1.7	16200/10/	1204
Resorufin Na salt	PMMA	0.2-0.5	4	16807 /11,12/	1081
Quinizarin	EtOH-MeOH	0.17	4.2	19436/13/	483/14/
Cresylviolet	PVA	0.15	7	16528/15/	2012
Cyanine HITCI	PVA	0.15	5.4	12658/16/	1106
Laser dye DCM	polystyrene	0/17/			$\sim$ 2300
2-Aminoanthracene	various	0/18/			$\sim$ 2500
Cresylviolet, neutr.	EtOH	0/12/			$\sim$ 3400

<sup>a</sup>The citation refers to the source of the  $\nu_0$  for jet-cooled molecule. Other  $\nu_0$  values are taken from the Table 2.

TABLE 2

The  $S_1-S_0$  transition frequencies of the free molecules as estimated from Eq. 1 by using the solvent-induced absorption band shifts at 20°C (N is the number of solvents, p and y are the regression coefficients, r is the linear correlation coefficient)

Compound	N	Slope, cm <sup>-1</sup>	$\nu_0$ , cm <sup>-1</sup>	r	$\nu_{0,\text{jet}}$ , cm <sup>-1</sup>
Tetraphenylporphine	5	p+y=-639	15613	0.994	15617/4/
Perylene	7	p+y=-4825	24112	0.986	24037/8/
Rhodamine 640(101)	7	p=-3040	18358	0.981	
perchlorate	3	y=-386		0.963	
Oxazine 4	6	p=-2919	17404	0.988	
perchlorate	7	y=-338		0.626	
Resorufin Na salt	7	p=-3275	17888	0.992	
	8	y=-136		0.351	
Quinizarin	4	p+y=-2413	19850	0.999	19919/14/
Cresylviolet	7	p=-5585	18540	0.964	
perchlorate	7	y=-267		0.319	
Cyanine HITCI	7	p=-3287	13764	0.958	
	10	y=+493		0.810	
Laser dye DCM	4	p+y=-8145	24050	0.999	
Cresylviolet, neutr.	8	p=-15000		0.948	

It has been shown/20/ on the basis of the Bakhshiev's theory /2/ that

$$y = 1.25 \cdot 10^4 \mu_g (\mu_g - \mu_e \cos \phi) / r^3 \quad (2)$$

$$p = \{-6.3 \cdot 10^3 (\mu_g^2 - 2\mu_g \mu_e \cos \phi + \mu_e^2) + 6.0 \cdot 10^4 (\alpha_g - \alpha_e)\} / r^3, \quad (3)$$

where  $\mu_g$  and  $\mu_e$  are the dipole moments of the ground and excited state in Debye units,  $\phi$  is the angle between these dipole moments,  $r$  is the Onsager cavity radius in Å,  $\alpha_g$  and  $\alpha_e$  are the polarizabilities of the ground and excited state in Å<sup>3</sup>.

In the case of non-polar solvents like n-alkanes, an equality holds between  $n^2$  and  $\epsilon$ , and thus  $Y=P$ . The  $\nu_0$  values obtained from the plots of the absorption band maxima versus the polarizability function by extrapolating the  $P$  to the zero are remarkably close to those of free molecules (Table 2).

Since ionic compounds cannot be dissolved in non-polar solvents, the slopes  $p$  and  $y$  have to be measured separately in two solvent sets by changing only one parameter while keeping the other nearly constant. Aprotic solvents with low nucleophilicity have been chosen in order to minimize the specific solvation effects. The solvent shifts in highly polar media with  $\epsilon > 30$  from acetonitrile ( $n=1.344$ ) to nitrobenzene ( $n=1.5513$ ) are very well correlated with the polarizability function  $P$  (Table 2).

The fit of the absorption band maxima versus the polarity function  $Y$  in a set of solvents with constant refractive indices ( $n=1.43$ ) from chloroform ( $\epsilon=4.8$ ) to propylene carbonate ( $\epsilon=65.1$ ) is usually poor because of ionic association and specific solvation effects (Table 2). However, this does not cause serious error in the extrapolated  $\nu_0$  value, since the influence of the dielectric constant is relatively small ( $y < 500 \text{ cm}^{-1}$ ). Consequently, the dipole moment difference between the  $S_1$  and  $S_0$  state for all molecules studied until now by hole-burning and fluorescence line narrowing techniques hardly exceeds several Debye units.

It is evident from the Table 1 that molecular impurities with the highest DWF-s are centrosymmetric and formally without dipole moments in both the ground and excited state (porphyrins, arenes, cyanine dyes).

Tetrapyrrolic pigments (porphyrins, phthalocyanines) possess outstandingly strong zero-phonon lines. Moreover, in contrast to the other organic impurities, zero-phonon holes have been observed even at 80K for tetraphenylporphine/3/ and phthalocyanine/21/. Porphyrins are characterized by unusually small matrix shifts of the  $S_1$ - $S_0$  transition frequency. The difference between the ground and excited state polarizabilities and the slope  $p = -639 \text{ cm}^{-1}$  for tetraphenylporphine are approximately by an order of magnitude smaller than the corresponding values for polycyclic arenes.

It remains still unclear, whether the diversity in DWF-s of polycyclic arenes, cyanine, oxazine, rhodamine and other dyes can be explained solely in terms of the changes in dipole moments and polarizabilities or, alternatively, the role of

torsional modes of the polymethine chain or the phenyl and amino substituents should be taken into account.

Transitions accompanied with pronounced intramolecular charge transfer display no zero-phonon component/18/. In this case extensive band shifts occur even in apolar solvents or in the solvents with constant  $\epsilon$  ( $p+y=-8145$  and  $p=-15000\text{cm}^{-1}$  for DCM and neutral cresylviolet, respectively) as a result of summation of both dispersion and dipole-induced-dipole contributions (Eq.3), when  $\mu_e \gg \mu_g$ . It seems plausible that molecules with solvent shifts more than  $2200\text{cm}^{-1}$  do not have zero-phonon transitions of measurable intensity in amorphous matrices.

In conclusion, it has been shown that useful predictions about the maximum zero-phonon hole depth at liquid helium temperatures can be made with the aid of room-temperature solvent shift measurements.

#### REFERENCES

1. K.K.Rebane and L.A.Rebane, in: Persistent Spectral Hole-Burning: Science and Applications, Ed. W.E.Moerner, Springer, Berlin-Heidelberg, 1988, 17.
2. N.G.Bakhshiev, Spectroscopy of Intermolecular Interactions, Nauka, Leningrad, 1972.
3. A.Furusawa, K.Horie and I.Mita, Chem.Phys.Lett., 1989, 161, 227.
4. U. Even, J.Magen, J.Jortner, J.Friedman and H.Levanon, J.Chem. Phys., 1982, 77, 4374.
5. G.Schulte-Roth, Thesis, Bayreuth University, 1986, 123.
6. P.S.H.Fitch, C.A.Haynam and D.H.Levy, J.Chem. Phys., 1980, 73, 1064.
7. U.Bogner, P.Schätz and M.Maier, Chem. Phys.Lett., 1985, 119, 335.
8. S.Leutwyler, Chem.Phys.Lett., 1984, 107, 284.
9. Y.Kanematsu, R.Shiraishi, S.Saikan and T.Kushida, Chem.Phys.Lett., 1988, 147, 53.
10. A.Renn, S.E.Bucher, A.J.Meixner and U.P.Wild, Chimia, 1985, 39, 389.
11. A.F.Childs and A.H.Francis, J.Phys.Chem., 1985, 89, 466.
12. R.van den Berg and S.Völker, Chem.Phys., 1988, 128, 257.
13. W.Breinl, Thesis, Bayreuth University, 1989, 133.
14. G.Smulevich, A.Amirav, U.Even and J.Jortner, Chem.Phys., 1982, 73, 1.
15. B.L.Fearey, T.P.Carter and G.J.Small, J.Phys.Chem., 1983, 87, 3590.
16. H.Nakatsuka, K.Inouye, S.Uemura and R.Yano, Chem.Phys.Lett., 1990, 171, 245.
17. J.M.Hayes, B.L.Fearey, T.P.Carter and G.J.Small, Intern.Rev. Phys.Chem., 1986, 5, 175.
18. I.Chiang, J.M.Hayes and G.J.Small, Anal.Chem., 1982, 54, 315.
19. I.A.Koppel and V.A.Palm, in: Advances in Linear Free Energy Relationships, Ed. N.B.Chapman and J.Shorter, Plenum Press, New York, 1972, 203.
20. I.Renge, U.Mölder and I.Koppel, Spectrochim.Acta, 1985, 41A, 967.
21. A.R.Gutiérrez, J.Friedrich, D.Haarer and H.Wolfrum, IBM Journ.Res.Developm., 1982, 26, 198.

## PERSISTENT HOLE BURNING STUDY OF CORE ANTENNA OF PHOTOSYSTEM II

M. Vacha, F. Adamec, M. Ambroz, J. Dian, L. Nedbal\* and J. Hala

Department of Chemical Physics,  
Faculty of Mathematics and Physics, Charles University,  
Ke Karlovu 3, 121 16 Prague 2, Czechoslovakia

\* Institute of Microbiology, CSAV  
Trebou 379 81, Czechoslovakia

The application of hole burning spectroscopy (HB) in the study of photosynthetic systems offers an independent method for determining excited state lifetimes of particular chromophores. The rate constants of excitation energy transfer (EET) in photosynthetic antennae can be directly determined by time resolved fluorescence spectroscopy. For most bacterial and higher plants antennae is of the order of  $10^{-12} \text{ s}^{-1}$  [1]. Efficient EET in pigment-protein complexes causes significant shortening (three orders of magnitude) of the excited state lifetimes  $T_1$  in comparison with isolated pigments. The hole widths obtained in hole burning spectroscopy are proportional to the total relaxation time  $T_2$  [2]:  $(T_2)^{-1} = (2T_1)^{-1} + (T_2^*)^{-1}$ . In the presence of fast EET the  $T_1$  contribution is dominant. The aim of this report is to compare the role of protein environment and efficiency of EET in photosystem II (PS II) core antenna chlorophyll protein complex (CPa2) in polyacrylamid gel with that of the core antenna in native PS II particles in buffer/glycerol glass (PS II part.).

Persistent hole burning (PHB) fluorescence spectra were measured on an apparatus consisting of a burning single frequency  $\text{cw}$  dye laser (DCM dye) and an excitation pulsed dye laser (Coumarine), an optical bath cryostat, a double grating monochromator and a cooled photomultiplier along with a boxcar integrator, as described in [3]. The preparation of the samples isolated from cyanobacteria *Synechococcus* was described in [3,4]. Low temperature (4.2 K) fluorescence spectra of antenna systems before burning are shown on fig.1a,b (dashed lines). Hole burning spectra were studied with the burning wavelengths in the region 675 - 695 nm. Typical PHB spectra obtained under saturating conditions are presented in fig.1a,b (full lines).

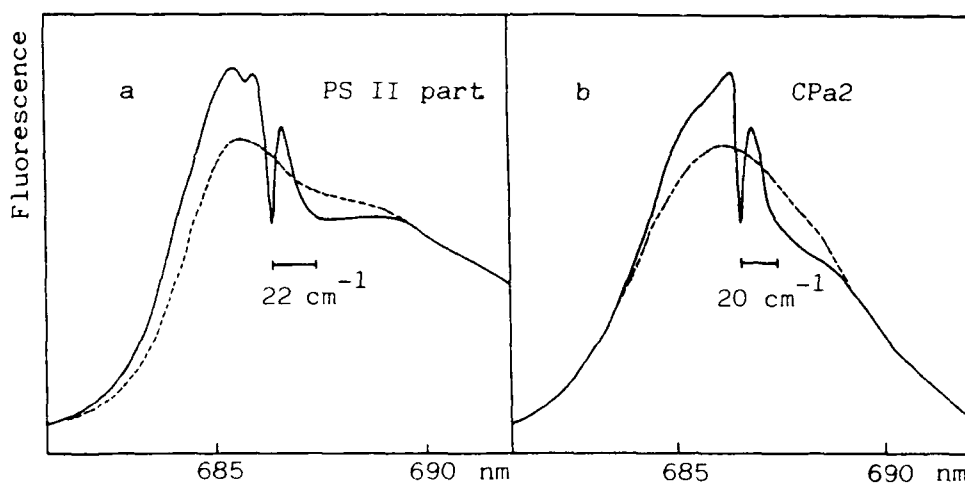


Fig.1 Fluorescence (dashed) spectra (excited at 440 nm) and hole burning (full) spectra (burned at 686.3 nm) of core antenna of photosystem II at 4.2 K: a - in polymere; b - in buffer/glycerol glass

Both spectra consist of an antihole, zero phonon hole (ZPH) and red shifted phonon side band hole (PSBH, real and pseudo- [4]). This structure is typical for nonphotochemical hole burning mechanism. Although the low temperature hosts in both systems are qualitatively different (polymer vs. glass), no qualitative

difference between the HB spectra suggests that the protein environment itself plays a dominant role in the HB mechanism. The dominant role of the protein is further supported by very small difference between protein phonon spectra (PSBH) of the two samples. The pigment-protein interaction is well characterized by an inhomogeneous distribution function (IDF) determined from the dependence of relative depths of saturated ZPH's on the burning wavelength [4] (fig.2). The observed shift between the maximum of the fluorescence spectrum and the maximum of IDF ( $\cong 23 \text{ cm}^{-1}$ ) corresponds well with the red shift ( $\cong 20\text{-}22 \text{ cm}^{-1}$ ) between ZPH and PSBH in fig 1a,b. The excited state lifetimes  $T_1$  shortened by fast EET were determined from the correct ZPH widths at 4.2 K [5]. The correct ZPH widths were obtained from the study of ZPH width as a function of burning fluence (total burning energy dose). Fig.3 shows this fluence experiment performed on PS II part. (the corresponding dependence for CPa2 was presented in [4]). The zero fluence extrapolated ZPH widths are  $1.0 \text{ cm}^{-1}$  for CPa2 and  $1.7 \text{ cm}^{-1}$  for PS II part, respectively. Related  $T_1$  values 10.6 ps and 6.2 ps, respectively, documented slower EET in chlorophyll-protein complex in gel.

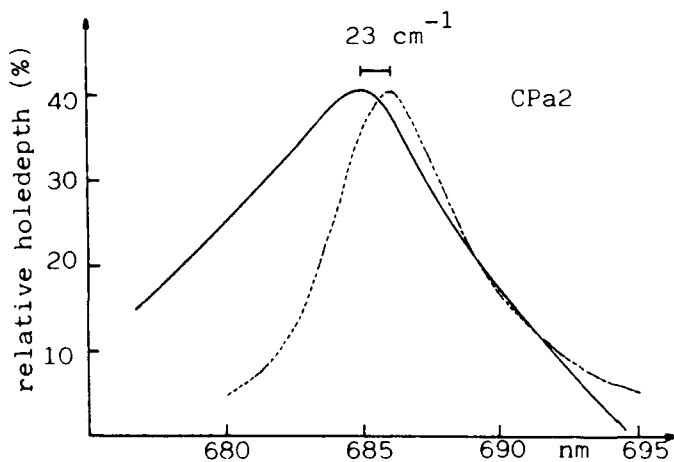


Fig.2 Relative holedepth of zero phonon hole as a function of burning wavelength (full line). Dashed line - corresponding fluorescence spectrum

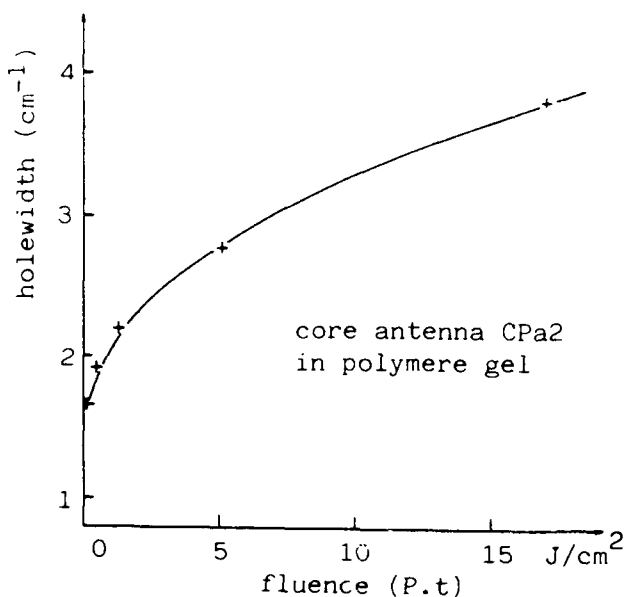


Fig.3 Width of zero phonon hole as a function of burning fluence (obtained for burning wavelength 676.4 nm at 4.2 K)

#### REFERENCES

- [1] H. Zuber, Photochem. Photobiol. 42 (1985) 821
- [2] S. Voelker, Annu. Rev. Phys. Chem. 40 (1989) 499
- [3] M. Vacha, F. Adamec, M. Ambroz, V. Baumruk, J. Dian, L. Nedbal and J. Hala, Photochem. Photobiol. 51 (1991) in press
- [4] M. Vacha, F. Adamec, M. Ambroz, J. Dian and J. Hala, Czech. J. Phys. (1991) in press
- [5] H. van der Laan, T. Schmidt, R.W. Visschers, K.J. Visscher, R. van Grondelle and S. Voelker, Chem. Phys. Lett. 170 (1990) 231

## Hole Burning in the Organic Triplet State: Side Holes in an Amorphous Glass

Hans Riesen and Elmars Krausz

*Research School of Chemistry, Australian National University*

*G.P.O. Box 4 Canberra 2601 A.C.T. Australia*

Overseas Fax: 61-6-249-0750

Hole-burning spectroscopy has been widely applied to the  $S_0$ - $S_1$  transition of organic molecules in amorphous hosts [1-3]. However, only very few reports on the hole-burning spectroscopy of the triplet state have appeared [4,5]. The low oscillator strength of the  $S_0$ - $T_1$  transition is the obvious handicap in performing such experiments. The oscillator strength of the  $S_0$ - $T_1$  transition can be dramatically increased by the heavy atom effect [6] making hole-burning experiments in the  $S_0$ - $T_1$  transition more feasible. A very pronounced heavy atom effect can be expected in ligand-centred singlet-triplet transitions of second and especially third row transition metal complexes leading to lifetimes in the  $\mu$ s range.

In the hole-burning spectrum of the  $S_0$ - $T_1$  transition it is in principal possible to observe sideholes that are separated from the resonant feature by  $\pm D$  for a chromophore with  $D \neq 0$  and  $E = 0$  and by  $\pm(D+E)$ ,  $\pm(D-E)$  and  $\pm 2E$  for a molecule with  $D \neq 0$  and  $E \neq 0$ . However, the first excited singlet state  $S_1$  and the phosphorescent triplet state  $T_1$  are well known to be poorly correlated in glasses, i.e. the  $S_1$ - $T_1$  separation is not constant within the inhomogeneous distribution. The spin sublevels of the triplet state may also not be correlated. In the case of a varying ZFS within the inhomogeneous distribution, sideholes will be broader than the resonant feature. If this variation is large enough, no distinct sidefeatures can be observed.

The present paper summarizes our work done on the  $S_0$ - $T_1$  transition in organic molecules and coordination compounds embedded in amorphous hosts, including the first observation of distinct sideholes in a truly amorphous material. A more detailed account of this work is to be given elsewhere [7,8].

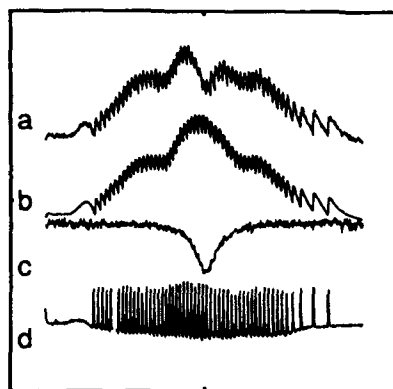


Figure 1

**The hole-reading technique**

A line of the  $\text{Ar}^+$  laser is tuned by changing the temperature of an intracavity etalon.

a is the observed excitation spectrum,

b the simultaneously measured laser power,

c is the ratio  $a/b$ , the hole spectrum.

d is the derivative of b, useful as a marker

The simple hole-burning technique used in this work is effectively illustrated in Fig. 1. The resolution is limited by the mode spacing of the  $\text{Ar}^+$  laser used, which is around 143 MHz for a Spectra Physics 164 laser.

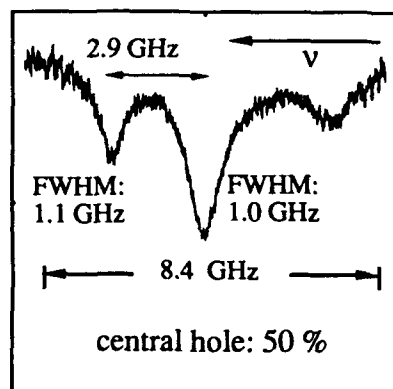


Figure 2

Coronene in 4:1 1-bromobutane/ethyl iodide at 1.6 K.

The 5145 Å laser line was etalon tuned.

The phosphorescence was monitored at  $5617 \pm 7$  Å.

The depth of the central hole [%] is indicated.

The expected sideholes at  $\pm D$  for  $E=0$  are very well pronounced ( $\pm 2.9$  GHz) in the particular case of coronene as seen in Fig. 2. This result does not come as a surprise. In phosphorescence line narrowing experiments sidebands could be observed [1]. Shallower holes were considerably narrower ( $\approx 500$  MHz). From an analysis of the data we evaluate a distribution of the ZFS of  $\pm 0.3$  GHz within the probed distribution. Coronene is a very rigid and symmetric molecule yet shows a 10% variation of the ZFS. This is significant, as we may then expect species that interact more strongly with their environment, such as nitrogen heterocycles to show a much larger spread.

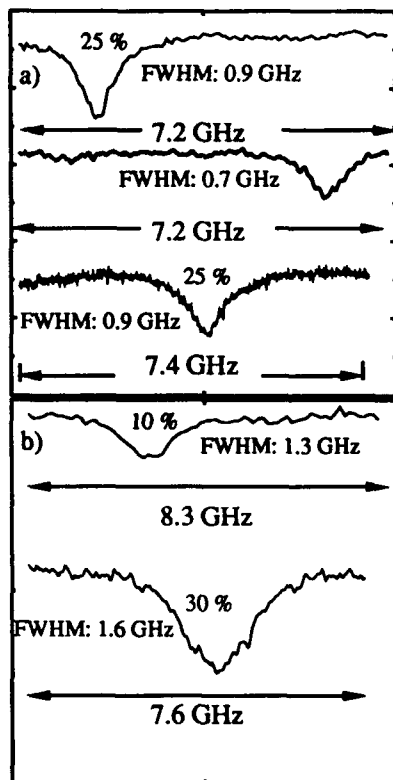


Figure 3

Hole-burning spectra at 1.6 K in 1-bromobutane for

- a) 2-iodoquinoline  
and b) 5-bromoacenaphthene

The 4578 Å laser line was scanned and phosphorescence was monitored at  $4883 \pm 2$  Å for the 2-iodoquinoline.

The 4880 Å laser line was scanned and phosphorescence was monitored at  $4957 \pm 5$  Å for the 5-bromoacenaphthene system. The hole depth and the measured holewidth (FWHM) are indicated.

No distinct sideholes could be detected for the 2-iodoquinoline and the 5-bromoacenaphthene systems in the experimental scanning range although in principal six sidefeatures could appear. We are able to conclude that the lack of distinct sideholes is most likely due to a non-correlation of the ZFS's. This result clearly indicates that ODMR data on triplet states in amorphous systems may well be prone to overinterpretation.

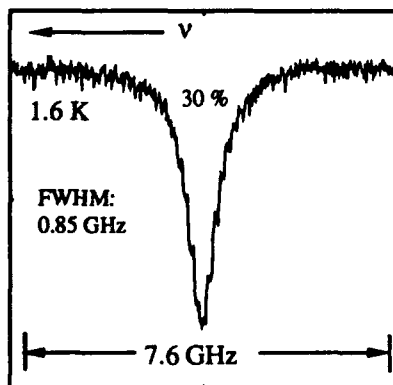


Figure 4

The hole-burning spectrum of

$[\text{Rh}(\text{ppy})_2\text{bpy}]^+$  in glycerol at 1.6 K.

The 4579 Å line of an Ar<sup>+</sup> laser was scanned and luminescence was monitored at  $4744 \pm 2$  Å.

No distinct sideholes can be observed within the scan range of  $\pm 3.8$  GHz from the resonant feature for the  $[\text{Rh}(\text{phpy})_2\text{bpy}]^+$ /glycerol (phby=phenyl pyridine) system as is illustrated in Fig. 4.. It is most likely that in coordination compounds of this kind the triplet state is very poorly correlated because of the additional degrees of freedom in the actual structure of the molecule. Thus sideholes of the same width as the resonant feature will only be rarely observed. It is possible to extract quantitative measures of the spread of ZFS's by performing hole burning and phosphorescence line narrowing experiments in magnetic fields where the Zeeman splittings are comparable to the ZFS's[7,8].

### References

- [1] R.I. Personov, "Spectroscopy and excitation dynamics of condensed molecular systems" eds. V.M. Agranovich and R.M. Hochstrasser (North-Holland, Amsterdam, 1983) p. 555.
- [2] W.E. Moerner, ed. "Persistent spectral hole-burning: science and application" (Springer, Berlin, 1989).
- [3] S. Völker, *Ann. Rev. Phys. Chem.* **40** (1989) 499.
- [4] S. Lin, J. Fünfschilling and I. Zschokke-Gränacher, *J. Luminescence* **46** (1990) 301.
- [5] K.K. Rebane and A.A. Gorokhovskii, *J. Luminescence* **36** (1987) 237.
- [6] S.P. McGlynn, T. Azumi and M. Kinoshita "Molecular spectroscopy of the triplet state" (Prentice Hall, Englewood Cliffs, 1969).
- [7] H.Riesen and E. Krausz, *Chem. Phys. Letters*, in press.
- [8] H.Riesen, E.Krausz, A.Zilian and H.U.Güdel, *Chem. Phys. Letters*, in press.

## Spectral Hole Burning: Dynamical Approach to Spectral Diffusion Problem

I. S. Osad'ko

Physics Department, V.I.Lenin State Pedagogical University,  
Moscow, 119435, USSR. Phone 247-10-04.

Herzog and Hahn [1] and Portis [2] while studying magnetic resonance in 1956 found hole broadening with time. This phenomenon was called "spectral diffusion". We can derive from Bloch equations the following expression for a hole in spin population:

$$\rho_{00}(\infty) = 1 - \frac{2\Lambda^2 T_1 T_2}{\Delta^2 + (1/T_2)^2 \cdot (1 + 4\Lambda^2 T_1 T_2)}. \quad (1)$$

Here  $\Delta = \omega - \omega_0$  is the difference between photon and resonance frequencies  $\omega$  and  $\omega_0$ ,  $\Lambda^2$  is the intensity of the electromagnetic field;  $T_1$  and  $T_2$  are times of the energy and phase relaxations. Halfwidth of the hole equals  $2/T_2$  at low intensity  $\Lambda^2$ . Therefore, Klauder and Anderson [3] suggested that spectral diffusion is the dependence of  $T_2$  on time. Experimental data obtained by Mims et. al. [4] confirmed this suggestion because the spin echo signal  $E(2\tau)$  had unusual dependence on the pause  $\tau$ :

$$E(2\tau) \propto \exp(-m\tau^2). \quad (2)$$

This result can easily be explained if we suppose that inverse dephasing time is a linear function of time:

$$2/T_2 = m\tau. \quad (3)$$

Klauder and Anderson [3] offered a stochastic theory for the dipolar correlation function of resonant spins which interact with an array of nonresonant ones. The interaction leads to the temporal dependence of the dephasing time  $T_2$  of the resonant spins. The stochastic theory for  $T_2$  was developed further [5] and extended over transitions in two level systems (TLS) of glasses [6] and optical transitions interacting with TLS [7,8].

Why do we reject the stochastic approach and use a dynamical one to consider a spectral diffusion problem for optical transitions in amorphous solids? There is an important reason for this.

As we know, a dipolar correlator  $\langle d(t)d(0) \rangle$  determines the temporal behaviour of both optical free induced decay and the intensity  $E(2\tau)$  of a photon echo signal. On the other hand, a Fourier-transform of  $\langle d(t)d(0) \rangle$  determines the optical band shape and the hole shape. Using the stochastic approach we cannot derive a *true optical band shape* which usually consists of a zero phonon line (ZPL) and a phonon side band (PSB). On the contrary, the dynamical theory yields true formulas both for ZPL and for PSB. These formulas are in a good agreement with experimental facts. As the halfwidth  $\gamma$  of ZPL is expressed via optical dephasing time  $T_2$  by means of a simple equation

$$1/T_2 = \gamma/2 + 1/2T_1, \quad (4)$$

we may hope that a dynamical theory can lead to a temporal dependence of  $T_2$  and the dependence can differ from that predicted by a stochastic theory. We must verify this hypothesis.

Within the scope of any dynamical approach the temporal behaviour of a dipolar correlator is determined by the dynamics of the impurity center, or what is more true, by a change of the Franck-Condon potential surface upon electronic excitation. This change is called electron-phonon interaction. In amorphous solids there are both phonons and excitations of TLS (so-called *tunnelons*). Therefore, there is a change in TLS upon electronic excitation as well. We will call this change the electron-tunnelon interaction and it must certainly influence the homogeneous optical band in amorphous solids.

Within the scope of the dynamical approach we can generalize the optical Bloch equations and derive novel equations for the density matrix which include formulas both for the total absorption band  $I^g$  and for the fluorescence band  $I^e$ . The equations look as follows [9]:

$$\begin{cases} \dot{\rho}_{10}(\Omega, t) = i(\Omega - i/2T_1)\rho_{10}(\Omega, t) + \Lambda(I^g(\Omega)\rho_{00}(t) - I^e(\Omega)\rho_{11}(t)), \\ \dot{\rho}_{01}(\Omega, t) = i(\Omega + i/2T_1)\rho_{01}(\Omega, t) + \Lambda(I^g(\Omega)\rho_{00}(t) - I^e(\Omega)\rho_{11}(t)), \\ \dot{\rho}_{00}(t) = -\Lambda \int_{-\infty}^{\infty} \frac{d\Omega}{\pi} (\rho_{10}(\Omega, t) + \rho_{01}(\Omega, t)) + \rho_{11}(t)/T_1, \\ \dot{\rho}_{11}(t) = -\rho_{00}(t). \end{cases} \quad (5)$$

Here  $I^g(\Omega)$  and  $I^e(\Omega)$  are functions of the absorption and fluorescence band shape. They are determined by the following eqs.:

$$\begin{aligned} I^g(\Omega) &= \pi \sum_{\alpha, \beta} P_\alpha \langle \alpha | \beta \rangle^2 \delta(\Omega + \Delta - \Omega_\beta + \Omega_\alpha); \\ I^e(\Omega) &= \pi \sum_{\alpha, \beta} P_\beta \langle \alpha | \beta \rangle^2 \delta(\Omega + \Delta - \Omega_\beta + \Omega_\alpha). \end{aligned} \quad (6)$$

Here  $|\alpha\rangle$  and  $\hbar\Omega_\alpha$  are eigenfunctions and energies of phonons and tunnelons in the ground electronic state.  $|\beta\rangle$  and  $\hbar\Omega_\beta$  are the same for the excited electronic state.  $P_\alpha$  and  $P_\beta$  are probabilities to find the system in quantum states  $|\alpha\rangle$  and  $|\beta\rangle$ , respectively.

Eqs.(5) are more complicated than the optical Bloch equations because eqs.(5) allow for realistic optical bands consisting of ZPL and PSB. If we neglect PSB then optical bands become:

$$I^g(\Omega) = I^e(\Omega) = \frac{\gamma/2}{(\Omega + \Delta)^2 + (\gamma/2)^2}. \quad (7)$$

Substituting eq.(7) into eqs.(5) and integrating  $\rho_{10}(\Omega, t)$  and  $\rho_{01}(\Omega, t)$  over  $\Omega$  we can derive from eqs.(5) the optical Bloch equations [9].

For a transient hole in the population of the ground level we find from eqs.(5) the following expression

$$\rho_{00}(\infty) = 1 - \frac{2\Lambda^2 T_1 I^g(0)}{1 + 2\Lambda^2 T_1 (I^g(0) + I^e(0))}. \quad (8)$$

This expression differs considerably from eq.(1) because eq.(8) describes a hole consisting of ZPL and PSB. For small intensity  $\Lambda^2$  the hole in population is proportional to a homogeneous absorption band  $I^g(0)$

$$\rho_{00}(\infty) = 1 - 2\Lambda^2 T_1 I^g(0). \quad (9)$$

With the help of eqs.(6)-(9) we can discuss such phenomenon as spectral diffusion. Indeed, for short-living phonons and tunnelons the probabilities  $P_\alpha$  and  $P_\beta$  are of the Boltzman type so that they depend only on temperature. For long-living tunnelons  $P_\alpha$  and  $P_\beta$  are functions of time. We can find a temporal behaviour of the tunnelon density matrix. Using it we can calculate the temporal behaviour of homogeneous optical bands determined by eqs.(6). An analysis of the theoretical results shows that

only intensities of peaks in optical band can depend on time. Homogeneous halfwidth of ZPL does not depend on time. This conclusion of the dynamical theory differs from that of the stochastic theory.

Does it mean that we cannot explain the temporal broadening of holes within the scope of the dynamical approach? No, it does not. A hole burnt in an inhomogeneous optical band is a convolution of the homogeneous absorption band  $I^g(\omega_p - \omega)$  and the function  $n(\omega_p - \omega, t_b)$  of the population of the ground level

$$h(\omega_p - \omega_b) \propto \int d\omega_0 \cdot I^g(\omega_p - \omega_0) \cdot n(\omega_b - \omega_0, t_b). \quad (10)$$

Here  $\omega_p$  and  $\omega_0$  are the frequencies of the probing and burning light,  $t_b$  is the burning time. Relaxation of long-living tunnelons in amorphous solids leads to excursion of resonant frequencies  $\omega_0$  of different molecules. This yields dependence  $n$  on the probing time  $t_b$  so that  $n = n(\omega_b - \omega_0, t_b, t_p)$ . Therefore, a halfwidth of a hole  $h(\omega_p - \omega_b)$  depends on the duration of a burning-probing cycle.

Thus, the dynamical theory for spectral diffusion leads to the time independent expression for the homogeneous halfwidth of ZPL and it ascribes temporal broadening of holes to temporal evolution of the population function  $n$ .

## References

1. B.Herzog and E.L.Hahn. *Phys. Rev.* *103* (1956) 148.
2. A.M.Portis. *Phys. Rev.* *104* (1956) 584.
3. R.Klauder and P.W.Anderson. *Phys. Rev.* *125* (1962) 912.
4. W.B.Mims, K.Nassau and J.D.McGee. *Phys. Rev.* *123* (1961) 2059.
5. P.Hu and S.R.Hartman. *Phys. Rev.* *B9* (1974) 1.
6. J.L.Black and B.I.Galperin. *Phys. Rev.* *B16* (1977) 2879.
7. W.O.Putikka and D.L.Huber. *Phys. Rev.* *B36* (1987) 3436.
8. M.Berg, C.A.Walsh, L.R.Narasimhan, K.A.Littau and M.D.Fayer. *J. Chem. Phys.* *88* (1988) 1564.
9. I.S.Osad'ko. *Zh. Exp. Theor. Fiz.* *98* (1990) 1045 (in russian).

# Holeburning Optical Magnetic Resonance Imaging

Stephan Schiller and R.L. Byer

Department of Applied Physics, Stanford University, Stanford, Ca 94305, USA

Tel. (415) 7252737

Scanning probe microscopy and gradient imaging are two techniques for imaging at sub-wavelength spatial resolution. Gradient imaging in the form of magnetic resonance imaging (MRI) has so far been demonstrated only in the radio- and microwave frequency domains [1]. An extension of MRI to optical frequencies for imaging (semi-) transparent objects is of interest because an optical photon detection process is inherently more sensitive than magnetic induction detection, potentially leading to increased spatial resolution. Rare-earth ions incorporated into a crystalline host are promising as a prototype system for demonstration of high spatial resolution OMRI.

In resonance imaging spatial resolution is obtained by "focussing" in the frequency rather than space domain and thus spatial resolution is not directly dependent on the wavelength of the exciting waves. A simple estimate for the minimum resolvable detail size can be given by considering magnetic resonance imaging of centers containing a Zeeman doublet (lower level 0 and upper level 1).

Figure 1: Principle of resonance imaging.

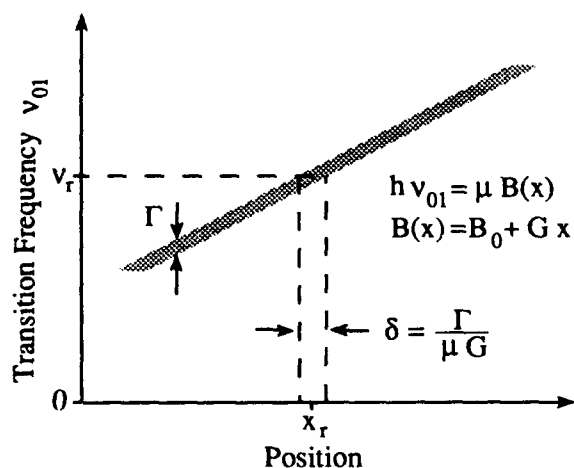


Fig. 1 illustrates the consequence of line broadening effects in resonance imaging, showing schematically the transition frequency of centers as a function of their location  $x$  in the gradient field of strength  $G$ . Any center in the object exhibits an absorption line profile of full-width (FWHM)  $\Gamma$ . For a partic-

ular excitation frequency centers within a slice of nonzero thickness around  $x_r$  are excited with probability depending on the lineshape, and the FWHM  $\delta$  of the spatial excitation profile is given by  $\delta = \Gamma / (\partial \nu_{01}(x_r) / \partial x)$ . For the linear Zeeman effect  $\delta = \Gamma / \mu G$ , where  $\mu$  is the magnetic moment. In practice, spatial resolution in nuclear and electron spin MRI is limited by the decrease in sensitivity with increasing resolution, due to the decrease in number of centers per image element.

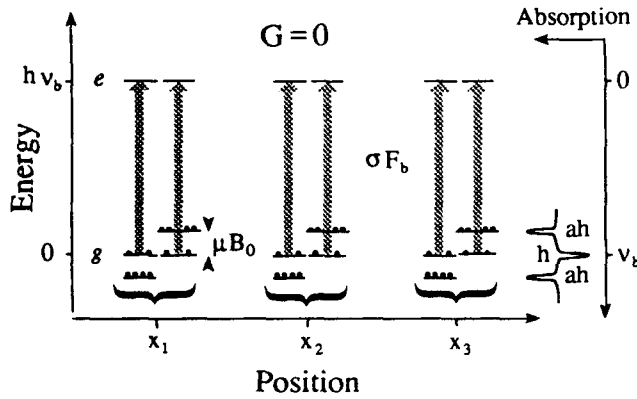
To estimate the feasibility of  $\mu\text{m}$ -resolution imaging of mm-size samples by OMRI, we take as realistic upper limit for gradient strength  $G = 3 \text{ T/cm}$  [2] and a magnetic moment  $\mu = 30 \text{ GHz/T}$ . The linewidth required to satisfy  $\delta < 1 \mu\text{m}$  is  $\Gamma < 10 \text{ MHz}$ .

A condensed matter system in which this condition is satisfied are rare-earth ions in crystalline hosts. At temperatures in the Kelvin range homogeneous linewidths can be less than 1 MHz. [3]. Inhomogeneous broadening, typically exceeding several GHz, then dominates the linewidth. High spatial resolution imaging is therefore not possible with simple implementations of OMRI, where a *single* optical transition frequency is used as a measure of external field strength and thus spatial location, e.g. in a laser absorption measurement. Instead techniques probing within the inhomogeneous broadening must be employed [3,4].

Spectroscopic methods of potential use in OMRI may be distinguished according to whether a Zeeman sublevel splitting (zero in absence of external field) or a ligand field level (multiplet or term) splitting is probed with high spectral resolution. Examples of the first class are optically detected magnetic resonance (ODMR) [5], Zeeman Raman scattering, Raman heterodyne NMR and ESR, holefilling MR, photon echo nuclear double resonance and quantum beat free induction decay [3].

Here we focus on holeburning Zeeman spectroscopy, which belongs to the second class. Unlike conventional MRI it is a noncoherent technique. The imaging process consists of a holeburning step (Fig. 2), the application of a field gradient and a hole reading step (Fig. 3). Consider centers that can be modeled by a three-level system consisting of a groundstate Kramers doublet, comprising levels 0 and 1, and a field-independent excited state

Figure 2: Sublevel population distribution after burning into the  $g \rightarrow e$ -transition with a laser field  $\nu_b$ . (thick arrow)



$e$ . The external field is a sum of a constant term and a gradient field that can be turned on or off,  $B(\mathbf{r}) = B(x) = B_0 + Gx$ . The homogeneous linewidth  $\Gamma_h$  of the  $0, 1 \rightarrow e$  transition is  $\pi\Gamma_h = 1/T_2 + \Gamma_e$ , with the dephasing time  $T_2$  and the decay rate  $\Gamma_e$  from the excited state to the groundstate.

In the holeburning process, population is transferred by a laser field of photon flux  $F_b$  and frequency  $\nu_b$  from one of the sublevels to the other via level  $e$ ; if the inhomogeneous broadening  $\Delta E$  is larger than the splitting  $\mu B$ , the sublevel of origin is either 0 or 1, depending on  $E_e$ , the reservoir then being 1 and 0, respectively. As a consequence the spectrum contains both holes and anti-holes whose lifetime is given by the intersublevel relaxation time  $\Gamma_{01}^{-1}$ . This type of holeburning mechanism was observed recently in the  $^4I_{9/2} \rightarrow ^2H_{11/2}, ^4G_{5/2}$  transitions of  $\text{Nd}^{3+}:\text{LaF}_3$  at 1.6 K [6].

The timescale for the creation of the (anti-) holes is  $\Gamma_e^{-1}$ . If the burn time is short, their width as measured by a probe beam is  $2\Gamma_h$ .

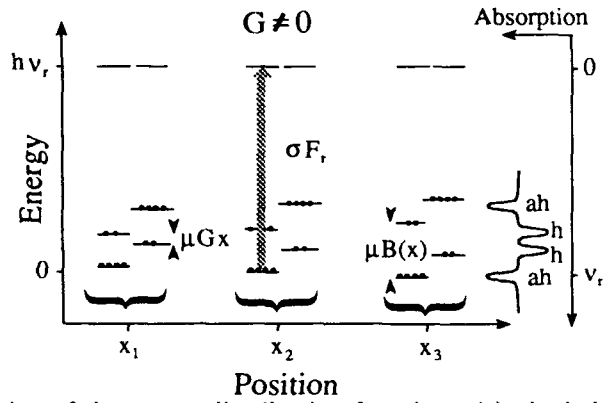
The essential step in holeburning OMRI is the application of the gradient field  $G$  between the burning and reading steps. In this way a position-dependent shift is impressed to the holes and anti-holes which encodes information about the ions' location along the gradient direction.

A fast and precise measurement of the (anti-) hole spectrum is essential for satisfactory performance of OMRI. This problem has been discussed in the context of frequency domain optical storage of substances exhibiting persistent spectral holeburning [7]. Important differences exist however, in that high resolution OMRI requires holewidths  $\Gamma_h$  below 1 MHz and small inhomogeneous broadening, while the opposite is true for storage applications.

We have calculated the measurement signal-to-noise ratio (SNR) for fluorescence and absorption detection assuming quantum-limited sensitivity.

The signal at the probe frequency  $\nu_r$  is a convolu-

Figure 3: Changes occurring in the absorption (or resonance fluorescence) spectrum when an inhomogeneous field  $Gx$  is applied.



tion of the center distribution function with the hole absorption lineshape, peaked in the slice located at  $x_r = (\nu_r - \nu_b)/\mu G$ :

$$S(\nu_r) \sim \int \frac{c(\mathbf{r})}{1 + 4(x - x_r)^2/\delta^2} dV.$$

The full-width at half maximum  $\delta = 2\Gamma_h/\mu G$ , can be identified with the spatial resolution introduced before. For fluorescence detection the average SNR associated with the value of center concentration in a slice of thickness  $\delta$  is

$$\text{SNR}_{\text{proj}} \approx \frac{\pi}{4} \sqrt{\eta_f \eta_{pm} \eta_c} \sqrt{N} \frac{d_0 \delta}{L},$$

where  $N = \pi F_r t_r \sigma_m c_d V \Gamma_h / 2\Delta E$ , with burn time  $t_r$ , peak absorption cross section  $\sigma_m$ , average center concentration  $c_d$ , sample volume  $V$ , hole depth  $d_0$  and total fluorescence detection efficiency  $\eta_f \eta_{pm} \eta_c$ . For frequency-modulation absorption spectroscopy the SNR is

$$\text{SNR}_{\text{proj}} = \frac{\pi M}{8} \sqrt{\eta_{pd} e^{-\beta(\nu_c)} \beta(\nu_c) / 2} \sqrt{N} \frac{d_0 \delta}{L}, \quad (1)$$

with the absorption coefficient  $\beta(\nu_c) = \pi \sigma_m \Gamma_h c_d V / 2A \Delta E$ ,  $A$  being the cross section of the sample perpendicular to the read beam,  $M$  the modulation index, and  $\eta_{pd}$  the total absorption detection efficiency.

Since the reading process involves population transfer, it destroys the holes and anti-holes. Therefore a useful signal is obtained only for a finite read time and consequently both SNR have upper limits, given by the condition of weak excitation probability,  $F_r t_r \sigma_m \ll 1$ ,  $M^2 F_r t_r \sigma_m \ll 1$ , respectively. The important dependences of the SNR are the linear decrease of signal to noise with resolution length  $\delta$  (due to the contribution  $\sim d_0 \delta$  of a particular slice to the absorption coefficient compared to the background response  $\sim L$ ) and the dependence on the ratio of homogeneous to inhomogeneous broadening,  $\Gamma_h/\Delta E$ , due

to the probing of a small homogeneously broadened packet within the inhomogeneous distribution.

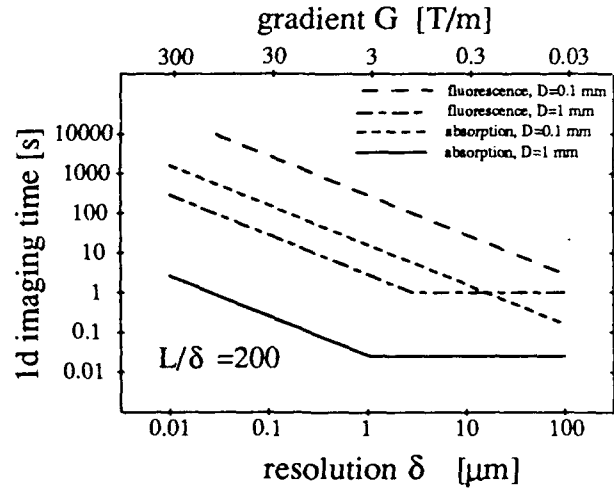
Fundamental limits for imaging speed arise from the times associated with the laser-induced population transfer (burning or pumping), and the absorption or fluorescence measurement of the non-equilibrium population. To obtain a full projection  $S(\nu_r)$ , the measurement is repeated  $L/\Delta x$  times, the number of pixels (slices) per projection. Two timescales are relevant to the scan time  $t_{\text{proj}}$ : the excited state lifetime  $\Gamma_e^{-1}$  and the inter-sublevel thermalization time  $\Gamma_{01}^{-1}$ . The first determines the duration of the holeburning process, the second whether a single burn step is sufficient for the entire scan. Here we assume  $\Gamma_{01}^{-1} > t_{\text{proj}}$ .

While the write step has equal length for the fluorescence and the absorption technique, the reading times differ. In fluorescence detection the accumulation of photon counts requires a time equal to several fluorescence decay times  $1/\Gamma_e$ . Thus we can estimate a lower limit for the scan time as the product of the number of pixels (slices) per projection and a time of the order of  $1/\Gamma_e$ ,  $t_{\text{proj}} \approx 5L/\Gamma_e \Delta x$ , where  $t_{\text{proj}} < \Gamma_{01}^{-1}$  and  $t_d \ll \Gamma_e^{-1}$  is assumed. Absorption detection is inherently faster than fluorescence detection since the measurement time is the pulse duration  $t_r$  itself [8], with a lower limit  $t_r > \Gamma_h^{-1}$ . Thus,  $t_{\text{proj}} \approx 5(1/\Gamma_e + L/\Gamma_h \Delta x)$ .

The above results can be combined to quantify the feasibility of high-resolution OMRI. In an actual application an image with a certain minimum spatial resolution and  $SNR_S^{\text{min}}$  per pixel is desired. If  $SNR_{\text{proj}} < SNR_S^{\text{min}}$ , averaging is necessary; if every projection is measured  $q$  times, the total imaging time and signal-to-noise ratio per projection become  $t_{1d} = q t_{\text{proj}}$ ,  $SNR_S = \sqrt{q} SNR_{\text{proj}}$ .

We have performed model calculations assuming the system to be imaged to be a crystalline host (e.g.  $\text{CaF}_2$ ,  $\text{LaF}_3$ ,  $\text{YAlO}_3$ ) doped with rare-earth ions at the 0.1%-level and take a gradient  $G_{\text{max}} = 3 \text{ T/cm}$ . Assuming a homogeneous linewidth  $\Gamma_h = 50 \text{ kHz}$  and a magnetic moment  $\mu = 30 \text{ GHz/T}$ , this implies a maximum attainable resolution of approximately 10 nm, about two orders of magnitude smaller than the optical wavelengths  $c/\nu_{b,r}$  involved in the spectroscopy of the  $4f^n \rightarrow 4f^n$  transitions of rare earth ions. Figure 4 shows the imaging time required to produce a one-dimensional image of center distribution, with SNR larger than  $SNR_S^{\text{min}}$ , as a function of resolution  $\delta$  for the two hole reading schemes. The number of pixels  $L/\delta$  is kept constant, implying a decreasing extension  $L$  of the sample in the gradient direction with decreasing resolution and a constant imaging time in the no-averaging regime. For the sample dimensions chosen in the figure, absorption detection is significantly faster than fluorescence detection. To achieve sufficient image quality in the  $\mu\text{m}$  regime and below, averaging is necessary, with

Figure 4: OMRI by holeburning spectroscopy: imaging time for 1d imaging of a rare-earth doped crystal of length  $L$  and thickness  $D$



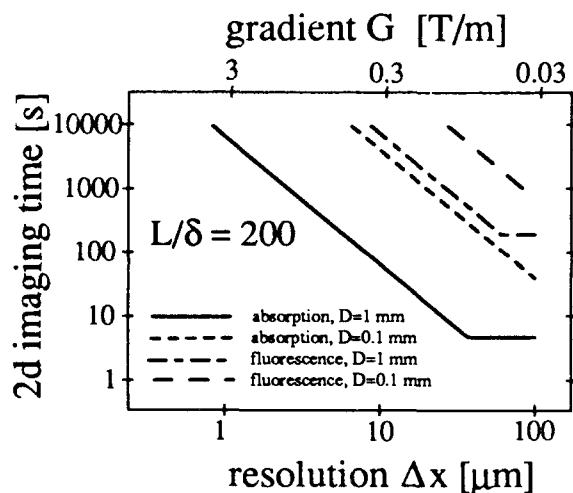
imaging times scaling inversely with  $\delta$  for both fluorescence detection and absorption detection with the read beam propagating perpendicular to the gradient. The parameter values are  $c_d = 10^{20} \text{ cm}^{-3}$ ,  $\Delta E = 5 \text{ GHz}$ ,  $1/\Gamma_e = 1 \text{ ms}$ , oscillator strength  $f = 10^{-8}$ ,  $\sigma_m = 3.4 \cdot 10^{-15} \text{ cm}^2$ ,  $M = 0.2$ ,  $\eta_f \eta_{pm} \eta_c = 10^{-2}$ ,  $\eta_{pd} = 0.5$ ,  $d_0 = 0.1$ .

Two- and three-dimensional OMRI is possible by applying well-known techniques used in computerized tomography (CT), that permit image reconstruction from multiple tomographic projections [9]. Consider 2-d imaging of an object of cylindrical shape with diameter  $L$  and thickness  $D$ . A single frequency scan  $S(\nu_r, \phi)$ , where  $\phi$  is the orientation angle of the object with respect to the gradient, gives the projection of the center density inside the disk onto the gradient direction. To obtain sufficient information to completely determine the image of to an accuracy  $\Delta x$ , a multiangle set of  $p = L/\Delta x$  such projections is required, at intervals  $\Delta\phi = \pi\Delta x/L$ . The reconstructed image  $R(x, y)$  is computed from the set  $\{S(\nu_r, \phi)\}$  using the filtered back-projection algorithm or other reconstruction techniques.

It has been shown [9,10], that the average signal-to-noise ratio per image pixel is related to the projection SNR by  $SNR_R = SNR_S \sqrt{\Delta x/L}$ , leading to  $t_{2d} = (L/\Delta x)^2 (SNR_R/SNR_{\text{proj}})^2 t_{\text{proj}}$ , which is valid for any OMRI technique based on tomography. Numerical values for the imaging time of a cylindrical section as a function of resolution have been plotted in Fig. 5 for two sample sizes and low  $SNR_R^{\text{min}} = 10$ .

Because of the decrease in SNR in the projection reconstruction process and the sequential measurement of the angular set of projections, the imaging time is several orders of magnitude longer than in the 1d case for given  $\delta$ . Also, averaging is now necessary below  $\delta \sim 20 - 100 \mu\text{m}$ . With  $L/\delta$  constant, the

Figure 5: Imaging time for 2d-holeburning OMRI.



scaling of  $t_{2d}$  in this case is  $\sim \delta^{-2}$  for fluorescence detection and FM spectroscopy using perpendicular propagation. Again, the latter technique is the faster one when the thickness  $D > 0.3$  mm.

An important result is the impossibility of reaching the theoretical resolution limit  $\delta_{min} = 2\Gamma_h/\mu G_{max}$  within a reasonable imaging time using holeburning OMRI because of the large ratio  $\Delta E/\Gamma_h$  of inhomogeneous to homogeneous broadening. Furthermore, it is evident from the figure that at least for the present parameter values, microscopic imaging at resolutions comparable to those attained in conventional microscopes is possible only using absorption detection.

For realistic sub-wavelength imaging ( $\delta = 1\mu\text{m}$ ,  $L=20\mu\text{m}$ ,  $D=1$  mm) imaging times of the order of 100 s would be desirable. This leads to the following requirements for the centers: linear electronic Zeeman effect in the ground state without hyperfine structure, homogeneous linewidth  $\Gamma_h \simeq 0.5$  MHz, hole lifetime  $1/\Gamma_{01} \simeq 10$  ms (comparable to  $t_{proj}$ ), inhomogeneous broadening  $\Delta E < 500$  MHz and oscillator strength  $f > 10^{-7}$ .

In conclusion, we have introduced optical resonance gradient imaging and discussed two holeburning laser spectroscopic techniques based on two-step incoherent pump/probe excitations. With increasing resolving power signal strengths are found to decrease rapidly, limiting resolution to the  $\mu\text{m}$ -regime for two-dimensional imaging. Alternative spectroscopic techniques have been discussed elsewhere [11].

## References

- [1] P. Mansfield and P.G. Morris, *NMR Imaging in Biomedicine* (Academic Press, New York, 1982); G.R. Eaton and S.S. Eaton, *Bull. Magn. Res.* **10**, 22-31 (1988)
- [2] K. Halbach, *Nucl. Instr. and Methods*, **169**,

- 1-10 (1980)
- [3] R.M. Macfarlane and R.M. Shelby, in *Spectroscopy of Solids Containing Rare Earth Ions*, A.A. Kaplyanskii and R.M. Macfarlane eds. (Elsevier, New York, 1987), pp. 51-184;
- [4] *Laser Spectroscopy of Solids*, W.M. Yen and P.M. Selzer eds. (Springer, New York, 1986)
- [5] S. Geschwind in *Electron Paramagnetic Resonance*, S. Geschwind ed. (Plenum Press, New York, 1972), Chapter 5; W.T. Lynch and D.W. Pratt, *Magn. Res. Rev.* **10**, 111-159 (1985); *Triplet State ODMR Spectroscopy*, R.H. Clarke ed. (Wiley, New York, 1982)
- [6] R.M. Macfarlane and J.C. Vial, *Phys. Rev. B* **36**, 3511-3515 (1987)
- [7] W.E. Moerner and M.D. Levenson, *J. Opt. Soc. Am. B* **2**, 915-924 (1985)
- [8] W. Lenth, C. Ortiz and G.C. Bjorklund, *Opt. Lett.* **6**, 351-353 (1981)
- [9] *Image Reconstruction from Projections*, G.T. Herman ed. (Springer, New York, 1979)
- [10] J.C. Gore and P.S. Tofts, *Phys. Med. Biol.* **23**, 1176-1182 (1978); D.A. Chesler, S.J. Riederer and N.J. Pelc, *J. Comp. Ass. Tomography* **1**, 64-74 (1977)
- [11] S. Schiller and R.L. Byer, to be published

Photon-Gated Photochemical Hole Burning in Zinc-Tetrabenzoporphyrin/Aromatic Cyanide System

Zhao Lizeng, Lu Zhengzhong, Zhang Xiulang, Zhang Dongxiang,  
Mi Xin, Nie Yuxin  
Institute of Physics, Academia Sinica  
Beijing 100080, China, Fax:(86-1)2562605

Wang Duoyuan, Hu Lingzhi, He Huizhu, Xie Jie, Zhang Junyi  
Institute of Photographic Chemistry, Academia Sinica  
Beijing 100101, China, Tel.2017061-512

The group of Moerner, et al., first reported two-color hole-burning by donor-acceptor electron transfer for a derivative of zinc-tetrabenzoporphyrin as a donor with halomethane acceptors in a poly(methyl methacrylate) (PMMA) thin film [1]. Their results have opened up a new class of materials for photon-gating.

We report a new example of photon-gated photochemical hole burning (PHB) in which donor-acceptor electron transfer is responsible for hole formation. The donor molecules are also derivatives of tetrabenzoporphyrin, one of which is meso-tetra(p-tolyl)-zinc-tetrabenzoporphyrin (TZT). The host matrix is PMMA. The acceptor can be one of several aromatic cyanide (AC) for example, cyanoanthracene, cyanonaphthalene, and cyanobenzene etc.. The TZT donor molecule was synthesized by a modified procedure and purified by extraction and liquid chromatography. The PMMA host used  $M_p \sim 10^5$ ,  $M_w/M_n = 2.0$ . Aromatic cyanide are obtained from Aldrich Chemicals. Optical samples were prepared by mixing the chloroform solution of TZT, AC and PMMA in appropriate ratio and evaporating the solvent on the optical glass. Concentration of the sample was adjusted to give thin film with the thickness of 50-150  $\mu\text{m}$ . The optical density at the intended wavelength was in the range of 0.3 - 1.0 at room temperature. Samples were placed in an optical immersion cryostat containing liquid helium. All PHB experiments were performed at 4.2K.

Two types of PHB experiments were carried out. In one, an  $\text{Ar}^+$  ion laser pumped ring dye laser (Spectra-Physics 380D) was used to provide  $\lambda_1$  for exciting the 0-0 component of the  $S_1 \rightarrow S_0$  transition of TZT molecule in PMMA. The dye laser provides narrow linewidth (0.5MHz) and scanning stabilized single frequency radiation for high resolution PHB experiments. In the second type of experiment, removing the etalons and unidirectional device from the laser cavity, the laser was a broadband dye laser which featured high power output and multimode 5GHz for an application of encoding multiple hole burning over a large

range of wavelength. Typical frequency-selective power  $P_1$  was 1-16  $\mu\text{W}$ . The gating radiation  $\lambda_2$  was provided by a 5-20mW beam from the  $\text{Ar}^+$  laser. Spectral hole detection was performed by scanning  $\lambda_1$  and detecting the sample transmission. Hole depth was determined from the acquired spectra as  $\Delta T/T_i$ , where  $\Delta T$  is the final minus the initial transmittance  $T_i$  at the laser wavelength  $\lambda_1$ .

The system of TZT/AC/PMMA has an inhomogeneously broadened absorption band of about  $370\text{cm}^{-1}$  centered at 625nm. When irradiated into the 0-0 absorption band, the system was found to readily undergo hole burning. It was observed, however, that the hole burning efficiency was much less on the blue edge of the absorption band than it was on the red edge. Fig. 1 shows a hole burned in TZT/AC/PMMA

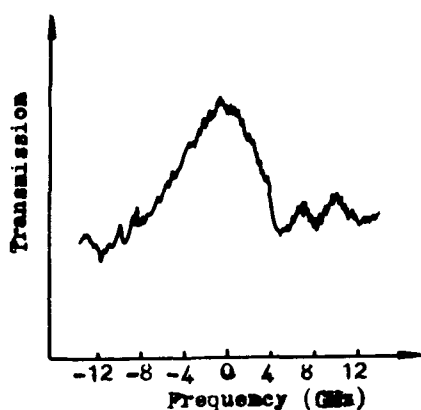


Fig. 1. Example of photo-gated PHB for TZT/AC/PMMA with  $P_1 = 16 \mu\text{W}$ ,  $P_2 = 16\text{mW}$  for 100s at  $\lambda_1 = 629.4\text{nm}$ .

with frequency-selective power  $P_1$  of 16  $\mu\text{W}$  and a gating light power  $P_2$  of 16mW for 100s. The hole depth and width were 46% and 7GHz, respectively. The multiplexing factor  $m$ , which is the ratio of the total inhomogeneous linewidth  $\Gamma_{\text{in}}$  divided by the hole width  $\Gamma_{\text{hole}}$  tended to 1600. Attempts to produce a measurable one-color hole under these conditions were unsuccessful. Only with much higher  $P_1$  and longer burnt time can single photon holes be burned. So we could use high detection power (1-10% of burning power) to gain adequate SNR.

A feature of this system is easy to make and keep a sample with appropriate donor-acceptor concentration ratio, as the acceptor AC has proper redox potential and much higher boiling point than that of halomethane the donor-acceptor concentration ratio can be controlled easily and the acceptable samples can be placed in air at room temperature for a long time. For example, the depth of a hole burned

in a sample which had been placed at room temperature for ten months and had been burned many times could still be up 134%.

Hole lifetime was measured. After 4 hours from burning, the hole depth decreased by 30% and then go down slowly. The experiment was limited by the time of keeping liquid helium.

A comparison of multiple hole burning between TZT/AC/PMMA and TZT/CHCl<sub>3</sub>/PMMA is shown in Fig. 2. The sample of TZT/AC/PMMA used

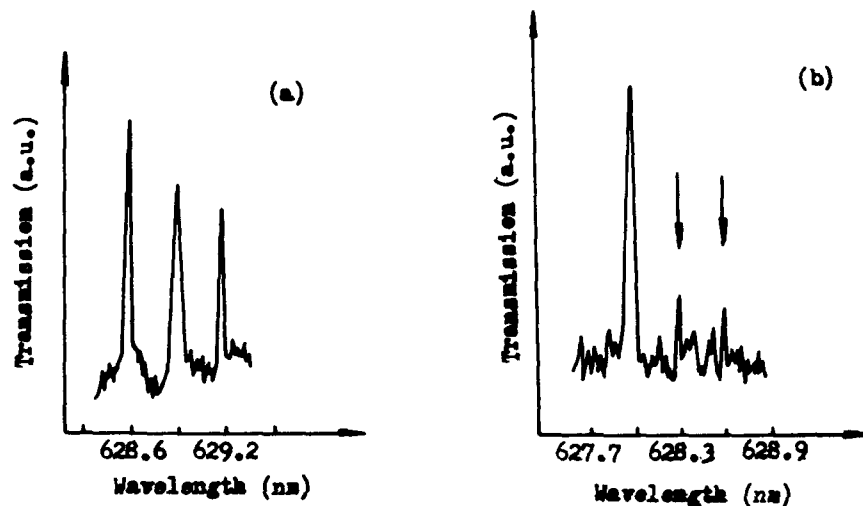


Fig. 2. A comparison of multiple hole burning between (a) TZT/AC/PMMA (b) TZT/CHCl<sub>3</sub>/PMMA with  $P_1=3.7 \mu\text{W}$  and  $P_2=10\text{mW}$  for 2min.

for the experiment had been placed in air at room temperature for three months. it was found that there were substantial differences in the hole-filling behavior accompanied by subsequent hole burning in these two systems. For TZT/CHCl<sub>3</sub>/PMMA the depth of previously burnt holes was considerably reduced by the subsequent hole burning at different wavelength, while for the system of TZT/AC/PMMA the following hole burnings had a less effect on the depth of the previous. Subsequent hole burning induced the hole filling via backreaction. Results described above shows as a acceptor AC is better than CHCl<sub>3</sub>. When a sample in which a gated hole had formed was irradiated only by the gating light for several minutes the depth of the burnt hole decreased. It suggests that the gating radiation would

cause the backreaction. Reducing gating power and irradiation time would be good for the reduction of hole filling. The detailed mechanisms for the hole filling and search for proper gating radiations and acceptors will be further studied in future work.

**Reference:**

- 1 T.P. Carter, C.Brauchle, V.Y. Lee and W.E. Moerner,  
J. Phys. Chem. **91** (1987) 3998.

## Preparation and properties of sol-gel thin films with Porphins

Hiroyuki INOUE, Takashi IWAMOTO, Akio MAKISHIMA  
 Department of Materials Science, Faculty of Engineering,  
 University of Tokyo, 7-3-1 Hongo, Bunkyo-ku, Tokyo 113, JAPAN  
 and  
 Makoto IKEMOTO, Kazuyuki HORIE  
 Department of Reaction Chemistry, Faculty of Engineering,  
 University of Tokyo, 7-3-1 Hongo, Bunkyo-ku, Tokyo 113, JAPAN

### INTRODUCTION

Recently the sol-gel process for preparing amorphous materials has been studied. The low processing temperatures enable us to dope the gel with functional organic molecules. Such molecules have poor thermal stability and cannot be included in traditional oxide glasses. Avnir et al.<sup>1,2)</sup> have been reported the preparation and optical properties of amorphous silica doped with rhodamine 6G and pyrene. Makishima and Tani<sup>3,4)</sup> have doped one with 1,4-dihydr-oxy-9,10-anthraquinone (DAQ) and showed photochemical hole burning (PHB) at 4.8 K. They have also demonstrated that other organic molecules can be successfully incorporated into sol-gel matrices. The number of potential applications of such materials is expected to be substantial.

Although materials have been synthesized, little is known about the structure of sol-gel matrix and the interaction between the molecule and the matrix. PHB has attracted considerable interest as a tool for high-resolution solid state spectroscopy.<sup>5-8)</sup>

The sol-gel thin film is expected to possess several advantages over gel bulks. Several studies<sup>9,10)</sup> suggest the differences of the structure and properties between bulks and thin films. However, due to the thickness, there have been rather few investigations attempting to obtain structural information directly. Recently the use of organic molecule appears to be one approach for supplying new insights regarding the chemistry of sol-gel materials.<sup>11,12)</sup> In this point of view PHB is expected to be high potential. We report here the preparation of sol-gel thin films doped with the porphine derivative and its application to PHB.

### EXPERIMENTAL

The reagents used were: tetraphenylporphine tetrasulfonic Acid (TPPS); tetrakis(4-carboxy-phenyl) porphine (TCPP); tetrakis(1-methylpyridinium-4-yl)porphine p-toluene-sulfonate (TMPyP); tetraethoxy-silane (TEOS); ethanol; hydrochloric acid; acetic acid; ammonia solution and sodium hydroxide. Molecular structures of TPPS, TCPP and TMPyP are illustrated in Figure 1. Starting solutions were prepared by mixing ethanol, TEOS, catalyst (HCl, CH<sub>3</sub>COOH, NH<sub>4</sub>OH or NaOH solution) and each porphine derivative dissolved in distilled water at room temperature. The solution was kept for several days at 20°C. Microscope cover glasses used as substrate were dipped into the solutions,

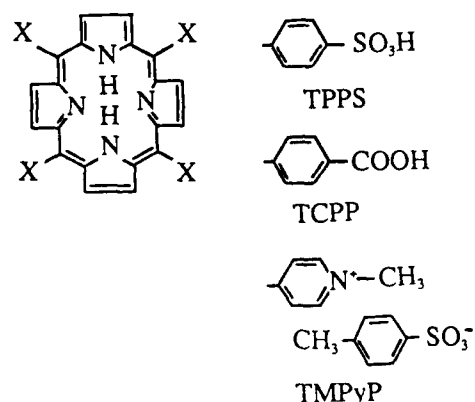


Figure 1 Molecular structures of porphine derivatives.

structure and dehydrate the water contents.

It is necessary for PHB measurement to adjust the concentration of TMPyP in the amorphous silica film to an optical density of about 0.4 at burning wave-length. It is critical to provide films about 1  $\mu\text{m}$  in thickness and these films are two or three orders thinner than gel bulks and polymer films. Therefore, we have to prepare the films with high TMPyP concentration. Figure 5 shows absorption and fluorescence spectra of the films with various [TMPyP]/[TEOS] molar ratio. Spectral profiles of fluorescence show no dependence on the excitation wavelength and are almost equal to the those of the solutions. It should be note that there is a tendency for intensity of the peaks to saturate in 0.005 [TMPyP] / [TEOS] and over. This saturation is mainly due to concentration quenching in high TMPyP concentration.

The hole is burned by the laser light irradiation with the intensity of  $0.44\text{mW}/\text{cm}^2$  at about 20K. An observable hole appears with 1min exposure. Figure 6 shows typical profiles of the hole at 647.6 nm. The efficiency of apparent quantum yield,  $\Phi$ , can be calculated from the initial slope,  $[d(A/A_0)/dt]_{t=0}$ , by using following equation,

$$\Phi = \frac{[d(A/A_0)/dt]_{t=0} A_0}{10^3 I_0 (1 - 10^{-A_0}) \epsilon R}$$

where  $A_0$  is the absorbance before irradiation,  $I_0$  is incident laser intensity,  $\epsilon$  is the molar extinction coefficient at hole burning wavelength and temperature, and R is the reciprocal initial fraction of photoreactive molecules within a homogenous line width. The value of apparent quantum yield for TMPyP is  $1.1 \times 10^{-5}$  calculated from the equation. The value of that for TMPyP at 4.4K

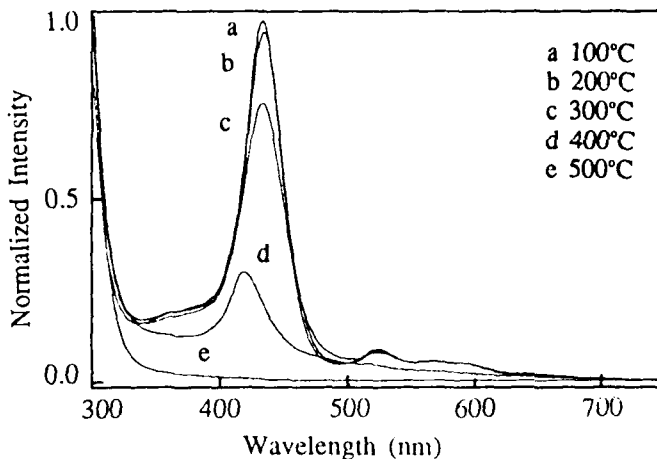


Figure 3 Absorption spectra of TMPyP doped amorphous silica films heat-treated at various temperatures.

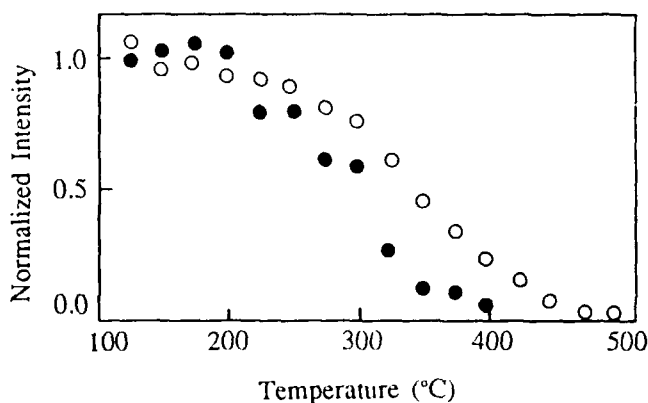


Figure 4 Change of absorbances at Soret band of TMPyP ○ and TPPS ● doped amorphous silica films heat-treated at various temperatures.

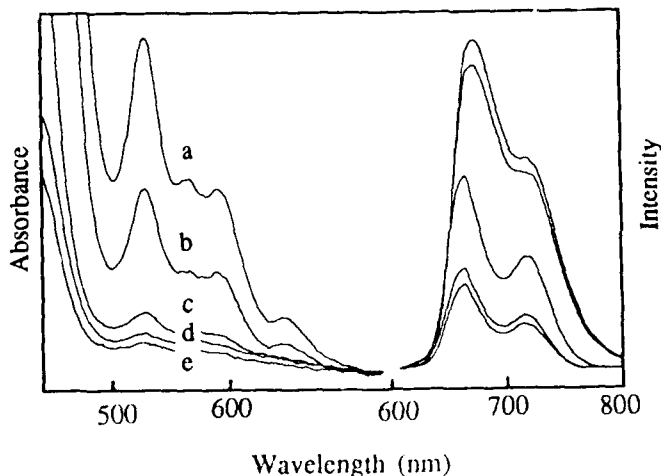


Figure 5 Absorption and fluorescence spectra of TMPyP doped amorphous silica films as a function of TMPyP concentration. a, [TMPyP]/[TEOS]=0.01; b, 0.005; c, 0.001; d, 0.0005; e, 0.0001.

withdrawn at 16mm/min and heated at 100 to 500°C. The process of dipping and heat-treatment was repeated if necessary.

Film thickness was measured using a Talystep apparatus. The influences of pH of the starting solution, temperature of heat-treatment and the concentration of porphin on the porphin in the thin films were investigated by the absorption and fluorescence spectra.

Photochemical hole burning was measured at about 20K. Details of the apparatus were given previously.<sup>7)</sup>

## RESULTS and DISCUSSION

We obtained homogeneous films doped with TPPS and TMPyP without macroscopic segregation. Figure 2 presents the characteristic absorption spectra of TMPyP doped amorphous silica films. The molar ratios of the starting solutions were TEOS:H<sub>2</sub>O:EtOH:HCl:TMPyP = 1:20: 14:0.1-0.0001:0.003. It is noteworthy that TMPyP in the film prepared from the solutions at pH 4.5 is neutral (H<sub>2</sub>L) form. This spectrum with 4 peaks in range of 500 to 700 nm, what is called a Q band, is typical one of the neural form. The absorption spectrum of TMPyP in the film from the solution at pH 2.5 corresponds to that in aqueous solution at pH 1. The color of the former is brown and the latter is yellow-green. The color of TPPS doped amorphous silica films is green, expect for one prepared from the starting solution with base-catalyst. The absorption spectra of TPPS doped amorphous silica films correspond to TPPS in aqueous solution at pH 1 and not to that of di-cation (H<sub>4</sub>L<sup>2+</sup>) form. The solution with base-catalyst gelled in a short time and it is difficult to prepare homogeneous films. TCPP was insoluble in water with acid-catalyst.

The porphins have neutral (H<sub>2</sub>L), mono-cation(H<sub>3</sub>L<sup>+</sup>) and di-cation (H<sub>4</sub>L<sup>2+</sup>) forms, which exist at different acidities, and the equilibrium constants are shown in Table 1. Only the neutral form is active in PHB. Under acidic condition TPPS and TMPyP are very soluble in water and TPPS is easily protonated at its central nitrogen atoms, H<sub>4</sub>L<sup>2+</sup> form. It is concluded that TMPyP is the best for our process in three porphine derivative.

Figure 3 shows the absorption spectra of TMPyP doped amorphous silica films as a function of temperature of heat-treatment for 10min. The change of the absorbance of Soret band is plotted in Figure 4 with the case of TPPS doped films. These results indicate that the TMPyP and TPPS in the silica matrix is stable up to ca. 200°C. It was found that the porphins doped amorphous silica film could be heat-treated up to 200°C to stabilize the

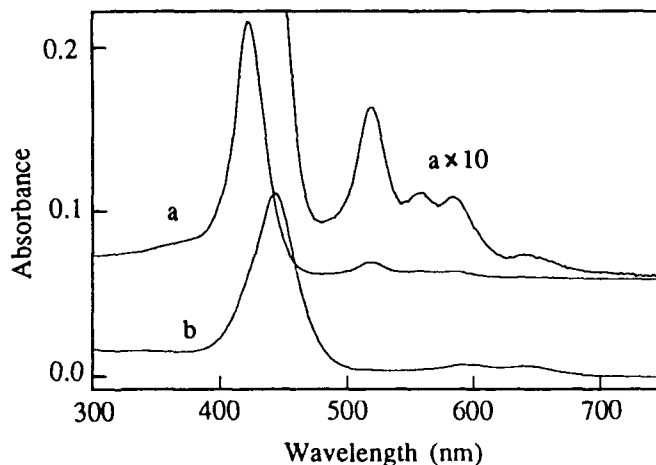


Figure 2 Absorption spectra of TMPyP doped amorphous silica films prepared from the starting solution at pH 4.5 (a) and 2.5 (b).

Table 1 The equilibrium constants for TPPS, TCPP and TMPyP.

	TPPS	TCPP	TMPyP	
pKa <sub>3</sub>	4.96	2.1	2.06	( H <sub>2</sub> L + H <sup>+</sup> ⇌ H <sub>3</sub> L <sup>+</sup> )
pKa <sub>4</sub>	4.86		0.8	( H <sub>3</sub> L + H <sup>+</sup> ⇌ H <sub>4</sub> L <sup>2+</sup> )
		pKac=6.7		

is  $1 \times 10^{-3}$  in amorphous silica reported by Tani et al. Our value is one-order lower in consideration of the temperature dependence. It is not clear at this time what is the origin for our low value of apparent quantum yield. The value of the energy difference between a zero-phonon hole and a pseudo-side hole,  $E_s$ , is  $21.8 \text{ cm}^{-1}$ . The  $E_s$  value is proved to be an inherent parameter to the matrix and indicates the temperature dependence of Debye-Waller factor at low temperature.<sup>7)</sup> This value of  $E_s$  is as large as that of poly(vinyl alcohol) and larger than those of other polymer matrices.

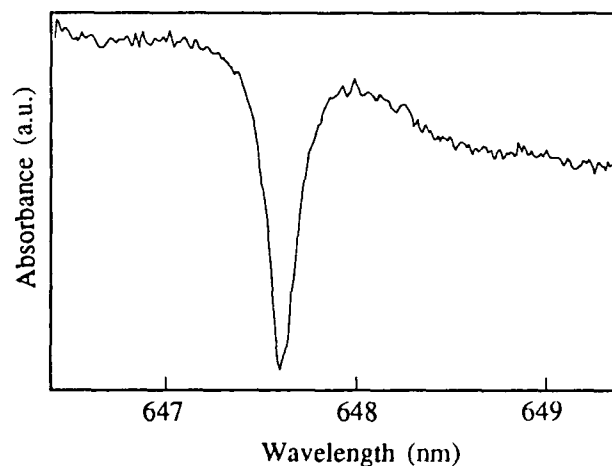


Figure 6 Typical photochemical hole of TMPyP in sol-gel thin film at about 20 K and 647.6 nm.

## REFERENCES

- 1) D.Avnir, D.Levy and R.Reisfeld, *J. Phys. Chem.*, **88** (1984) 5956.
- 2) D.Avnir, V.R.Kaufman and R.Reisfeld, *J. Non-Cryst. Solids*, **74** (1985) 395.
- 3) T.Tani, H.Namikawa, K.Arai and A.Makishima, *J. Appl. Phys.*, **58** (1985) 3559.
- 4) A.Makishima and T.Tani, *J. Am. Ceram. Soc.*, **69** (1986) C-72.
- 5) J.Friedrich, H.Wolfrum and D.Haarer, *J. Chem. Phys.*, **77** (1982) 2309.
- 6) A.Furusawa, K.Horie, K.Kuroki and I.Mita, *J. Appl. Phys.*, **66** (1989) 6041.
- 7) A.Furusawa, K.Horie and I.Mita, *Chem. Phys. Lett.*, **161** (1989) 227.
- 8) A.Furusawa, K.Horie and I.Mita, *Jpn. J. Appl. Phys.*, **28** (1989) 247.
- 9) C.J.Brinker, A.J.Hurd and K.J.Ward, *Ultrastructure Processing of Advanced Ceramics*, eds. J.D. Mackenzie and D.R.Ulrich (Wiley, New York, 1988) p.223.
- 10) C.J.Brinker, A.J.Hurd, G.C.Frye, K.J.Ward and C.S.Ashley, *J. Non-Cryst. Solids*, **121** (1990) 294.
- 11) J. Mckiernan, J.C.Pouxviel, B. Dunn and J.I.Zink, *J. Phys. Chem.*, **93** (1989) 2129.
- 12) J.C.Pouxviel, B. Dunn and J.I.Zink, *J. Phys. Chem.*, **93** (1989) 2134.

# Optimized Read/Write Conditions of PHB Memory

Norio Murase

Central Research Laboratory, Hitachi Ltd. Kokubunji, Tokyo 185, Japan  
Tel +81-423-23-1111

Kazuyuki Horie

Department of Reaction Chemistry, Faculty of Engineering,  
University of Tokyo, Hongo, Bunkyo-ku, Tokyo 113, Japan  
Tel +81-3-3812-2111

## 1. Introduction

PHB memory has been a good candidate for a future ultra high density memory for these ten years. This PHB memory is considered to realize the recording density of 1000 times higher than conventional optical memories because it can store wavelength-multiplicatively 1000 bits in a 1- $\mu$ m diameter recording spot. But not so many researchers are working on PHB memory compared to the number of researchers wrestling with realization of higher recording density of other types of memory such as magnetic or optical ones. One of the reasons is based on the doubt whether high speed readout is possible in such a high density recording in 1- $\mu$ m diameter spot. Therefore one of the most important research on PHB memory is the estimation of degree of coexistence between high recording density and high speed readout.

With respect to this point, two fundamental estimations have been proposed by Moerner et al.<sup>1,2)</sup> According to their results, even a memory of 10 times higher recording density than conventional optical memories can not be realized in case of 30 nsec/bit readout time for already-known single photon type PHB materials. But the above estimation was done under the conditions of 10  $\mu$ m for fixed laser spot diameter and 100 MHz for hole width. Furthermore, essentially inevitable noise was assumed to be shot noise only. Actually, a spot diameter is variable unless it's smaller than diffraction limit and hole width is usually larger than 3 GHz. And moreover, fluctuation in the distribution of photoabsorbing centers also becomes the origin of inevitable noise. For these reasons, the results might not be definitive.

In the present work, appropriate relationships between parameters are given and optimized conditions are pursued for the coexistence of both high density recording and high speed readout in PHB memory.

## 2. Theoretical Consideration

To achieve the above-mentioned purpose, we used a general equation at first for deriving signal to noise ratio theoretically.

Table 1 shows all parameters used for this consideration and their physical meaning. When transmitted light intensities before and after recording are changed into the currents  $i$  and  $i'$ , respectively, they are given by

$$i = q \cdot \eta_Q \cdot F_R \cdot A \cdot \exp(-\sigma \cdot N_\lambda \cdot L),$$

$$i' = q \cdot \eta_Q \cdot F_R \cdot A \cdot \exp(-\sigma \cdot N_\lambda' \cdot L).$$

Only two parameters,  $\eta_Q$  and  $N_\lambda$  (or  $N_\lambda'$ ), in these equations include inevitable noise sources. These two parameters are mean values with statistical distributions. Then, when we concentrate our attention on  $\delta_i$ , the inevitable noise for  $i$ , we only need to pick up these two types of parameters and it can be written by

$$\delta_i^2 = \left( \frac{\partial i}{\partial \eta_Q} \right)^2 \cdot \delta_{\eta_Q}^2 + \left( \frac{\partial i}{\partial N_\lambda} \right)^2 \cdot \delta_{N_\lambda}^2.$$

The first term of the right side is called shot noise and the second term is called material noise. Furthermore,  $\delta_{\eta_Q}$  and  $\delta_{N_\lambda}$  can be expressed as follows:

$$\delta_{\eta_Q} = \left( \sqrt{\frac{i \cdot \tau_R}{q}} / \frac{i \cdot \tau_R}{q} \right) \cdot \eta_Q,$$

$$\delta_{N_\lambda} = (\sqrt{N_\lambda \cdot A \cdot L} / N_\lambda \cdot A \cdot L) \cdot N_\lambda.$$

The signal  $S$  is given by the difference between  $i$  and  $i'$ . The rms noise  $N$  of  $S$  corresponds to  $\delta_s$ . Then signal to noise ratio SNR is expressed by

$$\text{SNR} = S / N = (i' - i) / \sqrt{\frac{q}{\tau_R} \cdot (i + i') + \frac{\sigma^2 \cdot L}{A} \cdot (i^2 \cdot N_\lambda + i'^2 \cdot N_\lambda')} \quad (1)$$

Hole depth  $\zeta$  can be defined by the degree of relative recording signal modulation and written by using  $N_\lambda$  and  $N_\lambda'$ ,

$$\zeta = (N_\lambda - N_\lambda') / N_\lambda,$$

and  $F_R$  could be written as

$$F_R \approx 1 / (\sigma \cdot T_1).$$

Finally, recording density  $D$  is given by

$$D = M / A.$$

By using these relations and an appropriate approximation, eq(1) can be transformed into

$$\tau_R = K / \left( \frac{1}{D} - \frac{1}{D_0} \right), \quad (2)$$

where  $D_0$  and  $K$  are defined as follows:

$$D_0 = \frac{M \cdot N_\lambda \cdot L}{2 \cdot \zeta + 2 \cdot \zeta \cdot \sigma \cdot N_\lambda \cdot L} \cdot \left( \frac{\zeta}{\text{SNR}} \right)^2,$$

$$K = \frac{(2 + \zeta \cdot \sigma \cdot N_{\lambda} \cdot L) \cdot T_1}{\eta_Q \cdot M \cdot \sigma \cdot N_{\lambda}^2 \cdot L^2} \cdot \left(\frac{\text{SNR}}{\zeta}\right)^2 \cdot \exp(\sigma \cdot N_{\lambda} \cdot L)$$

Eq(2) shows that recording density and readout speed are incompatible and their relation is described by a hyperbola with an asymptote of  $D = D_0$ . Moerner's result <sup>1)</sup> is derived by substituting infinite for  $D_0$  in eq(2), that means material noise  $\delta_{N_{\lambda}}$  is zero, and 100 MHz for a hole width.

Table 1. Parameters used for the theoretical consideration.

Parameter	Physical Meaning	Value
$F_R$	Readout light flux in photons /sec cm <sup>2</sup>	
$\tau_R$	Readout time for a single bit of information	
$\lambda$	Recording and readout wavelength	600 nm
A	Laser spot area	
L	Recording material thickness	
$N_{\lambda}$	Concentration of photoabsorbing centers within homogeneous width at wavelength $\lambda$ before recording	
$N_{\lambda}'$	Concentration of photoabsorbing centers within homogeneous width at wavelength $\lambda$ after recording	
$\sigma$	Absorption cross section of a photoabsorbing center	
$\eta_Q$	Detector quantum efficiency	0.75
q	Elementary electric charge	$1.6 \times 10^{-19}$ C
$T_1$	First excited state lifetime of photoabsorbing centers	10 nsec
M	Multiplicity	1000
C	Concentration of photoabsorbing centers	0.025 mol/l
$\epsilon$	Molar extinction coefficient of photoabsorbing centers	
D	Recording density	
$\zeta$	Hole depth	0.1
SNR	Required signal to noise ratio	20

### 3. Optimization and Discussion

According to the research works on PHB memory up to the present, recording performance with the hole depth  $\zeta$  of 0.1 and multiplicity M of 1000 can be attained under the most appropriate conditions. We concentrate our attention on the optimization of spot area, readout time and so on.

Relationships between microscopic quantity  $N_{\lambda}$ ,  $\sigma$  and macroscopic quantity C,  $\epsilon$  are

$$C = M \cdot N_{\lambda},$$

$$\epsilon = \frac{N_A \cdot \log e}{10^3} \cdot \frac{\sigma}{M},$$

where  $N_A$  is the Avogadro's number. When a laser beam is focused on a recording material, the relationship between  $A$  and  $L$  is expressed by

$$A = \pi \cdot r^2,$$

$$L = \pi \cdot r^2 / \lambda,$$

where  $r$  is the radius of laser spot. By using these equations and substituting the suitable values in Table 1 for all parameters except for  $D$  and  $\tau_R$ , the relationship between  $D$  and  $\tau_R$  is represented in Fig. 1.

Conventional magnetic memory has recording density of about 15 Mb/cm<sup>2</sup> and readout time of about 15 nsec/bit. And those of optical memory are about 150 Mb/cm<sup>2</sup> and 60 nsec/bit. In order to overcome these performances, readout time of PHB memory can be determined to be 10 nsec/bit, which is not within the abrupt rising up zone of readout time. At this point, recording density becomes about 20 Gb/cm<sup>2</sup>. Although this is theoretical consideration, PHB memory proved to have potential ability compared to magnetic and optical memories.

In this optimized case, spot diameter becomes to be about 2  $\mu$ m, but not 1  $\mu$ m. If a spot diameter is too small, statistical fluctuation of the concentration of photoabsorbing centers gives rise to serious noise and causes an insufficient SNR even for long readout time. Furthermore, this analysis also points out that optimized optical density is about 0.9 and required readout laser power is merely an order of 1  $\mu$ W.

Some factors which reduce this theoretical performance would exist. They are, for example, destructive reading, Gaussian distribution of inhomogeneous broadening and so on. These will be good targets of future researches and the present consideration must be a good guide for these researches.

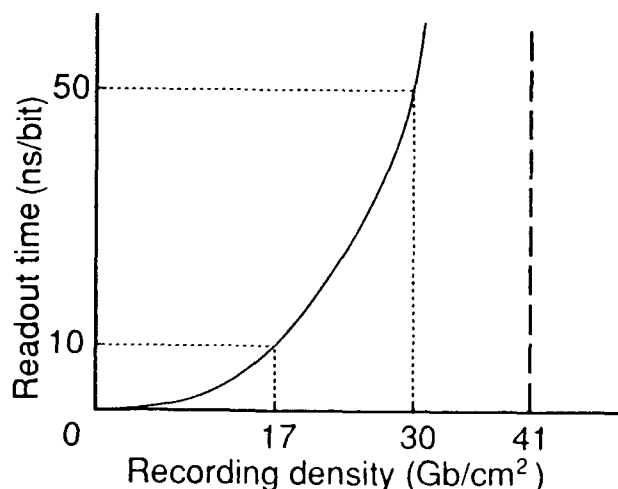


**Fig. 1. Readout performance of PHB memory considered by theoretical calculation**

#### References

- 1) W.E. Moerner and M.D. Levenson, J. Opt. Soc. Am. B, 2, 915(1985).
- 2) W. Lenth and W.E. Moerner, Opt. Commun., 58, 249(1986).

## Hole Multiplexing in Quinone Derivative Photochemical Hole Burning Systems

Motomu Yoshimura, Tetsuya Nishimura, Eiji Yagyu, Noriaki Tsukada and Tetsu Takeyama  
Central Research Laboratory, Mitsubishi Electric Corporation  
8-1-1 Tsukaguchi-Honmachi, Amagasaki, Hyogo 661, Japan  
+81-6-497-7084

### INTRODUCTION

We have been interested in PHB mechanism<sup>1,2</sup> in the quinone derivatives. The substituent effects of the guest molecules are examined on the hole multiplexing<sup>3</sup>, hole formation wavelength range and electric field effect<sup>4</sup>. We especially intend to know how densely multiple holes can be formed by wavelength tuning and Stark tuning.

First, the substituent effect on hole density and hole formation range in the wavelength dimension has been investigated. It has been proved to be important to select the proper substituents. Second, the Stark effect on the PHB reaction characteristics in the amorphous hosts has been investigated. Also in the quinone derivative systems, the Stark effect has been successfully observed. Five multiple holes in the electric field dimension have been produced at 4.2 K. The dipole moment difference  $\Delta\mu$  between in the ground state and in the excited state of the guest molecule has been estimated by the spectral hole shift due to the applied electric field.

### EXPERIMENTAL

The guest molecules examined were 1,4-dihydroxy anthraquinone (DAQ), 4-amino-2,6-bis(4-butylphenoxy)-1,5-dihydroxy anthraquinone (ABDAQ), 4-amino-2,6-bis(4-butylphenoxy)-1,5,8-trihydroxy anthraquinone (ABTAQ) and 4,8-diamino-2-(hexyloxyphenyl)-1,5-dihydroxy anthraquinone (DAHAQ). The alkyl or alkylphenyl groups and the hydroxy or amine groups were concerned with as the substituents to be examined. The latter groups are the active sites for PHB. And the host molecules examined were PMMA and poly-2-hydroxyethyl methacrylate (PHEMA) and polyvinyl butyral (PVB).

The samples were prepared as polymer film by casting the solution of the guest and host compounds. The concentration of the guest in the host polymer was in the range of  $10^{-3}$  to  $10^{-5}$  mol/mol. The thickness of the film was 50 to 300  $\mu\text{m}$ . The sample was set in a cryostat controlled at 4.2K. Tunable dye lasers were used as the light source of hole burning. Burning power was in the range of 2 to 35  $\text{mW}/\text{cm}^2$ . The hole profiles were detected by using a 1m monochromator and a photomultiplier and a lock-in amplifier. To apply the electric field, the sample film was mounted between two glass plates with transparent electrode on their inner side. The electric field was set on through a DC power supply, up to 100  $\text{kV}/\text{cm}$ , to the sample.

### RESULTS AND DISCUSSION

#### 1. Hole multiplexing in wavelength dimension

##### 1.1. Substituent effect on multiple hole formation

We examined hole multiplexing and density concerning with hole-hole interaction. In the DAQ/PMMA, the hole density was only 6 or 7 holes in 1 nm wavelength range as shown in fig. 1. In the ABDAQ/PMMA, that was only 3 or 4 holes in 1 nm wavelength range at most. On the contrary, we reported the dense hole formation of more than 12 holes in 1 nm wavelength range in the DAQ/PHEMA<sup>5</sup>. So, we achieved multiple hole formation of 300 in only 21 nm wavelength range of 566 to 587 nm efficiently. In the ABDAQ/PHEMA, the holes could be formed efficiently in the wavelength range of 580 to 608 nm at least<sup>6</sup>. The multiple holes of 350 were formed in the wavelength of 582 to 603 nm. Multiple holes could be produced more densely in the

ABDAQ/PHEMA than in the DAQ/PHEMA, that is 20 holes or so in 1 nm wavelength range could be formed independently each other as shown in fig. 2.

The hole densities for four systems are shown in table 1. In practice, it is suggested the hole density will depend on the dipole-dipole interaction modes between the guest and host molecules, the properties of the host polymer and the molecular size of the guest dye molecule.

Table 1 Hole densities in the DAQ/PMMA, ABDAQ/PMMA, DAQ/PHEMA and ABDAQ/PHEMA.

Guest \ Host	PHEMA	PMMA
	DAQ	12~13 holes/nm
ABDAQ	18~20 holes/nm	3~4 holes/nm

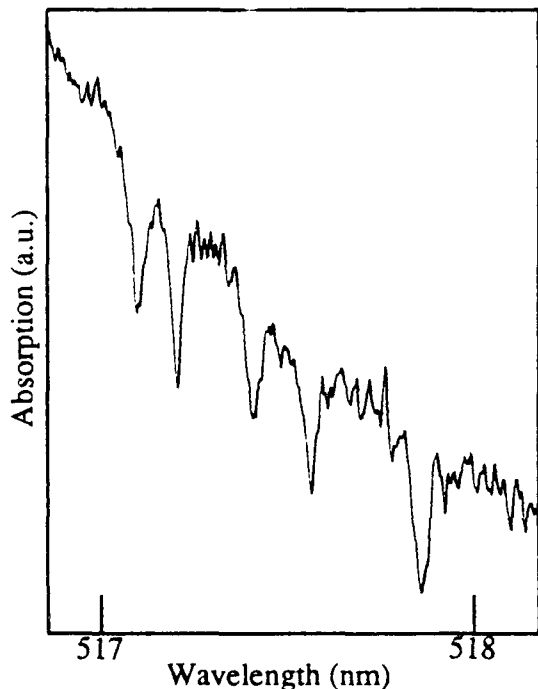


Fig. 1 Hole density in the DAQ/PMMA.

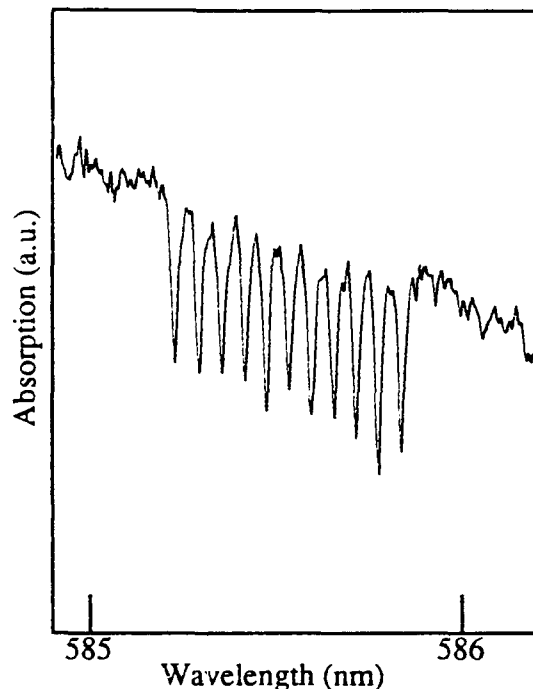


Fig. 2 Hole density in the ABDAQ/PHEMA.

### 1.2. Substituent effect on hole formation wavelength range

Here, we have examined how widely in the wavelength range the holes can be formed. In the previous section, holes could be formed in 566 to 587 nm in the DAQ/PHEMA, and in 582 to 603 nm in the ABDAQ/PHEMA. Furthermore, in the ABTAQ/PHEMA, the holes could be formed efficiently in the wavelength range of 600 to 620 nm. In the DAHAQ/PHEMA, the holes could be formed efficiently in the wavelength range of 640 to 675 nm. Fig. 3 shows a part of 300 of multiple holes in the wavelength range of 645 to 669 nm. And, multiple holes could be formed using a semiconductor laser as a light source in practice. From the results described hitherto, it is suggested that the wavelength range for hole formation can be widely controlled by selecting the substituents properly.

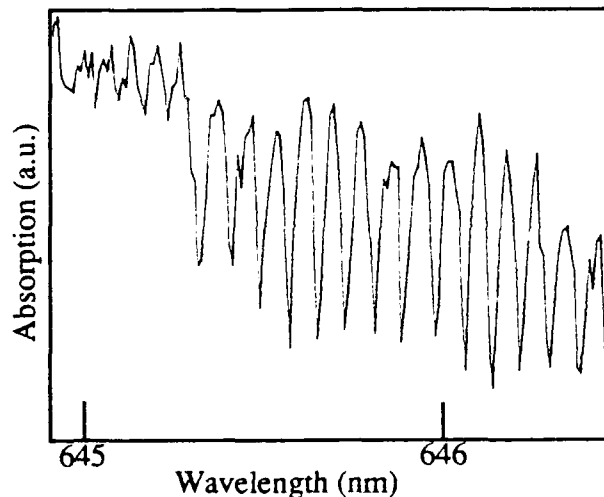


Fig. 3 Multiple hole formation in wavelength in the DAHAQ/PHEMA.

## 2. Hole multiplexing in electric field dimension

The shift  $\Delta\nu$  of the absorption band of the guest molecule by the Stark effect is, under a condition of up to an electric field strength of MV/cm, expressed as eq.(1) on changing the electric field  $E$  <sup>7</sup>,

$$h \Delta\nu = -f \Delta\mu \cdot E \quad (1)$$

where  $\Delta\mu$  is the dipole moment difference vector between in the ground state and in the excited state of the guest molecule. In an amorphous host, because the guest molecules orient randomly, the absorption bands of the guest molecules are shifted isotropically as denoted by eq.(1), so the hole is symmetrically broadening. Also, eq.(1) gives us the value of  $\Delta\mu$  from the results of the hole broadening.

### 2.1. Multiple hole formation in electric field dimension

One of interesting aspects of the Stark effect on the PHB hole is the multiple data storage in the electric field dimension. At first, the multiple hole formation in the electric dimension was investigated in the ABDAQ/PVB. The holes were burnt at five electric field strengths of -97.5 to +97.5 kV/cm at intervals of 48.75 kV/cm at the wavelength of 581.5 nm. The 5 multiple hole formation could be performed as shown in fig. 4. This result makes it sure that the multiple hole formation is possible in the electric field dimension in the quinone derivatives even at 4.2 K.

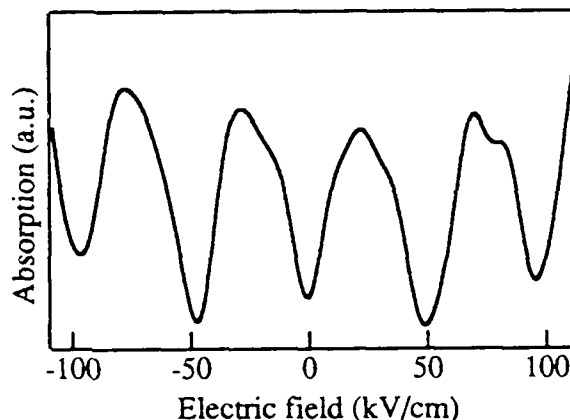


Fig. 4 Multiple hole formation in electric field in the ABDAQ/PVB.

### 2.2. Stark effect in quinone derivative PHB systems

The electric field dependence of the hole profile in the DAQ/PHEMA, ABDAQ/PHEMA and ABDAQ/PVB was examined. In the DAQ/PHEMA, as holes formed efficiently in the wavelength dimension, the efficient multiple hole formation also in the electric field dimension would be expected to be realized. An initial hole at the electric field strength of 18.5 kV/cm and at the wavelength of 576.22 nm was burnt. The hole width in the wavelength dimension was estimated at the FWHM of  $0.56 \text{ cm}^{-1}$  by the initial burnt hole profile. It is clearly seen that the electric field causes the hole broadening. The hole width in the electric field dimension was estimated at the FWHM of 22 kV/cm. By using eq.(1), the dipole moment difference of DAQ in this system was calculated at  $0.38D$  <sup>8</sup>. In the ABDAQ/PHEMA, the initial hole was burnt at the electric field strength of 26.5 kV/cm and the wavelength of 589.7 nm. The hole width in the wavelength dimension was estimated at  $0.86 \text{ cm}^{-1}$ . The Stark effect was also obviously observed in this system. By hole depth variation curve against the external electric field as shown in fig. 5, the hole width in the electric field dimension was estimated at 25 kV/cm. And, the dipole moment difference of ABDAQ in this system was calculated at  $0.51D$ . In the ABDAQ/PVB, the initial hole was burnt at the electric field strength of 56.3 kV/cm and wavelength of 589.7 nm. The hole width in the wavelength dimension was estimated at  $0.55 \text{ cm}^{-1}$ . By hole depth curve, the hole width in the electric field dimension was estimated at 38 kV/cm. And, the dipole moment difference of ABDAQ in this system was calculated at  $0.26D$  <sup>9</sup>. The FWHM's of the hole width in electric field and dipole moment differences measured in the three systems are summarized in the table 2 and 3.

As for the hole width in the electric field dimension, it appears that the hole width is narrower in PHEMA than in PVB by comparison of the results of the ABDAQ/PHEMA and

ABDAQ/PVB. The dipole moment difference of ABDAQ in PHEMA seems larger than in PVB. Such differences of the hole width and dipole moment difference of the guest molecule between in PHEMA and in PVB might be attributed to the difference of the dielectric constants of PHEMA and PVB. Also, the dipole moment difference  $\Delta\mu$  seems to be affected by the structure of the guest molecules by comparison of the  $\Delta\mu$  of DAQ in the DAQ/PHEMA and ABDAQ in the ABDAQ/PHEMA. The long substituent might make the  $\Delta\mu$  larger. It has been suggested that the value of the dipole moment difference depends on not only the guest molecular substituents of the quinone derivatives but also the host polymer structures. These results prove that the Stark effect is also useful for the analysis of the molecular characteristics.

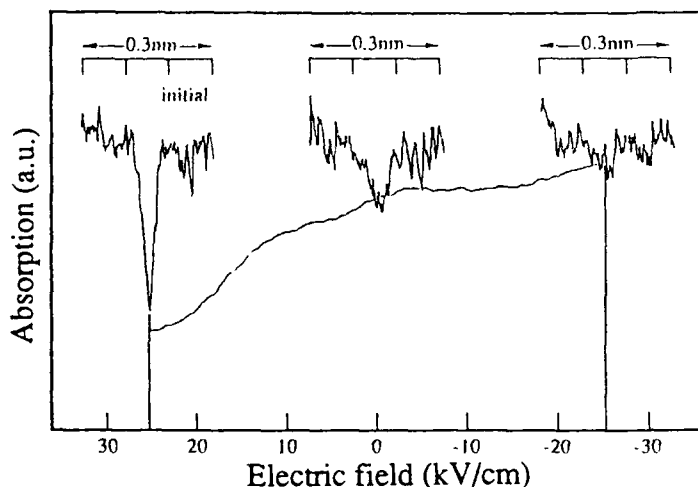


Fig. 5 Hole depth curve against the electric field in the ABDAQ/PHEMA.

Table 2 Hole FWHM's in the DAQ/PHEMA, ABDAQ/PHEMA and ABDAQ/PVB.

Guest \ Host	PHEMA	PVB
DAQ	$v_{1/2} = 0.56 \text{ cm}^{-1}$ $E_{1/2} = 22 \text{ kV/cm}$	—
ABDAQ	$v_{1/2} = 0.86 \text{ cm}^{-1}$ $E_{1/2} = 25 \text{ kV/cm}$	$v_{1/2} = 0.55 \text{ cm}^{-1}$ $E_{1/2} = 38 \text{ kV/cm}$

Table 3 Dipole moment differences in the DAQ/PHEMA, ABDAQ/PHEMA and ABDAQ/PVB.

Guest \ Host	PHEMA	PVB
DAQ	0.38D	—
ABDAQ	0.51D	0.26D

## ACKNOWLEDGMENT

This work was performed under the management of Mitsubishi Electric Corporation as a part of the R&D of Basic Technology for Future Industries supported by NEDO (New Energy and Industrial Technology Development Organization).

## REFERENCES

1. A.R.Guillierrez, J.Friedrich, D.Haarer and H.Walfrum, *IBM J. Res. Devel.* 26 (1982) 198.
2. W.E.Moerner, *J. Mol. Electron.* 1 (1985) 55.
3. J.Friedrich and D.Haarer, *Angew. Chem. Int. Ed. Engl.* 23 (1984) 113.
4. U.Bogner, P.Schatz, R.Seel and M.Maier, *Chem. Phys. Lett.* 102 (1983) 267.
5. M.Yoshimura, M.Maeda and T.Nakayama, *Chem. Phys. Lett.* 143 (1988) 342.
6. M.Yoshimura, T.Nishimura and N.Tsukada, *SPIE Proc.* 1078, Los Angeles (1989) 326.
7. A.J.Meixner, A.Renn, S.E.Bucher and U.P.Wild, *J. Phys. Chem.* 90 (1986) 6777.
8. T.Nishimura, E.Yagyu, M.Yoshimura, N.Tsukada and T.Takeyama, *SPIE Proc.* 1436, Los Angeles (1991) 31.
9. M.Maier, *Appl. Phys.* B41 (1986) 73.

## Antihole Formation in Intramolecular Rotational Tunnel Systems

G.Gradl, A. Feis, J. Friedrich

Institut für Phys. Chemie, Johannes Gutenberg-Universität

6500 Mainz, Germany

Phone: 06131-394212

Fax: 06131-393768

Hole burning in mixed crystals containing methyl groups can be used to determine the difference of the rotational tunnel splitting of the methyl groups in the ground and excited electronic state of the guest probe /1/. Two mechanisms were suggested: If the phototransformation of the probe is photochemical in nature, the difference in tunnel splitting shows up in the side hole pattern which appears upon thermal relaxation of the bleached ground state levels through spin conversion processes. On the other hand, if the phototransformation is purely photophysical in nature, the nuclear spin conversion occurs most probably in the excited triplet state and the tunnel splitting is reflected in the appearance of antiholes.

In this paper, we show that for dimethyl-s-tetrazine as a diluted guest in a n-octane host, the difference in the methyl tunnel splitting leads to the formation of two very sharp, perfectly Lorentzian antiholes. This splitting is 20 times as large as that for dimethyl-s-tetrazine in durene measured by Borczykowski et al. /1/. The absolute magnitude of the tunnel splitting in the ground state is comparable to  $kT$  leading to an intensity difference of the two antiholes from which the absolute magnitude of the tunnel splitting in the ground as well as in the electronically excited state can be determined.

Fig.1 shows the central hole and the two antiholes symmetrically shifted by 37 GHz. The intensity of the antihole at lower energy is larger by a factor of 2.5 as compared to the high energy antihole. The insert shows that the antiholes have a width on the order of 1.3 GHz and that their shape perfectly follows a Lorentzian. What do we learn from these observations? Following Borczykowski et al., we conclude that the phototransformation is based on a nuclear spin conversion process which occurs in the excited triplet state and which leads to a mutual transformation of the methyl tunnel states, i.e. the state with A symmetry is transformed to an E-symmetric state and vice versa. The corresponding methyl proton spin states are  $3/2$  (A) and  $1/2$  (E) /2/. Since the nuclear spin is conserved upon

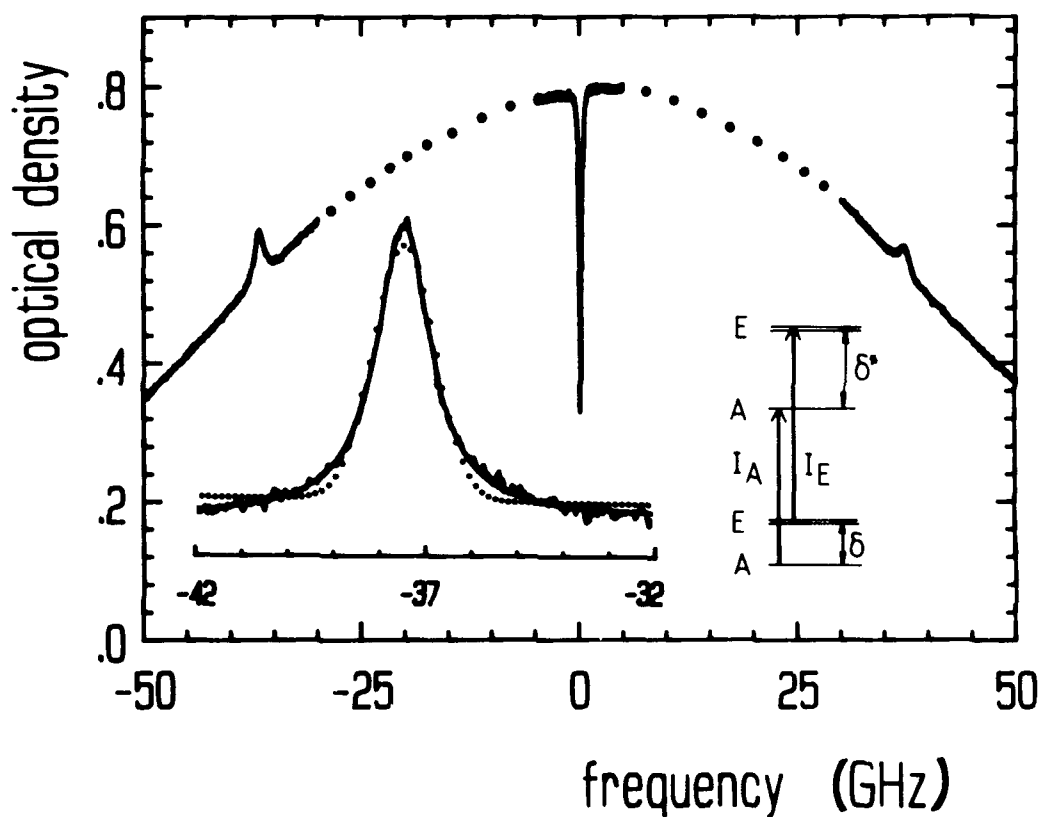


Fig. 1: Photophysical hole burning spectrum of dimethyl-s-tetrazine in *n*-octane at 4.2 K

excitation the absorption frequency of the transformed species differs from the excitation frequency by the difference in the tunnel splitting between the ground and excited state. The ground state relaxation from  $|1/2\rangle$  to  $|3/2\rangle$  is, at 4.2 K, on the order of 40 min. On this time scale equilibrium between the two states is established. As far as our experimental time scales are concerned, we can be sure that we start with equilibrated states.

The insert of Fig.1 shows the level scheme. In case the tunnel splitting in the ground state is on the order of  $kT$ , the intensities  $I_E$  and  $I_A$  of the antiholes at high and low energy, respectively, are influenced by the tunnel state Boltzmann factor. In our case the intensity ratio is roughly 2.5 at 4.2 K. From this ratio the absolute magnitude of the tunnel splitting  $\delta$  can be estimated.

$$I_E/I_A = 2n_E/n_A \approx 2 \exp(-\delta/kT)$$

The population of the states is denoted by  $n$ . The factor 2 accounts for the degeneracy of the E-state. We get  $\delta = 0.65 \text{ cm}^{-1}$ . According to our results in Fig.1, the high energy antihole is the one with lower intensity. Hence,  $\delta < \delta^*$ . Since  $\delta - \delta^* = 1.23 \text{ cm}^{-1}$ , the

splitting in the electronically excited state  $\delta^*$  equals  $1.88 \text{ cm}^{-1}$ . These are rather large values and are on the upper bound from what is known about methyl rotational tunnel splitting frequencies /2/. We argue that the large difference in tunnel frequencies indicates that it is the methyl groups attached to the probe which are measured and not those of the host crystal.

An interesting issue of our experiments is the fact that the antiholes are very sharp and perfectly Lorentzian. This result imposes restrictions on the nature of the interactions which cause the inhomogeneous broadening of the antiholes. They are, at 4.2 K, roughly four times as broad as the central hole. First of all, the Lorentzian line shape requires this interaction to be of long range, to be precise of dipole-dipole type and, moreover, the interacting centers must be isotropically and homogeneously dispersed /3,4/. We suggest the following picture: The main potential barrier of the methyl rotor is determined by intramolecular interactions between the electrons in the CH-bonds and the  $\pi$ -electrons of the ring as well as by nearby lattice molecules. This barrier is, however, modified by the strains created at the grain boundaries via elastic dipole-dipole interaction. The data show that the modulation of the tunnel splitting is rather small compared to its absolute magnitude. Hence a lowest order expansion of the tunnel splitting as a function of the barrier modulation is sufficient. Consider a probe molecule and let  $U_i(R)$  be the change of its methyl rotation barrier in the  $i$ 'th electronic state due to a defect at a distance  $R$ . Then, this defect will change the absorption energy of the probe by an amount of  $h\Delta\nu(R) = \hbar\Omega e^{-\lambda} [U_i(R) - U_0(R)]$ , with  $\lambda$  being the so called tunnel parameter, and  $\Omega$  is on the order of the zero point frequency of the methyl libration.  $\Omega$  and  $\lambda$  are considered as being fixed parameters, an assumption which is corroborated by the fact that the antihole splitting does not depend on the burn frequency within the inhomogeneous band. If  $\Delta\nu(R)$  is fluctuating in sign and is proportional to  $1/R^3$ , then the broadening of the antiholes will be Lorentzian provided the defects are uncorrelated. This model seems reasonable for n-octane: Compared to the range of the dipole-dipole interaction, the homogeneity and isotropy assumption does not seem to be crucial. On the other hand, the defect concentration is low enough (inhomogeneous broadening is small) so that the assumption of uncorrelated defects is reasonable. We stress that the sharp antiholes fade as the holes are burnt deeper. Instead, the phototransformed species is distributed over the whole inhomogeneous band. This is an indication that photochemical burning processes take over and that the lattice structure in the immediate neighborhood of the probe is heavily perturbed so that the tunnel frequency spreads out over a wide range.

The occurrence of sharp antiholes clearly demonstrates that the inhomogeneous line is

built from a convolution of interactions on various hierarchy levels. In our case it means that each site of the inhomogeneous line is itself inhomogeneously broadened by long range interactions with defects in the bulk. This result is in line with spectral diffusion experiments on similar systems /5/.

#### References:

- /1/ C. von Borczyskowski, A. Oppenländer, H.P. Trommsdorff, J.C. Vial, *Phys.Rev.Lett.* **65**, 3277 (1990)
- /2/ W. Press, in *Single-Particle Rotations in Molecular Crystals*, Springer Tracts in Modern Physics Vol. 92 (Springer, Berlin, 1981)
- /3/ A.M. Stoneham, *Rev.Mod.Phys.* **41**, 82 (1969)
- /4/ B.B. Laird, J.L. Skinner, *J.Chem.Phys.* **90**, 3274 (1989)
- /5/ J. Zollfrank, J. Friedrich, *J.Chem.Phys.* **93**, 8586 (1990)

# Subnanosecond Time Resolved Study of Accumulated Photon Echoes in Chlorin Doped Polymer Films at 1.2 K

Hansruedi Gyax, Ekkehard Görlach, Alexander Rebane, and Urs P. Wild

*Physical Chemistry Laboratory, Swiss Federal Institute of Technology, Zürich,  
ETH-Zentrum, 8092 Zürich, Switzerland, Tel.: +41 1 / 256 43 89; Fax: +41 1 / 252 34 02*

Organic impurity systems which exhibit effect of photoburning of persistent spectral holes have several interesting spectroscopic and prospective practical applications [1, 2]. A CW holographic technique for detecting of narrow hole shapes in thin polymer films doped with organic dye molecules can be used in combination with a variable-strength applied electric field to obtain information about the homogeneous line shapes and symmetry properties of the impurity centres [3]. This method serves also as a demonstration of the possibility of parallel optical computing [4].

An alternative approach to measure homogeneous line shape properties of low temperature impurity systems consists in the application of coherent optical transient techniques such as photon echoes and accumulated photon echoes [5]. A variation of an accumulated photon echo technique in photochemical hole burning media - photochemically accumulated stimulated photon echo (PASPE) [6] has been shown to be useful in measuring homogeneous dephasing times [7] as well as in writing ultrafast time domain holograms [8].

In the present work we describe an experiment where we have combined the principles of PASPE and time- and space domain holography with a sensitive subnanosecond time resolution detection using time-correlated single photon counting (TCSPC) apparatus. We also discuss the relation between the present time domain experiment and CW holographic hole burning.

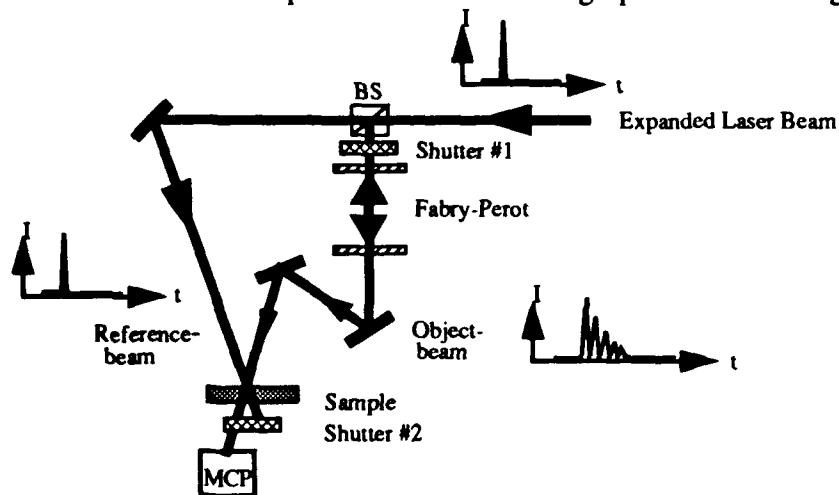


Fig. 1.

Fig. 1 shows the schematic of our experimental arrangement and Fig. 2 illustrates some of our results. The impurity system we study is chlorin doped into polyvinylbutyral film. The sample

is pressed between two glass plates covered with optically transparent electrodes and is positioned in a variable temperature (1 - 4.2 K) liquid He cryostat. In the experiment the excitation picosecond pulses are generated by a DCM dye laser synchronously pumped by a mode-locked Coherent Antares Nd-YAG laser. Echo signals are detected by using a multichannel plate photomultiplier tube (MCP). The necessary electronic clocking for the TCSPC apparatus is provided by a fast reference photodiode. The time separation between the pulses in the mode-locked pulse train is 13.22 ns. Fig. 2 presents linear (a) and logarithmic (b) plots of the excitation dye laser pulses.

### PASPE detected by TCSPC

Chlorin in PVB,  $T=1.2\text{K}$

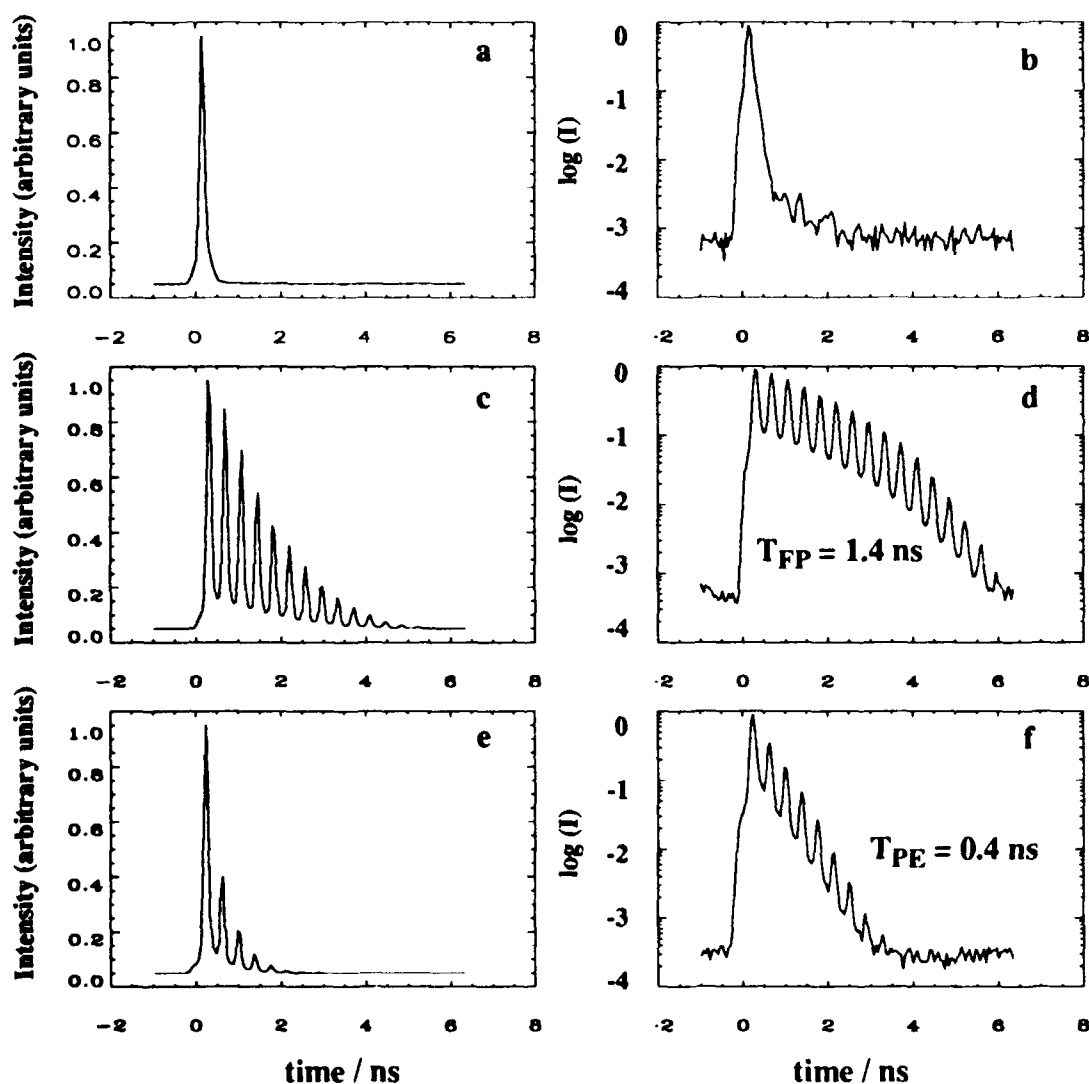


Fig. 2.

Our detection system provides 40 ps (FWHM) time resolution and low background signal level (background signal count rate  $< 10$  counts/sec). More details about the TCSPC apparatus are

given in [9].

In our holographic setup (Fig. 1) the incoming laser beam is expanded by a telescope and is then split into two parts. One of the two beams passes through a Fabry-Perot interferometer that consists of two flat mirrors. Inside the interferometer cavity the laser pulses reflect back and forth with a period that corresponds to the double round trip time between the two mirrors (380 ps). Each of the input laser pulses, is thus transformed at the output of the interferometer into an exponentially decaying sequence of equally spaced pulses (Fig. 2c). A Logarithmic plot of the time resolved interferometer output pulse sequence yields an exponential intensity decay constant,  $\tau_{FP} \sim 1.4$  ns (Fig. 2d). Note that  $\tau_{FP}$  depends only on the reflectivity coefficient of the mirrors ( $R=85\%$ ).

The beam containing the exponential pulse sequence overlaps with the second beam at the position of the sample. The timing of the excitation pulse in the second beam is adjusted so that it arrives at the sample about ten picoseconds before the first pulse from the interferometer-produced pulse sequence. The angle separation between the two beams is  $5^\circ$ .

The first step in probing the homogeneous dephasing properties of the impurity in our experiment consists in exposing the sample for about 30 seconds simultaneously to both beams with an average intensity of  $20 \text{ mW/cm}^2$ . The wavelength of the laser is tuned to the maximum absorption region of the inhomogeneously broadened 0-0 transition of the chlorin molecules (633 nm).

During the illumination the impurity concentration is bleached out mostly at the spatial locations of the sample where the two spatially overlapping beams give constructive interference. However, because the two pulses do not overlap in time, interference is induced by the coherent excitation of the molecules. This requires that at least some molecules excited by the first pulse have not yet dephased when the pulse-train arrives. Simultaneously the frequency spectrum of the pulse sequence is recorded in the sample within the  $1.5 \text{ \AA}$  spectral envelope of the original laser pulse. During the write-in at different frequencies, different spatial interference gratings are formed and the corresponding patterns are bleached out. At different frequencies the gratings may have different phases as well as different periods.

Taken separately each of the burnt-in monochromatic frequency gratings in the inhomogeneous distribution function carries basically the same information about the homogeneous line shape and is affected by the same line width broadening mechanisms (dephasing, spectral diffusion) as in the case of a CW holographic hole burning experiment. The depth and the contrast of the gratings decreases with increasing of the width of the homogeneous zero phonon line. Indeed, reading out the hologram from the direction of the second beam with a tunable narrow band laser would yield a holographic signal with a spectral profile of periodic sharp peaks corresponding to the transparency function of the Fabry-Perot interferometer. Each of the sharp peaks is the equivalent of a hole burnt with a CW narrow band laser, while the broad envelope profile of the multitude of the peaks corresponds to the overall spectral width of the laser pulses.

The special properties of the photon echo come into consideration when the time domain read-out of the holographic gratings is carried out in the next step of the experiment. For the read-out we illuminate the stored gratings with attenuated pulses ( $2 - 0.2 \text{ \mu W/cm}^2$ ) from the second beam while the beam passing through the interferometer is blocked (Shutter 1 is closed). Also,

Shutter 2, which had blocked the MCP plate from over-exposure by the intense signal during the writing, is now open.

The time domain holographic signal diffracted from the hole burning grating structure in the direction of the first beam and detected by the MCP is shown in Fig. 1e (linear scale) and 1f (log scale). The intensity of the PASPE pulses reproduce the exponential sequence but with a faster decay constant of a value of  $\tau_{\text{PASPE}} = 0.4$  ns. Note that the background noise in the detected signal due to detector dark counts and also due to ambient light scattering from the cryostat windows and the optical elements in the reference beam is about  $10^5$  times lower than the maximum measured signal level.

The difference between the decay rates of the original exponential pulse sequence (Fig. 1d) and that of the PASPE signal yields, by applying the relation,

$$4/T_2 = 1/\tau_{\text{PASPE}} - 1/\tau_{\text{FP}}$$

the homogeneous purely electronic zero phonon transition dephasing time value of  $T_2 \sim 2.3$  ns. This results correlates with the value estimated from earlier CW homogeneous line width measurements in chlorin in polyvinylbutyral film:  $T_2 \sim 2.0$  ns ( $T = 1.6$ K) [10] and  $T_2 \sim 1.4$  ns ( $T = 1.2$  K) [11]. The advantage we have in the present experiment is that the read out can be performed within a very short time which is, in principle, on the same timescale as the coherent response itself.

Similar considerations are valid if after burning-in the spectral grating structure the film is subject to a static electric field by applying voltage to the electrodes attached to the sample. Further experiments in this direction are currently in progress.

## References

- [1] L. A. Rebane, A. A. Gorokhovskii, and J. V. Kikas, *Appl. Phys. B* **29** (1982) 235.
- [2] J. Friedrich, and D. Haarer, *Angew. Chem. Int. Ed. Engl.* **23** (1984) 119.
- [3] A. J. Meixner, A. Renn, and U. P. Wild, *J. Chem. Phys.* **91** (1989) 6728.
- [4] U. P. Wild, C. De Caro, S. Bernet, M. Traber, and A. Renn, *J. Lum.* **48 & 49** (1991) 335 - 339..
- [5] D. A. Wiersma, in: *Photoselective Chemistry*, eds. J. Jortner, R. D. Levine, and S. A. Rice, *Advances in Chemical Physics*, XLVII, Wiley & Sons, New York, 1981.
- [6] A. Rebane, R. Kaarli, and P. Saari, *JETP Lett.* **38** (1983) 383.
- [7] A. Rebane, and D. Haarer, *Opt. Commun.* **70** (1989) 478.
- [8] A. Rebane, J. Aaviksoo, and J. Kuhl, *Appl. Phys. Lett.* **54** (1989) 93.
- [9] S. Canonica, J. Forrer, and U. P. Wild, *Rev. Sci. Instr.*, **56** (1985) 1754.
- [10] R. Locher, A. Renn, and U.P. Wild, *Chem. Phys. Lett.* **138** (1987) 405 - 409
- [11] F.A. Burkhalter, G.W. Suter, U.P. Wild, V.D. Samoilenko, N.V. Rasumova, and R.I. Personov, *Chem. Phys. Lett.* **94** (1983) 483 - 487

SPECTRAL HOLE-BURNING BETWEEN 2 K AND ROOM TEMPERATURE IN  
 $\text{Sm}^{2+}$  DOPED SUBSTITUTIONALLY DISORDERED MICROCRYSTALS

Keith Holliday, Changjiang Wei, Mauro Croci and Urs P. Wild

Physical Chemistry Laboratory, Swiss Federal Institute of Technology, ETH Zentrum,  
 CH-8092 Zürich, Switzerland. Tel. +41-1-2564384, Fax. +41-1-2523402

Photon gated spectral hole-burning was first observed in a samarium doped crystal,  $\text{BaFCl}:\text{Sm}^{2+}$  [1]. This material was of interest to the development of optical memories as the holes were found to be stable to room temperature thermal cycling. Holes could be burnt at liquid helium temperatures but as the temperature was raised the line quickly became homogeneously broadened. The addition of bromine to the melt succeeded in broadening the inhomogeneous linewidths to about 2 nm through substitutional disorder [2] and persistent holes were observed at 77 K [3]. Subsequently, a study of the parameters for spectral hole-burning in a  $\text{BaFCl}_{0.5}\text{Br}_{0.5}:\text{Sm}^{2+}$  crystalline powder was performed [4] and the highest temperature for which persistent hole-burning had been observed was raised to 133 K. Here we report spectral hole-burning at room temperature (figure 1) in a related compound,  $\text{Sr}_{0.5}\text{Mg}_{0.5}\text{FCl}_{0.5}\text{Br}_{0.5}:\text{Sm}^{2+}$ .

The hole-burning characteristics of this class of materials are dependent on the method of preparation [1] and, for instance, a separate study of  $\text{BaFCl}_{0.5}\text{Br}_{0.5}:\text{Sm}^{2+}$  observed holes at 183 K, decaying with a half-life of a few minutes [5]. The preparation method for the samples used here has previously been described [3].

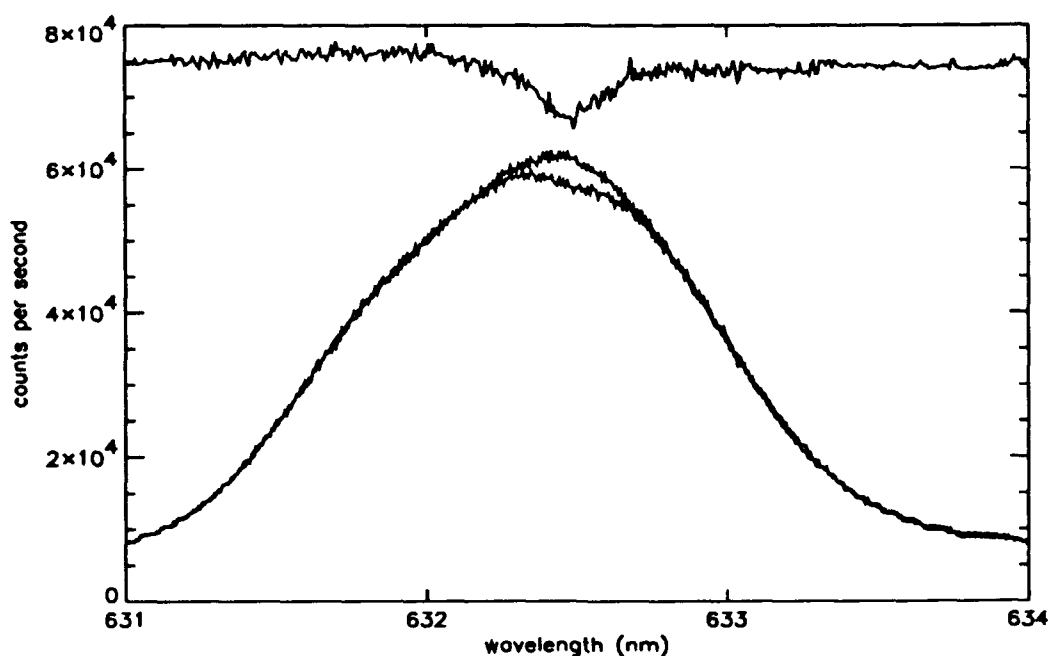


FIGURE 1. The  ${}^7F_0-{}^5D_1$  line in  $\text{Sr}_{0.5}\text{Mg}_{0.5}\text{FCl}_{0.5}\text{Br}_{0.5}:\text{Sm}^{2+}$  before and after room temperature hole-burning at 632.5 nm (laser scatter  $\sim 8000$  cps). The difference signal, above, is magnified by a factor of 2.

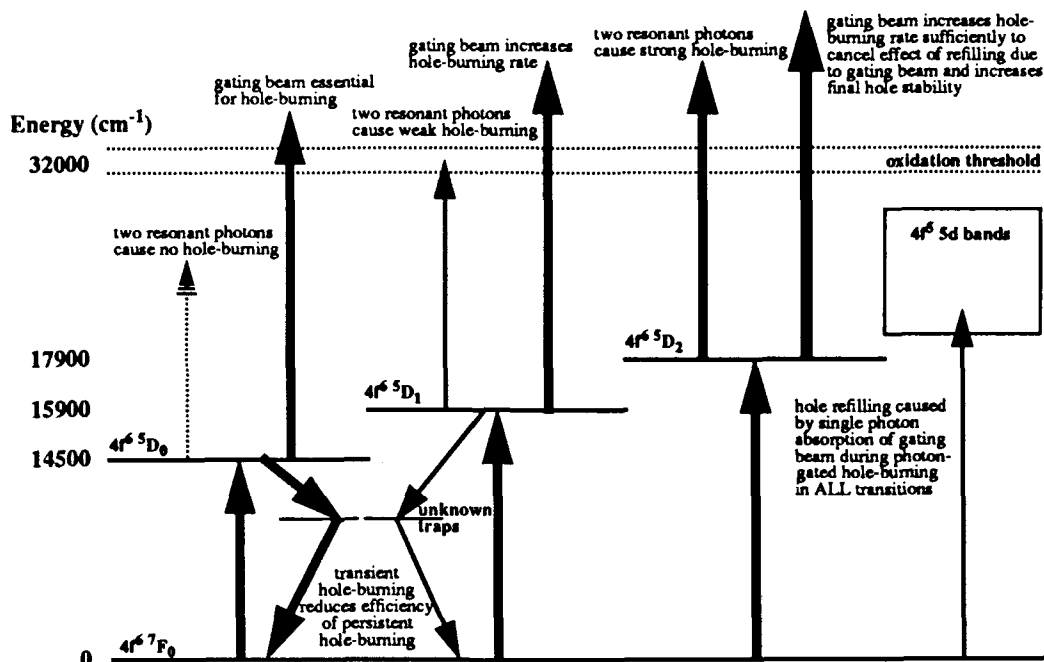


FIGURE 2. The hole-burning scheme in  $\text{BaFCl}_{0.5}\text{Br}_{0.5}:\text{Sm}^{2+}$  at 2 K.

The hole-burning system for  $\text{BaFCl}_{0.5}\text{Br}_{0.5}:\text{Sm}^{2+}$  at 2 K is shown schematically in figure 2. All three  $4f^6 \ ^7F_0 - ^5D_J$  electronic transitions exhibit hole-burning. Most measurements were taken for the  $^7F_0 - ^5D_2$  transition for which the emission signal was strongest as detection through cutoff filters becomes more difficult as the excitation wavelength approaches the fluorescence wavelength.

The temperature dependence of hole widths burnt in the  $^7F_0 - ^5D_2$  transition suggested two regions, the dependence being stronger above about 15 K. The power dependence of the hole width at 1.7 K showed that the homogeneous linewidth is neither lifetime (0.72 ms) nor laser linewidth (nominally 1 MHz) limited [4]. The dephasing mechanism below about 15 K is therefore attributed to a different mechanism to the dominant interaction at higher temperatures.

The temperature dependence of holes widths burnt in all  $^7F_0 - ^5D_J$  transitions between 15-90 K is shown in figure 3. Holes burnt at the same temperature in different transitions have similar widths and best fit analysis reveals hole widths for all transitions are described by  $T^{2.8 \pm 0.2}$ .

Holes burnt in the  $^7F_0 - ^5D_2$   $\text{Sm}^{2+}$  transitions of  $\text{Sr}_{0.5}\text{Mg}_{0.5}\text{FCl}_{0.5}\text{Br}_{0.5}$  and  $\text{Sr}_{0.65}\text{Ba}_{0.35}\text{FCl}_{0.5}\text{Br}_{0.5}$  show little variation from those burnt for the same transition in  $\text{BaFCl}_{0.5}\text{Br}_{0.5}$  (figure 4). Powers an order of magnitude greater were required to burn holes in  $\text{Sr}_{0.65}\text{Ba}_{0.35}\text{FCl}_{0.5}\text{Br}_{0.5}:\text{Sm}^{2+}$  but the hole width was little affected suggesting power broadening to be insignificant and the holes to be good probes of dephasing processes. As the hole widths for all compounds are similar, it is concluded that the magnitude and source of optical dephasing in this class of materials are equivalent.

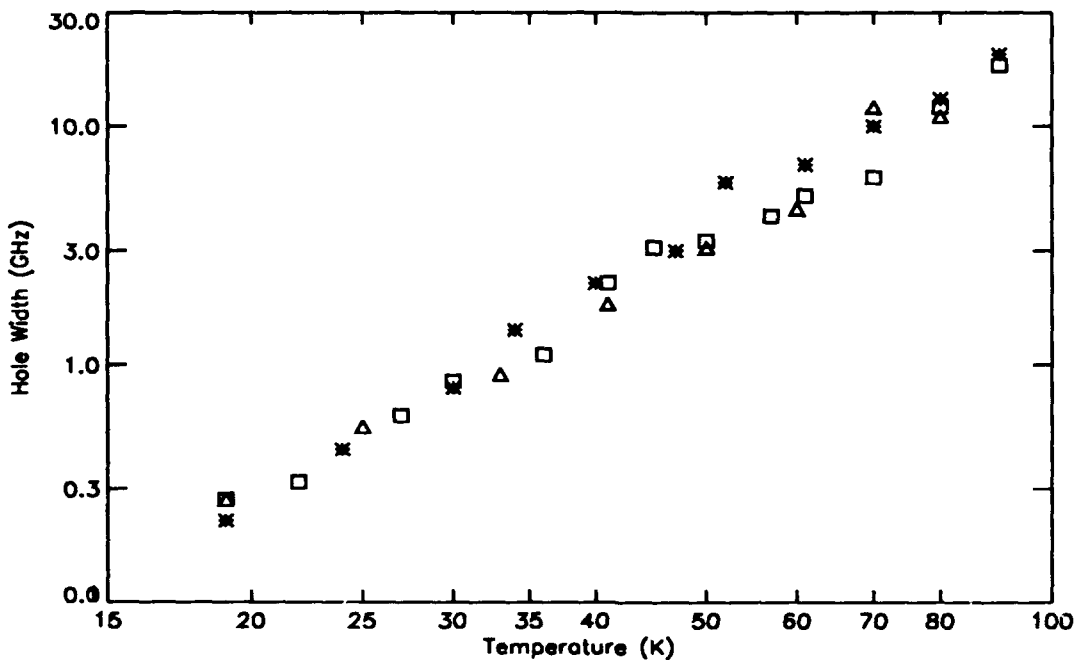


FIGURE 3. The temperature dependence of hole widths for the  ${}^7F_0-5D_0$  ( $\Delta$ ),  ${}^7F_0-5D_1$  ( $\square$ ) and  ${}^7F_0-5D_2$  ( $*$ ) transitions in  $BaFCl_{0.5}Br_{0.5}:Sm^{2+}$ .

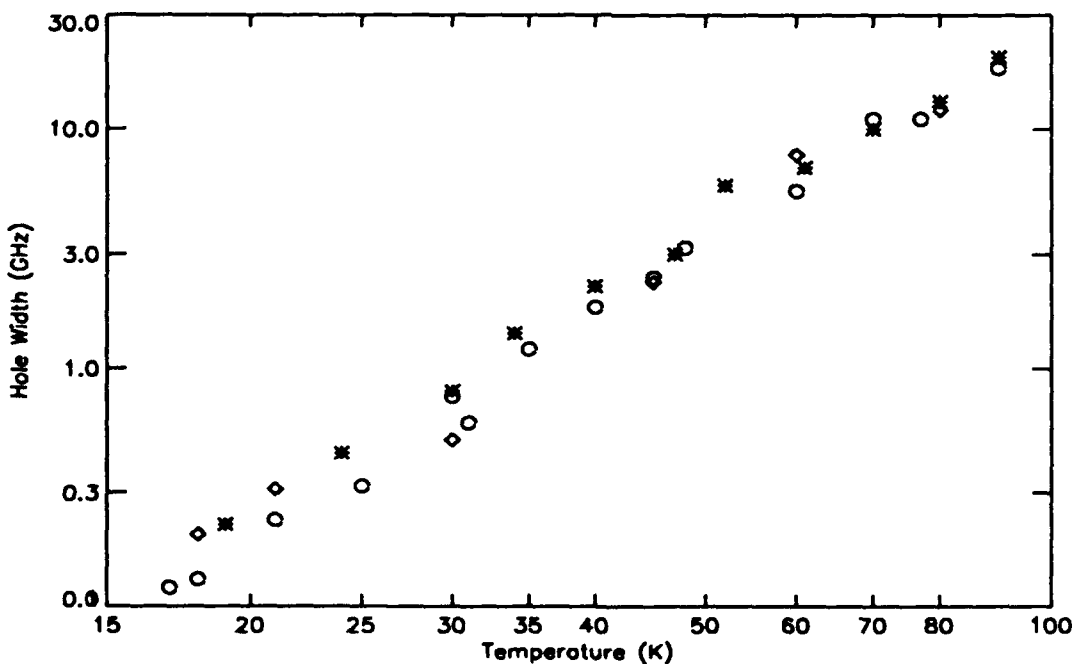


FIGURE 4. The temperature dependence of hole widths for the  ${}^7F_0-5D_2$  transitions in  $BaFCl_{0.5}Br_{0.5}:Sm^{2+}$  ( $*$ ),  $Sr_{0.5}Mg_{0.5}FCl_{0.5}Br_{0.5}:Sm^{2+}$  ( $\circ$ ) and  $Sr_{0.65}Ba_{0.35}FCl_{0.5}Br_{0.5}:Sm^{2+}$  ( $\diamond$ ).

The universality of the dephasing process is further demonstrated by room temperature hole-burning. Figure 1 shows a hole burnt at 300 K in the  ${}^7F_0-{}^5D_1$  line using 5 mW of light for 10 minutes, burnt and measured using a Coherent 899 autoscan dye laser. The best fit width, 0.26 nm, is twice the homogeneously broadened room temperature fluorescence linewidth, 0.13 nm [3], of the same transition in  $\text{BaFCl:Sm}^{2+}$ . The temperature dependence of the fluorescence linewidths of the  ${}^7F_J-{}^5D_J$  transitions in  $\text{BaFCl:Sm}^{2+}$  have been studied between 100-500 K [6] and the behaviour attributed to coupling of the impurity ions to a Debye distribution of phonons [7]. Though only one hole-burning measurement has been made in this region, it is reasonable to expect hole widths to confirm this assignment. At 90 K, discrepancy from the model is still small but at lower temperatures other contributions may dominate. It is thought that magnetic coupling between the halide ions and the  $\text{Sm}^{2+}$  impurities may make one such contribution.

The hole shown in figure 1 was remeasured two days later and it was found to have decayed to half its previous depth. It is conceivable, however, that this hole degradation was due to a small movement of the laser spot to a partially unburnt region of the sample in the intermediate time.

The initial results presented here show that homogeneous broadening processes may be studied using spectral hole-burning over more than three orders of magnitude by the introduction of disorder to the lattice. In the case of this class of systems the inhomogeneous broadening appears to be dominated by the contribution of the halide, rather than the cationic, disorder as inhomogeneous linewidths for all materials studied were 2-2.5 nm. Most importantly, however, the substitutional disorder does not appear to affect homogeneous processes. The observation of room temperature persistent spectral hole-burning has obvious implications for optical data storage and it is thought that similar investigations of other classes of disordered host/impurity systems could provide an ideal material.

### Acknowledgements

The authors would like to thank Professor J. Yu of the Changchun Institute of Physics for the kind gift of the samples used in this study and Dr. Bern Kohler for his invaluable assistance with the high temperature hole-burning experiments. This work was supported by the Swiss National Science Foundation.

### References

- [1] A. Winnacker, R. M. Shelby and R. M. Macfarlane, *Opt. Lett.* 10 (1985) 350
- [2] L. Zhang, J. Yu and S. Huang, *J. Lumin.* 45 (1990) 301
- [3] C. Wei, S. Huang and J. Yu, *J. Lumin.* 43 (1989) 161
- [4] C. Wei, K. Holliday, A. J. Meixner, M. Croci and U. P. Wild, *J. Lumin.*, in print
- [5] A. Oppenländer, F. Madeore, J.-C. Vial and J.-P. Chaminade, *J. Lumin.*, in print
- [6] B. Birang, A. S. M. Mahbub'ul Alam and B. Di Bartolo, *J. Chem. Phys.* 50 (1969) 2750
- [7] D. E. McCumber and M. D. Sturge, *J. Appl. Phys.* 34 (1963) 1682

Spectral hole burning between 2 K and room temperature  
in  $\text{Sm}^{2+}$  doped substitutionally disordered microcrystals

R. Bilmers, J. Davis, M. Squicciarini  
U.S. Naval Air Development Center  
Warminster, PA 18974

### Theory of Filter Operation

Filter operation is achieved by depleting the ground state population of molecules whose local environments are within the bandwidth of the hole-burning pump laser.

Hole-burning is achieved in these systems via a mechanism known as triplet-trapping which is shown in Figure 1. The first step in this mechanism is absorption from the ground singlet state,  $S_0$ , to the first excited singlet state,  $S_1$ , in the dye molecule. For most laser dyes, most of the population returns to the ground state via prompt fluorescence. Some of the population, however, is transferred to the lowest-lying triplet state,  $T_1$ , via spin-orbit coupling assisted intersystem crossing. Typical branching ratios for intersystem crossing are approximately 10%. The lifetime of the  $T_1$  to  $S_0$  transition in solid matrices at low temperatures is very long. Tompkin and Boyd<sup>1</sup> reported a 2.5 S lifetime for fluorescein in boric acid glass at 200 K. This metastable triplet level therefore acts to trap population and prevent it from returning to the ground state.

Polyatomic molecules exhibit picosecond relaxations between vibrational levels in the same electronic state. This means that only the zero-phonon line is saturable in this scheme. Tuning of this filter can be achieved because the ZPL is inhomogeneously broadened due to local-field effects in the amorphous host. Only molecules whose energies overlap the laser linewidth will absorb and be trapped in the triplet state, all others remain in the ground state to absorb unwanted photons at other wavelengths.

---

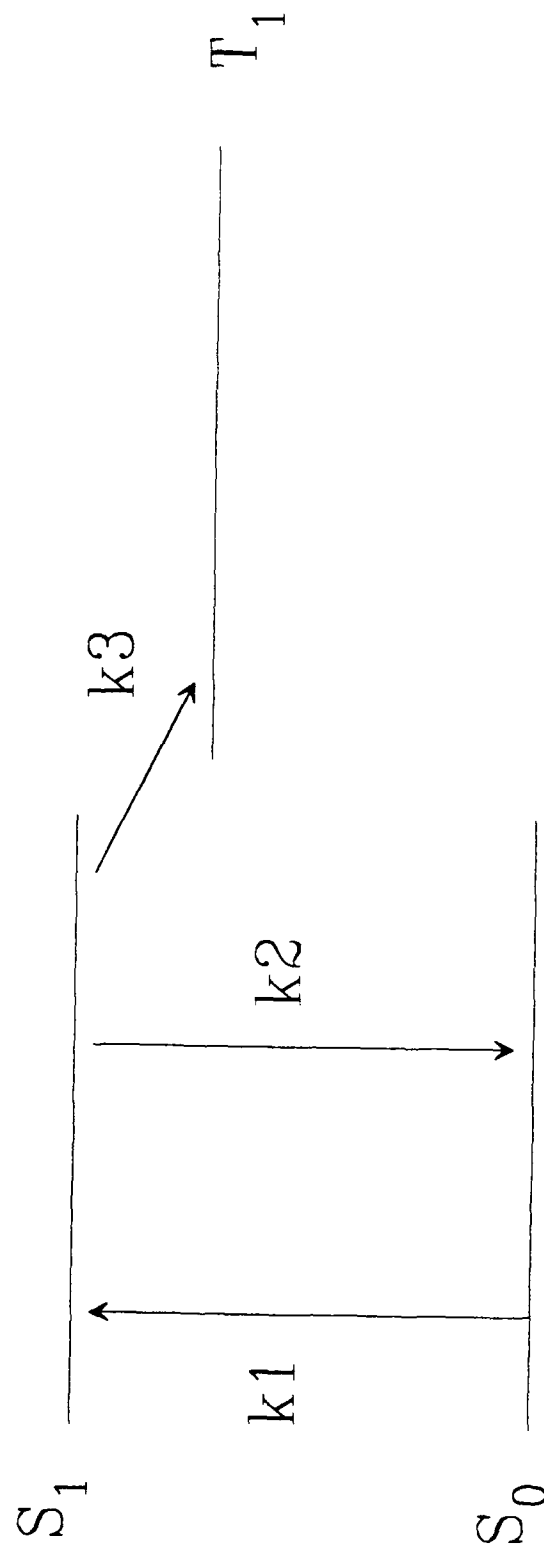
<sup>1</sup> Tompkin, W. R; Malcuit, M. S; Boyd, R. W; Applied Optics, **29** (1990), p. 3921

## Modeling Filter Performance

A model was developed to predict the performance of this filter for various dyes in various hosts. The model is based on the kinetics of the three-level system in Figure 1. While the details of the kinetic analysis will be dealt with in the presentation, the results of the analysis indicate that a pulsed laser with 100 KW of peak power and a repetition rate of 1000 Hz will yield a ground state depletion of 95% in Rhodamine after 110 consecutive pulses. The hole would be 30 - 50 % transmissive.

The width of the hole is also important to the filter performance. The width was modeled with a phonon-broadened term and a power broadened term. The phonon broadening was assumed to be proportional to  $T^{-1.3}$  with the constant of proportionality varying with host material. Several polymeric hosts were considered with phonon-broadened linewidths varying from 20 GHz to 125 GHz at 77 K. The power broadened linewidth was determined to be a function of the laser power, the transition dipole moment, the natural lifetime, and the total optical dephasing time. The power-broadened term is therefore dependent on the phonon-broadening in the system and so the holewidth was modeled as a function of both temperature and pump power for each dye/host system. The results show that Rhodamine 6G in Polyethylene at 77K pumped by a 100 KW laser pulse should exhibit a hole-burnt linewidth of approximately 40 GHz. The results of other systems will be discussed in the presentation.

Figure 1 - Three-Level Model Used to Explain "Triplet Trapping"



## Hole Burning of the Exciton Coupled Antenna Complex of *Rhodobacter Sphaeroides*

N. R. S. Reddy and G. J. Small  
Ames Laboratory-USDOE and Department of Chemistry,  
Iowa State University, Ames, Iowa 50011  
Tel: (515) 294-3859

Efficient energy transfer in light harvesting (LH) complexes forms an important part of the photosynthetic process that results in the conversion of light energy into chemical free energy. A number of factors are important for understanding the process that directs the optical excitation to the reaction center. Included are the nature of relevant excited states of chlorophylls (e.g. localised or delocalised), bath induced mechanisms for homogeneous broadening of transitions etc. . The  $Q_y$ -absorption ( $S_1$ ) of chlorophyllic molecules in protein complexes appears as inhomogeneously broadened bands with  $\Gamma_I \sim 50 - 200 \text{cm}^{-1}$  at liquid helium temperatures.

Hole burning has predominantly been used for the determination of homogeneous widths ( $\Gamma_H$ ), especially of the zero phonon line. In addition to contributions from linear electron-phonon coupling ( $\Gamma_{ep}$ ) and the excited state lifetime ( $1/2\pi T_1$ ), in photosynthetic systems excitonic level structure and scattering can contribute ( $\Gamma_{ex}$ ) significantly to  $\Gamma_H$ .

$$\text{i.e. } \Gamma = \Gamma_I + \Gamma_H = \Gamma_I + \Gamma_{ex} + \Gamma_{ep} + \Gamma_{T_1}$$

Burn wavelength dependent hole burned spectra only provide values of  $\Gamma_I$  and  $\Gamma_H$ . The problem of separating out the contributions of  $\Gamma_{ep}$  and  $\Gamma_{ex}$  to  $\Gamma_H$  still remains. Based on a novel vibronic satellite vibronic hole narrowing phenomenon, we have developed a method for determining  $\Gamma_{ex}$  in amorphous solids.

The LH antenna of *Rb. sphaeroides* is comprised of two main complexes, B800-B850 and B875, with the former peripheral to the latter, which surrounds and interconnects the reaction center. Based on their structures, significant excitonic interactions between the B850 molecules and also between the B875 molecules are expected to occur [1,2]. The absorption spectra for the mutant and wild type *Rb. Sphaeroides* are shown in fig 1 and 2 respectively. The absorption bands due to B800, B850 and B875 have widths of 170, 280 and 280  $\text{cm}^{-1}$  respectively. Figure 1 shows holeburned spectra obtained with  $\lambda_B$  (burn wavelength) tuned to within the B800 (a,b) and B850 (c) bands. The narrow ZPH at  $\lambda_B$  measured in high resolution has a width of

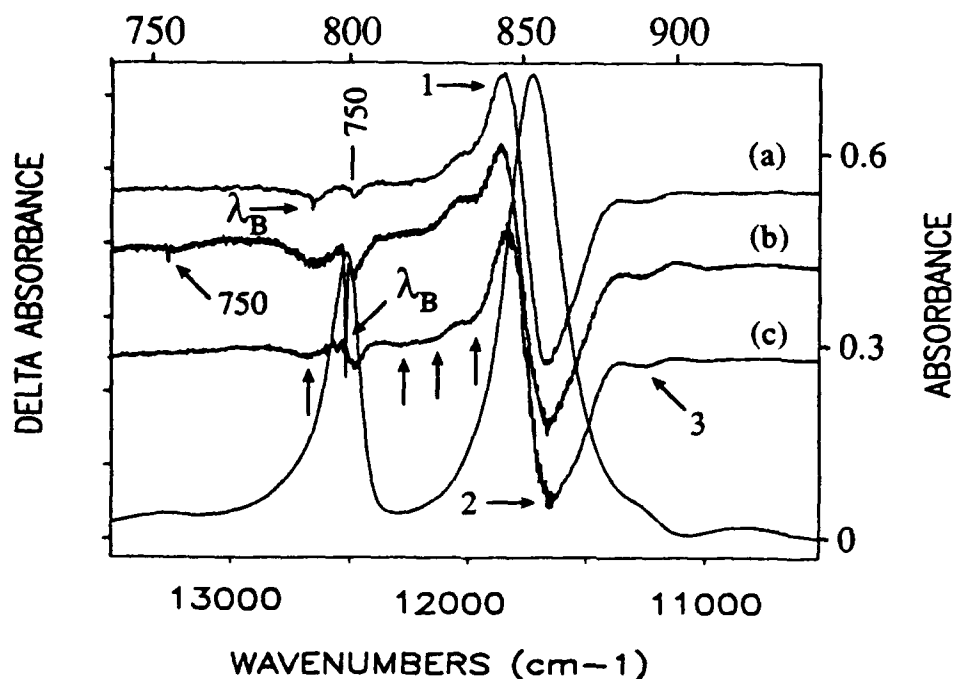


Figure 1. Absorption and hole burned ( $\Delta$  absorbance) spectra (4.2 K) of mutant NFCr chromatophores of *Rb. sphaeroides*. Typical burn conditions for obtaining the holeburned spectra were  $300 \text{ mW/cm}^2$  for 30 mins. The read resolution is  $2 \text{ cm}^{-1}$ . Burn laser frequency is denoted by  $\lambda_B$  in spectra (a) and (b) and in spectrum (c) =  $11760 \text{ cm}^{-1}$ . Hole marked 750 in (a) and (b) refer to the vibronic hole of the dominant intramolecular vibrational mode of BChl a building on B850 (a) and ZPH at (b) respectively. Feature 3 is the hole burned in the residual B875 band. Unlabelled vertical arrows refer to various vibronic holes building on the B850 hole. The upper horizontal scale gives the wavelength in nm and the right vertical axis refers to the absorption spectrum.

$4.2 \pm 0.5 \text{ cm}^{-1}$  corresponding to an excited state lifetime of  $2.3 \pm 0.1 \text{ ps}$  which agrees well with the B800 $\rightarrow$ B850 energy transfer time observed in picosecond experiments [3,4]. The broad hole labelled 2 is a non photochemical hole in B850 holewidth due to burning in B850 following its population primarily by energy transfer from B800. The broad B850 hole width ( $210 \pm 20 \text{ cm}^{-1}$ ) and the peak position are independent of  $\lambda_B$  within B850 band leading to [5]  $\Gamma_H(\text{minimum}) \sim 200 \text{ cm}^{-1}$ .

Holeburned spectra obtained as a function of  $\lambda_B$  within the B800 band prove that the broad holes in the near vicinity of the ZPH are vibronic satellite holes which build on the broad holes which build on B850 origin hole and that the electron phonon coupling for B800 band is weak. However, the vibronic satellite holes are significantly sharper than

the origin hole which they build upon. In spectrum (a) of figure 1, the  $750\text{ cm}^{-1}$  vibronic hole that builds upon the B850 hole has a width of  $60\text{ cm}^{-1}$ . The Franck-Condon factor for this vibration is determined to be 0.05 [6]. If the homogeneous broadening of B850 were due to strong linear electron phonon coupling or ultra-fast ( $<30\text{ fs}$ ) excited state relaxation, the vibronic hole should have the same width as the B850 origin hole. This 'discrepancy' can be explained if the homogeneous width is interpreted as due to excitonic interactions. The transition dipole moment, which directly determines the magnitude of exciton splittings, is apportioned between the origin band and the vibronic bands on the basis of Franck-Condon factors causing the vibronic hole to be "Franck-Condon factor narrowed" relative to the origin hole [7]. The B850 unit cell symmetry results in exciton level splittings but transitions to all levels may not be dipole allowed. However, diagonal energy disorder between symmetry related subunits of the unit cell will cause level mixing and removal of degeneracies when the energy disorder becomes comparable to the zero order exciton level splittings. If the homogeneous width of B850 band is taken to be equal to the hole width ( $210\text{ cm}^{-1}$ ), the excitonic contribution to the  $750\text{ cm}^{-1}$  vibronic hole is  $\sim 10\text{ cm}^{-1}$ . The vibronic relaxation contribution is less than  $10\text{ cm}^{-1}$  implying that the  $60\text{ cm}^{-1}$  width is mainly due to site inhomogeneous broadening  $\Gamma_I$ . This is consistent with the absorption linewidth being equal to  $280\text{ cm}^{-1}$ . Thus  $\Gamma_H = 210\text{ cm}^{-1}$  is a reasonable estimate for the *minimum* exciton bandwidth. This interpretation of the homogeneous width also explains why the energy transfer between the B800 $\rightarrow$ B850 energy transfer rate is only weakly temperature dependent. This is expected for Forster transfer when either or both of the homogeneous broadenings for the donor and acceptor states in the low temperature limit is  $\geq kT$  at room temperature ( $\sim 200\text{ cm}^{-1}$ ).

Similar effects were observed for the B875 band (wild type) leading to a  $\Gamma_H(\text{minimum})\sim 200\text{ cm}^{-1}$  for B875. From these spectra the BChl a modes participating in the Forster energy transfer process can be identified as  $750\text{ cm}^{-1}$  and  $910\text{ cm}^{-1}$  for the mutant (Fig 1) and  $1210\text{ cm}^{-1}$  for the wild type (Fig. 2). Our holeburning results on B875 predict the B850 $\rightarrow$ B875 energy transfer rate to be only weakly temperature dependent. In recent hole burning studies on the wild type *Rb. sphaeroides*, narrow ZPH could be burned on the low energy side of the B875 band (896 nm). The hole width observed in these spectra ( $3\text{ cm}^{-1}$ ) is inconsistent with the energy transfer times observed in time resolved experiments. Alternative interpretations for the holewidth are currently being developed.

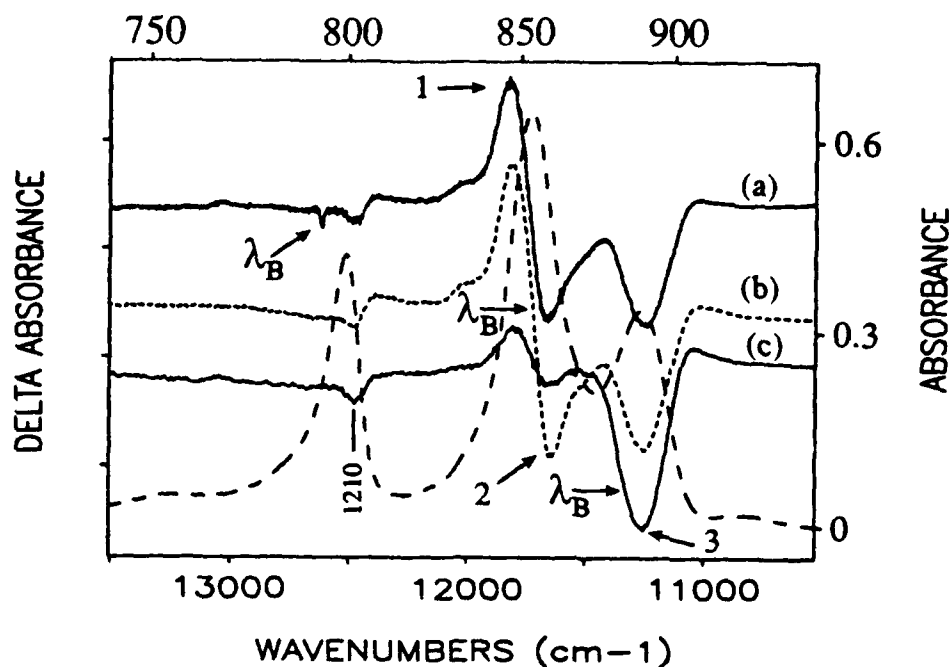


Figure 2. Absorption and hole burned ( $\Delta$  absorbance) spectra of wild type chromatophores. Typical burn conditions are as in Fig. 1. Burn laser frequency for spectrum (c) is  $11363 \text{ cm}^{-1}$ . The read resolution is  $4 \text{ cm}^{-1}$ . Hole marked 1210 refers to the vibronic holes due to intramolecular vibrational modes of BChl a building on B850.

## REFERENCES

- 1) C. N. Hunter, R. Van Grondelle and J. D. Olsen, *Trends Biochem. Sci.* 14 (1989) 72.
- 2) R. M. Pearlstein and H. Zuber, in: *Springer Series in Chemical Physics 42: Antennas and Reaction Centers of Photosynthetic Bacteria*, ed. M. E. Michel-Beyerle (Springer-Verlag, Berlin, 1985) p 53.
- 3) H. Zuber, *Photochem. Photobiol.* 42 (1985) 821.
- 4) H. Bergstrom, V. Sundstrom, R. Van Grondelle, T. Gillbro and R. Cogdell, *Biochim. Biophys. Acta* 936 (1988) 90.
- 5) J. M. Hayes, J. K. Gillie, D. Tang and G. J. Small, *Biochim. Biophys. Acta* 932 (1988) 287.
- 6) N. R. S. Reddy, G. J. Small, M. Siebert and R. Picorel, *Chem. Phys. Letts.* (in press).
- 7) R. M. Hochstrasser, *Molecular Aspects of Symmetry* (W. A. Benjamin, Inc., New York, 1966) Chapter 10.

## Free Volume Model of Thermally Induced Spectral Diffusion

Jun Tsuchiya, Jun-ichi Takahashi, and Hiroshi Tanaka

Central Research Laboratories, Idemitsu Kosan Co., Ltd.

1280 Kami-izumi, Sodegaura, Chiba 299-02 JAPAN.

telephone 81-438-75-7214

telefax 81-438-75-4373

### Introduction

An organic dye/polymer system, such as free base phthalocyanine ( $H_2Pc$ ) dispersed in polymethylmethacrylate (PMMA), has been interested in as a model material of new mass-storage for photochemical hole burning (PHB)[1]. There are, however, some unsolved problems in applying it to a practical memory system. That is, the influence of polymers as a matrix over the static and dynamic properties of the system, such as, thermally induced spectral diffusion (TISD), homogeneous and inhomogeneous line width, burning efficiency and so on, has not been solved yet. TISD among them has a strong correlation to micro environment of a polymer dispersing a dye. The disorders in amorphous polymers are seen in wide energy range whose upper limit is determined by the glass transition of polymers. However, the lower limit is still left unknown, although some phenomena are known which are affected by low energy excitation. Recently, hole burning spectroscopy was successfully applied to investigate in the lower energy region [2]. Thermally induced conformation changes of polymers are said to have energy of same size to cause TISD in the lower energy region. Koehler et al. succeeded in explaining the changes quantitatively from a combination of three independent processes, 1- phonon tunneling process, 2-phonon Raman scattering process and activation process [3]. The material parameters, however, that determine the changes are still unknown. We report TISD results of some dye/polymer systems and correlation between TISD and polymer properties.

## Experimental

The dyes employed in this study are tetraphenoxypthalocyanine (TPPc) and tetra-tert-butylphthalocyanine (TBPc). And the polymers employed are polystyrene (PS), poly(o-methylstyrene) (o-MePS), poly( $\alpha$ -methylstyrene) ( $\alpha$ -MePS), polymethylmethacrylate (PMMA), polyisobutylene (PIB), polyethylene (PE) and poly(4-methyl-1-pentene) (P4M1P). The dyes and polymers were dissolved in organic solvent like dichloromethane and toluene except for insoluble polymers like PE and P4M1P. The dye/polymer solution was cast and dried. And a sample film was heated to melt for eliminate trace of solvent. Hole burning was done at 6K with a pulsed dye laser (Lambda Physik FL2002) excited by a XeCl excimer laser (Lambda Physik EMG50). And samples were heated up to excursion temperature and cooled down to 6K. ZPH spectra were fitted by Lorentzian.

## Results and discussion

An example of TISD data is presented in Fig.1. The temperature dependency curve of hole width is well represented by straight line. However, in the case of some samples like TBPc/PE, there was a particular temperature that the discrepancy from the straight line began. In these cases, from the slope of straight line in lower temperature region, we obtained the irreversible broadening rate K. Obtained K and packing density  $\rho$  (by Bondi[4]) are listed in Table 1. The packing density  $\rho$  is calculated by dividing molar van der Waals volume of monomer by polymer volume of 1 mol monomer. Fig. 2 shows that obtained K were dependent on packing density  $\rho$ . This correlation suggests that TISD was dependent on micro unoccupied volume of polymer. The fitted curve is

$$K = 1.8 \times 10^2 \times \exp\left(\frac{4}{\rho - 1}\right)$$

which has the same form with Doolittle type equation for describing the viscosity of melting polymers. Cohen and Grest [5] showed that Doolittle type equation is derived from entropical re-orientation of unoccupied volume. Then, the correlation we found suggests that TISD was caused by re-orientation of unoccupied volume from conformational change in polymer matrix.

## Conclusion

TISD coefficients K were obtained from the slope representing TISD temperature dependency in lower region. We found the correlation between K and Bondi's packing density  $\rho$  was well fitted in Doolittle type equation. This correlation suggests that TISD was caused by reorientation of unoccupied volume in polymer.

## References

- [1] Gutierrez, A. R.; Friedrich, J.; Haarer, D.; Wolfrum, H., *IBM J. Res. Devel.*, **1982**, *26*, 198
- [2] Koehler, W.; Friedrich, J., *J. Chem. Phys.*, **1988**, *88* (10), 6655
- [3] Koehler, W.; Friedrich, J., *Europhys. Lett.*, **1988**, *7* (6), 517
- [4] Bondi, A., *J. Phys. Chem. Solids*, **1967**, *28*, 649
- [5] Cohen, M. H.; Grest, G. S. ;*Phys. Rev. B*, **1979**, *20* (3), 1077

**Table 1** Temperature coefficients of TISD K and packing density  $\rho$

dye	polymer	$K/10^{-2}\text{cm}^{-1}\text{K}$	$\rho^a$
TBPC	PIB	0.18	0.715
	PE	0.22	0.710
	PMMA	1.0	0.660
	PS	4.5	0.636
	P4M1P	2.7	0.606
TPPC	$\alpha$ -MePS	2.1	0.660
	o-MePS	2.4	0.644
	PS	4.0	0.636

a): Calculated by Bondi[4].

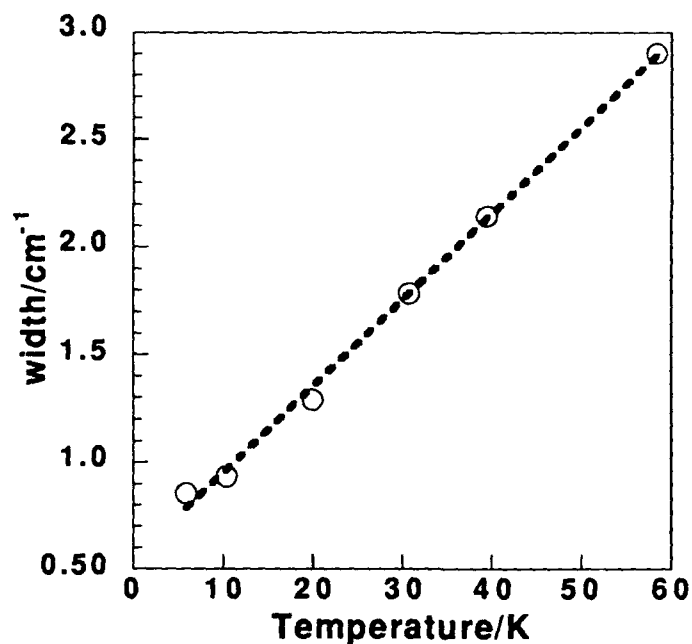


Fig. 1 Typical TISD data for TPPc/PS  
The slope is 4.0.

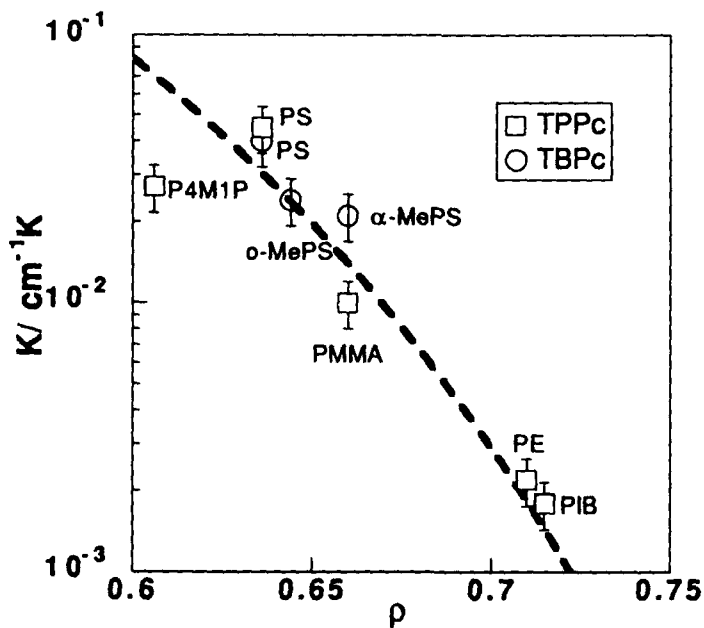


Fig. 2 Temperature coefficients of TISD (K)  
 $\rho$  is packing density of polymer calculated  
by Bondi [4].

Friday, September 27, 1991

# High Temperature and Photon Gating

**FA** 8:30am–10:30am  
DeAnza Room

A. J. Sievers, *Presider*  
*Cornell University*

Room Temperature Persistent Spectral Hole Burning using Dielectric Particles as Photonic Atoms, S. Arnold, Microparticle Photophysics Laboratory (MP<sup>3</sup>L), Department of Physics, Polytechnic University, 333 Jay St., Brooklyn, N.Y. 11201, Tel: (718)2603085

Persistent spectral hole burning at room temperature has recently been demonstrated using a 2-D collection of fluorescent spherical microparticles having a random distribution of sizes.<sup>1</sup> In this system, known as a Microparticle Hole Burning Medium (MHBM), the differences in the frequencies of Morphology Dependent Resonances (MDR) with size enables one to generate a fluorescence excitation spectrum which is heterogeneous.

MDR's are associated with photon confinement by a particle's "dielectric potential". In fact one can transform the usual electromagnetic vector wave equation into a Schrodinger equation which reveals modal functions which are analogous to wavefunctions of electrons in an atoms. However, unlike states in a conventional atom the modes of a "photonic atom" are virtual with the photon lifetime limited by leakage out of the particle.<sup>2</sup> The leakage can be extremely slow. Recent measurements reveal Q's approaching  $10^7$ .<sup>3,4</sup> Furthermore the theoretical analysis shows that each resonance occurs at a constant value of  $ka$ , where  $k$  is the magnitude of the wavevector in vacuum and  $a$  is the particle radius. Thus a collection of particles having a distribution of sizes of width  $\sigma_a$  when irradiated near a given resonance should display an inhomogeneous width  $\gamma_{ih} \approx \sigma_a \langle k \rangle / \langle a \rangle$ , where  $\langle k \rangle$  is the average wavevector of the radiation and  $\langle a \rangle$  is the average particle size. From the standpoint of hole burning the advantages of using a collection of particles as a hole burning memory are

- a. the homogeneous linewidth associated with leakage  $\gamma_h \approx \langle k \rangle / Q$  is narrow and virtually insensitive to temperature, and
- b. the inhomogeneous linewidth  $\gamma_{ih} \approx \sigma_a \langle k \rangle / \langle a \rangle$  associated with the size distribution width can be much broader since it is controlled independently.

Since fluorescence is incoherent we can model the fluorescence from such a collection of particles by adding the Mie absorption<sup>5</sup> from each of the particles. Fig.1 shows such a simulation for  $10^4$  doped polystyrene particles (refractive index =  $1.59 + 10^{-6}i$ ) having a mean radius  $\langle a \rangle$  of  $1.44 \mu\text{m}$  and a standard deviation to average size ratio  $\sigma_a / \langle a \rangle$  of 0.01. Although the absorption due to a given particle within the distribution shows distinct resonances at which the

absorption increases by more than a factor of 10, the collective absorption of all  $10^4$  particles (Fig.1, top curve) shows only small variations in intensity with wavelength. Now we suppose that an intense laser is projected onto the distribution at a wavelength  $\lambda_w$  of 588.3nm. As a consequence of photochemical bleaching the fluorescence from each particle will fall with exposure time with the rate of photolysis in proportion to the absorbed power,  $P$ . Using an exponential recipe the fluorescence from each particle is multiplied by  $F(a, \lambda_w) = \exp[-\beta P(a, \lambda_w)/P(\langle a \rangle, \lambda_w)]$ , where  $\beta$  is a parameter which is proportional the incident intensity of the photolyzing light, the quantum efficiency for photolysis and time. Fig.1 shows fluorescence excitation spectra with a hole at  $\lambda_w$ , distinct from the noise due to number fluctuations, after photolysis ( $\beta = 1$  or 20).

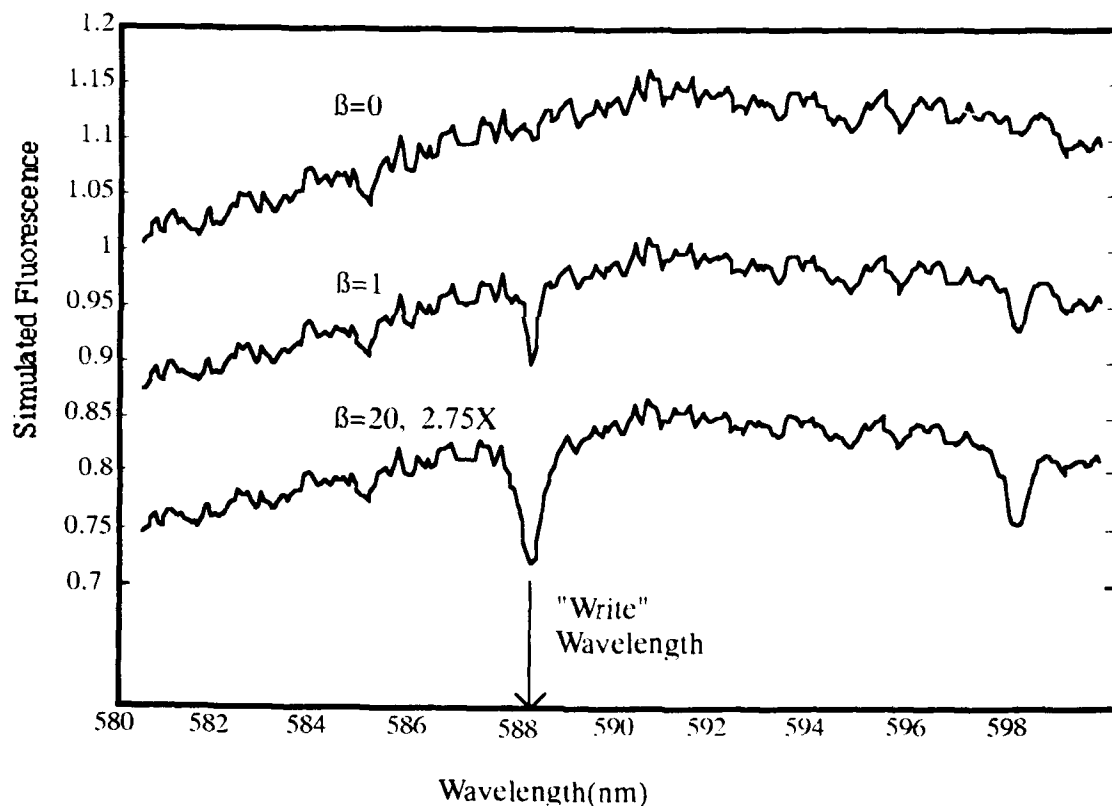


Fig.1. Fluorescence excitation spectra before ( $\beta = 0$ ) and after two simulated burns ( $\beta = 1$  and 20) on a particle distribution with  $\langle a \rangle = 1.44 \mu\text{m}$  and  $\sigma_a/\langle a \rangle = 0.01$ .

The hole at 588.3nm is apparent. The increased broadening of this hole with increasing  $\beta$  is due to saturation effects. As one can also see there is a subsidiary hole at 598nm.

To test our basic idea, experiments were carried out on Nile red dyed latex particles ( $\langle a \rangle = 12.1 \mu\text{m}$ ,  $\sigma_a = 2.2 \mu\text{m}$ , concentration  $\approx 10^{-4}\text{M}$ ). These particles were placed on a cover glass and irradiated on the stage of a fluorescence microscope with a tunable dye laser. The particles appeared to be in one layer with each particle touching at least one of its neighbors. The excitation spectrum of the fluorescence from approximately 2000 particles in an area of  $1\text{mm}^2$  is shown in Fig.2a. Following this scan at 0.4mW for 10 min. the laser wavelength was fixed at 572.5nm and the sample was irradiated for 5 min. at  $40\text{W}/\text{cm}^2$ . Fig.2b shows the resulting excitation spectrum taken under the same conditions as in Fig.2a. The overall reduction in luminescence of the scan in Fig.2b in comparison with

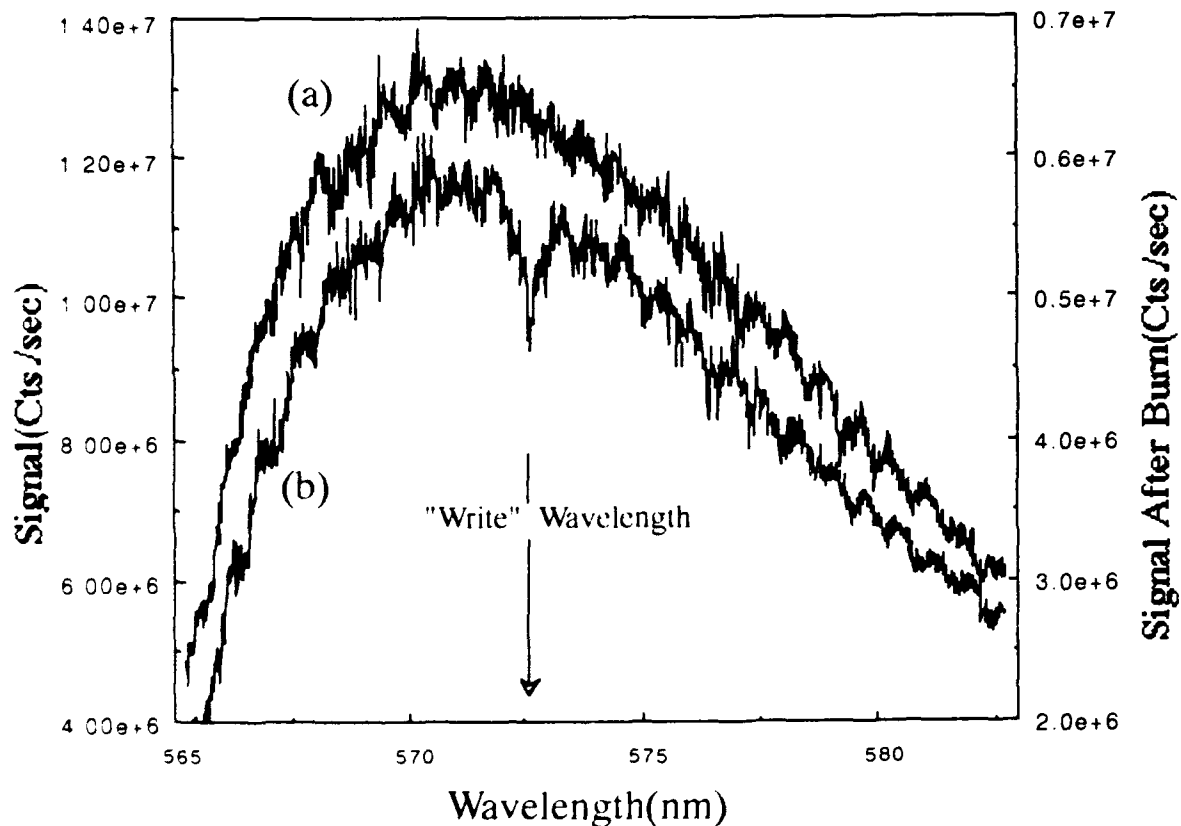


Fig 2 Fluorescence excitation spectra taken (a) before and (b) after projecting a relatively intense laser onto the sample at 572.5nm

Fig.2a is due to phoytolysis of the Nile red dye. The "hole" in the spectrum in Fig.2b at 572.5nm is apparent. The effect does not have a predominant surface sensitivity. Similar effects were obtained on an Al surface. The width of holes produced in these particles were approximately  $1\text{ \AA}$ , or  $\sim 2 \times 10^{-4}$  of the wavelength.

The width of the hole in Fig.2 is much larger than would be expected from the largest Q's measured on dielectric particles of  $10^7$ .<sup>2,3</sup> On this basis the hole width would be expected to be  $\sim 10^{-3} - 10^{-4} \text{ \AA}$ . The larger width in the microparticle hole burning spectra may be understood, however, in terms of a severe reduction in the photon lifetime within the particles at resonance due to absorption. The rate of decay for a trapped photon in the presence of absorption is approximately  $(c/n)\rho_a\sigma_a$ , where  $\rho_a$  is the density of absorbers,  $\sigma_a$  is the cross section for absorption, and  $c/n$  is the speed of light in a material of refractive index  $n$ .<sup>3,6</sup> If this absorption dominates over leakage then the width of a resonance divided by its frequency  $\omega_r$  will be  $(c/n)\rho_a\sigma_a/\omega_r$ . Since the width of a hole is related through a convolution to the width of a resonance, the ratio of the width of a hole to the frequency should be  $2(c/n)\rho_a\sigma_a/\omega_r$ . From the molar extinction of Nile red and the concentration of dye in our particles we calculate this ratio to be  $\sim 1.5 \times 10^{-4}$  in good agreement with the measured value of  $\sim 2 \times 10^{-4}$  and three order of magnitude above the lowest value which can be anticipated. Therefore we anticipate considerably sharper holes at reduced dye concentration.

It is interesting to note that interactions between neighboring particles do not seem to be an important source of line broadening at least down to the Angstrom level even though particles are touching. We have recently investigated this effect theoretically by the method of Fuller<sup>7</sup> for one particle in contact with another of a different size and find that as long as the exciting radiation is directed perpendicular to the line joining the particles there is no significant interparticle coupling.

1. S. Arnold, C.T. Liu, W.B. Whitten and J.M. Ramsey, *Opt. Lett.* **16**, 420(1991).
2. J.-Z. Zhang, D.L. Leach, and R.K. Chang, *Opt. Lett.* **13**, 270(1988).
3. S. Arnold and L.M. Folan, *Opt. Lett.* **14** 387(1989).
4. H.M. Nussenzveig, *Comments At. Mol. Phys.* **23**, 175(1989).
5. C.F. Bohren and D.R. Huffman, "Absorption and Scattering of Light by Small Particles", John Wiley, New York 1983
6. P.T. Leung and K. Young, *J. Chem. Phys.* **89**, 2894(1988).
7. K.A. Fuller, *Applied Optics*(in press)

## Room Temperature Persistent Spectral Hole Burning in Distributions of Optical Cavities: A Simple Fabry-Perot Model

Dee William Pack, The Aerospace Corporation, P.O. Box 92957, M2/251, Los Angeles, 213-336-5645  
Steve Arnold, Physics Department, Polytechnic University, 333 Jay St, Brooklyn, NY, 718-260-3085

### Cavity Spectra and Hole Burning

Efforts to create materials in which to burn holes at higher temperatures face an inherent contradiction: the need for inhomogeneous line broadening from host-guest interactions, vs. the desire to limit the homogeneous line broadening from thermal fluctuations of host-guest interactions (i.e. phonon broadening). A different approach to the question of how to burn holes at high temperatures was recently conceived and experimentally confirmed.<sup>1</sup> This approach relies on using distributions of chromophore-doped optical cavities as the hole burning medium. The effect was recently observed in dye-doped micro-spheres. As a simple model illustrating the important effects characteristic to these Mie theory cavity resonances in spheres, the Fabry-Perot is treated analytically and numerically in this work.

The dynamic consequences of confining emitting species in cavities has been an active topic of research in recent years. Spectroscopic aspects of doped cavities have received less attention, however. Placing optically active molecules within cavities imposes periodically varying structure on the molecular spectrum. The spectrum of dye molecules in a single cavity will contain sharp lines at wavelengths satisfying the cavity round trip equation, with widths that reflect the confinement time of the light inside the cavity. This may be thought of as the homogeneous linewidth imposed by the cavity. Arnold and co-workers<sup>1</sup> demonstrated that a distribution of cavity sizes (the radii of micro-spheres in Ref. 1) imposes an inhomogeneous spectral distribution, and that this can be taken advantage of to burn spectral holes at room temperature. Interest in this phenomena is sparked by its nature as a new type of hole burning effect, its possible utility for frequency domain optical memory, and its use to size and study the motion of distributions of micro-spheres.<sup>1</sup>

The spectrum of an optically active cavity is described by the function  $P(ka)$ , ( $k$  is  $2\pi/\lambda$ ,  $a$  is the cavity size), which has the appearance of the product of the molecular spectrum,  $M(k)$ , and the cavity spectrum,  $C(ka)$ :  $P(ka) = M(k) C(ka)$ . Strictly speaking,  $P(ka)$  will be altered by absorptive loss. Absorptive loss is neglected for the time being, as if the optically active material was behind the cavities, rather than inside. The effect of absorption can easily be introduced later, as a loss term that defines a lower, effective reflectivity. In what follows the molecular spectrum will be assumed to be homogeneously broadened, and wide enough so that it may be considered constant over the wavelength ranges considered. For a wide distribution of cavity sizes, the size dependence of the optical density would also need to be included, unless the number of absorbers was kept constant in the cavities of different sizes. Such complications are dispensed with for now. Standard hole burning theory provides a framework from which to proceed.<sup>2</sup>

We assume some distribution function of cavity sizes,  $N_0(a)$ , exists. The general formula for the spectrum of the ensemble of optically active cavities of size  $a$  is:

$$I_0(k) = \int \frac{N_0(a)}{N} P(ka) da \quad (1)$$

After irradiation, which photolyzes some of the molecules, the spectrum becomes:

$$I_b(k) = \int \frac{N_0(a)}{N} P(ka) \exp(-\beta P(k_w a)) da \quad (2)$$

where  $k_w$  denotes  $2\pi/\lambda_w$ , the subscript  $w$  referring to the writing or burning wavelength, and  $\beta$  is the burning parameter, which is the product of the burn-laser photon flux, the hole burning quantum efficiency, and the irradiation time.  $\beta$  will vary due to the modal spatial intensity variation inside the cavity. We do not treat this spatial hole burning effect in the following discussion. In the small  $\beta$  limit, adopted in what follows, this poses no concern. When  $\beta P(k_w a)$  is small, as would be the case for short burning time, Eq. (2) becomes:

$$I_b(k) = \int \frac{N_0(a)}{N} P(ka) [1 - \beta P(k_w a)] da \quad (3)$$

Recognizing  $I_0(ka)$  as one term in the above integral, adopting a uniform size distribution function ( $N_0(a)/N = 1$ ,  $a_1 \leq a \leq a_2$ ;  $N_0(a)/N = 0$ , elsewhere), and defining the hole's line shape as,  $I_h(k) = I_0(k) - I_b(k)$ , the expression for  $I_h(k)$  becomes:

$$I_h(k) = \beta \int_{a_1}^{a_2} P(ka) P(k_w a) da \quad (4)$$

### The Fabry-Perot Cavity

Examining the hole burning behavior of a distribution of planar cavities is useful because of the close analogies between their resonances and the somewhat less theoretically tractable Mie theory resonances of micro-spheres. In addition, optically active planar structures could potentially have use as a frequency domain optical memory material, as has been suggested for micro-spheres<sup>1</sup> (limitations unique to planar structures, such as diffractive loss will be discussed elsewhere).

The transmission spectral function for a non-absorbing etalon is:<sup>3</sup>

$$P(ka) = \frac{1}{1 + f \sin^2(n \cos(\theta) k a)} \quad (5)$$

where  $f$  is the contrast,  $f = 4R^2/(1-R^2)^2$ ,  $R$  is the reflectivity,  $n$  is the real part of the refractive index, and  $\theta$  is the incident angle of the reading and burning laser light and assumed to be zero for normal incidence in what follows. The hole spectrum for a uniform distribution of Fabry-Perot cavities is then described by:

$$I_h(k) = \beta \int_{a_1}^{a_2} \frac{1}{1 + f \sin^2(nka)} \frac{1}{1 + f \sin^2(nk_w a)} da \quad (6)$$

This function has some interesting limiting cases.

1. The low Q (low R) limit. For low reflectivity,  $R$ ,  $f \approx 4R^2 \ll 1$ , using,  $1/(1+x) \approx 1-x$  for  $x \ll 1$ , Eq. (6) becomes,

$$I_h(k) = \beta \int_{a_1}^{a_2} [1 - f \sin^2(nka)] [1 - f \sin^2(nk_w a)] da \quad (7)$$

After dropping constant terms and oscillating terms which integrate to zero, application of a Fourier cosine transform simplifies Eq. (7) to the familiar  $\text{Sin}(x)/x$  function:

$$I_h(k) = \frac{\beta f^2}{16} \frac{\text{Sin}[2n\Delta a(k-k_w)]}{(k-k_w)} \quad (8)$$

The linewidth in units of  $1/\lambda$ , is:  $\text{fwhm} = 1/(4n\Delta a)$ , and is dependent upon the width of the size distribution. The wider the distribution in cavity sizes ( $\Delta a = a_2 - a_1$ ), the narrower the hole width obtained. This is a feature unique to overlapping (low Q), periodic spectral functions. Holes burnt in this limit will be very weak, with a maximum depth of  $\beta f^2/16$ , where  $\beta$  and  $f$  are both small numbers. Practically, however, the extremely shallow depth limits the detectability of holes burnt in distributions of low Q cavities. The intensity of the total baseline decreases by a factor approximately equal to  $\beta$ , due to the appreciable absorption of all modes at the burning wavelength. This is another limitation on the utility of low Q cavity distributions.

Figure 1 plots the numerically integrated results of Eq. (6), illustrating the low Q hole shape for a distribution of  $10^5$  F-P cavities ranging in size from  $a = 20$ - $1000 \mu\text{m}$ , with  $R = 0.1$ ,  $n=1.5$ ,  $\beta = 0.10$ . The broad size distribution is necessary to realize a narrow linewidth, predicted to be:  $\text{fwhm} = 1/(4 \cdot 1.5 \cdot 0.098 \text{ cm}) \approx 1.7 \text{ cm}^{-1}$ . The linewidth of the  $\text{Sin}(x)/x$  function at its first two "zeros" (meaning the crossing around the y value of approximately 0.096078) in Fig. 1(B), is 0.119 nm. This is twice the fwhm linewidth for a  $\text{Sin}(x)/x$  function, giving a fwhm from the numerical

calculation of  $1.7 \text{ cm}^{-1}$ , in agreement with the analytical result for the low reflectivity limit. Hole widths are narrower than the resonance widths in this limit. The cost of this narrowness is considerable burning across the entire spectrum, and the shallowness of the hole.

**2. The high Q (high R) limit.** When reflectivity is high, the contrast is large, and successive resonances do not overlap appreciably. The hole spectrum described by Eq. (6) will then be close to Lorentzian, for  $nka \approx m\pi$ , where  $m$  is an integer. This will hold for a narrow size distribution, for the spectral shape in the vicinity of  $k = k_w$ . Using  $\text{Sin}^2(x) \approx x^2$ , and  $1/(1+fx) = (1/f) / ((1/f) + x)$ , the hole spectrum, Eq. (6) becomes:

$$I_h(k) = \beta \int_{a_1}^{a_2} \frac{1/f}{1/f + (nka - m\pi)^2} \frac{1/f}{1/f + (nk_w a - m\pi)^2} da \quad (9)$$

Eq. (9) is recognizable as the convolution of two Lorentzians. This yields a Lorentzian with a width twice that of the Fabry-Perot bandpass. In units of  $1/\lambda$  this width is:

$$\text{fwhm} = \frac{2}{\sqrt{f} \pi n \langle a \rangle} \quad (10)$$

where  $\langle a \rangle$  is the median cavity length. The hole shape tends towards a Lorentzian, with twice the width of the mean-size Fabry-Perot cavity resonance. This formula will apply whether the laser is on a resonance or not, although the hole will be weaker in the latter case.

Figure 2 compares the spectrum of a single Fabry-Perot resonance (A) with hole spectra from Eq. (6) for two size distributions. For the moment, we only consider the spectral region close to the burning wavelength, chosen to match the 590.164 nm resonance. The hole spectra are close to Lorentzian in shape, with a width twice that of the mean cavity resonance. Interestingly, this remains true for quite wide size distributions, although some deviation is noticeable for the 20-100  $\mu\text{m}$  distribution, pictured in Fig. 2 (C). Hole shapes for extremely wide distributions in the high Q limit take on a "cuspiest" appearance, but widths still do not differ greatly from the  $2/(f^{1/2}\pi n \langle a \rangle)$  value.

Figure 3 shows what happens off resonance from the burning frequency. Subsidiary holes may occur due to the repeating nature of the spectra of the cavities. An inverse relationship exists between the width of the size distribution, and the amplitude of the envelope of subsidiary holes. Higher cavity Q's also reduce the importance of the subsidiaries. Figs. 3 (A) - (C) illustrate this.

### Conclusions

Distributions of optical cavities can be exploited to create spectral holes at room temperature.<sup>1</sup> Choosing the simplest cavity, the plano Fabry-Perot, analytical equations have been derived for hole shapes in limit of both high and low Q cavities. In the high Q limit, the spectral hole shape is close to Lorentzian, with a width twice that of a cavity resonance. For distributions of cavities with low Q factors, only very weak resonant holes can be produced, possessing a  $\text{Sin}(x)/x$  line shape. While these calculations are for planar cavities, distributions of spherical cavities of the type examined by Arnold and co-workers are expected to have similar behavior in the high and low Q limits. Since micro-spheres have varying orders of resonances, their hole spectra will inevitably superimpose both cases. Other types of optical structures, such as fibers and waveguides, exhibit sharp, periodic resonances which might be exploited for optical memory purposes. In all of these systems, the fundamental limitation on data density imposed by the diffraction limit of light, is compounded by the need to have a wide distribution of cavity sizes. Broadening of the resonances through absorptive loss in the active medium is another limiting factor. Overcoming these limitations will be crucial to the utility of cavity assisted, room temperature holeburning as an optical memory technique.

### References

1. S. Arnold, C.T. Liu, W.B. Whitten and J.M Ramsey, *Opt. Lett.*, **16**, 420 (1991).
2. J. Friedrich, J.D. Swalen, and D. Haarer, *J. Chem. Phys.* **73**, 705 (1980); R. Jankowiak and G.J. Small, *Science*, **237**, 618 (1987); W.E. Moerner, editor, Persistent Spectral Hole-Burning: Science and Applications, (Springer-Verlag, Berlin, 1988).
3. J.M. Vaughan, The Fabry-Perot Interferometer: History, Theory, Practice and Applications, (IOP Publishing Ltd., Philadelphia, 1989); G. Hernandez, Fabry-Perot Interferometers, (Cambridge University Press, Cambridge, 1986). B. Chu, Laser Light Scattering, (Academic Press, New York, 1974).

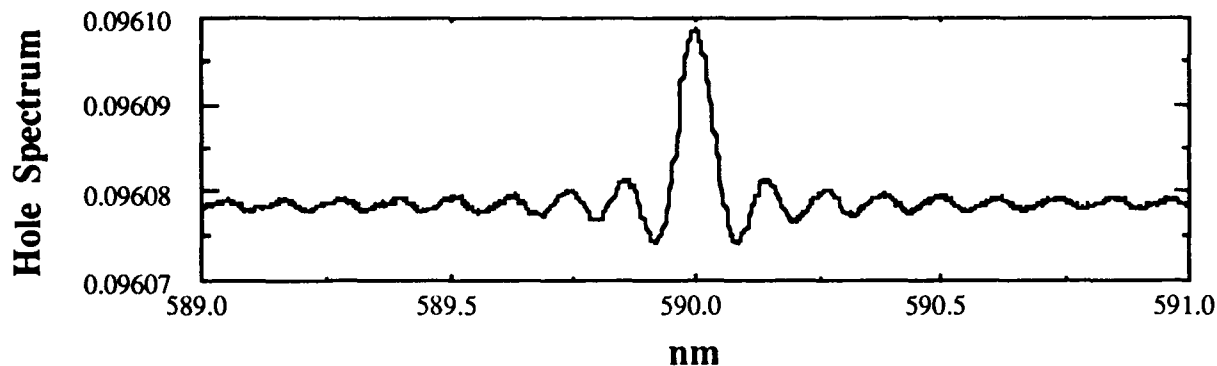


Figure 1. Hole burning in the low Q limit (low reflectivity,  $R$ ). Detail of the hole spectral function,  $I_h(\lambda) = I_0(\lambda) - I_b(\lambda)$  vs. wavelength (nm). The fwhm of the  $\text{sinc}/x$  type spectrum is closely equal to  $1/(4n\Delta a)$ , as predicted analytically.

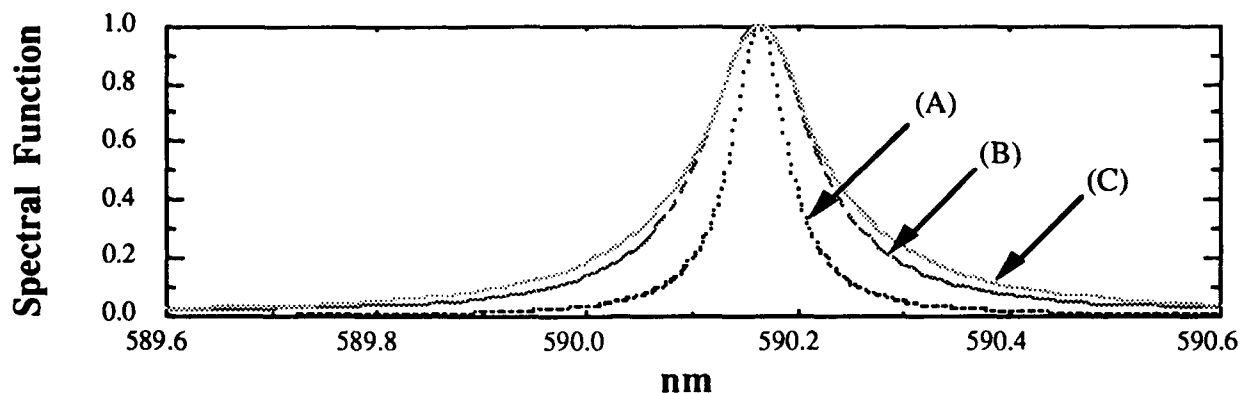


Figure 2. Spectral functions for: (A) resonance peak at 590.164 nm of a single  $a = 60 \mu\text{m}$ ,  $R = 0.95$  etalon; (B) hole spectral function,  $I_h(\lambda)$  for a  $\Delta a/\langle a \rangle = 10\%$  uniform distribution centered at  $60 \mu\text{m}$ ,  $a = 57\text{-}63 \mu\text{m}$ ,  $\beta = 0.10$ ,  $R = 0.95$ ,  $N = 1000$ ; (C) hole spectral function,  $I_h(\lambda)$  vs. wavelength (nm) for a  $\Delta a/\langle a \rangle = 133\%$  uniform distribution centered at  $60 \mu\text{m}$ ,  $a = 20\text{-}100 \mu\text{m}$ ,  $\beta = 0.10$ ,  $R = 0.95$ ,  $N = 1000$ . Holes are normalized to 1.0 for comparison to etalon transmission.  $n = 1.5$  for all.

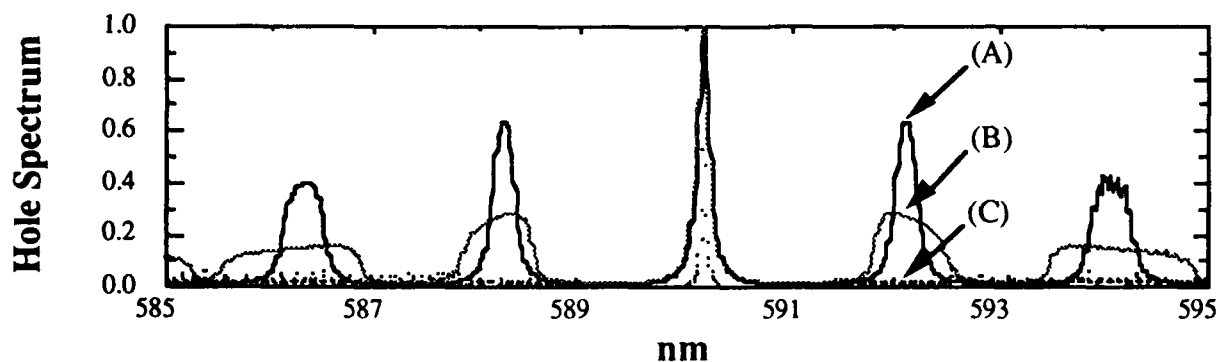


Figure 3. Hole Spectra,  $I_h(\lambda)$  for: (A)  $\Delta a/\langle a \rangle = 10\%$  uniform distribution centered at  $60 \mu\text{m}$ ,  $a = 57\text{-}63 \mu\text{m}$ ,  $\beta = 0.10$ ,  $R = 0.95$ ,  $N = 1000$ ; (B)  $\Delta a/\langle a \rangle = 33\%$  uniform distribution centered at  $60 \mu\text{m}$ ,  $a = 50\text{-}70 \mu\text{m}$ ,  $\beta = 0.10$ ,  $R = 0.95$ ,  $N = 1000$ ; (C)  $\Delta a/\langle a \rangle = 133\%$  uniform distribution centered at  $60 \mu\text{m}$ ,  $a = 20\text{-}100 \mu\text{m}$ ,  $\beta = 0.10$ ,  $R = 0.99$ ,  $N = 10,000$ . Holes are normalized to 1.0. Subsidiary holes are reduced by widening the size distribution and increasing Q.

## Inhomogeneous Broadening and Persistent Spectral Hole-Burning of Divalent Samarium Ions In Alkaline Earth Metal Halides

Jiahua ZHANG, Changchun Institute of Physics, Academia Sinica, 1 Yan-an Road, Changchun 130021, P.R.China, Phone, (0431) 52215-120

Xiangjun WANG, Tianjin Institute of Technology, Tianjin 300191, P.R.China, Phone, 318495

Shihua HUANG, Changchun Institute of Physics, Academia Sinica, 1 Yan-an Road, Changchun 130021, P.R.China, Phone, (0431) 52215-120

Jiaqi YU, Changchun Institute of Physics, Academia sinica, 1 Yan an Road, Changchun 130021, P.R.China, Phone, (0431) 52215-120

### 1. Introduction

Persistent spectral hole burning (PSHB) was discovered in organic molecular system in 1974 [1]. Five years later, PSHB in inorganic materials was discovered in NaF by R. M. Macfarlane et al [2]. In 1985, A. Winnacker et al [3] first observed photon gated spectral hole burning in  $\text{BaFCl}_2\text{Sm}^{2+}$  at 2K. Hole burning (HB) is useful in high resolution spectroscopy. It is also of crucial importance for the application to frequency domain optical storage. The storage density is proportional to the ratio of inhomogeneous linewidth ( $\Gamma_i$ ) to the homogeneous linewidth ( $\Gamma_h$ ),  $N = \Gamma_i / \Gamma_h$ . The inhomogeneous linewidth of  $^3D_1 - ^3F_4$  transition of  $\text{Sm}^{2+}$  is 16GHz and the hole width is 25MHz in  $\text{BaFCl}_2$  at 2K [3]. For this material, the inhomogeneous linewidth changes only moderately with the temperature; On the other hand, the homogeneous linewidth increases rapidly as the temperature rises. Then, a small value of  $N$  ( $\sim 2$ ) can be estimated when HB temperature is raised to 77K. That means, it is difficult to burn a hole in the inhomogeneous line in  $\text{BaFCl}_2\text{Sm}^{2+}$  at 77K. To maintain a reasonable storage capacity or to study HB at a quite high temperature, a large inhomogeneous linewidth is in great request.

In our previous work, the inhomogeneous linewidth of  $^3D_1 - ^3F_4$  transition of  $\text{Sm}^{2+}$  ions were broadened by adding Br ions to  $\text{BaFCl}_2$  matrix [4]. HB and fluorescence line narrowing (FLN) were observed in  $\text{BaFCl}_{1-x}\text{Br}_x\text{Sm}^{2+}$  at 77K. The variation of  $\Gamma_i$  and  $\Gamma_h$  with  $x$  was studied by HB and FLN in  $\text{BaFCl}_{1-x}\text{Br}_x\text{Sm}^{2+}$  at 77K [5]. In this paper, we report our results on  $\text{M}_1\text{M}_2\text{FCl}_{1-x}\text{Br}_x\text{Sm}^{2+}$  ( $\text{M}_1, \text{M}_2$  series) ( $\text{M}_1, \text{M}_2 = \text{Ca}, \text{Sr}, \text{Ba}, y=0 \sim 1$ ) series materials, in which HB was obtained at 77K. The dependence of the energy levels, inhomogeneous linewidth and homogeneous linewidth of  $^3D_1 - ^3F_4$  transitions on  $y$  were studied by fluorescence spectra and HB. A large inhomogeneous linewidth, i.e. a large ratio  $N$ , was obtained in a mixture which was formed by mixing the samples with different  $y$  together.

### 2. Experimental

$\text{Ca}_y\text{Sr}_{1-y}\text{FCl}_{1-x}\text{Br}_x\text{Sm}^{2+}$  (CaSr series) and  $\text{Sr}_y\text{Ba}_{1-y}\text{FCl}_{1-x}\text{Br}_x\text{Sm}^{2+}$  (SrBa series) powder samples were prepared by high temperature solid state reaction. Growth conditions are similar to that described by C. Wei [4]. In the growth, the chemical reagent used in this work is as follows,  $\text{CaF}_2$ ,  $\text{CaCl}_2$ ,  $\text{CaBr}_2$ ,  $\text{SrF}_2$ ,  $\text{SrCl}_2$ ,  $\text{SrBr}_2$ ,  $\text{BaF}_2$ ,  $\text{BaCl}_2 \cdot 2\text{H}_2\text{O}$ ,  $\text{BaBr}_2$  and  $\text{Sm}_2\text{O}_3$ . The nominal molar concentration of Sm in the samples is 0.01.

In measuring fluorescence spectra, 337.1 nm line of a nitrogen laser was used as an excitation source. Spex-1403 monochromator was used to detect the fluorescence. The data were processed by a microcomputer. A tunable dye laser, pumped by a pulsed Quanta-Ray DCR-2A Nd:YAG was used for HB study. Spectral holes were probed in a excitation spectrum which was measured by monitoring  $^3D_1 - ^3F_4$  emission with a D330 spectrometer, white scanning

$F_0 \rightarrow D_1$  transition. The samples were immersed in liquid nitrogen.

### 3. Results and Discussions

Persistent spectral hole can be burned in the three metastable  $^3D_1(J=0, 1, 2)$  excited states of the  $4f^6$  configuration. L. Zhang[5] has observed that the  $\Gamma_1$  values of  $^3D_1 \rightarrow F_0$  emission of  $Sm^{2+}$  increase obviously and approach a maximum with  $x$  close to 0.5 in  $BaFCl_xBr_{1-x}$ . In view of the result above, we add Ca, Sr and Ba ions in  $BaFCl_xBr_{1-x}$  to form CaSr series and SrBa series. Their fluorescence spectra were measured at 77K. The inhomogeneous linewidth and the energy( $E_0$ ) of  $^3D_1 \rightarrow F_0$  emissions in the two series are shown in table 1 and table 2, respectively. From the tables, we conclude that the  $\Gamma_1$  values increase slightly with  $y$  close to 0.5, while the energy  $E_0$  shifts to higher as  $y$  decreases. The result is discussed as follows,

Table 1 Values of  $\Gamma_1$ ( $cm^{-1}$ ) and  $E_0$ ( $cm^{-1}$ ) in CaSr series with different  $y$

$y$	0.2	0.4	0.5	0.55	0.7	0.8
$\Gamma_1$	33	32	35	38	38.5	39
$E_0$	14483	14480	14474	14466	14458	14450

Table 2 Values of  $\Gamma_1$ ( $cm^{-1}$ ) and  $E_0$ ( $cm^{-1}$ )( $J=0, 1, 2$ ) in SrBa series with different  $y$

$y$	0	0.25	0.4	0.5	0.65	0.75	1
$\Gamma_1$	26	27	28	31	28	29	24
$E_0$	14534	14528	14527	14512	14510	14502	14483
$\Gamma_1$	26	34	30	38	32	33	31
$E_0$	15879	15871	15871	15856	15852	15842	15819
$\Gamma_1$	26	26	26	34	35	27	20
$E_0$	17820	17809	17807	17791	17789	17781	17760

In  $BaFCl$ ,  $Sm^{2+}$ , the  $Sm^{2+}$  ions substitute the  $Ba^{2+}$  ion sites and have  $C_{\infty}$  symmetry.  $BaFCl_xBr_{1-x}Sm^{2+}$  has the same structure as  $BaFCl_xSm^{2+}$ [5] and the ligands Cl and Br around  $Sm^{2+}$  have different configurations with different probabilities for different  $x$ . The inhomogeneous line shape is determined by envelopes over contributions from different ligand configurations[5]. That indicates that the spread of energy levels is mainly dependent on the randomness of the nearest anions of Cl<sup>-</sup> and Br<sup>-</sup>. The randomness is the largest for  $x=0.5$ [5,6]. In MM series, the composition of anions, 0.5, is constant, so that  $\Gamma_1$  changed slightly when the composition of cations varies. This may be caused by two facts, the first, cations are located at farther sites than anions to  $Sm^{2+}$  ions; the second, electric field shielding may play a role.

Fig. 1 and Fig.2 show the dependence of  $E_0$  on  $y$  for CaSr series and SrBa series, respectively. It shows that the dependence is linear. In  $BaFCl_xBr_{1-x}Sm^{2+}$ , a linear dependence of  $E_0$  on  $x$  was found[6]. The relationships of  $E_0$  with  $x$  or  $y$  from experimental data are written as,

$$E_0 = 14550 - 24.7x (BaFCl_xBr_{1-x}) \quad (1)$$

$$E_n = 14498 - 58.1y \text{ (CaSr series)} \quad (2)$$

$$E_n = 14546 - 61.0y \text{ (SrBa series)} \quad (3)$$

$$E_n = 15885 - 61.0y \text{ (SrBa series)} \quad (4)$$

$$E_n = 17828 - 61.0y \text{ (SrBa series)} \quad (5)$$

The change of energy with  $x$  or  $y$  should be attributed to the increase of the anionic radius(cationic radius) with decreasing  $x(y)$ . The change of the ionic radius perturbs the crystal field[6].

According to the optical properties of the materials, it is possible to mix the samples with different  $x$  or  $y$  together in proper proportion to form a mixture with a large inhomogeneous linewidth. In Eq.(1)~(5), the energy changes faster with  $y$  than with  $x$ . In SrBa series,  $E_n$  ( $J=0, 1, 3$ ) changes with a same step. Therefore, three samples with  $y$  values of 0, 0.25 and 0.65 from SrBa series are selected to mix together in a reasonable proportion. The inhomogeneous line shape in the mixture should be determined by the overlapping of the inhomogeneous line shapes in the three samples. To  $F_3^4 - ^3D_2$  transition, the inhomogeneous linewidth of  $62.5\text{cm}^{-1}$  in the mixture is estimated by using the data of  $E_n$  and  $\Gamma$ , in table 2.

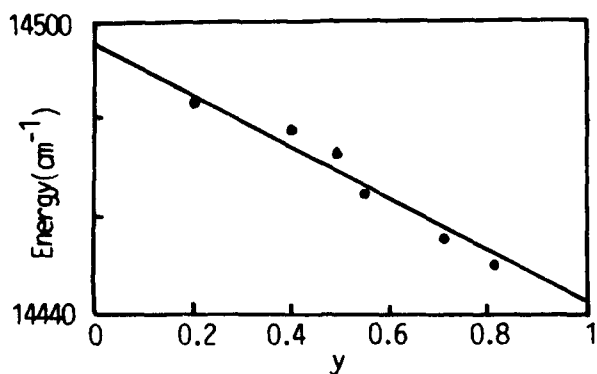


Fig. 1 Dependence of the energy of  $^3D_2 - F_4$  emission on  $y$  in  $\text{Ca,Sr}_{1-y}\text{FCl}_3\text{Br}_{0.5y}\text{Sm}^{3+}$  at 77K

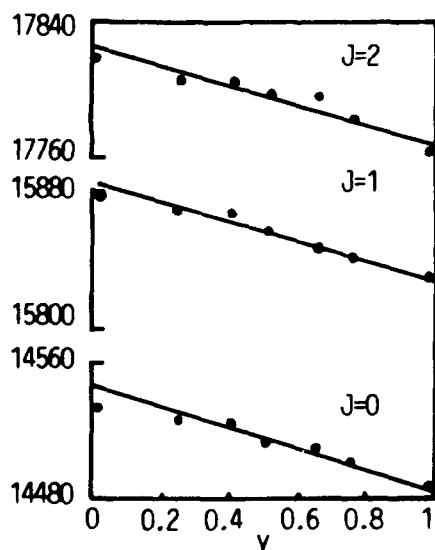


Fig. 2 Dependence of the energy of  $^3D_2 - F_4$  emission on  $y$  in  $\text{Sr,Ba}_{1-y}\text{FCl}_3\text{Br}_{0.5y}\text{Sm}^{3+}$  at 77K

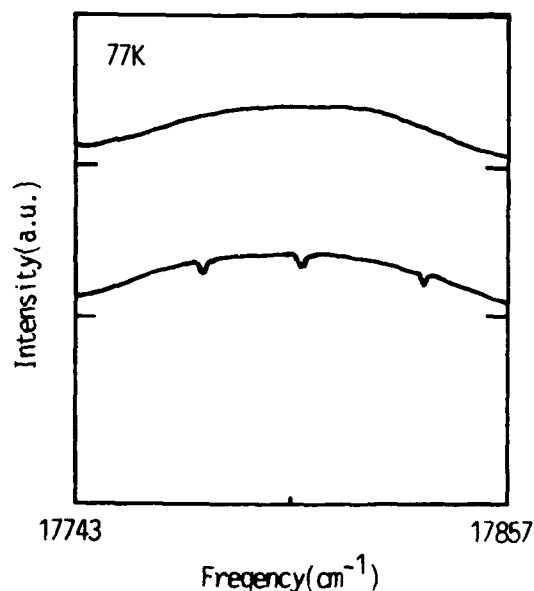


Fig.3 (a) The fluorescence excitation spectrum in a mixture (b) Three holes in the inhomogeneous line at 77K

Two-photon persistent spectral hole burning, which was described in detail by C. Wei [4],

is observed in  $F_0-{}^3D_1$  transition in the mixture at 77K. Fig.3(a) shows the excitation spectrum for  $F_0-{}^3D_1$  transition. The width of the spectral distribution is  $65\text{cm}^{-1}$ , which is in agreement with the estimation ( $62.5\text{cm}^{-1}$ ) above. Three spectral holes were burned in the inhomogeneous line as shown in Fig.3(b). Table 3 shows the energy, inhomogeneous linewidth, homogeneous linewidth of  $F_0-{}^3D_1$  transition and ratio  $N$  in the three samples and their mixture.  $\Gamma_n$  is determined by hole width ( $\Gamma_{\text{hole}}$ ) and laser linewidth ( $\Gamma_{\text{laser}}$ ) according to  $\Gamma_n = (\Gamma_{\text{hole}} - \Gamma_{\text{laser}})/2$ , in which  $\Gamma_{\text{laser}} = 0.2\text{cm}^{-1}$ . We see that  $\Gamma_n$  in each sample is less than  $0.5\text{cm}^{-1}$ . If  $\Gamma_n$  in the mixture is considered to be  $0.5\text{cm}^{-1}$ , the ratio  $N$  is as large as 130 in the mixture at 77K. By this way, the inhomogeneous line width can be broadened more by mixing the materials in which the energy of  ${}^3D_1 - F_0$  transition distributes widely.

Table 3 The values of  $E_n(\text{cm}^{-1})$ ,  $\Gamma_n(\text{cm}^{-1})$ ,  $\Gamma_n(\text{cm}^{-1})$  and  $N$  in the three samples in SrBa series and their mixture.

y	$E_n$	$\Gamma_n$	$\Gamma_n$	N
0	17821	26	0.5	53
0.25	17809	26	0.4	65
0.65	17789	35	0.38	82
Mixture	17800	65	0.5	130

#### 4. Conclusion

Fluorescence spectra and persistent hole burning were studied in  $\text{Ca}_x\text{Sr}_{1-x}\text{FCl}_3\text{Br}_{0.5}\text{Sm}^{2+}$  and  $\text{Sr}_x\text{Ba}_{1-x}\text{FCl}_3\text{Br}_{0.5}\text{Sm}^{2+}$  at 77K. Inhomogeneous line could be further broadened by mixing materials together. The results show that optical storage capacity could be significantly increased by this method.

#### References

- [1] V.M.Khartamov, R.I.Personov, L.A.Bykovskaya, Opt. Commun., 12, 191(1974)
- [2] K.M.Macfarlane, R.M.Shelby, Phys. Rev. Lett., 42, 788(1979)
- [3] A.Winnacker, R.M.Shelby, R.M.Macfarlane, Opt. Lett, 10, 350(1985)
- [4] C.Wei, S.Huang, and J.Yu, J. Lumin., 43, 161(1989)
- [5] L.Zhang, J.Yu, and S.Huang, J. Lumin. 45, 381(1990)
- [6] X.Wang, S.Huang, and D.Gao, Chinese J. Lumin., 12(1), 19(1991) (in Chinese)

## Room-Temperature Persistent Spectral Hole Burning in $\text{Sm}^{2+}:\text{SrFCl}_{0.5}\text{Br}_{0.5}$

R.Jaaniso and H.Bill

Department of Physical Chemistry, University of Geneva,  
30 quai E.Ansermet, CH-1211 Geneva 4, Switzerland

We report the first observation of spectral hole burning in the spectra of impurity centers at room temperature. The persistent holes are burned in the  ${}^5\text{D}_1\text{-}{}^7\text{F}_0$  (632 nm) and  ${}^5\text{D}_0\text{-}{}^7\text{F}_0$  (690 nm) transitions of  $\text{Sm}^{2+}$  ions in the title compound.

The search for the media showing persistent hole burning at liquid nitrogen<sup>1,2</sup> or at room temperatures is strongly motivated by the potential applications of this phenomenon in the frequency-selective optical data storage and processing, as has been demonstrated in a number of low-temperature experiments.<sup>3,4</sup> The extension of the temperature range of the hole burning method could also be of interest for scientific applications, especially in probing of disordered materials.

In our study, single crystal species with 1 at.% samarium, and having dimensions of  $0.2\text{-}5.5\text{ mm}^3$ , were used. From the structural point of view, they can be described as derivatives of PbFX type layer crystals with substitutionally disordered double layers of larger X (Cl,Br) halogens and with the  $\text{Sm}^{2+}$  impurities in the cationic sites.

The main spectral features of  $\text{Sm}^{2+}:\text{SrFCl}_{0.5}\text{Br}_{0.5}$   ${}^5\text{D}_1\text{-}{}^7\text{F}_0$  transition at room temperature are presented on Fig. 1. While the absorption spectrum or the nonselectively excited fluorescence spectrum has a width (FWHM) of  $\approx 30\text{ cm}^{-1}$ , the excitation spectrum of this transition, recorded spectrally selectively near the centre of the  ${}^5\text{D}_0\text{-}{}^7\text{F}_0$  fluorescence band,

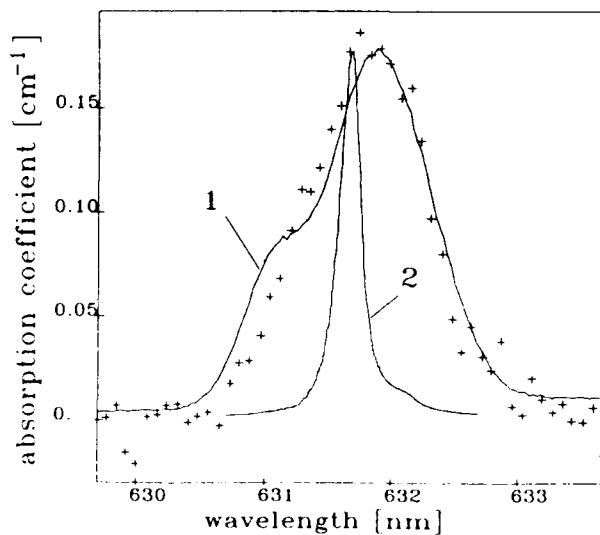


Fig. 1.  ${}^5\text{D}_1\text{-}{}^7\text{F}_0$  transition spectra: (+) - absorption, (1) - fluorescence at 476.5 nm excitation, (2) - excitation spectrum, recorded selectively at 690.1 nm. The units of ordinate axis correspond to the absorption spectrum.

shows the width of  $4.8 \text{ cm}^{-1}$ . The first value is therefore determined by the inhomogeneous broadening in the partially disordered host, while the second one demonstrates strong correlation between the frequencies of above mentioned transitions, and sets the upper limit to the homogeneous width of  ${}^5\text{D}_1\text{-}{}^7\text{F}_0$  line.

Persistent hole burning was observed with a resonant narrow-band dye laser ( $0.15 \text{ cm}^{-1}$  bandwidth) for typical exposures of  $\approx 10\text{--}100 \text{ s}$  at the intensities of  $\approx 10 \text{ W/mm}^2$  in case of  ${}^5\text{D}_1\text{-}{}^7\text{F}_0$  transition. Holes were detected in the excitation spectrum by monitoring the fluorescence of  ${}^5\text{D}_0\text{-}{}^7\text{F}_2$  line around  $730 \text{ nm}$ .

The first hole in the spectrum of a fresh (non-irradiated) sample was always relatively small (Fig. 2a), reaching at long exposure times the depth of 2-5%, depending on the sample. The main properties of hole burning in  $\text{Sm}^{2+}:\text{SrFCl}_{0.5}\text{Br}_{0.5}$  were studied on samples which had been pre-irradiated in an  $\text{Ar}^+$  laser beam ( $1.5 \text{ W}$  at  $514\text{--}458 \text{ nm}$ ), typically for 5-10 min. They can be summarized as follows:

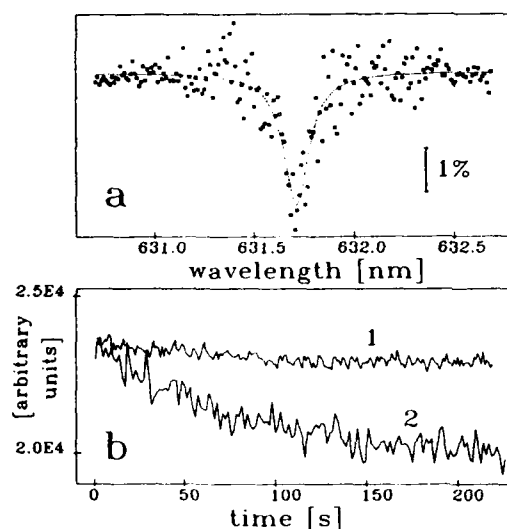


Fig. 2. (a) - Spectral hole in  ${}^5\text{D}_1\text{-}{}^7\text{F}_0$  transition - the difference of two spectra, measured before and after 180 s exposure at  $631.7 \text{ nm}$  (fresh sample), (b) - hole burning kinetics before (1) and after (2) the sample irradiation with an  $\text{Ar}^+$  laser green-blue light.

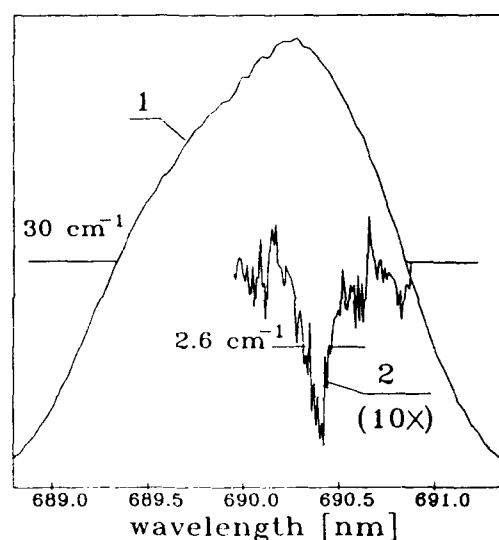


Fig. 3. Inhomogeneous spectrum of  ${}^5\text{D}_0\text{-}{}^7\text{F}_0$  transition (1), and a spectral hole (2) burned at  $690.4 \text{ nm}$  (15 min. exposure at  $\approx 50 \text{ W/mm}^2$ ).

1) After the irradiation by the  $\text{Ar}^+$  laser green-blue light, strongly absorbed by the  $f\text{-}d$  transitions of  $\text{Sm}^{2+}$ , the resonant holes with a maximum depth of 15-20% could be burned in all samples studied (Fig.2b).

2) The smallest holewidth obtained was  $3.5 \text{ cm}^{-1}$  for the  ${}^5\text{D}_1\text{-}{}^7\text{F}_0$  transition and  $2.6 \text{ cm}^{-1}$  for the  ${}^5\text{D}_0\text{-}{}^7\text{F}_0$  transition (Fig. 3). Slight variations in holewidth were

observed due to the sample dependence, the more defective crystal pieces showing the wider (but still narrower than  $5 \text{ cm}^{-1}$ ) holes.

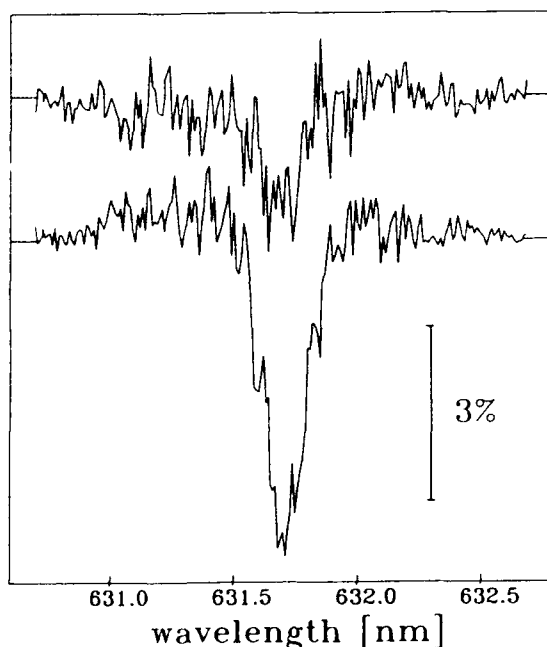


Fig. 4. Two holes burned with the same dose but different intensity in the  $^5D_1-^7F_0$  transition. For the upper hole the intensity was reduced by a factor of 3 with the respective increase in the exposure time. The hole areas are in the ratio close to 1:3.

The two-photon character together with the intensity redistribution within the inhomogeneous band suggest the burning mechanism to be similar to that observed first in BaFCl host at  $T=2\text{K}^5$  - the two-step photoionization of  $\text{Sm}^{2+}$  with the following electron trapping on  $\text{Sm}^{3+}$  in another lattice site. There may be two essential differences in the details of this mechanism at or near the room temperature: the phonon-assisted photoionization may have lower threshold and the ionization efficiency may be increased by the charge compensating movement of  $\text{F}^-$  ions.<sup>6</sup> The lack of redistribution in case of the first hole burned in the fresh sample and the appearance of  $\text{Sm}^{3+}$  traps after the sample irradiation indicate that some bulk or surface traps of other origin should also be present.

The correlation between the energies of different f-f transitions were also studied and nearly linear dependence between the energies of two transitions were obtained with a "correlation width" of  $1-2 \text{ cm}^{-1}$ .

3) The hole formation was accompanied by the increase of signal in the other parts of inhomogeneous profile. In accordance with this, the second hole, burned at a shifted resonant wavelength, partly filled the first hole which has been burned in the same sample spot.  
4) No spontaneous hole filling was observed during the time intervals of  $\approx 1 \text{ h}$ .  
5) The holes could be erased with  $\text{Ar}^+$  laser green-blue light i.e. the photochromic process is reversible.

6) The pre-saturation dependence of the hole depth (or area) from the burning intensity was clearly not linear, but approximately quadratic (Fig. 4), showing that the absorption of two photons occurs in the elementary burning act.

The comparison with the "pure" SrFCl host shows that, while the Cl-Br disorder increases the inhomogeneous broadening (caused by the variations in the local static fields) by a factor of  $\approx 10^2$ , it does not affect the homogeneous linewidths  $\Gamma_h$  (determined by dynamical modulation) at room temperature. For mixed crystals the values of  $\Gamma_h$  should be equal or smaller than the halfwidths of the narrowest holes.<sup>3,4</sup> 1.75 cm<sup>-1</sup> and 1.3 cm<sup>-1</sup> for the  $^5D_1-^7F_0$  and  $^5D_0-^7F_0$  transitions, correspondingly. In case of SrFCl host the value of  $\Gamma_h=1.55\pm 0.15$  cm<sup>-1</sup> was obtained for both transitions.

---

<sup>1</sup> C.Weï, S.Huang, and J.Yu, *J.Luminescence* **43**, 161 (1989).

<sup>2</sup> A.Furusawa and K.Horie, *J.Chem.Phys.* **94**, 80 (1991).

<sup>3</sup> *Persistent Spectral Hole-Burning: Science and Applications*, ed. by W.E.Moerner, *Topics in Current Physics*, Vol. 44 (Springer-Verlag, Berlin, 1988).

<sup>4</sup> *Zero Phonon Lines and Spectral Hole Burning in Spectroscopy and Photochemistry*, ed. by O.Sild and K.Haller (Springer-Verlag, Berlin, 1988).

<sup>5</sup> A.Winnacker, R.M.Shelby, and R.M.Macfarlane, *Optics Lett.*, **10**, 350 (1985).

<sup>6</sup> R.L.Fuller and D.S.McClure, *Phys. Rev. B* **43**, 27 (1991).

Suppression of Dephasing by Deuteration of Amorphous Host  
Materials: The Case of Porphyrin-doped Polymers

by

Kazuaki Sakoda and Masayuki Maeda  
Electronic & Imaging Materials Research Laboratories,  
Toray Industries, Inc.  
1-1, Sonoyama 1-chome, Otsu, Shiga 520, Japan  
Tel. (0775)33-8426

As is widely recognized, the dephasing of an optical impurity doped in an amorphous host is mainly brought about by the interaction with two level systems (TLS)<sup>1)</sup>. Because the microscopic structure of TLS is not clear and statistically distributed in usual cases, it is quite difficult at present to specify the relevant factors which govern the the relaxation of TLS's in a given material. However, we know that the relaxation is substantially the tunneling of atoms in the material. According to ref.2, the tunneling relaxation rate is proportional to  $\exp(-2\lambda)$ , where  $\lambda$  is given by

$$\lambda = \left(\frac{mV}{2}\right)^{\frac{1}{2}} \frac{d}{\hbar} \quad (1)$$

Here,  $m$  is the mass of the tunneling atom or atoms,  $V$  the potential barrier height,  $d$  the tunneling distance. From this equation, we may expect an isotope effect on TLS's relaxation, and hence on the dephasing of the optical impurity. Because hydrogen is the lightest atom and most likely to tunnel in a usual organic

system, the deuteration of the organic amorphous host may result in the suppression of the dephasing. We show that this is really the case for polyvinylalcohol(PVA) doped with an ionic porphyrin.

In order to estimate the effect of the deuteration on the dephasing rate, we compared the linewidths of zero phonon holes burned in PVA and deuterated PVA( $d_3$ -PVA, see Fig.1) doped with tetrasodium tetrasulfonatophenylporphin (TSPP, see Fig.2) between 20K and 84K. As we reported previously<sup>3)4)</sup>, zero phonon holes can be burned in TSPP-doped PVA at relatively wide temperature range, which is a consequence of weak temperature dependence of the Debye-Waller factor in this kind of materials<sup>5)</sup>.

The photochemical holes were burned in the  $Q_x$  band of the samples with a CW ring dye laser. The laser power density was  $0.6\text{mW/cm}^2$  and the irradiation time was adjusted so as to burn a hole whose depth was less than 10% of the initial optical density. The linewidths of the holes were measured by conventional transmission spectroscopy with 1m single monochromator.

The results are shown in Fig.3. We found that the deuteration brought about a decrease of the linewidth by 30 to 50%. Since the dephasing rate is proportional to the width of the zero phonon hole, we can conclude that the deuteration of the host polymer results in the suppression of the dephasing as was expected. Besides, we also found that the width  $\Gamma$  depends on temperature  $T$  as

$$\Gamma \propto T^a \quad a \cong 1.7 \quad (2)$$

for both samples, which is consistent with the temperature dependence of the dephasing rate determined by photon echo experiment for a similar material system<sup>5)</sup>.

### References

1. S. Voelker, J. Lumin., 36, 251(1987).
2. J. L. Black and B. I. Halperin, Phys. Rev. B16(6), 2879(1977)
3. K. Sakoda, K. Kominami and M. Iwamoto, Jpn. J. Appl. Phys., 27, L1304(1988) .
4. K. Sakoda, K. Kominami and M. Iwamoto, Jpn. J. Appl. Phys., 28, Suppl. 28-3, 229(1989).
5. S. Saikan, A. Imaoka, Y. Kanematsu, K. Sakoda, K. Kominami and M. Iwamoto, Phys. Rev. B41(5), 3185(1990).

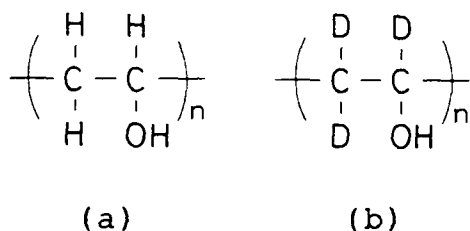


Fig.1 Chemical structures of (a) PVA and (b) deuterated PVA ( $d_3$ -PVA).

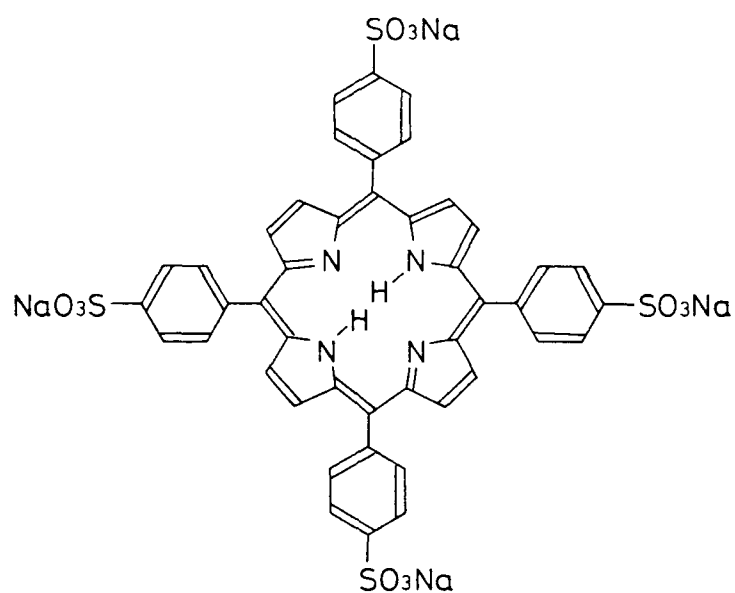


Fig.2 Chemical structure of TSPP.

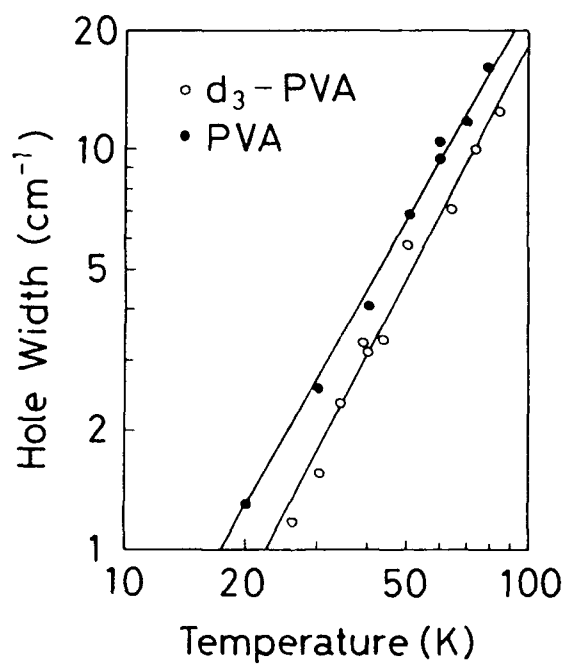


Fig.3 Temperature dependence of the full width at half maximum of zero phonon hole.

A New Type Photon-Gated Photochemical Hole Burning  
by Two-Color-Sensitized Photoreaction

Kazuyuki Horie, Shinjiro Machida, and Takashi Yamashita\*

Faculty of Engineering, University of Tokyo, Hongo 7-3-1,

Bunkyo-ku, Tokyo 113, Japan. TEL (03)3812-2111 ex.7312

\*Research Center for Advanced Science and Technology,

University of Tokyo, Komaba 4-6-1, Meguro-ku, Tokyo 153, Japan.

TEL (03)3481-4561

Photochemical Hole Burning (PHB) has attracted considerable interest not only as a tool for high resolution spectroscopy of amorphous solid at low temperature but also as a possible means for frequency-domain high-density optical storage.<sup>1)</sup> Many recent investigations have been devoted to a photon-gated mechanism because it allows nondestructive readout in utilizing PHB for a practical optical memory system. The mechanisms of previously reported photon-gated PHB systems are two-step photoionization, photodecomposition, and photoinduced donor-acceptor electron transfer reactions.<sup>1)</sup>

In this presentation, we report the first observation to our knowledge of a new mechanism for photon-gated PHB: two-color photosensitization of the photoreactive matrix polymer that involves triplet-triplet energy transfer process from higher excited triplet state of sensitizer to photoreactive energy acceptor groups. The present system consists of a zinc 9,18,27,36-tetra(4-tolyl)-tetrabenzoporphine (ZnTTBP), and a glycidyl azide polymer (GAP) cross-linked with trimethylol propane and isophorone diisocyanate.

Fig.1 illustrates the schematic energy diagram and the most probable mechanism for the observed photon-gated PHB. The site-selection light (CW DCM dye laser, at the wavelength of  $\lambda_1$ ) and the gating light (Ar<sup>+</sup> laser, at  $\lambda_2$ ) excite ZnTTBP molecules, the energy donor, to a higher excited triplet state,  $T_n$ . The energy of the  $T_n$  is transferred from

ZnTTBP to a nearby azide group resulting in its excitation to the lowest triplet state,  $T_1$ . The excited azide group decomposes and generates a nitrogen molecule and nitrene. The decomposition and subsequent reactions induce a drastic change in the interaction between the ZnTTBP molecules and the surrounding matrix and causes the change in the resonant frequencies of the molecules to form a spectral hole.

Fig.2 shows typical hole profiles burnt by two-color and one-color irradiations at 20K. Traces (a), (b), and (c) show the two-color holes formed by 12sec, 36sec, and 60sec irradiation, respectively with the intensities of  $38 \mu\text{W}/\text{cm}^2$  at  $\lambda_1$  and  $8\text{mW}/\text{cm}^2$  at  $\lambda_2$ . Trace (d) shows the transmittance after 300sec irradiation of only  $\lambda_1$ , with the intensity of  $380 \mu\text{W}/\text{cm}^2$ . In spite of the total irradiated energy of  $\lambda_1$  is 50 times larger than the case of trace (c), no observable hole is formed in trace (d). It was not until 600 sec irradiation that one-color hole was observed in our experiments (shown in trace (e)). The ratio for the quantum efficiency of hole formation of (a) to (e) based on  $\lambda_1$  is about 500. Trace (f) shows that the addition  $\lambda_2$  ( $8\text{mW}/\text{cm}^2$ )

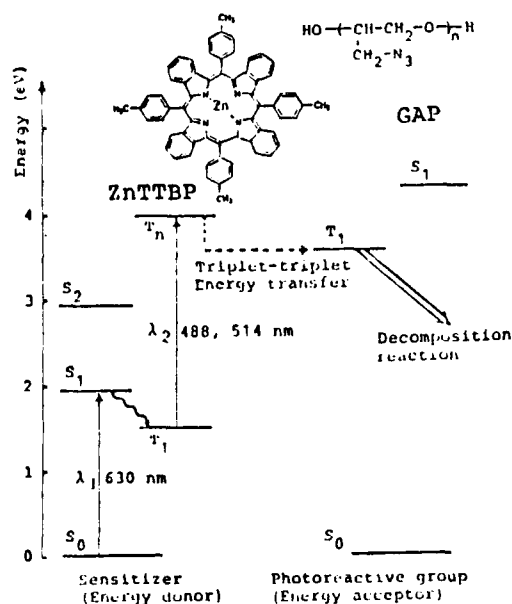


Fig.1. Schematic energy diagram and the most probable mechanism for the observed photogated PHB.

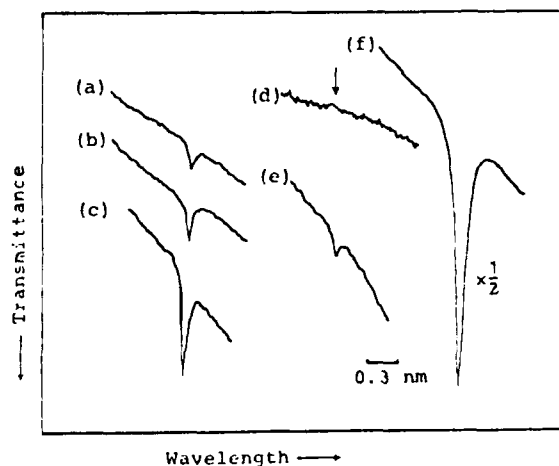


Fig.2. Hole profiles of ZnTTBP/GAP system for various burning conditions. (a), (b), and (c): 12sec, 36sec, and 60sec irradiation of 2-color ( $58 \mu\text{W}/\text{cm}^2$  at  $\lambda_1$  and  $8\text{mW}/\text{cm}^2$  at  $\lambda_2$ ). (d) and (e): 300sec and 600sec irradiation of  $\lambda_1$  only ( $380 \mu\text{W}/\text{cm}^2$ ). (f): 2-color (600sec,  $380 \mu\text{W}/\text{cm}^2$  at  $\lambda_1$  and  $8\text{mW}/\text{cm}^2$  at  $\lambda_2$ ). Sensitivity for the trace (f) is half of those for others.

to  $\lambda_1$  of the same condition as trace (e) formed a very deep hole (hole depth: 34%).

Fig.3 shows the change in the transmittance of the whole absorption band before (a) and after (b,c) a long-time two-color irradiation with the intensities of  $75\text{mW}/\text{cm}^2$  both at  $\lambda_1$  and  $\lambda_2$  at 20K. Trace (b) shows that 30min irradiation at 633nm formed a broad hole on the longer-wavelength side of the inhomogeneous absorption band and an anti-hole on the

top of the absorption band. Trace (c) of the transmission spectrum after further 30min irradiation at the top of the anti-hole (627nm) becomes similar to the initial one (trace (a)) and the area of the absorption band is unchanged. In the case of  $\text{ZnTTBP-CHCl}_3/\text{PMMA}$  system, which shows photon-gated PHB by electron transfer mechanism,<sup>1)</sup> similar experiment showed that 30min irradiation of  $\lambda_1$  and  $\lambda_2$  (both  $38\text{mW}/\text{cm}^2$ ) made the whole absorption band drastically smaller. These facts indicate that ZnTTBP molecules themselves do not change to other chemical species during hole formation in GAP.

Photodecomposition of azide is sensitized via both singlet and triplet states.<sup>2)</sup> It is quite reasonable that  $T_1$  of ZnTTBP that has much higher energy than  $T_1$  of azide sensitizes the decomposition of GAP. The nitrene generated by the decomposition of azide group has high reactivity and undergoes hydrogen extraction, addition, insertion, or other reactions.<sup>2)</sup> Though the type of reaction of nitrene in the present case is not yet clear, it can be said that the triplet-triplet energy transfer from the two-color-excited

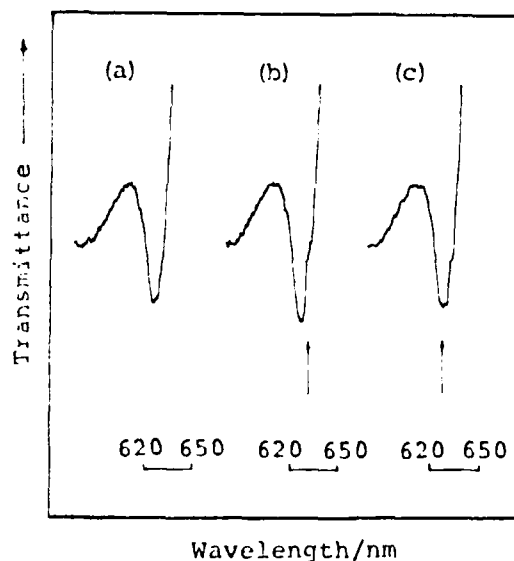
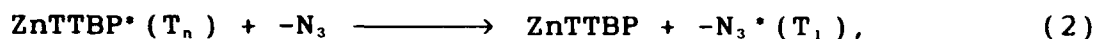
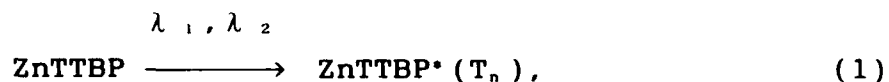


Fig.3. Transmission spectra of the whole absorption band before (a) and after (b,c) 2-color irradiation. (b): 30min,  $75\text{mW}/\text{cm}^2$  both at  $\lambda_1$  (633nm) and  $\lambda_2$  (488, 514nm). (c): 30min irradiation on sample (b),  $75\text{mW}/\text{cm}^2$  both at  $\lambda_1$  (627nm) and  $\lambda_2$  (488, 514nm).

ZnTTBP molecules to the nearby azide groups occurs and that the decomposition of the azide group and subsequent reactions change the guest-host interaction leading to a hole formation:



The results reported here is expected to offer a new class of photon-gated PHB based on a two-color photosensitization of photoreactive groups via triplet-triplet energy transfer. This type of mechanism has a great advantage of providing a large variety of sensitizer and reactive group pairs and of expanding the kinds of chemical reactions which can be used for PHB. The photosensitization mechanism of PHB by using photoreactive matrix polymers also provides a new possibility of measuring PHB spectra of various dye molecules with high efficiency which have zero-phonon line but do not undergo photochemical reactions. This would increase the importance of PHB spectroscopy for chemists and physicists as well as the expectation to utilize PHB for frequency-domain optical storage.

#### References

- 1) W. E. Moerner ed.. Persistent Spectral Hole-Burning; Science and Applications (Springer, Berlin, 1988).
- 2) N. J. Turro, Modern Molecular Photochemistry (Benjamin/Cummings, 1978) Chapt. 13.

## Persistent Photon-gated Spectral Holeburning In A New Donor-Acceptor Electron Transfer System

Mingzhen TIAN, Baozhu LUO, Wenlian LI, Shihua HUANG, Jiaqi YU  
Changchun Institute of Physics, Academia Sinica, 1 Yan-an Road, Changchun  
130021, P.R.China, Phone:(0431) 52215 Ext.120

### 1.Introduction

Due to the interest in the frequency-domain optical storage application, recent researches on spectral holeburning concentrated on the two-colour photon-gated persistent holeburning[1,2]. Some organic systems have been investigated [3-7]. A representative one is TZT as a donor and  $\text{CHCl}_3$  as an acceptor in PMMA film undergoing donor-acceptor electron transfer, which offered a significant mechanism for persistent holeburning in organic system [4,5]. But there is an insurmountable problem in the system. As  $\text{CHCl}_3$  is volatile at room temperature, its concentration can not be controlled and the sample is difficult to further study. Here we report the holeburning system composed of metal-tetrabenzoporphyrin derivatives (MTBP) as the donors and a solid electron acceptor, p-hydroxybenzaldehyde (PHBA), which can easily be made into a stable "dry" film and in which the concentration of each component can be modified easily.

In a donor-acceptor system,  $\Delta G$ , the equilibrium free energy releasing during electron transfer is given by the following relation[8]:

$$\Delta G = F [E(D,ox) - E(A,red)] - E_n - e^2/R_c E \quad (1)$$

Substituting  $E(D,ox) = 0.36 \text{ eV}$  (for donor, ZnTBP),  $\lambda_1 = 632.8 \text{ nm}$  and  $\lambda_2 = 532 \text{ nm}$  to (1), we estimate the  $E(A,red)$  value to select acceptor. On one hand, it is expected that electron transfer occurs at the state excited by two-colour photons ( $\Delta G < 0$ ). So we got the lowest limit of the reduction potential,  $-3.51 \text{ eV}$ . The more easily the acceptor is reduced, the stronger the driving force of the electron transfer is. On the other hand, we expect the donor-acceptor pair not undergoing electron transfer under one-colour excitation ( $\Delta G > 0$ ). So we get the highest limit of the reduction potential,  $-1.6 \text{ eV}$ . If  $E(A,red)$  is larger than  $-1.6 \text{ eV}$ , electron transfer will occur at a lower state excited by  $\lambda_1$  only. According to this estimation, we chose PHBA [ $E(A,red) = -1.61 \text{ eV}$ ] as an electron acceptor. We have observed two-colour photon-gated holes at  $4.2 \text{ K}$  and  $20 \text{ K}$  in our samples with the excitation of the selecting light ( $\lambda_1$ ) near  $630 \text{ nm}$  and gating light ( $\lambda_2$ ) at  $532 \text{ nm}$  or  $514.5 \text{ nm}$ .

### 2. Experiments

Four kinds of MTBP, Zn-tetraphenylbenzoporphyrin, Mg-tetrabenzophenylporphyrin, Zn-tetranaphthalenebenzoporphyrin, Zn-tetratoylbenzoporphyrin were synthesized, and PHBA was commercially obtained. Four kinds of film samples were prepared by the means of dissolution and evaporation at room temperature. Experiments have been done for each sample, but our discussion will focus on the representative sample 1, Zn-tetraphenylbenzoporphyrin/PHBA/PMMA. The absorption spectra of each sample were examined. Fig.1 shows the

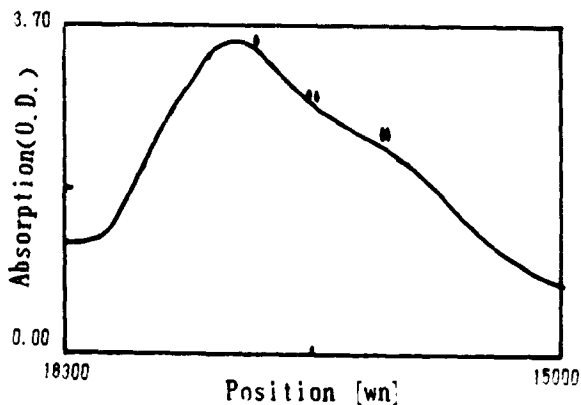


Fig.1  $S_0 \rightarrow S_1$  absorption band of ZnTPBP/PHBA/PMMA at 20K.

absorption band of  $S_0 \rightarrow S_1$  transition in sample 1 whose inhomogeneous line width is about  $700 \text{ cm}^{-1}$  with the peak position at  $630 \text{ nm}$ . At  $4 \text{ K}$  and  $20 \text{ K}$ , holes were burnt at the positions indicated by arrows in Fig.1. To burn gated holes, we simultaneously expose the samples to two lasers, one is selecting light  $\lambda_1$  and the other is gating light  $\lambda_2$ . The detection of the holes was performed by monitoring the transmission. Temperature-cycling experiments were performed between  $20 \text{ K}$  and  $60 \text{ K}$ , and thermal erasing was observed.

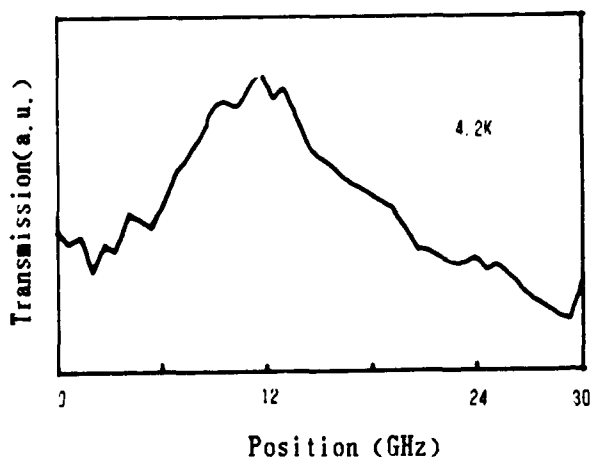


Fig.2 Photon-gated PHB in ZnTPBP/PHBA/PMMA system at  $4.2 \text{ K}$ .

For hole burning material applied to optical storage,  $\Gamma_i/\Gamma_h$  is one of the essential parameters affecting the storage density.  $\Gamma_i/\Gamma_h = 2600$  of the sample 1 is rather high among the organic systems yet reported.

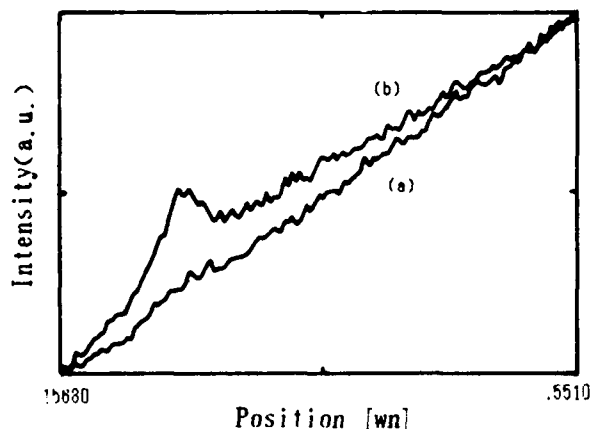


Fig.3 Gating effect of second photon in ZnTPBP/PHBA/PMMA system at  $20 \text{ K}$ .

A MTBP molecule is excited by  $\lambda_1$  from the ground state  $S_0$  to the first singlet excited state  $S_1$  where the intersystem crossing to the lowest triplet state  $T_1$  occurs with a high yield. Then  $\lambda_2$  excited the molecules at  $T_1$  to higher triplet states  $T_n$  where electrons are ejected from MTBP and trapped by PHBA. Thus a persistent hole was formed. If  $\lambda_2$  is absent, the excited

### 3. Results and Discussions

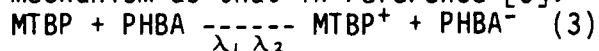
A hole was burnt at  $4 \text{ K}$  (Fig.2) with  $\lambda_1 = 630 \text{ nm}$ ,  $P_1 = 32 \mu\text{W}$  and  $\lambda_2 = 514.5 \text{ nm}$ ,  $P_2 = 8 \text{ mW}$ , the diameter of laser spot was about  $5 \text{ mm}$  and burning time  $t = 100 \text{ s}$ . The full width at half maximum of the hole ( $\Gamma_h$ ) is  $8 \text{ GHz} = 0.27 \text{ cm}^{-1}$ . The hole depth was defined as:

$$d = \Delta\alpha/\alpha_i = (\alpha_i L)^{-1} \cdot \Delta T/T_i \quad (2)$$

where  $\Delta\alpha$  is the difference of the absorption coefficients at the burning frequency before and after burning,  $L$  is the sample thickness, and  $\Delta T/T_i$  is the relative change of transmittance at the burning position. From (2) and Fig.2, we got the hole depth  $d = 2.5\%$ .

Fig.3 shows the gating effect of the second photon,  $\lambda_2$ . Trace (a) gives the transmission after  $15 \text{ s}$  irradiation with only  $\lambda_1 = 15663.5 \text{ cm}^{-1}$  and power  $P_1 = 100 \mu\text{W}$ ; no observable hole was formed. Trace (b) shows a hole with depth  $d = 1.6\%$  and width  $\Gamma_h = 6 \text{ cm}^{-1}$  burnt by simultaneously irradiating both  $\lambda_1 = 15663.5 \text{ cm}^{-1}$  with the same power as in trace (a) and  $\lambda_2 = 532 \text{ nm}$  with power  $P_2 = 26 \text{ mW}$  for  $15 \text{ s}$ . Here we can see the gating effect is obvious.

We expect that photon-gated hole-burning in our materials has the same mechanism as that in reference [5]:



electrons of MTBP molecules will transit to  $S_0$  from  $T_1$  by intersystem crossing and no persistent hole will be formed.

For the gating effect is related to T---T absorption so the most efficient wavelength of the gating light locates at the peak position of the T---T absorption band, 480nm for ZnTPBP[9]. Restricted by the experiment apparatus gating light we used, 532nm or 514.5nm, is not rather efficient for burning.

In the material system, it is very important to select an electron acceptor with suitable reduction potential matching our electron donor mentioned in section 1. We prepared a sample whose ingredients are the same as that in sample 1, but lacking PHBA. No hole was observed under the same condition as that in Fig.3 (b). It indicates that our sample is the DA-ET system

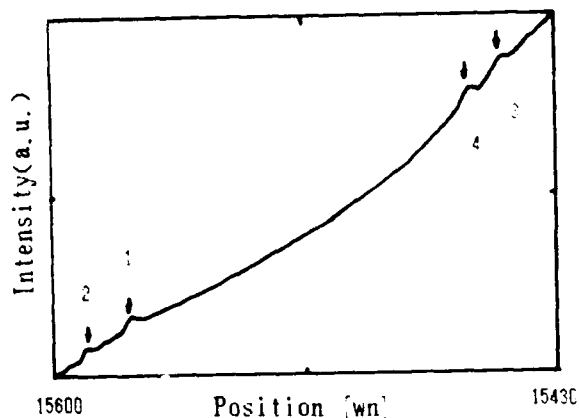


Fig.4 Multiholes burnt in the order of the numbers under the same condition at 20K.

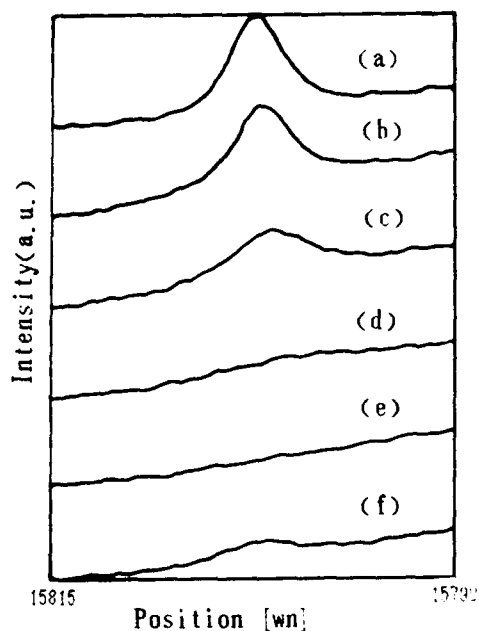


Fig.5 Thermal cycling of a photon-gated hole at 632.8nm.

To study the interaction between the holes in a wide inhomogeneous absorption band, we burnt four holes at different positions as shown in Fig.4. In all cases,  $P_1=100\mu W$ ;  $\lambda_2=532$  nm,  $P_2=26mW$ ;  $t=15s$ .  $\lambda_1$  was changed in the order of the numbers in Fig.4. It shows that four holes are nearly identical in hole depth and width and no antihole formed. Thus we can get the following conclusion: two nearby holes are distinguishable and do not affect each other when their distance in wavenumber is not smaller than 2.4 times of hole width such as position 3,4 in Fig.4; when holeburning at position 3 was followed by holeburning at position 4 formation of hole 4 did not bring about the erasing of the hole 3.

In Fig.5(a), we burnt a considerably deep hole with He-Ne laser (632.8nm) and YAG laser(532nm) at 20K,  $\Gamma_h=5cm^{-1}$   $d=14\%$ . After burning, we raised the temperature of the sample in a cryostat slowly and detected the hole at 30K, 40K, 50K and 60K as curves (b),(c),(d),(e) in Fig.5 respectively, then cooled the sample back to 20K and detected the hole as curve (f) in Fig.5. The hole was erased by heating and not detectable at 60K. A small part of the hole recovered after the thermal cycling.

In summary, we report only results on sample 1 here, while we have gotten the agreeable results on our other samples. Detailed researches on related problems such as the exact process of the hole formation, light erasing, effect of matching between donor and acceptor energy levels are in progress.

## References

1. W.E.Moerner: "Persistent Spectral Hole-burning: Science and Applications" Springer-Verlag Berlin, 1988
2. W.E.Moerner: Jpn. J. Appl. Suppl. 28-3, 221 (1989)  
(International Symposium on Optical Memory, Kobe, Japan, 26-28 Sept.1989)
3. H. W. H. Lee, M. Gehrtz, E. Marinero, W. E. Moerner: Chem. Phys. Lett., 118, 611(1985)
4. T. P. Carter, C. Brauchle, V. Y. Lee, M. Manavi, W. E. Moerner: Opt. Lett., 12, 370(1987)
5. T. P. Carter, C. Brauchle, V. Y. Lee, M. Manavi, W. E. Moerner: J. Phys. Chem., 91,3998(1987)
6. W. P. Ambrose, W. E. Moerner: Chem. Phys., 144, 71(1990)
7. H. Suzuki, T. Shimada, T. Nishi, H. Hiratsuka: Jpn. J. Appl. Phys., 29, L1146(1990)
8. Verhoeven, J. W. Pure: Appl. Chem., 58,1285(1986)
9. M. P. Tsvirko, V. V. Sapunov, K. N. Solovev: Opt. Spektrosk, 34, 1094(1973)



Friday, September 27, 1991

## Time Domain

**FB** 10:45am-12:30pm  
DeAnza Room

*W. M. Yen, Presider*  
*University of Georgia*

## Temporal Accessing of Frequency-Domain Optical Storage: Specific Approaches and General Considerations

Thomas W. Mossberg  
Department of Physics, University of Oregon  
Eugene, Oregon 97403; (503) 346-4779

The ultimate memory device would be one in which a bit of data is stored in every atom or molecule within a storage material. Such a memory would have an incredible storage capacity of somewhere in the range of  $10^{22}$  bits/cm<sup>3</sup>. Traditional optical memories, whether two- or three-dimensional, can never hope to achieve atomic-level storage densities for the simple reason that minimally sized storage cells always have edge dimensions on the order of or larger than the wavelength of light employed. In the case of visible light, cubic wavelength scale storage volumes contain billions of atoms.

A new class of optical memories has recently been proposed [1-4] which holds the promise of making near atomic-level data storage a reality. This approach to storage, generically referred to as frequency-selective optical data storage, works by addressing atoms spectrally as well as spatially. It turns out that the constituent atoms/molecules within many materials display spectrally narrow resonances (with a width referred to as  $\Delta f_h$ ), and that the resonances of individual atoms/molecules are spread throughout a rather broad frequency range (referred to as  $\Delta f_i$ ). Thus atoms located within a minimally sized spatial volume can be subdivided and hence addressed on the basis of their frequencies. In some materials, up to  $\Delta f_i/\Delta f_h \approx 10^7$  frequency subdivisions can be made, making it possible to subdivide the billions of atoms/molecules within a minimally sized spatial storage volume into separately addressable groups containing only a few hundred atoms each. The atoms/molecules belonging to each spectral group are generally positioned randomly throughout the spatially addressed storage volume with which they are associated.

Frequency-selective approaches to optical data storage can be divided into two types both of which can in principle achieve the same ultimate storage density. In one type (referred to here as *directly addressed* [1,2]), lasers involved in the storage and retrieval process must be frequency shifted to address and mark each of the spectrally distinguishable subgroups of atoms/molecules. Within a spectral storage channel, an on bit is represented through a write-induced change in the absorptivity of the storage material. The drawbacks associated with this approach to frequency selective memory follow from the need to rapidly tune the read and write lasers to specific absolute frequencies. Also, it follows from fundamental physics that a spectral storage channel of width  $\Delta f_h$  cannot be individually accessed in a time shorter than about  $\Delta f_h^{-1}$ . This fact limits the input/output rate of directly addressed frequency-selective optical memories to about  $\Delta f_h$  bits/sec. In the other type of frequency-selective memory (referred to here as *temporally addressed* [4-10]), writing is accomplished with a laser of fixed carrier frequency that is amplitude or frequency modulated so as to encode a string of bits onto its temporal envelope. The maximum permissible modulation rate is material dependent and is given by  $\Delta f_i$ . Each spatially

addressable volume of the storage material is exposed to the writing laser for a time that can be as long as  $\Delta f_h^{-1}$ . During this time  $\Delta f_i/\Delta f_h$  bits, one for each available spectral channel, can be encoded and stored. Note that the storage of all these bits occurs in a temporal interval equal to that required to store a single bit in the direct addressing scheme described above. In temporally addressed frequency-selective storage, the Fourier spectrum of the bit stream is recorded in the spectral channels of the storage material and all spectral channels are written in parallel. The Fourier spectrum is represented through frequency-dependent changes in the storage material's absorption profile. The parallelism implicit in temporal addressing endows it with a potential factor of  $\Delta f_i/\Delta f_h$  speed advantage over direct addressing. With temporal addressing, input/output must occur at a rate of  $\Delta f_i$  bits/sec in order to utilize the full storage potential of a given material. In cases where,  $\Delta f_i$  exceeds obtainable input/output rates, only  $\Delta f_m/\Delta f_h$  bits, where  $\Delta f_m$  is the maximum achievable input/output rate, can be stored using the simple temporal addressing scheme discussed here. Temporally addressed data is recalled by stimulating the storage material to emit a coherent optical signal having the same duration and temporal envelope as the stored bit stream. Write-induced changes in the storage material's spectral absorption profile are never directly observed. Hybrid approaches utilizing both direct and temporal addressing may avoid many of the limitations of either approach considered separately. We note that variations of the temporal addressing scheme can be employed in the storage of holographic movies [4], delayed phase conjugation of images [11], and in the convolution and cross-correlation of temporal [12] or spatial [13] waveforms.

In the following, we give further details concerning the temporal addressing approach to frequency selective optical data storage. The direct addressing approach has been discussed extensively elsewhere [2,3].

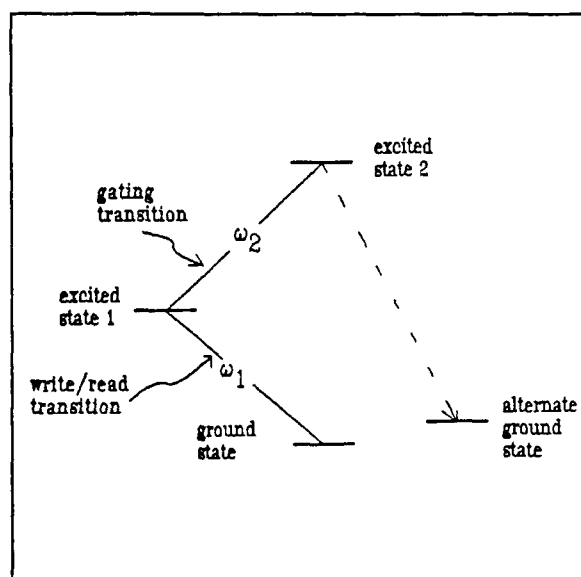


Figure 1a

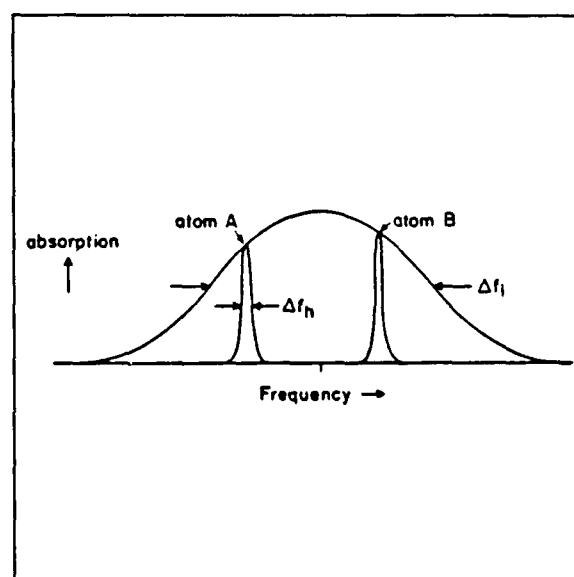


Figure 1b

We assume that the storage material is three-dimensional and contains active atoms/molecules that are modified so as to change their absorptivity in the data storage process. In materials studied to date, the active species has constituted anywhere from a fraction of one percent to nearly the entire bulk of the storage material. One highly favorable arrangement of internal energy levels for the active atoms/molecules is shown in Fig. 1a. In this case, the ground state consists of a single level lacking nearly degenerate subcomponents, and the write/read transition exhibits strong inhomogeneous broadening. Inhomogeneous broadening of the read/write transition implies (see Fig. 1b) that individual active atoms/molecules within the material are distributed in frequency over an interval large compared to their individual spectral response widths. Illumination of the material at the gating transition frequency transfers atomic/molecular population residing in excited state 1 to excited state 2. Once in excited state 2, a large fraction of the population decays by spontaneous processes to the alternate ground state. The alternate ground state may be the ground state of a photochemically altered species or, in the case of atoms, a low-lying and long-lived state. Ultimate storage times cannot be greater than the time required for population in the alternate ground state to relax back to the ground state.

The generic level configuration just described may also be suitable for directly addressed frequency-selective optical memories. Generally speaking, to realize a memory with a fixed number of spectral channels, direct (temporal) addressing is to be preferred in the case of materials with large (small) values of  $\Delta f_h$ . In the case of larger  $\Delta f_h$ , the intrinsic speed of direct addressing memories improves and difficulties associated with precise laser frequency control are eased. Conversely, in the temporal addressing case, large values of  $\Delta f_h$  necessitate large (eventually impossibly large) input/output bit rates. The input/output rate must be at least  $N_b$  times  $\Delta f_h$ , where  $N_b$  denotes the number of bits to be stored in a given spatial storage location. As discussed above, an upper limit on  $N_b$  is set by the need to keep the input/output rate less than  $\Delta f_i$ .

A simple configuration for a temporally addressed memory is shown in Fig. 2. In this case, the storage material is in the form of a disk so that its spatial storage channels can be addressed as in traditional optical memories. Within the one spatial storage cell shown in Fig. 2, multiple bits corresponding to the number of spectral channels available are written. The thickness of the storage material and/or the concentration of active atoms/molecules within it is to be adjusted so that a weak input beam is attenuated by approximately 50 percent as the beam passes through the storage material. Fulfillment of this condition allows for output signals of optimal size relative to the input beams. Two pulses are involved in the storage of a bit stream in a single spatial storage cell (see Fig. 3). The first pulse, referred to here as the preparation pulse, excites the active atoms/molecules into a superposition state involving the ground state and excited state 1. The intensity of this pulse should be adjusted so that it transfers roughly half of the ground state atoms within its bandwidth to excited state. The preparation pulse may be temporally short compared to the bandwidth of the bit stream to be stored, or it may be longer and swept in frequency across the bandwidth of the bit stream. The second (data) pulse consists of the actual bit stream to be stored. Its intensity, like that of the preparation pulse, should be adjusted so that it

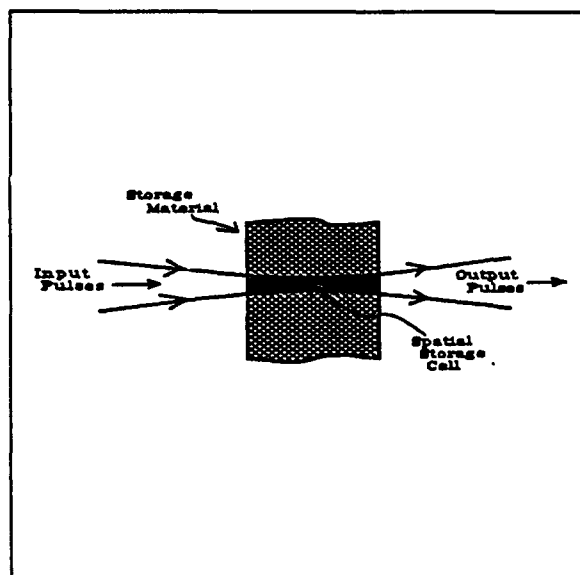


Figure 2

population distributions in the ground state and in excited state 1. If excited state 1 decays exclusively to the ground state, the stored information will disappear over the lifetime of excited state 1. For the information to be retained, the excited state population must be prevented from recombining with the population in the ground state. In some materials, the ground state contains sublevels and the excited state decays back to them in a way which differs from the way in which the writing pulses depopulate them. In these cases, information can be retained as a frequency dependent non-thermal distribution of population among the ground state sublevels [6,8]. In the level scheme shown in Fig. 1, long term data storage is achieved by applying a gating pulse, resonant with the transition between excited states 1 and 2, following the writing pulses and before excited state 1 decays. If excited state 2 decays primarily to the alternate ground state, the complementary populations created during the storage sequence will be prevented from recombining over the ground state - alternate ground state thermalization time. The use of a gating pulse is also important because it allows the read function to be non-destructive [3].

would by itself transfer approximately half of the population in the ground state and within its bandwidth to excited state 1. The central frequency of both storage pulses should lie within the inhomogeneous absorption profile of the storage material. The total temporal interval between the start of the preparation pulse and the end of the data pulse should be less than approximately  $\Delta f_h^{-1}$ . The combined action of the preparation and data pulses acts to record the Fourier transform of the data pulse as a feature of the absorption profile of the storage material. If the preparation pulse is not short, the transform is recorded in a complex form.

Immediately following the writing sequence, the bit stream is stored in complementary frequency-dependent

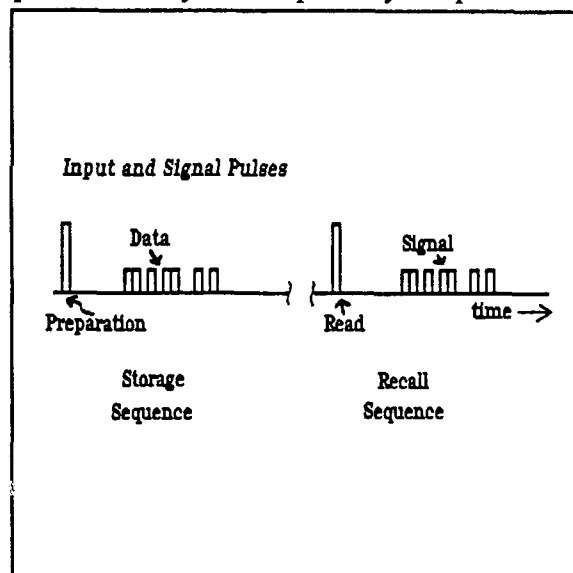


Figure 3

The recall sequence consists of an input read pulse followed by a signal pulse. The read pulse must be essentially identical to the preparation pulse; however, it may in principle be resonant with a transition coupling the ground state with another excited state. In cases studied to date, the read pulse and the preparation pulse have been resonant with the same transition. If a second transition is to be employed, its inhomogeneous broadening must be correlated with the inhomogeneous broadening of the transition used in the writing sequence. The read pulse stimulates the storage material to emit a signal pulse having the same temporal envelope as the data pulse. The signal pulse is a coherently emitted signal, and as such it is highly directional. If all input pulses are collinear (Fig. 2), the signal pulse will have directional properties essentially identical to the data pulse. In general, the wavevector of the signal pulse will be related to the wavevectors of the input pulses according to

$$\mathbf{k}_s = \mathbf{k}_d + \mathbf{k}_r + \mathbf{k}_p$$

where  $\mathbf{k}_p$ ,  $\mathbf{k}_d$ ,  $\mathbf{k}_r$ , and  $\mathbf{k}_s$  represent the wavevectors of the preparation, data, read, and signal pulses, respectively. To maximize the intensity of the signal pulse, the process must be phase matched, i. e. the input pulse directions must be arranged so that the magnitude of  $\mathbf{k}_s$  from the equation above is equal to  $n\omega_s/c$ , where  $n$  is the index of refraction of the storage material,  $\omega_s$  is the frequency of the signal pulse, and  $c$  is the speed of light. Under ideal conditions, the number of photons emitted in the signal pulse will be about 1/100 of the number of active atoms/molecules in the spatial storage cell, and the intensity of the signal pulse will be about 1/100 of the intensity of the data pulse.

Temporally addressed frequency-selective optical data storage has been demonstrated in the laboratory [5,6,8,10], and the basic optical physics related to the storage and retrieval process is now well understood. The question of whether this form of memory will ever find significant application will depend primarily on the success or failure of attempts to find suitable storage materials. All long term storage materials demonstrated to date are useful only when cooled to near liquid helium temperatures (4 K) in order to make  $\Delta f_n$  reasonably small. While this situation is unlikely to change, the enormous potential speed and capacity of temporally addressed frequency-selective optical memories should more than justify the relatively minor costs associated with cooling. Materials exhibiting the ideal level system shown in Fig. 1 have not yet been found. This is not particularly surprising nor discouraging since workers to date have concentrated on understanding the storage process itself. True materials limitations will only become apparent when materials experts become acquainted with the system needs discussed here and have a chance to apply their knowledge to the problem. If an ideal material is found, near atomic scale memories with storage densities up to  $10^{14}$  -  $10^{18}$  bits/cm<sup>3</sup> and input/output rates in the multigigahertz range may become achievable.

## References

1. A. Szabo, U. S. Patent No. 3,896,420 (July 22, 1975). G. Castro, D. Haarer, R. M. MacFarlane, and H. P. Trammendorf, U. S. Patent No. 4,101,976 (July 18, 1978).
2. W. E. Moerner, *J. Molec. Elec.* **1**, 55 (1985).
3. W. E. Moerner, W. Lenth, G. C. Bjorklund, in *Persistent Spectral Holeburning: Science and Applications*, Topics in Current Physics, vol. 44, Springer-Verlag, p 251 (1988). Note: The analysis of frequency-selective optical storage presented in this review is limited in that not all possible approaches are considered and limiting assumptions are unnecessarily made. This is particularly true in the case of temporal addressing.
4. T. W. Mossberg, *Opt. Lett.* **7**, 77 (1982), and U. S. Patent No. 4,459,682 "Time-Domain Frequency-Selective Optical Memories," (July 10, 1984).
5. N. W. Carlson, Y. S. Bai, W. R. Babbitt, and T. W. Mossberg, *Phys. Rev. A* **30**, 1572 (1984); Y. S. Bai, W. R. Babbitt, and T. W. Mossberg, *Opt. Lett.* **11**, 724 (1986).
6. W. R. Babbitt and T. W. Mossberg, *Opt. Commun.* **65**, 185 (1988).
7. W. R. Babbitt, Y. S. Bai, and T. W. Mossberg, *Proc. of SPIE*, v. 639 (April 1986).
8. M. K. Kim and R. Kachru, *Opt. Lett.* **14**, 423 (1989).
9. M. Mitsunaga, M. K. Kim, and R. Kachru, *Opt. Lett.* **13**, 536 (1988).
10. M. Mitsunaga and N. Uesugi, *Opt. Lett.* **15**, 195 (1990).
11. N. W. Carlson, W. R. Babbitt, and T. W. Mossberg, *Opt. Lett.* **8**, 623 (1983).
12. W. R. Babbitt and T. W. Mossberg, *Appl. Opt.* **25**, 962 (1986).
13. M. K. Kim and R. Kachru, *Opt. Lett.* **12**, 593 (1987).

**Time-domain optical data storage  
using  $\text{Eu}^{3+}$  ions in crystals**

**Masaharu Mitsunaga**

**NTT Basic Research Laboratories**

**Musashino-shi, Tokyo 180, Japan**

The photon-echo memory[1], or the time-domain optical data storage, resembles the hole-burning memory[2] in that the inhomogeneous absorption line of a material is employed as a storage medium and the information is stored in it as a frequency-dependent absorption change with the resolution determined by the homogeneous width. Having the common memory capacity  $N$  given by the inhomogeneous-to-homogeneous width ratio, both types of memories share common problems like low-temperature operation, spectral diffusion and so on. Although a storage medium is common, storage techniques are definitely different for the two memories. The photon-echo memory utilizes the temporal interference effect between a reference pulse and a data pulse and their interference pattern is stored as a population grating in the frequency domain. In this sense this is a time-domain analog of holography where the spatial interference pattern between a reference beam and a data beam is stored in a medium as a population grating in the real space. Like the spatially diffracted beam from the read beam gives the information stored in the hologram, the "temporally diffracted pulse", or the photon echo, after the read pulse can give the information stored in the inhomogeneous distribution.

Due to this interference effect, the holography and the photon-echo memory store the quantity  $\mathcal{E}_R^* \mathcal{E}_D$  where  $\mathcal{E}_R$  and  $\mathcal{E}_D$  denote the amplitudes of the reference beam and the data

beam, respectively, whereas the ordinary optical memory and the hole-burning memory store  $|\mathcal{E}_D|^2$ . In this respect, one may call ordinary optical memory and hole-burning memory incoherent-type memories and holography and photon-echo memory coherent-type memories.

Some advantages of coherent-type memories over incoherent-type memories can be summarized as follows: 1) optical amplitude storage (including phase) instead of intensity storage, 2) simultaneous retrieval of multiple-bit information, 3) immunity from defect (The amount of information is not affected by the defect in the storage medium. Only the signal intensity is reduced.) 4) application to spatial or temporal phase conjugation, and 5) ability of signal processing.

We have been investigating the feasibility of time-domain optical data storage using photon-echo technique in rare-earth ions, especially  $\text{Eu}^{3+}$ , in crystals such as  $\text{YAlO}_3$  and  $\text{Y}_2\text{SiO}_5$ . Among rare-earth ions, Eu ions show 1) ultralong dephasing time ( $> 100 \mu\text{s}$ )[3] or ultranarrow homogeneous width ( $< 1 \text{ kHz}$ ), 2) inhomogeneous width of  $\sim 10 \text{ GHz}$  which, combining with the homogeneous width, gives the memory capacity  $N \sim 10^7$ , 3) long storage time ( $\sim \text{hours}$ ) 4) small photon echo envelope modulation. These properties make the Eu-doped crystal a perfect sample in investigating the time-domain data storage.

So far we have achieved a 248-bit temporal data storage using cw photon echo technique[4,5] and also bit-by-bit storage technique[6]. The stored information could be retrieved by the read pulse and the input data was reproduced without any error. Storage time of well above 1 hour was confirmed.

Instead of writing and reading the information in the same domain, time-domain or frequency-domain, an alternative approach may be to write in the frequency domain and read in the time domain. This is called spectrally programmed stimulated photon echo[7].

By using a single-frequency tunable cw laser, one can burn in the inhomogeneous line any desired hole pattern by frequency-scanning and intensity-modulating the laser. One can then apply a pulsed laser to obtain a coherent transient response as a Fourier transform of whatever is programmed in the inhomogeneous line. Aside from a memory device, this system can be regarded as an all-optical function generator that produces any desired pulse shape (or pulse train). Since only a small spotsize is needed for this experiment, several thousand different pulseshapes (or temporal data) can be generated by one crystal.

#### ACKNOWLEDGMENTS

The author is indebted to Ryuzi Yano and Naoshi Uesugi for their comments and experimental help.

#### REFERENCES

1. T. W. Mossberg, *Opt. Lett.* **7**, 77 (1982); W. R. Babbitt, Y. S. Bai, and T. W. Mossberg, *Proc. Soc. Photo-Opt. Instrum. Engr.* **639**, 240 (1986).
2. *Persistent Spectral Hole-Burning: Science and Applications*, Topics in Current Physics 44, Editor W. E. Moerner, Springer Verlag, 1988.
3. R. M. Macfarlane and R. M. Shelby, *Opt. Commun.* **39**, 169 (1981).
4. M. Mitsunaga, R. Kachru, E. Xu and M. K. Kim, *Phys. Rev. Lett.* **63**, 754 (1989); M. Mitsunaga, *Phys. Rev.* **A42**, 1617 (1990).
5. M. Mitsunaga and N. Uesugi, *J. Lumin.* **48/49**, 459 (1991).
6. M. Mitsunaga and N. Uesugi, *Opt. Lett.* **15**, 195 (1990).
7. M. Mitsunaga and N. Uesugi, *Opt. Lett.* **16**, 264 (1991).

## INCOHERENT LIGHT READ-OUT OF SPECTRAL HOLOGRAMS

A. Débarre, J.-C. Keller, J.-L. Le Gouët, and P. Tchério

Laboratoire Aimé Cotton, C.N.R.S.II, Bâtiment 505, 91405 Orsay Cedex

It is known that one has investigated two types of approach to Persistent Spectral Hole Burning (PHB), and to potential application for optical data storage. In both methods, a structure is stored within the inhomogeneously broadened optical absorption line of the guest ions or molecules in a host matrix at low temperature.

In the first method, monochromatic laser irradiation results in the reduction of the sample absorption coefficient at a given frequency. The burnt spectral hole is then detected by monitoring the transmission of the laser beam when its frequency is scanned over the absorption band. In view of application to optical data storage, spectral hole burning can be regarded as the physical process for addressing a bit of binary encoded information at a given position within the absorption band. The maximum number of independent addresses in the absorption band is given by the ratio between the inhomogeneous width  $\Delta_i$  and the homogeneous width  $\Delta_h$  of the optical transition.

The other PHB method belongs to coherent transient spectroscopy. It is derived from Stimulated or three-pulse Photon Echo (SPE). Interaction with the first two pulses engraves a sinusoidal modulation in the absorption band. This hologram-type structure spreads over all the inhomogeneous width. Its period equals the inverse time separation between the first two pulses. The third pulse of the SPE sequence acts as a probe. It gives rise to an emission which is the frequency-to-time Fourier transform of the engraved spectral hologram. The duration of this emission is given by the inverse inhomogeneous width and its delay with regard to illumination by the probe equals the inverse period of the hologram. In conventional PHB, holes can be burnt at different locations in the absorption band. In a similar way, holograms with different periods can be stored together. When probed by a single pulse, the sample radiates a train of bursts of light. Each burst originates from a definite spectral hologram. In a sample of dye molecules embedded in a polymer host, the inverse inhomogeneous width is usually as short as 100 fs. This is the minimum duration of the light bursts, and this is the time resolution which has to be attained in signal emission triggering and in signal detection, in order to take advantage of the storage capabilities of the sample. Two requirements have to be met. The first one is to produce probe laser pulses in

the femtosecond range. The second one is to keep a 100fs resolution all along the signal processing. Fulfilment of this latter condition is presently out of reach of electronic systems. It can be circumvented by using an optical sampling technique such as cross-correlation between the signal and a reference pulse. Then the hologram structure is probed repetitively and the signal is analyzed point after point as a function of the time interval since illumination by the probe. When intensity cross-correlation is used, the time resolution is limited by the duration of the probe and of the reference [1]. Since fast sampling is compatible with slow detectors, the necessity of using so short pulses has to be questioned. As a matter of fact, probing by long duration broadband pulses and sampling by field cross-correlation is enough to gain the required short time resolution, which is then determined by the coherence time of the light and not by the pulse duration. Signal analysis by field cross-correlation has already been achieved [2] using heterodyne detection. The signal amplitude depends upon the the phase shift between the signal and the reference. The optical paths of these pulses have thus to be controlled with interferometric precision.

We report on the retrieval of optically stored spectral holograms. The *sampling analysis of the signal* is also based upon a field cross-correlation technique. The field cross-correlation function is deduced from the contrast of an interference pattern built between the signal and the reference. We insist that contrary to the case of heterodyne detection, no interferometric control of the optical paths is needed. Subpicosecond data retrieval is obtained with both picosecond and nanosecond probe pulses. A sampling point is acquired in nearly 50ms. In the nanosecond regime, owing to the low repetition rate of the laser ( $15s^{-1}$ ), single shot sampling is practicable. In the picosecond regime, the result is a statistical average over a large number of probing processes. Storage of spectral holograms involves a "write" pulse and a train of "data" pulses, which propagates along the wave vectors  $\mathbf{k}_1$  and  $\mathbf{k}_2$  respectively. An engraved hologram is associated with the interference of each "data" with the "write" pulse. The probe pulse propagates along  $\mathbf{k}_1$  and the signal is emitted along  $\mathbf{k}_2$ . The reference pulse is beam-split from the probe pulse, with an adjustable time-delay. The experiment is performed in a polystyrene plate doped with octaethylporphine. The upper trace on Figure 1 represents the recorded field cross correlation between the reference and an elementary data train which is reduced to a sequence of two pulses. The FWHM of the data is 240fs. On the lower trace of the figure is displayed the single

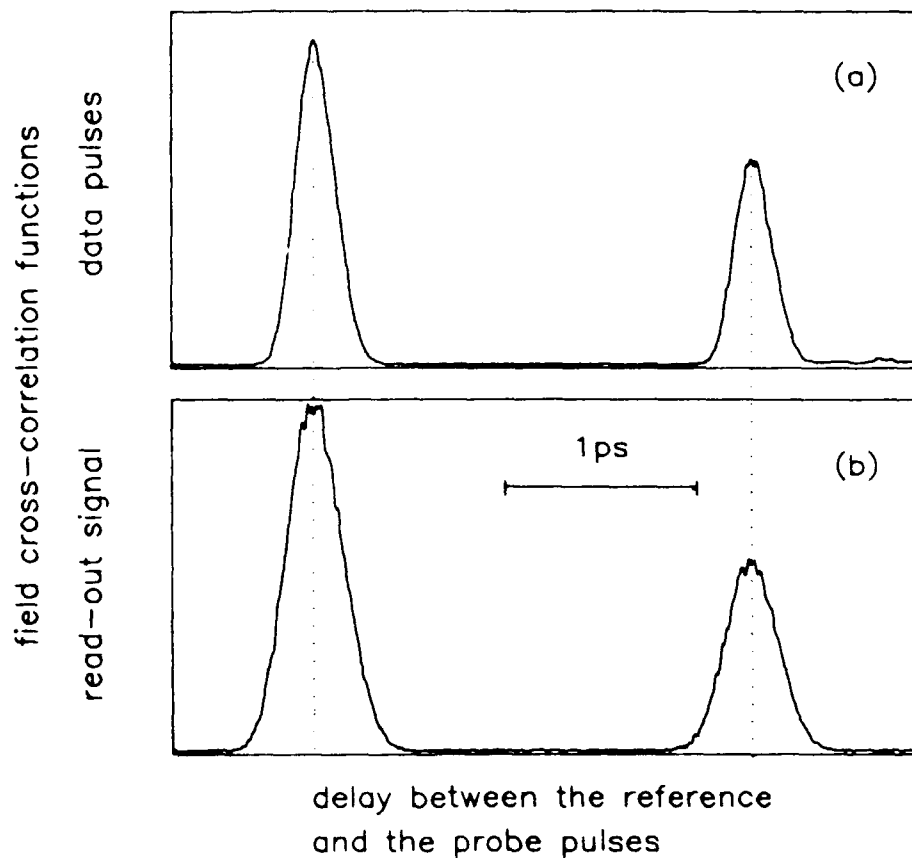


Figure 1

scan recording of the field crosscorrelation between the reference and the restored signal, when the sample is probed by a nanosecond laser with a coherence time of 120fs. The time separation between the restored peaks coincides with the delay between data pulses. Their width (360fs) is a little smaller than expected (450fs) by calculating the convolution of the data with the probe and the absorption band ( $\Delta_1^{-1} = 260\text{fs}$ ).

[1] A. Rebane, J. Aaviksoo, and J. Kuhl; *Appl. Phys. Lett.*, **54** 93 (1989).

[2] S. Saikan, T. Kishida, A. Imaoka, K. Uchikawa, A. Furasawa, H. Oosawa; *Opt. Lett.*; **14**, 841 (1989).

[3] A. Débarre, J.-C. Keller, J.-L. Le Gouët and P. Tchénié; *J. Opt. Soc. Am.* **8**, 153 (1991).

## Frequency - Domain Measurements of Spectral Hole Patterns Burned with Phase - Coherent Pulses

C. Michael Jefferson, Alfred J. Meixner

IBM Almaden Research Center  
650 Harry Road  
San Jose, CA 95 120  
phone (408) 927 2141, (408) 927 2808

### *Introduction*

Several investigations have shown that in some systems stimulated photon echoes may be obtained over times much longer than the excited state relaxation time  $T_1$ <sup>1,2</sup>. It has been claimed that the mechanism for this anomalously long storage time is the formation of a frequency dependent modulation of the ground state population which persists because of spectral hole-burning<sup>1</sup>. Such a population grating produced by coherent multipulse excitation and spectral hole-burning has been measured only in a few cases<sup>3</sup>.

We have investigated the frequency dependence of such hole patterns stored in the ground state population with respect to the parameters of both the excitation sequence and those of the guest-host system. We compare our results to a theoretical model obtained using density matrix formalism to describe an inhomogeneously broadened distribution of two level systems with a relaxation path into an additional reservoir state to allow for spectral hole-burning.

We chose two pulse stimulation of the inhomogeneously broadened band as a format for studying stored population gratings because the structure of such gratings is especially simple. In our experiments we were able to accurately control the pulse amplitudes, durations, separations and the relative optical phases. We will show that the phase relationship of the stimulating pulses has a profound effect on the structure of the population grating.

### *Experimental*

We performed these experiments at 6 K in  $Eu^{3+}:YAlO_3$  (0.25%), a system which has both long dephasing ( $T_2 = 58\mu s$  at 1.5 K) and excited state lifetime ( $T_1$  on the order of 1 ms).<sup>4</sup> This system allows spectral hole-burning because of hyperfine levels which serve as a population reservoir. The spectral holes persist for many hours at liquid helium temperatures<sup>1</sup>. We excited the inhomogeneously broadened  ${}^7F_0 - {}^5D_0$  transition of the  $Eu^{3+}$  ions at 581.6 nm with pairs of 40 ns pulses. These pulses were separated by 60 ns and had a rise and fall time of approximately 11 ns. We were able to adjust the optical phase of the second pulse relative to the first by either  $0^\circ$  or  $180^\circ$ . The phase-coherent pulses were created by acousto-optic modulation<sup>5</sup> of the cw beam of an actively stabilized ring dye laser with an estimated bandwidth of 1 MHz. We applied 1000 pulse pairs to the sample separated by 2 ms. This time was chosen so as to allow complete relaxation of the excited state after each excitation state. By using this many burning cycles we were able to resolve structural details in the resulting population grating over the entire measurement range. Transmission spectra were measured by scanning the laser frequency over a spectral range of 200 MHz and recording the detected light power on a digital oscilloscope.

## Results and Discussion

The spectral hole patterns in Fig.1 were obtained by dividing the transmission spectra by previously recorded reference spectra. Details concerning the data treatment will be published elsewhere. Both hole patterns exhibit a broad envelope which reflects the spectral width of the 40 ns wide pulses. The strong modulation at 10 MHz corresponds to the inverse of the time between the leading edges of the excitation pulses (100 ns) rather than their separation (60 ns). In Fig.1a there was no phase shift between the pulses and in Fig.1b, the second pulse had a 180° phase shift. The hole patterns show a distinct qualitative difference. In Fig.1a there is a deep spectral hole component at the center frequency whereas in Fig.1b there is instead an increase of absorption. Overlaying the hole spectra shows that the deep hole components in Fig.1a and 1b are shifted by 5 MHz with respect to each other. We believe that this is the first time that the effect of the relative optical phase of the excitation pulses has been observed in spectral hole patterns.

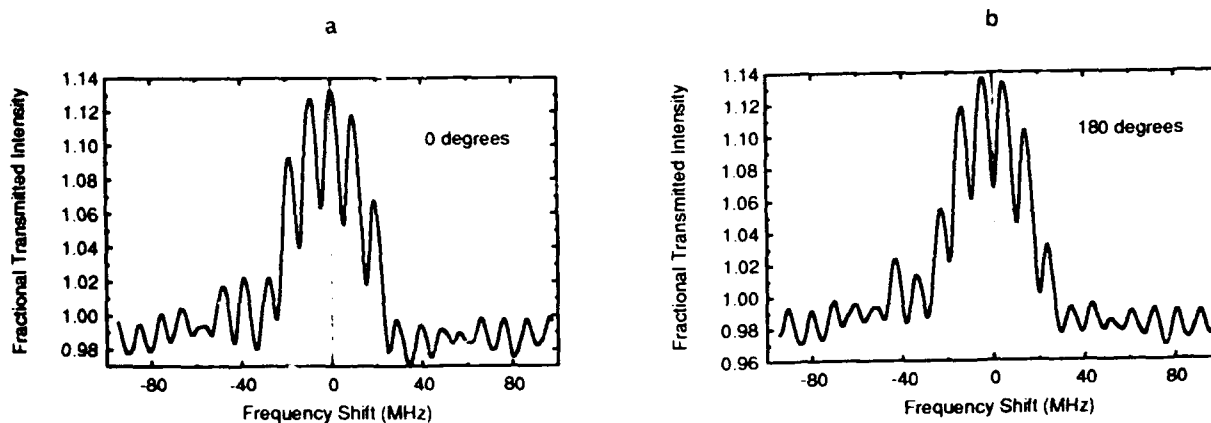


**Figure 1.** Measured spectral hole patterns burned by 1000 phase-coherent pulse pairs. Pulses were 40 ns duration and separated by 60 ns. Relative optical phase of the second pulse was either 0° or 180°.

With a few exceptions<sup>5,6</sup> the usual practice has been to neglect the phase in the theoretical treatment of photon echoes and time domain hole-burning. As a result, we have found it necessary to rederive expressions for the macroscopic polarization and the ground and excited state population which explicitly include the optical phase in order to explain our experimental data.

We use the time dependent Schrodinger equation to derive expressions for the density matrix elements which include the optical phase. Dephasing and relaxation is introduced into these equations in the usual manner.<sup>7</sup> This formalism is applied to an inhomogeneously broadened system and the variation of the phase as a function of the frequency is taken into account. We use this model to calculate an explicit expression for the ground state population  $\rho_{11}(\Delta)$ , following two pulse stimulation and subsequent relaxation of the excited state.

$$\rho_{11}(\Delta) = 1 - \eta \frac{\sin^2(\chi(\Delta)\tau)}{2} (1 + e^{-t'/T_2} \cos(\phi - \Delta(t' + \tau))). \quad (1)$$

Here  $\rho_{11}(\Delta)$  is the density matrix element for the ground state population as a function of the frequency offset,  $\Delta$ , from the center frequency of the laser pulses. The hole-burning efficiency is described by  $\eta$ . Note that the Rabi frequency  $\chi(\Delta) = \mu E(\Delta)/\hbar$  is itself a function of the offset frequency,  $\Delta$ . The transition dipole moment is described by  $\mu$  and is assumed to be constant.  $E(\Delta)$  is the Fourier transform of the electric field

of the excitation pulses. Both excitation pulses have identical duration,  $\tau$ , and the time between pulses is  $t'$ . By this definition the time between the leading edges of the pulses is  $(t' + \tau)$ , and the optical phase of the second pulse relative to the first is  $\phi$ .

In our calculation we have neglected relaxation only during excitation, and we have assumed that the excitation sequence is much shorter than the energy relaxation time,  $T_1$ . The  $\sin^2$ -term provides the envelope of the spectral hole pattern. Note that this is an inherently non-linear function, which is, in the limit of weak excitation, proportional to the product of the frequency spectra of the excitation pulses. The term in parentheses describes a modulation or "grating" which has a period given by  $(t' + \tau)^{-1}$  and a phase equal to the phase difference of the pulses. The modulation depth depends only on the ratio between the pulse separation  $t'$  and the dephasing time  $T_2$  in our approximation.

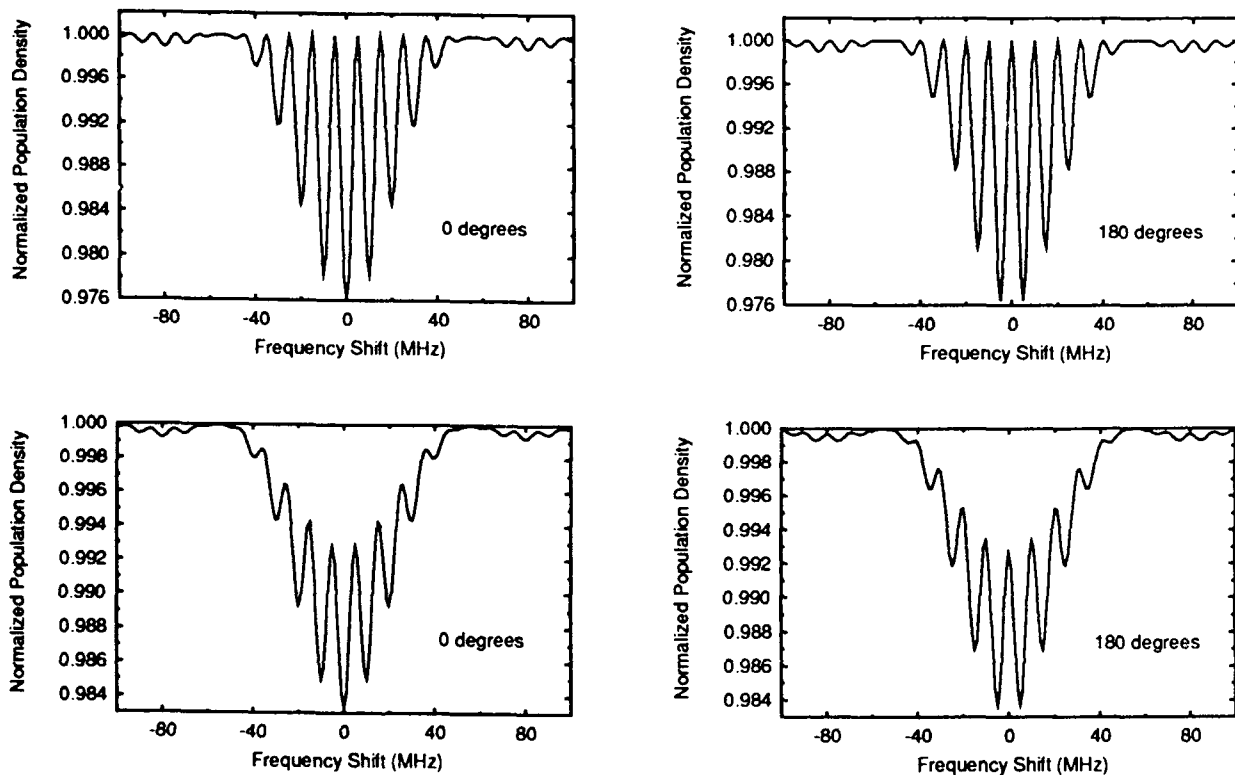


**Figure 2.** Calculated population gratings using Eq.(1) with our experimental parameters. Left side figures have  $0^\circ$  optical phase difference between the pulses; right side figures have  $180^\circ$  phase shift. The lower traces include the effect of 2 MHz laser jitter.

In the upper half of Fig.2 we have plotted Eq.(1) using our experimental parameters. We note that there is a substantial difference between the observed and predicted modulation depths. According to Eq.(1) the modulation depth is reduced by dephasing. In our experiments, the ratio of  $t'/T_2$  is far too small to account for the observed decrease in modulation depth. We believe that this decrease is due to frequency jitter of the laser. In the lower half of Fig.2 we have plotted a simulation of the population grating calculated from Eq.(1) with the addition of a statistically jittering laser frequency, described by a Gaussian probability function. If the laser is assumed to have a 2 MHz rms bandwidth, then the calculated population grating is in excellent agreement with the data, in both the  $0^\circ$  and  $180^\circ$  phase cases. Another difference between the

calculated population gratings and the measured spectra is the presence of strong modulation far from the center frequency. We believe that this is due to the hyperfine levels<sup>4,8</sup> which cause side holes and antiholes which could also be modulated.

The theoretical model which describes our measurements has two important implications for time domain spectral hole-burning: i) The modulation depth and hence the strength of the stimulated echo depend on the ratio  $t'/T_2$ . If the stimulated echo is due to accumulation of a number of pulse pairs with different  $t'$ , as is often done, then the amplitude of the stimulated echo will decay due to the dephasing term in Eq.(1).<sup>9</sup> ii) It is also clear that the effect of phase and frequency jitter of the laser during the excitation process or in the course of accumulation will tend to reduce the modulation depth and consequently also reduce the amplitude of the stimulated echo.

### **Summary**

We have performed experimental measurements of the ground state population gratings created by excitation of an inhomogeneously broadened system with resonant pulse pairs whose relative phases could be varied. We have compared our results to a theoretical model and found good agreement. Our investigations have shown that many aspects of time domain spectral hole-burning may be better understood by considering the details of the actual spectrum of the ground state population grating in the frequency domain.

### **References**

1. W.R. Babbitt, T.W. Mossberg, *Opt. Comm.* 65 (1988) 185
2. M.K. Kim, R.Kachru, *Opt. Lett.* 14 (1989) 423
3. A. Rebane, R. Kaarli, P.Saari, A. Anjialg, K. Timpmann, *Opt. Comm.* 47 (1983) 173.
4. R.M. Macfarlane, R.M. Shelby in "Spectroscopy of Solids Containing Rare Earth Ions", A.A. Kaplyanskii, R.M. Macfarlane Editors, North-Holland 1987
5. W.S. Warren A.H. Zewail, *J. Chem. Phys.* 78 (1983) 2279
6. T.W. Mossberg, R. Kachru, S.R. Hartmann, A.M. Flusberg, *Phys. Rev. A* 20 (1979) 1976
7. Amnon Yariv "An Introduction to the Theory and Applications of Quantum Mechanics", Wiley 1982, p. 160
8. W.R. Babbitt, A. Lezama, T.W. Mossberg, *Phys. Rev. B* 39 (1989) 1987
9. M. Mitsunaga, N. Uesugi, *Opt. Lett.* 15 (1990) 195

**Photon-echo in Er-doped fibers:  
a new approach to femtosecond time-domain  
optical signal processing**

V.L. da Silva, Y. Silberberg, J.P. Heritage, E.W. Chase,  
M.A. Saifi, and M.J. Andrejco

*Bellcore, 331 Newman springs Road, Red Bank, New Jersey 07701-7040  
Tel: (908) 758-3130, FAX: (908) 741-2891*

Recently, interest in photon echo has been revived because of its potential application in time-domain optical memories<sup>1</sup>. Several demonstrations have been reported in gases and also bulk organic and inorganic materials at cryogenic temperatures<sup>2-4</sup>. In this paper, we report the observation of accumulated photon echo in Er doped optical fibers and demonstrate that these fibers can be used to store information on the subpicosecond time scale.

Optical fibers have proved to be very attractive for studies of nonlinear optical phenomena such as optical Kerr effect, stimulated Raman and Brillouin scattering, four wave-mixing and even second harmonic generation<sup>5</sup>. The great advantage of optical fibers over bulk media is in the ability to focus the light in a small core area and to propagate it without diffraction over lengths that can be as long as kilometers. By using rare-earth doped fibers, other new, stronger nonlinearities than those originated from the silica base are introduced by the dopant. As a consequence, coherent effects should be important when pulses shorter or comparable to the dephasing time of the impurity ions propagate in the fiber. Er-doped fibers are particularly important in optical communications because the  $I_{15/2} - I_{13/2}$  transition at 1.53  $\mu\text{m}$  coincides with the minimum loss region of silica based fibers. These fibers can be pumped by diode lasers and have been used as amplifiers and as lasers in the 1.53  $\mu\text{m}$  region.

The homogeneous, inhomogeneous and fluorescence lifetimes for the  $I_{15/2} - I_{13/2}$  transition of erbium in aluminosilicate fibers at 4.2°K were measured to be 80 psec, 0.6 psec and 10 msec, respectively<sup>6</sup>. That suggests that these fibers should be a suitable medium for storage of tens of bits with subpicosecond duration. The use of Er doped fibers for these applications offer a major advantage in terms of significant simplification of alignment and cooling requirements. Er-doped fibers are also compatible with many highly developed fiber-based components, including amplifiers, couplers and connectors, and should be investigated as a possible

alternative for time-domain optical signal processing.

In our experiment, depicted in Fig.1, a NaCl:OH<sup>-</sup> color-center laser with additive-pulse mode-locking<sup>7</sup> is used as the optical pulse source for the photon-echo experiment. These pulses are less than 200 fsec long and can be tuned into the  $I_{15/2} - I_{13/2}$  transition of the Er ions at 1.53  $\mu\text{m}$ . The laser pulse repetition rate is 82 MHz while the Er relaxation time  $T_1$  is 10 msec. That means that approximately  $10^6$  pulse pairs are coupled into the fiber within  $T_1$ , which satisfies the condition for accumulated photon echo<sup>8</sup>.

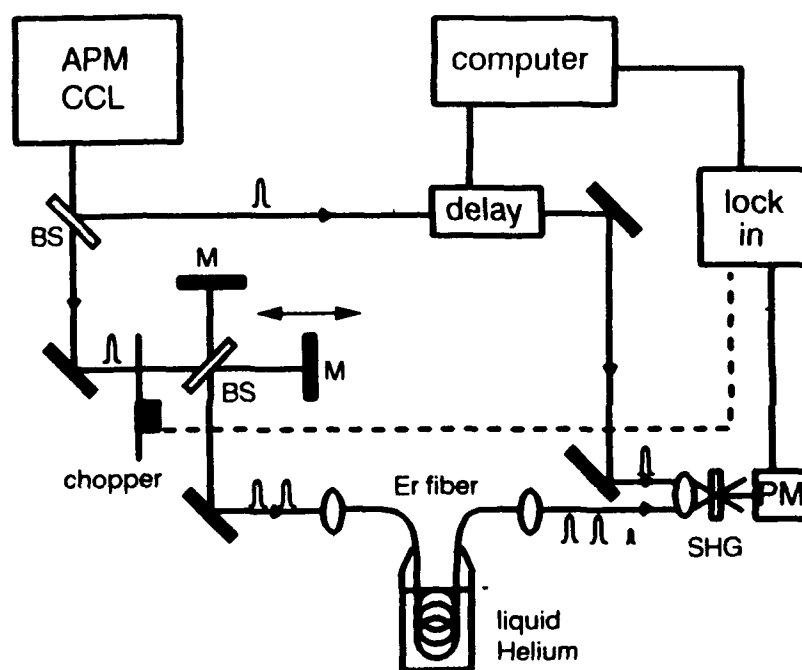


Fig. 1 Experimental set up for observation of photon-echo in an Er-doped fiber.

The fiber used had a silica cladding and an Er-doped germanium-calcium-aluminum silicate core<sup>9</sup>, with a diameter of 5  $\mu\text{m}$ . The peak absorption was 10 dB/m at 1.530  $\mu\text{m}$  at room temperature. A 4.5 m section of this fiber was coiled to a 4 cm diameter, spliced to dispersion shifted fiber pigtails and immersed in liquid helium. Note that using a fiber system eliminated the need for windows, vacuum and other difficulties associated with cryogenic optical systems.

A Michelson interferometer was used to generate a pulse pair which was coupled to the fiber. The average power coupled to the fiber was about 4 mW. The output from the tested fiber was time-resolved by cross-correlating it with a delayed pulse of the laser, as shown in fig. 1. The echo pulse obtained in this experiment had a duration of 800 fsec. It is likely that this pulse is broadened by the dispersion in the fiber, estimated to be about 10 psec/Km nm. The echo duration was measured

to be only 500 fsec in a 0.8 m long fiber, where dispersion effects should be minimal. Since the excitation pulses are only 200 fsec in duration, this echo duration is a signature of the 10 nm inhomogeneous linewidth. Although we did not measure the value of the homogeneous lifetime  $T_2$  in our fiber, it seemed to be significantly longer than the 80 psec measured in aluminosilicate fibers<sup>6</sup>, as we could not detect a significant drop in echo intensity even for pulse separations of 200 psec. This difference can be attributed to the special glass composition of the fiber in our experiment<sup>9</sup>. These results suggests the possibility of storage and recording of information as long as hundreds of picoseconds with 0.5 psec resolution.

In order to verify the possibility of using Er doped fibers in time-domain optical memories<sup>1</sup>, we substituted one of the excitation pulses with a double-peaked pulse. Although in our experiment the echo is generated through the accumulating effect of many pulses, we can still demonstrate the correlation between the shapes of the echo and the excitation pulses, which provides the basis for these signal processing applications. In our experiment the second excitation pulse serves also as the read pulse. The double-peaked pulse, with 3 psec separation, was obtained by exploiting the birefringence of a 10 mm long KTP crystal, which was introduced into one of the arms of the interferometer. The relative intensity of the two peaks was adjusted by rotating the crystal. A polarizer was inserted before the fiber in order to assure that both excitation pulses were linearly polarized in the same direction. An Er-doped fiber amplifier was used in this experiment to amplify the input pulses before they enter the fiber under test, in order to enhance the generated echo.

Figure 2a shows the echo generated when the double-pulse is the first to enter the fiber. As expected, the echo pulse shape is a time-reversed replica of the first excitation pulse. Figure 2b shows a similar experiment where the double pulse was arriving second. The echo clearly shows a triple peaked signal; in the small signal limit, this echo can be shown to be the autoconvolution of the second excitation pulse<sup>2</sup>. In both cases we observed significant distortion in the ratio between the peaks, particularly when the excitation intensity was increased. We believe that the distortions are the result of higher nonlinear effects induced in a strongly saturated system and will be discussed later.

In conclusion, we have verified that complex pulse shapes can be stored and recalled in erbium doped fibers. Our data suggests that the erbium-doped fiber system is a suitable medium for processing complex signals with maximum duration of hundreds of picoseconds and resolution of only 0.5 psec.

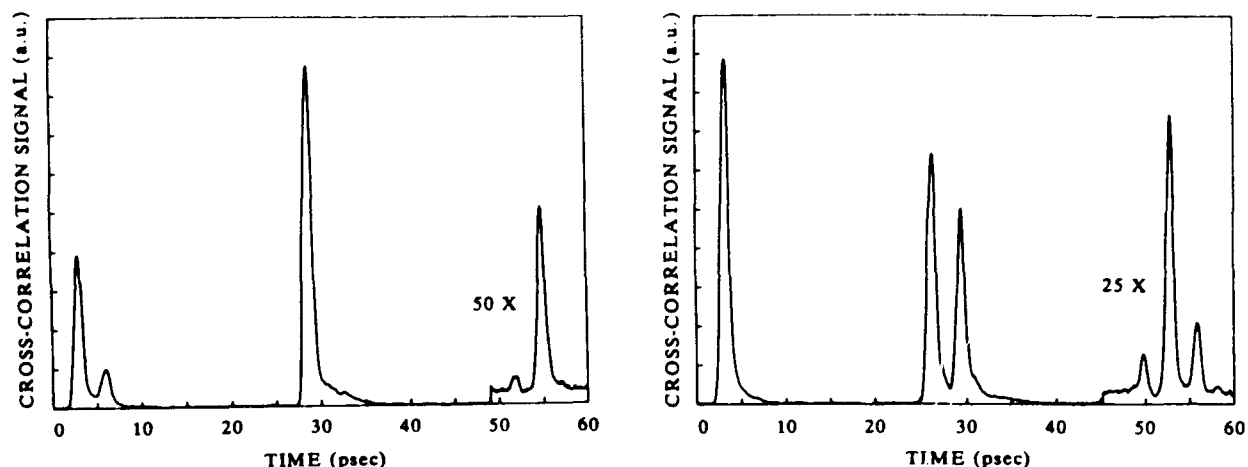


Fig. 2. (a) An echo experiment with a double-peaked leading pulse. The echo is a time-reversed replica of the leading pulse. Distortion is caused by higher order saturation effects. (b) An echo experiment with a double-peaked trailing edge. The triple-peaked echo is the auto-convolution of the second pulse.

### References

1. T.W. Mossberg, *Opt. Lett.* **7**, 77 (1982).
2. N.W. Carlson, L.J. Rothberg, A.G. Yodh, W.R. Babbitt, and T.W. Mossberg, *Opt. Lett.* **8**, 483 (1983); N.W. Carlson, Y.S. Bai, W.R. Babbitt, and T.W. Mossberg, *Phys. Rev. A* **30**, 1572 (1984); Y.S. Bai, W.R. Babbitt, N.W. Carlson, and T.W. Mossberg, *Appl. Phys. Lett.* **45**, 714 (1994); W.R. Babbitt and T.W. Mossberg, *Opt. Comm.* **65**, 185 (1988).
3. A. Rebane, R. Kaarli, P. Saari, A. Anijalg, and K. Timpmann, *Opt. Comm.* **47**, 173 (1983); A. Rebane, J. Aaviksoo, and J. Kuhl, *Appl. Phys. Lett.* **54**, 93 (1989).
4. M.K. Kim and R. Kachru, *Opt. Lett.* **12**, 593 (1987); M.K. Kim and R. Kachru, *Opt. Lett.* **14**, 423 (1989).
5. see for example G.P. Agrawal, *Nonlinear fiber optics*, Quantum Electronics - Principles and Applications Series, Academic Press (1989).
6. E. Desurvire, J.L. Zyskind, and J.R. Simpson, *IEEE Phot. Tech. Lett.* **2**, 246 (1990).
7. C.P. Yakymyshyn, J.F. Pinto, and C.R. Pollock, *Opt. Lett.* **14**, 621 (1989).
8. W.H. Hesselink and D.A. Wiersma, *J. Chem. Phys.* **75**, 4192 (1981).
9. M.A. Saifi, M.J. Andrejco, W.I. Way, A. Von Lehman, A.Y. Yan, C. Lin, F. Bilodeau, and K.O. Hill, in the Technical Digest of the Optical Fiber Communication Conference 1991, paper FA6.



Friday, September 27, 1991

## Mechanisms: 1

**FC** 2:00pm–3:15pm  
DeAnza Room

G. J. Small, *Presider*  
*Iowa State University*

## Hole Burning in the Vibrational Spectrum of Crystals and Glasses

A. J. Sievers

518 Clark Hall, Laboratory of Atomic and Solid State Physics, Cornell University

Ithaca, NY 14853, phone: 607-255-6422

Persistent IR spectral holes can be generated in the vibrational degrees of freedom of small molecules matrix isolated in crystals<sup>(1)</sup> and glasses<sup>(2,3)</sup> even though no electronic excitation is involved, i.e., a non-photochemical process. The union of the IR lead salt diode laser and broad band FT interferometric methods has produced a new high resolution spectroscopic technique for investigating both the statics and dynamics of molecules in solids. These low power single mode diode lasers (~10 to 100  $\mu\text{W}$ ) provide a near ideal cw source for investigating persistent IR spectral holes (PIRSHs). They can be produced and probed with a single laser, focused to an intensity at the sample typically up to 100  $\text{mW}/\text{cm}^2$ . Persistent spectral changes which occur far from the laser line can be monitored with an FTS probe beam at 60 MHz resolution.

Vibrational hole burning in crystalline hosts can be divided into four generic kinds of effects. The simplest persistent effect is where the vibrational hole and antihole are distributed inside the original inhomogeneously broadened line, as observed for the tetrahedral molecule  $\text{ReO}_4^-$  in alkali halide crystals. Hole burning occurs because the inhomogeneous static strain fields in the crystal at the same site makes the two molecular orientations, which are separated by a large potential barrier, inequivalent. As long as these neighboring ground state configurations differ by more than a laser linewidth, there is a possibility of reorientation during the continued excitation and de-excitation of the vibrational transition for one molecular orientation. Hence, as long as the relaxation time back to the ground state is much longer than the excited state lifetime, the absorption at the laser frequency will decrease, producing a persistent hole.

A second kind of vibrational hole burning, in which the antihole is removed in frequency from the inhomogeneously broadened line, has been observed for the  $\text{CN}^-$  molecule in alkali halide crystals. Since the  $\text{CN}^-$  ion isolated in a perfect KBr crystal tunnels among a number of equivalent positions, it does not show persistent effects. However, when another impurity such

as  $\text{Na}^+$  is a near neighbor to  $\text{CN}^-$  the stretch mode of  $\text{CN}^-:\text{Na}^+$  and that with the molecule rotated by 180 degrees ( $\text{NC}^-:\text{Na}^+$ ) are inequivalent. One of these is the ground state configuration. Persistent hole burning studies as a function of temperature have shown that the other configuration is 140 K above the ground state energy value with these two states separated by a barrier height of 1400 K. By burning at the vibrational ground state transition frequency and monitoring the entire IR spectrum with a high resolution FT interferometer, it has been possible to carry out spectroscopic and hole burning measurements on both configurations. For example, vibrational Stark effect measurements indicate that the effective dipole moments in each arrangement are different.

Manifold burning represents a third kind of process. The asymmetrical bending mode transition of  $\text{NO}_2^-$  in KCl and KBr consists of a complex spectrum made up of five absorption lines, four components symmetrically spaced around a weak central line. Hole burning at any of the four components produces additional satellite holes in the other three, indicating that all four lines stem from the same dynamical properties of an individual molecule. Such experiments have shown that the complex spectrum is produced by rotational tunneling of the N about the O-O axis, which is fixed in the octahedral cage, and that the hole burning is associated with the reorientation of the O-O axis in the crystal.

Finally, the fourth effect consists of burning at one vibrational mode frequency while monitoring the persistent changes produced in the other internal or external modes with a high resolution FT interferometer. This procedure has been used effectively to identify the localized phonon modes of the particular defect-lattice system. When  $\text{NO}_2^-$  is doped into KI, in addition to the internal vibrational modes of the molecule, three low lying far IR excitations are found at frequencies in the gap between the optic and acoustic phonon branches. By doping the crystal with molecules containing an isotopic mixture of N-14 and 15, as well as O-16 and 18, and then monitoring the forest of far IR lines in the KI gap region while sequentially burning on each of the isotope-shifted IR bending modes with the diode laser, the far IR isotope shifts of all of the gap-mode isotopic combinations have been identified. The different isotope shifts show for the first time that two of the far IR transitions are from translational localized modes of the  $\text{NO}_2^-$ , while the third has a mixed translational-librational character. Such information is crucial for any

lattice dynamical calculation of this low symmetry defect-lattice system. The general conclusion is that vibrational hole burning can be expected to influence the entire spectrum produced by the defect, including the impurity induced absorption in the phonon spectrum.

The chalcogenide glasses are the first class of glassy systems to exhibit non-electronic persistent hole burning. Glasses of  $\text{As}_2\text{S}_3$ , Se,  $\text{As}_2\text{Se}_3$  as well as the alloy Ge-As-Se have all been doped with small molecules and examined by PIRSH burning to characterize the general dynamical properties of the glassy state. The results are quite revealing. All molecule:glass combinations show PIRSH burning and spontaneous hole filling at low temperatures. We find that a diverse set of impurities in a single host all display very similar relaxation behavior, while identical impurities in different hosts show strikingly different behavior. These results demonstrate the dominant role of the host in determining the hole relaxation behavior. A similar pattern emerges for the hole widths in the various systems in that the temperature dependence of the width appears to be determined solely by the host, independent of the defect involved.

When the spontaneous hole filling is monitored for PIRSHs burned in the SeH vibrational band for glasses of 10 different chemical compositions in the Ge-As-Se system at 1.5 K, the dominant spectral hole relaxation rate is found to increase by over three orders of magnitude as the average atomic coordination number varies from 2 to 2.8. However, it is observed that the quantitative time dependent form of the non-exponential hole relaxation depends solely on the average coordination number, independent of chemical composition. Given the complexity of glassy systems, it is both surprising and intriguing that the average coordination number can predict spectral hole relaxation behavior.

### References

1. A. J. Sievers and W. E. Moerner, in *Persistent Spectra Hole Burning: Science and Applications*, W. E. Moerner, ed., (Springer-Verlag Publishing Co., New York, 1988).
2. S. P. Love and A. J. Sievers, in *Advances in Disordered Semiconductors, Vol. II*, F. Fritzsche, ed., (World Scientific Pub. Co., Singapore, 1990).
3. S. P. Love, et al., *Phys. Rev. Letters* **65**, 1792 (1990).

## Hydrogen Bonds in a Polymer Investigated by Picosecond Infrared Hole Burning

H. Graener

University of Bayreuth, Physics Department

P.O. Box 101251, D-8580 Bayreuth, Germany

In the past spectral hole burning was intensively investigated for dye molecules in solid matrices. The long-lived photochemical holes at low temperature gave valuable and detailed information on the structural properties of the molecular surrounding, e.g. polymer matrices. More recently, persistent photochemical hole burning at low temperatures was extended to the infrared for smaller molecules in rare gas<sup>1</sup> or glass matrices and to hydrogen bonded polymers.<sup>2</sup>

Recently we observed transient spectral holes in the infrared absorption spectrum of a polymer at ambient temperature.<sup>3</sup> The analysis of the hole parameters gives valuable information on the hydrogen bonds in the disordered system. Our experimental technique is a double-resonance spectroscopy with intense tunable picosecond pulses. Details of the measuring system have been described recently.<sup>4</sup>

In short, a first strong IR excitation pulse (energy  $\sim 50 \mu\text{J}$ , duration  $11 \pm 2$  ps, bandwidth  $8\text{--}20 \text{ cm}^{-1}$  (depending on frequency) is resonantly tuned to the OH absorption band and focused into the sample. A second time-delayed weak probing pulse (energy  $< 1 \mu\text{J}$ , the other parameter as for the pump) with adjustable frequency serves to measure the sample transmission  $T(\nu, t_D)$  as a function of delay time  $t_D$  and/or probe frequency  $\nu$  (energy transmission  $T$  of the probe pulse). A peak intensity of  $2 \times 10^{10} \text{ W/cm}^2$  is estimated for the focal plane of the pump beam.

The samples are polymer (PVB) films (thickness  $20\text{--}60 \mu\text{m}$ ) with high optical quality. The preparation has been described recently.<sup>4</sup> The dried polymer films are fixed between  $\text{CaF}_2$  optical windows using poly(chlorotrifluoroethylene) oil as an index-matching fluid and placed in a cryostat.

The conventional IR absorption spectrum of PVB shows a broad asymmetric band with a maximum around  $3470\text{ cm}^{-1}$  and a steep wing to the high frequency side. On the low frequency side the absorption decreases more slowly by a factor of 10 from the maximum to  $3100\text{ cm}^{-1}$ .

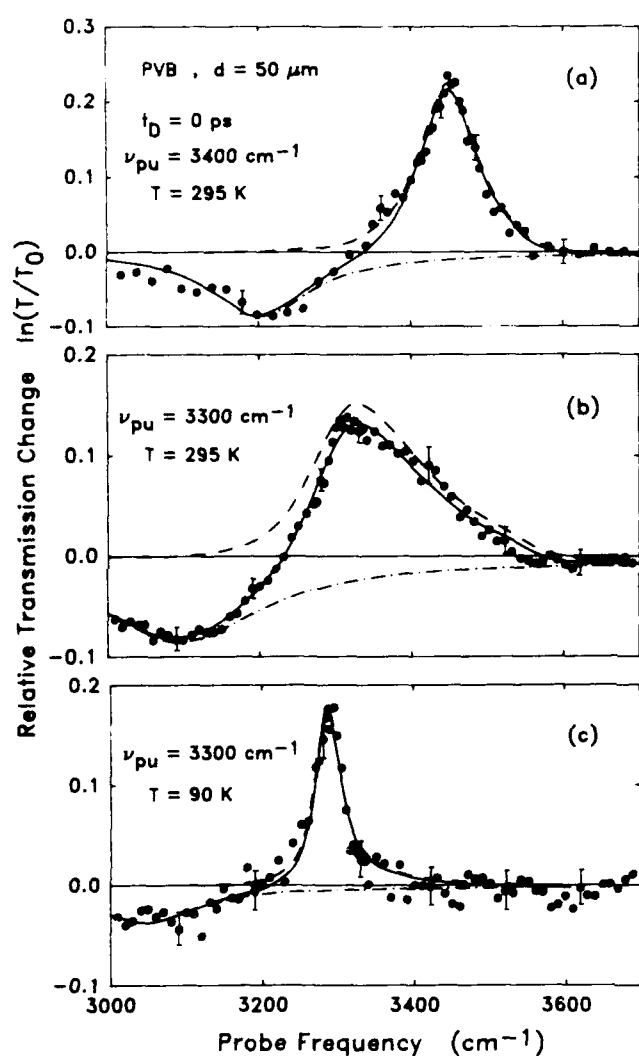


Fig. 1:

Transient probe spectra in the OH region of PVB taken during the excitation process:

a) pump frequency  $\nu_{\text{pu}} = 3440\text{ cm}^{-1}$ ,  $T = 295\text{ K}$ ;

b)  $\nu_{\text{pu}} = 3300\text{ cm}^{-1}$ ,  $T = 295\text{ K}$ ;

c)  $\nu_{\text{pu}} = 3300\text{ cm}^{-1}$ ,  $T = 90\text{ K}$ .

The solid lines represent fitted theoretical curves for the determination of the hole width; two spectral components (dashed lines) are considered respectively for the fundamental transition and excited state absorption.

Fig. 1 presents three experimental results. The relative transmission change  $\ln(T/T_0)$  is plotted versus probe frequency. For Fig. 1a (sample temperature  $295\text{ K}$ ) the pump pulse was tuned to  $3400\text{ cm}^{-1}$  near the center of the absorption maximum of the OH stretching vibration band. Clearly visible is the transmission increase (spectral hole) around the pump frequency and the

inverse hole around  $3200 \text{ cm}^{-1}$ . Tuning the pump pulse to  $3300 \text{ cm}^{-1}$  (Fig. 1b) the spectral hole and the inverse hole are red-shifted by approximately  $100 \text{ cm}^{-1}$ . Additionally a broadening of the transmission increase is observed. For Fig. 1c the sample was cooled down to 90 K and excited at  $3300 \text{ cm}^{-1}$ . The center frequency of the hole (compared to Fig. 1b) is only slightly shifted, whereas the hole width notably decreases.

A summary of the temperature dependence of the hole width is given in Fig. 2. The hole width  $2\Gamma$  (HWHM) is plotted on a semilogarithmic scale versus the reciprocal temperature. The upper (solid) line refers to measurements with a pump frequency of  $3300 \text{ cm}^{-1}$ . For the measurements of the lower (dashed) line the pump pulse was tuned to  $3440 \text{ cm}^{-1}$ . One observes in both cases an exponential decrease of the hole width  $1/T$ , but larger ordinate values for the low frequency pumping. Assuming a dependence of the form  $\Gamma \sim \exp(-hc\nu_2/kT)$  as suggested by anharmonic exchange coupling<sup>5</sup> to the bridge stretching vibration  $\nu_2$  one gets slopes of respectively  $\nu_2 = 141 \pm 17 \text{ cm}^{-1}$  ( $\nu_{\text{pu}} = 3300 \text{ cm}^{-1}$ ) and  $135 \pm 15 \text{ cm}^{-1}$  ( $\nu_{\text{pu}} = 3440 \text{ cm}^{-1}$ ).

Further time-resolved measurements show that the lifetime of the hole and the inverse hole is  $5 \pm 2 \text{ ps}$  and independent of temperature (80 - 300 K) within the accuracy of the experiment. The short lifetimes of the holes is directly related to the different physical mechanisms as compared to persistent holes observed in similar systems, which are of photochemical nature.<sup>2</sup> In our observation the population difference between the ground state and the excited OH vibration gives the dominant contribution. So the observed lifetime of the holes is the population decay time of OH stretching vibration.

The extrapolation of the observed exponential temperature dependence of the hole width to 10 K yields values much too low compared to the width of the observed persistent holes of other systems. On the other hand, the observed vibrational lifetime  $T_1 = 5 \pm 2 \text{ ps}$  suggests a lower limit for the hole width of  $\approx 1 \text{ cm}^{-1}$  (HWHM) that nicely compares with the reported width of persistent IR holes at low temperature.<sup>2</sup> For higher temperatures  $> 100 \text{ K}$ , lifetime broadening is insignificant.

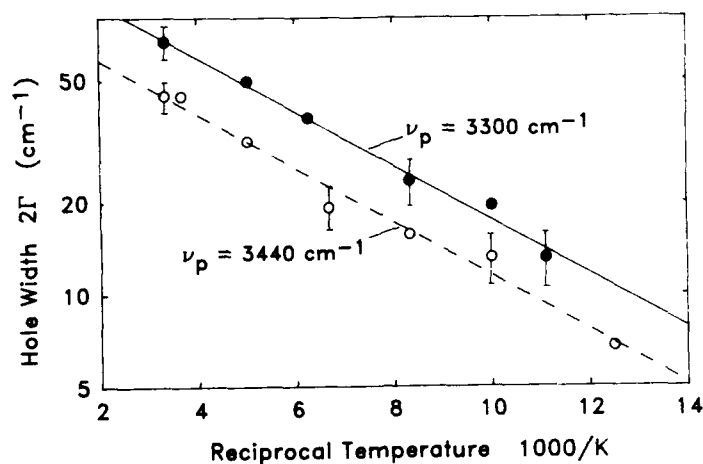


Fig. 2: Hole width  $2\Gamma$  (HWHM) on a logarithmic scale versus reciprocal temperature for two values of the pump frequency: experimental points. The calculated lines yield slopes of  $\nu_2 = 135 \pm 15 \text{ cm}^{-1}$  (dashed line,  $\nu_{pu} = 3400 \text{ cm}^{-1}$ ) and  $141 \pm 17 \text{ cm}^{-1}$  (solid line,  $\nu_{pu} = 3300 \text{ cm}^{-1}$ ).

Further comparison between the persistent (photochemical)<sup>1,2</sup> and our transient (photophysical) holes give nice agreements. In both cases the hole width increases with decreasing pump frequency: also a frequency dependence of the hole depth is related to the absorption cross section. For our PVB samples, many of the findings can be explained by a local variation of the strength of the hydrogen bonds that also accounts for the inhomogeneous character of the OH absorption band.

The close relationship between transient and persistent spectral holes suggested by our investigation is not surprising since a transient (population) hole is a necessary precursor of a persistent (photochemical) hole.

<sup>1</sup> S.P. Love and A.J. Sievers. Chem. Phys. Lett. 153 (1988) 379

<sup>2</sup> J.S. Shirk, R.G.S. Pong and A.W. Snow. J. Chem. Phys. 90 (1989) 3380

<sup>3</sup> H. Graener, T.-Q. Ye and A. Laubereau. Phys. Rev. B 41 (1990) 2597

<sup>4</sup> H. Graener, R. Dohlus and A. Laubereau. Chem. Phys. Lett. 140 (1987) 306

<sup>5</sup> S.F. Fischer and A. Laubereau. Chem. Phys. Lett. 55 (1978) 189.

## Spectral and Temporal Dynamics of Nonequilibrium Phonons in YAG:Pr<sup>3+</sup>

Xiao-jun Wang and W.M. Dennis

Department of Physics and Astronomy  
University of Georgia  
Athens, GA 30602

Tel: (404) 542 2882, FAX: 404-542-2492

We have investigated the spectral and temporal dynamics associated with phonon decay in the YAG:Pr<sup>3+</sup> system at a range of temperature between 9 and 25 K. Nonequilibrium phonons were generated using defect induced one phonon absorption (DIOPA) of far infrared (FIR) radiation<sup>1</sup>. Phonon detection was achieved optically using a variation of absorption vibronic sideband phonon spectroscopy<sup>2</sup>.

Far infrared radiation in the frequency range 30 - 113 cm<sup>-1</sup> was generated using a transversely excited atmospheric pressure CO<sub>2</sub> laser pumped superradiant cell. This configuration produces 50 ns FIR pulses with single pulse energies in the range 1 - 10 mJ. The optical detection pulses were generated using a YAG:Nd<sup>3+</sup> pumped dye laser. The generation and detection beams were incident on the sample in a counterpropagating geometry with the phonon generated fluorescence collected at 90°. The sample was mounted in a two stage cold cycle refrigerator allowing the temperature to be varied between 9 and 300 K. The sample temperature was determined optically.

Figure 1 shows the spectral and temporal evolution of the decay products of 66 cm<sup>-1</sup> phonons. The decay products form two distinct peaks at 23 and 43 cm<sup>-1</sup> with distinct time evolutions. These features cannot be explained in terms of anharmonic decay processes which should lead to a single broadband distribution centered at half the generation frequency. Monochromatic phonon generation at 43, 111 and 113 cm<sup>-1</sup> also resulted in decay products with a spectral distribution similar to that in figure 1.

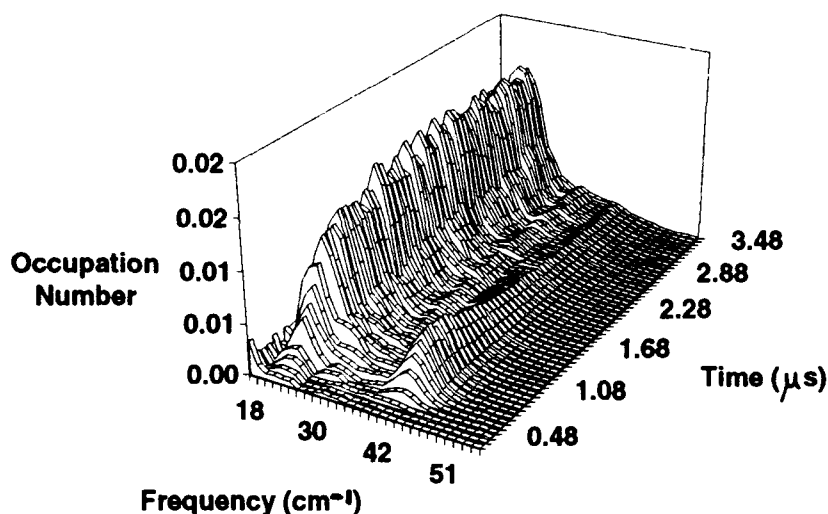


Figure 1. Time resolved phonon spectrum of the decay products of  $66\text{ cm}^{-1}$  phonons. Two spectral features at  $23$  and  $43\text{ cm}^{-1}$  can be clearly distinguished.

We interpret this behavior as due to inelastic phonon scattering processes. The phonon peaks described above cannot be correlated to states of the  $\text{Pr}^{3+}$  ion as reported in the literature<sup>3</sup>. However, an examination of the excitation spectrum of  $\text{Pr}^{3+}$  at a temperature of  $9\text{ K}$  reveals the presence of two states at  $23$  and  $43\text{ cm}^{-1}$ . These states appear to be  $\text{Pr}^{3+}$  ions in distorted sites or possibly pair states. We feel that it is not unreasonable that  $\text{Pr}^{3+}$  ions in distorted sites should exhibit a greater cross-section for phonon scattering than those in regular sites. In the case of  $43$  and  $113\text{ cm}^{-1}$  phonon generation we were able to detect the presence of narrowband frequency phonon distributions at  $20$  and  $70\text{ cm}^{-1}$  corresponding to inelastic scattering off the  $23$  and  $43\text{ cm}^{-1}$  states, respectively.

In the presence of inelastic scattering, the frequency dependence of the phonon lifetime should deviate from the  $\omega^5$  behavior expected for anharmonic decay. This was observed for phonons of frequencies  $< 70\text{ cm}^{-1}$  where the frequency dependence of the phonon lifetime rolled over towards an  $\omega^2$  dependence. Deviations from  $\omega^5$  at low

frequencies have been observed previously<sup>4</sup> and have been attributed to phonon transport out of the interaction region. We can dismiss this as a factor as the integrated phonon energy over the timescale of our experiment remains constant. Furthermore phonon transport experiments show that transport out of the interaction region occurs by heat conduction which occurs on a timescale of tens of microseconds.

We have investigated the dependence of phonon lifetime ( $\tau$ ) with temperature for the case of  $43 \text{ cm}^{-1}$ . A strong temperature dependence was observed as is shown in figure 2.

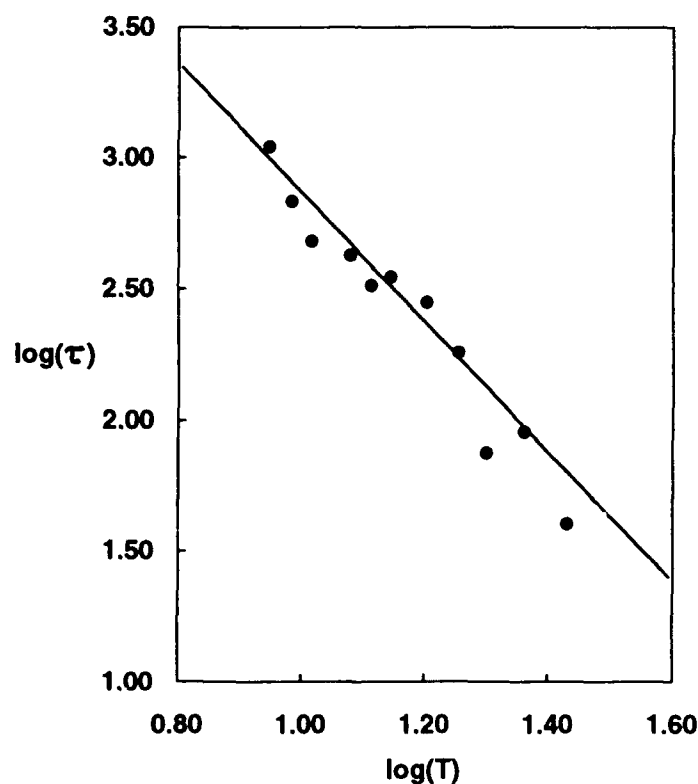


Figure 2. Plot of  $\log(\tau)$  versus  $\log(T)$ , where  $\tau$  is in ns. The solid line shows the best fit to a  $T^{-3}$  dependence over the range 9 - 25 K

The data show reasonable agreement with a  $T^{-3}$  dependence as expected for thermally induced phonon decay processes in the regime where  $\omega \gg T$ . We note that the above criterion is only a good approximation at temperatures below 20 K for the case of

43 cm<sup>-1</sup> phonons<sup>5</sup>. The detailed nature of the phonon processes involved and corrections to the T<sup>-3</sup> behavior at higher temperatures are currently under investigation.

This work was supported by National Science Foundation Grant Nos. DMR-8717696 and DMR-9015468. Equipment support was provided National Science Foundation Grant DMR-8914955.

#### REFERENCES

1. W.A. Tolbert, W.M. Dennis and W.M. Yen, Phys. Rev. Lett. **65**, 607 (1990).
2. R.S. Meltzer, J.E. Rives and G.S. Dixon, Phys. Rev. **B 28**, 4786 (1983).
3. J. B. Gruber, M.E. Hills, R.M. Macfarlane, C.A. Morrison and G.A Turner, Chem. Phys. **134**, 241 (1989).
4. R. Baumgartner, M. Englehardt and K.F. Renk, Phys. Rev. Lett. **47**, 1403 (1981).
5. Y. B Levinson, *Nonequilibrium phonons in nonmetallic crystals*. W. Eisengmenger and A.A. Kaplyanski, eds. (North-Holland Amsterdam, 1986), chapter 3.

Persistent spectral holeburning induced by ion-tunneling in  
hydrogenated  $\text{CaF}_2:\text{Pr}^{3+}$  and  $\text{SrF}_2:\text{Pr}^{3+}$  crystals.

R. J. Reeves\* and R. M. Macfarlane

IBM Research Division

Almaden Research Center

650 Harry Road, San Jose, CA 95120-6099

(408) 927-2428

The crystal systems of  $\text{CaF}_2:\text{Pr}^{3+}$  and  $\text{SrF}_2:\text{Pr}^{3+}$  into which  $\text{H}^-$ ,  $\text{D}^-$ , or  $\text{T}^-$  ions have been diffused exhibit persistent spectral holeburning when particular  $\text{Pr}^{3+}$  ion centers are resonantly excited.<sup>1</sup> The  $\text{H}^-$  ions replace lattice and interstitial  $\text{F}^-$  ions.<sup>2</sup> The holeburning is caused by  $\text{H}^-$  (or  $\text{D}^-$ ,  $\text{T}^-$ ) ion motion in the lattice following the  $\text{Pr}^{3+}$  excitation and the holes have lifetimes of at least several hours at low temperatures.

The group of centers that undergo this process have rhombic symmetry and are modified from the predominant  $\text{C}_{4v}$   $\text{H}^-$  hydrogenic center by the addition of extra hydrogenic ions in the near neighbor coordination cube. A number of centers are produced because there are several different positions where these extra ions can be located. The degenerate E ground state of the  $\text{C}_{4v}$  parent center is split by the rhombic field resulting in singlet ground states for the  $\text{Pr}^{3+}$  ion. Of particular interest is the fact that the centers differ greatly from one another in the strength of the rhombic distortion and hence the splitting,  $\Delta$ , of the ground state E level. This has dramatic consequences for the magnetic properties of the ground states and for the pseudoquadrupole splittings of  $^{141}\text{Pr}$ .

Four centers labeled  $\text{C}_s(1) - \text{C}_s(4)$  were studied in both  $\text{CaF}_2:\text{Pr}^{3+}:\text{D}^-$  and  $\text{SrF}_2:\text{Pr}^{3+}:\text{D}^-$  crystals. The centers remain quasi-axial and the  $^{141}\text{Pr}$ ,  $I = \frac{5}{2}$

hyperfine levels can be described by the spin Hamiltonian parameter  $2D$  with splittings between levels of  $2D$  and  $4D$ . Table 1 summarizes the spectral data for the centers under study.

Table 1  
Spectral and hyperfine data for the  $C_S$  centers in  $CaF_2:Pr^{3+}:D^-$   
and  $SrF_2:Pr^{3+}:D^-$  crystals

Crystal	Center	Wavelength (nm)	$\Delta$ ( $cm^{-1}$ )	$2D_{obs}$ (MHz)	Holeburning Mechanism <sup>a</sup>
CaF <sub>2</sub>	C <sub>S</sub> (1)	601.24	0.53	633	1
	C <sub>S</sub> (2)	604.79	9.5	52	2
	C <sub>S</sub> (3)	606.40	18.5	32 <sup>b</sup>	1
	C <sub>S</sub> (4)	602.29	20.2	26.9 <sup>b</sup>	1
SrF <sub>2</sub>	C <sub>S</sub> (1)	598.40	3.3	164	2
	C <sub>S</sub> (2)	601.80	8.3	64	2
	C <sub>S</sub> (3)	603.46	16.3	32 <sup>b</sup>	1
	C <sub>S</sub> (4)	599.82	21.3	24.9 <sup>b</sup>	1

- <sup>a</sup> 1 – Transient optical pumping of the  $Pr^{3+}$  hyperfine levels at temperatures less than 4K. Persistent holeburning at temperatures above 4K.  
2 – Persistent holeburning at all temperatures above 2K.

- <sup>b</sup> Hyperfine splittings measured by Optically Detected Nuclear Magnetic Resonance.

The holeburning spectra for the centers studied in  $CaF_2:Pr^{3+}:D^-$  and  $SrF_2:Pr^{3+}:D^-$  crystals are shown in figures 1 and 2 respectively. The temperature was 2K in all cases except for the  $C_S(1)$  center in  $CaF_2:Pr^{3+}:D^-$  where it was 5K. In each case there is a central hole at the laser frequency and either six additional side holes or antiholes depending upon the mechanism for holeburning. The origin of the side structure is the pseudoquadrupole splittings of the  $Pr^{3+}$  ground

state. The different splittings result from the variations in the energy  $\Delta$  of the first excited electronic state above the ground state. The magnitude of the splitting for each center is given in the table.

Figure 1.

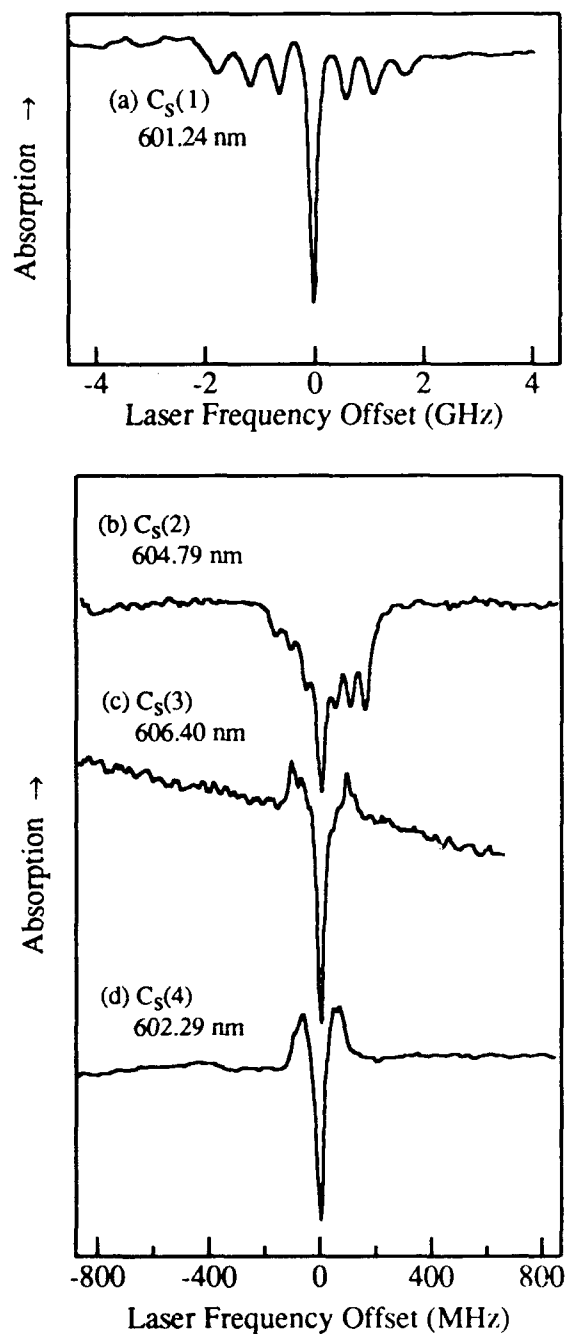
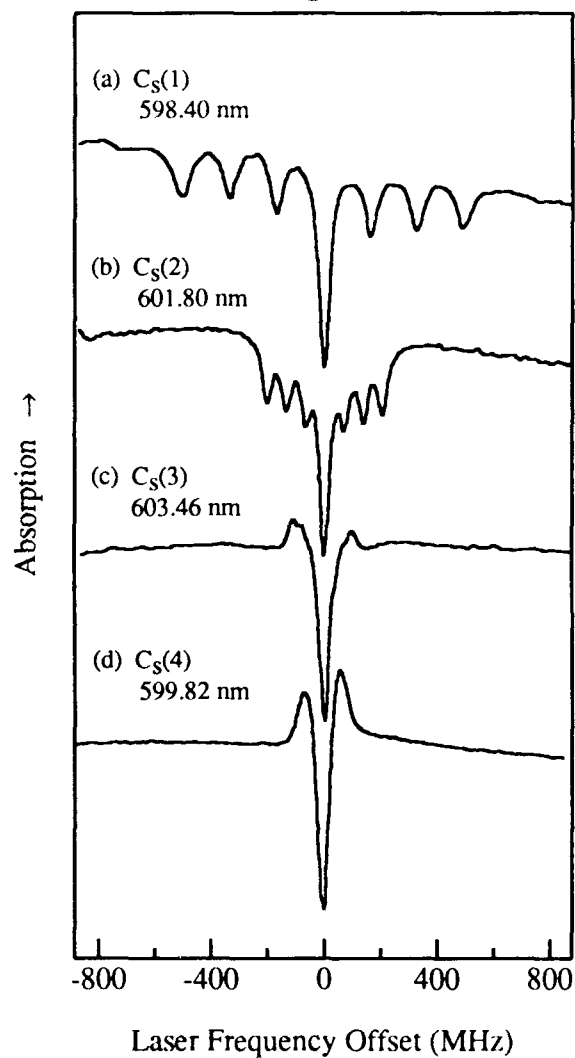


Figure 2.



Figures 1 and 2. Holeburning spectra for the four centers under study in a  $\text{CaF}_2:\text{Pr}^{3+} \text{D}^-$  and  $\text{SrF}_2:\text{Pr}^{3+} \text{D}^-$  crystal respectively.

Below 4K, the holeburning mechanism for the  $C_S(1)$  center in  $CaF_2:Pr^{3+}:D^-$  and the  $C_S(3)$  and  $C_S(4)$  centers in both crystals was optical pumping of the hyperfine levels. All centers exhibited persistent holeburning at temperatures above 4K. Figure 3 shows a schematic model of the  $C_S(1)$  center and the proposed mechanism for the hydrogenic ion motion. Note that in this case the optical transition wavelength of the photoproduct is not shifted but it absorbs in a different polarization. It appears necessary to have at least two hydrogenic ions in the near vicinity of the  $Pr^{3+}$  ion for persistent holeburning to occur. As would be expected from the proposed mechanism, the tunneling rate and hence the rate of holeburning depends on the mass of the hydrogenic ion.

In summary, we have observed persistent spectral holeburning in an inorganic crystal that is caused by light induced ionic motion and we have used this to measure pseudoquadrupole splittings for many of the centers.

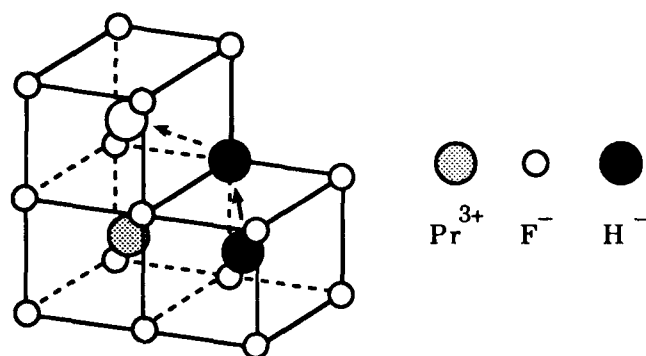


Figure 3. Schematic model of the  $C_S(1)$  center and the ionic motion that leads to persistent spectral holeburning.

\* Present Address: Center for Laser Research, Oklahoma State University, Stillwater, Oklahoma 74078.

- 1 R. M. Macfarlane, R. J. Reeves, and G. D. Jones, *Opt. Lett.* **12**, 660 (1987).
- 2 R. J. Reeves, G. D. Jones, and R. W. G. Syme, *Phys. Rev. B* **40**, 6475 (1989).

Friday, September 27, 1991

## Mechanisms: 2

**FD** 3:45pm–5:15pm  
DeAnza Room

Urs P. Wild, *Presider*  
*Swiss Federal Institute of Technology, Switzerland*

Linear electron-phonon interaction in dye-doped polymers  
: Boson peak frequencies in polymers

Seishiro Saikan

Department of Physics, Faculty of Science, Osaka University,  
Toyonaka, Osaka 560, Japan  
(06-844-1151 ext. 4149)

This talk presents a review of our recent experimental results on femto-second accumulated photon echo in dye-doped polymers. The aim of this research is to clarify the parameter that is most important in affecting seriously the linear electron-phonon coupling in these samples, and to find the materials which have extremely weak linear electron-phonon coupling. The latter research is needed for the improvement of the PHB memory materials. We have so far demonstrated experimentally that Fourier-transform spectroscopy [1] based on the femtosecond accumulated photon echo is most useful for these studies. Furthermore, the detection sensitivity for the accumulated photon echoes has been improved significantly with the use of the phase modulation technique [2].

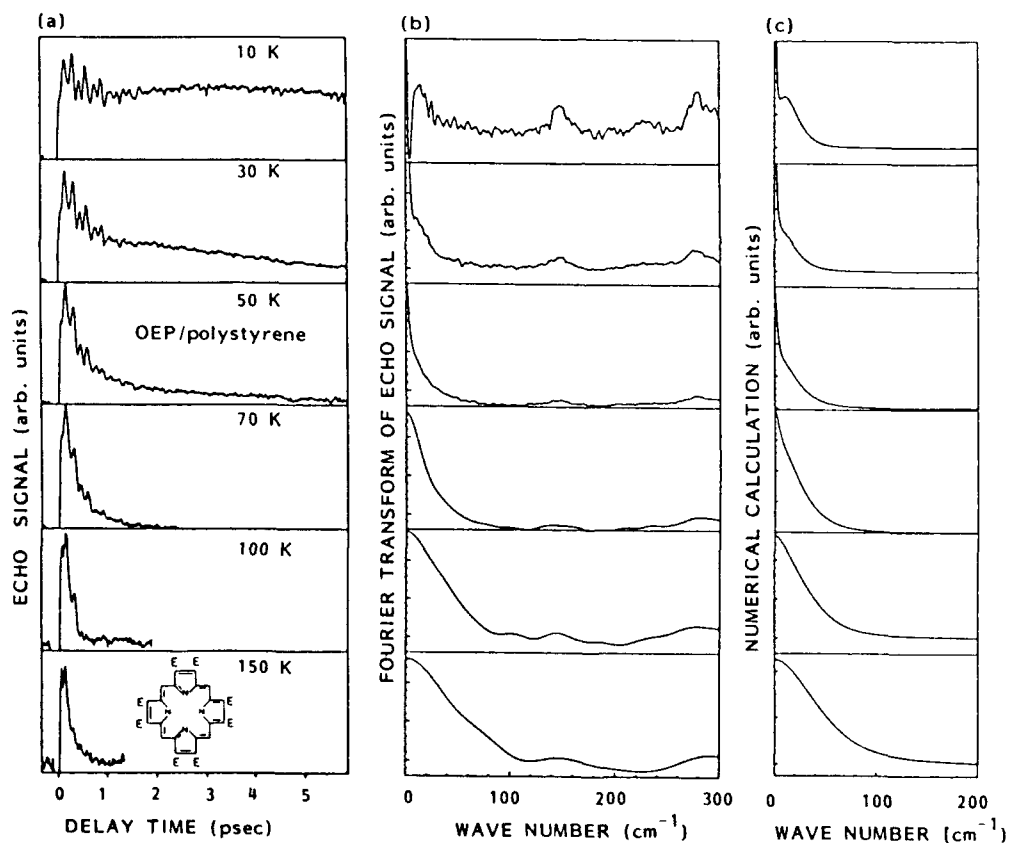


Fig.1. (a) Temperature dependence of the accumulated photon echo in octaethyl porphine doped in polystyrene. (b) Fourier cosine transformed spectrum of (a). (c) Numerical simulations. The intensities of the zero-phonon lines at 10 and 30 K are off scale in (b) and (c).

First we investigated the temperature dependent variation of the homogeneous absorption spectrum and checked the validity of the linear electron-phonon interaction theory.[3] The experimental results in OEP doped in polystyrene are shown in Fig.1, in which (a) is the observed echo signals, (b) is the Fourier transformed spectra, and (c) is the numerical simulation according to the theory of the linear electron-phonon interaction. As the temperature increases, the relative strength of the zero-phonon line decreases gradually and vanishes near the temperature of 60 K in this sample. Above this temperature, the broadening of the phonon sideband spectrum was observed. From the good agreement between the Fourier-transformed spectrum and the numerical simulation, it should be stressed that once the phonon sideband spectrum and the Debye-Waller factor are determined at a sufficiently low temperature, the homogeneous spectrum at any temperature can be predicted accurately.

In the linear electron-phonon coupling theory, the Debye-Waller factor  $\alpha$  is an important parameter. With the use of this factor, we can characterize the dye-doped polymer samples. Under the approximation of the single phonon mode,  $\alpha$  is defined as

$$\alpha = \exp(-S_0 \coth \frac{\hbar\omega}{2kT})$$

where  $S_0$  is the Huang-Rhys factor and  $\omega$  is the phonon frequency. Hence the most preferable materials for PHB optical memories should have a smaller Huang Rhys factor and a higher phonon frequency. Fig.2 shows the experimental results on the temperature dependence of the Debye-Waller factor in three samples. The dots denote the measured values and the solid lines denote the numerical fit to the theory. From this numerical fitting, we can estimate the two parameters  $S_0$  and  $\omega$ . It also indicates that although the two samples of TPP/PMMA and TCPP/PVOH have almost the same value for the Huang-Rhys factor, the Debye-Waller factor declines steeply in the former sample. This is due to the relatively low phonon frequency in the PMMA polymer. Therefore it is important to know the polymer dependence of the phonon frequency in order to find the materials which maintain a large value of the Debye-Waller factor up to higher temperatures. [4]

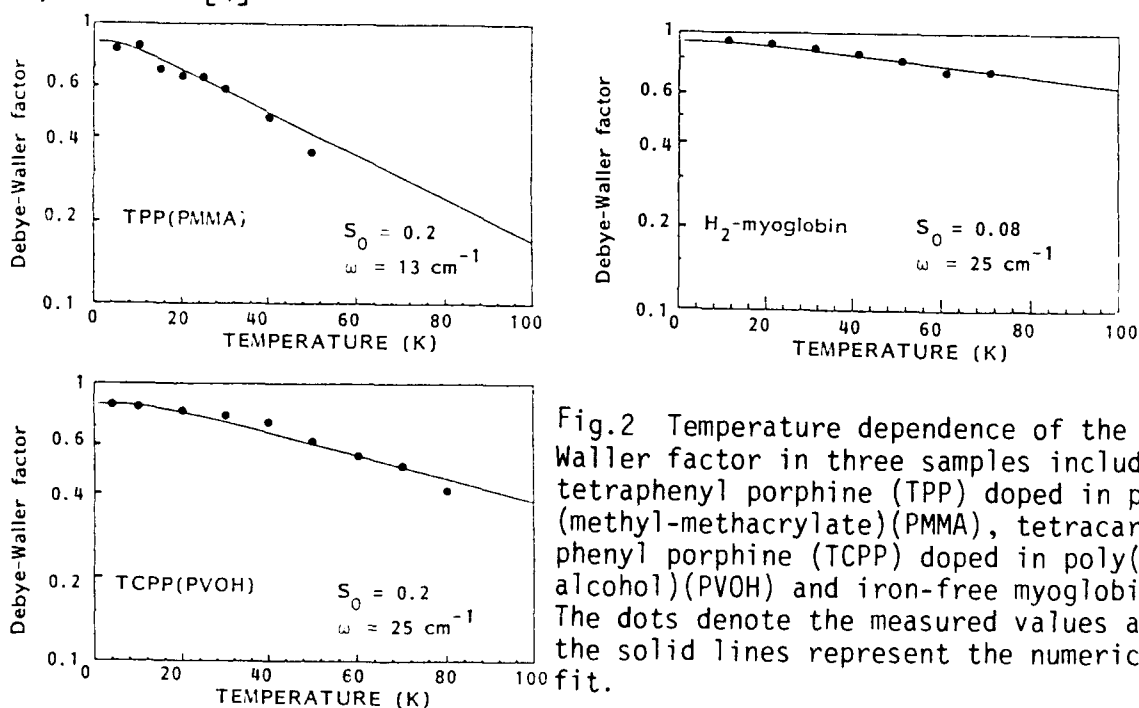


Fig.2 Temperature dependence of the Debye Waller factor in three samples including tetraphenyl porphine (TPP) doped in poly (methyl-methacrylate)(PMMA), tetracarboxy phenyl porphine (TCPP) doped in poly(vinyl alcohol)(PVOH) and iron-free myoglobin. The dots denote the measured values and the solid lines represent the numerical fit.

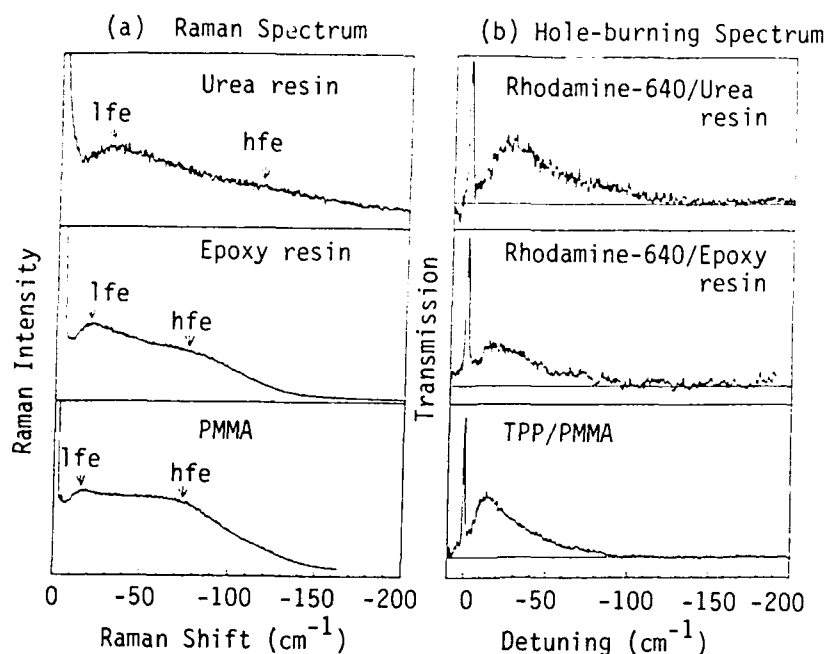


Fig.3 Comparison between the Raman scattering spectra and the hole burning spectra. The hole-burning spectra were measured for same polymer doped with rhodamine-640 or tetraphenylporphine (TPP).

Low-frequency Raman scattering has revealed that a low-frequency peak occurs in the spectra of all amorphous and vitreous solids. This low-frequency peak has been called the boson peak, since the boson occupation factor affects the peak height and Raman spectral shape. Recently, the low-frequency mode in amorphous materials has been interpreted from the viewpoint of a fracton vibration. Fig.3(a) shows the low-frequency depolarized Raman spectra in three polymers of urea resin, epoxy resin and PMMA. The hole burning spectra, shown in Fig.3(b), were also measured for the same polymers doped with rhodamine-640 or TPP dyes. The characteristic feature of the Raman spectra of the polymers is that there appears two spectral edges in the spectra and the  $\omega^\mu$  dependence is observed in the spectral range between the two edges. The low frequency peak corresponds to the boson peak. We have tentatively termed the two spectral edges in the Raman spectrum the low-frequency fracton edge (lfe) and the high-frequency fracton edge (hfe), respectively. It is evident that the low-frequency fracton edge nearly coincides with the peak frequency of the phonon sideband spectrum. Table 1 shows the polymer dependence of the boson peak frequency. [5] This table also indicates that hydrogen-bonded polymers have higher boson peak frequencies, and that there seems to exist a maximum of the boson peak frequency at around 30 cm<sup>-1</sup> in organic polymers. The former result explains the reason as to why the Debye-Waller factor is enhanced when the dyes are doped in polyvinyl alcohol. Furthermore, if there exists an upper-limit in the boson peak frequencies in polymers, we must search for materials which have smaller Huang-Rhys factor for the improvement of PHB memory materials.

Table 1 Polymer dependence of Boson peak frequency

	Polymer	Boson peak frequency
1	polystyrene	14 $\text{cm}^{-1}$
2	poly(methyl methacrylate)	13
3	poly(ethyl methacrylate)	13
4	poly(butyl methacrylate)	16
5	poly(lauryl methacrylate)	16
6	poly(vinyl acetate)	12
7	poly(2-hydroxyethyl methacrylate)	23
8	poly(vinyl alcohol)	25
9	poly(acrylic acid)	25
10	urea formaldehyde resin	23
11	dextran	30

Recently, we have reported that the higher-order structure of the micro-environment surrounding the dye molecule helps weaken the linear electron-phonon coupling strength. For example, we have found that the Huang-Rhys factor in iron-free myoglobin, which is one of the naturally occurring dye-polymer systems, is an extremely small 0.08. The temperature dependence of Debye-Waller factor in this sample is shown in Fig.2. The large value of 0.7 for the Debye-Waller factor at 77 K means that even at liquid nitrogen temperature the absorption spectrum of this sample mainly consists of the zero-phonon line. As far as the dye-polymer system is concerned, the iron-free heme proteins are, to the best of our knowledge, one of the samples with the weakest linear electron-phonon coupling at 77 K. The more detailed results on the linear electron-phonon coupling in iron-free heme proteins will be presented in this conference by Lin et al.

#### References

- [1] Fourier-transform spectroscopy in dye-doped polymers using femtosecond accumulated photon echo, S.Saikan, N.Nakabayashi, Y.Kanematsu and N.Tato, Phys.Rev. B38 (1988) 7777
- [2] Phase modulation technique for accumulated photon echo S.Saikan, K.Uchikawa and H.Ohsawa, Opt.Lett. 16 (1991) 10
- [3] Linear electron-phonon interaction in dye-doped polymers S.Saikan, A.Imaoka, Y.Kanematsu and T.Kishida Chem.Phys.Lett. 162 (1989) 217
- [4] Temperature dependence of Debye-Waller factor in dye-doped polymers S.Saikan, A.Imaoka, Y.Kanematsu, K.Sakoda, K.Kominami and M.Iwamoto Phys.Rev. B41 (1990) 3185
- [5] Polymer dependence of boson peak frequency studied by hole burning and Raman spectroscopies, S.Saikan, T.Kishida, Y.Kanematsu, H.Aota, A.Harada and M.Kamachi, Chem.Phys.Lett. 166 (1990) 358

**Iron-free Cytochrome C and Myoglobin in Buffer Glass as Weakly-coupling Mesoscopic Molecular System: Holeburning, Absorption and Fluorescence Spectra and their Temperature Properties**

Toshiro TANI, Youichi SAKAKIBARA, Hisao TAKAHASHI and Kyonosuke YAMAMOTO

Electrotechnical Laboratory, Umezono 1-1-4, Tsukuba-shi, Ibaraki 305, Japan (Tel: 0298-58-5451, Fax: 0298-58-5459)

Persistent spectral hole burning is a useful tool to detect zero-phonon line and phonon sideband of organic dye molecules doped in glasses and polymers, which are usually covered under inhomogeneous broadening. These observation bring us information on the electron-phonon interaction such as Debye-Waller factor  $a$  in these molecular systems. From the viewpoint of the issue of materials designing for wavelength-multiplexed optical memory and also with naive interest to obtain efficient sharp holes, we have paid much attention to the molecular systems in the category of rather weaker inter/intra-molecular coupling.

Basically the decrease of linear electron-phonon interaction brings us efficient zero-phonon hole formation and the decrease of the quadratic one does the sharpening of the hole. Using quinizarin derivatives and porphyrin family, we have been investigating various hole-forming dye-doped systems by modifying the molecular structure of dye as well as matrix<sup>1)</sup>. Glass matrices are surveyed from organic solvents through modified polymers to inorganic sol-gel glasses<sup>2,3)</sup>. We have been trying to classify and comprehend the properties of holes, including spectral diffusion, as well as photoreaction processes of hole formation in relation to the local structure of materials<sup>4,5)</sup>.

We consider at the moment as follows: Though the zero-phonon hole formation and its capabilities are mostly determined by the properties of guest molecule, however, the structure of guest-host interacting clusters which include some intermediate, or mesoscopic, range of matrix molecules around each photoactive center should also be taken into account for more holistic comprehension. The former can be related to the intra-molecular interaction whereas the latter the inter-molecular one. This approach of the mesoscopic structural control of molecular interactions, or molecular assemblies, already proposed is useful not only from the viewpoint of material optimization but also for surveying new materials<sup>4,6)</sup>.

Recent results of persistent hole-burning of chromoproteins, iron-free cytochrome c ( $H_2$ :CyC) and iron-free myoglobin ( $H_2$ :Mb) doped in buffer glass will be described here. We think these would be typical examples of functional mesoscopic system in which for instance extremely weak linear electron-phonon coupling is realized. We have already observed in our preliminary work that highly efficient zero-phonon hole has been formed in  $H_2$ -cytochrome c and the hole-filling experiment by temperature cycling indicates the guest-host coupling seems very weak<sup>7)</sup>. This is quite in contrast with the earlier hole burning experiment<sup>8)</sup>

on the natural hemeproteins in which the observed hole spectra are broad, as broad as the absorption band. The extraction of iron from the central porphyrin has brought us remarkable improvement of the functions. Incidentally the guest is the central porphyrin here and all the substituents, protein chain and probably water and/or glycerol molecules within some mesoscopic range consist of the functional host.

Samples are prepared in accordance with the method of Vanderkooi and Erecinska<sup>9)</sup>. They are obtained in the solution of 0.5M PO<sub>4</sub> buffer with pH 7.4 and mixed with glycerol to 3~4 times in volume. They are degassed and sealed in the glass cells with 1 to 3 mm optical path length. The optical densities of the Q<sub>x</sub>(0-0) bands are from 0.03 to 0.3 at room temperature. Results are itemized as follows with description rather stressed on the difference of the characters noted in the two systems;

1. Broad band excitation and emission spectra of fluorescence in H<sub>2</sub>:CyC and H<sub>2</sub>:Mb at 4.8 K are shown in Fig. 1 in relation to the Q<sub>x</sub>(0-0) transitions. The two structures of the peak at 620 nm and the shoulder at 625 nm (see also Fig. 2) in H<sub>2</sub>:Mb for instance are notable. These seem to be 0-0 transition, indicating there exists at least two sites in the hydrophobic heme pockets or the cages made of polypeptide chain. Emission spectra by quasi site-selective excitation into Q<sub>x</sub>(0-1) band at 565 nm and 562 nm support it. This specified feature is similar in both systems.

2. The hole burning profiles and the efficiencies and hole filling experiments by temperature cycling at peak and shoulder are almost similar, also indicating that their electronic origins are common each other.

3. In case of H<sub>2</sub>:CyC the shoulder is sensitive to the condition of the sample whereas not in case H<sub>2</sub>:Mb.

4. If we look at the results in 2 more precisely to compare the two systems, there is surely the difference. The dye-matrix coupling in the sense of extrinsic TLS seems to be weaker in H<sub>2</sub>:CyC than in H<sub>2</sub>:Mb from the temperature hole filling experiments (Fig. 3).

5. Figure 2 shows the hole spectra and their difference spectra obtained by the intense burning at peak the wavelength for each. In H<sub>2</sub>:CyC there appears anti-hole or product states absorption just at the shorter wavelength side of the burning, whereas not in H<sub>2</sub>:Mb. In the latter case the product states seem to appear in wide spread at longer wavelength region. Second, another new band appears at 603 nm in H<sub>2</sub>:CyC. This band also seems to be fluorescent (see Fig. 1).

6. Another remarkable difference in H<sub>2</sub>:CyC and H<sub>2</sub>:Mb is the strong temperature dependence of Q<sub>x</sub>(0-0) band observed in the latter (Fig. 4).

7. As for the linear electron-phonon couplings, the temperature dependence of  $\alpha$  in H<sub>2</sub>:Mb/buffer glass is obtained from the novel accumulated photon echo experiment<sup>10)</sup>:  $\alpha$  at 0 K limit is 0.92 and it is still 0.7 at 77K. It is estimated that Huang-Rhys factor S<sub>0</sub> is 0.08 and the dominant phonon energy is 25 cm<sup>-1</sup>. Though the numbers could not be determined in case of H<sub>2</sub>:CyC due to the generation of the product band (Fig. 2), the coupling intensity seems to be nearly the same.

8. Based on these observation the temperature dependence of

hole spectrum is measured in H<sub>2</sub>:Mb (Fig. 5) and the persistent hole can be observed up to 140 K though the efficiency seems to become low. The temperature dependence of T<sub>2</sub> estimated from that of the hole width  $\Gamma_n$  by assuming  $\Gamma_n = 2/\pi T_2$  follows a T<sup>-b</sup> dependence where b is 2.2 (Fig. 6), in agreement with that of echo data. The deviation observed above 120 K is due to the increased contribution from phonon sidebands.

9. The shift  $\Delta$  of the pseudo-phonon sidehole obtained from intense burning is 25 cm<sup>-1</sup> which is in good agreement with 7. In ordinary burning conditions, we could not detect any trace of phonon sidehole in both H<sub>2</sub>:Mb and H<sub>2</sub>:CyC.

In summary we have obtained extremely weak linear electron-phonon coupling systems, probably the weakest at the moment among organic systems, though existing in nature but sufficiently artificially. This is caused by the reduction of the nonradiative relaxation in the porphyrin moiety and the hydrophobic environment of the heme pocket. The weakness in the coupling is almost comparable to that in Shpol'skii matrix. As for the quadratic coupling, the reduction of the linear one may also decrease its intensity though of course remains further investigation.

There exist some structural differences; protoporphyrin IX is connected to the cysteins of the polypeptide chain through the two thioether linkages in H<sub>2</sub>:CyC whereas no chemical bond in H<sub>2</sub>:Mb. The  $\alpha$ -helix content and the charge distribution are also different each other. We consider so far the higher order structures of the in H<sub>2</sub>:CyC is less tight than in H<sub>2</sub>:Mb causing inclusion of H<sub>2</sub>O molecule(s) and/or PO<sub>4</sub>'s in the protein or the pocket, which eventually leads to the notable characteristics in the former.

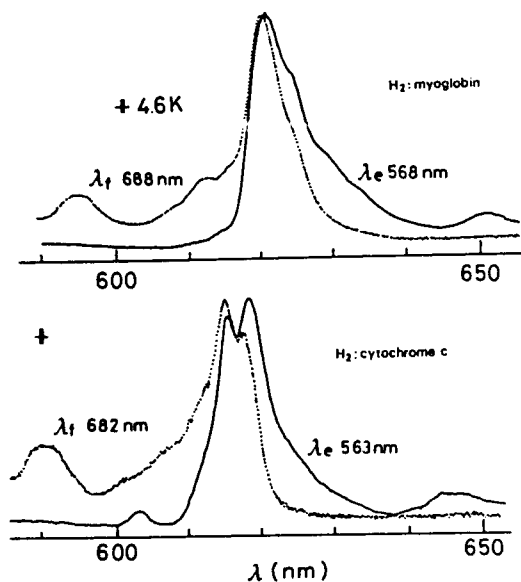


Fig. 1 Excitation (.....) and emission (—) spectra at 4.6 K.

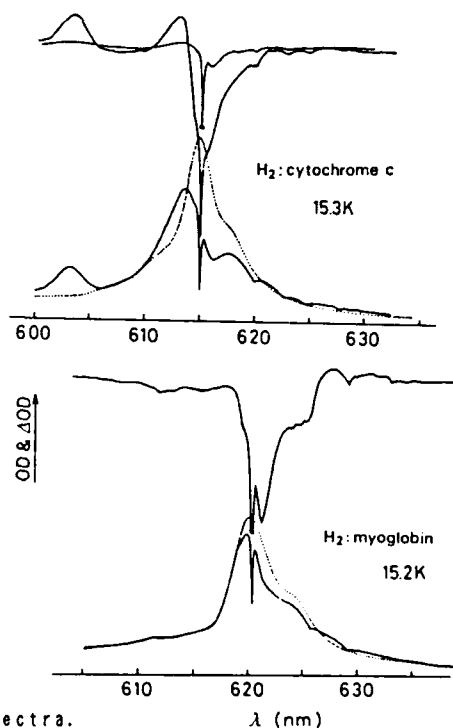


Fig. 2 Hole spectra and their difference spectra.

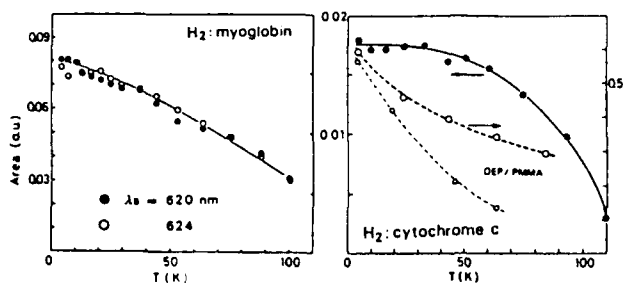


Fig. 3 Hole filling by temperature cycling. The results of octaethylporphyrin doped in PMMA are also shown for comparison.

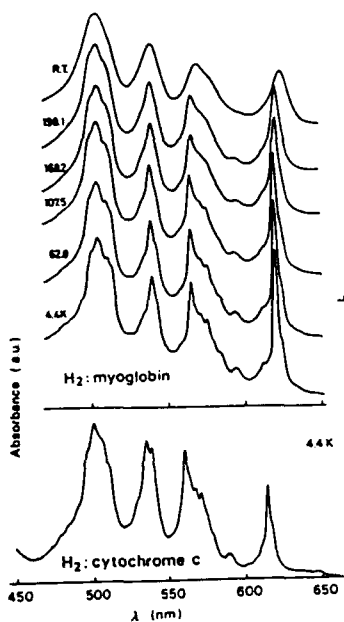


Fig. 4 Temperature dependence of absorption spectra.

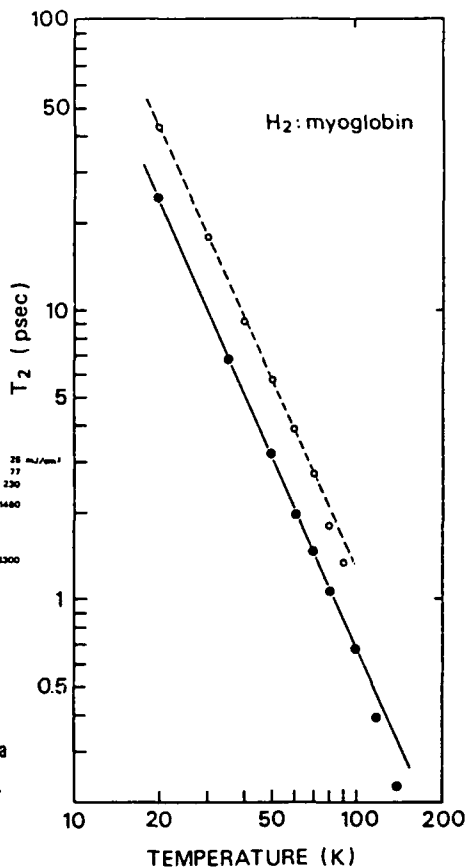
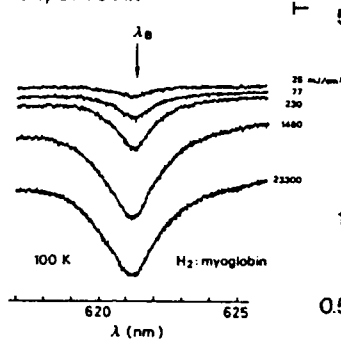


Fig. 6 Temperature dependence of  $T_2$  deduced from hole burning.  $\circ$ 's are obtained from accumulated photon echo experiment.

#### REFERENCES:

- 1) Y. Iino, T. Tani, M. Sakuda, H. Nakahara and K. Fukuda, *Chem. Phys. Lett.*, **140**, 76 (1987); T. Tani, Y. Iino, M. Sakuda, H. Nakahara and K. Fukuda, *J. Lumines.*, **38**, 739 (1987).
- 2) T. Tani, A. Itani, Y. Iino and M. Sakuda, *J. Chem. Phys.*, **88**, 1272 (1988).
- 3) T. Tani, H. Namikawa, K. Arai and A. Makishima, *J. Appl. Phys.*, **58**, 3559 (1985); A. Makishima and T. Tani, *J. Amer. Cer. Soc.*, **69**, C-72 (1986).
- 4) T. Tani, A. Itani, Y. Iino and M. Sakuda, *Proc. ISOM'89, Tokyo 1987, Jpn. J. Appl. Phys.*, **26**, Suppl. 26-4, 77 (1987); T. Tani, Y. Sakakibara and K. Yamamoto, *Proc. ISOM'89, ibid.*, **28**, Suppl. 28-3, 239 (1989).
- 5) U. Itoh and T. Tani, *Appl. Opt.*, **27**, 739 (1988).
- 6) T. Tani, in "Polymers for Microelectronics -- Science and Technology --", **38**, ed. Y. Tabata, I. Mita, S. Nonogaki, K. Horie and S. Tagawa, 481 (1990, Kodansha).
- 7) T. Tani, Y. Sakakibara and K. Yamamoto, *Mol. Cryst. Liq. Cryst.*, **183**, 475 (1990).
- 8) J. Pahapill and L. Rebano, *Chem. Phys. Lett.*, **158**, 283 (1989).
- 9) J. M. Vanderkooi and M. Erecinska, *Eur. J. Biochem.*, **60**, 199 (1975).
- 10) J. W-l. Lin, T. Tada, S. Saikan and T. Tani, to be published in *Phys. Rev.* **8**.

# The study of weak linear electron-phonon coupling in iron-free hemeproteins

J.W-I.Lin, T.Tada, S.Saikan and T. Kushida

Department of Physics, Faculty of Science, Osaka University

Toyonaka, Osaka 560, Japan

(06-844-1151 ext. 4149)

T.Tani

Electrotechnical Laboratory

Umezono 1-1-4, Tsukuba, Ibaraki 305, Japan

## Summary

The present interest in the PHB optical memories has motivated research into finding materials which have weak electron-phonon coupling between the guest impurity and the host system. The magnitude of the linear electron-phonon coupling strength can be obtained from the Debye-Waller factor, the relative strength of the zero-phonon line and phonon sideband of the homogeneous spectrum. The Debye-Waller factor can be determined readily in crystals; in amorphous solids, however, the large inhomogeneous spectral broadening masks the individual homogeneous spectrum. Out of the many nonlinear spectroscopic techniques, our group utilized the femtosecond accumulated photon echo technique with phase modulation<sup>1</sup> to examine the polymer dependence of the electron-phonon coupling in amorphous dye-doped polymer systems.

Previous results<sup>2</sup> from low frequency Raman scattering and PHB spectroscopy indicate a larger Debye-Waller factor for a higher "boson peak"

frequency. However, most organic polymers examined exhibit a peak frequency no higher than  $30 \text{ cm}^{-1}$ . Considering the fact that the Debye-Waller factor is dependent on both the mean phonon frequency (boson peak frequency) and the linear electron-phonon coupling coefficient (Huang-Rhys factor), it is desirable to search for dye-polymer samples which have an extremely small Huang-Rhys factor in order to improve the temperature characteristics of the PHB memory materials.

Our own measurements<sup>3</sup> have indicated that the dye-polymer sample of TCPP/PVOH exhibits weak linear electron-phonon coupling, as evident from the theoretical fit against the measured values for the Debye-Waller factor. As seen in Fig. 1, the Huang-Rhys factor comes to 0.2 with  $25 \text{ cm}^{-1}$  for the mean phonon frequency in this sample. Recently, however, we have discovered that iron-free myoglobin and iron-free cytochrome-C both have weaker linear electron-phonon couplings.

In these chromoprotein samples, the protein polypeptide chain wraps the iron-free heme chromophores in the protein's tertiary structure. The iron-free heme chromophores exist in a hydrophobic environment with the librational degrees of freedom assumed limited by the tight wrapping of the polypeptide chain. In Fig. 2, the absorption and fluorescence spectra for iron-free myoglobin show a lack of any significant Stokes shift, indicating that the adiabatic potentials for the ground and excited states have no significant shift in their equilibrium positions in the configuration coordinates. This fact predicts a small value for the Huang-Rhys factor.

Fig. 3 shows the temperature dependence of the photon echo signal for iron-free myoglobin. At 10K, the spike, which represents the phonon sideband, is largely absent and the exponential decay, which represents the zero phonon line contributions, takes up most of the echo signal. Even at near liquid nitrogen temperatures, the exponential decay portion is a significant part of the signal, in contrast to other dye-polymer samples. Fig. 4 shows the theoretical fit of the Debye-Waller factor for the iron-free myoglobin sample. The plot shows a significant weakening of the electron-phonon coupling, as evident from the Huang-Rhys factor of 0.08.

We have attributed the weakness of the linear electron-phonon coupling to the hydrophobic environment of the polypeptide chain interior and the tight wrapping of the chromophores by that chain.<sup>4</sup>

<sup>1</sup> Opt. Lett. **16**, 10 (1991)    <sup>2</sup> Chem. Phys. Lett. **166**, 358 (1990)    <sup>3</sup> Phys. Rev. **B41**, 3185 (1990)    <sup>4</sup> *Extremely weak linear electron-phonon coupling in iron-free heme proteins studied by phase modulated photon echo*, to be published in Phys. Rev. B.

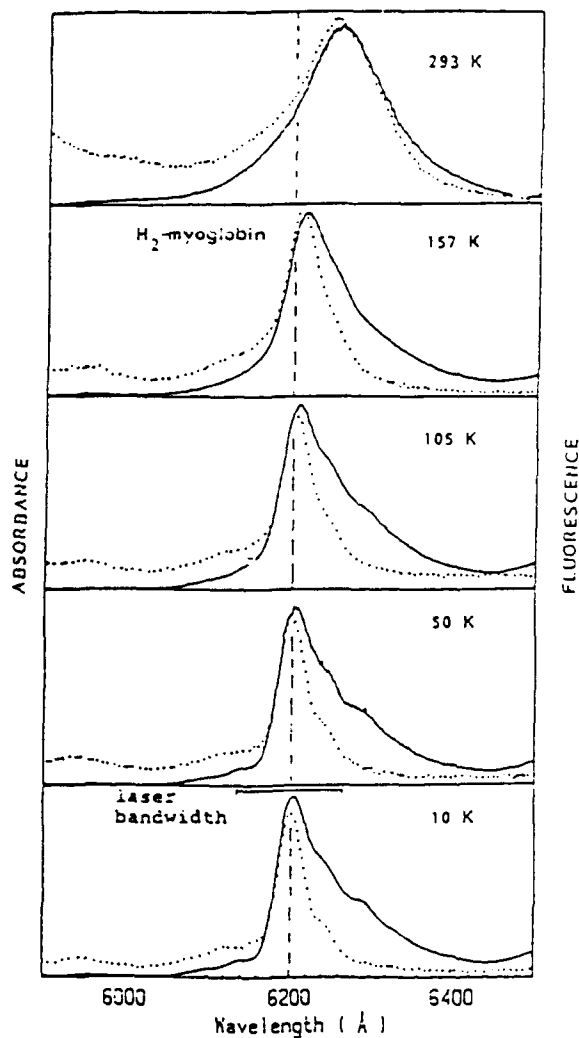
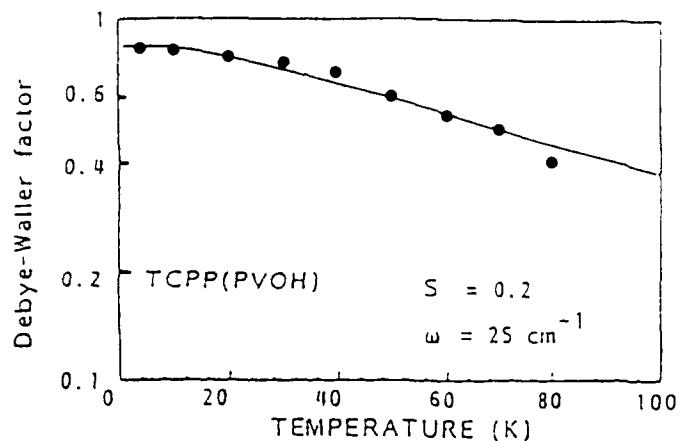


Fig. 1 Temperature dependence of the Debye-Waller factor for tetracarboxyphenyl porphyrin (TCPP) doped in poly(vinyl-alcohol) (PVOH). The dots denote the measured values and the line denotes the numerical fit to the theory.

Fig. 2 Temperature dependence of the fluorescence (solid) and absorption (dots) spectra in iron-free myoglobin. The Stokes shift is rarely observed over the wide temperature range from liquid helium temperature to near room temperature. The laser bandwidth used for the echo measurement is depicted in the spectrum at 10K.

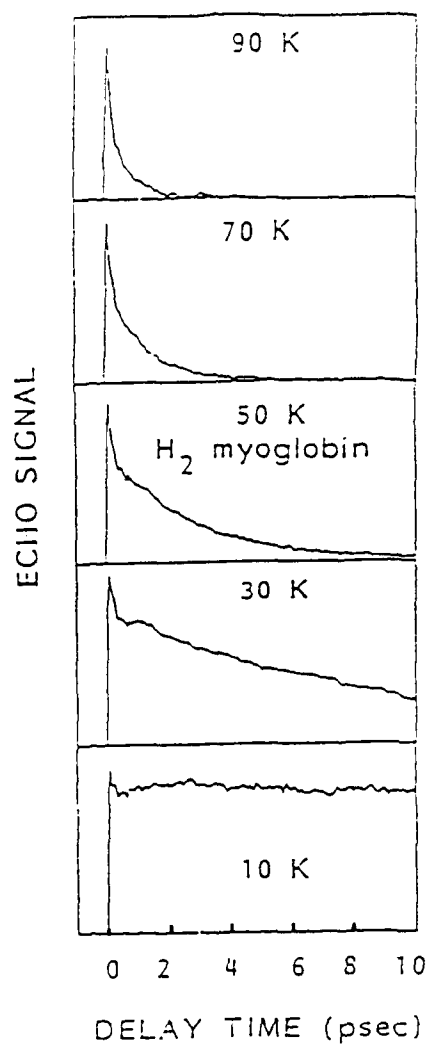


Fig. 3 Temperature dependence of the accumulated photon echo in iron-free myoglobin. The exponential decay due to the zero-phonon line is clearly visible at 90 K.

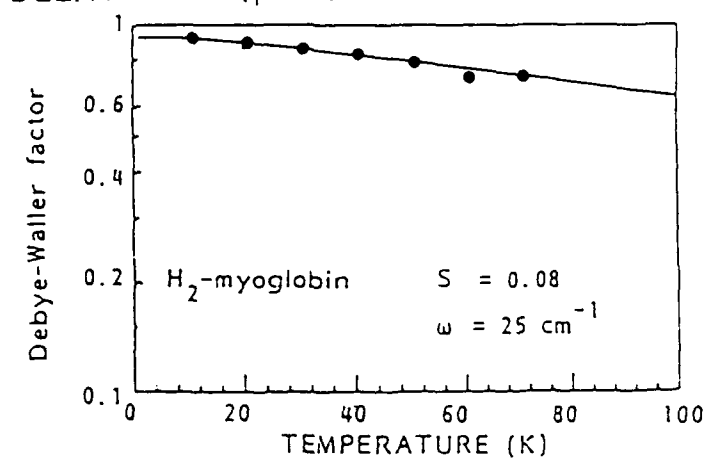


Fig. 4 Temperature dependence of the Debye-Waller factor for iron-free myoglobin. The dots denote the measured values and the line denotes the numerical fit to the theory.

## Spectral Hole-Burning in the Storage Hierarchy ?

Roger F. Hoyt  
IBM Research Division  
Almaden Research Center K65.802  
650 Harry Road  
San Jose, CA 95120-6099  
408.927-2118

## Abstract

The challenges and opportunities for a spectral hole-burning-based storage device are discussed in the environment of contemporary computer systems which rely on a hybrid 'Storage Hierarchy' for high capacity and performance.

## 1. Introduction

Rapid storage and retrieval of information is a key factor in the design and performance of present-day computers. For example, nearly all sectors of the business world (banks, airlines, insurance companies, etc.) now critically rely on computer storage subsystems to provide efficient 'on-line' service to their customers. World-wide, computer storage industry revenues are well over \$40B a year and growing. In addition to applications in so called 'high-end' mainframe systems, storage peripherals also play important roles in the mid-range and low end. This last category, which has clearly emerged since 1980, has fostered the growth of new companies who solely develop and manufacture storage devices for workstation, personal computer and lap-top computer applications.

The capacity and performance of computer storage devices span a rather broad spectrum, depending upon system requirements and applications. A large mainframe computer system may have an 'online' storage capacity requirement of 100 Gigabytes or more, with access times and data transfer rates of 10 msec and 4.5 MByte/sec respectively. This may be compared with the 40 MByte capacity, 20 msec access time and 2 MByte/sec transfer rates characteristic of storage units for low end personal computers. Typical prices of \$5 to \$10 per Megabyte are expected to continue to decrease substantially.

Current research and development for computer storage devices are exploring a number of alternatives to today's mainline technologies. The goal of these activities is to identify storage methods which may develop into products to provide improved performance, while satisfying system needs such as nonvolatility, greater capacity, lower cost, etc. Two examples of concepts which are now emerging as storage technologies are disk arrays (high performance), and magneto-optic storage (removable, high capacity). Some other examples of areas under active investigation by many groups include nonvolatile semiconductors, ferroelectric RAM, STM storage, holographic memories, and persistent spectral hole-burning. We discuss here briefly the environment of a current computer system and how a storage device based on spectral hole-burning may find an application niche.

## 2. The Storage Hierarchy

A typical architecture of a present day computer system consists of a main processor which continually exchanges data with a high speed semiconductor cache 'memory'. This 'memory' consists of high performance static RAM chips with capacity of perhaps several hundred KBytes, giving the fastest response times of 10's of nsec's., and is volatile to loss of power. Supporting this is the computer's main storage memory, which consists of several hundred MBytes. This main memory is fabricated from high-performance dynamic RAM (current products use 4 MBit or 16 Mbit chips) with performance times of around 60 nsec's. Like SRAM, DRAM is also volatile in the case of power loss.

The next level of storage which exists in a computer system is a combination of more DRAM and magnetic hard disk storage (DASD). The DRAM cache exists in the DASD storage controller to provide improved performance. It does this by acting as a high speed buffer to the disk file, thereby masking the seek and latency of the disk file itself. The combination of this with the capacity of the DASD provides a very powerful and cost effective solution to the computer's storage requirements. Since the storage mechanism of the disk is magnetic recording, it is stable and non-volatile. The capacity of this storage can range anywhere from a few hundred MBytes for a very small system to many hundred GBytes or more. Proper coordination between the semiconductor cache and magnetic DASD by the system software can result in a fast response time for system loaded with a large number of users. Native data transfer rates of 4.5 MByte/sec for a disk file today is typical. However, recently, the use of arrays of DASD are today resulting in data rates larger by a factor of 10 to 20 or higher. The combination of DRAM with battery back-up ('Solid State Disks') also offers a way by which higher performance disk-like storage may be achieved. For many applications, though, the higher cost of this approach generally makes widespread use difficult.

The final stage in the storage hierarchy is generally that of so-called archival storage. This is generally accomplished using magnetic tape devices. Tape is removable and non-volatile, and provides the useful solution to long term backup, software distribution, etc. More recently, in some instances write-once and read-write optical devices (optical 'libraries') may begin to satisfy some of the archival tape-like applications. In general, the data rates of these systems are similar to that of DASD, with capacities up to a terabyte or more (due to the removable nature of the media).

## 3. Spectral Hole-Burning

The first proposal for information storage using spectral hole-burning was made in 1975 (Ref. 1). Since then, a number of reviews have been written, summarizing progress in the field and the requirements for realizing a practical system (Ref's. 2 + 3). Currently, several laboratories worldwide are carrying out research focussed on many of the fundamental problems yet to be solved to realize a storage device which may be compatible with computer architectures (Ref. 4). We discuss here the main requirements for computer systems as they are compared with hole-burning's potential promises:

### 1. High Speed

With the advent of DASD Arrays offering data transfer speeds of 100 MB/sec and beyond, it is key that any hole-burning based storage system must offer an easier solution. Recent studies

of hole-burning in the time domain may be an important pointer to the best path to take to achieve GB/sec rates and higher (Ref. 5).

## 2. High Capacity

From the first, persistent spectral hole-burning has offered the possibility for wavelength multiplexed information storage on the same physical spot on the storage material. This would allow higher areal density for a given optical system, in comparison with the single bit per spot of magneto-optic storage. Progress in this area is being made (Ref. 6), and offers the hope that a system which realizes the capacity enhancement from the ratio of the inhomogeneous to the homogeneous linewidths may someday be demonstrated. Important trade-offs of signal to noise ratio versus capacity must be considered in detail, as well as suitable signal processing and coding.

## 3. Nonvolatility

In the last few years, spectral hole-burning on materials at temperatures well above cryogenic temperatures has been observed (Ref.7) Some of these materials or their derivatives may become technically interesting. However, a key factor for constructing a practical storage device based on hole-burning remains the development of a suitable material which is stable and not subject to data loss because of loss of power, cooling, etc. (Ref.'s 7 + 8)

## 4. Data Formatting

An important feature of practical storage devices is the manner in which the stored information is formatted and stored. Most all devices do this in a serial manner. For example on a disk file a data 'record block' could be 512 Bytes long, with data stored serially along the track. In a spectral hole-burning storage device, it would probably be more convenient to store data as parallel images, to be written and read in parallel. Some groups are currently making interesting progress in exploring this concept (Ref. 9).

## 5. Crosstalk

The integrity of stored data must not be contaminated by the information stored in adjacent 'blocks'. Interesting concepts are currently being explored through clever optical design and processing to minimize this (Ref. 10).

## 6. Cost

The ever lowering cost of storage, both for semiconductors and magnetic storage, makes this a difficult, moving target for an alternative technology such as hole-burning to beat. The reduced costs of optical components and the proper materials, may at some point make a hole-burning-based solution attractive. It will, however, be a real challenge for the technology.

## SUMMARY

Persistent spectral hole-burning offers the possibility for use in mainline computer storage with high capacity and very high performance. Many serious technical problems remain to be overcome before a practical operating system can be built. During this time, mainline

technologies based on semiconductors and magnetic recording will continue to improve in performance and cost. The challenge for hole-burning will be to outpace these in suitable application areas, particularly those involving massively parallel storage.

#### References

1. A. Szabo, "Frequency Selective Optical Memory", U.S. Patent No. 3,896,420 (1975).
2. W.E. Moerner (editor) in "Persistent Spectral Hole Burning: Science and Applications", Topics in Current Physics, Springer, Berlin 1988.
3. S.V. Pappu, Int. Journal of Optoelectronics (U.K.), Vol. 5, No. 3, p. 251, 1990.
4. Asian Wall Street Journal Weekly, p. 8, June 11, 1990. (Mitsubishi)  
Comline Electronics, p. 1, March 16, 1990. (SONY)  
The Institute (IEEE), p. 10, Feb. 1991. (NTT)
5. W.R. Babbitt and T.W. Mossberg, Optics Communications, Vol. 65, p. 185, 1986.
6. M. Mitsunaga and N. Uesugi, Optics Letters, Vol. 15, No. 3, p. 195, 1990.
7. K. Sakoda, K. Kominami, and M. Iwamoto; 'High Temperature Photochemical Hole Burning', presented at the International Symposium on Optical Memory, Kobe Japan, Sept. 1989.
8. S. Arnold et al., Optics Letters, Vol. 16, No. 6, p. 420, 1991.
9. A. Renn and U. Wild, Applied Optics, Vol. 26, No. 19, p. 4040, 1987.
10. A. Renn, A. Meixner, and U. Wild, J. Chem. Phys., Vol. 93, No. 4, p. 2299, 1990.



Friday, September 27, 1991

## Poster Session: 2

**FE** 5:15pm-6:45pm  
DeAnza Room

PERSISTENT HOLE BURNING SPECTROSCOPY APPLICATIONS ON  
PHTHALOCYANINE LANGMUIR-BLODGETT FILMS

F. Adamec, M. Ambroz, E. Brynda<sup>\*</sup>, J. Dian, M. Vacha and J. Hala

Department of Chemical Physics,  
Faculty of Mathematics and Physics, Charles University,  
Ke Karlovu 2, 121 16 Prague 2, Czechoslovakia

<sup>\*</sup> Institute of Macromolecular Chemistry, CSAV  
160 00 Prague 6, Czechoslovakia

Phthalocyanine Langmuir Blodgett (LB) films represent ultra thin monomolecular layers with molecules in tight contact. Most of the phthalocyanine molecules in LB films are ordered in domains where they occupy well defined (parallel) positions. There is also a minority of non-ordered molecules in off-domain positions in LB films. This fact is well documented in X-ray diffraction and transmission electron diffraction [1]. Moreover, significant inhomogeneous broadening of absorption spectra of LB film has been observed (see fig.1), in comparison with absorption spectra of isolated molecules. On the other hand the observed fluorescence is very weak, nevertheless its spectral profile well corresponds to that of isolated molecules. This phenomenon can be well explained on the basis of strong aggregation and/or fast excited energy transfer (EET) [2]. Persistent hole burning (PHB) (in fluorescence excitation spectra) has recently been applied on LB film of related porphyrin - poly-heptyl-cyanoacrylate matrix

[3]. The PHB study of tetraazoporphyrin in LB films suggested this EET interpretation. The role of EET in free base phthalocyanines was also discussed in [4] together with the analysis of off-resonant holes in fluorescence spectra. The aim of this paper is to determine the excited state lifetimes  $T_1$  strongly influenced by fast EET from PHB measurements (in fluorescence excitation spectra).

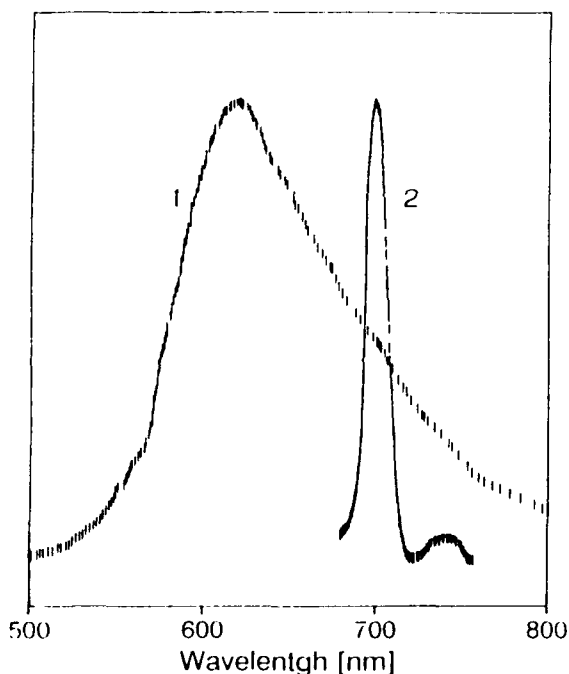


Fig.1 Absorption (300 K) - 1 and fluorescence (4.2 K) - 2 spectra of  $H_2$ -phthalocyanine LB film

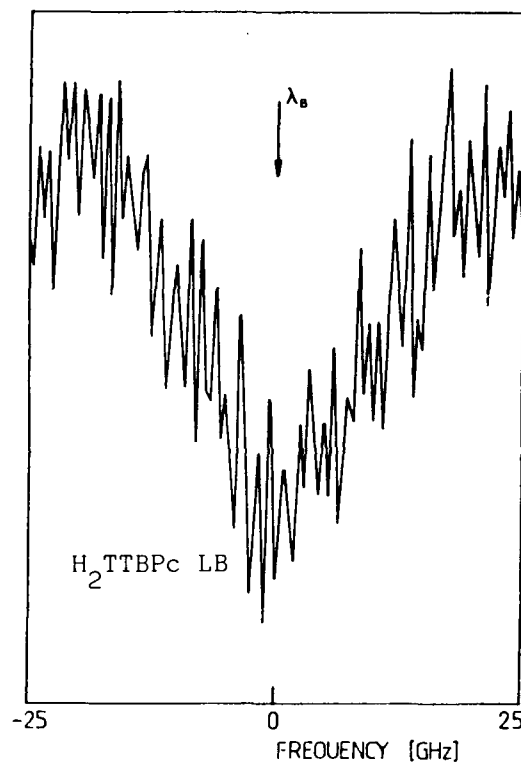


Fig.2 Persistent hole burned in fluorescence excitation spectrum at 4.2 K

The studied LB films (multilayers of 20-50 monomolecular layers on quartz plates without any polymere matrix) were prepared from phthalocyanine xylene solutions according to [1]. The PHB experiments were performed on an apparatus consisting of a *cw* ring dye laser and an optical cryostat. Fluorence was resolved using cut-off and interference filters along with a

cooled photomultiplier and a photon counter. The burning wavelengths have been tuned into the maximum of the absorption band ( $\cong 616$  nm), fluorescence was detected near its (0-0) band maximum (697-707 nm). The scanning intervals of the excitation spectra were  $\cong 100$  GHz. The applied burning power (P) ranged from 0.1 to 10  $\text{mW}\cdot\text{cm}^{-2}$ , burning exposition times (t) from 30 to 300 s. Typical PHB spectrum obtained after subtraction of the excitation spectra before and after burning is presented in fig.2. Fig.3 shows the measured holewidth as a function of burning fluence (P.t). It is evident that the obtained holewidth is virtually constant within the whole presented exposition range. The holewidths obtained on LB films at 4.2 K are approx. two orders of magnitude higher than those observed on isolated phthalocyanines in polymeres [5]. The holewidth  $0.7 \pm 0.1$   $\text{cm}^{-1}$  corresponds to the relaxation time of 15 ps.

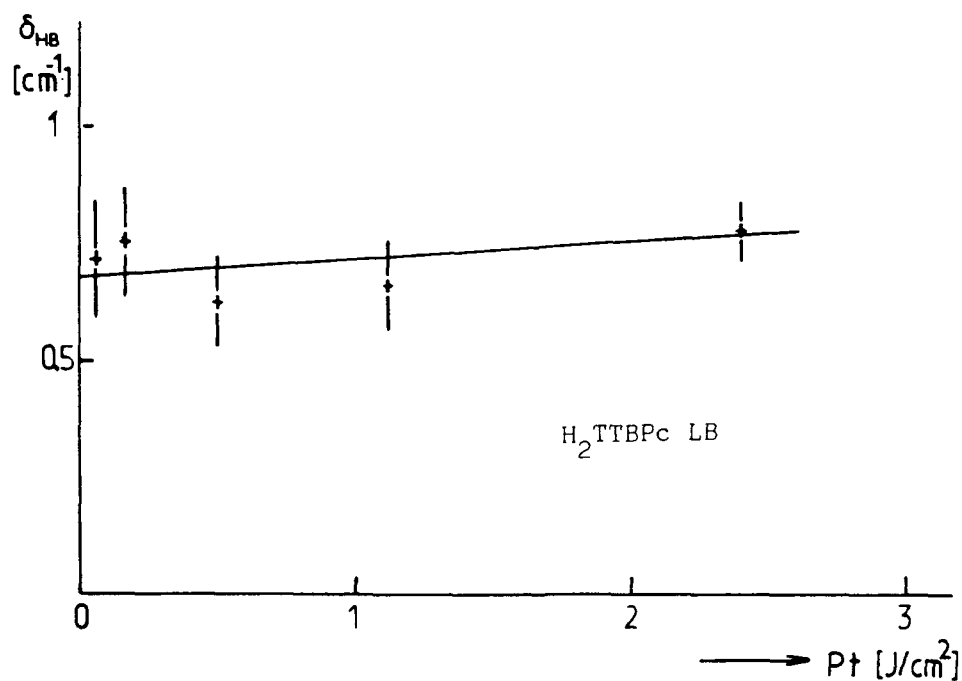


Fig.3 Holewidth as a function of burning fluence P.t at 4.2 K

This relaxation time is interpreted as a rate constant (at 4.2 K) of EET from domains to non-ordered molecules which is in agreement with results obtained in [7]. The temperature dependence function of the holewidth of porphyrins in tight contact [6,8] differs qualitatively from that of isolated porphyrins in amorphous matrices. This function depends strongly on geometrical arrangement of the molecules (distance, orientation, local vibrations, etc.) and is subject of detailed theoretical (based on the Foerster EET model) and experimental (temperature dependence 1.5-20 K) study (to be published).

#### REFERENCES

- [1] E. Brynda, L. Kalvoda, I. Koropeccky, S. Nespurek and J. Rakusan, *Synthetic Metals* 37 (1990) 327
- [2] M. Floersheimer and H. Hoehwald, *Thin Solid Films* 159 (1988) 115
- [3] J. Bernard, M. Orrit, R.I. Personov and A.D. Samoilenko, *Chem. Phys. Lett.* 164 (1989) 377
- [4] F. Adamec, M. Ambroz, E. Brynda, J. Dian, M. Vacha and J. Hala, *Proc. SPIE* 1402 (1990) 82
- [5] G. Schulte, W. Grond, D. Haarer, R. Silbey, *J. Chem. Phys.* 88 (1988) 679
- [6] H. van der Laan, T. Schmidt, R.W. Visschers, K.J. Visscher, R. van Grondelle and S. Voelker, *Chem. Phys. Lett.* 170 (1990) 231
- [7] I. Yamazaki, N. Tamai, T. Yamazaki, A. Murakami, M. Mimuro, Y. Fujita, *J. Phys. Chem.* 92 (1988) 5035
- [8] J. Hala, M. Vacha, J. Dian, O. Prasil, J. Komenda, submitted for publication

## Kinetics of Hole Burning in Inhomogeneously Broadened Spectra: the Origin of Nonexponentiality and Problem of Burning Efficiency Dispersion

E.I.Al'shits, B.M.Kharlamov, N.I.Ulitsky

Institute of Spectroscopy, USSR Academy of Sciences,  
142092, Troitzk, Moscow Region, USSR, phone:3340236

High inhomogeneous broadening of impurity spectra in amorphous media reflects one type of dispersion, characteristic for disordered systems: dispersion of electronic transition frequency. In principle, there can exist a pronounced dispersion of other parameters: homogeneous line width ( $\Gamma$ ), Debay-Waller factor ( $\alpha$ ), hole burning efficiency ( $\phi$ ), etc. The problem of the burning efficiency dispersion (BED) was extensively discussed in the recent years ([1-6] and references therein). The nonexponentiality of the burning kinetics was treated in some publications [1-3,6] as an evidence of such dispersion. But burning kinetics is always nonexponential in strongly inhomogeneously broadened systems, if a burning laser line width  $\Delta\nu_l$  is much less than  $\Gamma$ . That was found experimentally and treated theoretically in one of the first publications on a hole burning [7] (see, also [8]). All other sources of the nonexponentiality are, in fact, additional to this one. So, it's not easy to attain experimentally the BED parameters on such background. The procedure of a numerical fitting of the burning kinetic with BED, developed in [4,5], is correct, but it looks unreliable due to many fitting parameters.

In this paper we describe the special experimental procedure, eliminating above mentioned "background" source of nonexponentiality in the burning kinetics. Some preliminary results of the kinetic measurements on systems with so called nonphotochemical hole burning (NPHB) are presented.

### Description of the burning kinetics and experiment.

Let us consider a simplified case: the distribution function of impurity centers  $N(\nu_0)$  is much broader than zero phonon line (ZPL) ( $N(\nu_0)=\text{const}$ ) and a phonon wing is very weak ( $\alpha=1$ ). The hole profile is the convolution:

$$D(\nu, E) = \int d\nu_0 \cdot \varepsilon(\nu - \nu_0) \cdot \Delta N(\nu_0, E), \quad (1)$$

where:  $\varepsilon(\nu)$  is ZPL profile,  $\Delta N(\nu_0, E) = N_0 - N(\nu_0, E)$ , and  $E = I \cdot t \cdot \phi$  ( $I \cdot t$  is a burning fluence).

Let us neglect the back reaction and consider two limiting cases:

1) Laser line is much narrower than ZPL:  $\Gamma_l \ll \Gamma$  (situation, typical for hole burning experiments). It is easy to show then:

$$D(\nu, E) \simeq \text{const} \cdot \int d\nu_0 \cdot \varepsilon(\nu - \nu_0) \cdot \{1 - \exp[-E \cdot \varepsilon(\nu_0 - \nu_l)]\}. \quad (2)$$

Burning kinetics is strongly nonexponential in this case.

2) Laser line is much broader than ZPL ( $\Gamma_l \gg \Gamma$ ):

$$D(\nu, E) \simeq \text{const} \cdot \{1 - \exp[-E \cdot \varphi(\nu_l - \nu)]\}, \quad (3)$$

where  $\varphi(\nu)$  is the exciting laser line profile. Burning kinetics in this case is exponential. It is preferable to realize such experimental scheme in a searching for above mentioned dispersion of parameters.

Experiments were performed on Mg-tetrazaporphin in ethanol solution at 4.2 K. The peak hole depth was registered as a function of a burning time at constant laser power in two different modes: with relatively broad ( $\Gamma_l \simeq 2.5 \text{ cm}^{-1}$ ), and narrow

( $\Gamma \approx 0.01 \text{ cm}^{-1}$ ) laser line. Home made dye laser with R-6G, pumped by  $\text{Ar}^+$ -ion laser (ILA-120), was used in experiments. Typical results are presented on Fig.1.

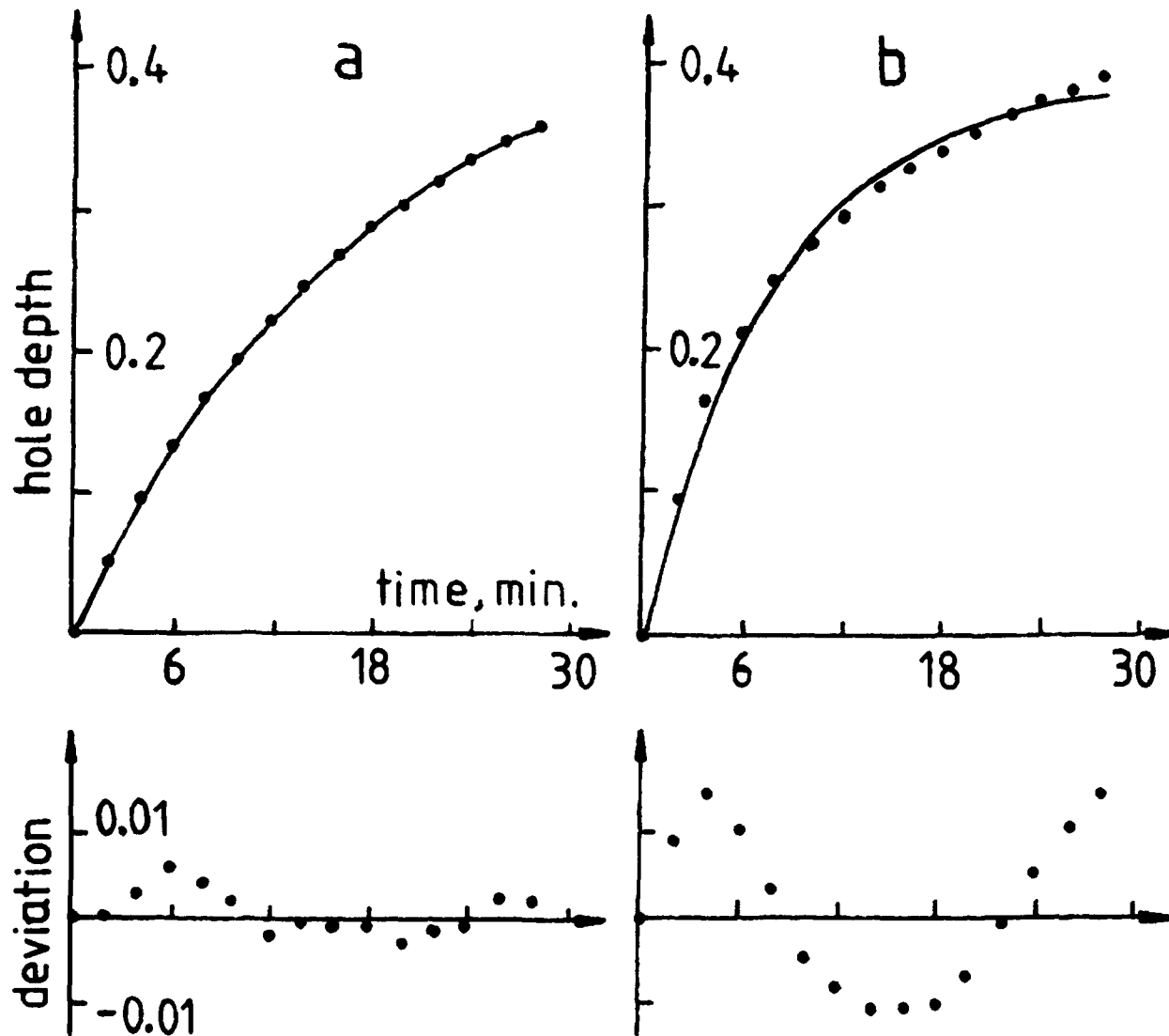


Fig.1. The kinetics of the peak hole depth growth:  
 a) burning laser line width  $\Delta\nu=2.5 \text{ cm}^{-1}$ , registration system resolution  $\Delta\nu=0.5 \text{ cm}^{-1}$ , burning power density  $P \approx 0.2 \text{ mW/cm}^2$ .  
 b) burning laser line width and registration system resolution  $\Delta\nu=0.01 \text{ cm}^{-1}$ , burning power density  $P \approx 5 \text{ } \mu\text{W/cm}^2$ .  
 The circles are experimental points. The full lines correspond to the fitting curve:  $A\{1-\exp(-Bt)\}$ , where A and B are least square fitting parameters. The deviation from the fitting model is depicted in the lower part of the figure.

The hole growth kinetics for the broad band burning is exponential within the limits of the experimental accuracy. The kinetics for narrow band burning is definitely nonexponential, as had been expected in accordance with (2).

Exponential curve on Fig.1a) testifies for the absence of a pronounced BED. This result is nontrivial for the system with NPHB. Efficiency of NPHB depends strongly on matrix. It was expected, that a high disorder of glassy matrix should lead to a noticeable BED. This experiment shows that an influence of the BED on the burning kinetics on the Mg-tetrazaporphin/ethanol system is at least one order of magnitude less, than the influence of the inhomogeneity (Eq.(2)). Now experiments are in progress on other objects, where a more pronounced BED is expected.

### References

1. R.Jankowiak, R.Richert, H.Bassler, J.Phys.Chem., **89**, 4569, (1985);
2. C.Aubert, J.Funfschilling, I.Zschokke-Granacher, T.A.Wieldman, W.Siebrand, Chem.Phys.Lett., **122**, 465, (1985);
3. A.Elschner, R.Richert, H.Bassler, Chem.Phys.Lett., **127**, 105, (1986);
4. Y.Kanematsu, R.Shiraishi, A.Imaoka, S.Saikan, T.Kushida, J.Chem.Phys., **91**, 6579, (1989);
5. A.Elschner, H.Bassler, J.Lumin., **43**, 33, (1989);
6. M.J.Kenney, R.Jankowiak, G.J.Small, Chem.Phys., **146**, 47, (1990);
7. B.M.Kharlamov, R.I.Personov, L.A.Bykovskaya, Opt.i Spectr., **39**, 240, (1975);
8. W.Kohler, J.Friedrich, Chem.Phys.Lett., **134**, 200, (1987);

## Spectral diffusion decay for strongly interacting spins in glasses

U. Zürcher and R. Silbey, Department of Chemistry,  
Massachusetts Institute of Technology, Cambridge, MA 02139

Thermal properties of glasses are successfully described with a model consisting of two-level systems (spins) coupled to a phonon bath [1], [2]. In most treatments, it is assumed that the spin-phonon interaction is weak. However, recent detailed examinations have revealed that this assumption is not justified [3] and that, therefore, the spin-phonon interaction is important for understanding physical properties of glassy materials [4], [5]. In this paper, we examine the implications of strong spin-phonon interaction on the spectral diffusion [6].

In the strong coupling limit, the spins are dressed with virtual phonons and interact with each other like electric dipoles [7],

$$\mathcal{H}_{int} = \sum_{k \neq l} \left( \frac{\vec{\sigma}^k \cdot \vec{\sigma}^l}{r_{kl}^3} - 3 \frac{(\vec{\sigma}^k \cdot \vec{r}_{kl})(\vec{\sigma}^l \cdot \vec{r}_{kl})}{r_{kl}^5} \right), \quad (1)$$

where  $r_{kl}$  denotes the spatial distance between the spins labeled  $k$  and  $l$ , and  $\vec{\sigma}$  has the components  $\sigma_\nu$ ,  $\nu = x, y, z$ . Following Klauder and Anderson [6], we retain the  $\sigma_x \sigma_x$  terms in Eq. (1) to define the local field at site  $k$ ,

$$H^k = \gamma \sum_{l \neq k} \frac{1}{r_{kl}^3} \sigma_x^l. \quad (2)$$

The local fields renormalize the energy splittings between upper and lower spin states,

$$E^k \rightarrow E^k + H^k. \quad (3)$$

Because the spin-phonon interaction is assumed to be strong the local fields  $H^k$  are much larger than the bare level splittings  $E^k$  and thereby dominate the energy scale.

The local fields change due to spin flips induced by the residual spin-phonon interaction. For strongly interacting spins, the spin-phonon relaxation rates depend on the local fields, and the spectral diffusion has to be determined in a selfconsistent way.

In the standard terminology [6], spins which have the same value  $H_0$  of the initial local field at time  $t = 0$  are called "A-spins," and are distinguished from all others ("B-spins"). In an inhomogenously broadened line, B-spins outnumber A-spins. The spectral diffusion

is the conditional probability  $p(H, t; H_0, 0)$  that the local field has value  $H$  at time  $t$  if that value was  $H_0$  at time  $t = 0$ ; it contains the statistical properties of the local fields only. However, the  $A$ -spins all have different local environments. Therefore, the spectral diffusion is calculated by first considering the stochastic process  $H(t)$  at the site of an  $A$ -spin, and then, in the second step, averaging over all different local environments of  $A$ -spins. That is, the spectral diffusion is defined for an *average*  $A$ -spin whose local field is a *macroscopic* variable. This leads to a separation of time scales: the individual spins relax to thermal equilibrium much faster than macroscopic local fields change.

Thus, for calculating the spectral diffusion, in Eq. (2), we replace the spin variables by quantities averaged over a short time interval  $[t, t + \delta t]$ ,

$$H^k(t) = \gamma \sum_{l \neq k} \frac{1}{r_{kl}^3} \hat{\sigma}^l(t), \quad (4)$$

$$\hat{\sigma}^l(t) = \frac{1}{\delta t} \int_t^{t+\delta t} d\tau \sigma_z^l(\tau). \quad (5)$$

The time averaged quantities  $\hat{\sigma}^k(t)$  are given by

$$\hat{\sigma}^k(t) = \sigma_{eq}^k(H^k(t)) + \delta\sigma^k(t), \quad (6)$$

where  $\sigma_{eq}^k(H^k)$  are equilibrium expectation values of  $\sigma_z^k$ ,

$$\sigma_{eq}^k(H^k) = \tanh\left(\frac{E^k + H^k}{2T}\right), \quad (7)$$

and  $\delta\sigma^k(t)$  are small deviations thereof. Correspondingly, the local fields split into slowly varying parts  $\bar{H}^k(t)$  and rapidly varying fluctuations  $\delta H^k(t)$ ,

$$H^k(t) = \bar{H}^k(t) + \delta H^k(t). \quad (8)$$

We show elsewhere [8] that the small fluctuations can be modelled by Gauss-Markov processes which are completely specified by their mean values,  $\langle \delta H^k(t) \rangle = 0$ , and correlation functions,

$$\langle [\delta H^k(t + \Delta t) - \delta H^k(t)] [\delta H^l(t + \Delta t) - \delta H^l(t)] \rangle = \delta^{kl} D_s \Delta t. \quad (9)$$

Here,  $\delta^{kl}$  is the Kronecker symbol, and  $D_s$  is the short time diffusion constant which in this treatment, is a parameter dependent on temperature. The temporal changes in the slowly varying parts  $\bar{H}^k(t)$  come about by those in the spin expectation values  $\sigma_{eq}^k(H^k(t))$  which, in turn, depend on the spectral diffusion. That is, the spectral diffusion is determined in a selfconsistent way. More specifically, we assume a Gaussian distribution,

$$p(H, t; H_0, 0) = \frac{1}{\sqrt{\pi w(t)}} \exp\left[-\frac{(H - H_0)^2}{w(t)}\right], \quad (10)$$

and solve selfconsistently for the width  $w(t)$ .

The spectral diffusion is given by

$$p(H, t; H_0, 0) = \langle\langle \delta \left[ H - \gamma \sum_{l \neq k} \frac{1}{r_{kl}^3} \sigma_{eq}^l (H^l(t)) \right] \rangle\rangle. \quad (11)$$

Here,  $\langle\langle \cdot \rangle\rangle$  denotes the average over both the short time fluctuations  $\{\delta H^l(\tau)\}_{l \neq k}$ ,  $0 \leq \tau \leq t$ , and long time fluctuations  $\{\bar{H}^l(\tau)\}_{l \neq k}$ ,  $0 \leq \tau \leq t$ , subject to the initial condition  $H_0 = \gamma \sum_{l \neq k} (1/r_{kl}^3) \sigma_{eq}^l (H^l(0))$ . We insert the Fourier representation of the  $\delta$ -function, and truncate a cumulant expansion after the second term. Assuming an identical distribution  $\rho(H(0))$  for the initial local fields at all spin sites and a uniform spatial distribution of spins, we find

$$w(t) = \lambda \int_0^t d\tau \int_{-\infty}^{\infty} dH_0 \rho(H_0) \int_{-\infty}^{\infty} dH p(H, \tau; H_0, 0) [\sigma'_{eq}(H)]^2. \quad (12)$$

Here, the prime denotes the derivative with respect to the argument and  $\lambda = 8\pi\gamma^2 D_s n / 3r_{min}^3$ , where  $n$  is the density of spins and  $r_{min}$  is the shortest distance between neighboring spins. Eqs. (10) and (12) determine the temporal behavior of the width  $w(t)$ .

For simplicity, we set the bare level splittings equal to zero,  $E^k = 0$ . We choose for the distribution of the initial local fields two Gaussians centered at  $\bar{H}_0$  and  $-\bar{H}_0$ , respectively,

$$\rho(H_0) = \frac{1}{2\sqrt{\pi}u} \left\{ \exp \left[ -\frac{(H_0 - \bar{H}_0)^2}{u} \right] + \exp \left[ -\frac{(H_0 + \bar{H}_0)^2}{u} \right] \right\}. \quad (13)$$

Thus, the width  $w(t)$  depends on the three parameters  $T$ ,  $\bar{H}_0$ , and  $u$ .

In the high temperature limit,  $T \rightarrow \infty$ , the width increases linearly in time,

$$w(t) = \frac{\lambda}{4T^2} t. \quad (14)$$

So that in agreement with the results of Klauder and Anderson [6], the conditional probability  $p(H, t; H_0, 0)$  decays diffusively. We note that the high temperature result is independent of the distribution of the initial local fields. This changes drastically in the case of low temperatures to which we now proceed.

In the case in which  $\bar{H}_0 \gg 2T$  and  $\sqrt{u} \ll 2T$  (in suitable units), we find

$$w(t) = T^2 \ln \left\{ \frac{1}{1 - (4\lambda/T^2) \exp \left[ -\left(2\bar{H}_0/T - u/T^2\right) t \right]} \right\}, \quad 0 \leq t \leq t_1, \quad (15)$$

where  $t_1$  is determined by  $\sqrt{w(t_1) + u} = \bar{H}_0 - 2T$ . For  $t \gg t_1$ , we find

$$w(t) \simeq \left( \frac{3\lambda}{2\pi T} \right)^{2/3} t^{2/3}, \quad t \rightarrow \infty. \quad (16)$$

That is, the local fields remain narrowly distributed for long times, and then spread very fast during a short time. Asymptotically,  $p(H, t; H_0, 0)$  decays more slowly than diffusively.

For the two other cases,  $\tilde{H}_0 \ll 2T$ ,  $\sqrt{u} \ll 2T$  and  $\sqrt{u} \gg 2T$ , we find a crossover from a diffusive regime for short times,  $w(t) \propto t$ ,  $t \rightarrow 0$ , to a subdiffusive regime for very long times,  $w(t) \propto t^{2/3}$ ,  $t \rightarrow \infty$ . A more detailed discussion is given in [8].

In summary, we examined carefully the relevant time scale for dephasing experiments in glasses. At low temperatures, strong spin-phonon coupling leads to deviations from simple diffusive behavior of the local fields. In a certain region of parameter space, a large part of the spectral diffusion decay occurs during a short time.

*Acknowledgments:* One of us (U.Z.) gratefully acknowledges financial support from the Swiss National Science Foundation.

## References

1. P. W. Anderson, B. I. Halperin, and C. M. Varma, *Philos. Mag.* **25**, 1 (1972).
2. W. A. Phillips, *J. Low Temp. Phys.* **7**, 351 (1972).
3. M. W. Klein, *Phys. Rev. B* **29**, 5825 (1984); *ibid* **31**, 1114 (1985);  
*Phys. Rev. Lett.* **65**, 3017 (1990).
4. C. C. Yu and A. J. Leggett, *Comments Condens. Mat. Phys.* **14**, 231 (1988).
5. C. C. Yu, *Phys. Rev. Lett.* **63**, 1160 (1989).
6. J. R. Klauder and P. W. Anderson, *Phys. Rev.* **125**, 912 (1962).
7. K. Kassner and R. Silbey, *J. Phys.: Condens. Mat.* **1**, 4599 (1989).
8. U. Zürcher and R. Silbey, to be published.

## **Electro - Optical, Multi-Stable Switches Based on Persistent Spectral Holes**

**David M. Hanson, Department of Chemistry  
State University of New York, Stony Brook, NY 11794-3400  
516-632-7884**

Photochemical or photophysical transformations induced by highly monochromatic laser radiation can drastically reduce the concentration of molecules absorbing at a particular wavelength within an inhomogeneously broadened absorption band. These spectral holes can be broadened, removed, shifted or split by the application of an external electric field under appropriate conditions. This property provides a nonlinear response in sample transmission, absorption, or diffraction and can be coupled with feedback to produce novel electro-optical devices. These devices include electrically activated, frequency selective, monostable, bistable, or multistable switches.

The most novel of these devices utilizes a holographic grating produced by spectral hole burning to provide frequency selectivity. The grating only exists for light in a small range of frequencies determined by the hole linewidth. This range of frequencies can be tuned by an applied electric field. With the field off and the laser tuned away from the spectral hole, no diffraction occurs. When the field is switched on, the hole is tuned into resonance with the laser, the grating is formed, and the diffracted beams appear. The intensity of the diffracted beams can be modulated by varying the frequency separation between the hole center and the laser. This frequency tunable grating can be incorporated into an optical waveguide to couple light into or out of the guide or to switch the light from one guide to another. This tunable switch can separate and direct light beams of different frequencies by varying the voltage that is applied to tune the spectral hole.

A bistable electro-optical switch can be produced by using the intensity of the diffracted beam in a feedback loop to adjust the voltage that is applied. This feedback causes the intensity of the diffracted beam to be a nonlinear and multi-valued function of input intensity. Consequently the output intensity can be either high or low for a given input intensity depending upon whether the switch is set high or low (bistable) by a prior light pulse. By suitably adjusting the spectral profile of the hole, similar multi-valued switches can be produced.

The principles, feasibility, and practicality of these devices are described along with experimental results.

Marker Mode Structure in the  
Primary Donor State of Bacterial Reaction Centers

P. Lyle and G.J. Small

Ames Laboratory-USDOE and Department of Chemistry,  
Iowa State University Ames, IA 50011 (U.S.A.) (515)294-3859

T.J. DiMugno and J.R. Norris

Department of Chemistry, The University of Chicago Chicago, IL 60637 (U.S.A.) (515)702-9646

Underlying structure for the primary donor absorption profiles of isolated reaction centers *Rhodospseudomonas viridis* and *Rhodobacter sphaeroides* (P960 and P870) has recently been uncovered by transient hole burning experiments [1]. A Franck-Condon progression of an intermolecular special pair marker mode ( $\omega_{sp}$ ) was found to originate in the low energy shoulder of the absorption spectra and peak at the one quantum transition. The theory of Hayes and Small [2] for fitting hole burned spectra was extended to include the coupling of the marker mode. Briefly, the theory defines a single site absorption function as being made up of a sum of 0-, 1-, ... phonon lineshape functions composed of a gaussian distribution for the low energy side and a lorentzian for the high energy side. By constructing a gaussian distribution whose full-width at half maximum is equal to the inhomogeneous broadening and convolving with the single site absorption function, the absorption spectrum is obtained. By further convolving these functions with an exponential decay function of the single sites centered at the burn frequency the absorption spectra after burning a time  $\tau$  is obtained. Important parameters include the Huang-Rhys factor for the phonons and marker mode  $S, S_{sp}$ , the mean phonon frequency  $\omega_m$ , the marker mode frequency  $\omega_{sp}$ , the width of the one phonon profile  $\Gamma$ , the zero-

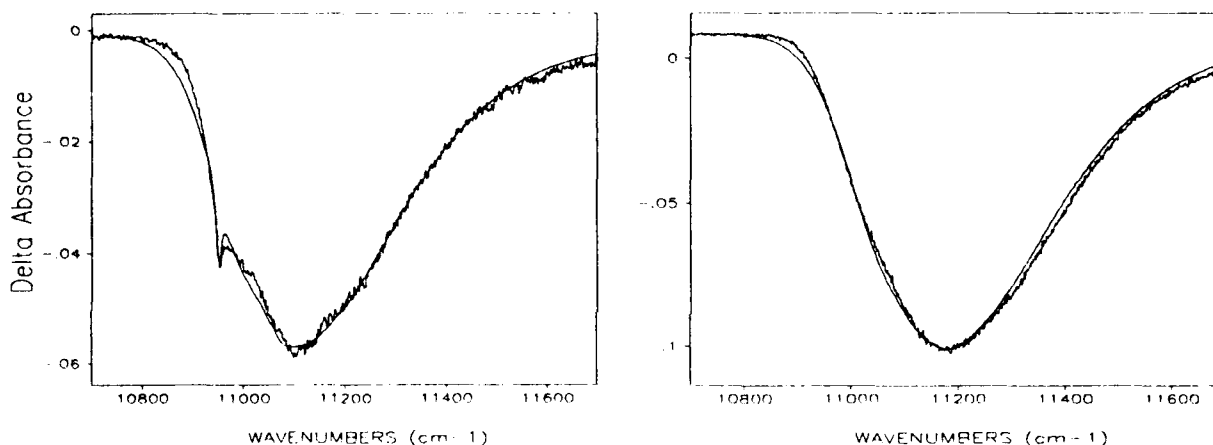
phonon width  $\gamma$ , and the inhomogeneous broadening  $\Gamma_I$ . Most of the parameter values required in the fit can be obtained from experiment. An important test for the theory is how well it can account for the burn wavelength dependence of the hole spectrum.

The above experiments on bacterial reaction centers were extended in this study to include the fully deuterated wild type *Rb. sphaeroides* and also a series of mutants of *Rb. capsulatus* (mutations at positions M208 and L181).

Hole burned spectra along with the respective fits for the deuterated reaction centers of *Rb. sphaeroides* are shown in the figure. The parameters found to fit the data are  $S=2.2$ ,  $S_{sp}=1.0$ ,  $\omega_m=25\text{cm}^{-1}$ ,  $\omega_{sp}=125\text{cm}^{-1}$ ,  $\Gamma=20\text{cm}^{-1}$ ,  $\gamma=5\text{cm}^{-1}$ , and  $\Gamma_I=130\text{cm}^{-1}$ . These can be compared to the parameter values for protonated *Rb. sphaeroides*:  $S=2.2$ ,  $S_{sp}=1.5$ ,  $\omega_m=30\text{cm}^{-1}$ ,  $\omega_{sp}=115\text{cm}^{-1}$ ,  $\Gamma=30\text{cm}^{-1}$ ,  $\gamma=5\text{cm}^{-1}$ ,  $\Gamma_I=170\text{cm}^{-1}$ . Even though some differences exist in the parameters, fits for the protonated reaction center obtained with the deuterated parameters are similar to the published spectra (not shown). In fact, the only significant difference is in the inhomogeneous broadening. This result strengthens the dynamical interpretation of the marker mode as a localized low frequency intermolecular vibration of the special pair primary electron donor since deuteration would be expected to have a small effect on such a mode.

Mutants of bacterial reaction centers have importance in determining how electron transfer proceeds in the reaction center by inducing small changes to the structure which can be compared to wild type. Preliminary studies are in progress in our lab on P870 of the reaction center mutants of *Rb. capsulatus*. As for the above bacterial reaction centers, these mutants also show evidence for marker mode structure. However this structure is

far less pronounced than observed for P960 and P870 of *Rps. viridis* and *Rb. sphaeroides*, which may indicate that  $\omega_{sp} \lesssim 110 \text{ cm}^{-1}$ . Zero-phonon holes were seen for some of these mutants, however more experiments are needed to characterize their depths and intensities for comparison with ultra-fast spectroscopic studies [3]. Differences in the low temperature spectra are seen and fits are under way to characterize the hole burning parameters.



Calculated and Experimental hole spectrum for the deuterated reaction center of *Rb. sphaeroides*. The spectrum on the left is for the burn wavelength on the low energy side of the primary donor absorption profile and the spectrum on the right is for the burn wavelength shifted  $\sim 400 \text{ cm}^{-1}$  to higher energy.

1 Johnson, S.; Tang, D.; Jankowiak, R.; Hayes, J.M.; Small, G.J. and Tiede, D.M. (1990) *J. Phys. Chem.*, 94, 5849-5855.

2 Hayes, J.M.; Gillie, J.K.; Tang, D.; Small, G.J. *Biochim. Biophys. Acta* 932 (1988), 287-305.

3 Chan, C-K; Chen, L. X-Q; DiMugno, T.J.; Hanson, D.K.; Nance, S.L.; Schiffer, M.; Norris, J.R. and Fleming, G.R. (1991) *Chem. Phys. Lett.* 176, 366-372.

## SOLVATION EFFECTS OF ORGANIC DYES IN POLYMERS: WAVELENGTH DEPENDENCE OF THE STARK EFFECT

Eric Vauthey, Keith Holliday, Changjiang Wei, Alois Renn and Urs P. Wild

*Physical Chemistry Laboratory, Swiss Federal Institute of Technology, ETH Zentrum, CH-8092 Zürich, Switzerland. Tel. +41 1 256 4384, Fax. +41 1 252 3402*

The wavelength dependence of the electric field effect on holes burnt in the absorption spectrum of Nile red (NR) and cresyl violet (CV) in polyvinylbutyral (PVB) and polyvinylformal (PVF) films has been investigated. The holes were detected using the holographic method [1].

Fig.1 shows a three dimensional surface plot of a holographically detected hole burnt in the absorption spectrum of NR in PVB. The hole was burnt in the centre of the frequency tuning range with no externally applied electric field. The plot was constructed from a sequence of external electric field scans at varying

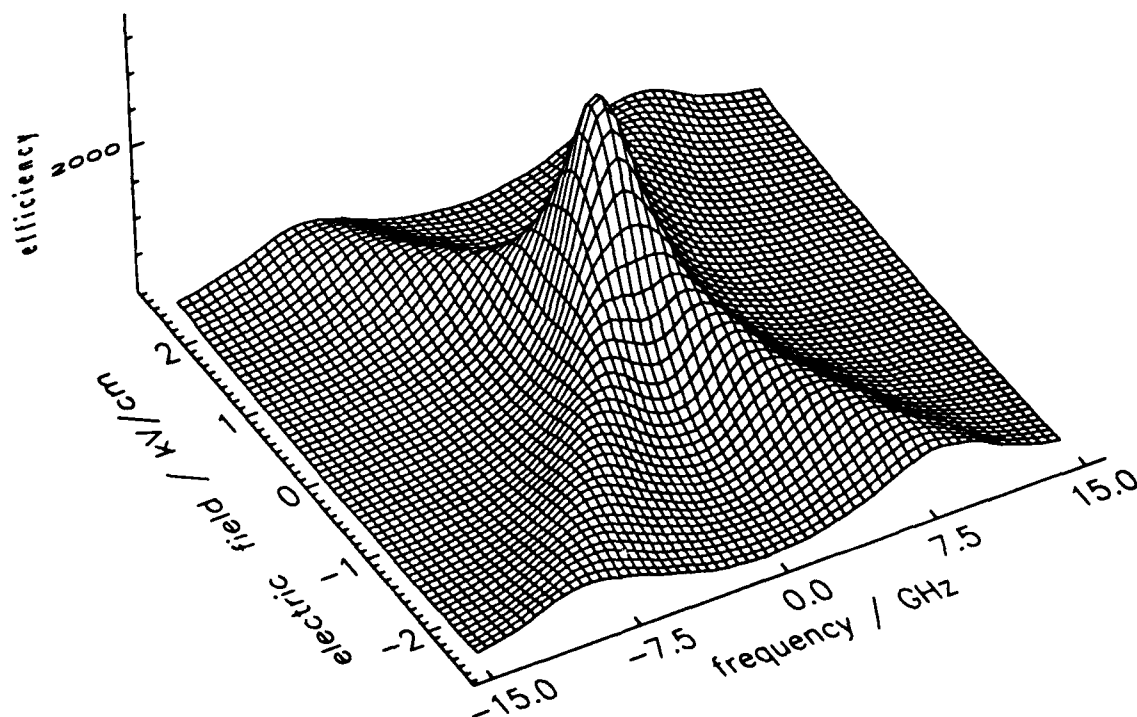


**FIGURE 1.** Stark effect on a hole burnt using the parallel geometry at 600 nm and at zero electric field in the NR/PVB system at 1.7 K.

frequency offsets. A cut parallel to the frequency axis shows the hole profile at the corresponding electric field strength. The external electric field was applied parallel to the polarisation of the laser light and so the splitting of the hole indicates a small angle,  $\theta$ , between the effective dipole moment difference and the transition moment [2]. In this case, when the external field is applied perpendicular to the laser polarisation the hole broadens but does not split.

From these two sets of Stark effect data, the effective magnitude of the molecular dipole moment difference between the ground and the excited state,  $\Delta\mu_e$ , can also be determined [3]. This contains contributions from the isolated molecular dipole moment difference,  $\Delta\bar{\mu}_M$ , and a matrix induced part. In previous investigations [2], the matrix induced contributions were described by the mean value of an isotropic distribution.

In the case of NR in PVB, however, fits of the sets of data to the theoretical functions [2] for each orientation could be made using a single parameter to represent  $\Delta\mu_e$ . The value of  $\Delta\mu_e$  was found to vary with wavelength, from 4.1 at 610 nm to 4.7 at 580 nm (fig. 2), while  $\theta$  was constant ( $\theta=23\pm 2^\circ$ ).

The dependence of  $\Delta\mu_e$  upon wavelength is an indication of the effect of the matrix on the molecular dipole moment difference. NR is a dye which shows large solvent shifts dependent on the polarity of the solvent, the transition energy decreasing with increasing solvent polarity, suggesting that NR has a large value of  $\Delta\bar{\mu}_M$ . Semi-empirical CNDO calculations show that NR also has a large ground state dipole moment of 6 D. This dipole moment causes local orientation of the impurity environment and thus local fields are strongly correlated with the orientation of the guest molecules. The dipole moment decreases with the strength of the interaction indicating that the matrix induced part of  $\Delta\mu_e$  points in the opposite direction to the purely molecular part. This also explains the lower value of  $\Delta\mu_e$  observed when the host matrix is changed to PVF (fig. 2) which has a larger dielectric constant ( $\epsilon=3.4$ ) than PVB ( $\epsilon=3.0$ ). In PVF, the Debye-Waller factor of NR is relatively small, making observation of the zero-phonon line difficult. For this reason, the Stark effect was investigated at only one wavelength. At 602 nm the measured dipole moment difference is 3.9 D and the angle  $\theta$  is the same as in PVB.

The same procedure was performed for CV in the two host matrices. The effective dipole moment difference was again found to decrease with increasing wavelength (fig. 2) but a distribution of matrix induced dipole moments had to be

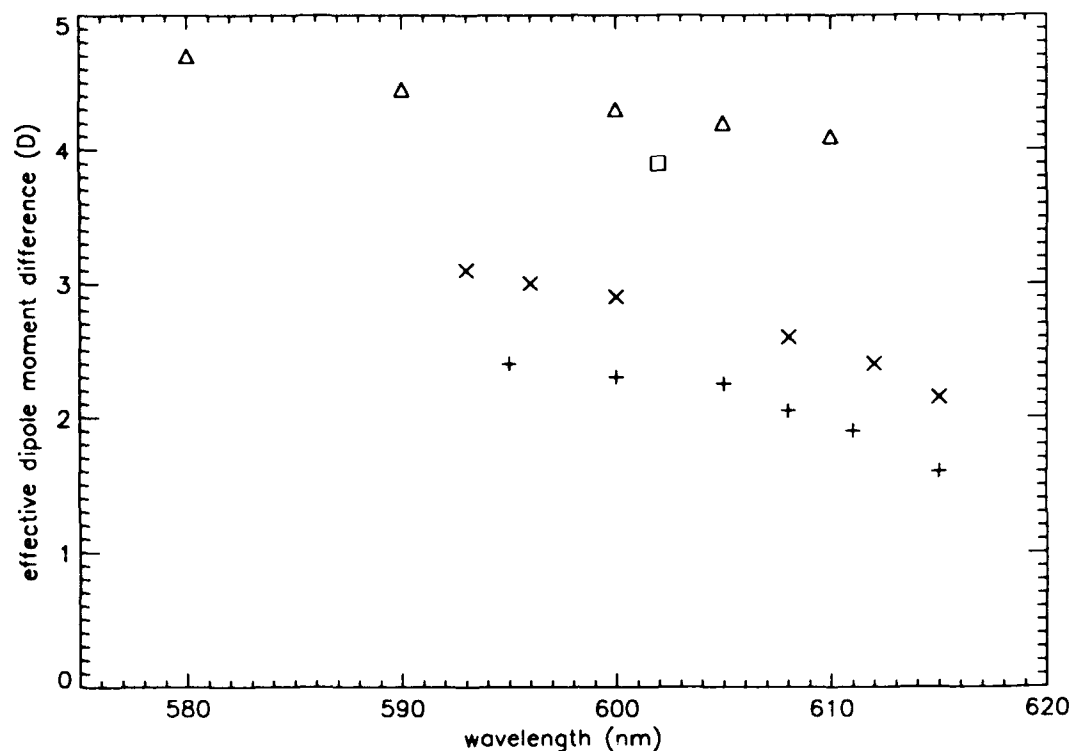


**FIGURE 2.** Wavelength dependence of the effective molecular dipole moment difference for CV in PVB (X) and PVF (+) and for NR in PVB ( $\Delta$ ) and PVF ( $\square$ ).

introduced to fit the data. The magnitude of the mean value of the distribution increased with increasing wavelength. When the dielectric constant of the host polymer was increased, from PVB to PVF, the magnitude of the mean value of the distribution again increased whilst, as for NR,  $\Delta\mu_e$  was found to decrease.

In previous studies [2], a three-dimensional isotropic distribution of matrix fields was used to fit Stark effect data in similar systems. However, the wavelength dependence of the effective molecular dipole moment difference indicates that such an isotropic distribution of matrix induced dipole moments does not describe the studied systems properly. The hole splittings for CV show that the induced dipole moment is larger in the red part of the spectrum. As a consequence, the sum of the distribution of induced dipole moment differences must point in the direction opposite to  $\Delta\bar{\mu}_M$ . The larger spread of induced dipole moments observed for CV in PVF suggests that the anisotropy of the local fields is stronger than in PVB, in agreement with the relative dielectric constants of PVB and PVF. Similarly, the large isotropy of the induced dipole moment observed for

CV is explained by the smaller ground state dipole moment, 1 D from CNDO calculations.

However, the magnitude of the induced dipole moment,  $\Delta\mu_i (=|\Delta\bar{\mu}_M - \Delta\bar{\mu}_e|)$ , depends on the local electric field and on the polarisability difference between the excited and the ground state of the molecule. The transition energy of the molecule also depends on the local field. This is the reason why  $\Delta\mu_i$  varies with transition energy. According to a simple electrostatic model [4],  $\Delta\mu_i$  is given by:

$$\Delta\mu_i = -\Delta\mu_M + (\Delta\mu_M^2 - 2.\Delta\omega.\Delta\alpha.h.c)^{1/2}$$

where  $\Delta\omega$  is the frequency shift of the transition and the isotropic polarisability difference is given by  $\Delta\alpha$ . Hence, for equal values of  $\Delta\omega$  and  $\Delta\alpha$ , the induced dipole moment difference is smaller for molecules with larger  $\Delta\mu_M$ . This explains the smaller change with wavelength of  $\Delta\mu_e$  in NR. Finally, from the wavelength dependence of  $\Delta\mu_i$ , it is possible to estimate the polarisability difference. The values obtained for CV and NR are in good agreement with those measured for similar molecules using different [5] or similar [6] techniques.

The variation of molecular parameter magnitudes with wavelength is expected to be a general phenomenon for guest molecules in amorphous hosts and a fuller model will be published elsewhere [4]. An understanding of this effect is important for the development of a molecular computer [7].

1. A. Renn, A.J. Meixner, U.P. Wild and F.A. Burkhalter, *Chem. Phys.* **93** (1985) 157.
2. A. Renn, S.E. Bucher, A.J. Meixner, E.C. Meister and U.P. Wild, *J. Lumin.* **39** (1988) 181.
3. A.J. Meixner, A. Renn, S.E. Bucher and U.P. Wild, *J. Phys. Chem.* **90** (1986), 6777.
4. E. Vauthey, K. Holliday, C. Wei, A. Renn and U.P. Wild, to be published.
5. J.H. Meyling, P.J. Bounds and R.W. Munn, *Chem. Phys. Lett.* **51** (1977) 234.
6. L. Kador, S. Jahn, D. Haarer and R. Silbey, *Phys. Rev. B* **41** (1990) 12215.
7. U.P. Wild, C. De Caro, S. Bernet, M. Traber and A. Renn, *J. Lumin.* **48** (1991) 335.

## Elucidation of Photophysics and Photochemistry in Polyacene Photoadducts

by

Mark A. Iannone and Gary W. Scott  
Department of Chemistry  
University of California, Riverside  
Riverside, CA 92521

(714) 787-3212

### Summary

Recently we have reported studies of low-temperature spectroscopy of a series of polyacene photoadducts.<sup>1-4</sup> A principal technique has been that of photochemical hole burning at 1.5K. The photochemistry involves the photodecomposition of the adduct back to the constituent polyacenes. In the present paper we extend this work on the photophysics and photochemistry of AT and also report new results on BrAT.

For AT, photodecomposition occurs in  $S_1$  over a relatively high barrier,<sup>1,5</sup> typically at temperatures  $>200\text{K}$  or at high excess excitation energies ( $\lambda < 280\text{ nm}$ ). Decomposition may also occur from upper triplet or singlet states, well-above the energies of the lowest excited states in these manifolds.

Intersystem crossing from the  $S_1$  state of AT occurs at room temperature with a reported yield<sup>5</sup> of 0.53. The  $T_1$  state, however, is not dissociative. The present paper shows conclusively that, at low temperatures, photodecomposition of AT and BrAT occurs predominantly by absorption of a second photon by the  $T_1$  state, thereby exciting a dissociative  $T_n$  state.

Samples were prepared as previously described<sup>1-3</sup> by photochemical synthesis of AT and, in an analogous fashion, BrAT. After purification by recrystallization, these molecules were blended into PMMA matrices to form sample films. Photochemical hole burning experiments were carried out on these films by immersing them in liquid helium at 1.5K or 4.2K. Frequency-

doubled dye lasers were used as excitation sources with bandwidths ranging from 0.1 to 5  $\text{cm}^{-1}$ . Action spectra for enhancement of hole burning were obtained by burning spectral holes in the uv while using a different second color in each experiment.

Fluorescence spectra were obtained with a commercial spectrofluorimeter at  $\sim 1$  nm resolution. Sample films were typically held at 12K in a closed cycle refrigerator. Fluorescence lifetimes were obtained using  $\sim 500$  ps, frequency-doubled dye laser pulses for excitation. Triplet-triplet absorption spectra for comparison with the two-color hole burning action spectra were obtained with a diode array spectrophotometer.

### Photochemical Hole Burning

AT undergoes PHB when irradiated on the red edge of the 0-0 absorption band.<sup>1,2</sup> In the present work, we were able to burn a relatively deep hole in this band and to observe broad antiholes to the red of the absorption band as well as weak satellite holes to the blue of the zero phonon hole. The anti-holes were readily assigned to anthracene and tetracene absorption due to photodecomposition of the AT. The hole area in the AT spectrum due to photolysis gave rise to an equal amount of tetracene produced, confirming the photochemical nature of these holes.

Satellite holes to the blue of the zero phonon hole may be assigned to vibronic levels in the  $S_1$  state. Excited vibrational states were clearly observed at  $709 \pm 4$   $\text{cm}^{-1}$ ,  $969 \pm 4$   $\text{cm}^{-1}$  and  $1387 \pm 4$   $\text{cm}^{-1}$  above the origin hole. These vibrations may be assigned to an in-plane skeletal distortion, an in-plane bend, and a C-C stretch of the naphthalene chromophore, respectively.

Two-color PHB experiments were performed on AT and BrAT. At low repetition rates (0.17 Hz) a gating efficiency of 5 was obtained for AT irradiating with 440-nm light while photolyzing in the UV. Similar results were obtained with BrAT.

Gating efficiencies were also obtained at several different wavelengths of the second color. The action spectrum, although noisy, peaks at  $\sim 440$  nm for both AT and BrAT, similar to the T-T absorption spectrum described below.

The above results strongly favor a two-photon decomposition mechanism at low temperatures. The first photon is absorbed in an  $S_1 \leftarrow S_0$  transition while the second excites a  $T_n \leftarrow T_1$  absorption with an intervening intersystem crossing step. To confirm this mechanism, we carried out an experiment in which both photons were of the same color ( $\sim 326$  nm) and determined the hole burning rate vs. source intensity. In a constant energy experiment, a two-photon process is expected to give a linear dependence on intensity while a one-photon process should show no intensity dependence. However, in the present instance, a triplet bottleneck gives a different intensity-dependent hole depth. A quantitative model is developed for this case and is compared with experimental results on AT. Only the two-photon, triplet-triplet absorption mechanism agrees with the experimental results.

### **Emission Spectra and Kinetics**

Fluorescence and phosphorescence spectra of AT and BrAT in PMMA film at 15K were obtained. Both showed emission spectra due to the naphthalene chromophore. The AT fluorescence intensity was much stronger than that of the phosphorescence under conditions of steady state illumination. For BrAT, the reverse was true due to the heavy atom effect of the nearby bromine atom.

The heavy atom effect also influenced the emission lifetimes. For AT, the fluorescence lifetime was  $60 \pm 4$  ns while for BrAT it was  $18.4 \pm 1.5$  ns. The phosphorescence lifetimes, measured at 15K, were  $3.20 \pm 0.03$ s for AT and  $1.19 \pm 0.04$ s for BrAT.

### **Triplet-Triplet Absorption Spectra**

The T-T absorption spectra of AT and BrAT were obtained and compared with T-T absorption spectra of 2,3-dimethylnaphthalene. All 3 spectra show the same vibronic development, and they all peak in the visible at  $\sim 440$  nm. From these spectra, the fractional triplet state population of AT could be determined. This information allowed us to calculate the

intersystem crossing quantum yield which, for AT, turns out to be  $\Phi_{isc} = 0.77$  at 15K. This gives a radiative lifetime for AT, using the fluorescence lifetime, of  $\tau_{rad} \geq 260$  ns, in reasonable agreement with the published value for 2,3-dimethylnaphthalene<sup>6</sup> (205 ns).

### References

1. Iannone, M; Scott, G.W.; Brinza, D.; Coulter, D.R J. Chem. Phys. 1986, **85**, 4863.
2. Scott, G.W.; Iannone, M.A.; Mackay, R.A.; Yamashita, T. Proc. Soc. Photo-Opt. Instrum. Eng. 1990, **1213**, 155.
3. Iannone, M.A.; Scott, G.W. J. Chem. Phys. 1988, **89**, 2640.
4. Iannone, M.A.; Scott, G.W. Chem. Phys. Letts., 1990, **171**, 569.
5. Yamamoto, S.-A.; Grellmann, K.-H. Chem. Phys. Letts. 1982, **92**, 533.
6. Berlman, I.B. Handbook of Fluorescence Spectra of Aromatic Molecules; Academic Press:New York, 1971.

Fluorine Spin Diffusion Barrier in  $\text{Pr}^{3+}:\text{LaF}_3$  Observed by Cross Relaxation

L.L. Wald and E.L. Hahn  
 Department of Physics, University of California  
 Berkeley, California, 94720 (415) 642-4859

M. Lukac  
 Josef Stefan Institute, Jamova 39,  
 Ljubljana, 61000, Yugoslavia Ph. (61) 214-399

Photon echo measurements made at 2 °K on the  $^3\text{H}_4 - ^1\text{D}_2$  transition in  $\text{Pr}^{3+}:\text{LaF}_3$  show that magnetic dipolar couplings between the Pr and F nuclei account for the 56 kHz homogeneous linewidth of this transition.<sup>1</sup> The homogeneous broadening arises from the enhanced  $^{141}\text{Pr}$  nuclear moment ( $I=5/2$ ) interacting with the local field fluctuations of the  $^{19}\text{F}$  nuclear moments undergoing mutual spin flip transitions. Such resonant fluctuations should, in the absence of a fluorine spin diffusion barrier, produce a homogeneous linewidth of about 200 kHz which is, in fact, roughly what is observed for the inhomogeneous broadening of the  $\text{Pr}^{3+}$  hyperfine levels and is considerably broader than that obtained by the photon echo measurements. Shelby et al<sup>2</sup> proposed a simple model analogous to the spin diffusion barriers responsible for narrowing the homogeneous lines in certain electron paramagnetic resonance transitions<sup>3</sup>. In such systems, the field produced by the electron magnetic dipole moment (2-3 orders of magnitude larger than the enhanced nuclear moment associated with the ground state of  $\text{Pr}^{3+}$  in  $\text{LaF}_3$ ) de-tunes the nearest neighbors from each other, prohibiting mutual spin flips among them. Thus, the fields produced by the neighboring spins are static and their interaction with the paramagnetic ion contributes to the inhomogeneous linewidth and not to homogeneous broadening. The de-tuned neighbors are referred to as the "frozen core." Application of this picture to the case of  $\text{Pr}^{3+}:\text{LaF}_3$  is supported by the calculation of Devoe et al.<sup>4</sup> Their Monte Carlo calculation of the  $\text{Pr}^{3+}$  optical dephasing times shows that the observed homogeneous linewidth could be explained by deleting the nearest neighbor F spins from the lattice of rapidly fluctuating fluorine moments, in effect, treating them as part of a frozen core.

We give direct evidence for the presence of a spin diffusion barrier in  $\text{Pr}^{3+}:\text{LaF}_3$  by examining the cross relaxation between the Pr and the F nuclei in a magnetic field chosen so that a pair of the Pr hyperfine energy levels matches the F splitting or a multiple of the F splitting. This is achieved by observing the effect of the F cross relaxation (or harmonic cross relaxation) on the optical pumping signal from the  $^1\text{D}_2 - ^3\text{H}_4$  optical transition.<sup>5</sup> Fig. 1 shows the calculated energy splittings from the spin hamiltonian for  $\text{Pr}^{3+}:\text{LaF}_3$  and the

effect of cross relaxation on the laser absorption. We examine directly the cross relaxation between the Pr and F spins by NMR and measure the coupling rate.

The Pr spins that cross relax can be maintained at an infinite spin temperature by applying one or more external RF fields in a way that does not directly effect the F spins, as shown in Fig. 2. The degree to which the saturated Pr system heats the F spin system (which initially is in equilibrium with the lattice at 2 °K) is examined by NMR measurement of the bulk F spin polarization. The Pr<sup>3+</sup> hyperfine levels and F transitions are shown in Fig. 2 for the single and double F spin flip crossings at B = 2.80 kgauss and 5.02 kgauss respectively.

A three reservoir system is involved where  $\beta_{Pr}$  represents the inverse spin temperature of the two Pr hyperfine levels participating in the coupling,  $\beta_F$  represents the bulk fluorine inverse spin temperature,  $\beta_0$  is the equilibrium (lattice) inverse spin temperature, and  $1/\tau$  represents the coupling rate between the bulk fluorine spins and the Pr spins. The F NMR signal obtains mainly from the bulk F spins that couple only by spin diffusion to the rare Pr spins. When Pr-F cross relaxation is observed through its effect on the optical pumping cycle, the opposite is true. In this case, the Pr populations are monitored and are coupled directly only to the nearest neighbor fluorines. These fluorine nuclei in turn must overcome any spin diffusion barriers associated with the frozen core in order for any effect to be seen among the bulk fluorines.

If the Pr spins are saturated ( $\beta_{Pr} = 0$ ), the coupled spin temperature equations for the three spin reservoirs give the relation

$$\beta_F / \beta_0 = (1 + \epsilon T_{IF} / \tau)^{-1},$$

at equilibrium, where  $\epsilon = 1/3(N_{Pr} / N_F) = 6 \times 10^{-4}$  is the ratio of the Pr spin system heat capacity to that of the F system.

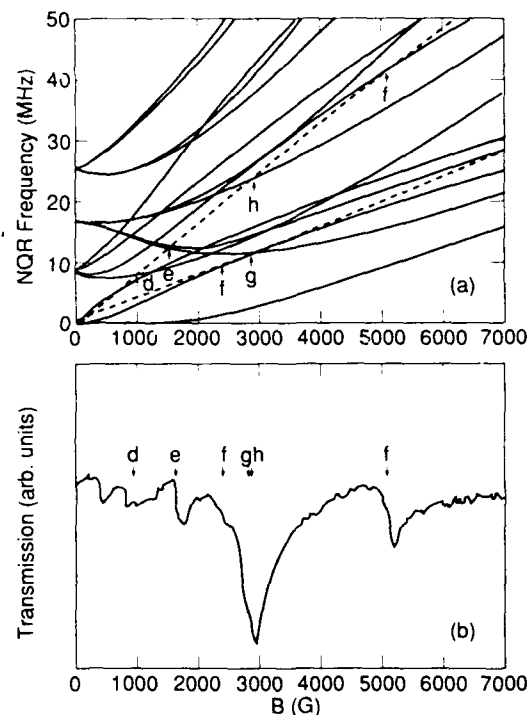


FIG. 1 (a) Numerical calculation of Pr<sup>3+</sup> ground state NQR splittings (solid line) for B parallel to a C<sub>2</sub> axis. The dashed lines are the fluorine transition and the double fluorine spin flip transition. Arrows show where the energy conserving cross relaxation occurs. (b) Optical transmission during a magnetic field sweep at a rate of 500 gauss/sec.

In the absence of a spin diffusion barrier and assuming a long spin  $T_1$  ( $> 15$  min at  $2^\circ\text{K}$ ) for the F nuclei, we expect the saturated Pr levels to depolarize the F system with a time constant  $\tau/\epsilon$  where  $\tau$ , in this case, is roughly the  $T_2$  of the fluorine spins. Using the measured  $T_2 = 15$   $\mu\text{s}$ , we estimate the bulk F polarization would then disappear in 0.02 seconds. Instead we measure  $\tau > 10$  s, indicating a diffusion barrier.

A 0.5 at. %  $\text{Pr}^{3+}:\text{LaF}_3$  crystal at  $2^\circ\text{K}$  is placed in a static magnetic field B directed along a crystal  $C_2$  axis. The crystal was mounted in a pair of capacitor plates which produce a voltage parallel to the same  $C_2$  axis. This allows a Stark modulated optical pumping cycle (SMOP) to be employed.<sup>6</sup> The crystal is inside two RF coils mutually perpendicular to B. The coil along the  $C_3$  axis is tuned to the fluorine NMR frequency and connected to a standard pulsed NMR apparatus which records the fluorine free induction decay. The other coil is untuned and is driven by a broadband RF power amplifier which allows the saturation of one or more Pr hyperfine transitions.

The level crossing condition is found by varying the magnetic field and observing either the laser transmission as in ref. 5 or by using the Stark modulation technique.<sup>6</sup> The magnetic field is then fixed at the level crossing condition and the  $\text{Pr}^{3+}$  hyperfine spectrum is measured by optically detected NMR using the SMOP method.<sup>6</sup> The observed spectrum is in good agreement with the  $\text{Pr}^{3+}$  spin Hamiltonian.<sup>5</sup>

Having achieved level crossing, the laser beam is then blocked, and the appropriate Pr levels are saturated as shown in Fig. 2. For the single F flip crossing the two different RF fields are applied in alternating 5 ms bursts to avoid the generation of any difference frequencies that would tend to saturate the F spins directly. After saturating the Pr spins for 15 minutes, the F NMR signal is recorded and compared to its equilibrium value.

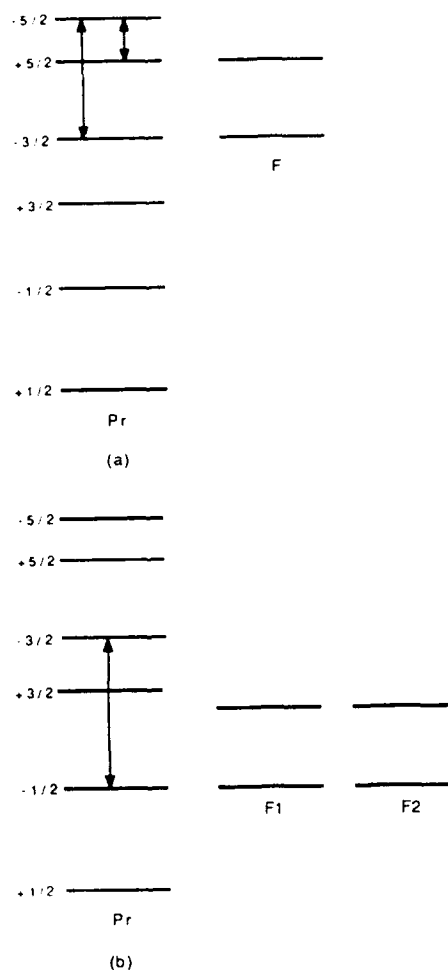


FIG. 2 (a) Pr and F energy levels for the case of the single fluorine flip level crossing at 2800 gauss. The  $m$  values shown correspond to the levels at zero field. At these fields the  $m$  values are mixed. The applied RFs used to saturate the  $5/2 - 3/2$  transition are shown. (b) Same as (a) but for the double fluorine spin flip transition at 5000 gauss. The sum of the two fluorine transition energies match with the  $5/2$  to  $3/2$  Pr transition.

For the single F spin flip level crossing at 2.80 kgauss there was no measurable change in the fluorine free induction decay signal. Given that a 5% change could have been detected, we estimate for  $T_1 = 900$  s that  $\tau > 10$  s. This lower bound for  $\tau$  is two to three orders of magnitude longer than the cross relaxation time expected in the absence of a spin diffusion barrier. We ascribe this weak cross relaxation rate to the presence of a spin diffusion barrier. For the double fluorine spin flip crossing at 5.02 kgauss, we observe a 30% reduction in the fluorine free induction decay. This gives a  $\tau$  of 2 s which implies that the diffusion barrier affects the much weaker resonant two spin flip cross relaxation rate to a lesser extent.

The two spin flip dipole-dipole cross relaxation rate involves a matrix element determined from second order perturbation theory which is a factor of  $(B_{\text{dipolar}} / B_0) \sim 10^{-3}$  smaller than the single flip process.<sup>7</sup> Nevertheless, this process couples to the bulk fluorines as well or better than the single flip process. This fact is consistent with the existence of a frozen core. The two flip process allows the coupling to circumvent the barrier presented by the frozen core provided the de-tuning does not extend beyond the first nearest neighbor fluorines. It is possible to imagine that the Pr splitting may match the sum of the two fluorine splittings without the fluorine splittings being equal to one another. If the outer F is coupled strongly to the bulk fluorines then the double flip process overcomes the spin diffusion barrier. The two de-tuned fluorines can be thought of as coupled together via their non-resonant dipole-dipole interaction but de-tuned from one another since they see a different values of the Pr dipolar field. Any calculation of the rate for this process would be complicated by the presence of several nearest neighbor fluorines, the mixture of the Pr  $m_z$  levels, the fact that the F and Pr spins have different quantization axis, and the isotropic nature of the Pr gyromagnetic moment.

In conclusion our observation of a weak Pr - F cross relaxation serves as an additional confirmation of the frozen core model.

1. R.M. Macfarlane, R.M. Shelby, and R.I. Shoemaker, Phys. Rev. Lett. 43, 1726 (1979).
2. R.M. Shelby, and R.M. Macfarlane, Opt. Commun. 27, 399 (1978).
3. W.B. Mims, in Electron Paramagnetic Resonance, ed. S. Geschwind (Plenum, New York) p 291.
4. R.G. Devoe, A. Wokaun, S.C. Rand and R.G. Brewer, Phys. Rev. B 23, 3125 (1981).
5. M. Lukac, F.W. Otto, and E.L. Hahn, Phys Rev A 39, 1123 (1989).
6. M. Lukac, and E.L. Hahn, J. Lumin. 42, 257 (1988).
7. N. Bloembergen, S. Shapiro, P.S. Pershan, and J.O. Artman, Phys. Rev. 114, 445 (1959).

## Crystalline Model Systems Probing Dynamics and Electric-Field Effects

*T. Attenberger and U. Bogner,  
Institute of Physics III, University of Regensburg,  
Postfach 397, 8400 Regensburg, Germany, T. 943-2109*

Recently in studies of fluorescence excitation and persistent spectral hole burning (PSHB) of single molecules in crystalline environment spectral jumps have been observed at 1.5 K providing new insights into the low temperature dynamics of the condensed phase [1]. The connection between PSHB and the phonon-induced dynamics in asymmetric double-well-potentials (DWP) has been used in a photophysical model of PSHB explaining also phonon detection by refilling of a spectral hole observed *after* irradiation with nanosecond heat pulses [2]. These DWP have been originally introduced in order to explain anomalous acoustic and thermal properties of amorphous materials by the so-called two-level systems, the existence of which is due to tunneling in DWP with *appropriate* parameters. The photophysical model is based on spectral shifts (matrix-shift-variations) caused by phonon-induced crossing of the barriers which can occur in *all* DWP if the phonon frequency is high enough.

Because of the problems connected with the statistical distribution of the barrier heights in amorphous materials we started to investigate crystalline organic [3] and inorganic [4] model systems with discrete barrier heights. Concerning inorganic materials we used  $\text{KI} : \text{S}_2^-$ ,  $\text{SrF}_2 : \text{Pr}^{3+} : \text{D}^-$  and neutron-irradiated sapphire.  $\text{KI} : \text{S}_2^-$  is a well-known system for barrier crossing and  $\text{SrF}_2 : \text{Pr}^{3+} : \text{D}^-$  was selected as a special model system in which not the light-absorbing species ( $\text{Pr}^{3+}$ ) itself but the neighbouring  $\text{D}^-$  ions are involved in the DWP. Neutron-irradiated  $\alpha\text{-Al}_2\text{O}_3$  is not only interesting because of the ballistic propagation of very high frequency phonons in sapphire but it is an interesting material also because it is an example of material optimization for possible applications in storage and in photonics since two-color, photon-gated PSHB in the IR with high thermoresistance (up to 670 K) was discovered [5]. For basic physics organic crystalline systems like perylene/n-heptane proved to be universally applicable model systems which turned out to be ideal for the study of correlations, not only between different dynamical effects but also between these dynamical effects and electric-field-induced level shifts [3]. These systems are ideal because the parameters determining all these effects are substantially different for the different antiholes (photoproduct lines) and the original lines.

In the present paper we will provide results concerning information about the physical nature of the DWP in these organic model systems and for the example perylene/n-heptane we will demonstrate that the universality involves also that PSHB in the background between the discrete lines of this Shpol'skii system yields exactly the same results (concerning dynamics and also concerning electric field effects) as in the case of amorphous materials so that these model systems represent a connecting link between crystalline and amorphous materials.

In our experiments the thickness of the sample was about 50  $\mu\text{m}$ . The sample cell usually consisted of two suprasil windows. For investigations of the electric field effects we used transparent indium tin oxide layers on the windows as transparent electrodes. The microcrystalline n-paraffines consisted of

lamellas, which in such a thin layer are mainly parallel to the windows [6]. Perylene in n-heptane, n-hexane and n-pentane are Shpol'skii systems in which the perylene (see left insert of Fig. 1) occupies distinct substitutional sites in the lattice by replacing n-paraffine chains, so that multiple structures with several pure electronic zero-phonon lines are observed in the low temperature spectra. In the case of perylene/n-heptane we investigated in particular the strong line II at 445.25 nm which has an inhomogeneous broadening of  $5 \text{ cm}^{-1}$ . Line II corresponds to a site in which the perylene molecule is replacing three n-heptane molecules (demonstrated for comparison in the left insert of Fig. 1) and in which the long axis of the perylene molecules is perpendicular to the n-heptane chains.

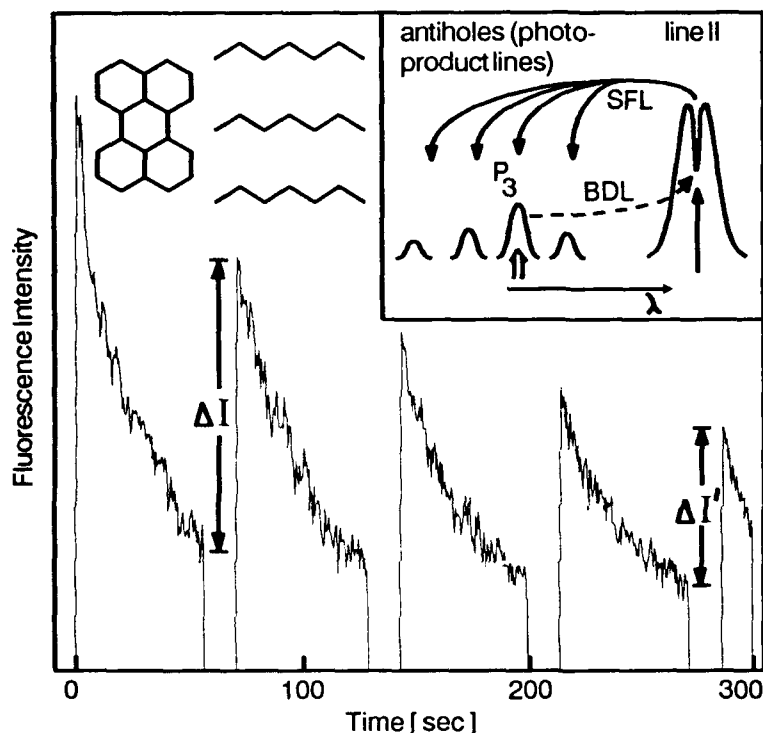


*Fig. 1. Repeated burning of perylene/n-heptane in line II with the single frequency ring dye laser (SFL). After each burning intervall the antihole (photo-product line)  $P_3$  is completely reverted by selective excitation with the broad-band dye laser (BDL). For  $\Delta I$  and  $\Delta I'$  see text.*

By excitation with a single frequency ring dye laser (SFL) we obtained PSHB in line II with creation of 8 antiholes (photoproduct lines  $P_1 - P_8$ ) shifted to higher energies up to  $100 \text{ cm}^{-1}$  and in the photoproduct lines we observed relative hole-burning efficiencies  $\eta'$  up to 6 orders of magnitude higher than in line II ( $\eta' = 1$ ), which has a very low burning efficiency so that it was necessary to focuss the full power (60 mW) of the SFL (width  $< 20 \text{ MHz}$ ) to an area of about  $0.3 \text{ mm}^2$  in order to obtain a hole depth of about 50 % in 20 sec. [3]. Concerning the laser-induced reverting of the photoproducts into the hole in line II we performed the following experiments.

With the SFL a hole was burned in line II and monitored by fluorescence excitation of the first vibronic transition which is shifted  $355 \text{ cm}^{-1}$  relative to the pure electronic transition. In addition a broad-band linear dye laser (BDL) with a width larger than 60 GHz was focussed on the same area of the sample (with a somewhat larger focus as compared to that of the SFL). After *one* frequency scan of the BDL in the spectral range of all P-lines the narrow hole (width  $\sim 200 \text{ MHz}$ ) in line II was completely refilled even after several times repeating burning and refilling. By burning and probing different parts of the spectral range of the P-lines we also proved that there is no direct phototransformation between the different P-lines but that all perylene molecules are reverted back

into line II. From these results we conclude that in the burning and refilling process only the perylene molecules themselves change their position. In the case of dynamical processes concerning the n-heptane molecules also the combination of changes involving *several* n-heptane molecules would be effective (there is no outstanding site of *one* of the n-heptane molecules forming the cage walls but because of the lattice symmetry there are always at least two n-heptane molecules in comparable sites in the cage walls). In this case we would not obtain a complete refilling of the hole in line II.

The experimental procedure of the second experiment is shown schematically in the right insert of Fig. 1 (only 4 of the 8 P-lines are drawn for simplicity). In this experiment only the strongest line  $P_3$  is reverted completely by selective excitation with the BDL. It can be seen in Fig. 1 that the fluorescence increase  $\Delta I$  between the end of the preceding burning process gets *smaller* with each cycle (see  $\Delta I'$  in Fig. 1) of burning and reverting. Therefore it can be ruled out that the appearance of the different P-lines is due to *different* rigid cage configurations since for constant burning times in this case always the same number of molecules would be switched into line  $P_3$  and also back to line II. This conclusion is confirmed by the observation that simultaneous PSHB in  $P_3$  and line II produces an increased population of the other P-lines.

The results provide the information that the DWP involved in PSHB and reverting are formed by the dye molecules moving relative to the *rigid* host cage between different discrete positions. For each cage, there is always the same distinct position corresponding to line II, with the highest value of the total intermolecular potential energy of the van der Waals interaction between dye and cage. This position represents the lowest lying minimum, i. e. the global minimum of all DWP. After photoexcitation and subsequent radiationless relaxation processes (which provide phonon cascades, including excitation of very high frequency local phonons) the dye can be clicked in a higher lying minimum, which represents another distinct position (corresponding to a P-line) with reduced value of the total interaction energy. The reduced barrier height  $W_r$  for the reverse phonon-induced barrier crossing process, means a strong asymmetry of the DWP and it results in a substantial increase of  $\eta'$  for the P-lines.

We have performed PSHB not only in the discrete lines but also in the weak continuous background. This continuous background is attributed to perylene molecules adsorbed on the surface of the n-heptane microcrystals which have a lamellar structure. We observed that the holes in the background show exactly the same low temperature dynamics as holes in amorphous polymers like polyvinylbutyral. We observed that these holes are spontaneously filled in part even at 1.3 K while the holes in line II could be filled only by heating the sample. For example after heating for 5 min to 2.4 K one of the weak P-lines completely disappeared and by this thermal reverting the hole in line II was filled a little bit. If the sample is heated for a time  $t_r$  to a temperature  $T_r$ , then the barrier with height  $W_r$  can be crossed by thermally activated reverting. The value of  $W_r$  can be calculated by the approximation formula [7]

$$W_r = kT_r \ln(t_r/\tau_0). \quad (1)$$

We use the characteristic time  $\tau_0 = 8$  ps which was determined for perylene in paraffin-like Langmuir-Blodgett films by the heat pulse technique [8]. With  $t_r = 5$  min we calculated the lowest value  $W_r = 52 \text{ cm}^{-1}$  [3], whereas for the background we can estimate with Eq. (1) that there must be barrier heights even below  $30 \text{ cm}^{-1}$ . The holes in the background are completely refilled after heating the

sample for 5 min to about 45 K and therefore the highest values of  $W_r$  for the background must be in the order of  $950 \text{ cm}^{-1}$ . On the basis of the correlation between  $W_r$  of the different P-lines and their burning efficiencies [3] this broad distribution of barrier heights results in an extreme large distribution of burning efficiencies.

This broad distribution of barrier heights is also interesting in connection with the electric field effects. The coefficients  $\delta v_s/E$  of the electric field induced hole splittings (which were observed in all discrete lines of perylene in n-heptane [6] including meanwhile also the P-lines [3]) are correlated with the barrier height  $W$  [3]. In this correlation high values of  $\delta v_s/E$  correspond to low values of  $W$ . The correlation is based on the fact that the dispersion interaction induced spectral shift and the van der Waals interaction energy are determined by the short range interaction between *fluctuating* dipoles [3]. In addition the large value of the electric-field induced level-shift measured for one of the P-lines is even exceeding the corresponding average values obtained for perylene in the polar matrix butanol and reaches approximately 70 % of those values reported recently [9] for selected polar polymers. The background is showing exactly the same electric-field-induced change of the holes as in amorphous materials, i. e. application of an electric field broadens the hole so that the hole structure can disappear completely if the electric field is high enough. This effect is interesting for technical applications such as optical data storage because it provides the possibility to use the electric field dimension as a second dimension, in addition to the frequency dimension. Apparently the broad distribution of electric-field-induced level shifts is based on the broad distribution of barrier heights. On the other hand this reasoning demonstrates the advantages of perylene/n-heptane as a model system because the correlations between the discrete values of the barrier heights and the discrete values of other parameters, connected e. g. with the variability of the dispersion interaction, can be determined separately for different wavelengths.

### References

1. M. Orrit and J. Bernard, *Phys. Rev. Lett.* **65**, 2716 (1990); W. P. Ambrose and W. E. Moerner, *Nature*, **349**, 6306 (1991); W. E. Moerner and W. P. Ambrose, *Phys. Rev. Lett.* **66** 1376 (1991).
2. U. Bogner, *Phys. Rev. Lett.* **37**, 909 (1976); U. Bogner and R. Schwarz, *Phys. Rev.* **B24**, 2846 (1981).
3. T. Attenberger and U. Bogner, to be published.
4. T. Attenberger, I. Sildos, G. Jones, U. Bogner and Max Maier, *Radiation Effects and Defects in Solids*, **119**, 320 (1991).
5. M. Aizengendler, U. Bogner, I. Dolindo, J. Kikas and I. Sildos, to be published.
6. T. Attenberger, U. Bogner and Max Maier, *Chem. Phys. Lett.* **180**, 207 (1991).
7. J. J. Prejean and J. Souletie, *J. Physique* **41**, 1335 (1980).
8. T. Attenberger, K. Beck and U. Bogner, *Proceedings of the Third Int. Conf. on Phonon Physics*, edited by S. Hunklinger, W. Ludwig, and G. Weiss (World Scientific; Singapore, London; 1990) p. 555.
9. Y. Kanaan, T. Attenberger, U. Bogner, M. Maier, *Appl. Phys.* **B51**, 336 (1990).

## Light- and Thermoinduced Spectral Diffusion in Organic Amorphous Systems Measured via Hole Burning Stark Spectroscopy.

E.I. Al'shits, B.M. Kharlamov, N.I. Ulitsky

Institute of Spectroscopy, USSR Academy of Sciences,  
142092, Troitzk, Moscow Region, USSR, phone:3340236

Spectral diffusion (SD) is extensively investigated in the past years by means of hole burning method. In particular, evidences of thermo- [1] and lightinduced [2] SD are found. At the same time authors of [3] have found a strong dependence of the burned hole width on the burning fluence. As known, the classical model of a burning kinetics ( hole broadening in this model is connected with saturation of the hole in the distribution function of impurity centers ) predicts enough weak hole broadening at the initial stage of burning [4]. It leads to a conclusion about possible additional mechanisms of hole broadening on an initial burning stage. One of such mechanisms can be SD, induced by the burning light (LISD). The influence of the burning power and fluence on the hole broadening was investigated by means of high sensitive Stark spectroscopy on chlorin in polyvinylbutyral (Chl/PVB). Thermoinduced SD (TISD) is investigated also, model of this process is proposed.

Experiments were performed on the Chl/PVB films, supplied by semitransparent Stark electrodes at temperatures  $2 \div 30$  K. The single frequency He-Ne laser LGN-209 was used for a hole burning. The burning power was  $1 \div 70 \mu\text{W}/\text{cm}^2$ . During registration process it was decreased down to  $10^{-9} \text{W}/\text{cm}^2$ . Field curves were measured: the dependence of the sample transmittance in the hole maximum on the applied voltage. The field curve width is linearly connected

influence of the hole filling light with power  $\simeq 1 \text{ mW/cm}^2$ . Effective LISD should somewhere increase the hole width in such conditions. But measured hole widths were practically the same, as in the previous experiments. So, the set of the presented data testifies the negligible influence of LISD on the hole formation in the spectrum of Chl/PVB.

Thermoinduced SD was measured using a temperature cycling method [1]: after hole burning and measurement at temperature  $T_b$  the sample was annealed at  $T_a$ , cooled back to  $T_b$  and measured again with 15 - 20 min delay.  $T_b$  was changed from 5 K to 20 K,  $T_a$ -from  $T_b+5 \text{ K}$  to  $T_b+30 \text{ K}$ . The results are presented on Fig.1.

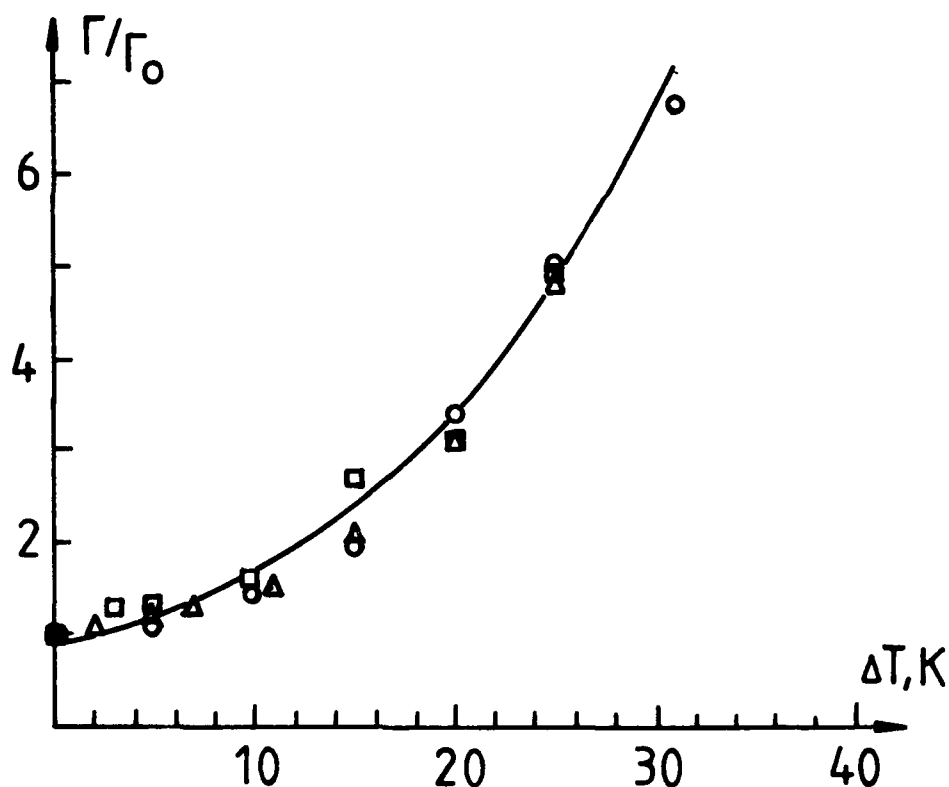


Fig.1. Dependence of the irreversible hole broadening on the annealing temperature  $\Delta T = T_a - T_b$ . Experimental points for the holes, burned at different temperatures are presented as:

○ -  $T_b = 5 \text{ K}$ ;    △ -  $T_b = 15 \text{ K}$ ;    □ -  $T_b = 20 \text{ K}$ .

with the hole spectral width [5]. It is easy to calculate the hole spectral width, using measured field curve width and the known change of the static dipole moment at electronic transition. It is evident, that theoretical limit should exist on the minimal registerable hole depth ( $D_{min}$ ) and, therefore on the minimal burning fluence ( $Pt_{min}$ ). Analytic formulas were obtained in [6] for  $D_{min}$  and  $Pt_{min}$  under standard experimental conditions, at relatively general assumptions. Estimation, based on this equations, gives for chlorin at 5 K:  $D_{min} \simeq 5 \cdot 10^{-4}$  and  $Pt_{min} \simeq 10 \mu\text{J}/\text{cm}^2$ . The values, reasonably close to this limits, were obtained in pure experiments:  $D_{min} \simeq 2 \cdot 10^{-3}$  and  $Pt_{min} \simeq 60 \mu\text{J}/\text{cm}^2$ . The minimal hole width  $\Gamma = 0.02 \text{ cm}^{-1}$  (at 5 K) was found using measured value of the field curve width. Increase of the fluence up to  $0.1 \text{ J}/\text{cm}^2$  (and the hole depth by  $\simeq 30\%$  of the initial optical density of the sample) results in a hole width increase by  $\simeq 2.5$  times. The experimental dependence of the hole width on the burning fluence is in a very good agreement with the classical model [4], e.g. any additional hole broadening on an early stage of the burning is not observed.

Special experiments were performed to check a possible role of LISD in more broad range of fluences. As known, the 0-0-absorption band of the Chl photoproduct is shifted  $1600 \text{ cm}^{-1}$  from the educt one, and the rate of the back reaction is  $\simeq 10^2$ - $10^3$  times higher. It makes possible hole measurements in the conditions of the stationary hole burning - hole filling process. The equilibrium state appears under simultaneous influence of the burning laser light and broad band irradiation in the product absorption band. In such experiments an effective burning fluence was approximately an order of magnitude higher than maximum fluence in the previous experiments, and it is necessary to add the

In our case hole broadening  $\Gamma/\Gamma_0$  depends nonlinearly on  $T_a$ . The data can be fitted equally good both by an exponent with the activation temperature  $\Delta T \simeq 14.5 \pm 2$  K (full line on Fig.1) and by a power function with the exponent  $\alpha \simeq 2.2 \pm 0.1$ . The measured hole broadening law is in contradiction with a linear behavior, predicted by classical SD model, and experimentally obtained in [1]. The source of this contradiction is still unclear. Our data can be treated in frames of activation model of the relaxation of two level systems (TLS), responsible for SD.

There are different models of SD, based on TLS theory. Roughly we can distinguish two types of models, treating SD in frames of equilibrium or nonequilibrium evolution of TLS-ensemble. Special experiments were performed with multiple temperature cycling, before and after hole burning. The results of those experiments can be treated noncontradictory only in frames of a model of equilibrium TLS evolution.

#### References:

1. G.Schulte, W.Gron, D.Haarer, R.Silby, J.Chem.Phys., **88**, 679, (1988);
2. W.Richter, Th.Sesselmann, D.Haarer, Chem.Phys.Lett., **159**, 235, (1989);
3. R.van der Berg, A.Visser, S.Volker, Chem.Phys.Lett., **144**, 105, (1988) and references therein;
4. L.Kador, G.Schulte, D.Haarer, J.Phys.Chem., **90**, 1264, (1986);
5. V.K.Ivanov, R.I.Personov, N.V.Rasumova, Opt. i Spektr., **58**, 2, (1985);
6. E.I.Al'shits, N.I.Ulitsky, B.M.Kharlamov, Izv.Akad.Nauk Estonia, (1991), in press;

## Stark Effect on Persistent Spectral Holes Measured by Electric Field Modulation Technique

Toshiyuki Shimada and Hiroyuki Suzuki

*NTT Opto-Electronics Laboratories*  
*Shirakata Shirane, Tokai-mura, Naka-gun, Ibaraki-ken 319-11, Japan*  
*Tel. 81-292-87-7425 Fax. 81-292-87-7870*

### Introduction

An external field applied to dye doped polymers which have inhomogeneous dispersion in their absorption spectra causes a shift in the absorption of the dye molecules. This, in turn, changes the line shapes of persistent spectral holes<sup>1)</sup>. The Stark effect has been applied to optical storage<sup>2)</sup> and optical computing<sup>3)</sup>. It has been also used as a powerful tool for investigating such physical profiles of materials as the difference between the effective molecular electric dipole moments in the host matrix in the ground and excited states which is related to hole burning<sup>4),5)</sup>.

In this paper, we used an electric field modulation technique to measure the Stark effect on wide and shallow spectral holes. The technique enables us to detect weak Stark effects on spectral holes in dye doped polymers using a weak electric field at about 6 K.

### Stark Effect on Persistent Spectral Holes : Principle and Discussion

The Stark effect is regarded as a perturbation in the photon absorption process of guest molecules. The line shape of a spectral hole is described by a Lorentzian function. An external electric field ( $E_S$ ) causes a frequency shift of the absorption of the  $i$ -th guest molecule as,

$$\Delta\omega_i = (1/\hbar)[(\epsilon + 2)/3]\Delta\mu_{mol,i}E_S \quad (1)$$

where  $\epsilon$  is the dielectric constant of the host polymer<sup>4)</sup>, and  $\Delta\mu_{mol,i}$  is the difference between the electric dipole moments in the ground and excited states. The dispersion of the directions of  $\Delta\mu_{mol,i}$  causes a change in the line shape of a burnt hole<sup>4)</sup>. For dye molecules doped in a polymer host matrix,  $\Delta\mu_{mol,i}$  is the sum of the permanent molecular dipole moment difference and the results from the local electric field of the host matrix. The Stark effect on spectral holes has been analyzed when all the  $\Delta\mu_{mol,i}$  values are equal but the directions are isotopically dispersed, and  $\Delta\mu_{mol,i}$  and the molecular transition moment  $D_i$  have a fixed angle  $\theta$ <sup>6)</sup>. The line shape of a hole depends on  $\theta$  in addition to  $\Gamma$ ,  $\omega$  and  $\Delta\omega$ , where  $\Gamma$  and  $\omega$  are the initial width and the center frequency of the hole, respectively.

Figure 1 (a) and (b) show the calculated line shapes of a spectral hole in an external electric field at 2 K and 6 K, respectively. In the calculation, the following assumptions were made:

- (1) The external electric field is vertical to the electric field of the laser light.
- (2) The  $\theta$  value is 0.
- (3) The two holes have the same area.
- (4) The holewidth dependence on temperature ( $T$ ) is expressed by  $\Gamma = \Gamma_0(T - T_0)^a$ , where  $\Gamma_0$  denotes the width at  $T = T_0$ , and  $a$  is a constant between 1 and 2<sup>7)</sup>.

The figure indicates that the Stark effect induced by a weak external field at the higher temperature is difficult to detect by means of conventional transmission measurements.

When the external electric field is alternated as shown in Fig.1 (c), the line shape of the hole changes in response to the electric field. By detecting only the difference between the line shapes with and without the field we can obtain the spectra shown in Fig.1 (d). It should be noted that this technique detects the Stark effect directly. The experimental results obtained using the electric field modulation technique are described in the following section

## Experimental

The samples were prepared by casting dyes with polymer using dichloromethane as a solvent as previously described<sup>8)</sup>. The sample thickness was of the order of  $10^2 \mu\text{m}$ . They were cooled to approximately 6 K in a He cryostat. The laser for burning and probing holes was a single-frequency ring dye laser (bandwidth 500 kHz). Two types of measurement were made using (a) the laser double beam technique<sup>9)</sup> and (b) the electric field modulation technique (Fig. 2). The scanning range of the laser was expanded to about 60 GHz. The experimental setup for supplying the external electric field was similar to that reported previously<sup>5)</sup>, except that the electric field was alternated. The signal was phase-sensitively detected by a lock-in amplifier.

## Results and Discussion

Figure 3 (a) shows a spectral hole measured using the laser double beam technique (metal-free tetraphenylporphine (TPP) in poly-vinylbutyral (PVB)). The concentration of TPP is  $5 \times 10^{-3} \text{ M}$ , and the thickness of the sample is  $178 \mu\text{m}$ . The hole was burnt by tuning the dye laser to 660 nm and irradiating the sample at a power of  $20 \mu\text{W}/\text{cm}^2$  for 30 sec at 5.2 K. A hole was detectable but it was unclear due to the low signal to noise ratio. In contrast to Fig. 3 (a), a very clear signal is detected in the zero background using the modulation technique (Fig.3 (b)) for the same hole (the external electric field was vertical to that of the laser light and had an amplitude of 56 kV/cm at a modulation frequency of 35 Hz). The modulation frequency was sufficiently high in the experiment because the laser light scanning rate was 0.1 GHz/sec. The wings on either side of the strong center signal should be negative (see Fig.1 (d)), but we only measured the amplitude of the signal so they appear to be positive. The signs of the wings can be corrected by detecting the phase of the signal. The sensitivity of this technique is higher by about 10 dB than that of the laser double beam technique.

The dependence of the modulated signal on the amplitude of the external electric field is shown in Fig. 4. The sample is PVB doped with pyropheophorbide a methyl ester (PPME; Fig. 5) (concentration:  $6 \times 10^{-4} \text{ M}$ ). The sample thickness is  $400 \mu\text{m}$ . The fact that a hole is detectable even though the external field is as weak as 2.5 kV/cm at 6 K (Fig. 4 (a)) shows that this technique is very effective for measuring the Stark effect on spectral holes. This technique is also effective for measuring the Stark effect in the  $E_S // E_O$  geometry as well as for samples whose materials are easily affected by a field. It should be noted that the maximum obtainable amplitude of the field in the  $E_S // E_O$  geometry is practically lower than that in the  $E_S \perp E_O$  geometry.

## Conclusions

The Stark effect on persistent spectral holes in dye doped polymers was measured using a sensitive modulation technique. The electric field required for PPME/PVB, for example, was only of the order of kV/cm at 6 K. The technique is, therefore, useful for measuring the Stark effect on systems which are easily affected by an electric field. It also enables the Stark effect to be measured at considerably higher temperatures than previously achieved.

## References

- 1) U. Bogner, P. Schätz, R. Seel and Max Maier, Chem. Phys. Lett., **102**, 267 (1983).
- 2) U. P. Wild, S. E. Bucher and F. A. Burkhalter, Appl. Opt., **24**, 1526 (1985).
- 3) U. P. Wild, A. Renn, C. DE Caro and S. Bernet, Appl. Opt., **29**, 4329 (1990).
- 4) L. Kador, D. Haarer and R. Personov, J. Chem. Phys., **86**, 5300 (1987).
- 5) A. Renn, S. E. Bucher, A. J. Meixner, E. C. Meister and U. P. Wild, J. Lumin., **39**, 181 (1988).
- 6) A. J. Meixner, A. Renn, S. E. Bucher and U. P. Wild, J. Phys. Chem., **90**, 6777 (1986).
- 7) *Persistent Spectral Hole-Burning: Science and Applications*, ed. W. E. Moerner (Springer-Verlag Berlin Heidelberg, 1988).
- 8) T. Nishi, K. Arishima, H. Tabei and H. Hiratsuka, Jpn. J. Appl. Phys., **27**, 225 (1988).
- 9) T. Shimada, H. Suzuki, T. Nishi, K. Arishima and H. Hiratsuka, Chem. Phys. Lett., **158**, 435 (1989).

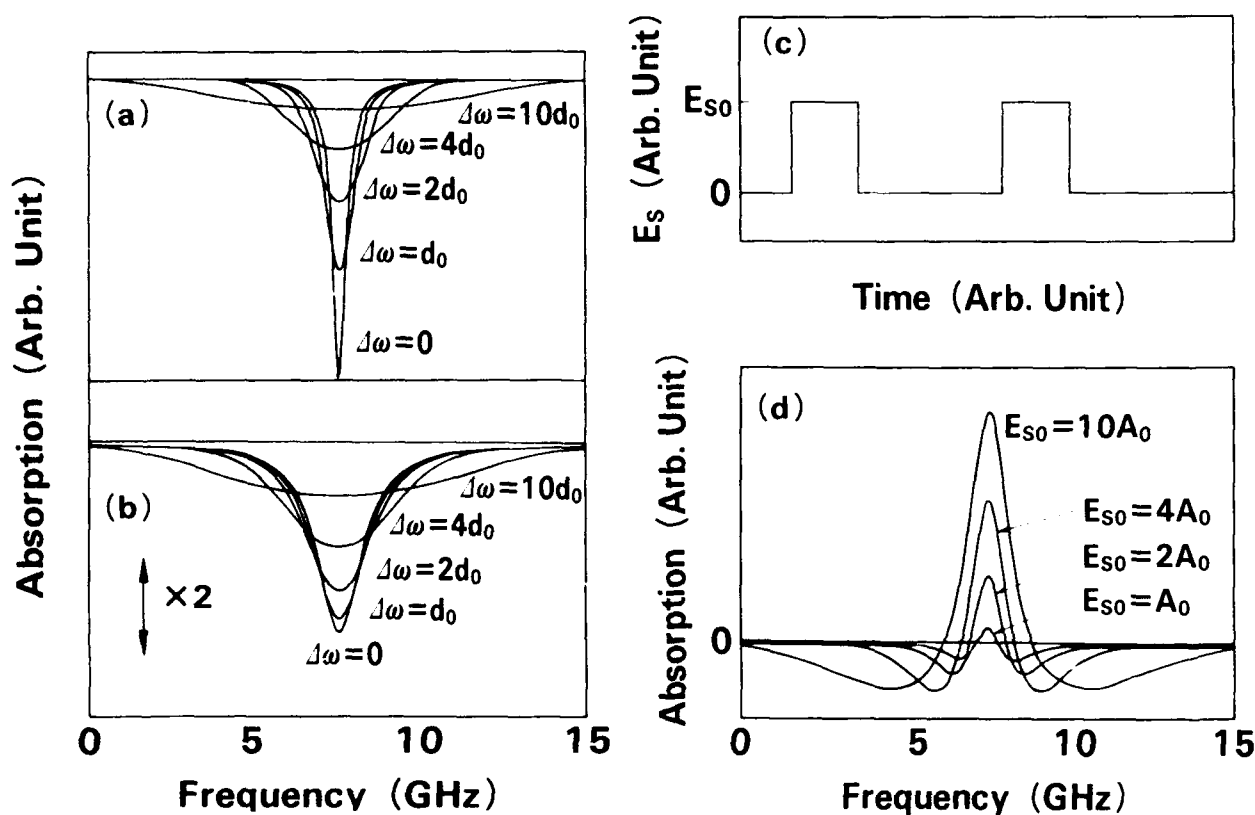


Fig.1. Calculated line shapes of a hole for  $E_s \perp E_0$ ,  $\theta = 0$  at (a)  $T = 2$  K and (b)  $T = 6$  K.  $\Delta\omega$  is the averaged  $|\Delta\omega|$  value (see eq. (1)) and  $d_0 = 0.75$  GHz. (c) The alternated external electric field. (d) The difference spectra between the line shapes for  $E_s = 0$  and  $E_s = E_{s0}$  (see (c)).  $A_0 = (\hbar / \Delta\mu)[3 / (\epsilon + 2)]d_0$ .

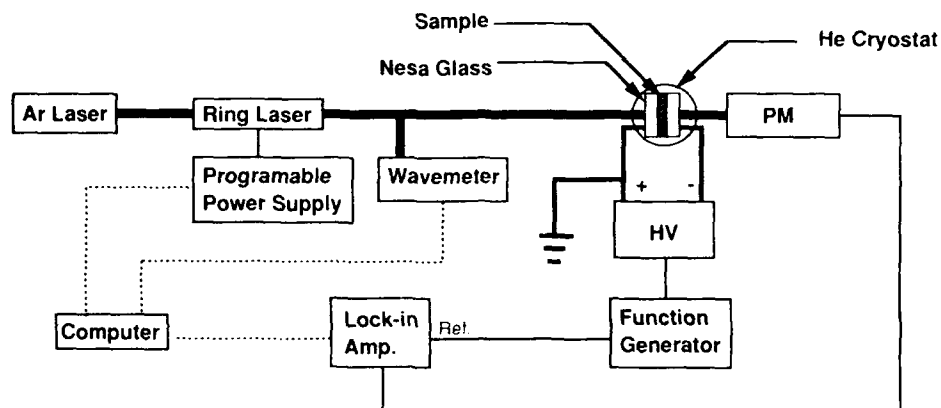


Fig.2. Set up for the electric field modulation technique.

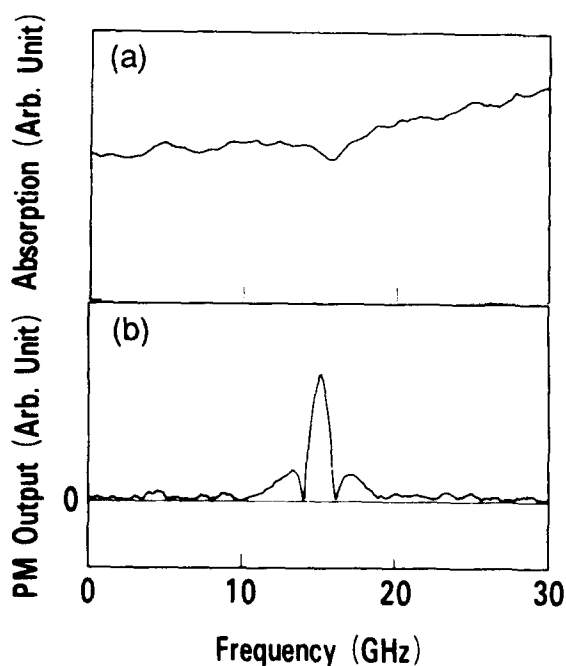


Fig.3. A spectral hole burnt in TPP/PVB ( $5 \times 10^{-3}$  M, thickness  $178 \mu\text{m}$ ), measured with (a) the laser double beam technique and (b) the electric modulation technique. The hole was burnt by tuning the dye laser to  $660 \text{ nm}$  and irradiating the sample at  $20 \mu\text{W}/\text{cm}^2$  for 30 sec at  $5.2 \text{ K}$ .

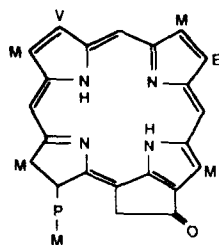


Fig.5. The structure of *pyropheophorbide a methyl ester*. M:  $-\text{CH}_3$ , E:  $-\text{CH}_2-\text{CH}_3$ , V:  $-\text{CH}=\text{CH}_2$ , P:  $-\text{CH}_2-\text{CH}_2-\text{COOH}$ .

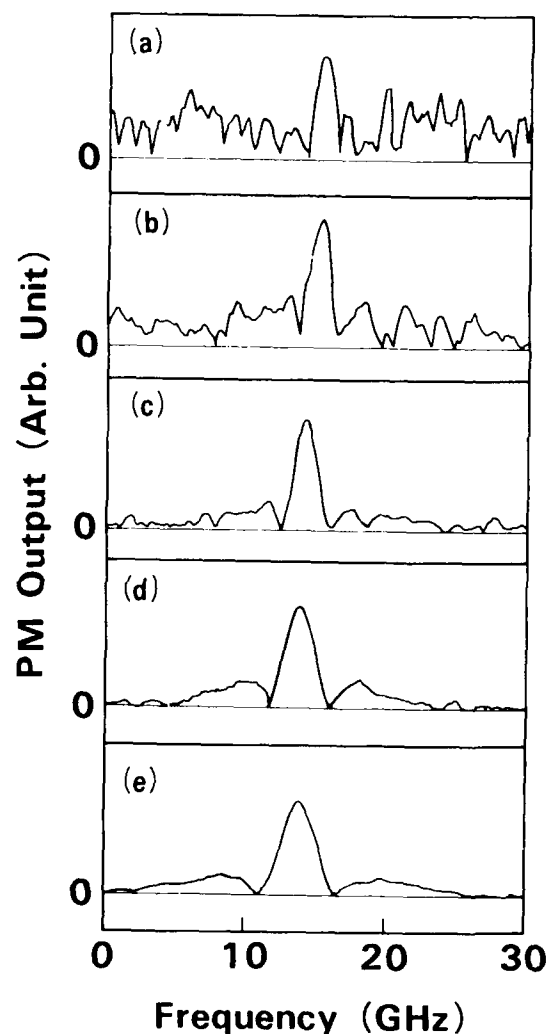


Fig.4. The dependence of the modulated signal on the amplitude of the external electric field in PPME/PVB. The amplitudes of the electric field are: (a)  $2.5 \text{ kV}/\text{cm}$ , (b)  $5 \text{ kV}/\text{cm}$ , (c)  $7.5 \text{ kV}/\text{cm}$ , (d)  $15 \text{ kV}/\text{cm}$ , and (e)  $20 \text{ kV}/\text{cm}$ , respectively.

## The New Systems of Organic Photon-gated Photochemical Hole Burning

Wang Duoyuan, Hu Lingzhi, He Huizhu  
Institute of Photographic Chemistry, Academia Sinica  
P.O. Box 772, Beijing 100101, China. Tel. 2017061-512

Zhao Lizeng, Mi Xin, Ni Yuxin  
Institute of Physics, Academia Sinica  
P.O. Box 603, Beijing 100080, China. Tel. 288390

Recent material research has been devoted to search for two-color or photon-gated photochemical hole burning mechanisms in inorganic as well as organic materials. A mechanism for photon-gated spectral hole burning by donor-acceptor electron transfer in a material composed of meso-tetra-p-tolyl-tetrabenzoporphyrinato)zinc (TZT) (Donor) with halomethanes(acceptor) in poly(methylmethacrylate) (PMMA) thin film at 1.4K was reported by Carter et al.<sup>[1]</sup>

In this paper, we report a new series of organic systems, RZT/AC/PMMA, for photon-gated photochemical hole burning(PGPHB) by donor-acceptor electron transfer at 4.2K. The donor molecules(RZT) are meso-tetraaryl derivatives of zinc-tetrabenzoporphyrin, aryl=phenyl(PZT), p-tolyl(TZT) and a-naphthayl(NZT) respectively. The acceptor can be one of several aromatic cyanides(AC) instead of halomethane, for example, cyanobenzene, cyanonaphthalene, or cyanoanthracene. Optical samples are prepared by mixing the chloroform solution of donor, acceptor and PMMA in a appropriate ratio and then evaporating of the solvent on a optical glass at room temperature. The concentration of samples were adjusted to give thin film between 50-100um with an OD value at intended  $\lambda_1$  in the range of 0.5-0.7 at room temperature. Acceptable samples were then placed in an optical immerion crystate containing liquid helium. All PGPHB experiments were performed at 4.2K.

An Ar<sup>+</sup> ion laser pumped ring RhB dye laser with a 3GHz linewidth was used to provide  $\lambda_1$  for exciting the 0-0 component of the S<sub>1</sub> - S<sub>0</sub> transition of RZT molecules in PMMA. This laser beam was not focused and beam diameter at sample was about 4mm. The gating irradiation  $\lambda_2$  was provided by 2-21 mW beam from the Ar<sup>+</sup> ion laser. The intensities of both beam at the sample were adjusted by a combinations of neutral density filter. The  $\lambda_1$  power P<sub>1</sub> was between 1-21 uW for burning and reading. The detection of holes burnt was performed by scanning  $\lambda_1$  and detecting the sample transmission with a photomultiplier(EMI 9635QA) and lock-in amplifier(EG&G PARC 5209) and the results were recorded by an X-Y recorder(YEW3036). Hole depth was determined from the required spectra as  $\Delta T/T_i$  values, where  $\Delta T$  is the difference between final and initial transmittance T<sub>i</sub> at the laser frequency.

Three characteristics were observed in these new systems for PGPHB as following:

1. The new systems of RZT/AC/PMMA have a broadened inhomogeneous absorption band variations from 330 to 390  $\text{cm}^{-1}$  centered at 627 nm dependence on the concentration of donor and acceptor in PMMA. The full width at half maximum (fwhm) for 0-0 component of the  $S_1 - S_0$  transition of RZT is larger 10-30% than that of TZT/ $\text{CHCl}_3$  /PMMA system and a saturated phenomenon of inhomogeneous linewidth variation was observed, while both concentration of donor and acceptor increasing simultaneously in a constant ratio of donor/acceptor. The latter is useful for selecting proper composition of acceptable thin film sample for high performance PGPHB.

2. The new systems appear a typical photon-gating characteristics. The representative photon-gated characteristics for the various systems are listed in table 1.

Table 1 The characteristics of PGPHB in RZT/AC/PMMA systems

RZT	$\lambda$ (Å)	$P_1$ ( $\mu\text{W}$ )	$P_2$ (mW)	$\Delta T/T_i$ (%)	fwhm (Å)	t (min.)	G
	6231.0	4.0	21	22	1.07	1	
	6278.0	4.0	21	27	0.45	1	
HZT	6282.0	4.0	21	54	0.64	2	
	6300.0	4.0	21	29	0.40	2	
	6353.5	4.0	21	8	0.50	2	
-----							
	6232.5	4.0	21	62	0.56	2	
	6278.5	4.0	21	228	0.57	2	
	6300.5	4.0	21	124	0.35	2	
PZT	6353.5	4.0	21	19	0.38	2	
	6301.5	21	0	11	----	2	
	6304.5	21	16	103	0.79	2	9.4
-----							
	6238.0	4.0	21	23	0.30	2	
	6278.0	4.0	21	121	0.35	2	
	6350.0	4.0	21	24	0.30	2	
TZT	6300.5	4.0	0	0	0	2	
	6300.0	7.6	0	0	0	2	
	6302.0	19	0	10	----	2	
	6298.0	19	16	118	0.77	2	11.8
-----							
	6231.0	4.0	21	74	0.64	2	
	6278.0	4.0	21	100	0.45	2	
	6300.0	4.0	21	71	0.41	2	
NZT	6352.0	4.0	21	46	0.56	2	
	6302.5	21	0	17	----	2	
	6306.0	21	16	77	0.72	2	11.0

Each value was obtained by a sample with a certain ratio for RZT/AC in PMMA, using 2 min. irradiation for both  $\lambda_1$  and  $\lambda_2$ . The gating ratio,  $G$ , as the ratio of depth of a two-color hole to the depth of a one-color hole, for equal  $\lambda_1$  irradiation times and burnt intensities. As showing in table 1, one-color hole burnt can only observed in the condition of higher selecting frequency powers ( $P_1$ ), no observable hole is formed in the case of lower  $P_1$  values. It shows that these system exhibit very low efficiency for single-photon reaction either in excited singlet states or in the lowest excited triplet states of donor molecules. However, two-photon photochemical reaction by donor-acceptor electron transfer in upper excited triplet states could be easily occurred to produce persistent spectral hole burning in the presence of gating beam.

It is just required to add proper threshold for photon-gated hole burning to overcome the destructive readout with the reading irradiation in the single photon mechanism [2].

3. The new systems can be easily burnt for multiple photon-gated hole burning. A typical multiple PGPHB is observed in the lower hole burning powers ( $P_1 = 1.1 \mu\text{W}$ ,  $P_2 = 2.3 \text{mW}$ ) and shorter burnt time ( $t=1 \text{min.}$ ) for PZT/AC/PMMA system which exhibits a higher sensibility and a less effect on the depth of the previous burnt holes in multiple hole burning as showing in Fig.1.

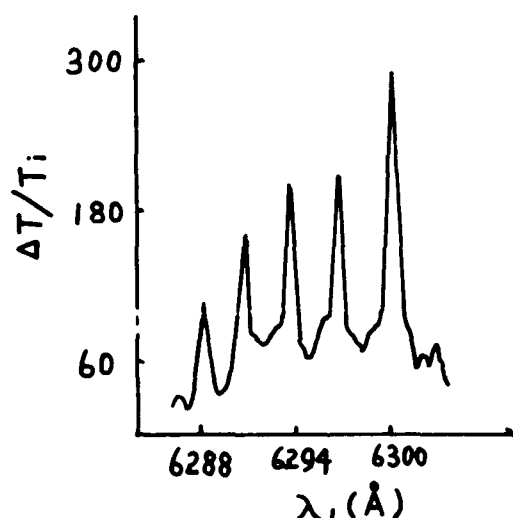


Fig.1 The multiple PGPHB for PZT/AC/PMMA at 4.2 K.  
 $P_1 = 1.1 \mu\text{W}$ ,  $P_2 = 2.3 \text{mW}$ ,  $t=1 \text{min.}$

The holes depth are 100-300% with  $0.34-0.50 \text{ \AA}$  (fwhm), especially up to 300% deep hole can be burnt to appear the

overall efficiency of gated hole formation which is proportional to the hole depth is very high. It implies that the intrinsic probability for electron transfer from the upper triplet levels of donor to the nearby aromatic cyanide acceptors in the system of PZT/AC/PMMA is as well larger than that for TZT/CHCl<sub>3</sub> /PMMA system.

#### References

- [1]. T.P.Carter ,C.Bräuchle,V.Y.Lee,M.Manavi and W.E.Moerner, J. Phys.Chem. 91 (1987) 3998.
- [2]. W.E.Moerner and M.D.Levenson, J. Opt. Soc. Am. B: Opt. Phys. 2 (1985) 915.

Effect of intersystem crossing enhancement on the hole-burning process of metal-free porphyrin

Youichi Sakakibara, Toshiro Tani

Electrotechnical Laboratory, 1-1-4 Umezono, Tsukuba-shi, Ibaraki 305, Japan, (Phone 0298-58-5456)

Youkoh Kaizu

Department of Chemistry, Tokyo Institute of Technology, O-okayama, Meguro-ku, Tokyo 152, Japan

The photochemical reaction in the hole-burning process of metal-free porphyrins has been ascribed to the photoinduced tautomerism of central two protons through the triplet state<sup>1)</sup>. For further understanding of the reaction mechanism, one of the useful approaches is to modify the lifetimes of the excited states without changing energy levels. The population of electronic states under laser-excitation will be influenced considerably, but the electronic structure itself will not change so much. The quantum yield of the hole-formation will be also influenced if it depends mainly on the population of the state where the reaction starts. In this study, we modified the lifetimes by enhancing the intersystem crossing rates with a paramagnetic effect of copper(II) atom. The starting point of the reaction will be discussed with the quantum yields and the population of the states.

The metal-free porphyrins used were tetra-tolylporphyrin ( $H_2TTP$ ) monomer and its dimer shown in figure 1 which is covalently linked to copper(II) tetra-tolylporphyrin moiety ( $CuTTP$ ) with  $-(CH_2)_3-$  chain. These porphyrins were dispersed in PMMA as cast films with concentrations  $2.2 \times 10^{-3}$  mol/l (monomer) and  $3.1 \times 10^{-3}$  mol/l (dimer), and thickness 0.80 mm (monomer) and 0.75 mm (dimer).

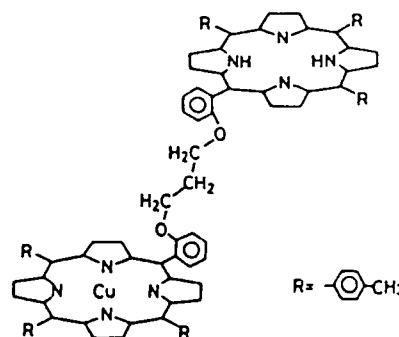


Figure 1. Open conformation

The absorption spectra of Q-band at 4.4 K are shown in figure 2. The spectrum of the dimer may be regarded as the simple 1:1 superposition of  $H_2TTP$  and  $CuTTP$  as in the case of solution<sup>2)</sup>. As  $CuTTP$  has no absorption in the region longer than 625 nm<sup>2)</sup>, the longest wavelength absorption band of the dimer must consist solely of the Qx(0-0) band of the  $H_2TTP$  moiety. Thus, in burning this band, we have only to take account of the excitation of the  $H_2TTP$  moiety. As is shown in table 1, the half width of this band of the dimer is 1.3 times larger than that of the monomer. The conformational variation between the counter-

part CuTTP and the H<sub>2</sub>TTP, in addition to the amorphous polymer matrix, may bring some inhomogeneous broadening due to the fluctuation of dimer coupling.

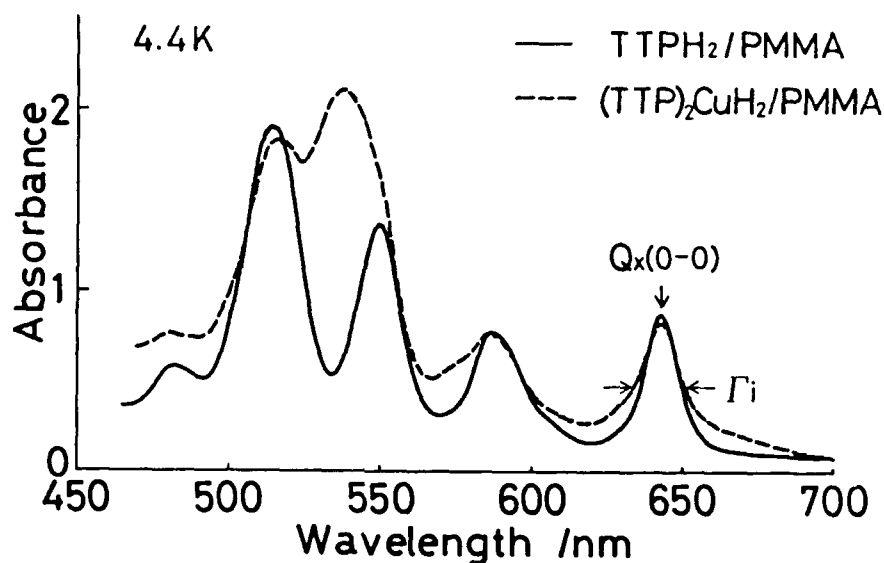


Figure 2. Absorption spectra

The hole-burning was done with both a nano second pulse laser (Quanta-Ray DCR-11, PDL-3; pulsedwidth 6 ns, repetition 10 Hz, linewidth  $0.07 \text{ cm}^{-1}$ ) and a cw laser (COHERENT CR-699-29; linewidth  $< 10^{-4} \text{ cm}^{-1}$ ) on the Qx(0-0) absorption band indicated with the arrow in figure 2. The burning conditions were made as equal as possible in using the same laser. Holes were detected as transmission spectra with a high-resolution monochromator (JOBIN YVON THR1500; resolution  $0.05 \text{ cm}^{-1}$ ). Figure 3 shows the fluence dependence of the holearea with the pulse laser. Several times amount of fluence is necessary for the dimer to grow to the same extent. As the absorbances of both samples are almost the same, this result indicates that the quantum yield of the dimer is smaller than that of the monomer. Quantum yields estimated from the initial stages are summarized in table 1. The yield of the dimer decreased only to 1/5 (pulse) or 1/3 (cw) times compared with that of the monomer. By comparing this fact

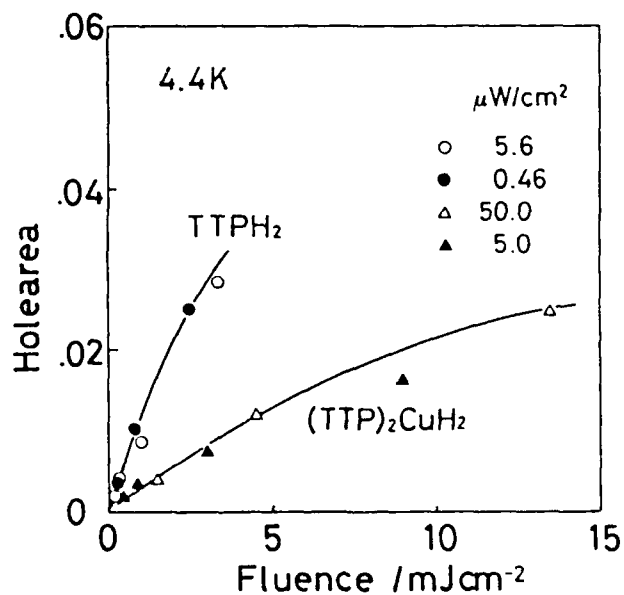


Figure 3. Fluence vs. holearea

Table 1 Holewidth, quantum yield, and inhomogeneous width

	width(cm <sup>-1</sup> )		quantum yield		inhomo.width (cm <sup>-1</sup> )
	pulse	cw	pulse	cw	
monomer	0.25	0.25	2 × 10 <sup>-3</sup>	3 × 10 <sup>-3</sup>	330
dimer	0.36	0.29	4 × 10 <sup>-4</sup>	1 × 10 <sup>-3</sup>	440

with the change of population estimated from a simple rate equation, we suggest that the photochemical reaction may start from the excited singlet state rather than the triplet state. We can easily estimate the population of each level under steady state condition. The rate equations are

$$dN_S(t)/dt = \sigma I N_0(t) - k_N N_S(t) - k_F N_S(t) - k_{ISC} N_S(t), \quad (1)$$

$$dN_T(t)/dt = k_{ISC} N_S(t) - k_T N_T(t), \quad (2)$$

where  $N_0(t)$ ,  $N_S(t)$ ,  $N_T(t)$  are number of molecules at ground( $S_0$ ), singlet( $S_1$ ), triplet( $T_1$ ) states respectively, and their total number is  $N$ ;  $k_N$ ,  $k_F$ ,  $k_{ISC}$ ,  $k_T$  are rates of the nonradiative transition from  $S_1$  to  $S_0$ , the fluorescence, the intersystem crossing, and the total of the phosphorescence and the nonradiative transition from  $T_1$  to  $S_0$  respectively, as are shown in figure 4;  $\sigma$  is absorption cross section and  $I$  is intensity of laser. As for the product state, a term  $-k_P N_S(t)$ , where  $k_P$  is a rate for the product state, must be added to the right side of (1) if the reaction for hole-formation starts from  $S_1$ ; and  $-k_P N_T(t)$  to (2) if it starts from  $T_1$ . Assuming  $k_P \ll k_N, k_F, k_{ISC}, k_T$ , these terms can be negligible. The steady state approximation gives

$$N_0 = N/a, \quad (3)$$

$$N_S = ((\sigma I / (k_F + k_N + k_{ISC})) (N/a)), \quad (4)$$

$$N_T = (k_{ISC} / k_T) ((\sigma I / (k_F + k_N + k_{ISC})) (N/a)), \quad (5)$$

where

$$a = 1 + \sigma I / (k_F + k_N + k_{ISC}) + (k_{ISC} / k_T) (\sigma I / (k_F + k_N + k_{ISC})). \quad (6)$$

Thus, we can estimate the population of each level if each  $k$  is available. Not available itself, we use the values from the previous reports though our present situation in PMMA at 4.4 K is somewhat different. In toluene at room temperature<sup>2)</sup>, the fluorescence lifetime ( $\tau_F$ ) of the monomer were 11.7 ns, while that of the dimer were shortened to 3.1 ns. The quantum yield ( $\phi_F$ ) of the fluorescence of the monomer was 0.12 and the dimer 0.026. The decay lifetimes ( $\tau_T$ ) of the triplet state of the monomer was 1.1 ms and the dimer 1.1  $\mu$ s. As the intersystem

crossing of the H<sub>2</sub>TTP moiety in the dimer is promoted by the paramagnetic effect from the CuTTP moiety, both the singlet and the triplet lifetimes become shortened. As for the intersystem crossing yield ( $\phi_{ISC}$ ), we adopt 0.70 for both the monomer and the dimer which is from the value of H<sub>2</sub>TPP<sup>3)</sup> because the value of H<sub>2</sub>TTP itself is not known. Using the next relations;

$$\tau_F = 1/(k_F+k_N+k_{ISC}), \quad (7)$$

$$\phi_F = k_F/(k_F+k_N+k_{ISC}), \quad (8)$$

$$\phi_{ISC} = k_{ISC}/(k_F+k_N+k_{ISC}), \quad (9)$$

each  $k$  can be calculated. Under the weak excitation condition, (3),(4),(5) are written as

(monomer)	(dimer)
$N_0 = (1-7.7 \times 10^{-4} \sigma I)N$	$(1-7.7 \times 10^{-7} \sigma I)N$
$N_S = 1.2 \times 10^{-8} \sigma IN$	$3.1 \times 10^{-9} \sigma IN$
$N_T = 7.7 \times 10^{-4} \sigma IN$	$7.7 \times 10^{-7} \sigma IN$

The S<sub>1</sub> population decreases to 1/3.8 and T<sub>1</sub> to 1/1000 at the same laser intensity. Assuming that quantum yield depends mainly on the population of starting state, the decrease of quantum yields to 1/5 - 1/3 suggests that the photochemical reaction may start from the S<sub>1</sub> state. The discussions so far does not deny the protons tautomerism reaction itself. We can consider, at the moment, two possibilities for this reaction from the singlet state; one is the allowed energy transfer between the S<sub>1</sub> states of the two tautomer due to the local inhomogeneity of the matrix, and the other is the tunneling from S<sub>1</sub> to non-adiabatic S<sub>0</sub> potential of the tautomer.

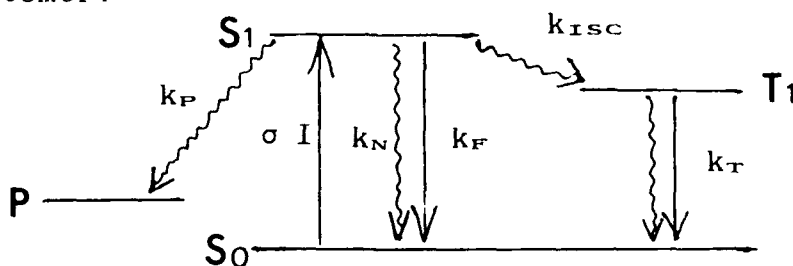


Figure 4.

#### References

- 1) S.Voelker, J.H.van der Waals, Mol.Phys.32,1703(1976)
- 2) O.Ohno, Y.Ogasawara, M.Asano, Y.Kajii, Y.Kaizu, K.Obi, and H.Kobayashi, J.Phys.Chem.91,4269(1987).
- 3) Y.Kajii, K.Obi, I.Tanaka, S.Tobita, Chem.Phys.Lett.111,347(1984)

## PHOTON ECHO DECAY AND OPTICAL STORAGE IN Pr DOPED YAlO<sub>3</sub>

Stefan Kröll\*

Dept. of Atomic Physics, Lund Institute of Technology,  
P. O. Box 118, S-221 00 Lund, Sweden

Ravinder Kachru

Molecular Physics Laboratory, SRI International, Menlo Park, CA 94025

\* This work was performed at Molecular Physics Laboratory, SRI International

Homogeneous dephasing processes and optical storage in Pr doped YAlO<sub>3</sub> crystals have been examined using photon echoes produced by gated continuous wave laser excitation.

The two-pulse photon echo decay time of the <sup>3</sup>H<sub>4</sub> - <sup>1</sup>D<sub>2</sub> transition in 0.1% Pr<sup>3+</sup>:YAlO<sub>3</sub> has been measured as a function of excitation pulse energy. The excitation energy dependence of the decay time is essentially the same for the first and the second pulse in the excitation sequence. This is different from the behaviour recently observed in Eu<sup>3+</sup>:Y<sub>2</sub>O<sub>3</sub> and Tb<sup>3+</sup>:LiYF<sub>4</sub> [1-3], where mainly the second pulse intensity affected the two-pulse photon echo decay time.

By frequency chirping write and read pulses, photon echo data storage and recall of about 50 bits at a single location have been performed using a continuous wave dye laser and a copropagating geometry for the excitation beams [4]. Single-shot storage and recall was performed with very good signal-to-noise ratio. The bit rate in the data sequence was ≈20 MHz. The decay rate and storage experiments are separately described below.

### Photon echo decay in the <sup>3</sup>H<sub>4</sub> - <sup>1</sup>D<sub>2</sub> transition in 0.1% Pr<sup>3+</sup>:YAlO<sub>3</sub>

The excitation sequence for the two-pulse photon echoes was generated by acousto-optically gating a CR699-21 ring dye laser. The excitation pulse duration was, for most cases, 900 ns and the pulse energy was varied between 2 and 40 nJ yielding photon-echo decay times ranging approximately from 70 to 20 μs (photon-echo decay time here stands for 4 times the 1/e decay time). Different excitation energies were produced by attenuating the excitation pulses by neutral density filters or by changing the acousto-optic modulator voltage. The two approaches produced the same decay time within 10%. Strong first and weak second pulse or weak first and strong second pulse also gave the same decay time within 10%. To obtain long decay times both excitation pulses had to be weak. At low excitation energies the observed decay time significantly exceeded the literature value for the homogeneous dephasing time (35 μs). Since the first and second pulse energy affect the decay time in the same way the energy dependence can, to our understanding, not, as recent excitation energy dependent photon-echo decay time measurements in Eu<sup>3+</sup>:Y<sub>2</sub>O<sub>3</sub> and Tb<sup>3+</sup>:LiYF<sub>4</sub>, be attributed to instantaneous spectral diffusion. In those measurements mainly the second pulse energy influenced the decay time [1-3]. By examining two crystals of different thickness (0.4 mm and 1.0 mm) we have

concluded that optical density effects [5] are not the main reason for the observed energy dependence in Pr:YAlO<sub>3</sub>. The measured photon-echo decay times can be parametrized as a function of the sum of the excitation energy in the two pulses but not as a function of the energy in one of them only. Also we have verified that the decay times cannot be parametrized as a function of echo intensity or as a function of excitation pulse area [6].

We have attempted to separate the decay rate ( $\Gamma$ ) of the photon echo as

$$\Gamma = \gamma(\text{radiative}) + \gamma(\text{magnetic}) + \gamma(\text{excitation})$$

where  $\gamma(\text{radiative})$  is the inverse of two times the 185  $\mu\text{s}$  radiative lifetime of the <sup>1</sup>D<sub>2</sub> state,  $\gamma(\text{magnetic})$  is the decay rate contribution induced by nuclear spin-flips in the Al lattice atoms and  $\gamma(\text{excitation})$  is an excitation energy dependent decay rate.  $\gamma(\text{magnetic})$  can be quenched by the application of a magnetic field.

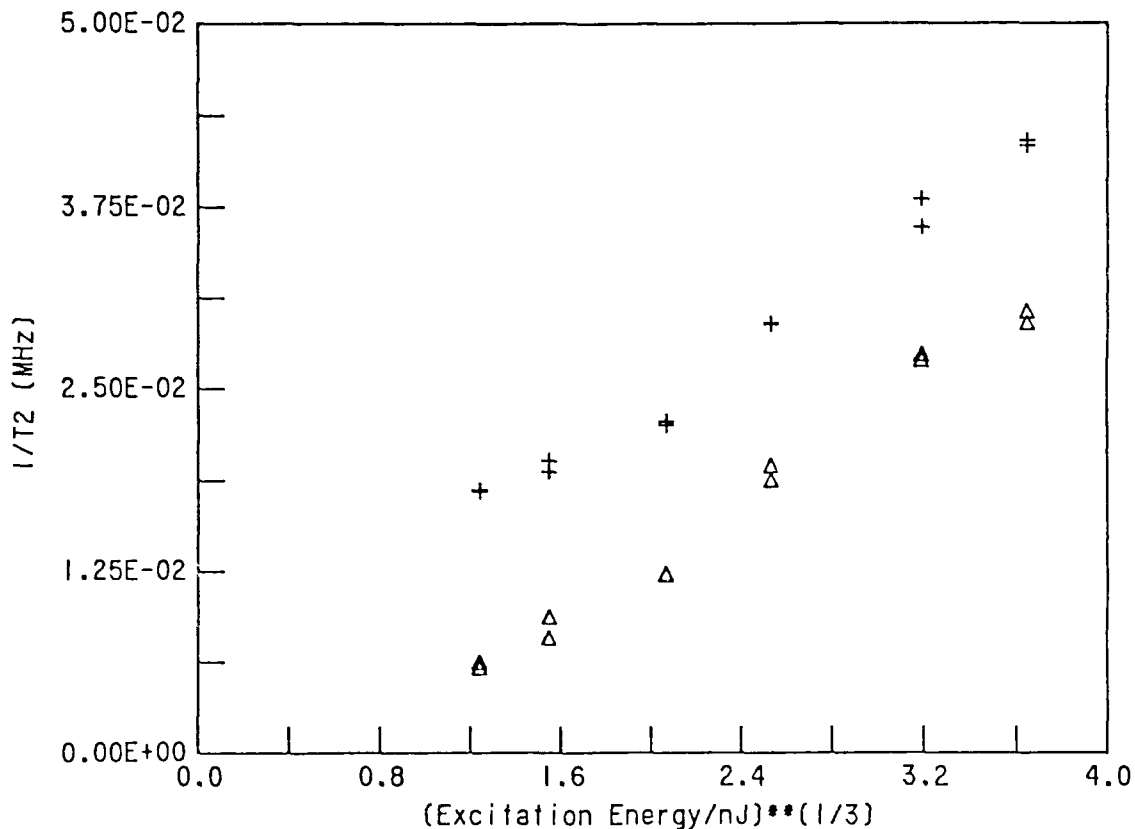


Fig. 1. Photon-echo decay rate versus excitation energy raised to 1/3 with ( $\Delta$ ) and without (+) magnetic field.

Fig. 1 shows the decay rate vs excitation energy raised to 1/3 with ( $\Delta$ ) and without (+) magnetic field [7]. The decay contribution removed by the magnetic field is approximately independent of excitation pulse energy. This may indicate that the mechanism for the excitation energy dependent decay is an

interaction of non-magnetic origin, however, the magnetic fields used here have been rather small (<150 Gauss). Surprisingly a resonance could be observed for the photon echo decay time versus magnetic field. A few years ago Wokaun and coworkers [8] looked for resonances in photon echo decay as a function of magnetic field for the  $^3H_4 - ^1D_2$  transition at magnetic fields which produced magnetic field induced level crossings. No resonances were, however, observed. The resonance observed in this work does not appear to be connected to magnetic field induced level crossings though. Further investigations of the observed resonance are in progress.

### Photon-echo data storage using a frequency chirped continuous wave laser

In comparison with persistent spectral hole-burning (PSHB), photon echo storage has the advantage that, for a given transition, the bitrate is limited by the inhomogeneous transition line-width instead of, as in PSHB, by the homogeneous line-width. If the data input sequence in photon-echo storage is modulated at a high rate, write and read pulses must have large Fourier widths in order to recall the Fourier components of the stored data sequence. Pulsed lasers have commonly been used to produce short Fourier broadened pulses with an energy sufficient for storing and recalling the data sequences. To decrease the energy needed in the write and read pulses frequency chirping of these pulses can be used [9]. We have recently used this approach on the  $^3H_4 - ^1D_2$  transition in  $Pr^{3+}:YAlO_3$ . By changing the voltage across an intra-cavity mounted ADP crystal the dye laser output frequency could be changed by approximately 75 MHz. All pulses were copropagating thus eliminating all beam overlap problems. A gated Pockels' cell at the detection side protected the photomultiplier tube against the excitation pulses. With a data-rate of 20 MHz and single data-bit energies of 200 pJ single-shot storage and recall of data sequences of about a microsecond duration was performed. Read and write pulse energies then were around 25 nJ.

### References

1. Jin Huang, J. M. Zhang, A. Lezama and T. W. Mossberg, "Excess dephasing in photon-echo experiments arising from excitation-induced electronic level shifts", *Phys. Rev. Lett.* **63**, 78 (1989).
2. Jin Huang, J. M. Zhang and T. W. Mossberg, "Excitation-induced frequency shifts and frequency-dependent dephasing in  $Eu^{3+}:Y_2O_3$ ", *Opt. Commun.* **75**, 29 (1990).
3. G.K. Liu and R.L. Cone, "Laser-induced instantaneous spectral diffusion in  $Tb^{3+}$  compounds as observed in photon echo experiments", *Phys. Rev.* **B41**, 6193 (1990).
4. S. Kröll, L.E. Jusinski and R. Kachru, "Frequency chirped copropagating multiple bit stimulated echo storage and retrieval in  $Pr^{3+}:YAlO_3$ ", *Opt. Lett.*, **16**, 517 (1991).
5. R.W. Olson, H.W.H. Lee, F.G. Patterson and M.D. Fayer, "Optical density effects in photon echo experiments", *J. Chem. Phys.* **76**, 31 (1982).

6. S. Kröll, E. Y. Xu and R. Kachru, "Influence of excited state  $\text{Pr}^{3+}$  of the  $\text{Pr}^{3+}:\text{YAlO}_3$   $^1\text{D}_2$ - $^3\text{H}_4$  transition", Phys. Rev. B, accepted for publication.
7. S. Kröll, E. Y. Xu and R. Kachru, in progress.
8. A. Wokaun, S.C. Rand, R.G. DeVoe and R.G. Brewer, "Anti-crossings in solid-state laser spectroscopy", Phys. Rev. B23, 5733 (1981).
9. Y.S. Bai, W.R. Babitt and T.W. Mossberg, "Coherent transient pulse-shape storage/recall using frequency-swept excitation pulses", Opt. Lett. 11, 724 (1986).

## HOLE BURNING IN LONG CHAIN MOLECULAR AGGREGATES

**R. Hirschmann, J. Friedrich**

Institut für Physikalische Chemie, Johannes Gutenberg-Universität,

D-6500 Mainz, Germany

Phone: (06131)-39-4212

The salts of pseudoisocyanine (PIC) have very specific optical properties. Under certain conditions (concentration, temperature) the PIC-molecules form linear aggregates in solution. Since the coupling between the molecules comprising the aggregate is very strong, the excited states are delocalized over a large range. A coherence length on the order of 1000 Å is not uncommon. These excitonic states carry momentum and, hence, the physics of these systems shows novel phenomena as compared to small probe systems. Such phenomena are, for instance, extreme motional narrowing of inhomogeneous line broadening and a very specific temperature dependence of the homogeneous width due to exciton-phonon-scattering processes in which both, energy as well as momentum, have to be conserved.

We first focus on the line narrowing phenomena. Line narrowing in PIC-aggregates can be observed at various levels of resolution. Most obvious is the narrowing of the inhomogeneous absorption band of the monomer: As the monomers aggregate, a sharp band (or several sharp bands) appears at the red edge of their absorption band (J-band). Its width is narrowed by a factor on the order of ten as compared to the monomer. This phenomenon has already been discovered by Scheibe and Jelly in 1936 /1,2/. The narrowing factor is roughly given by  $N^{1/2}$ , where  $N$  is the number of PIC-molecules within the coherence length /3/. From the measured width, one determines  $N$  to be on the order of 100. Two of these narrowed absorption lines are shown in Fig.1. The sample is PIC-iodide in ethyleneglycol-water glass.

Recently it has been discovered that spectral holes could be burnt into the J-bands /4/. This offered the opportunity to measure the homogeneous linewidth of the exciton band. In determining the homogeneous width from a hole burning experiment, spectral diffusion broadening is usually a problem /5,6/. Spectral diffusion occurs because the glass matrix is a non ergodic system and may change its configuration during the burning and detection period. This is a severe problem for small probe systems. However, for extended states, as in the PIC-aggregates, it plays no significant role. Since spectral diffusion is an inhomogeneous line broadening contribution it is averaged out to a large degree by a fast

As to the exciton-phonon-scattering it is obvious from Fig.2 that such processes cannot take place between 300 mK and 10 K. It seems that in this temperature range there are no phonons which satisfy the required energy and momentum conditions. The rather large residual width in this temperature range of  $0.36 \text{ cm}^{-1}$  is attributed to the fluorescence decay. Due to the superradiant behaviour of the coherently coupled molecules in the chain [7], this decay is very fast and accounts for the 29 ps as deduced from the observed linewidth. Around 15 K the hole starts to broaden. Obviously, a phonon gets populated which satisfies the required conditions. This phonon has an energy of  $27 \text{ cm}^{-1}$ . We attribute it to an acoustic phonon of the chain. Above 55 K, the first optical phonon which is able to scatter comes in and leads to a steep increase of the width with increasing temperature. Along these lines of reasoning the fit curve is a superposition of the thermal population factors of the two phonons and a constant, which accounts for the low temperature width. This contrasts with glasses doped with small probe molecules, where the homogeneous width increases according to a power law with exponents between 1 and 2.

In summary, PIC-salts show very specific optical properties, which originate from a large coherence length of the excited states. As the cations of the PIC-salts are varied, the coherence length changes and hence these properties can be experimentally controlled to some extent.

## References

- /1/ G. Scheibe, *Ang. Chemie* **49** (1936) 563
- /2/ E. E. Jelley, *Nature* **138** (1936) 1009
- /3/ E. W. Knapp, *Chem. Phys.* **85** (1984) 73
- /4/ S. de Boer, K. J. Vink, D. A. Wiersma, *Chem. Phys. Lett.* **137** (1987) 91
- /5/ W. Breinl, J. Friedrich, D. Haarer, *J. Chem. Phys.* **81** (1984) 3916
- /6/ M. Berg, C. A. Walsh, L. R. Narasimham, K. A. Littau, M. D. Fayer, *J. Chem. Phys.* **88** (1988) 1564
- /7/ F. Spano, S. Mukamel, *J. Chem. Phys.* **91** (1989) 683

AD-A260 224

ORGANIZATION OF THE 1991 SOCIETY OF AMERICA PHOTONIC  
SCIENCE TOPICAL MEET... (U) OPTICAL SOCIETY OF AMERICA  
WASHINGTON DC J W QUINN 22 MAY 92 AFOSR-TR-92-0514

4/4

UNCLASSIFIED

AFOSR-91-0176

NL

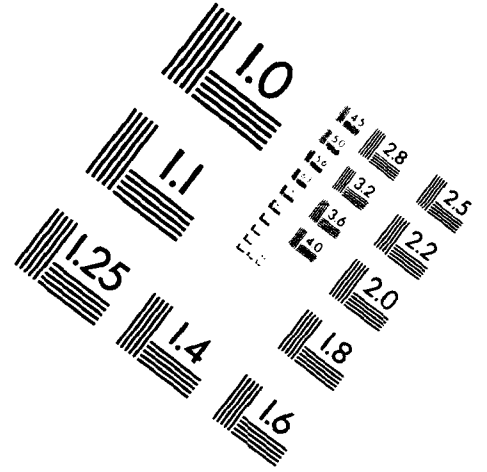
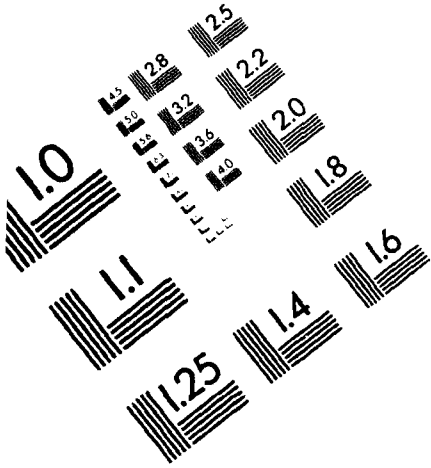
END  
FILMED  
DTIC



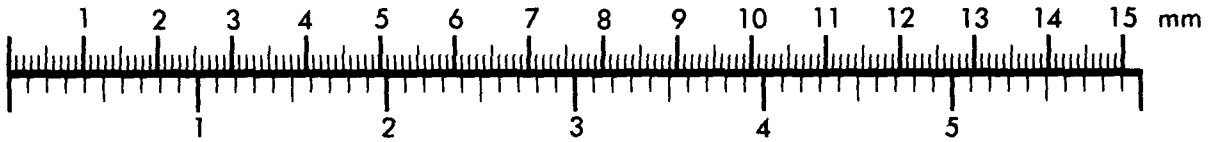
**AIM**

**Association for Information and Image Management**

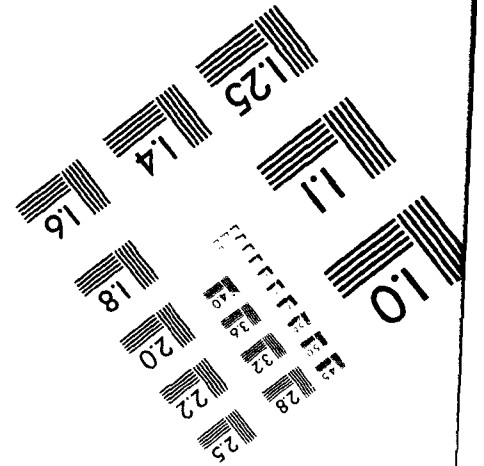
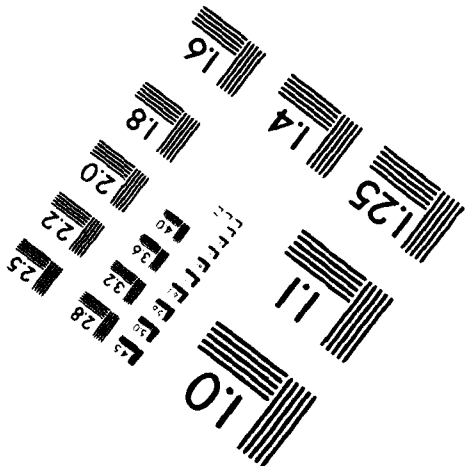
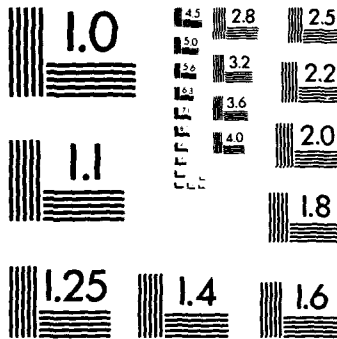
1100 Wayne Avenue, Suite 1100  
Silver Spring, Maryland 20910  
301/587-8202



Centimeter



Inches



MANUFACTURED TO AIM STANDARDS  
BY APPLIED IMAGE, INC.

moving exciton. This is directly seen in the lower part of Fig.1: The evolution of a hole was measured over five orders of magnitude in time. Its shape is shown at the beginning of the observation period and at the end. Though the hole experiences a significant change, its width remains constant. For small probe systems, the situation is quite different: There, the width may increase in such a time span by more than a factor of two.

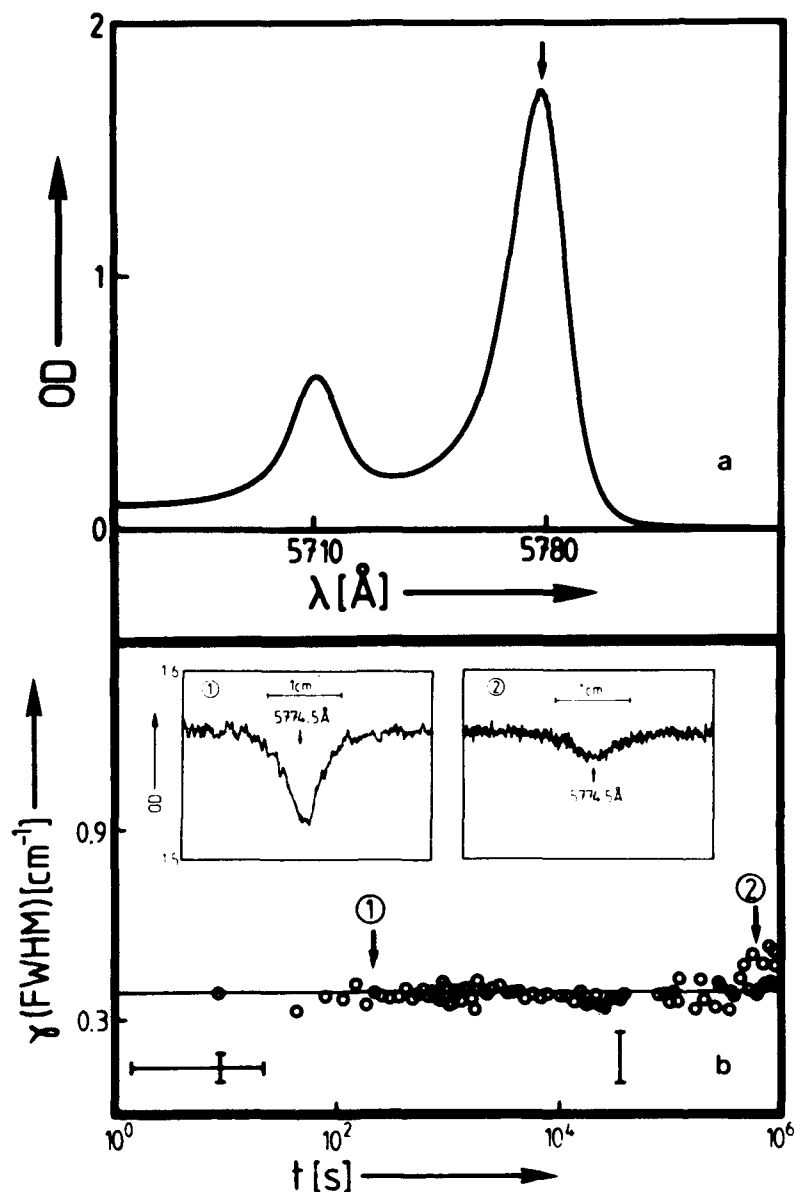


Fig. 1

- a) Exciton peaks in pseudoisocyanine
- b) Spectral diffusion behavior of a hole burnt into the longwavelength exciton band (arrow).

A similar narrowing phenomenon occurs for holes which broaden when external pressure is applied. The broadening under pressure is inhomogeneous, too, and, hence, is narrowed by the moving exciton. This is exactly what is observed in PIC-aggregates.

All these experiment demonstrate that inhomogeneous contributions to the hole width are of no importance. Then, it is straight forward to measure the homogeneous width with the hole burning technique. The result is shown in Fig.2

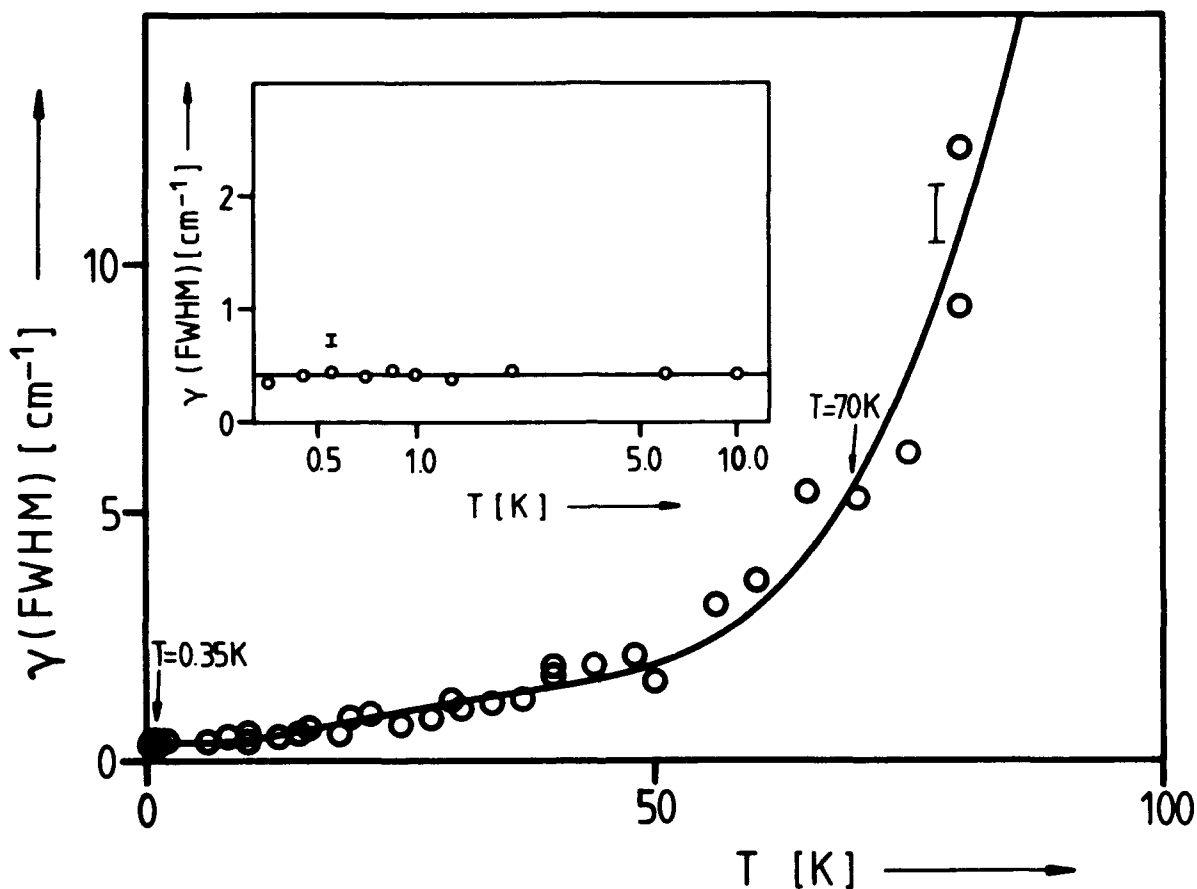


Fig. 2: Hole width, extrapolated to zero energy absorption, as a function of temperature.

The thermal behaviour of the homogeneous width of extended states in glasses is also very different from small probe systems. There are two reasons for this: First, the TLS-interaction with the exciton seems to be small, hence, the dephasing is caused by phonon-scattering-processes. Second, in these processes, not only the energy but also the momentum has to be conserved.

That the TLS-exciton interaction does not play an important role, is obvious: A TLS-relaxation is a rather local event, and, hence, does not have a large influence on an extended state with a coherence length of 1000 Å or so.



Saturday, September 28, 1991

# Linewidth and Relaxation

**SA** 8:30am–10:30am  
DeAnza Room

Michael Fayer, *Presider*  
*Stanford University*

## Molecular Theory of Inhomogeneous Broadening in Glasses

J. L. Skinner

Department of Chemistry

University of Wisconsin

Madison, WI 53706

The absorption spectra of impurities in liquids, glasses, and crystals are often inhomogeneously broadened. This means that different impurities reside in different environments, which are static on the relevant time scale, and which perturb the energy levels of the impurities to produce a distribution of transition energies. This inhomogeneous broadening overwhelms the intrinsic linewidth of an individual impurity (the homogeneous linewidth), and is therefore a complicating feature of high-resolution spectroscopy. On the other hand, from a technological perspective inhomogeneous broadening is interesting because it is necessary for hole-burning, and hence for optical storage. And from a scientific perspective it is also interesting since it provides a probe of the local disorder in complicated condensed phase systems. In this talk I will discuss a molecular theory of inhomogeneous broadening in an attempt to understand this effect within a microscopic statistical mechanics framework.

The theory begins by considering an impurity (solute), which in each of its vibronic states interacts in a pairwise manner with surrounding solvent molecules. Specifying the pair interaction potential energy for each solute state, the solvent density, the solute-solvent radial distribution function (which is proportional to the probability of finding a solvent molecule a given distance away from the solute), and the solvent-solvent radial distribution

function, is sufficient to describe with reasonable accuracy the distribution of energy levels for each solute state. In addition, for a pair of states one can determine the conditional probability that if a solute has energy  $E$  in one state it has energy  $E'$  in another. Depending on the correlation between these two energy distributions this conditional probability will be narrow or broad, and one can understand its behavior from a knowledge of the molecular interactions and solvent structure.

A simple absorption experiment measures only the difference between two energy levels, and hence cannot provide direct information about the energy distributions or conditional probabilities described above. However, within the molecular theory one can instead consider the *transition* energy distributions between different pairs of levels, and the conditional probabilities that if a solute has a transition energy  $\Delta E$  for one transition it has transition energy  $\Delta E'$  for another transition. This latter conditional probability is precisely what is measured in a variety of nonlinear experiments. For example, in nonresonant fluorescence line narrowing one selects the energy of the  $S_0$ - $S_1$  transition with narrow-band excitation, and then frequency resolves the fluorescence to a vibronic level in  $S_0$ . In phosphorescence line narrowing one again selects the energy of the  $S_0$ - $S_1$  transition with narrow-band excitation, and then (after intersystem crossing) frequency resolves the resulting phosphorescence from  $T_1$  to  $S_0$ . In a photochemical holeburning experiment one can burn a narrow hole in  $S_0$ - $S_1$  and then measure the absorption spectrum of the photoproduct, or antihole. In photochemical or photophysical holeburning one can burn a narrow hole in a vibronic transition and then probe the hole width of a different vibronic transition. Finally, in a closely related type of experiment, one can burn a narrow hole in  $S_0$ - $S_1$ , perturb the solute environment by changing the pressure or electric field, and then monitor the resulting hole width change. Each of these experiments can in principle be described by our molecular theory, and I will discuss several examples in some detail. The analysis of these experiments with this molecular theory provides information about the local structure of glasses, and about solute-solvent interactions.

Inhomogeneous broadening also plays a role in energy transfer experiments in disordered systems. If one considers energy transfer between two like chromophores, the efficiency of transfer depends on both the distance between the pair and the transition energy difference of the pair. For example, for incoherent phonon-assisted energy transfer the rate is proportional to the phonon weighted density of states, which increases with increasing energy gap. On the other hand, for coherent or resonant energy transfer and Anderson localization problems, the process is most efficient with zero energy gap. In either case the transfer efficiency will depend strongly on whether or not the transition energy distributions for the two chromophores are correlated, which in general will be the case, since two nearby chromophores are interacting with the same solvent molecules. We have extended our molecular theory to describe this situation, and several examples will be discussed.

### References

1. Microscopic theory of reversible pressure broadening in hole-burning spectra of impurities in glasses, B. B. Laird and J. L. Skinner, *J. Chem. Phys.* **90**, 3274 (1989).
2. On the microscopic nature of inhomogeneously broadened spectra of chromophores in glasses and crystals, B. B. Laird and J. L. Skinner, *J. Chem. Phys.* **90**, 3880 (1989).
3. A molecular theory of inhomogeneous broadening, including the correlation between different transitions, in liquids and glasses, H. M. Sevian and J. L. Skinner, *Theoretica Chimica Acta* (in press).

Time-resolved transient hole-burning in disordered systems

Silvia Volker  
University of Leiden  
The Netherlands

Microsecond-living transient holes have been burned and probed, as a function of time and temperature, with a diode laser. Results are discussed in terms of spectral diffusion and compared with experiments on longer time scales in glassy and crystalline systems.

Accumulated photon echoes as a probe of radiationless  
relaxation processes in Nd-doped glasses

Keith W. Ver Steeg, Roger J. Reeves, Richard C. Powell

University Center for Laser Research  
413 Noble Research Center  
Oklahoma State University  
Stillwater, OK 74078  
(405) 744-6575

Accumulated photon echoes (APE) were used to measure the dephasing rates of  $\text{Nd}^{3+}$  in various inorganic glasses as a function of excitation wavelength, sample temperature, and laser power. Although dephasing processes of optical transitions in solids are of considerable interest, they are poorly understood, largely due to the lack of experimental data on femtosecond and picosecond time scales. The APE technique using sub-picosecond laser sources has made it possible to measure in the time domain dephasing rates of inhomogeneously broadened transitions in amorphous systems.<sup>1,2</sup> This technique therefore acts as a complement to dephasing experiments done in the frequency domain, such as spectral holeburning. Other researchers have used similar stimulated echo techniques to optically store binary information in solid state materials.<sup>3,4</sup> Thus the results of this work provide information useful to the understanding of fundamental physical processes affecting the characteristics of spectral holeburning and in addition they may have direct application to optical storage techniques based on photon echoes.

In this experiment, a Nd-YAG laser was mode locked, pulse compressed, and frequency doubled, to provide a 82 MHz pulse train that synchronously pumped a tunable dye laser. This system produced nearly transform lim-

ited 350-400 femtosecond pulses tunable from 570 to 610 nm. The dye laser wavelength was tuned across the inhomogeneously broadened  $^4I_{9/2} \rightarrow ^4G_{5/2}$  transition of neodymium, and the accumulated photon echoes colinear with the probe beam were detected with a silicon photodiode and phase sensitive amplifier. The measured APE signal, which has a characteristic decay rate of  $2/T_2$ , was stored in a computer and fitted to a single or double exponential function. APEs from  $Nd^{3+}$  ions in silicate, fluoride, and germanate glasses (with  $Nd^{3+}$  molar% concentrations of 3, 5, and 4, respectively) were measured at temperatures between 10K and 100K. The results provided information about how the APE decay rate varies as a function of wavelength and temperature depending on the glass structure.

A typical result is shown in Figure 1 for lithium germanate glass. The dephasing rate increases as the laser source is tuned to shorter wavelengths. Assuming that the dominant dephasing process involves radiationless relaxation to lower Stark components within the  $^4G_{5/2}$  manifold, the results show that these processes are more probable for larger energy gaps. The trends are similar for the silicate and fluoride glasses. The optical dephasing rate for a given excitation frequency and temperature increases from germanate to silicate to fluoride glasses.

The data are interpreted in terms of single phonon radiationless relaxation processes. The variations from host to host are associated with the differing phonon density of states and electron-phonon coupling in each material. The echo decays for all three glasses were found to be single exponential (Figure 2). Oscillations of the APE signal intensity were observed near zero time pulse-probe delay for the fluoride glass (Figure 3) and are attributed to optical density effects.<sup>5</sup>

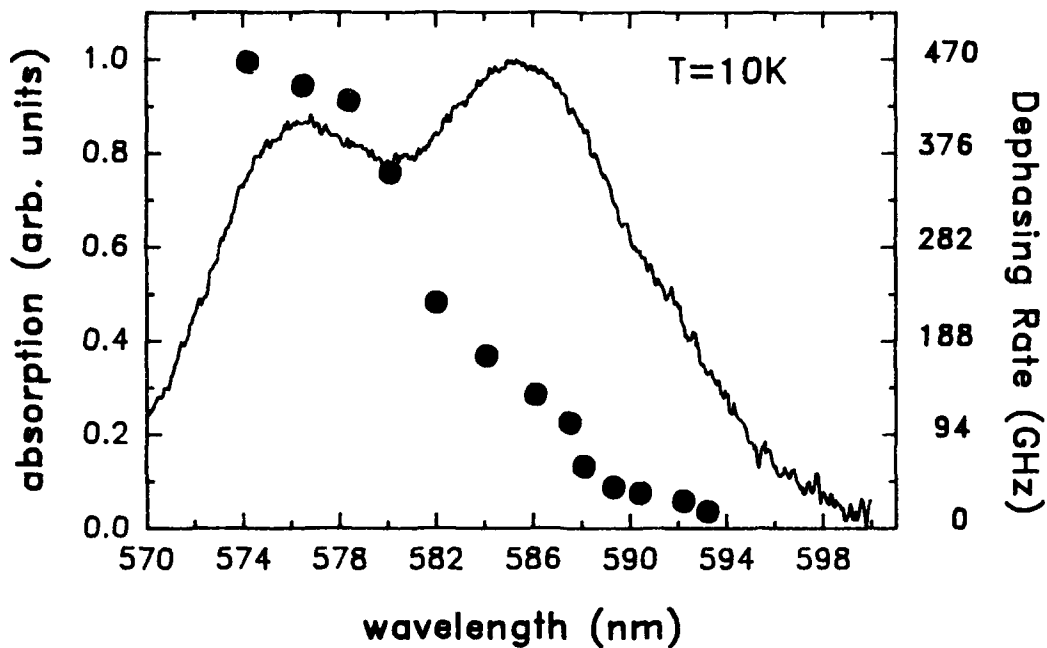


Figure 1 APE dephasing rate versus excitation wavelength for  $\text{Nd}^{3+}$  doped lithium germanate glass at 10K. The solid line is the low temperature absorption spectrum of the sample.

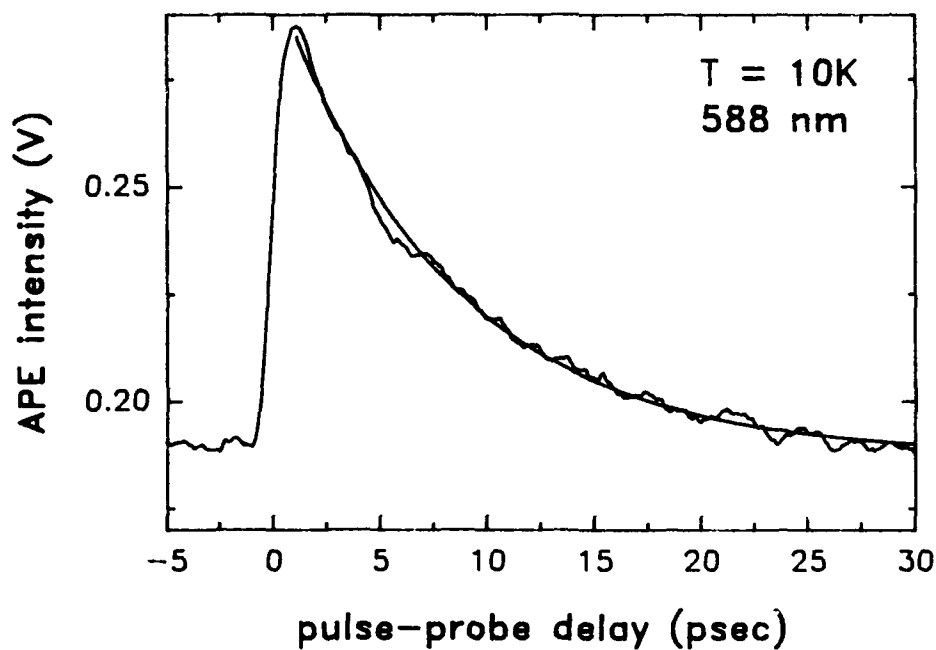


Figure 2 APE decay curve for  $\text{Nd}^{3+}$  doped lithium germanate glass at 10K. The fitted line is single exponential.  $T_2 = 16.1$  ps.

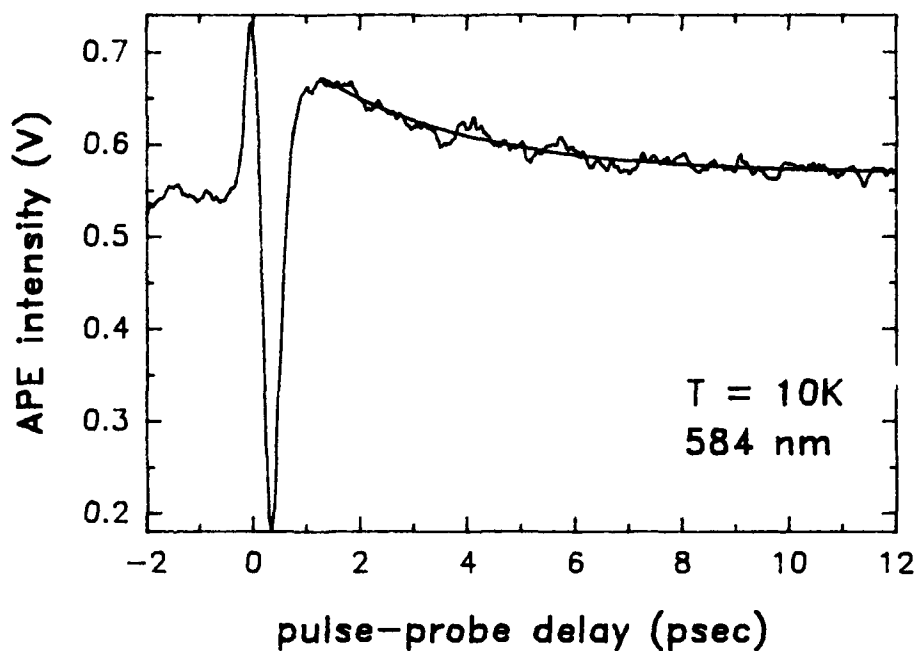


Figure 3 APE decay curve for  $\text{Nd}^{3+}$  doped fluoride glass at 10K. Fitted line is single exponential.  $T_2 = 5.6$  ps.

#### ►References

- 1 R.M. Shelby, *Opt. Lett.* **8**, 88 (1983).
- 2 H.W.H. Lee, *J. Lumin.* **45**, 99 (1990).
- 3 M. Mitsunaga, N. Uesugi, *Opt. Lett.* **15**, 195 (1990).
- 4 S. Saikan, T. Kishida, A. Imaoka, K. Uchikawa, A. Furusawa, H. Oosawa, *Opt. Lett.* **14**, 841 (1989).
- 5 S. Saikan, H. Miyamoto, Y. Tosaki, A. Fujiwara, *Phys. Rev. B* **36**, 5074 (1987).

## Persistent Spectral Hole-Burning of $\text{Pr}^{3+}$ ions in $(\text{ZrO}_2)_{1-x}(\text{Y}_2\text{O}_3)_x$ mixed crystals

K. Tanaka, T. Okuno, and T. Suemoto

*The Institute for Solid State Physics, The University of Tokyo, Roppongi 7-22-1, Minato-ku, Tokyo 106, Japan. (Tel. 03-3478-6811 ext. 5141 or 5142)*

H. Yugami, and M. Ishigame

*Research Institute for Scientific Measurements, Tohoku University, Katahira 2-1, Aoba-ku, Sendai 980, Japan. (Tel. 022-227-6200 ext. 2522)*

Many persistent spectral hole-burning (PSHB) experiments on various organic glasses and polymers doped with organic molecules reveal that the temperature dependence of the homogeneous linewidth ( $\Gamma_h$ ) is  $T^{1.3}$  at low temperatures (0.3 K ~ 20 K)<sup>1,2)</sup>. In contrast to organic molecules, very few PSHB data exist for rare earth ions in inorganic materials while data by fluorescence line-narrowing (FLN) above ~10K are considerably accumulated<sup>3)</sup>. Macfarlane and Shelby observed PSHB in  $\text{Pr}^{3+}$ - and  $\text{Eu}^{3+}$ -doped silicate glasses and reported that  $\Gamma_h$  of them have a  $T^{1.0}$  - dependence<sup>2,4)</sup>. Similar results were obtained by Van der Zaag et al.<sup>5)</sup>. In pure crystals,  $\Gamma_h$  is theoretically expected to have a  $T^7$  - dependence in the low temperature region and a  $T^2$  - dependence above the Debye temperature (Raman process)<sup>6)</sup>.

In spite of the relatively long history of research in this field, there are many unsolved problems concerning the condition for possibility of the persistent hole, and mechanism which controls the hole width and its temperature dependence. These problems are profoundly related to inhomogeneous properties or disorder in the host material. However, most of works in the past did not treat the disorder in a systematic way. In order to clarify this point, it is necessary to study PSHB under systematic control of the disorder and to reveal how  $T^7$  - dependence of  $\Gamma_h$  in pure crystals changes into  $T^\alpha$  - dependence ( $1 \leq \alpha \leq 2$ ) in glasses. YSZ (yttria stabilized zirconia),  $(\text{ZrO}_2)_{1-x}(\text{Y}_2\text{O}_3)_x$ , is suitable for this purpose as mentioned below.

It is well known that YSZ is a typical superionic conductor of the oxygen ion<sup>7)</sup>, having many oxygen vacancies for the charge compensation. YSZ is considered to have an intermediate property between crystalline and amorphous materials: X-ray diffraction measurements of YSZ crystals show clearly the  $\text{CaF}_2$  structure, while the diffuse neutron scattering measurements indicate random displacements of oxygen ions<sup>8)</sup>. Such a distribution of oxygen ions will

act as a random potential on optical centers (such as  $\text{Pr}^{3+}$ ,  $\text{Eu}^{3+}$ , etc.) replacing  $\text{Y}^{3+}$  sites. This type of disorder can be controlled by changing the composition.

In the present study, polycrystalline samples of YSZ ( $\text{Y}_2\text{O}_3$ : 10 mol%) containing a small amount of  $\text{Pr}^{3+}$  ions (2 mol%) were used. Three absorption bands ( $\alpha$ ; 6115A,  $\beta$ ; 6085A,  $\gamma$ ; 5825A) have been observed in  $\text{Pr}^{3+}$  doped YSZ. They are assigned to crystal field (CF) components of the  $^3\text{H}_4 \Rightarrow ^1\text{D}_2$  transition of  $\text{Pr}^{3+}$  ions by the analogy with the free-ion electronic energy diagram <sup>2), 9)</sup>. Inhomogeneous linewidths of these bands are  $200 \sim 300 \text{ cm}^{-1}$ , which are a little narrower than those in silicate glasses, but much broader ( $10^2 \sim 10^3$  times) than in pure crystals, such as  $\text{CaF}_2$  or  $\text{LaF}_3$ . This suggests that YSZ considerably has a glassy property as far as the effect on the electronic transitions is concerned. When excitation is made into these absorption bands, a structured broad emission band is observed around 6400 A, consisting of four components at least. The energy positions and widths of the peaks in the excitation spectrum for the 6400 A emission are almost the same as those in the absorption spectrum. The origin of the 6400 A emission band is assigned to the transition from the lowest CF component of  $^1\text{D}_2$  to several higher CF components of  $^3\text{H}_4$ .

Holes were burned into the absorption band of  $\text{Pr}^{3+}$  ions by irradiating with a single frequency dye laser (CR 699-21) with a frequency jitter width of  $\sim 1$  MHz. A typical laser intensity on the sample under burning was  $\sim 100 \text{ W/cm}^2$ . The hole was detected by measuring the emission excitation spectrum of the 6400 A band with a beam attenuated by a factor of  $50 \sim 100$ . Signals were obtained by a lock-in detection technique and accumulated  $20 \sim 30$  times by a digital storage oscilloscope synchronized with a ramp signal which scans the laser wavelength. Typical measuring time of the holes was 5 minutes.

Long-lived holes can be burned in the region from 6093 A to 6146 A which corresponds to the  $\alpha$  band. Figure 1 shows typical hole spectra at 4.2K, 6K, 9K, 14K, and 18.7K obtained by the irradiation of the 6135 A laser light ( $\sim 100 \text{ W/cm}^2$ ). Burning time was 2 minutes in all cases. As the temperature is raised, the width of the hole becomes wider and the depth shallower. We hardly burn out holes above 25K. Moreover, it is confirmed that burned holes disappear when the temperature is raised up to 50 K (erase process). As for the origin of holes, two types of mechanisms have been known to bring about long-lived holes in glasses containing rare earth ions; optical pumping mechanism and non-photochemical process which involves an optically induced rearrangement of the local structure of the glasses <sup>2),4),5)</sup>. In the former case, anti-holes are observed in any case and holes are stable only at the low temperatures ( $\leq 4 \text{ K}$ ). In YSZ, anti-holes can not be recognized and holes can be burned at relatively high

temperatures ( $\sim 20$  K). Therefore, the optical induced local lattice rearrangement is likely to give rise to holes in YSZ.

We found that the hole can not be burned in the higher energy absorption bands ( $\beta$  and  $\gamma$  bands). The width of the hole did not depend on the excitation wavelength under the same burning time. As for the reason why holes can not be burned in the  $\beta$  and  $\gamma$  bands, we tentatively consider as follows: Electrons excited into the higher CF level of  $^1D_2$  by the light corresponding to the  $\beta$  or  $\gamma$  band quickly relax into the lowest CF level of  $^1D_2$  before changing the local structure around  $Pr^{3+}$  ions. And this level have so different inhomogeneous distribution function<sup>10)</sup> from that of  $\beta$  or  $\gamma$  band that the electrons distribute all around the inhomogeneous linewidth of the lowest level, leading to no hole as a result.

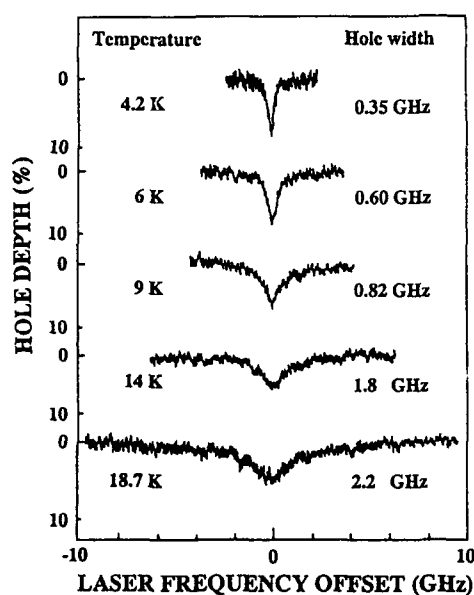


**Fig.1** Hole spectra burned at 6135A in YSZ:Pr<sup>3+</sup>(2 mol %).

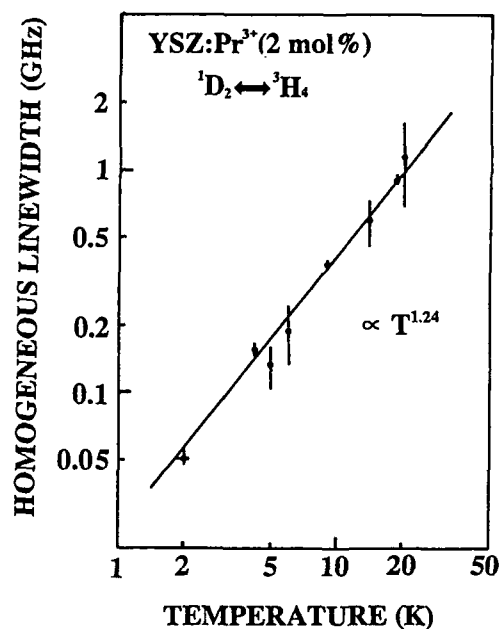


**Fig.2** Temperature dependence of the homogeneous linewidth.

The homogeneous linewidth,  $\Gamma_h$ , is obtained by calculating  $H(0)/2$ , where  $H(0)$  is the zero-burning limit value of the hole width.  $H(0)$  is determined by extrapolating the data for various burning times ( $t_b$ ) to  $t_b \rightarrow 0$ . In Fig.2 are shown values of  $\Gamma_h$  for the  $\alpha$  band of  $Pr^{3+}$  ions by closed circles against temperatures ( $T$ ) in log-log scale. Data points are fitted to a function of  $\Gamma_h = \alpha T^\beta$  by the least-squares method and the result is shown by a straight line in the figure. One can find a  $T^{1.24 \pm 0.1}$  dependence of  $\Gamma_h$ . It is well known that  $\Gamma_h$  (Hz) is represented by using energy relaxation time  $T_1$  and pure dephasing time  $T_2^*$  as  $\Gamma_h = 1/\pi (1/2T_1 + 1/T_2^*)$ . The value of  $T_1$  for the lowest CF component of  $^1D_2$  was determined as

$\sim 110 \mu\text{s}$  at 4.2 K by measuring the transient response of the 6400 Å emission. By using this  $T_1$ ,  $1/(2\pi T_1)$  gives  $\sim 1 \text{ KHz}$ , which is  $10^5 \sim 10^6$  times smaller than the observed hole width. Therefore, it is concluded that the homogeneous linewidth is determined mainly by  $T_2^*$  for the  $\alpha$  band in  $\text{Pr}^{3+}$ -doped YSZ in this temperature region. The temperature dependence of  $\Gamma_h$  in YSZ is similar to that obtained in various polymers and amorphous materials, rather than in other rare earth doped crystals. This means that in phase relaxation processes YSZ has a similar nature to amorphous materials.

For molecular systems in polymers and glasses, several models including a coupling of electrons to two level systems (TLS) are proposed and  $T^{1.3}$  -dependence of  $\Gamma_h$  is explained <sup>11)</sup>. In YSZ, existence of TLS has already been suggested from specific-heat measurements at the low temperature <sup>12)</sup>. A probable candidate which acts as TLS is the tunneling motion of mobile vacancies, which contributes to the ionic conductivity in YSZ. It is very probable that the temperature dependence of  $\Gamma_h$  of  $\text{Pr}^{3+}$  ions in YSZ also originates from the interaction with TLS. To make clear the hole-burning mechanism and the origin of the temperature dependence of the homogeneous linewidth, it will be effective to study holes in YSZ systems with different composition, i.e. with different degrees of disorder.

### References

- [1] K.K.Rebane and A.A.Gorokhovskii, *J. Luminescence* **36** (1987), 237.
- [2] R.M.Macfarlane and R.M.Shelby, *J. Luminescence* **36** (1987), 179.
- [3] W.M.Yen and R.T.Brundage, *J. Luminescence* **36** (1987), 209 and references therein.
- [4] R.M.Macfarlane and R.M.Shelby, *Optics Communications* **45** (1983), 46.
- [5] P.J.Van der Zaag, B.C.Schokker, Th.Schmidt, and R.M.Macfarlane, *J. Luminescence* **45** (1990), 80.
- [6] B.Di. Bartolo, in: *Optical Interactions in Solids* (John Wiley & Sons, 1968), Chap. 15.
- [7] R.M.Dell and A.Hooper, in: *Solid Electrolytes, General principles, Characterization, Material, Application*, P.Haglmaller and W.V.Goog eds. (Academic Press, New York, 1978) p.291.
- [8] D.Steele and B.E.F.Fender, *J. Phys. C* **7** (1974), 1.
- [9] G.H.Dieke : *Spectra and Energy Levels of Rare Earth Ions in Crystals* (Interscience, 1968).
- [10] K.K.Rebane and L.A.Rebane, in : *Persistent Spectral Hole-Burning: Science and Applications* (Springer-Verlag, Berlin, 1988), Chap 2.
- [11] J.M.Hayes, R.Jankowiak, and G.J.Small, in : *Persistent Spectral Hole-Burning : Science and Applications* (Springer-Verlag, Berlin, 1988), Chap 5.
- [12] W.N.Lawless, *Phys. Rev. B* **22** (1980), 3122.

Optical Pumping Detection of Anomalous NQR Spectra of  $\text{Pr}^{3+}$  in  $\text{Pr}^{3+}:\text{LaF}_3$ 

L.L. Wald, and E.L. Hahn

Department of Physics, University of California  
Berkeley, California, 94720 (415) 642-4859

M. Lukac

Josef Stefan Institute, Jamova 39,  
Ljubijana 61000, Yugoslavia (61) 214-399

The nature of inhomogeneous broadening in rare earth systems plays an important role in the dynamical optical properties of ions in crystals. For this reason much of the work on the nature of the inhomogeneous broadening in rare earth doped systems has concentrated on the investigation of ion-ion interactions such as spectral transfer and up conversion processes.<sup>1-3</sup> Variations in homogeneous optical dephasing times across the inhomogeneous optical line have also been reported.<sup>4</sup> These studies concentrate on the variations of collective effects of ion-ion interactions at different positions in the inhomogeneous optical line in relatively heavily doped rare earth systems. We report variations in optically detected NQR (ODNQR) linewidths and shifts of  $\text{Pr}^{3+}$  hyperfine transitions in the optical ground state as a function of position in the inhomogeneous optical line and for satellite transitions of the  $^1\text{D}_2$ - $^3\text{H}_4$  transition in lightly doped (0.5 at. %)  $\text{Pr}^{3+}:\text{LaF}_3$ . A systematic increase in the broadening of the Pr hyperfine transitions is observed as the laser is tuned toward the wings of the inhomogeneous optical transition without a shift of the NQR center frequency. The principle contribution to the 200kHz (FWHM) inhomogeneous width of the Pr hyperfine levels is explained by magnetic dipole-dipole interactions between the Pr nuclei and the neighboring fluorine spins. This contribution remains constant across the Stark broadened optical transition. Thus we show the existence of an additional broadening mechanism. We postulate that this broadening is due to the interaction of the  $^{141}\text{Pr}$  nuclear quadrupole moment with the electric field gradients associated with random point defects. In the case of the satellite transitions associated with ion pairs, the point defect is simply the second Pr ion and thus will produce a unique quadrupole shift. We measure the ODNQR spectra for these satellite

transitions and find the hyperfine transitions shifted and narrower than in the wings of the main optical line.

A 0.5 at. %  $\text{Pr}^{3+}:\text{LaF}_3$  crystal at  $2^\circ\text{K}$  is mounted in a pair of capacitor plates which produce a voltage parallel to the crystal  $C_2$  axis. This allows a Stark modulated optical pumping cycle to be employed.<sup>4</sup> In this technique, a 100kHz sawtooth voltage is applied to the plates. No voltage is applied for the first half of the cycle, during which a hole is burned in the optical spectrum (resulting in no absorption). This is followed by a fast (compared to the rate of optical pumping) ramp voltage during which absorption from those ions swept into resonance with the laser by the ramp is detected. The enhanced absorption from anti-holes is also detected. The ramp voltage Stark modulates the ions through a span of 100 MHz in our experiment. The ions sampled during the ramp part of the cycle experience a lesser degree of holeburning since they are in resonance with the laser for a smaller fraction of the cycle. The resulting modulated transmission is lock-in detected and recorded. We refer to the amplitude of this signal as the SMOP amplitude.

The crystal is placed inside an untuned RF coil connected to a power amplifier and RF sweep generator. The laser polarization can be applied either along the crystal  $C_2$  axis, allowing the  $\Gamma(1)-\Gamma(1)$   $\sigma$  transition, or perpendicular to the crystal  $C_2$  axis, in which case this  $\sigma$  transition is forbidden by symmetry. However, due to symmetry breaking crystal field distortion in the vicinity of the ion pairs, the ion wavefunctions are slightly mixed, allowing the perpendicular polarization to produce a weak  $\pi$  polarized transition for these ions.<sup>6</sup> Since the polarizers are not perfectly aligned, some of the much stronger  $\sigma$  transitions always occur during measurements made with the  $\pi$  orientation. While this does not present a problem far from the main optical transition, it allows the  $\sigma$  transitions of the main optical line to overwhelm any  $\pi$  transition satellites in this region.

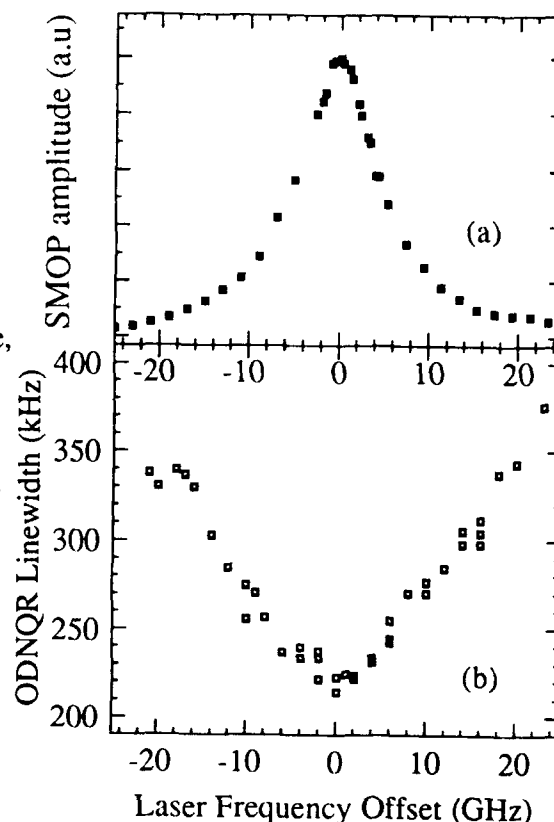


Fig. 1 (a) The main, inhomogeneously broadened optical line of  $\text{Pr}^{3+}:\text{LaF}_3$ . (b) Variation of the NQR width (FWHM) of the 16.67 MHz  $5/2$  to  $3/2$  hyperfine transition of Pr as a function of position in the inhomogeneous optical line.

The two peak structure of the 5/2 to 3/2 Pr hyperfine splitting observed for two of the optical doublets (Fig.3 and Fig.4) may arise from two overlapping satellite ions unresolvable under the inhomogeneous optical line. Another possibility is that the doublet is a manifestation of Pr-Pr magnetic dipolar coupling between an ion pairs. The ODNMR spectrum of the Pr 3/2 to 5/2 hyperfine transition associated with the satellite marked s in Fig.2 is narrower (280 kHz FWHM) than that found in the wings of the main optical line and is shifted by 10 kHz to 16.57 MHz. This is a small shift compared to the >100 kHz of additional Pr NQR linewidth broadening seen in the wings of the main optical line. It appears that a small but discrete shift in the Pr NQR resonant frequency occurs for an ion pair relative to the NQR transition for a single Pr ion.

The  $\text{Pr}^{3+}$  hyperfine ground state is described by a spin Hamiltonian which is a combination of the magnetic pseudo quadrupole interaction and a "real" quadrupole interaction arising from the interaction of the  $^{141}\text{Pr}$  nuclear quadrupole moment with the crystal field gradient. We propose that the ODNQR linewidth variations and shifts at different positions in the optical line arise from the latter. An order of magnitude estimate of the relative contributions of the pseudo quadrupole contribution and the "real" quadrupole contribution can be made by estimating the electric field gradient at the Pr site using La NQR data for  $\text{LaF}_3$ .<sup>7</sup> The field gradient obtained in this way should be about the same as the gradient at the Pr site, since the two ions occupy the same site (although the Pr ion undoubtedly distorts its surroundings to some extent.) The relative values of the Sternheimer anti-shielding factor for the two ions is also unknown. An order of magnitude estimate made in this way indicates that the contribution from the pseudo quadrupole interaction in  $\text{Pr}^{3+}$  is roughly 50x larger than that produced by the  $\text{LaF}_3$  field gradient. Despite the relatively small value of the Pr nuclear quadrupole moment, the shifts and broadenings we measure are of a size commonly encountered in nuclear quadrupole spectroscopy.

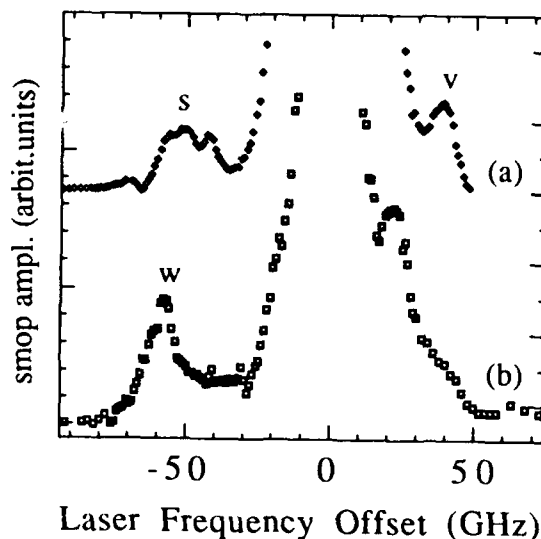


Fig.2. SMOP amplitude as a function of the laser frequency in the vicinity of the  $^3\text{H}_4\text{-}^1\text{D}_2$  ( $\Gamma(1)\text{-}\Gamma(1)$ ) transition for both the  $\sigma$  (allowed) (a), and the  $\pi$  polarizations (b). The vertical scale for (b) is enhanced by roughly a factor of 100.

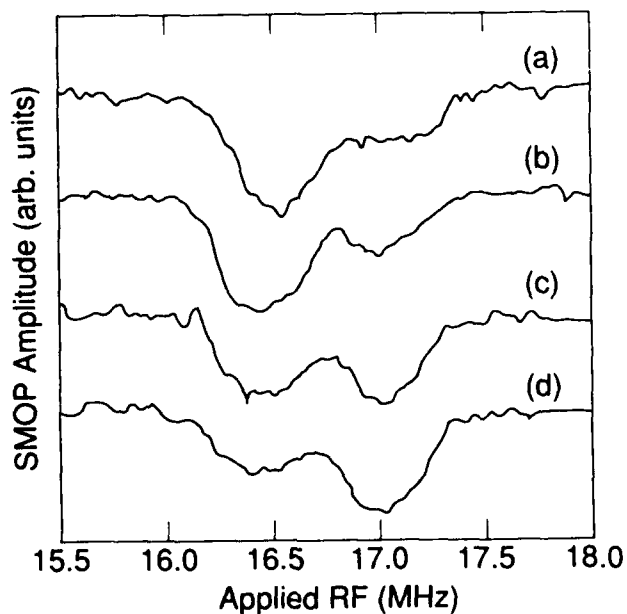


Fig. 3. The  $5/2$  to  $3/2$  Pr hyperfine transition spectrum of the satellite transition marked w in Fig. 2. Laser polarization is in  $\pi$  orientation. Laser frequency offset of (a) -50 GHz. (b) -60 GHz. (c) -65 GHz (d) -70 GHz.

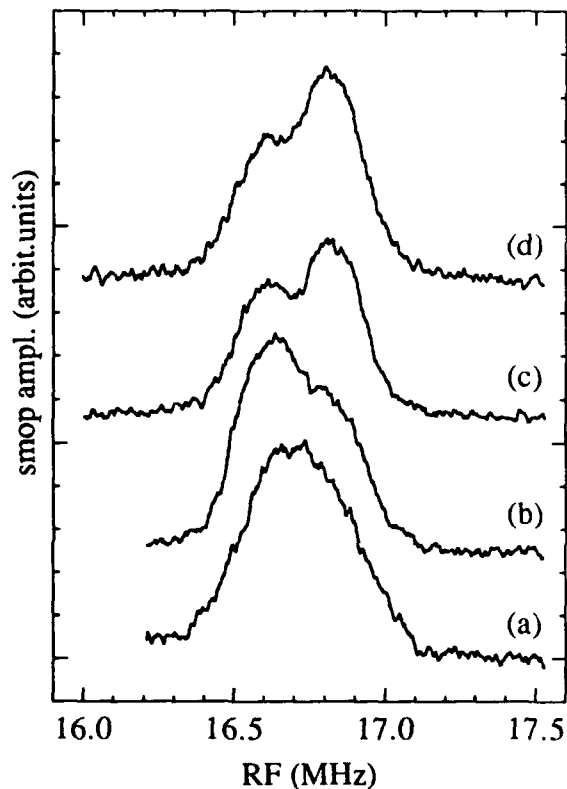


Fig. 4. The  $5/2$  to  $3/2$  Pr hyperfine transition spectrum of the satellite transition marked v in Fig. 2. Laser polarization is in  $\sigma$  orientation. SMOP signal is inverted relative to Fig.3 due to an instrumental effect Laser frequency offset of (a) +35 GHz. (b) +40 GHz. (c) +45 GHz. (d) +49 GHz.

1. W.M. Yen, in Spectroscopy of Solids Containing Rare Earth Ions, eds. A.A. Kaplyanskii and R.M. Macfarlane (North-Holland, New York, 1987).
2. R. Flach, D.S. Hamilton, P.M. Selzer, and W.M. Yen, Phys. Rev. B 15, 1098 (1980).
3. A.J. Silversmith, Liren Lou, and W.M. Yen, Phys. Rev. B 26, 2656 (1982).
4. R.M. Shelby and R.M. Macfarlane, Phys. Rev. Lett. 45, 1098 (1980).
5. M. Lukac and E.L. Hahn, J. Lumin. 42, 257 (1988).
6. M. Lukac and E.L. Hahn, Optics Comm. 70, 195 (1989).
7. K. Lee, A. Sher, L.O. Anderson, and W.G. Proctor, Phys. Rev. B 150, 168 (1966).

## HOLE-BURNING STUDY OF OPTICAL HEATING IN LOW-TEMPERATURES GLASSES

A.A. Gorokhovskii<sup>a</sup>, G.S. Zavt<sup>b</sup>, V.V. Palm<sup>b</sup> and A.L. Stolovich<sup>b</sup>

<sup>a</sup> *Institute for Ultrafast Spectroscopy and Lasers and Physics Department of The City College of New York, 138th Str. & Convent Ave., New York, NY 10031, USA  
Tel. 212/650-5525*

<sup>b</sup> *Institute of Physics, Estonian Academy of Sciences,  
142 Riia Str., Tartu, Estonia, 202400, USSR*

### **Introduction.**

Zero-phonon lines (ZPL) in the spectra of impurities in solids are extremely narrow and intense. Due to these unique features, an impurity - guest can serve as a very sensitive probe of both the quasistatic structural disorder (inhomogeneous broadening) and dynamical processes (homogeneous broadening) in the matrix - host<sup>1</sup>. Site selective high resolution spectroscopy, in particular, persistent hole burning, can be successfully used to remove inhomogeneous broadening<sup>1,2</sup> and can provide useful information about relaxation and propagation of elementary excitations in solids. For glasses at low temperatures actual excitations are phonons and two-level systems<sup>3</sup> (TLS). The following properties of the persistent hole in the pure-electronic absorption band of an impurity introduced in a glassy matrix should be mentioned in this respect: (i) at low temperatures the width is determined mainly by the electron-TLS interaction<sup>4,5</sup>; (ii) the hole intensity and width are highly sensitive to external perturbations, particularly, to thermal ones; (iii) the optical dephasing time is usually shorter than and spectral diffusion time is usually longer than the typical times determining the thermalization processes in glasses. Therefore, the hole spectra can be used as a suitable 'intrinsic thermometer' in time-resolved studies.

Recently we demonstrated<sup>6</sup> an extremely high sensitivity of a hole in the spectrum of the organic impurity in amorphous polymer to a relatively weak optical excitation that is not in resonance with optical absorption spectra of this impurity, but falls within the vibronic band of another impurity or within an infrared vibrational band of the matrix-host. Photoexcitation generates nonequilibrium phonons that change the TLS populations distribution and results in the (partly reversible) hole width increasing, intensity reducing and shape changing i.e. hole shows photoinduced spectral diffusion. In the present paper we will discuss results of the photoinduced spectral diffusion study in the conditions of good and weak thermal link between sample and helium bath in the temperature range 0.6-5 K.

### **Experimental.**

We studied samples of amorphous polystyrene (PS) doped with impurities of two types: H<sub>2</sub>-octaethylporphin (OEP, concentration  $\approx 7 \times 10^{17} \text{ cm}^{-3}$ ) and ClAl-phtalocyanine (Pc,  $5 \times 10^{16} \text{ cm}^{-3}$ ). The persistent hole is burnt in the OEP 0-0 absorption band of S<sub>1</sub> - S<sub>0</sub> transition ( $\lambda_{\text{max}}=618.5 \text{ nm}$ ,  $\sigma=150 \text{ cm}^{-1}$ ) by a single - mode dye laser (0.01 - 0.1 mW/cm<sup>2</sup>) at  $\lambda_0=619 \text{ nm}$ . The hole shape is Lorentzian with width  $\delta_0=0.03 \text{ cm}^{-1}$  at T=1.45 K (Fig 1a). After hole burning, the sample was in the same direction illuminated by He-Ne laser radiation (632.8 nm,  $\leq 50 \text{ mW/cm}^2$ ) that matches

the 0 -1 vibronic (intramolecular vibration  $\approx 1100 \text{ cm}^{-1}$ ,  $OD \approx 0.4$ ) band of the Pc impurity but is outside the OEP absorption band. The kinetics of the hole filling and recovering were studied by measuring the transmission at the center of the hole under excitation by a 632.8 nm beam modulated by an acoustooptic modulator. Two experimental setups were used: in setup #1 the sample was immersed in liquid He, while in setup #2 a weak link between He<sup>3</sup> and a sample placed in vacuum was used. The temperature was varied in the first case from 1.45 to 4.2 K, in the second, from 0.6 to 5 K. The main results can be summarized as follows.

(1) Under illumination, the hole depth decreases and width grows (Fig. 1, a and b). For small change in the transmission at the hole center  $I$ ,  $\Delta I/I \leq 0.1$ , the hole shape remains Lorentzian while for large changes the significant deviations from this shape are observed (Fig 1b). The effect is observed only if the holeburning and illuminating tracks overlap in setup #1 while such overlapping is not needed in setup #2. (2) The change of the hole depth depends linearly on the illumination intensity in a wide range of the hole depth change,  $\Delta I/I = 0-0.95$ . (3) The time dependence of the hole depth change  $\Delta I(t)$  for  $\Delta I/I \leq 0.1$  follows the exponential law for both the filling and recovery kinetics (Fig. 2), however, the recovery kinetic significantly depends on the illumination intensity (Fig. 3). The characteristic time  $\tau$  in both setups grows with temperature approximately as  $T^3$  for  $T > 1.2$  and remains constant at lower temperatures (Fig. 4). However, this time is not intrinsic: it depends on the sample thickness and essentially increases for the case a of weak link with the helium bath (Fig. 2b and d). (4) After switching off the illumination, the hole recovers only partially (Fig. 1c and 3). For longer times a very slow (roughly logarithmic) recovery process is observed: the hole increases and narrows (Fig. 1d) that is opposite to the usual spectral diffusion<sup>4,5,7</sup>.

### Model and discussion.

Suppose, that after hole burning the system is subjected to an external time-dependent perturbation which changes the impurity ZPL shape function  $\sigma_0(\omega)$  to  $\sigma_1(\omega)$  but does not change the homogeneous distribution. Then for weak burning the hole shape is determined as<sup>8)</sup>

$$F(\Omega - \Omega_0) = \langle \int d\omega \sigma_0(\Omega_0 - \omega) \sigma_1(\Omega - \omega) \rangle \quad (1)$$

where  $\Omega_0$  is the laser frequency and the average is over all the values of the transition energy  $\omega$ . At  $T < 5 \text{ K}$  the system studied is in the slow modulation regime of line broadening<sup>4,8)</sup>,  $\Gamma(E) < \delta(T)$ , where  $\Gamma$  is the reciprocal lifetime of the TLS upper level. In this case Exp.(1) leads to

$$F(\Omega - \Omega_0, t) = \int_{-\infty}^{\infty} d\mu \exp\{ i(\Omega_0 - \Omega)\mu - \delta_0(T)|\mu| - \sum_j \text{th}(E_j / 2T) \int dr \Delta f(E_j, r, t) [1 - \cos(V_j(r)\mu)] \}$$

$$\delta_0(T) = (\pi^2/3) \overline{PT} |V_0|^2 a^3, \quad V_j(r) = V_0 a^3 \Delta_j / (r^3 E_j) \quad (2)$$

Here  $E_j$  is the energy of  $j$ th TLS,  $\Delta_j$  is the asymmetry parameter,  $a$  - mean distance between host molecules,  $\Delta f(E, r, t)$  - change of the population factor for the upper level of TLS. It is seen that the change of the hole parameters is controlled by the temporal and spatial evolution of the TLS population numbers.

The light absorption in the vibronic band, followed by fast ( $\approx 1$  ps) radiationless processes, leads to the creation of nonequilibrium phonons with a broad spectral distribution. In addition, TLS are excited by high-frequency phonons through Raman and a relaxation absorption processes. As a result, a nonequilibrium density of phonons,  $\Delta n(\omega, \mathbf{r})$ , and of TLS,  $\Delta f(E, r, t)$ , arises in the illumination beam track. The next relaxation stage is much slower and described by coupled kinetic equations in the diffusion approximation with sources  $\Delta n$  and  $\Delta f$ . The solution for  $\Delta f(E, r, t)$  in Exp.(2) contains two terms  $\Delta f_1 + \Delta f_2$ . The first term is a propagating part describing essentially a diffusion of the phonons which interact resonantly with TLS (the sample heating). It is assumed that all phonons have a unique temperature  $T^*(r, t)$ , i.e. the process is controlled by thermal diffusivity  $D(T) = K(T)/C(T)$  where  $K(T)$  - thermal conductivity,  $C(T)$  - heat capacity, and the diffusion time  $\tau_D = \beta L^2/D(T)$ , where  $L$  - mean size of the excited region,  $\beta \approx 1$ . Since for glasses at  $T = 1 - 10$  K,  $D(T) \sim T^{-3}$  and at  $T < 1$  K,  $D(T) \sim T^{-0.1}$  the observed dependence of  $\tau$  upon the temperature can be readily explained. In the case of good cooling (setup #1),  $L \approx 1$  mm is the sample thickness or the illuminating beam diameter and at  $T=1.5$  K for PS one has  $\tau \approx 10$  ms. In the case of weak link (setup #2) the distance between the laser beam and the point of the heat drain ( $\approx 10$  mm) plays the role of the  $L$  and one has  $\tau \approx 1$  s. At relatively high illumination intensity we overheat the sample and  $D$  becomes intensity dependent. That brings about the nonexponential recovery kinetic and the need to solve a nonlinear equation for a quantitative description.

The second (non-propagating) term  $\Delta f_2$  is due to excited TLS and leads to the deviation of the relaxation kinetic from the diffusional model at late stages and to the slow recovery after switching off the illuminations due to TLS cooling. Moreover, the change of the hole shape can be also ascribed to nonequilibrium TLS since such TLS should be localized in a small volume around the absorbing Pc molecules. Calculations assuming the Poisson distribution are in qualitative agreement with the experiment.

1. See, e.g. *Zero-Phonon Lines and Spectral Hole Burning in Spectroscopy and Photochemistry*, ed. by O.Sild and K.Haller, Springer-Verlag, Berlin, Heidelberg (1988).
2. See, e.g. *Persistent Spectral Hole-Burning: Science and Applications*, ed. by W.E. Moerner, Springer-Verlag, Berlin, Heidelberg (1988).
3. See, e.g. *S. Hunklinger and A.K. Rayenhandhori*, in: *Progress in Low Temperature Physics*, ed. by D.E. Brewer, North-Holland, 1986, p.265.
4. See, e.g. *K.K. Rebane and A.A. Gorokhovskii*, *J. Luminescence* **38**, 267 (1987).
5. *J. Friedrich and D. Haarer*, in: *Optical Spectroscopy of Glasses*, ed by I. Zchokke, Riedel (1986), p.149.
6. *A.A. Gorokhovskii, G.S. Zavt and V.V. Palm*, *JETF Lett.*, **48**, 369 (1988).
7. *K.A. Littau and M.D. Fayer*, *Chem. Phys. Lett.*, **176**, 551 (1991).
8. *M.A. Krivoglaz*, *Soviet Phys. JETF* **61**, 1284 (1985).

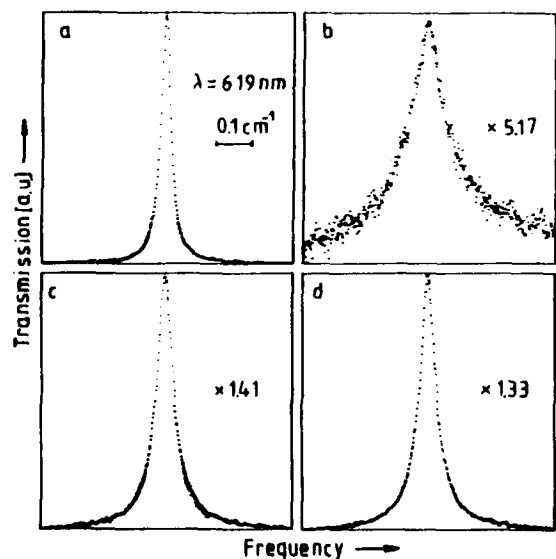


Fig 1. Hole shape: *a*-original hole; *b* - during illumination,  $P=40 \text{ mW/cm}^2$ ; *c* - 30 s after illumination is turned off; *d* - 1200 s later.

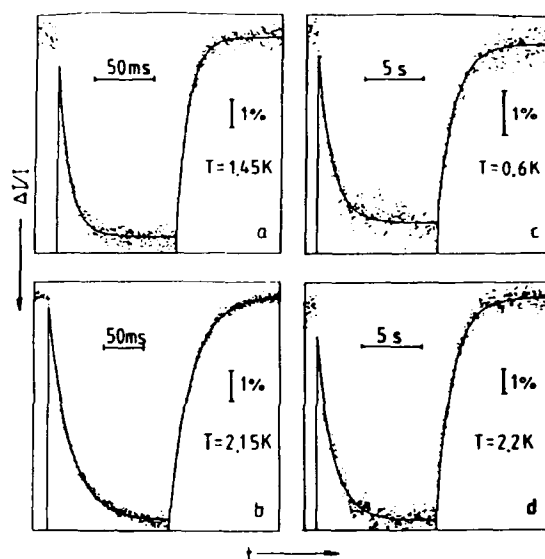


Fig. 2 Kinetics of the change in the transmission  $I$  at the hole center at various temperatures; *a, b* - setup #1, *c, d* - setup #2.  $P=5 \text{ mW/cm}^2$ .

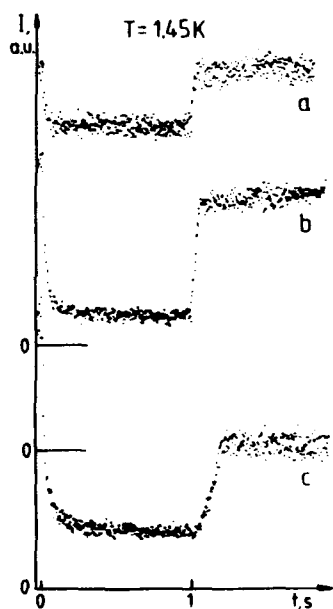
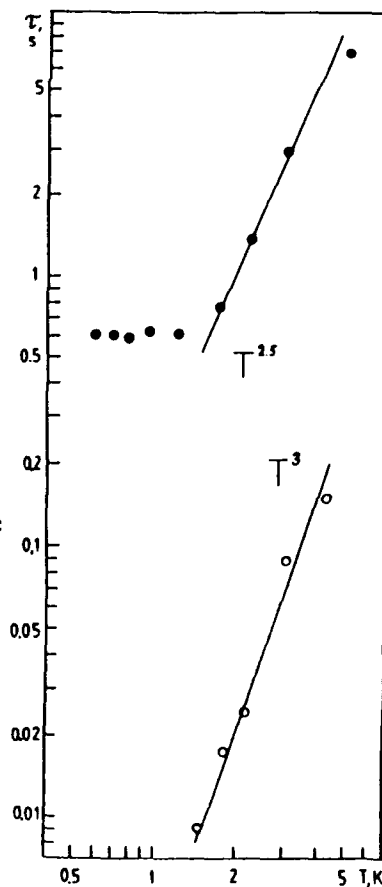


Fig. 3. Kinetics at different intensity of illumination  $P$ ; *a* -  $15 \text{ mW/cm}^2$ , *b* -  $35 \text{ mW/cm}^2$ , *c* -  $50 \text{ mW/cm}^2$ .

Fig. 4. Temperature dependence of the relaxation time; open circles - setup #1, solid circles - setup #2.





Saturday, September 28, 1991

## Novel Spectroscopies and Systems

**SB** 11:00am-1:00pm  
DeAnza Room

W. E. Moerner, *Presider*  
*IBM Almaden Research Center*

Applications of spectral hole-burning spectroscopies to the excited electronic states and transport dynamics of photosynthetic units

G. J. Small

Ames Laboratory-USDOE and Department of Chemistry

Iowa State University

Ames, Iowa 50011

Hole-burning methodologies suitable for the study of excited electronic state structure, energy and electron transfer dynamics, electron-phonon coupling, and heterogeneity of photosynthetic units are discussed.

The critically important picosecond and sub-picosecond events of photosynthesis occur in the photosynthetic unit which is comprised of an antenna (light harvesting) and reaction center complex. The major photocatalysts are chlorophylls (Chls) which operate off their  $Q_y(S_1)$ -state. The early time events are energy (optical excitation) transfer within and between different complexes of the antenna and from the antenna to  $P^*$  (excited state of a special Chl pair) of the reaction center whose population initiates primary charge separation. An understanding of these events requires a firm understanding of the excited state electronic and vibrational structures of a protein-pigment complex, the coupling of electrons and electronic transitions to the protein phonons, vibrational and phonon relaxation times and the structural heterogeneity afforded by the "glass-like" protein. Conventional spectroscopic techniques provide little information of this type because the  $Q_y$ -absorption bands at low temperatures carry widths of  $\sim 100$ - $500\text{ cm}^{-1}$ , depending on the nature of the pigment and protein.

Recently, spectral hole burning spectroscopies (nonphotochemical, photochemical and transient population bottleneck) have been applied with considerable success to the primary donor state absorption profiles of the reaction centers of photosystem I [1] and photosystem II [2-4] of green plants (P700 and P680, respectively) and P870 and P960 of the purple bacteria *Rhodobacter sphaeroides* and *Rhodospseudomonas viridis* [5-7]. The antenna complexes studied include those of photosystem I [8,9], the base-plate BChl *a* (bacteriochlorophyll *a*) protein complex of the green algae *Prosthecochloris aestuarii* [10], the B800-B850 and B875 BChl *a* proteins of *Rb. sphaeroides* [11-13] and the phycobilisomes of *Masticogladus laminosus* [14]. Hole burning has led to an improvement in the resolution of the  $Q_y$ -absorption bands of 2-4 orders of magnitude and the observation of zero-phonon holes (ZPH) has led to the first determinations of energy and electron transfer dynamics from a well-defined level (*total zero-point*).

Of equal or greater interest than the ZPH is the entire hole profile and, specifically, the burn wavelength ( $\lambda_B$ ) dependence of the profile. This is because the  $\lambda_B$ -dependent hole spectra contain important information on the site inhomogeneity ( $\Gamma_I$ ) and linear electron-phonon ("delocalized" protein and intermolecular "localized" pigment modes) coupling ( $\Gamma_{ep}$ ) contributions to the absorption width. It was the photochemical hole burned spectra of P870 and P960 which led to the development of an accurate theory for hole profiles which is valid for arbitrarily strong electron-phonon coupling [15,16]. In addition to the contributions from  $\Gamma_I$  and  $\Gamma_{ep}$  to the absorption width ( $\Gamma$ ), there can be a significant contribution from exciton level structure and inter-exciton level scattering ( $\Gamma_{ex}$ ) in antenna protein complexes. Very recently a methodology for untangling the contributions from  $\Gamma_{ep}$  and  $\Gamma_{ex}$  has been developed [11,12]. It is based on "Franck-Condon factor narrowing" of intramolecular vibronic satellite holes which build on the origin band hole.

This talk assumes little knowledge on the structures and dynamics of photosynthetic units and will begin with an introduction to the subject and a brief review of current unsolved problems. By way of model calculations, the theory for spectral hole profiles will be discussed and then applied to the hole spectra of P870 of the *fully* deuterated reaction center of *Rb. sphaeroides*. These spectra are compared with those of the protonated reaction center and the relevance of the results to the excited state structure and dynamics of the special pair discussed. New results for the reaction center of PS II will be presented and discussed from the viewpoints of energy transfer and primary charge separation kinetics and the question of whether or not P680 is a "special pair" of Chls as is the case for the purple bacteria. The talk will end with a discussion of what spectral hole burning has revealed about excitonic interactions and energy transfer in antenna complexes.

## Acknowledgment

Ames Laboratory is operated for the U.S. Department of Energy by Iowa State University under contract No. W-7405-Eng-82. This article was supported by the Chemical Sciences Program of the Office of Basic Energy Sciences.

## References

1. J. K. Gillie, P. A. Lyle, G. J. Small and J. H. Golbeck, *Photosynthesis Research* 22 (1989) 233.
2. R. Jankowiak, D. Tang, G. J. Small and M. Seibert, *J. Phys. Chem.* 93 (1989) 1649.
3. D. Tang, R. Jankowiak, M. Seibert and G. J. Small, *Photosynthesis Research* 27 (1991) 19.
4. D. Tang, R. Jankowiak, M. Seibert, C. F. Yocum and G. J. Small, *J. Phys. Chem.* 94 (1990) 6519.
5. S. G. Johnson, D. Tang, R. Jankowiak, J. M. Hayes, G. J. Small and D. M. Tiede, *J. Phys. Chem.* 94 (1990) 5849.
6. D. Tang, S. G. Johnson, R. Jankowiak, J. M. Hayes, G. J. Small and D. M. Tiede, in *Perspectives in Photosynthesis* (1990); J. Jortner and B. Pullman, Eds.; Kluwer Academic: Dordrecht.
7. D. Tang, S. G. Johnson, J. M. Hayes, R. Jankowiak, D. Tiede and G. J. Small, *J. Phys. Chem.* 93 (1989) 5953.
8. J. K. Gillie, B. L. Fearey, J. M. Hayes, G. J. Small and J. H. Golbeck, *Chem. Phys. Lett.* 134 (1987) 316.
9. J. K. Gillie, G. J. Small and J. H. Golbeck, *J. Phys. Chem.* 93 (1989) 1620.
10. S. G. Johnson and G. J. Small, *J. Phys. Chem.* 95 (1991) 471.
11. N. R. S. Reddy and G. J. Small, *J. Chem. Phys.*, in press.
12. N. R. S. Reddy and G. J. Small, *Chem. Phys. Lett.*, in press.
13. H. van der Laan, Th. Schmidt, R. W. Visschers, K. J. Visscher, R. Van Grondelle and S. Volker, *Chem. Phys. Lett.* 170 (1990) 231.
14. W. Köhler, J. Friedrich, R. Fischer and H. Scheer, *J. Chem. Phys.* 89 (1988) 871.
15. J. M. Hayes, J. K. Gillie, D. Tang and G. J. Small, *Biochim. Biophys. Acta* 932 (1988) 287.
16. S. G. Johnson, I.-J. Lee and G. J. Small, in *Chlorophylls* (1991); H. Scheer, Ed.; CRC Publishers.

MICROWAVE-INDUCED HOLE BURNING OF THE 638 NM ZERO-PHONON TRANSITION  
AND FREQUENCY-DEPENDENT DEPHASING OF THE N-V CENTER IN DIAMOND

Max Glasbeek and Eric van Oort

Laboratory for Physical Chemistry, University of Amsterdam  
Nieuwe Achtergracht 127, 1018 WS Amsterdam, The Netherlands  
Phone: (31) 20 5256996; Fax: (31) 20 5255698

In recent years the microscopic description of inhomogeneous broadening of electronic transitions of chromophores in crystals and glasses has attracted much interest [1-3]. In the phenomenological model proposed by Selzer [1], it is assumed that the energies of the initial and final states involved in the optical transition exhibit a one-to-one correlation. In an alternative approach by Lee et al [2], the two states are considered as completely uncorrelated. Very recently, a more general microscopic theory has been presented by Laird and Skinner [3]. In the latter theory the aforementioned models are obtained as limiting cases. So far relatively few experiments have been reported which focus on the origin of inhomogeneous broadening.

In this paper, we report on experiments in which hole burning of the optical zero-phonon line of the chromophore is accomplished by the resonant microwave pumping of the spin transition of the probe molecule in its triplet ground state. Using a narrow-band laser in the optical-microwave double resonance experiments, it will be demonstrated that as a result of the hole burning process additional fine structure splittings in the triplet ground state can now be resolved. A variation of the fine structure splitting with the laser excitation wavelength indicative of site selection is reported. On the other hand, the inhomogeneous broadening of the zero-field ODMR transition of the molecular probe is found to be insensitive to the laser wavelength. It is discussed that the results are compatible with the idea of a partial correlation of the energies of the initial and final states in the optical transition.

The chromophore studied in this paper is the nitrogen-vacancy (N-V) center in diamond. The center consists of a substitutional nitrogen atom adjacent to a carbon vacancy [4]. In absorption and emission the defect gives rise to a zero-phonon transition peaking at 638 nm. In a series of recent studies it has been established that the defect has an electron triplet spin ground state,  $^3A$  [5-7]. The 638 nm zero-phonon line (ZPL) is attributed to a  $^3A \rightarrow ^3E$  transition. In this Letter we also report results of spin coherent transient measurements of the diamond N-V center under conditions that narrow-band laser excitation near its 638 nm zero-phonon absorption (rather than broad-band excitation as in previous work [6,7]) is applied. A major result is that the irreversible spin dephasing rate (characteristic of the homogeneous line width of the triplet ground state spin transition) appears to depend strongly on the laser wavelength used in the double resonance experiment. It is discussed that the frequency-dependent dephasing is a manifestation of the presence of microscopic strain in the crystal.

The diamond sample was the same as used in previous work [5]. A description of the optical-microwave experimental set-up is given elsewhere [8]. The experiments were performed at a temperature of 1.4K. In most narrow-band excitation experiments the laser line width was about 60 GHz; when the laser width was limited to 1 MHz the observed line narrowing phenomena described below were essentially similar to those for the 60 GHz width excitation, although the S/N ratio was much worse. Laser excitation was within the 638 nm ZPL (FWHM  $\approx$  900 GHz) of the N-V center using a Coherent CR-590 dye laser pumped by a cw Ar<sup>+</sup>-ion laser with 50 mW output power.

Fig. 1 shows characteristic optically detected microwave resonance (ODMR) spectra as observed in zero magnetic field for the diamond N-V defect using broad band and narrow-band ( $\sim$  60 GHz) laser excitation within the ZPL, respectively. The observation of ODMR is explained as follows [6]. Optical excitation of the defect gives rise to a significant spin alignment in the  $^3A$  ground state. Microwave resonance involving the  $^3A$  spin transition influences the population distribution of the ground state spin levels and this in turn affects the net number of N-V centers that are photo-excited to the fluorescent  $^3E$  state. As a result, by scanning the microwave frequency a change in the fluorescence intensity is observed when spin resonance among the ground state spin levels is induced. The splitting of the ODMR line is resolved upon narrow band laser excitation only (cf Fig.1). As detailed recently [9], from the

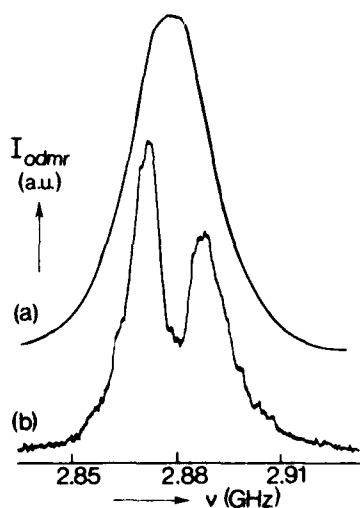


Fig.1. Phase-sensitively detected ODMR of the N-V center under conditions of (a) broad-band excitation at 514 nm, (b) narrow-band excitation at 637.8 nm. Fluorescence detection is at 660 nm.  $T = 1.4$  K.

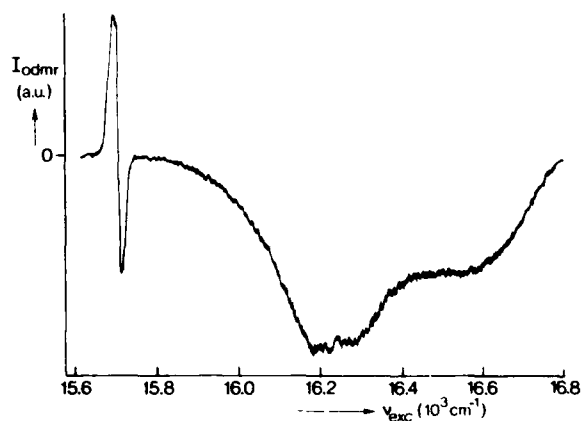


Fig.2. Double resonance excitation spectrum of the N-V center, when the microwave frequency is 2880 MHz. Fluorescence detection is at 660 nm.  $T = 1.4$  K.

anisotropic behavior of the splitting in the presence of an externally applied magnetic field, it could be proved that the splitting reveals a lifting of the local axial symmetry ( $E \neq 0$ ). The magnitude of the  $E$ -splitting appeared to change linearly with the excitation energy:  $\delta|E|/\delta\epsilon = 5.0 \cdot 10^3$  MHz, where  $\epsilon$  is the strain. The excitation wavelength dependence of the 2880 MHz zero-field ODMR signal is displayed in Fig.2. Remark that the ZPL now consists of positive and a negative part and a microwave-induced hole in between. Evidently, the narrow-band excitation experiments allow for the photo-selection of subensembles for which the  $E$ -splitting in the ODMR spectrum is not masked by inhomogeneous broadening effects arising from random strain (this strain being responsible for a continuous spread in the value of the fine structure  $E$  parameter). Note that this result at first sight seems to suggest that N-V centers having the same optical transition energy also seem to have preferred  $E$ -splittings or, equivalently, the  $E$ -splitting and the optical transition energy seem to be correlated. Such a result would be in favour of the model put forward by Selzer [1] and is never anticipated according to the model of Lee et al [2] (which is based on a multi-level system consisting of completely uncorrelated energies). However, it should be emphasized that the subset of N-V centers preselected by the laser, and which is further interrogated by means of ODMR, does not give rise to a line-narrowing effect in ODMR in proportion with the laser frequency line width. On the contrary, the inhomogeneous line width of the  $E$ -split ODMR transitions invariably differs by only a factor of about three from the ODMR line width obtained under broad band excitation (10 MHz versus 30 MHz), even if the laser frequency width is diminished to a few MHz. Thus, despite the photo-selection which allows the observation of an  $E$ -splitting, a significant inhomogeneous broadening effect still remains. This result qualitatively fits in the model, advanced by Laird and Skinner [3], implying that correlations between the absolute energies of the probed molecules can be obtained starting from a microscopic model.

Optically detected spin echo decays under the condition of cw narrow-band optical excitation of the N-V centers were also measured [6]. The observed transients fitted a mono-exponential decay, the

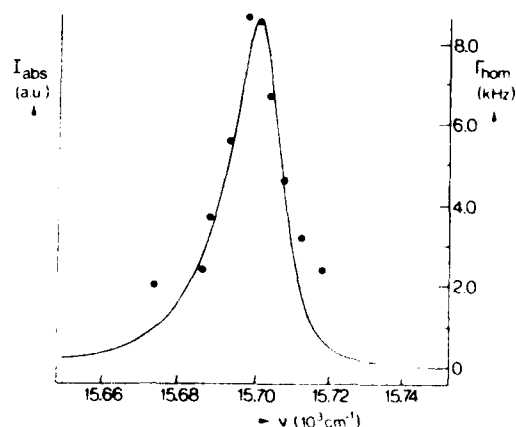


Fig.3. ZPL absorption of the N-V center in diamond (solid curve). Dots represent homogeneous line width,  $\Gamma$ , as determined from optically detected spin echo decay measurements at  $T = 1.4$  K.

characteristic phase memory time being strongly dependent on the excitation wavelength of the laser. In Fig.3 we plot the experimental homogeneous line width  $\Gamma$  ( $= 1/\pi T$ ) as a function of the laser energy used to optically excite the defect. The ZPL observed in the optical absorption spectrum is included in the figure. Clearly, the variation of the spin dephasing rate constant as a function of the excitation energy follows the shape of the ZPL. Recently, it has been shown that for the diamond N-V centers the irreversible spin dephasing is due to a magnetic dipolar induced cross-relaxation among resonant N-V centers [6,7]. The random crystal strain will cause an inhomogeneous spread in the zero-phonon optical transition energy and the ODMR transition energy. Optical excitation within the ZPL of a subset of defects will produce in ODMR the response of a preselected subset (see above) and in the spin echo decay experiment its characteristic dephasing behavior. The latter will be strongly dependent on the spacing between resonant N-V centers. On the other hand, experimentally we find that the dephasing rate, and thus the intercenter spacing, follows the strain distribution profile. Put in other words, the concentration of defects is highest in strain fields that are most probable. It follows that the average distance of resonant N-V centers is larger than the typical correlation length of the strain field and the results of the spin dephasing measurements therefore provide evidence for the presence of microscopic strain in the crystal [10]. The observed variation of the optically detected spin dephasing rate with the excitation energy is the spin analogue of the frequency-dependent dephasing rates reported for a number of optical transitions [11-13].

## References

1. P.M. Selzer, in: Laser Spectroscopy of Solids, eds. W.M. Yen and P.M. Selzer (Springer, Berlin, 1981).
2. H.W.H. Lee, C.A. Walsh, and M.D. Fayer, J.Chem.Phys. 82, 3948 (1985).
3. B.B. Laird and J.L. Skinner, J.Chem.Phys. 90, 3880 (1990).
4. G. Davies and M.F. Hamer, Proc.R.Soc.London SerA 348, 285 (1976).
5. E. van Oort, N.B. Manson, and M. Glasbeek, J.Phys.C 21, 4385 (1988).
6. E. van Oort and M. Glasbeek, Phys.Rev.B 40, 6509 (1989).
7. E. van Oort and M. Glasbeek, Chem.Phys. 143, 131 (1990).
8. M. Glasbeek and R. Hond, Phys.Rev.B 23, 4220 (1981).
9. E. van Oort, B. van der Kamp, R.Sitters, and M. Glasbeek, J.Lumin. 48/49, 803 (1991).
10. L. Root and J.L. Skinner, J.Chem.Phys. 81, 5310 (1984) ; *ibid*, Phys.Rev.B 32, 4111 (1985).
11. R.M. Macfarlane and R.M. Shelby, Opt.Comm. 39, 169 (1981).
12. R.M. Shelby and R.M. Macfarlane, Phys.Rev.Lett. 45, 1098 (1980).
13. G.K. Liu, R.L. Cone, M.F. Joubert, B. Jacquier, and J.L. Skinner, J.Lumin. 45, 387 (1990).

## Hole-Burning of Dye-Molecules Adsorbed on Metal Oxide Powders

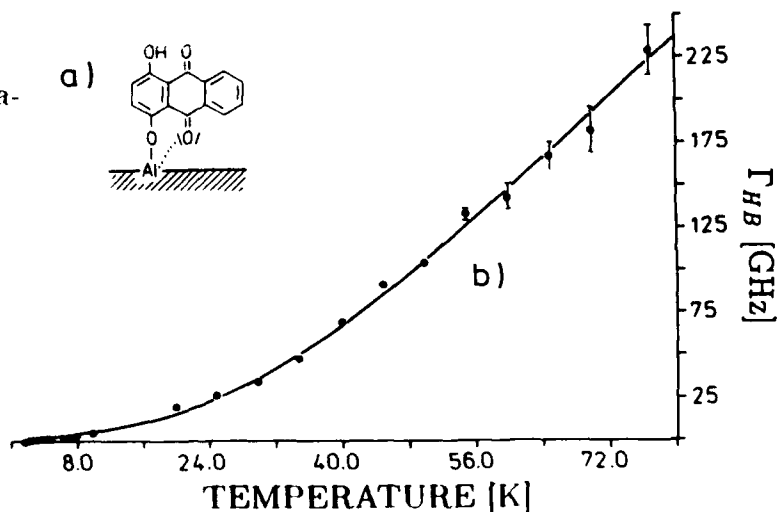
Th. Basché and C. Bräuchle  
 Institut für Physikalische Chemie, Universität München  
 Sophienstraße 11, (Tel.: 089 - 5902 301)  
 8000 München 2, Germany

First preliminary persistent spectral hole-burning (PSHB) investigations of dye-molecules adsorbed onto the disordered surfaces of metal oxide powders or porous glasses<sup>1,2,3</sup> indicated that these systems seem to behave quite similar to doped glasses. The optical absorption is strongly inhomogeneously broadened due to the disorder of the surface and at 1.5 K holewidths in the  $1 \text{ cm}^{-1}$  range - even an order of magnitude broader than in glasses - have been reported. In the following we will give a short summary of our latest more detailed investigations of surface adsorbed dye-molecules which on the one hand reaffirm that these systems indeed behave in many respects as 3-D disordered systems but on the other hand point to some remarkable specific features of adsorbed dye-molecules.

A comparison of the holewidth  $\Gamma_{\text{hole}}$  of two systems differing in the type of bonding to the surface, Cresyl Violet (CV) physisorbed to  $\gamma$ -alumina and Quinizarin (Q) chemisorbed to  $\gamma$ -alumina (see Fig.1.a for the proposed adsorption model), suggest that  $\Gamma_{\text{hole}}$  of surface adsorbed molecules may be connected with the strength of the chemical bond between the dye-molecule and the adsorbens.  $\Gamma_{\text{hole}}$  for CV/ $\gamma$ -alumina ( $0.85 \text{ cm}^{-1}$ ) was found to be the same order of magnitude as for other physisorbed molecules but appreciably broader than for Q/ $\gamma$ -alumina ( $0.035 \text{ cm}^{-1}$ ). One possible explanation for this phenomenon relies on the assumption that physisorbed molecules have a higher mobility on the surface and therefore tend to increased spectral diffusion. Alternatively, physisorbed molecules may occupy a wider range of local environments and sample a broader distribution of TLS's (two-level tunneling systems) leading to wider spectral holes.

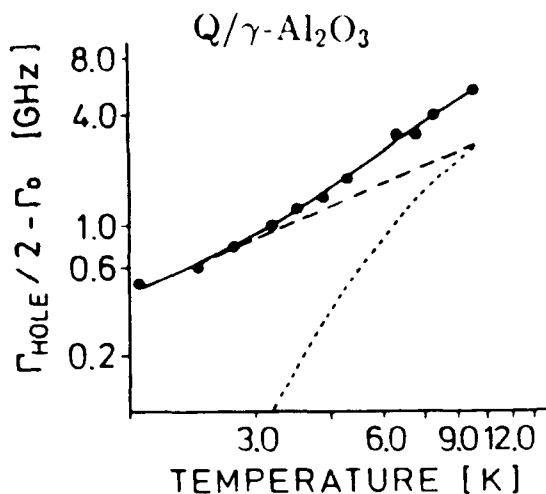
The existence of surface TLS mentioned above is evidenced by the temperature dependence of the hole-burning linewidth  $\Gamma_{\text{HB}} = \Gamma_{\text{hole}}/2 + \Gamma_0$  which was measured for Q/ $\gamma$ -alumina. The phrase hole-burning linewidth ( $\Gamma_{\text{hole}}$ ) refers to the possibility that spectral diffusion may contribute to  $\Gamma_{\text{hole}}$ <sup>4</sup>. In Fig.1.b  $\Gamma_{\text{HB}}$  is given between 1.6 and 77 K.

**Figure 1.** a) Binding model of quinizarin adsorbed to the surface of  $\gamma$ -alumina. b) Hole-burning linewidth  $\Gamma_{\text{HB}}$  of Q/ $\gamma$ -alumina as a function of temperature. Solid line: Fit to Eq.2.



For the moment we will concentrate on the  $T$  range between 1.6 and 10 K which is given enlarged in Fig.2. With regard to the inherent disorder of the  $\gamma$ -alumina surface we fitted the

**Figure 2.**  
Log-log plot of  $\Gamma_{\text{HB}}$  of  $Q/\gamma$ -alumina between 1.6 and 10 K. The solid line is the best non-linear least squares fit of the experimental data to Eq.2. The dashed lines are the  $T^\alpha$  contribution (---) and the exp. activated contribution (- - -) of the fit to Eq.2.



low temperature data to empirical model functions successfully used to describe 3-D glassy systems. First  $\Gamma_{\text{HB}}$  was fitted to the well known algebraic power law given in Eq.1

$$\Gamma_{\text{HB}} = a T^\alpha \quad (1)$$

which yields  $\alpha = 1.3$  in many organic and inorganic systems and which is explained by the assumption that the low energy excitations specific of amorphous materials (TLS) dominate the excited chromophores' dynamics at low temperatures. From the best fit to the experimental data we derived  $\alpha = 1.5$ . The data can be slightly better approximated by Eq.2

$$\Gamma_{\text{HB}} = a T^\alpha + b \exp(-\Delta E/kT) \quad (2)$$

as was seen in a statistical analysis ( $\chi^2$  test) of the data. This model function which was introduced by Jackson and Silbey<sup>5</sup> describes the dephasing by two processes whereby the exponential activated contribution is attributed to coupling of the electronic excitation to librational modes of the chromophore or pseudolocal glass modes. The best fit to Eq.2 yields  $\alpha = 1$  and  $\Delta E = 12 \text{ cm}^{-1}$ . The corresponding fit function is shown in Fig.2 where also the two contributions of Eq.2 are drawn separately. Independent of the actual correct approximation (Eq.1 or 2) this investigation clearly shows that a slowly varying  $T$  dependence has to be included in the fitting model to account for the observed glasslike dynamics at low temperatures. Neglecting contributions from the bulk, it is reasonable to assume that surface TLS in  $\gamma$ -alumina are connected with the wide distribution of OH groups known to exist on the surface.

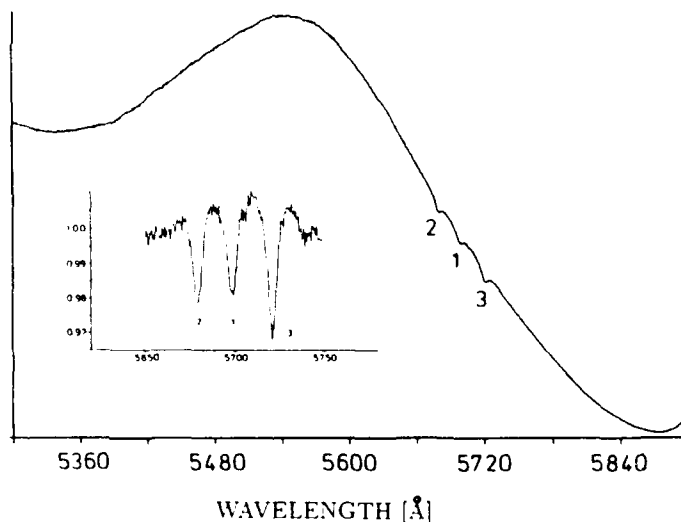
As is seen in Fig.1.b it was possible to burn stable holes even at  $T \geq 77\text{K}$  in  $Q/\gamma$ -alumina. Burning of stable holes at liquid nitrogen temperatures, which may be of interest for frequency domain optical storage applications<sup>6</sup> without the technological limitations connected with storage at  $T \leq 4.2 \text{ K}$ , seems to be a common feature for dye-molecules adsorbed on metal oxide powders as it was also observed for all other systems

studied as e.g. CV/ $\gamma$ -alumina or Oxazine 170/Silica 60. This is in contrast to polymeric host-guest systems where high-T hole burning is only observed with specific guest molecules as substituted porphyrins or phthalocyanins<sup>7</sup> and e.g. not with CV or Q.

To burn and detect stable holes at  $T \geq 77$  K several criteria must be met. The ratio of the inhomogeneous to the homogeneous linewidth should be  $\gg 1$  and therefore, as the inhomogeneous width is nearly independent of temperature between 1.6 and 77 K,  $\Gamma_{\text{hole}}(77 \text{ K})$  should be small compared to  $\Gamma_{\text{inhom}}$ . Furthermore, as a very important parameter the linear electron-phonon coupling as well as its temperature dependence should be weak.

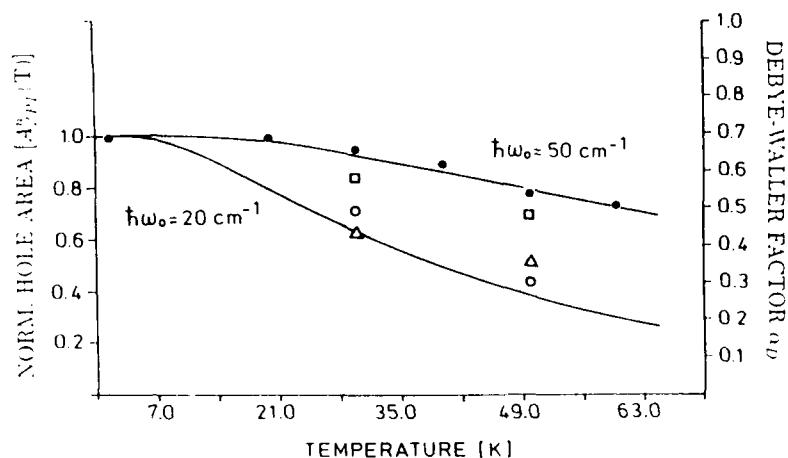
In Fig.1.b the result of a fit of  $\Gamma_{\text{inh}}$  between 1.6 and 77 K to the model function in Eq.2 is given. Hereby  $\alpha$  was fixed to 1.5 and  $\Delta E$  to  $87 \text{ cm}^{-1}$ . The latter value corresponds to the energy of a weak low frequency mode seen in the line narrowed fluorescence spectrum of Q/ $\gamma$ -alumina. The result suggests that at  $T \approx 30$  K an activated process induced by a low frequency adsorbate mode begins to contribute to the dephasing. In the low power limit  $\Gamma_{\text{hole}}$  was measured to be  $15 \text{ cm}^{-1}$  at 77 K. The multiplexing factor  $m$  [ $m = \Gamma_{\text{inhom}} / \Gamma_{\text{hole}}(T)$ ] is an important parameter with regard to frequency domain optical storage. With  $\Gamma_{\text{inhom}} = 1000 \text{ cm}^{-1}$  and  $\Gamma_{\text{hole}}(77\text{K}) = 15 \text{ cm}^{-1}$  we obtained  $m = 67$  which is inevitably several orders of magnitude lower than at 1.6 K but to our knowledge higher than in other systems at 77 K. In Fig.3 a fluorescence excitation spectrum of Q/ $\gamma$ -alumina is shown with three holes burnt at 77 K. As the electron-phonon coupling is weak even at 77 K, the zero-phonon (ZPL) holes are not mutually influenced by their phonon sidebands (PSB).

**Figure 3.** Fluorescence excitation spectrum of Q/ $\gamma$ -alumina between 5300 and 5900 Å with three spectral holes burnt and recorded at 77 K (Burning conditions:  $P = 12 \text{ mW/cm}^2$ ,  $t = 500 \text{ s}$ ). The inset shows an enlarged part of the spectrum.



The temperature dependence of the Debye-Waller factor  $\alpha_D(T)$  was determined by burning a deep hole at high temperatures (65 K) and measuring the area of the ZPL hole at lower temperatures down to 1.6 K. By lowering the temperature, intensity is redistributed from the PSB band to the ZPL thus leading to an increase of the ZPL hole area which is proportional to  $\alpha_D(T)$  at a given temperature. In Fig.4. the normalized hole area  $A_{\text{ZPL}}^0$  of Q/ $\gamma$ -alumina as

**Figure 4.** Normalized hole-area  $A_{PH}^n$  and Debye-Waller factor  $\alpha_D$  of Q/ $\gamma$ -alumina ( $\bullet$ ) as a function of temperature. The solid lines are calculated by Eq.3 using the indicated values of  $\hbar\omega_0$  and  $S = 0.37$ . Also given are data points of different porphyrin/polymer systems according to ref.7.



a function of temperature is shown. With an estimated  $\alpha_D(1.6 \text{ K}) = 0.7$  the data points can also be scaled with regard to  $\alpha_D(T)$ . Also given in Fig.4 is a curve calculated from Eq.3 which holds if only one low energy mode (phonon) dominates the linear electron-phonon coupling.

$$\alpha_D(T) = \exp[-S \coth(\hbar\omega_0/2kT)] \quad (3)$$

$S(0.37)$  is the Huang-Rhys factor and  $\hbar\omega_0$  was set to  $50 \text{ cm}^{-1}$  corresponding to the energy difference between the peaks of the ZPL- and the PSB hole. Whereas  $S$  lies in a typical range of systems with weak linear electron-phonon coupling, the phonon sideband frequency  $\hbar\omega_0$  is much higher than in polymer systems (Fig.4), leading to a weaker temperature dependence of  $\alpha_D$ . The importance of  $\hbar\omega_0$  is demonstrated by the curve calculated with the same  $S$  as above but  $\hbar\omega_0 = 20 \text{ cm}^{-1}$  which is typical value found in polymer matrices. The data points ( $\square$ ) in Fig.4 are probably due to a smaller  $S$  in this particular system.

Summarizing, we have shown that the structural disorder of the surface of metal oxide powders as  $\gamma$ -alumina is reflected in the dynamics of adsorbed probe molecules at low temperatures. The results indicate a generally weak linear electron-phonon coupling for adsorbed molecules which allows PSIIB at  $T \geq 77 \text{ K}$ .

1. U. Bogner, P. Schätz and M. Maier, *Chem. Phys. Lett.* **119**, 335 (1985).
2. Th. Basché and C. Bräuchle, *J. Phys. Chem.* **92**, 5069 (1988).
3. P. J. van der Zaag, Th. Schmidt, H. van der Laan, A. Visser and S. Völker, *Mol. Cryst. Liq. Cryst.* **183**, 105 (1990).
4. L. R. Narasimhan, K. A. Littau, D. W. Pack, Y. S. Bai, A. Elschner and M. D. Fayer, *Chem. Rev.* **90**, 439 (1990).
5. B. Jackson and R. Silbey, *Chem. Phys. Lett.* **99**, 331 (1983).
6. W. E. Moerner, W. Lenth and G. C. Bjorklund, in *Persistent Spectral Hole Burning: Science and Applications*, Ed.: W. E. Moerner, (Springer, Berlin 1988)
7. A. Furusawa, K. Horie, T. Suzuki, S. Machida and I. Mita, *Appl. Phys. Lett.* **57**, 141 (1990).
8. M. H. L. Pryce, in *Phonons in Perfect Lattices and in Lattices with Point Imperfections*, Ed.: R. W. Stevenson, (Oliver and Boyd, Edinburgh 1966).

## FLUORESCENCE EXCITATION OF SINGLE MOLECULES

M. Orrit and J. Bernard

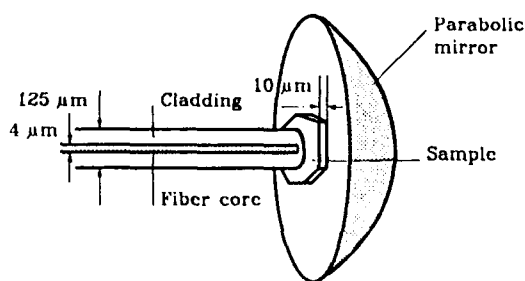
Centre de Physique Moléculaire Optique et Hertzienne  
C.N.R.S. et Université de Bordeaux I  
351, Cours de la Libération, 33405 Talence, France  
(Tel. 56 84 62 09 ; Fax 56 84 69 70)

A few years ago, many people would have deemed the optical observation of single molecules nearly impossible. Yet, new experiments at room [1] and at liquid helium temperatures [2,3] have started to remove this psychological barrier. Several applications to trace detection and sensing, to spectroscopy of localized neighborhoods and to optical addressing of local spots in solids may now be envisioned. The purpose of this presentation is to show that single molecules can be studied at helium temperatures by means of a fairly simple setup, at least in the very favorable case of pentacene in terphenyl crystal. We thus hope to stimulate further work either on this model system or on more difficult ones with more sophisticated detection methods.

The main difficulties in dealing with single molecules arise from the weakness of the signal. During the long accumulation times, the molecular resonance frequency must be fixed : As hole burning and spectral diffusion will interrupt the accumulation, the host-guest couple should be chosen so that both processes are minimal.

In the first single molecule detection experiments [1], Moerner and Kador measured the absorption signal of a single pentacene molecule in a p-terphenyl crystal directly. However, the relative absorption signal as given by the ratio of molecular cross-section to beam section was in the range  $10^{-3}$ - $10^{-4}$ , and strong photon noise from the necessarily weak probing beam limited the signal-to-noise ratio, even with the highly sensitive difference method they used. This situation can change in next years with the advent of squeezed light and twin-photon sources [4]. In our study of the same host-guest couple, we used the fluorescence of pentacene. If the illuminated volume is small enough, a single molecule's emission dominates Raman scattering and residual

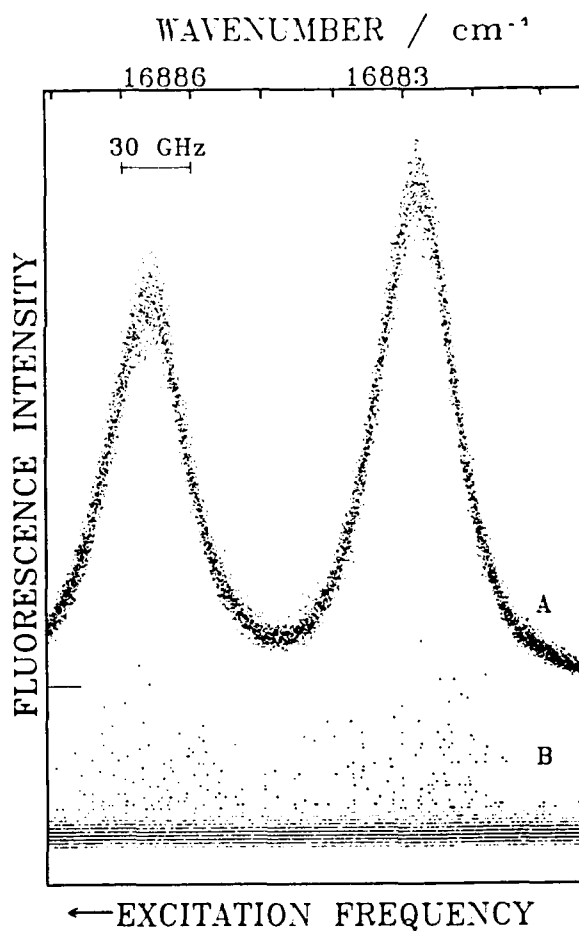
*Figure 1 : Schematic diagram of the sample crystal at the end of a single-mode optical fiber. The fluorescence from the small excited volume is collected by the parabolic mirror and reflected to the photodetector.*



fluorescence from the host crystal. The selection of a small volume of crystal was achieved by means of a single-mode optical fiber to the tip of which a sublimation-grown crystal was contacted. The excited volume was about  $200 \mu\text{m}^3$ , which amounted to a few hundreds of pentacene molecules at the low concentration used ( $10^{-9}$  mol/mol). The fluorescence was collected by a large-aperture parabolic mirror inside the cryostat (see figure 1) and focused on the photomultiplier tube through a red-pass cutoff filter.

The fluorescence excitation spectrum of our sample is shown on Fig.2B in the region of sites  $O_1$  and  $O_2$  [5]. The spectrum is compared to that of a larger, macroscopic crystal (a few  $\text{mm}^3$ , with a concentration of about  $10^{-6}$  mol/mol, on Fig.2A). The nearly Gaussian bands of Fig.2A resolve into sharp peaks of individual pentacene molecules, seen as dots on Fig.2B. The

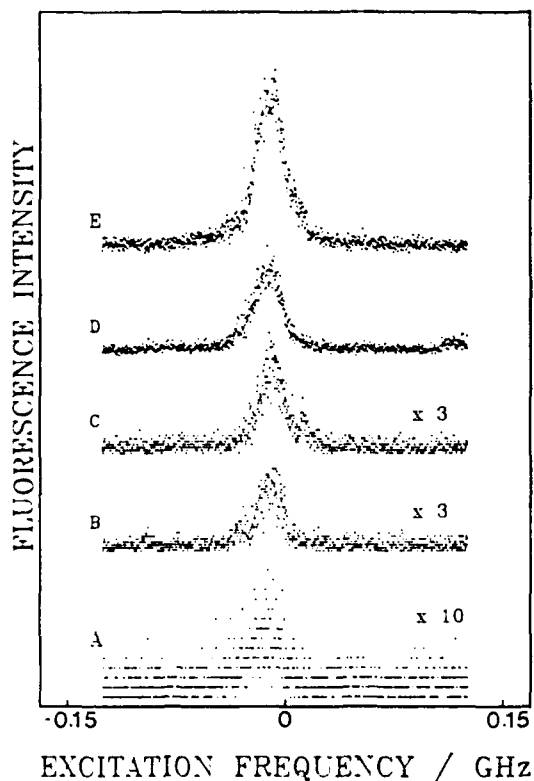
*Figure 2 : Fluorescence excitation spectra of two different samples of p-terphenyl crystal doped with the absorbing impurity pentacene. Spectrum A from a comparatively large crystal (a few  $\text{mm}^3$ ) displays the broad inhomogeneous bands  $O_1$  and  $O_2$ , corresponding to the many possible environments of individual molecules. Spectrum B is from our small sample (see Fig.1). Well above the weak background from dark counts and residual emission, about a hundred dots appear at frequencies scattered over the inhomogeneous profile : due to the limited number of molecules sampled, only a few environments are represented. The dots, which are not resolved at the frequency scale of the figure, are the resonance lines of single pentacene molecules, as shown on Fig.3. Different peak intensities may be due to different positions within the Gaussian exciting beam.*



signal/noise ratio is sufficient to measure the Lorentzian profile and the width of the resonances. The distribution, intensity, shape and width of these peaks are consistent with their attribution to single molecules. However, this may be proven definitely by looking at the time-correlation properties of the emitted light. Due to transitions from the excited singlet to the metastable triplet state, the fluorescence signal is interrupted by dark periods, when the molecule is in the triplet state. The resulting photon bunching causes the correlation function of the fluorescence to decay exponentially : taking into account the triplet lifetime of pentacene in this system ( $40 \mu\text{s}$  [5]), the observed correlation is compatible only with a single molecule [3].

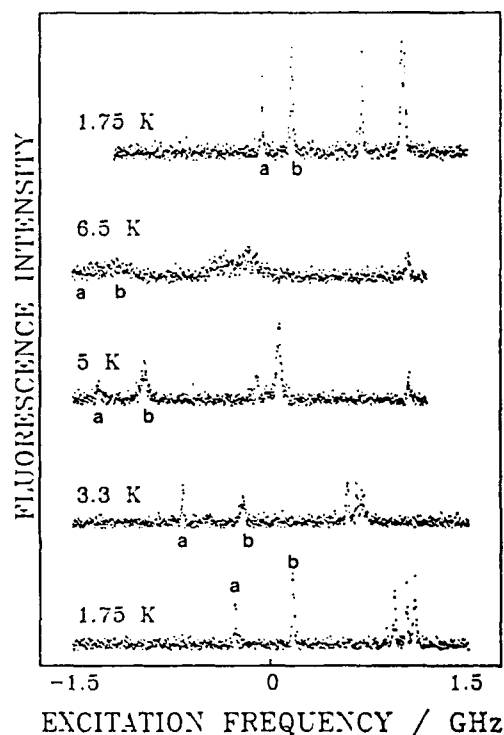
The measured widths of single molecule peaks ranged from 10 to 20 MHz. Figure 3 shows the shape of one of the broader peaks as a function of the exciting power, from  $70 \mu\text{W}/\text{cm}^2$  (bottom) to  $3 \text{ mW}/\text{cm}^2$  (top): extrapolation to zero power yields a width of more than 20 MHz. More recently, Moerner and Ambrose [6,7] found a much lower width of 7.8 MHz, compatible with the homogeneous width deduced from photon echoes measurements [5]. We tentatively attribute the discrepancy to additional broadening of the resonance of our molecule, probably by spectral diffusion processes such as those investigated in [6] : spectral diffusion can be much stronger in our contacted sample due to cooling-induced defects than in the unsupported samples of [6,7], where the inhomogeneous broadening is much less.

*Figure 3 : Shape of a single molecule's excitation line as a function of the exciting power (from bottom to top, approximately 70, 300, 700, 1500, 3000  $\mu\text{W}/\text{cm}^2$ ). The lowest spectra are magnified for the sake of comparison. Since the light power is rather weak, the triplet is not saturated and the width (about 20 MHz) is nearly independent of the power, while the peak height still increases with power. The homogeneous width expected from photon echoes would be 8 MHz. The difference could arise from spontaneous (spectral diffusion) or photo-induced motion in the molecule's remote surroundings.*



Single molecule peaks can be studied as the temperature changes, as shown on Fig.4. Around 4 K, the activation of librations [8] starts to broaden the peaks considerably, but even below this temperature, different behaviors may be observed on different molecules as Figure 4 shows : here the line labelled "b" broadens between 1.8 K and 3.5 K while line "a" remains narrow. It is fair to assume that defects in the local surroundings of molecules "a" and "b" are activated differently as the temperature is raised. Other possible behaviors will be discussed in the presentation.

*Figure 4 : Temperature dependence of the excitation peaks of a few molecules. The sample underwent a thermal cycle lasting some 20 minutes (from bottom to top), while spectra were recorded at different temperatures. The general shift of all structures is a pressure effect. Between 1.75 K and 3.3 K, line b is seen to broaden, whereas the lines of the other molecules remain narrow. Moreover, the relative positions of lines a and b have changed after the cycle, which is an evidence of activated spectral diffusion.*



#### References

- [1] E Brooks Shera, N.K. Seitzinger, L. M. Davis, R. A. Keller and S. A. Soper, Chem. Phys. Lett. 174 (1990) 553.
- [2] W.E. Moerner and L. Kador, Phys. Rev. Lett. 62 (1989) 2535
- [3] M. Orrit and J. Bernard, Phys. Rev. Lett. 65 (1990) 2716.
- [4] A. Heidmann, R. J. Horowicz, S. Reynaud, E. Giacobino and C. Fabre, Phys. Rev. Lett. 59 (1987) 2555.
- [5] H. de Vries and D. A. Wiersma, J. Chem. Phys. 69 (1978) 897.
- [6] W. P. Ambrose and W. E. Moerner, Nature 349 (1991) 225.
- [7] W. E. Moerner and W. P. Ambrose, Phys. Rev. Lett. 66 (1991) 1376.
- [8] T. E. Orlovski and A. H. Zewail, J. Chem. Phys. 70 (1979) 1390 (see p.1413).

## OBSERVATION OF SPECTRAL DIFFUSION IN SOLIDS USING A SINGLE MOLECULE

W. P. Ambrose,\* T. Basche' and W. E. Moerner

IBM Research division, Almaden Research Center, K95/801, 650 Harry Rd,  
San Jose, CA 95120 Phone: (408) 927-2426

Recent advances in high-efficiency fluorescence excitation spectroscopy of pentacene in p-terphenyl crystals<sup>1-3</sup> have improved the signal to noise ratio for the detection of single pentacene defects, thus confirming single pentacene detection using absorption techniques.<sup>4</sup> Using 1-10  $\mu\text{m}$  thick crystals, tightly focused laser beams, and high collection efficiency, background emission noise is significantly reduced below the fluorescence emission rate of single pentacene defects. To observe single molecules, the laser is tuned out into the wings of the pentacene  $O_1$  site inhomogeneous line until the number of defects per homogeneous linewidth is less than 1. With the improved detection sensitivity, we have observed two classes of pentacene defects present in both the red and blue wings of the inhomogeneous line: class I consist of stable, time-independent defects with lifetime limited homogeneous linewidths below 4 K, and class II have time varying resonance frequencies.

Figure 1 shows a time sequence of excitation spectra, which were obtained in a fixed laser focal spot. The spectra contain three time-independent class I peaks, which form stable ridges along the time axis near -130, -70, and +10 MHz. In the 0 to 150 MHz region is a single class II defect whose frequency varies from one scan to the next. Indeed, this same molecule can appear several times in the same 2 min laser scan, or almost not at all. Notice that in the same  $\sim 50 \mu\text{m}^3$  volume of crystal and at nearly the same frequency there are both class I defects as well as spectrally migrating class II defects. We broadly use the term "spectral diffusion" to refer to the changes in resonant frequency that occur as a function of time for class II single pentacene defects.

When the laser frequency is held constant near a time varying defect, the detected fluorescence turns on and off discontinuously as the molecule spectrally jumps into and out of resonance with the fixed laser frequency. Figure 2 shows that when the excitation power level is varied at a fixed frequency, the rate of spectral jumps does not appear to be influenced. The mean times between jumps in Fig. 2 (a) and (b) of 80 and 61 seconds do not decrease by the factor of 5.3 increase in the fluorescence excitation rate. Hence, the spectral jump rate does not appear to be influenced by the optical excitation rate and thus cannot be regarded as a light-induced process that can produce spectral hole burning. The change in resonant frequency for class II defects appears to be a spontaneous process at low temperatures.

The absence of fluorescence in Fig. 2 only means that the defect is not absorbing at the laser frequency. To follow the shifts in resonance frequency directly, we scanned the laser frequency more rapidly in order to measure the spectral position of the defect at 1 to 3 second intervals. A digital waveform recorder locates the peak in each scan and records this resonance frequency as a function of time, as in Fig. 3. Figure 3 (a) shows how the resonance frequency of a spectrally jumping class II defect evolves with time at a fixed temperature of 4.18 K. The optical transition energy appears to

have a preferred set of values and performs spectral jumps between these values that are discontinuous on the 2.7 second time scale of the measurement in Fig. 3.

One important physical measurement that would help to identify the source of the spectral diffusion effect would be temperature dependence of the jump rate. Pieces of the 4.18 K data in Fig. 3 (a) are expanded in Fig. 3 (b) and (c) for comparison with the shorter trend at a higher temperature of 5.77 K (Fig. 3 (d)). For this single defect, the residence time between the largest jumps is 80 seconds at 4.18 K, and 40 seconds at 5.77 K. This defect was confined to a 300 MHz range for over 5000 seconds at 4.18 K. At 5.77 K the spectral range initially expanded to 400 MHz, and after the 800 second time interval shown in Fig. 3 (d), this defect began to diffuse rapidly outside this range to lower frequencies, and became confused with other single molecules.

The results for both class I and class II defects does not support the observation of spectral hole-burning. One is thus led to consider what might have been the source of spectral hole burning observed during the earlier study of statistical fine structure (SFS) for pentacene in p-terphenyl.<sup>5</sup> The SFS studies utilized the powerful absorption technique of FM spectroscopy to observe the small spectral variations near the center of the inhomogeneous line on a zero background. In fact, the size of the observed spectral holes even after extended irradiation were on the order of 1 part in 1000 of the total absorption. One interpretation of this result is that of all the pentacene molecules with center frequencies within one homogeneous linewidth of the laser frequency, only 0.1 % had a photoinduced pathway leading to changes in resonance frequency.

If it is correct that only 0.1 % of all molecules can participate in hole-burning, then in the single molecule regime one might expect on average to find a molecule capable of light induced resonant frequency changes for only one in 1000 molecules, and to date, only several hundred single molecules have been studied in detail. It is therefore quite possible that specific single molecules will be found that clearly undergo photoinduced spectral changes. It will be most interesting to perform detailed studies of the local environment around such molecules using Stark, stress, Zeeman, and other perturbations to determine the symmetry and interactions that lead to spectral hole formation.

In contrast to the scarcity of single molecules able to undergo hole-burning, the appearance of single molecules of pentacene in p-terphenyl which spontaneously change resonant frequency with time is much more common. This surprising observation of spectral jumping may be analogous to spectral diffusion processes that play a crucial role in the physics of glasses and other amorphous materials. Here, the single-molecule technique allows the spectral changes to be followed in real time for only one center, without any averaging over an inhomogeneous distribution that may obscure the effect. The spectral changes take many forms, from discontinuous jumping, to quasi-continuous wandering, to creeping towards line center in small discontinuous jumps. Also, the fraction of spectrally diffusing molecules clearly increases with distance from the center of the inhomogeneous line. Thus, the occurrence of class II defects appears to be associated with sites that have some degree of local disorder so that the local strain or electric field is far from the equilibrium value.

Since the resonance frequency of a single molecule in a solid is extremely sensitive to the local strain (and other local fields) at the position of the molecule, the

spectral jumps may occur because the class II pentacene molecules are coupled to an (unidentified at present) set of degrees of freedom in the nearby host crystal that are excited at 1.5 K. Further, these degrees of freedom interact with phonons, as evidenced by the increase in jumping rate and range at higher temperatures. Unfortunately, the diversity of behavior observed has made a detailed determination of the temperature dependence of questionable value at this time.

Possible sources for the class II behavior should reflect the fact that it is connected with disorder in the crystal. One possible source for the effect could be librational tunneling of the central phenyl ring of the nearby p-terphenyl molecules about the p-terphenyl molecular axis. The spectral diffusing effects reported here may therefore result from discrete librational motions of the central phenyl ring of p-terphenyl driven by phonon assisted tunneling in an asymmetric double well potential that has become allowed due to the local disorder. Migration of He atoms, vacancies or anharmonic local modes may also occur in the disordered regions of the crystal.

### REFERENCES

- \* Present address Los Alamos National Laboratory, M888, Los Alamos, NM 87545  
Phone: (505) 665-2092
- 1. M. Orrit and J. Bernard, Phys. Rev. Lett. **65**, 2716 (1990).
- 2. W. P. Ambrose and W. E. Moerner, Nature **349**, 225 (1991).
- 3. W. E. Moerner and W. P. Ambrose, Phys. Rev. Lett. **66**, 1376 (1991).
- 4. W. E. Moerner and L. Kador, Phys. Rev. Lett. **62**, 2535 (1989).
- 5. W. E. Moerner and T. P. Carter, Phys. Rev. Lett. **59**, 2705 (1987).

### FIGURES

Figure 1. Single pentacene defect fluorescence excitation spectra time dependence. Upper half: wire plot of individual spectra, lower half: contour plot of same data obtained with 2 min per spectrum, laser power 1.5 nW, and 0 MHz detuning = 592.539 nm. The appearance of class I defects at negative detuning and class II defects at positive detunings has no significance.

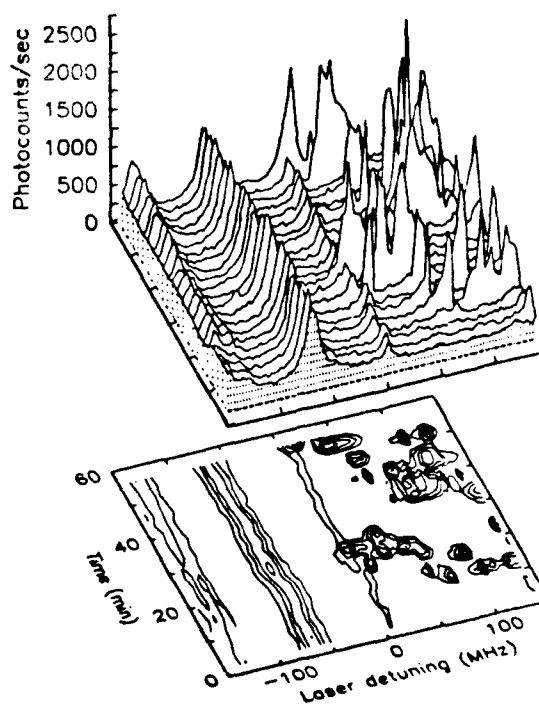


Figure 2. Spectral jump rate power independence. Spectral jumps are observed in the fluorescence signal of a single pentacene defect with a fixed wavelength of 592.362 nm at laser powers of (a) 0.89 nW and (b) 36 nW. The single molecule emission rate increases by a factor of 5.3 (the (b) ordinate is increased by a factor of 5.3 for comparison) for the factor of 40 increase in excitation power; however, the jump rate is qualitatively unchanged.

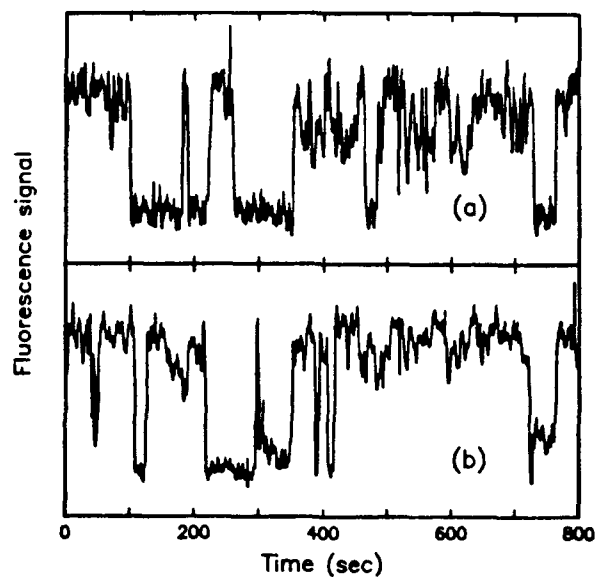
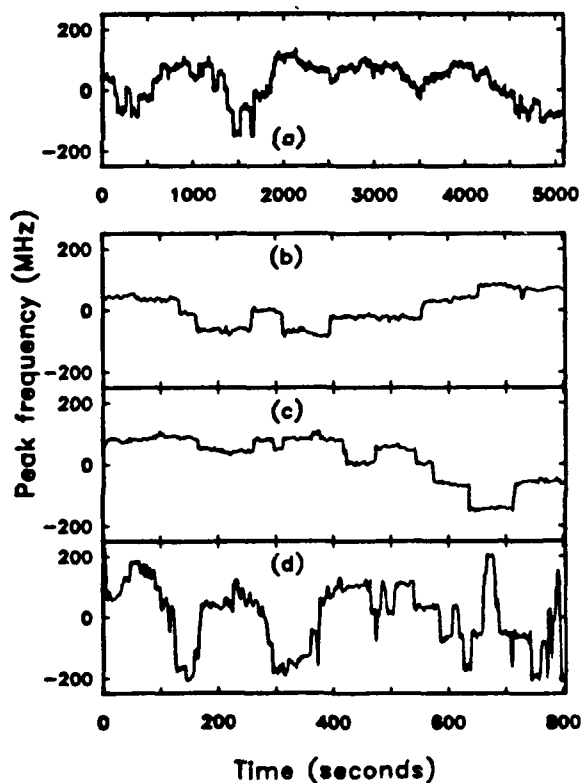


Figure 3. Qualitative increase in spectral jump rate with temperature. Peak-frequency trends for a single class II pentacene defect near 592.410 nm wavelength at a temperature of  $4.18 \pm 0.04$  K ((a), (b), and (c)), and at a higher temperature of  $5.77 \pm 0.02$  K (d). (b) and (c) are the 0 to 800 second and 800 to 1600 second sections of the data in (a) expanded for comparison with the 0 to 800 second data at 5.77 K in (d). Note that the jump rate for the largest jumps at 5.77 K in (d) is nearly twice the jump rate at 4.18 K in (b) and (c).









**A**damec, F. — ThE2, FE1  
 Al'shits, E. I. — FE2, FE10  
 Ambrose, W. P. — SB5  
 Ambroz, M. — ThE2, FE1  
 Andrejco, M. J. — FB5  
 Arnold, Steven — FA1, FA2  
 Attenberger, T. — FE9

**B**aozhu, Luo — FA7  
 Basché, Thomas — SB3, SB5  
 Bernard, J. — SB4  
 Bernet, Stefan — ThC3, ThC4  
 Bill, H. — FA4  
 Billmers, R. — ThE13  
 Bogner, Uo — FE9  
 Bräuchle, C. — SB3  
 Brynda, E. — FE1  
 Byer, R. L. — ThE5

**C**hase, E. W. — FB5  
 Chronister, Eric L. — ThA5  
 Croci, Mauro — ThE12  
 Crowell, Robert A. — ThA5

**D**a Silva, V. L. — FB5  
 Davis, J. — ThE13  
 Débarre, A. — FB3  
 Dennis, W. M. — FC3  
 DiMagno, T. J. — FE5  
 Dian, J. — ThE2, FE1  
 Dongxiang, Zhang — ThE6  
 Duoyan, Wang — ThE6, FE12

**F**ayer, Michael — ThA2, SA  
 Feinberg, Jack — ThC2  
 Feis, A. — ThE10  
 Friedrich, Josef — ThD5, ThE10, FE15

**G**lasbeek, Max — SB2  
 Görlach, Ekkehard — ThE11  
 Gorokhovskii, A. A. — SA6  
 Gradl, Gerhard — ThD3, ThE10  
 Graener, H. — FC2  
 Gruzdev, N. V. — ThA6  
 Gygax, Hansruedi — ThE11

**H**aarer, Dietrich — ThA1, ThA3  
 Hahn, E. L. — FE8, SA5  
 Hala, J. — ThE2, FE1  
 Hanson, David M. — FE4  
 He, Huizhu — ThE6, FE12  
 Henshaw, Philip D. — ThB2  
 Heritage, J. P. — FB5  
 Hirschmann, R. — FE15  
 Holliday, Keith — ThE12, FE6  
 Horie, Kazuyuki — ThE7, ThE8, FA6  
 Hoyt, Roger F. — FD4  
 Hu, Lingzhi — ThE6, FE12  
 Huang, Shihua — FA3, FA7  
 Huber, D. L. — ThA  
 Huizhu, He — ThE6, FE12

**I**annone, Mark A. — FE7  
 Ikemoto, Makoto — ThE7  
 Inoue, Hiroyuki — ThE7  
 Ishigame, Mareo — SA4  
 Iwamoto, Takashi — ThE7

**J**aaniso, R. — FA4  
 Jefferson, C. Michael — ThC, FB4  
 Jiahua, Zhang — FA3  
 Jiaqi, Yu — FA3, FA7  
 Jie, Xie — ThE6  
 Junyi, Zhang — ME6

**K**aarli, Rein — ThB3  
 Kachru, R. — FE14  
 Kador, Lothar — ThD4  
 Kaizu, Youkoh — FE13  
 Keller, J.-C. — FB3  
 Kharlamov, B. M. — FE2, FE10  
 Kohler, Bern — ThC3, ThC4  
 Kohler, Bryan E. — ThD3  
 Krausz, Elmars — ThE3  
 Kröll, Stefan — FE14  
 Kushida, T. — FD3

**L**e Gouet, J. L. — FB3  
 L'Esperance, Drew M. — ThA5  
 Li, Wenlian — FA7  
 Lieberth, M. — ThA3  
 Lin, J. W.-I. — FD3  
 Lingzhi, Hu — ThE6, FE12  
 Lis, Steven A. — ThB2  
 Lizeng, Zhao — ThE6, FE12  
 Lu, Zhengzhong — ThE6  
 Lukac, M. — FE8, SA5  
 Luo, Baozhu — FA7  
 Lyle, P. — FE5

**M**acfarlane, R. M. — ThA4, FC4  
 Machida, Shinjiro — FA6  
 Maeda, Masayuki — FA5  
 Maier, Max — ThD1  
 Makishima, Akio — ThE7  
 Meixner, Alfred J. — FB4  
 Meltzer, R. S. — ThA4  
 Mi, Xin — ThE6, FE12  
 Mingzhen, Tian — FA7  
 Mitsunaga, M. — ThB, FB2  
 Moerner, W. E. — SB, SB5  
 Mossberg, Thomas W. — FB1  
 Müller, K. P. — ThA1  
 Murase, Norio — ThE8

**N**edbal, L. — ThE2  
 Ni, Yuxin — ThE6, FE12  
 Nishimura, Tetsuya — ThE9  
 Norris, J. R. — FE5

**O**kuno, Tsuyoshi — SA4  
 Ollikanien, Olavi — ThB1  
 Orrit, M. — SB4  
 Osadko, I. S. — ThE4

**P**ack, Dee William – FA2  
 Palm, V. V. – SA6  
 Personov, R. I. – ThD2  
 Powell, Richard C. – SA3

**R**ebane, Alexander – ThB1, ThC2, ThC4, ThE11  
 Rebane, Karl K. – ThB1  
 Reddy, N. R. S. – ThE14  
 Reeves, Roger J. – FC4, SA3  
 Renge, Indrek – ThE1  
 Renn, Alois – ThC1, ThC3, ThC4, FE6  
 Richter, W. – ThA3  
 Riesen, Hans – ThE3

**S**aari, Peeter – ThB3  
 Saifi, M. A. – FB5  
 Saikan, Seishiro – FD1, FD3  
 Sakakibara, Youichi – FD2, FE13  
 Sakoda, Kazuaki – FA5  
 Schiller, Stephan – ThE5  
 Scott, Gary W. – ThD, FE7  
 Shihua, Huang – FA3, FA7  
 Shimada, Toshiyuki – FE11  
 Sievers, A. J. – FA, FC1  
 Silberberg, Y. – FB5  
 Silbey, R. – FE3  
 Skinner, James – SA1  
 Small, G. J. – ThE14, FC, FE5, SB1  
 Sónajalg, Heiki, – ThB3  
 Squicciarini, M. – ThE13  
 Stolovich, A. L. – SA6  
 Suemoto, Tohru – SA1  
 Suzuki, Hiroyuki – FE11

**T**ada, T. – FD3  
 Takahashi, Hisao – FD2  
 Takahashi, Jun-ichi – ThE15  
 Takeyama, Tetsu – ThE9  
 Tanaka, Hiroshi – ThE15  
 Tanaka, Koichiro – SA4  
 Tani, Toshiro – FD2, FD3, FE13  
 Tchénio, P. – FB3  
 Tian, Mingzhen – FA7  
 Tsuchiya, Jun – ThE15  
 Tsukada, Noriaki – ThE9

**U**litsky, N. I. – FE2, FE10

**V**acha, M. – ThE2, FE1  
 Vainer, Yu. G. – ThA6  
 van Oort, Eric – SB2  
 Vauthey, Eric – FE6  
 Ver Steeg, Keith W. – SA3  
 Volker, S. – SA2

**W**ald, L. L. – FE8, SA5  
 Wang, Duoyuan – ThE6, FE12  
 Wang, Xiangjun – FA3  
 Wang, Y. P. – ThA4  
 Wang, Xiao-jun – FC3  
 Wannemacher, R. – ThA4  
 Wei, Changjiang – ThE12, FE6  
 Wenlian, Li – FA7

Westerfield, Curtis – ThD3  
 Wild, Urs – ThC1, ThC3, ThC4, ThE11, ThE12,  
 FD, FE6

**X**iangjun, Wang – FA3  
 Xie, Jie – ThE6  
 Xin, Mi – FE12  
 Xiulang, Zhang – ThE6

**Y**agyu, Eiji – ThE9  
 Yamamoto, Kyonusuki – FD2  
 Yamashita, Takashi – FA6  
 Yen, W. M. – FB  
 Yoshimura, Motomu – ThE9  
 Yu, Jiaqi – FA3, FA7  
 Yugami, Hiroo – SA4  
 Yuxin, Ni – FE12

**Z**avt, G. S. – SA6  
 Zhang, Dongxiang – ThE6  
 Zhang, Jiahua – FA3  
 Zhang, Junyi – ThE6  
 Zhang, Xiulang – ThE6  
 Zhao, Lizeng – ThE6, FE12  
 Zhengzhong, Lu – ThE6  
 Zollfrank, J. – ThD5  
 Zürcher, U. – FE3

## TECHNICAL PROGRAM COMMITTEE

**W. E. Moerner, Chair**  
*IBM Almaden Research Center*

**Michael Fayer**  
*Stanford University*

**J. Friedrich**  
*University of Mainz, Federal Republic of Germany*

**Dietrich Haarer**  
*University of Bayreuth, Federal Republic of Germany*

**Kazuyuki Horie**  
*The University of Tokyo, Japan*

**Michael Jefferson**  
*IBM Almaden Research Center*

**Roger Macfarlane**  
*IBM Almaden Research Center*

**Masaharu Mitsunaga**  
*NTT Basic Research Laboratories, Japan*

**Thomas W. Mossberg**  
*University of Oregon*

**R. I. Personov**  
*Moscow Institute of Spectroscopy, USSR*

**K. Rebane**  
*Estonian Academy of Sciences, USSR*

**Seishiro Saikan**  
*Osaka University, Japan*

**Kazuaki Sakoda**  
*Toray Industries, Inc., Japan*

**Gary Scott**  
*University of California, Riverside*

**Albert Sievers**  
*Cornell University*

**Robert Silbey**  
*Massachusetts Institute of Technology*

**James Skinner**  
*University of Wisconsin*

**G. J. Small**  
*Iowa State University*

**Toshiro Tani**  
*Electrotechnical Laboratory, Japan*

**S. Volker**  
*University of Leiden, The Netherlands*

**Urs Wild**  
*ETH, Switzerland*

**William M. Yen**  
*University of Georgia*

AFOSSR-TR- 89-02

# **PERSISTENT SPECTRAL HOLE- BURNING: SCIENCE AND APPLICATIONS**

*Sponsored by*  
**Optical Society of America**

**POSTDEADLINE  
PAPERS**

**SEPTEMBER 26-28, 1991  
MONTEREY, CALIFORNIA**

**93 2 2 038**

**Persistent Spectral Hole-Burning: Science and Applications**  
**Postdeadline Papers**  
**September 26-28, 1991**

- PD1 Optical Spectra of Single Impurity Molecules in a  
Polymer: Spectral Diffusion and Persistent Spectral  
Hole-Burning; Th. Basche and W. E. Moerner.....328**
- PD2 Spectral Gain Cross Saturation and Hole-Burning in  
Wideband Erbium-Doped Fibre Amplifiers; M. Tachibana,  
R. I. Laming, P. R. Morkel, and D. N. Payne.....332**
- PD3 The Irreversible Burning of Infrared Spectral Line by  
Laser Action on Silica Contained Matters;  
Anatolii M. Bondar and Anel F. Mukhamedgalieva.....333**
- Key to Authors.....335**

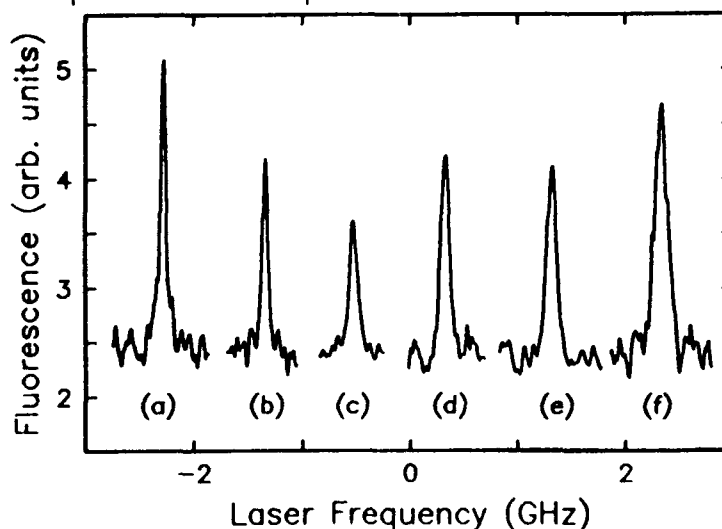
## Optical Spectra of Single Impurity Molecules in a Polymer: Spectral Diffusion and Persistent Spectral Hole-Burning

Th. Basché and W. E. Moerner  
IBM Research Division, Almaden Research Center  
650 Harry Road, San Jose, CA 95120 (408-927-2426)

Recent advances in the optical detection and spectroscopy of single impurity centers in crystals has provided the possibility of obtaining information about defect-solid interactions on a truly local level. For the system composed of pentacene impurity molecules in the crystal p-terphenyl, single molecules have been studied using both absorption<sup>1</sup> and fluorescence excitation<sup>2</sup> techniques at liquid helium temperatures. The superior signal-to-noise of the latter technique has led to direct observations of the lifetime-limited Lorentzian homogeneous profile of a single pentacene impurity<sup>3</sup> as well as the surprising observation of spontaneous spectral diffusion<sup>4</sup>. Spectral diffusion, or changes in the resonance frequency of an impurity molecule with time as a result of low-energy excitations (two-level system transitions (TLS)),<sup>5</sup> is generally expected in amorphous hosts. Indeed, the presence of TLSs in amorphous solids is intimately connected with nonphotochemical mechanisms for persistent spectral hole-burning (PSHB) in amorphous materials<sup>6-8</sup>. Using perylene impurity molecules in poly(ethylene), we have observed the optical spectra of single molecules in a polymeric host for the first time. At 1.5K, individual perylene molecules show the expected spectral diffusion; moreover, we observe light-induced changes in resonance frequency, i.e., persistent spectral hole-burning, which allows one to envision optical storage on the single-molecule level.

Samples were prepared by predissolving zone-refined perylene in acetone; mixing with low-density poly(ethylene) (PE) powder (25 % crystallinity), drying at 50 C for 30 min under high vacuum, hot pressing by hand at 140-150 C between glass slides, and quenching to 77 K for 1 min. The resulting 10-20  $\mu\text{m}$  thick samples had excellent optical clarity (low scattering), little or no aggregate formation as tested by low-resolution optical absorption, and perylene/PE mass ratios of  $9.5 \times 10^{-2}$ . The samples were mounted in a low-temperature optical cryostat at the joint focus of a lens providing the excitation beam and a parabolic mirror collecting the emitted fluorescence as described in detail elsewhere<sup>9</sup>. The tunable excitation laser ( $\approx 2-3$  MHz linewidth) used UV pumping of Stilbene 420 laser dye to generate wavelengths near the center and to the red of the inhomogeneous line of the perylene (0-0)  $S_1 \leftarrow S_0$  transition in PE (442-449 nm). The emitted fluorescence was long-pass filtered with a Schott KV500 low-fluorescence filter to reject Rayleigh scattered radiation. Fluorescence excitation spectra were obtained by scanning the dye laser and recording the red-shifted fluorescence with a GaAs phototube and a photon counter.

**Figure 1.** Fluorescence excitation spectra of various single molecules of perylene in poly(ethylene) at 1.5 K.



By tuning the laser to the long-wavelength side of the inhomogeneous line, isolated single-molecule spectra are easily observed, as in trace (a) of Figure 1. Moreover, even with low laser probing intensity, a variety of linewidths are observed at 1.5 K, as shown in traces (a)-(f). The observed linewidths range from  $52 \pm 2$  MHz in trace (a) to  $142 \pm 5$  MHz in trace (f), and all these values are larger than the lifetime-limited width of 23.4 MHz. The different linewidths occur without correlation with position relative to the center of the inhomogeneous line and without correlation with the probing intensity. In fact, trace (a) of Figure 1 was recorded with the highest probing power of 9 nW (in a  $\approx 5 \mu\text{m}$  diameter laser focal spot). It appears that spectral diffusion on the 1-50 MHz scale is occurring during the 2 s required to measure the lineshape. In addition, there may be a pure dephasing (nondiagonal) contribution to the width at this temperature due to the TLS transitions present at 1.5 K; however, in the standard model, this contribution to the width is generally assumed to be the same for all molecules. In addition to the range of linewidths, we also observe spectral diffusion which appears as discontinuous jumps in resonance frequency on the scale of several hundred MHz between or during the 25 s laser scans in a fashion similar to the previous work on pentacene in *p*-terphenyl<sup>4</sup>.

Usually, persistent spectral hole-burning (PSIIB) in solids refers to optical modification of an inhomogeneous line where the number of centers in resonance is much greater than one. Due to photochemical changes in the excited centers or to photophysical (nonphotochemical) alterations in the nearby host, a narrow spectral "hole" or dip can develop because the altered centers no longer absorb at the laser wavelength. (By definition, "persistent" requires that the alteration persists longer than any excited state lifetime.) In the single-molecule regime, however, only the isolated homogeneous absorption profile of a single center is present. When photochemical or photophysical changes occur as a result of optical excitation, the resonance frequency of the single molecule may move far away from the laser scan range, that is, the absorption line simply disappears.

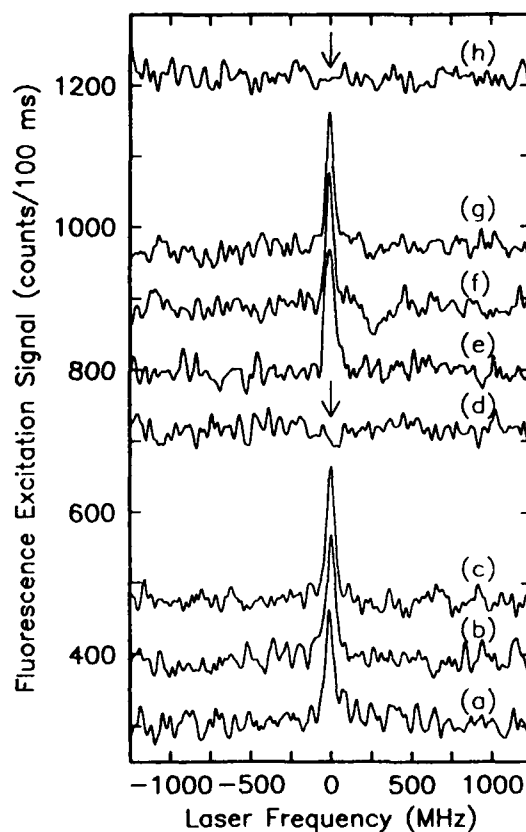
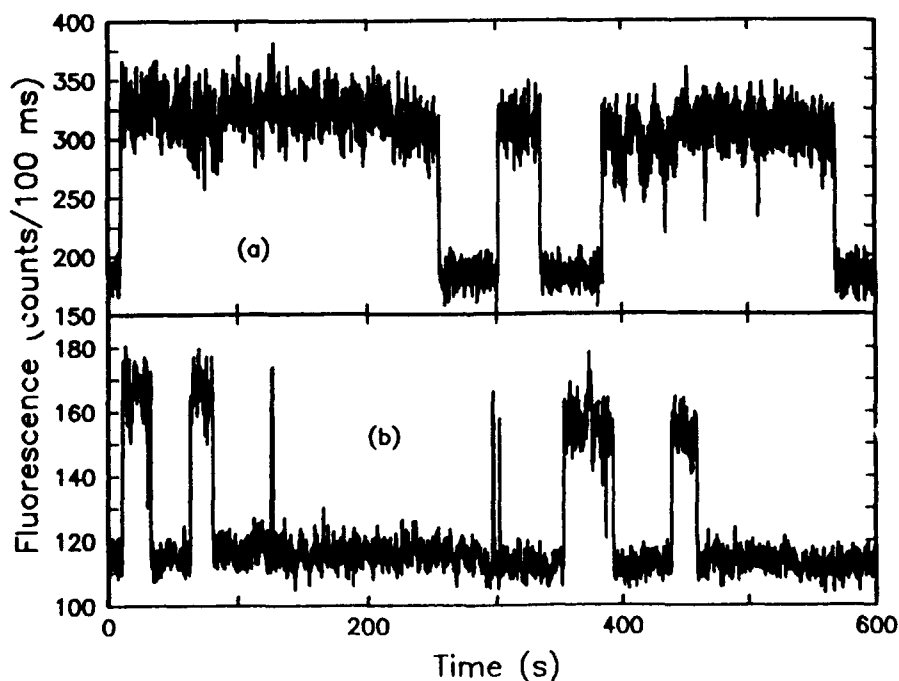


**Figure 2.** Fluorescence excitation spectra of a single molecule showing PSIIB. See text for description.

Figure 2 shows an example of persistent spectral hole-burning for a single perylene molecule in PE. The molecule was deliberately chosen to have little spontaneous spectral jumping from one resonance frequency to another. Before the traces shown in the figure, the molecule was scanned 5 times and no significant changes were observed. Traces (a), (b), and (c) show three additional scans of the molecule. After trace (c), the laser was tuned into resonance with the molecule using the scanning power of 9 nW; within 30 sec the size of the emitted fluorescence suddenly dropped to the background level indicating hole-burning. Trace (d) was then acquired, which shows that the resonance frequency shifted by more than  $\pm 1.25$  GHz as a result of the light-induced change. A further scan some minutes later (trace (e)) showed that the molecule surprisingly returned to the original wavelength within 10 MHz. Further scans (traces (f) and (g)) revealed no further changes in resonance frequency. After trace (g), the laser was again tuned into resonance until the fluorescence dropped; a final scan (trace (h)) showed that the molecule was again absent from the range of the laser scan.

To provide more evidence that the persistent spectral hole-burning process shown in Fig. 2 is laser-driven and not very slow serendipitous spectral diffusion, studies of the kinetics of the process were performed. Figure 3 shows time scans with a fixed laser frequency. In trace (a), the laser was tuned into resonance with the molecule in the first 10 s at a power level of 4.5 nW. The eventual drop in resonance frequency is the hole-burning event; the return of the emitted fluorescence indicates that the molecule has returned to the original wavelength, only to be burned again, and so on. In trace (b) of the figure, the laser power level was increased to 27 nW; now the time in resonance, although stochastic, is clearly shorter. This indicates that the average rate of PSIB for this perylene impurity in PE increases with laser power. Additional studies<sup>10</sup> on a variety of single molecules at a variety of laser power levels over many thousands of seconds of observation yields a confirmation of this power dependence. Even though the actual burn and return times are stochastic, the average burn time for one center decreases with increasing laser power, while the average return time is uncorrelated with laser power.

Figure 3. Time dependence of emitted fluorescence at (a) low power and (b) high power.



The generally accepted model for persistent spectral hole-burning of impurity molecules with no photochemistry in amorphous hosts<sup>8</sup> involves transitions among TLS near the impurity as a result of the optical excitation, while spontaneous (phonon-assisted) transitions of TLS far from the impurity affect the dephasing or optical linewidth. Since a transition of a TLS near the impurity should produce a large change in the local strain field, the resulting shift in the optical resonance frequency should be large, while frequency shifts from distant TLS produce small frequency shifts. Our data provide direct evidence for this picture, since the spontaneous spectral diffusion occurs over a small frequency scale on the order of 10-500 MHz, while the shifts from PSHB are much larger. The return of the optically excited center to exactly the same wavelength in Fig. 2 is surprising, since it suggests that coupling to exactly one nearby TLS is involved in the hole-burning process. If this is true, the single impurity molecule may serve as a direct probe of a single TLS.

The ability to optically modify the absorption of single impurity centers in a solid leads naturally to the possibility of optical storage at the single-molecule level. One could imagine a very thin layer of a material with a very broad inhomogeneous line so that single molecules are isolated and spread over a large range of frequency space. The resonance frequencies constitute the addresses of all the bits to be encoded in a single focal volume. A binary sequence of "1"s and "0"s can be produced by altering or ignoring each single molecule adsorption. Of course, to achieve areal density higher than current persistent spectral hole-burning schemes, a method of producing optical beams much smaller than the diffraction limit must be utilized. This concept, while highly speculative at the present time, provides several advantages and disadvantages. Among the advantages are the extreme areal density (up to perhaps  $10^{14}$  bits/cm<sup>2</sup>) and the greatly increased signal from each molecule resulting from use of sub-diffraction-limited beams (the SNR scales as  $\sqrt{\sigma P/\Lambda}$ , where  $\sigma$  is the peak absorption cross section, P is the laser power, and  $\Lambda$  is the beam area. Some disadvantages are the required low temperatures, stochastically variable burning times, and variable frequency locations of the individual bits from laser spot to laser spot. Nevertheless, the single-molecule persistent spectral hole-burning reported here not only provides a unique window into photophysics of the amorphous state, but it also allows such novel optical storage schemes to be contemplated.

The authors wish to acknowledge crucial prior work by W. P. Ambrose and partial support from the U. S. Office of Naval Research.

1. W. E. Moerner and L. Kador, *Phys. Rev. Lett.* **62**, 2535-2538 (1989).
2. M. Orrit and J. Bernard, *Phys. Rev. Lett.* **65**, 2716 (1990).
3. W. E. Moerner and W. P. Ambrose, *Phys. Rev. Lett.* **66**, 1376 (1991).
4. W. P. Ambrose and W. E. Moerner, *Nature* **349**, 225 (1991).
5. See *Amorphous Solids: Low Temperature Properties*, W. A. Phillips, editor (Springer, Berlin, 1981).
6. J. M. Hayes, R. P. Stout, and G. J. Small, *J. Chem. Phys.* **74**, 4266 (1981).
7. J. Friedrich and D. Haarer, "Structural Relaxation Processes in Polymers and Glasses as Studied by High Resolution Optical Spectroscopy," in *Optical Spectroscopy of Glasses*, I. Zschokke, Ed. (D. Reidel, 1986), pp. 149-198.
8. G. J. Small, Ch. 5 of *Persistent Spectral Hole-Burning: Science and Applications*, W. E. Moerner, editor, Topics in Current Physics Vol. 44 (Springer, Berlin, Heidelberg, 1988).
9. W. P. Ambrose, Th. Basché, and W. E. Moerner, *J. Chem. Phys.*, (Nov. 15, 1991).
10. Th. Basché and W. E. Moerner, to be published.

## SPECTRAL GAIN CROSS SATURATION AND HOLE-BURNING IN WIDEBAND ERBIUM-DOPED FIBRE AMPLIFIERS

M.Tachibana\*, R.I.Laming, P.R. Morkel and D.N. Payne  
 Optoelectronics Research Centre, The University, Southampton, UK.  
 Tel: (+703) 593583 Fax: (+703) 593142

\*Now at Seiko Instruments Inc., 563 Takatsuka-Shinden, Matsudo, Chiba 271, Japan,  
 Tel: (+473) 91 3126, Fax: (+473) 92 2026

**ABSTRACT** Cross saturation characteristics are investigated in broadband 1.48 $\mu\text{m}$  pumped and 980nm pumped, gain-shaped EDFAs. "Gain-shaping" is shown to give a more uniform spectral gain compression on saturation. In addition room temperature spectral gain hole-burning is observed for the first time.

**INTRODUCTION** One of the major applications of erbium-doped fibre amplifiers (EDFA) is likely to be in WDM systems<sup>1</sup>. In this case it is desirable to flatten and maximise the gain bandwidth of the EDFA. To date two techniques have been employed, either by the use of a pump wavelength of  $\sim 1.48\mu\text{m}$  combined with careful choice of pump power and fibre length<sup>2</sup> or by "gain-shaping", incorporating an optical filter in the middle of the amplifier<sup>3</sup>. Applied to either alumino-silicate, germano-alumino-silicate or ZBLAN<sup>4</sup> EDFAs results in 3dB gain bandwidths of  $\sim 35\text{nm}$ . In addition it is important to understand and optimise the cross saturation characteristics of the EDFA. Thus the number of WDM channels can be maximised whilst the gain penalty for each channel and interchannel crosstalk effects are minimised.<sup>5,6</sup>

In this paper, we report an efficient, 1.48 $\mu\text{m}$  diode pumped fibre amplifier. The use of a germano-alumino-silicate erbium-doped fibre as well as careful choice of pump power, pump wavelength and fibre length creates an amplifier characterised by a 25dB gain and 35nm 3dB bandwidth for only 15mW of pump power. Cross saturation characteristics are investigated for saturating signals at various wavelengths across the gain band and different pump powers. In general the gain spectrum decreases non-uniformly, with shorter wavelengths suffering the largest penalty. In addition saturation characteristics show little dependence on the saturating wavelength, only small spectral gain hole-burning is observed confirming the near homogeneous nature of the erbium transition in germano-alumino-silicate glass. Comparison with similar results for a "gain-shaped", 980nm pumped EDFA shows this to be a preferable technique yielding a more uniform decrease in gain spectrum.

**EXPERIMENTAL** The amplifier consisted of 35m of germano-alumino-silicate erbium-doped fibre which was characterised by an  $\text{Er}^{3+}$ -doping level of  $\sim 160\text{ppm}$ , a NA of 0.2 and  $\lambda_{\text{cutoff}}$  at 930nm. The signal source was an ELED which allowed measurement of gain spectra between 1.52 $\mu\text{m}$  and 1.57 $\mu\text{m}$ . Its power was maintained to be less than 200nW within the gain band of  $\text{Er}^{3+}$ , thus ensuring small-signal operation. A further signal from either a DFB-LD or a tunable external cavity LD was mixed with the probe signal through a 3dB fibre coupler. This large signal was sufficient to saturate the amplifier and permitted the measurement of spectral gain under saturated conditions<sup>3</sup>. Pump light at  $\sim 1.485\mu\text{m}$  was obtained from 2 diode lasers. This was combined with the two signals via a dichroic fibre coupler and injected into the amplifier fibre. All free fibre ends were angle polished to suppress optical feedback.

The amplifier output was coupled to a monochromator and detected with lock-in techniques to allow discrimination of the broad-band (ELED), saturating signals (DFB or tunable laser) and ASE by virtue of their different modulation frequencies. Output spectra were obtained for various pump powers, under both small-signal and saturated operation and for several wavelengths of saturating signal. At the end of experiments, the fibre was cut back and spectrum of the broad-band (ELED) signal measured such that the gain spectrum could be obtained

## The irreversible burning of infrared spectral line by laser action on silica contained matters

Anatolii M. Bondar'  
 Institute of Metallurgy,  
 Academy of Science of the USSR  
 Leninsky prospect, 49  
 Moscow 117334, USSR  
 Fax: 7 (095) 135-86-80  
 Anel F. Mukhamedgalieva  
 Moscow Mining Institute  
 Leninsky prospect, 6  
 Moscow 117935, USSR

*The effect of CO<sub>2</sub> laser focused radiation (the wave length of 10.6 μm, power density of 10<sup>3</sup>-10<sup>5</sup> W/cm<sup>2</sup>) on melted quartz and silica contained minerals - nepheline KNa<sub>3</sub>[AlSiO<sub>4</sub>]<sub>4</sub>, microcline K[AlSi<sub>3</sub>O<sub>8</sub>], kaolinite Al<sub>4</sub>[Si<sub>4</sub>O<sub>10</sub>](OH)<sub>8</sub>, etc., has been investigated. The materials mentioned above undergo the laser radiation in the low frequency rang of ungomogeneously broadened infra red absorption line of asymmetric valent Si-O-Si vibrations.*

*Infrared spectra of irradiated samples and those of sublimate demonstrate the phenomena of irreversible spectral line "burning out", i.e. absorption coefficient decrease over the range of laser radiation frequency. The spectral line laser "burning out" phenomena have been observed as characteristic, "step" on the low frequency range of Si-O valent vibrations intensive band and as absorption coefficient decrease on the frequency of laser radiation (943 cm<sup>-1</sup>) /1,2/. In analogous experiments made for nepheline, kaolinite and others silica contained minerals also the absorption decrease in infrared spectrum of irradiated samples zones has been observed /3/. Both the absorption spectra of thermal melts (usually and sun melted) of the same samples, prepared for comparison and those of vacuum ounced laser melted samples have not shown such a decrease.*

*Different types of laser and nonlaser thermal source action indicate the specific laser action on silica-contained minerals - by laser action, instead of thermal heating, selective destruction of Si-O covalent bond occurs.*

*To concretize the mechanism of this bond destruction the electron spin resonance (ESR) investigation of quartz irradiated by CO<sub>2</sub> laser has been made. ESR spectra of crystalline powder (particle size of 10-100 μm) before and after irradiation at the room temperature have been registered. Irradiation of 10.6 μm lead to appearance of intensive wide asymmetric line ( $\Delta H = 90 mT$ ,  $g = 2.5$ ) and more slight narrow line on the right side of wide line with  $g = 1.943$ ;  $H = 328 mT$ . The time behaviour of wide line indicates, that this line is connected with appearance of paramagnetic centers on the surface of powder particles. The narrow line may be identified with paramagnetic center  $\equiv Si-O\cdot-Si \equiv$ , of  $\equiv Si-O-Si \equiv$  bonds. The destruction of these bonds leads to appearance of nonbridging oxygens to change of Si-O vibrations frequency forming the causing of absorptions at the laser action frequency. Thus, the observed spectral line "burning" is obviously caused by nonequilibrium heating and resonant selective destruction of solid covalent bonds, and this provides "clearing" of matter at the laser action frequency.*

1. A.F. Mukhamedgalieva, A.M. Bondar', T.A. Ziborova, "The "burning out" of lines from infrared absorption spectra of microcline  $K[AlSi_3O_8]$  by CO<sub>2</sub> laser radiation". Thesis of reports of the 3 All-Union Conference on physical of interaction the optical radiation on condensed matters, 12-15 november, 1974, Leningrad; p.59 (1974), Moscow, (in russian)

2. A.F. Mukhamedgalieva, A.M. Bondar', T.A. Ziborova, "The effect of IR absorbtion spectrum "deformation" caused CO<sub>2</sub> laser radiation". Sov.Phys., Journal of Technical Physics 46, 873-874 (1976) (in russian)

3. A.F. Mukhamedgalieva, A.M. Bondar', "Laser-stimulated reactions on the surface of quartz and some minerals". Sov. Phys., Surface, physics, chemistry and mechanics 5, 125-129 (1983) (in russian)

**Key to Authors**

Basche, Th. 328  
Bondar, Anatolii 333  
  
Laming, R. I. 332  
  
Moerner, W. E. 328  
Morkel, P. R. 332  
Mukhamedgalieva, Anel F. 333  
  
Payne, D. N. 332  
  
Tachibana, M. 332